

Hyperbolic Knot Theory

Jessica S. Purcell

SCHOOL OF MATHEMATICS, 9 RAINFOREST WALK, ROOM 401, MONASH
UNIVERSITY, VIC 3800, AUSTRALIA
E-mail address: jessica.purcell@monash.edu

2010 *Mathematics Subject Classification*. Primary 57M25, 57M27, 57M50, 30F40. Secondary 57N10, 57Q15

Key words and phrases. Hyperbolic geometry, knot theory, 3-manifolds

Contents

| | |
|---|-----------|
| Introduction | vii |
| Preface | ix |
| Why I wrote this book | ix |
| How I structured the book | x |
| Prerequisites and notes to students | xi |
| Acknowledgments | xii |
| Chapter 0. A Brief Introduction to Hyperbolic Knots | 1 |
| 0.1. An introduction to knot theory | 1 |
| 0.2. Problems in knot theory | 3 |
| 0.3. Exercises | 15 |
| Part 1. Foundations of Hyperbolic Structures | 17 |
| Chapter 1. Decomposition of the Figure-8 Knot | 19 |
| 1.1. Polyhedra | 19 |
| 1.2. Generalizing: Exercises | 25 |
| Chapter 2. Calculating in Hyperbolic Space | 29 |
| 2.1. Hyperbolic geometry in dimension two | 29 |
| 2.2. Hyperbolic geometry in dimension three | 37 |
| 2.3. Exercises | 39 |
| Chapter 3. Geometric Structures on Manifolds | 43 |
| 3.1. Geometric structures | 43 |
| 3.2. Complete structures | 49 |
| 3.3. Developing map and completeness | 60 |
| 3.4. Exercises | 61 |
| Chapter 4. Hyperbolic Structures and Triangulations | 65 |
| 4.1. Geometric triangulations | 65 |
| 4.2. Edge gluing equations | 69 |
| 4.3. Completeness equations | 73 |
| 4.4. Computing hyperbolic structures | 78 |
| 4.5. Exercises | 79 |
| Chapter 5. Discrete Groups and the Thick–Thin Decomposition | 83 |
| 5.1. Discrete subgroups of hyperbolic isometries | 83 |

| | |
|--|------------|
| 5.2. Elementary groups | 88 |
| 5.3. Thick and thin parts | 91 |
| 5.4. Hyperbolic manifolds with finite volume | 93 |
| 5.5. Universal elementary neighborhoods | 95 |
| 5.6. Exercises | 101 |
| Chapter 6. Completion and Dehn Filling | 105 |
| 6.1. Mostow–Prasad rigidity | 105 |
| 6.2. Completion of incomplete structures | 106 |
| 6.3. Hyperbolic Dehn filling space | 109 |
| 6.4. A brief summary of geometric convergence | 117 |
| 6.5. Exercises | 122 |
| Part 2. Tools, Techniques, and Families of Examples | 125 |
| Chapter 7. Twist Knots and Augmented Links | 127 |
| 7.1. Twist knots and Dehn fillings | 127 |
| 7.2. Double twist knots and the Borromean rings | 131 |
| 7.3. Augmenting and highly twisted knots | 134 |
| 7.4. Cusps of fully augmented links | 140 |
| 7.5. Exercises | 146 |
| Chapter 8. Essential Surfaces | 149 |
| 8.1. Incompressible surfaces | 149 |
| 8.2. Torus decomposition, Seifert fibering, and geometrization | 154 |
| 8.3. Normal surfaces, angled polyhedra, and hyperbolicity | 156 |
| 8.4. Pleated surfaces and a 6-theorem | 164 |
| 8.5. Exercises | 171 |
| Chapter 9. Volume and Angle Structures | 173 |
| 9.1. Hyperbolic volume of ideal tetrahedra | 173 |
| 9.2. Angle structures and the volume functional | 182 |
| 9.3. Leading–trailing deformations | 184 |
| 9.4. The Schläfli formula | 190 |
| 9.5. Consequences | 190 |
| 9.6. Exercises | 192 |
| Chapter 10. Two-Bridge Knots and Links | 195 |
| 10.1. Rational tangles and 2-bridge links | 195 |
| 10.2. Triangulations of 2-bridge links | 199 |
| 10.3. Positively oriented tetrahedra | 207 |
| 10.4. Maximum in interior | 213 |
| 10.5. Exercises | 222 |
| Chapter 11. Alternating Knots and Links | 225 |
| 11.1. Alternating diagrams and hyperbolicity | 225 |
| 11.2. Checkerboard surfaces | 237 |

| | |
|--|------------|
| 11.3. Exercises | 241 |
| Chapter 12. The Geometry of Embedded Surfaces | 243 |
| 12.1. Belted sums and mutations | 243 |
| 12.2. Fuchsian, quasifuchsian, and accidental surfaces | 247 |
| 12.3. Fibers and semifibers | 253 |
| 12.4. Exercises | 259 |
| Part 3. Hyperbolic Knot Invariants | 261 |
| Chapter 13. Estimating Volume | 263 |
| 13.1. Summary of bounds encountered so far | 263 |
| 13.2. Negatively curved metrics and Dehn filling | 266 |
| 13.3. Volume, guts, and essential surfaces | 279 |
| 13.4. Exercises | 288 |
| Chapter 14. Ford Domains and Canonical Polyhedra | 291 |
| 14.1. Horoballs and isometric spheres | 292 |
| 14.2. Ford domain | 299 |
| 14.3. Canonical polyhedra | 305 |
| 14.4. Exercises | 309 |
| Chapter 15. Algebraic Sets and the A -Polynomial | 311 |
| 15.1. The gluing variety | 311 |
| 15.2. Representations of knots | 316 |
| 15.3. The A -polynomial | 323 |
| 15.4. Exercises | 327 |
| Bibliography | 329 |
| Index | 339 |

Introduction

Knots appear in scientific literature as early as 1771, in work of Vandermonde. In approximately 1833, Gauss developed the linking number of two knots, and his student Listing published work on alternating knots in 1847. Tait was one of the first to try to classify knots up to equivalence, creating the first knot tables in the 1870s and 1880s. For more on the history of knots, see for example the detailed article by Epple [Epp98], or the survey articles by Przytycki [Prz98] and Silver [Sil06].

Since the early work of Tait, knot theory has been influenced by and influential in the mathematical fields of topology, algebra, quantum field theory, and in geometry. There are several books that investigate knots from topological, algebraic, and quantum perspectives; some of my favorites are those of Rolfsen [Rol90], Burde and Zieschang [BZ85], Murasugi [Mur96], and Lickorish [Lic97]. This book focuses on knots from a geometric perspective, particularly hyperbolic geometry, and overlaps more with books on hyperbolic geometry than knot theory, particularly in the early chapters that develop prerequisites in hyperbolic geometry. See, for example, [BP92, Rat06, Thu97].

The study of the geometry of knots, particularly hyperbolic geometry, began with work of Robert Riley in the 1970s [Ril75], and developed further in the late 1970s and early 1980s, with work of William Thurston [Thu79].

By Thurston's work, a knot complement has one of three forms: Either it is a *torus knot*, which can be drawn as an embedded curve on a Heegaard torus in the 3-sphere, or a *satellite knot*, which lies in a tubular neighborhood of another knot, or it is *hyperbolic* [Thu82]. Torus knots are relatively well-understood, and satellite knots are often studied by considering other knots. Hyperbolic knots, however, are not well-understood in general, and yet they are extremely common. For example, of all prime knots up to 16 crossings, classified by Hoste, Thistlethwaite, and Weeks, 13 are torus knots, 20 are satellite knots, and the remaining 1,701,903 are hyperbolic [HTW98]. Of all prime knots up to 19 crossings, 15 are torus knots, 380 are satellite knots, and the remaining 352,151,858 are hyperbolic [Bur20].

Moreover, if a knot complement admits a hyperbolic structure, then that structure is unique, by work of Mostow and Prasad in the 1970s [Mos73, Pra73]. More carefully, Mostow showed that if there is an isomorphism between the fundamental groups of two closed hyperbolic 3-manifolds, then there is an isometry taking one to the other. Prasad extended this work to

3-manifolds with torus boundary, including knot complements. Thus if two hyperbolic knot complements have isomorphic fundamental group, then they have exactly the same hyperbolic structure. Finally, Gordon and Luecke showed that two knot complements with the same fundamental group are equivalent [**GL89**] (up to mirror reflection).

Thus a hyperbolic structure on a knot complement is a complete invariant of the knot. If we could completely understand hyperbolic structures on knot complements, we could completely classify hyperbolic knots. This book is an introduction to the mathematics involved.

Preface

Why I wrote this book

This book is an introduction to hyperbolic geometry in three dimensions, with motivations and examples coming from the field of knots. It is also an introduction to knot theory, with tools, techniques, and topics coming from geometry. As I write, I believe it is the only book that attempts to be both.

To be clear, there are dozens of excellent books on knot theory, available from undergraduate to graduate levels, many of them classics that I learned from and continue to learn from. There are also several excellent books on hyperbolic geometry, particularly from the three-dimensional viewpoint. The aim of this book is to fill in a gap between them: to feature the contributions of hyperbolic geometry to knot theory, and the contributions of knot theory to hyperbolic geometry. It also aims to put techniques and tools from both fields into one place.

In recent years, the field of hyperbolic 3-manifolds has matured, with many open conjectures resolved in the early 2000s. The result is that we now have better insight than ever into the structure of hyperbolic manifolds. This insight can be applied to broad classes of 3-manifolds, including many knot and link complements. On the other hand, the area of knot theory has also ballooned in recent years, with new tools arising from algebra, homology theory, quantum topology, representation theory, as well as geometry. As new knot and link invariants arise, and new applications of knot theory to other fields develop, it is natural to ask how such invariants interact. In particular, how do these invariants interact with hyperbolic geometry, which contains some of the strongest information on knots and links? There are many open questions and conjectures about the interaction of hyperbolic geometry with other knot invariants, and many mathematicians are interested in learning hyperbolic geometry specifically as it applies to knot theory. This book is a more direct introduction to the hyperbolic geometry of knots.

Hyperbolic geometry was first applied to the study of knots and their complements in the 1970s. Since then, hyperbolic geometry has played an important role in the classification of knots, with invariants such as volume and canonical decomposition developing directly from geometry.

However, the contribution of knot theory to hyperbolic geometry should not be understated. Complements of knots and links have been the playground of the 3-dimensional hyperbolic geometer for decades, aided by diagrams and topology, and by computational software such as SnapPea by Weeks, to find hyperbolic structures on knots. Many conjectures in hyperbolic geometry are based upon geometric properties that were first observed in knots. Many results in hyperbolic geometry have been proved first by restricting to families of knots, especially twist knots, two-bridge knots, and alternating knots, all of which feature prominently in this text.

This book is a hands-on introduction to this mixing of fields, geometry and knots.

How I structured the book

The book starts with an introductory chapter giving basic definitions required from knot theory, and motivating some of the problems discussed in this book.

The first example of a hyperbolic knot, identified by Riley, is the unique prime knot with crossing number four, known as the figure-8 knot. In chapter 1, we give an introduction to the complement of the figure-8 knot, and describe how to decompose it into two polyhedra. The exercises outline a generalization of this decomposition to all knots, and lead the reader through complications that arise when generalizing. This decomposition, particularly for the figure-8 knot, will then serve as a running example for later chapters.

In chapters two through six, we develop the basics of geometric structures on manifolds, particularly in dimensions two and three. Much of this material overlaps with other texts on hyperbolic geometry. Here, we try to keep our presentation heavily illustrated by examples, especially examples from knot theory. More specifically, chapter 2 gives an introduction to the hyperbolic plane and hyperbolic 3-space, and gives properties and examples of calculations that we will need in the text. It is purposely brief, as it is not meant to be a comprehensive introduction to these spaces, but only to equip the reader with the tools required to calculate and compute in hyperbolic geometry. Chapter 3 introduces geometric structures on manifolds, and works through examples in two dimensions, including careful examples of the torus and the 3-punctured sphere. Chapter 4 returns to 3-manifolds and knots, building the first examples of hyperbolic structures on knot complements by way of triangulations. The chapter covers Thurston's gluing and completeness equations, again using the figure-8 knot as a running example. Chapter 5 delves a little more deeply into properties of hyperbolic isometries, with a main goal of proving the thick-thin decomposition of hyperbolic 3-manifolds. This decomposition implies that thin parts of hyperbolic 3-manifolds can always be identified with knots or links in some

3-dimensional space. Finally, in chapter 6, incomplete structures on hyperbolic 3-manifolds are investigated carefully. The main result is that such structures can often be viewed as Dehn fillings of hyperbolic manifolds.

Chapters seven through twelve focus on families of knots and links that have been particularly amenable to study through hyperbolic geometry, and to tools used to study these knots and links, including tools coming from more general 3-manifold topology. Chapter 7, just after the chapter on hyperbolic Dehn filling, discusses knots described by Dehn filling links in the 3-sphere; many of these links have very explicit hyperbolic geometry. This chapter explores consequences of Dehn fillings for these families. Chapter 8 then provides an interlude, with results from 3-manifold topology, defining essential surfaces, normal surfaces, and returning to hyperbolic geometry via angle structures. Chapter 9 develops the powerful tool of angle structures and volumes of 3-manifolds. The main result in the chapter is a proof of the theorem of Casson and Rivin relating volumes of angle structures to hyperbolic geometry. Angle structures have had great success as applied to the family of two-bridge knots, and this is the subject of chapter 10. The chapter develops topological descriptions of the knots as gluings of tetrahedra, and works through a proof that these tetrahedra are geometric using the theorems of chapter 9. In chapter 11, we study alternating links. This chapter gives a proof, using properties of these knots, of the theorem of Menasco that a prime alternating knot with more than one twist region is hyperbolic. Chapter 12 discusses the geometry of surfaces embedded in knot and link complements, including three and four punctured spheres, and checkerboard surfaces.

The final chapters, chapters thirteen through fifteen, explore some of the more important knot and link invariants arising from hyperbolic geometry. One of the most important geometric invariants of a hyperbolic knot is its volume, and chapter 13 is devoted to volumes of knots and links. It contains methods to bound the volume of a knot. Chapter 14 discusses the Ford domain and canonical polyhedral decomposition, also called the Epstein–Penner decomposition of a manifold. This decomposition provides a tool that can be used to identify when two 3-manifolds are isometric; for example it is used by the software SnapPea (and SnapPy). Chapter 15 gives a brief introduction to the overlap of hyperbolic geometry and algebraic geometry, introducing gluing and character varieties of knots, and the A -polynomial, which is a polynomial invariant directly related to the hyperbolic geometry of a knot.

Prerequisites and notes to students

I have tried to keep prerequisites to a minimum. A basic course in topology is required, as well as some knowledge of basic algebraic topology, particularly the fundamental group and covering spaces. Occasionally, experience with Riemannian geometry will be helpful, but it is not required, with

one exception: we assume standard results from a first course in Riemannian geometry in parts of chapter 13. We also occasionally assume basic results in differential topology, such as the fact that smooth manifolds admit tubular neighborhoods, and that submanifolds can be isotoped to meet transversely.

Also, this book is written to be interactive, with examples and exercises. I hope you work through the examples as they are presented, and generalize them in exercises. Many important results are saved for exercises.

Acknowledgments

The first form of this book appeared as lecture notes for a unit at Brigham Young University (BYU). The subject was inspired by my participation in a workshop on interactions between hyperbolic geometry, quantum topology, and number theory held at Columbia University in 2009. I have also given related graduate student workshops at Iowa in 2014, at Melbourne in 2016, and at Luminy in 2018. I thank the organizers of these workshops for inviting me, and various agencies for supporting the workshops, and for supporting fundamental research in mathematics.

I learned much of the material in the first part of this book as a graduate student under the direction of Steve Kerckhoff, reading notes of William Thurston from the 1970s that were ghost-written by Kerckhoff and Bill Floyd [Thu79]. Learning along with me were fellow graduate students David Futer and Henry Segerman. Many of their insights and elucidations helped me develop my own understanding; those insights are contained in this book, and I thank Steve, David, and Henry for them. I also owe thanks to Henry Segerman and Saul Schleimer for figures, particularly figures 6.4, 6.5, 6.6, and 12.6. Thanks to Saul Schleimer for figures 12.5, and to David Bachman, Saul Schleimer, and Henry Segerman for figure 12.7. Discussions with David Futer about various parts of this book, especially two-bridge knots, have been invaluable. I also thank Jim Cannon, who attended my course on this material, and provided ideas for helping students get involved with exercises, and I thank Kenneth Perko, Abhijit Champanerkar, Ilya Kofman, Yi Wang, and Yair Minsky for feedback on drafts of the book.

I owe the most thanks to the many people who have worked through various drafts and incarnations of this book, especially Emma Turner and Mark Meilstrup, who gave great feedback during the original 2010 BYU course, and Sophie Ham, Max Jolley, Josh Howie, Emily Thompson, John Stewart, and Ensil Kang, who read through many chapters carefully and helped me fix exposition and errors. I also thank students who have worked through drafts of this book with others, including students at the University of Warwick, at Michigan State University, Temple University, and at Oklahoma State University.

Remaining errors are, of course, my own. Please tell me about them.

Jessica S. Purcell

CHAPTER 0

A Brief Introduction to Hyperbolic Knots

This book gives an introduction to knots, links, and hyperbolic geometry. Before we begin, we need to define carefully what we mean by knots and links, and that is done in this chapter. We also introduce classical problems in knot theory, and problems motivated by geometry, especially hyperbolic geometry. This chapter is meant to motivate future chapters, and it has many references to content covered in more detail later in the book, where we address some of these problems. Many of the questions described in this chapter have partial answers, and many are still wide open.

0.1. An introduction to knot theory

The earliest study of knots seems to be by Gauss, Listing, and especially Tait, who published several papers on knot theory in the years 1876 through 1885. In a preface to his work on knot theory, republished in his 1898 Scientific papers [Tai98], Tait writes:

“The subject [knot theory] is a very much more difficult and intricate one than at first sight one is inclined to think, and I feel that I have not succeeded in catching the key-note.”

Since Tait’s work, advances in knot theory have come through applications of topology, algebra, and invariants arising in quantum field theory, but no single mathematical field has led to simple tools that apply to all knots. In other words, perhaps mathematicians still have not succeeded in catching the “key-note.” Perhaps there is no “key-note” in knot theory. However, there are definitely mathematical techniques that work well when applied to particular problems or particular families. This book introduces techniques arising from geometry.

0.1.1. Basic terminology. To begin, we need careful definitions of the objects involved.

DEFINITION 0.1. A *knot* $K \subset S^3$ is a subset of points homeomorphic to a circle S^1 under a piecewise linear (PL) homeomorphism. We may also think of a knot as a PL embedding $K: S^1 \rightarrow S^3$. We will use the same symbol K to refer to the map and its image $K(S^1)$.

More generally, a *link* is a subset of S^3 PL homeomorphic to a disjoint union of copies of S^1 . Alternatively, we may think of a link as a PL embedding of a disjoint union of copies of S^1 into S^3 .

A PL homeomorphism of S^1 is one that takes S^1 to a finite number of linear segments. Restricting to such homeomorphisms allows us to assume that a knot $K \subset S^3$ has a regular tubular neighborhood, that is there is an embedding of a solid torus $S^1 \times D^2$ into S^3 such that $S^1 \times \{0\}$ maps to K . An embedding of S^1 into S^3 that cannot be made piecewise linear defines an object called a *wild knot*. Wild knots may have very interesting geometry, but we will only be concerned with the classical knots of definition 0.1 here.

In fact, rather than working with PL embeddings and homeomorphisms, we obtain the same results working with smooth ones. That is, we could require instead in definition 0.1 that a knot be a smooth embedding of S^1 into S^3 , and we obtain an equivalent theory. We will assume this fact throughout the book, working with both PL and smooth maps, with very little mention of this fact.

DEFINITION 0.2. We will say that two knots (or links) K_1 and K_2 are equivalent if they are *ambient isotopic*, that is, if there is a (PL or smooth) homotopy $h: S^3 \times [0, 1] \rightarrow S^3$ such that $h(*, t) = h_t: S^3 \rightarrow S^3$ is a homeomorphism for each t , and

$$h(K_1, 0) = h_0(K_1) = K_1 \quad \text{and} \quad h(K_1, 1) = h_1(K_1) = K_2.$$

Such a map h is called an *ambient isotopy*.

A PL (or smooth) embedding of S^1 into S^3 defines two 3-manifolds, one open and one compact, as in the following definition.

DEFINITION 0.3. For a knot K , let $N(K)$ denote an open regular neighborhood of K in S^3 . The *knot exterior* is the manifold $S^3 - N(K)$. Notice that it is a compact 3-manifold with boundary homeomorphic to a torus.

The *knot complement* is the open manifold $S^3 - K$, homeomorphic to the interior of $S^3 - N(K)$.

Similarly, if L is a link the *link exterior* is $S^3 - N(L)$, and the *link complement* is $S^3 - L$.

It was an open question for many years as to whether two knots with homeomorphic complements must be equivalent (up to reflection). This was proved in the affirmative by Gordon and Luecke in 1989 [GL89].

THEOREM 0.4 (Gordon–Luecke Theorem). *If two knots have complements that are homeomorphic by an orientation-preserving homeomorphism, then the knots are equivalent.*

The complement of a knot and the complement of its reflection are homeomorphic, by the orientation-reversing reflection homeomorphism. However, the knot itself may not be equivalent to its reflection. In fact, hyperbolic geometry tools do not distinguish knots and their reflections, and so we

often only consider knots up to reflection in this book. If we disregard reflections, the Gordon–Luecke theorem states that knots are determined by their complements.

The same is not true for links. There are infinitely many inequivalent links whose complements are homeomorphic. However, the ways in which such links can be constructed are relatively well-understood; see, for example [Gor02].

DEFINITION 0.5. A *knot diagram* (or *link diagram*) is a 4-valent graph with over/under crossing information at each vertex. The diagram is embedded in a plane $S^2 \subset S^3$ called the *projection plane*, or *plane of projection*.

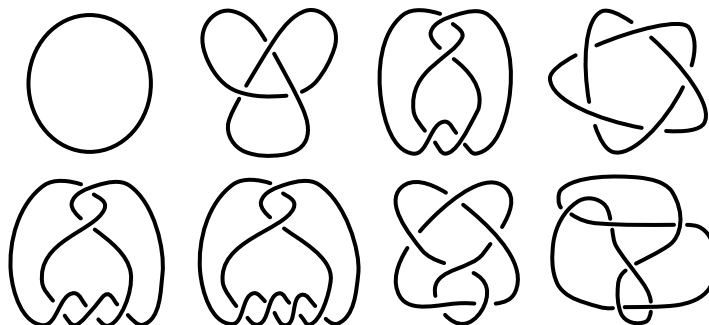


FIGURE 0.1. Knots with at most six crossings.

Figure 0.1 shows diagrams of the eight knots with at most six crossings. Classically, a knot has been described by a diagram. Tait’s works give many diagrams. In modern work, knots also appear without diagrams, for example when they arise as periodic orbits of a dynamical system [BW83], or from a gluing of polyhedra [CDW99, CKP04, CKM14].

However, many open problems in knot theory still concern knot diagrams. One goal of chapter 1, and then the next few chapters, is to give a method to pass from a knot or link *diagram* to a topological and then geometric description of the knot or link *complement*. That is, we start with a 4-valent graph describing a knot or link K , and obtain a mathematically rigorous decomposition of the 3-manifold $S^3 - K$ into simple 3-dimensional pieces, which will be useful for applying tools from geometry and 3-manifold topology.

0.2. Problems in knot theory

There are many open problems in knot theory, and as new mathematical fields are brought to bear upon these problems, new questions and problems arise. This section gives a few highlights of the most classical problems, and also problems that seem most amenable to geometric techniques. Probably the most long-standing problem, and also one of the most broad, is the following.

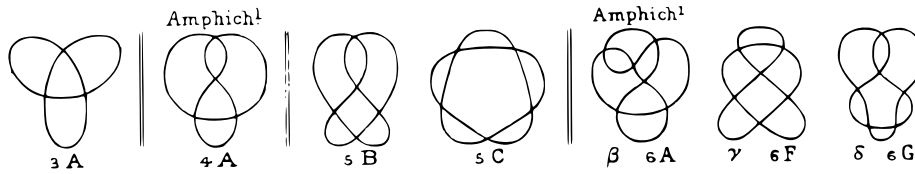


FIGURE 0.2. A very small portion of P. Tait's 1884 tables of knot diagrams, from [Tai 4]. The original contains a full page with such diagrams, with additional pages of diagrams in [Tai 5].

0.2.1. The classification problem. When do two different descriptions of knots yield equivalent knots? When do they have homeomorphic complements?

When the description of a knot is given by a diagram, this is the problem that Tait encountered while trying to list all knots with a fixed number of crossings. See figure 0.2, which is modified from the 1884 paper [Tai 4].

There are a few moves that can be performed on a diagram that do not change the equivalence class of the underlying knot. For example, if the diagram contains a single crossing that forms a loop, as shown on the left of figure 0.3, that loop can be untwisted to simplify the diagram.

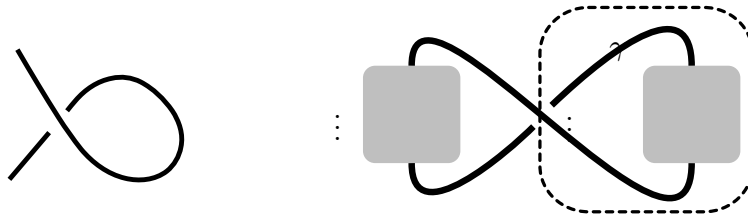


FIGURE 0.3. On the left, a nugatory crossing. On the right, a more general reducible crossing.

DEFINITION 0.6. A single crossing forming a loop, as on the left of figure 0.3, is called a *nugatory crossing*.

More generally, a *reducible crossing* is a crossing through which we may draw a circle γ on the plane of projection such that γ meets the diagram only at one point, at the crossing. See figure 0.3, right.

A diagram is *reduced* if it contains no reducible crossings.

Note that reducible crossings can be removed by isotoping the diagram. We typically will assume that our knot diagrams are reduced.

There are other well-known moves to change a diagram into an equivalent diagram. These include the three moves shown in figure 0.4, called Reidemeister moves.

The Reidemeister moves appear in work of Maxwell in the 1800s (see, for example, [Epp98]). In the 1920s, Reidemeister [Rei27] and Alexander

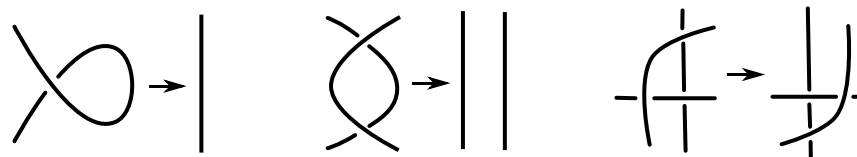


FIGURE 0.4. Three Reidemeister moves do not change knot equivalence.

and Briggs [AB27] independently gave rigorous proofs that two equivalent diagrams can always be related by a sequence of such moves.

The *crossing number* of a knot is the minimal number of crossings in all diagrams of the knot. A minimal crossing diagram will necessarily be reduced. However, a reduced diagram is not necessarily a minimal crossing diagram. For example, figure 0.5 shows the reduced diagram of a knot that can, with a little work, be simplified to the *unknot*, i.e. the simple circle with no crossings. This diagram was discovered by Goeritz in 1934 [Goe34].

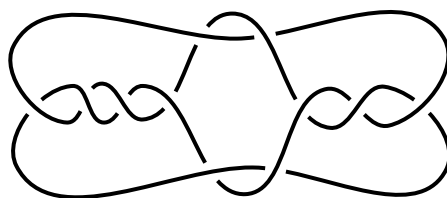


FIGURE 0.5. This diagram of the unknot was discovered in 1934 by Goeritz.

In fact, the diagram of figure 0.5 is an example of a knot diagram that cannot be simplified by Reidemeister moves without first increasing the number of crossings of the diagram.

In addition to attempting to remove crossings, other moves can be performed on diagrams to simplify the classification problem. For example, there is a way of joining two simple diagrams into one more complicated diagram, shown in figure 0.6.

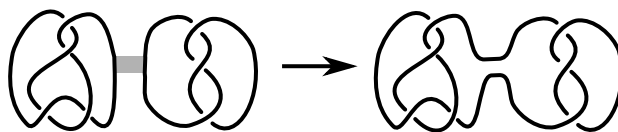


FIGURE 0.6. The knot sum of two knots.

Starting with two diagrams side-by-side, take a rectangle embedded in the plane of projection that has one side on one diagram, avoiding crossings, an opposite side on the other diagram, again avoiding crossings, and the final two sides disjoint from the two diagrams. Form the new diagram by removing the two edges of the rectangle that lie on the knots, and joining

the knots along the two opposite sides of the rectangle. The resulting knot is called the *knot sum*. It is also sometimes called the *connected sum of the knots*.

Given a knot sum of two knot diagrams, consider the embedded curve γ in the plane of projection of the diagram that encircles exactly one of the original diagrams, cutting through the rectangle in the definition of the knot sum. This curve γ meets the diagram of the knot sum in exactly two points, and it bounds disks on both sides (thinking of the projection plane as $S^2 \subset S^3$), and both discs contain crossings. We say that a diagram is *prime* if no such curve γ exists. That is, a knot or link diagram is *prime* if, for every simple closed curve γ in the plane of projection, if γ meets the knot exactly twice transversely away from crossings, then γ bounds a region of the diagram with no crossings.

Curves such as γ above detect knot sums. When knots are classified by diagram, listed according to crossing number, typically only prime diagrams are included.

The problem of listing all knots by crossing number, without duplicates, is a difficult one. There are 1,701,936 prime knots with at most 16 crossings, classified by Hoste, Thistlethwaite, and Weeks in 1998 [HTW98]. More recently, Burton classified 352,152,252 prime knots up to 19 crossings [Bur20]. These knots can be downloaded with the 3-manifold software Regina [BBP⁺19]. In both instances, the knots are only classified up to reflection in the plane of projection.

DEFINITION 0.7. A *knot invariant* is a function from the set of knots to some other set whose value depends only on the equivalence class of the knot. A *link invariant* is defined similarly.

The crossing number of a knot is an example of a knot invariant.

Knot and link invariants are used to prove that two knots or links are distinct, or to measure the complexity of the link in various ways. We will revisit examples of knot invariants below, particularly geometric ones.

Notice that the number of knots with a given crossing number grows very rapidly. There does not seem to be a natural way of enumerating knots within a fixed class of crossing number. And while the crossing number was one of the first knot invariants to be studied by knot theorists, it does not seem to relate well to other knot invariants, particularly those that arise in geometry. For these reasons and others, other ways of classifying knots have arisen over the years, which we will discuss further below.

In this book we will apply geometry to the problem of the classification of knots. It has been known since the early 1980s, due to work of Thurston [Thu82], that the complement of a knot decomposes into pieces, each admitting a 3-dimensional geometry. By using geometric properties of knot complements, we can often distinguish knots. This brings us to the second problem in knot theory that we discuss here.

0.2.2. The problem of determining geometry of the complement. Briefly, the complement of a knot is *hyperbolic* if and only if it admits a complete metric with all sectional curvatures equal to -1 . We will give other equivalent definitions of hyperbolic knots in later chapters, which will often be more useful for calculations, computations, and examples.

For now, it is known that when a knot complement is hyperbolic, its hyperbolic metric is unique. That is, hyperbolic knot complements that are homeomorphic must also be isometric under any hyperbolic metrics placed upon their complements. Moreover, a large number of knots are hyperbolic, and many that are not hyperbolic decompose into hyperbolic pieces.

More precisely, consider the following families of knots.

DEFINITION 0.8. A *torus knot* is a knot that can be embedded (without crossings) on the surface of an unknotted torus in S^3 . See figure 0.7.

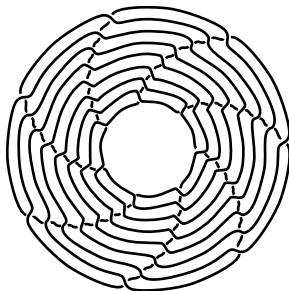


FIGURE 0.7. A torus knot

By an unknotted torus, we mean the neighborhood of an unknot in S^3 , with no crossings.

DEFINITION 0.9. A *satellite knot* is a knot that can be embedded in a regular neighborhood of another knot in S^3 . See figure 0.8.

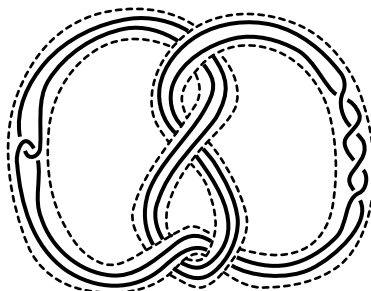


FIGURE 0.8. An example of a satellite knot. The dotted line forms the boundary of a neighborhood of a different knot, and the satellite lives inside that neighborhood.

The complement of a torus knot admits a 3-dimensional geometry that is not hyperbolic, due to work of Thurston [Thu82]. He also showed that the complement of a satellite knot cannot be hyperbolic, but can be cut along a torus to decompose into pieces that admit 3-dimensional geometry, which could possibly be hyperbolic. For example, the knot complement in figure 0.8 can be cut along the dashed solid torus into two hyperbolic pieces, as we will see later in this book.

Thurston showed that every knot in S^3 that is neither a torus knot nor a satellite knot must have hyperbolic complement [Thu82].

Thus hyperbolic geometry can be a useful tool in the classification problem of knots — in theory.

In practice, we need tools and techniques to determine when a knot complement is hyperbolic. For example, if a knot is given by a messy diagram, how does one determine whether or not it is equivalent to a torus or satellite knot? How can we determine whether its complement is hyperbolic? And if it is hyperbolic, how can we find a hyperbolic metric?

Thurston outlined a procedure for finding a hyperbolic metric using the diagram of the figure-8 knot in his 1979 lecture notes [Thu79]. This process was generalized by others, for example [Men83], and even made algorithmic, in Weeks' 1985 PhD thesis [Wee85]. There is now software that determines, given a knot diagram, whether or not the knot complement is hyperbolic. This is the computer program SnapPy, which is freely available [CDGW16].

Indeed, using computational tools, Burton has determined that of all prime knots with up to 19 crossings, 352,151,858 are hyperbolic, and only 395 are not hyperbolic [Bur20]. These are split into 14 torus knots and 380 satellite knots.

The next four chapters of this book concern the problem of determining a hyperbolic metric on a knot complement. We will step carefully through the necessary definitions and procedures, using Thurston's decomposition of the figure-8 knot complement as an example. This will give our first potential method to find a hyperbolic metric.

Chapters 5 and 6 give additional methods and tools from hyperbolic geometry to find or deform a hyperbolic metric. These first six chapters form the foundation required to discuss hyperbolic geometry and knots in more detail.

Of course, these chapters require some work. The fact that software exists that can compute hyperbolic geometry of knots begs the question, why work through such computations by hand at all? Why not just work with the computer? There are many reasons, related to additional open problems. One reason is the next problem.

0.2.3. The problem of determining geometry for families of knots. A computer program computes hyperbolic geometry for one knot at a time, or for a finite number of knots. But what can be said about infinite families of knots? For example, how does one determine the hyperbolic

geometry of knots with descriptions given by infinite classes of diagrams? If two knots in a family are “similar” is their geometry also similar?

Potential answers to such questions seem to depend very heavily on the family of knots given. For example, for fixed c , it does not seem to be the case that the (finite) family of knots with crossing number c have very similar hyperbolic geometry.

On the other hand, certain infinite families of knots do exist with very similar hyperbolic geometry, and others at least seem to have geometry that reflects properties of the diagrams. We will discuss such knots and their properties, for example in chapters 7, 10, and 11, with careful proofs. For now, we will present a definition of one such family.

DEFINITION 0.10. A *bigon* is a region of a graph bounded by exactly two edges and exactly two vertices.

For example, figure 0.9 shows several bigons connected end-to-end in a portion of a diagram graph of a knot.



FIGURE 0.9. A twist region of a diagram

DEFINITION 0.11. A *twist region* of a diagram of a knot is a maximal portion of the knot diagram where two strands twist around each other, as in figure 0.9.

More precisely, recall that a diagram of a knot is a 4-valent graph with over/under crossing information at each vertex. A twist region is a string of bigon regions in the diagram graph, arranged end-to-end at their vertices, which is maximal in the sense that there are no additional bigon regions meeting the vertices on either end. A single crossing adjacent to no bigons is also a twist region. We will further restrict so that all twist regions are alternating, meaning crossings alternate over and under while following a strand of the twist region. If not, the second Reidemeister move applied to the diagram removes two crossings from the twist region.

The condition that twist regions be maximal ensures that there is only one way to put together exactly two twist regions in a diagram.

DEFINITION 0.12. The *twist knot* $J(2, n)$ is the knot with a diagram consisting of exactly two twist regions, one of which contains two crossings. The other twist region contains $n \in \mathbb{Z}$ crossings. The direction of crossing depends on the sign of n .

Twist knots $J(2, 2)$, $J(2, 3)$, $J(2, 4)$, and $J(2, 5)$ are shown in figure 0.10.

The family of twist knots $J(2, n)$ has very nice hyperbolic geometry, which we discuss in chapter 7. In particular, as n approaches infinity, we

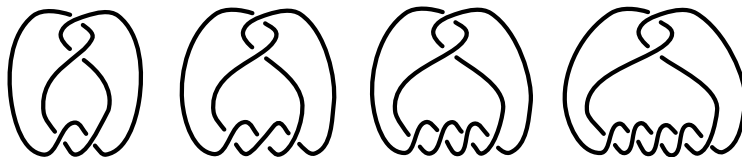


FIGURE 0.10. Twist knots $J(2,2)$ (the figure-8 knot), $J(2,3)$ (the 5_2 knot), $J(2,4)$ (the 6_1 or Stevedore knot), and $J(2,5)$

will see that the hyperbolic geometry of twist knot complements limits, in a precise sense, to the hyperbolic geometry of the Whitehead link complement; the Whitehead link is shown in figure 0.11.

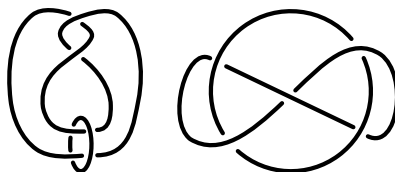


FIGURE 0.11. Two diagrams of the Whitehead link.

More generally, any family of knots containing higher and higher numbers of crossings in a twist region will have complements converging to a link with a simple circle encircling that twist region. Knots with high numbers of crossings in twist regions are called *highly twisted*. Again these are discussed in chapter 7.

Given a diagram of a link, we can combine twist regions by performing a sequence of moves on the diagram called *flypes*.

DEFINITION 0.13. Let γ be a simple closed curve meeting the diagram of K transversely exactly four times away from crossings, with two intersections adjacent to a crossing on the outside of γ . A *flype* is a move on the diagram that rotates the region inside γ by 180° , moving the crossing adjacent to γ to become a crossing adjacent to γ but between the opposite two strands. See figure 0.12.

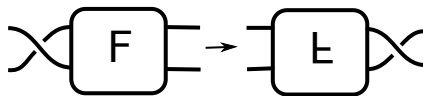


FIGURE 0.12. A flype.

Now, suppose a simple closed curve γ in the plane of projection meets a diagram transversely exactly four times away from crossings, and suppose also that the curve is adjacent to crossings on both sides. Then we can perform a flype to move one of the crossings to the opposite side of the

curve, to form a bigon. If the bigon is not alternating, remove both crossings, producing a diagram with fewer crossings. Otherwise, there are two cases. Either the curve γ encloses only bigons on one side to begin with, and the flype produces a diagram that is unchanged, or the flype has moved a crossing out of one twist region, on one side of γ , into a distinct twist region on the other side of γ . Performing the same flype a finite number of times will move all crossings in the twist region on one side of γ into the twist region on the other side, thus reducing the number of twist regions of the diagram. Thus by performing a finite number of flypes, we obtain a diagram with a minimal number of twist regions. Such a diagram is called *twist-reduced*.

Every knot has a twist-reduced diagram with some number of twist regions. On the other hand, for a fixed positive integer T , there are only finitely many ways of combining twist regions to form a twist-reduced diagram with T twist regions. The collection of twist-reduced diagrams with T twist regions forms an infinite family of diagrams. Two highly twisted diagrams with the same pattern of twist regions will have similar hyperbolic geometry, in ways that can be quantified. Thus rather than classifying knots by crossing number, from a geometric perspective it may make more sense to classify knots by number of twist regions in a twist-reduced diagram, or *twist-number*. This brings us to another (broad and vaguely-worded) problem.

0.2.4. The problem of enumerating knots by geometry. Enumerating knots by twist region may make more geometric sense than enumerating by crossing number, because highly twisted knots have diagrams that relate well to their geometry, in a sense that will be made precise in chapter 7. Given any knot, is there always a diagram that encodes hyperbolic geometry?

Schubert considered a family of knots in 1956 [Sch56]. He called the knots *2-bridge knots*. They can be described diagrammatically by taking four parallel strands, and twisting pairs of the strands into sequences of twist regions, then capping off either end with two “bridges.” A general form of such a diagram is shown in figure 0.13; see also chapter 10.

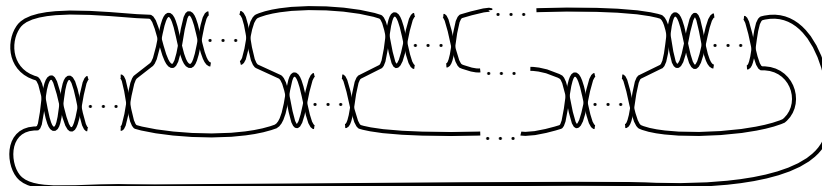


FIGURE 0.13. A general form of a 2-bridge knot.

Although Schubert’s work pre-dates the first work on the hyperbolic geometry of knots by nearly two decades, his 2-bridge knots turn out to

be very amenable to hyperbolic geometry techniques. We will see early on in this book that any knot exterior $S^3 - N(K)$ can be decomposed into a collection of truncated tetrahedra. Equivalently, $S^3 - K$ is formed by gluing tetrahedra whose vertices have been removed. This is called an *ideal triangulation* of the knot exterior, or sometimes simply a *triangulation*.

In the case of 2-bridge knots, we will see that a triangulation of the knot complement can be read easily off the diagram. Not only that, we will see in chapter 10 that the edges and faces of the triangulation can be made totally geodesic under the hyperbolic metric, and the tetrahedra can be straightened simultaneously to be convex, with piecewise geodesic boundaries. Thus the combinatorics of the diagram of a 2-bridge knot gives a combinatorial method of describing the geometry of the 2-bridge knot. This is very powerful.

It would be great to be able to extend these techniques to all knots, and some progress has been made with applications to other families, such as n -bridge knots for higher n . However, few families seem to be quite as nice as 2-bridge knots.

There is still much ongoing work on triangulating knot exteriors and determining geometric properties of triangulations. We will discuss some of the techniques and applications in chapter 9.

We have mentioned above that any knot exterior can be triangulated. In fact, any 3-manifold with torus boundary components can be decomposed into truncated tetrahedra. When the tetrahedra are convex hyperbolic tetrahedra, we say the triangulation is *geometric*. The software SnapPy has a census of orientable manifolds built up of at most nine geometric tetrahedra [CDGW16]. Some of these are knot complements.

This leads to a new way of classifying hyperbolic knots: by the number of geometric tetrahedra required to triangulate their exterior. This method of enumerating knots has been employed in [CDW99, CKP04, CKM14].

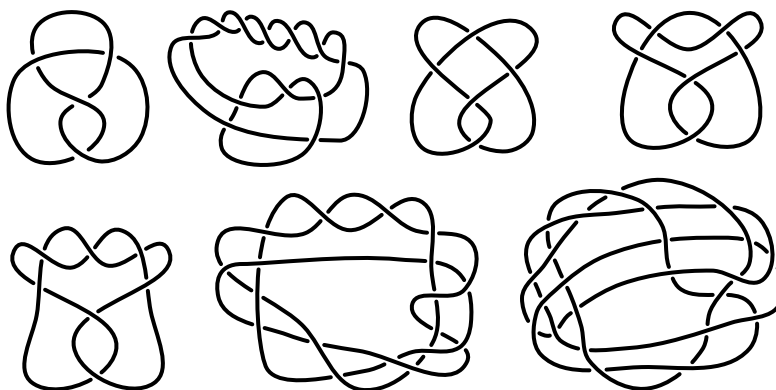


FIGURE 0.14. The seven simplest hyperbolic knots, built of at most four geometric tetrahedra.

To date, 502 hyperbolic knots, built of at most eight geometric tetrahedra, have been classified. The diagrams of these knots often have large numbers of crossings. The knots built of at most four tetrahedra are shown in figure 0.14.

Classifying knots by triangulations of their exteriors seems to be more difficult than classifying them by diagrams. This is because, given a triangulation of a 3-manifold with torus boundary, it is not obvious that the underlying space is a knot complement for a knot K in S^3 . We will discuss some techniques to detect whether such a manifold is a knot complement in chapter 8.

0.2.5. The problem of finding geometric diagrams. Twist knots and 2-bridge knots have standard diagrams that encode a great deal of information about the geometry of the knot. Does every knot have such a diagram? (Probably not.) Does every knot have a diagram from which we may read some geometric information?

Alternating knots are another family of knots that seem to be amenable to hyperbolic geometric techniques.

DEFINITION 0.14. An *alternating diagram* is a diagram of a knot or link that has an orientation such that, when following the knot in the direction of the orientation, the crossings alternate between over and under. An *alternating knot or link* is a knot or link that has an alternating diagram.

We will see in the exercises in chapter 1 that alternating knot complements decompose into pieces with the same combinatorics of the diagram. In chapters 11, 12, and 13 we will use this decomposition to determine some geometric information on the knot complement.

How useful is this work broadly? All knots with at most seven crossings have alternating diagrams. Tait began his work [Tai98] by assuming diagrams were alternating (although he did publish diagrams of eight- and ten-crossing non-alternating examples in 1877). However, the proportion of alternating knots in diagrams enumerated by crossing number rapidly drops to zero [ST98, Thi98]. As for knots enumerated by geometric triangulations, non-alternating examples seem to be even more common; a non-alternating example appears as the second knot on the list in figure 0.14. Thus unfortunately, alternating knots and links are not very common.

An open research question is, how many of the techniques presented in these chapters for determining geometry of alternating links generalize to other knots and links? There has been much work in recent years in extending this work to other families of knots, and some success. We are far from using such techniques to find hyperbolic geometry of all knots, though.

0.2.6. The problem of determining geometric invariants. One way of distinguishing knots is to compute invariants for each of them. If the invariants disagree, then the knots cannot be equivalent.

Several knot invariants arise classically, such as the crossing number that we encountered above. Many additional knot invariants arise through geometry. One aim of this book is to discuss such invariants, and give tools to calculate them.

One of the most straightforward knot invariants that arises in geometry is the volume of a knot. We will show in chapter 5 that any knot complement that admits a hyperbolic structure has finite volume. Thus volumes of knots give knot invariants.

For those knots whose diagrams are particularly amenable to geometric techniques, such as twist knots, 2-bridge knots, and alternating knots, there are known methods to estimate volume using the combinatorics of the diagram. This is discussed along the way, but especially in chapter 13, where we bring to bear several tools in geometry to give two-sided bounds on volumes.

How powerful is volume as a knot invariant? It can be easy to calculate numerically, using the software SnapPy [CDGW16], for example. Such computations can be rigorously verified to lie in a fixed error range using interval arithmetic, as in [HIK⁺16]. Thus computing volume is a useful tool for distinguishing knots with distinct volume. However, there are many distinct knots that cannot be distinguished by volume; they have the same volume. We give some methods of constructing such knots and links in chapter 12.

Then, is there a better geometric knot invariant than volume to distinguish knots? In chapter 14, we describe the *canonical decomposition* of a hyperbolic knot complement. This is a decomposition consisting of convex polyhedra. We will show that when two knots have the same canonical decomposition, they must necessarily have homeomorphic complements, and thus by the Gordon–Luecke theorem, they must be equivalent (up to reflection). Thus the canonical decomposition is a complete invariant for hyperbolic knots. Unfortunately, it is not easy to compute in general, and provable forms of canonical decompositions are only known for a few infinite families of knots, including 2-bridge knots [Gue06a]. Canonical decompositions of alternating knots are still unknown in general, for example.

Finally, we discuss very briefly one polynomial invariant. In most standard books on knot theory, there will be chapters on polynomial invariants, particularly the Alexander polynomial and the Jones polynomial. We will not treat such polynomials here; they arise from techniques that do not use hyperbolic geometry. There is one polynomial invariant of knots that depends heavily on hyperbolic geometry, however. This is the *A*-polynomial. We devote chapter 15 to a discussion of the *A*-polynomial, its definition and computation for a few examples. We will see that it relates to hyperbolic structures on a knot complement and the deformations of such structures.

0.2.7. The problem of relating geometric invariants to other invariants. What of the invariants that are being omitted from this book?

We mentioned above Alexander and Jones polynomials. There are also more modern algebraic knot invariants, such as Khovanov homology and Floer homologies, and quantum invariants such as colored Jones polynomials.

Many open problems in knot theory, driving much of the ongoing research in the field, concern relating invariants of knots arising from other fields of mathematics to hyperbolic geometry and hyperbolic knot invariants. We will not discuss in detail these open problems, because defining non-hyperbolic invariants will take us too far afield. However, one motivating factor for writing this book was to help mathematicians, particularly students, get up to speed with their hyperbolic geometry, in order to investigate the relations of geometry to other invariants in knot theory.

0.3. Exercises

EXERCISE 0.1. Find a sequence of isotopy moves of the diagram of the Goeritz knot, figure 0.5, that reduces it to the standard diagram of the unknot with no crossings.

EXERCISE 0.2. Download and install the software SnapPy [CDGW16]. Use it to sketch diagrams of a few knots, and determine whether the knot is hyperbolic. Do this for at least one hyperbolic knot and at least one non-hyperbolic knot.

EXERCISE 0.3. Convince yourself by drawing several examples that every 4-valent planar graph can be assigned over/under crossing information at each vertex to obtain an alternating knot. Now try to prove this fact. (This may require some graph theory.)

EXERCISE 0.4. Show that a connected sum of two knots is always a satellite knot.

Part 1

**Foundations of Hyperbolic
Structures**

CHAPTER 1

Decomposition of the Figure-8 Knot

In this chapter, we begin developing tools to work with knots and links and the 3-manifolds they define. We give a geometric method, explained carefully by example, to decompose a knot or link complement into simple pieces. The methods here are an introduction to topological techniques in 3-manifold geometry and topology, and an introduction to some of the tools used in the field.

One goal of this chapter is to present a method that will allow us to pass from a knot or link *diagram* to a description of the knot or link *complement*. That is, we start with a 4-valent graph describing a knot or link K , and obtain a mathematically rigorous decomposition of the 3-manifold $S^3 - K$ into simple 3-dimensional pieces, which pieces will be useful for applying tools from geometry and 3-manifold topology.

1.1. Polyhedra

Sometimes it is easier to study manifolds, including knot complements, if we split them into smaller, simpler pieces, for example 3-balls. We are going to decompose the figure-8 knot complement into two carefully marked 3-balls, namely ideal polyhedra. The diagram of the figure-8 knot that we use is shown in figure 1.1. The decomposition we describe appears in Thurston's notes [Thu79], and with a little more explanation in [Thu97]. The procedure has been generalized to all link complements, for example in [Men83]. This work is essentially what we present below in the text and in exercises.

DEFINITION 1.1. A *polyhedron* is a closed 3-ball whose boundary is labeled with a finite graph, containing a finite number vertices and edges, so that complementary regions, which are called *faces*, are simply connected.

An *ideal polyhedron* is a polyhedron with all vertices removed. That is, to form an ideal polyhedron, start with a regular polyhedron and remove the points corresponding to vertices.

We will cut $S^3 - K$ into two ideal polyhedra. We will then have a description of $S^3 - K$ as a gluing of two ideal polyhedra. That is, given a description of the polyhedra, and gluing information on the faces of the

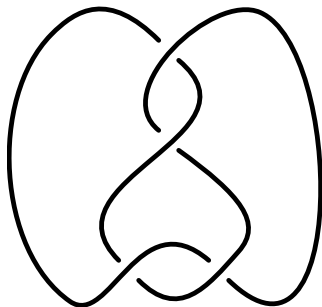


FIGURE 1.1. A diagram of the figure-8 knot.

polyhedra, we may reconstruct the knot complement $S^3 - K$. Although we use the example of the figure-8 knot, in the exercises, you will walk through the techniques below to determine decompositions of other knot complements into ideal polyhedra, and to generalize to all knots.

1.1.1. Overview. Start with a diagram of the knot. There will be two polyhedra in our decomposition. These can be visualized as two balloons: One balloon expands above the diagram, and one balloon expands below the diagram. As the balloons continue expanding, they will bump into each other in the regions cut out by the graph of the diagram. Label these regions. In figure 1.2, the regions are labeled A , B , C , D , E , and F . These will correspond to faces of the polyhedra.

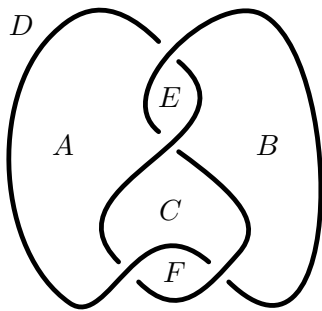


FIGURE 1.2. Faces for the figure-8 knot complement.

The faces meet up in edges. There is one edge for each crossing. It runs vertically from the knot at the top of the crossing to the knot at the bottom (or the other way around). The balloon expands until faces meet at edges. Figure 1.3 shows how the top balloon would expand at a crossing. The edge is drawn as an arrow from the top of the crossing to the bottom. Faces labeled T and U meet across the edge. Rotating the picture 180° about the edge, we would see an identical picture with S meeting V .

It may be helpful to examine the meeting of faces at an edge by 3-dimensional model. Henry Segerman has come up with a paper model to

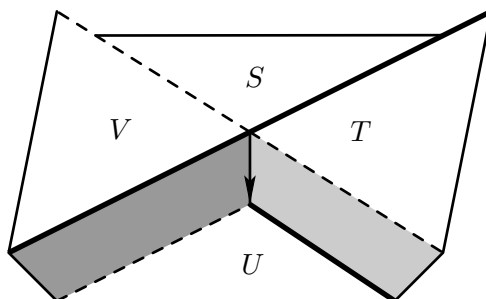


FIGURE 1.3. The knot runs along diagonals. Faces labeled U and T meet at the edge shown, marked by an arrow.

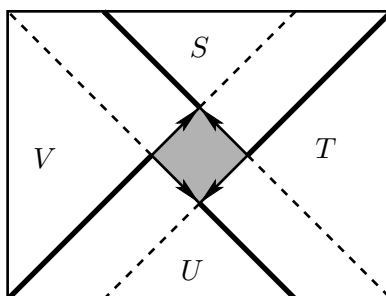


FIGURE 1.4. Cut out the shaded square. Start with a pair of parallel lines. Fold the thick part of the line in a direction opposite that of the dashed part of the line. Fold parallel thick and dashed lines in opposite directions. Correct folding results in a model that looks like figure 1.3.

illustrate the phenomenon of figure 1.3. Start with a sheet of paper labeled as in figure 1.4. Cut out the shaded square in the middle. Now fold the paper until it looks like that in figure 1.3. By rotating the paper model, we can see how faces meet up.

Stringing crossings such as this one together, we obtain the complete polyhedral decomposition of the knot. This is the geometric intuition behind the polyhedral expansion. We now explain a combinatorial method to describe the polyhedra.

1.1.2. Step 1. Sketch faces and edges into the diagram.

Recall a diagram is a 4-valent graph lying on a plane, the plane of projection. The regions on the plane of projection that are cut out by the graph will be the faces, including the outermost unbounded region of the plane of projection. We start by labeling these, as in figure 1.2.

Edges come from arcs that connect the two strands of the diagram at a crossing. These are called *crossing arcs*. For ease of explanation, we are going to draw each edge four times, as follows. Shown on the left of

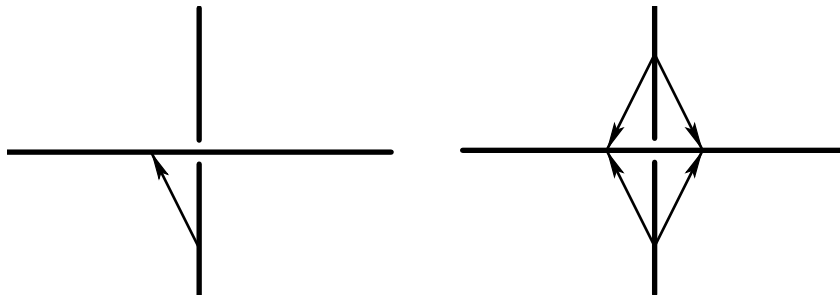


FIGURE 1.5. A single edge.

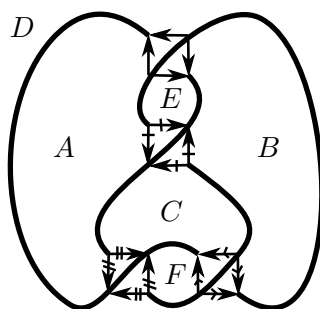


FIGURE 1.6. Edges of the figure-8 knot complement.

figure 1.5 is a single edge corresponding to a crossing arc. Note that the edge is ambient isotopic in S^3 to the three additional edges shown on the right in figure 1.5.

The reason for sketching each edge four times is that it allows us to visualize easily which edges bound the faces we have already labeled. In figure 1.6, we have drawn four copies of each of the four edges we get from crossing arcs of the diagram of the figure-8 knot. Note that the face labeled A , for example, will be bordered by three edges, one with two tick marks, one with a single tick mark, and one with no tick marks.

REMARK 1.2. Orientations on the edges can be chosen to run in either direction; that is, arrows on the edges can run from overcrossing to undercrossing or vice versa, as long as we are consistent with orientations corresponding to the same edge. We have chosen the orientations in figure 1.6 to simplify a later step, and to match a figure in chapter 4. The opposite choice for any edge is also fine.

1.1.3. Step 2. Shrink the knot to ideal vertices on the top polyhedron.

Now we come to the reason for using *ideal* polyhedra, rather than regular polyhedra. Notice that the edges stretch from a part of the knot to a part of the knot. However, the manifold we are trying to model is the knot complement, $S^3 - K$. Therefore, the knot K does not exist in the manifold.

An edge with its two vertices on K must necessarily be an ideal edge; that is, its vertices are not contained in the manifold $S^3 - K$.

Since the knot is *not* part of the manifold, we will shrink strands of the knot to ideal vertices. That is, retract each knot strand to a single point. This may cause some confusion at first, because the strand of the knot is not homeomorphic to a single point. However, we are considering the *complement* of the strand. The complement of the strand on the boundary of the ball is homeomorphic to the complement of a single point on the boundary of the ball, so we replace strands by ideal vertices (single removed points).

Focus first on the polyhedron on top. Each component of the knot we “see” from inside the top polyhedron will be shrunk to a single ideal vertex. These visible knot components correspond to sequences of overcrossings of the diagram. Compare to figure 1.3 — note that at an undercrossing, the component of the knot ends in an edge, but at an overcrossing the knot continues on. Moreover, note that at an overcrossing, the knot passes the same edge twice, once on each side.

In terms of the four copies of the edge in figure 1.5, when we consider the polyhedron on top, we may identify the two edges which are isotopic along an overstrand, but not those isotopic along understrands. See figure 1.7.

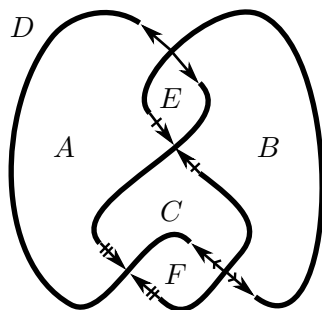


FIGURE 1.7. Isotopic edges in top polyhedron identified.

Shrink each overstrand to a single ideal vertex. The result is pattern of faces, edges, and ideal vertices for the top polyhedron, shown in figure 1.8. Notice that the face D is a disk, containing the point at infinity.

1.1.4. Step 3. Shrink the knot to ideal vertices for the bottom polyhedron.

Notice that underneath the knot, the picture of faces, edges, and vertices will be slightly different. In particular, when finding the top polyhedron, we collapsed overstrands to a single ideal vertex. When you put your head underneath the knot, what appear as overstrands from below will appear as understrands on the usual knot diagram.

One way to see this difference is to take the 3-dimensional model constructed in figure 1.4. Figure 1.3 shows the view of the faces meeting at an

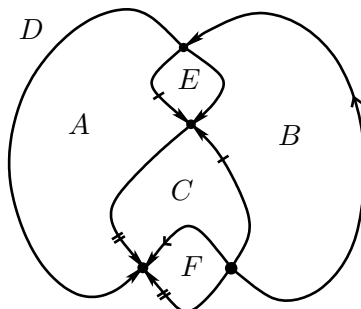
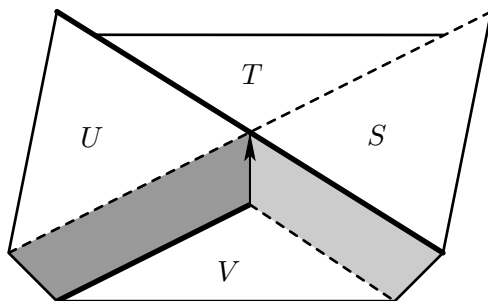


FIGURE 1.8. Top polyhedron, viewed from the inside.

edge from the top. If you turn the model over to the opposite side, you will see how the faces meet underneath. Figure 1.9 illustrates this. Note U now meets V , and S meets T .

FIGURE 1.9. 3-dimensional model, opposite side as in figure 1.3. Now faces V and U meet along an edge.

In terms of the combinatorics, edges of figure 1.5 that are isotopic by sliding an endpoint along an understrand are identified to each other on the bottom polyhedron, but edges only isotopic by sliding an endpoint along an overstrand are not identified.

As above, collapse each knot strand corresponding to an understrand to a single ideal vertex. The result is figure 1.10.

One thing to notice: we sketched the top polyhedron with our heads inside the ball on top, looking out. If we move the face D away from the point at infinity, then it wraps *above* the other faces shown in figure 1.8.

On the other hand, we sketched the bottom polyhedron with our heads outside the ball on the bottom. If we move the face D away from the point at infinity, it wraps *below* the other faces shown in figure 1.10.

1.1.5. Rebuilding the knot complement from the polyhedra.

Figures 1.8 and 1.10 show two ideal polyhedra that we obtained by studying the figure-8 knot complement. We claim that they glue to give the figure-8 knot complement. That is, attach face A on the bottom polyhedron to the

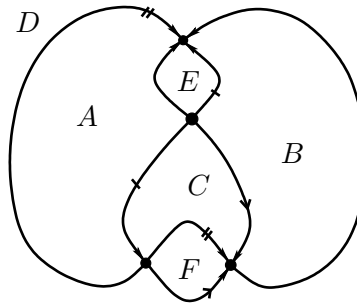


FIGURE 1.10. Bottom polyhedron, from the outside.

face labeled A on the top polyhedron, ensuring that the edges bordering face A match up. Similarly for the other faces.

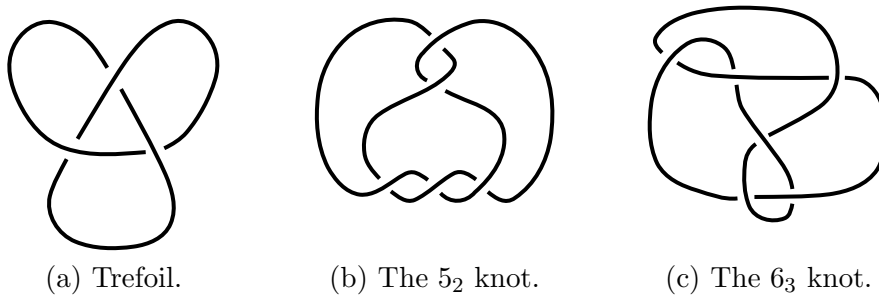
This process of gluing faces and edges gives exactly the complement of the knot. By construction, faces glue to give the faces illustrated in figure 1.6, and edges glue to give the edges there, except when we have finished, all four edges in an isotopy shown in that figure have been glued together.

1.2. Generalizing: Exercises

This polyhedral decomposition works for any knot or link diagram, to give a polyhedral decomposition of its complement.

EXERCISE 1.1. As a warm-up exercise, determine the polyhedral decomposition for one (or more) of the knots shown in figure 1.11. Sketch both top and bottom polyhedra.

Your solution should consist of two ideal polyhedra, i.e. marked graphs on the surface of a ball, with faces and edges marked according to the gluing pattern. For example, the complete diagrams in Figures 1.8 and 1.10 form the solution for the figure-8 knot.



(a) Trefoil.

(b) The 5_2 knot.(c) The 6_3 knot.

FIGURE 1.11. Three examples of knots.

EXERCISE 1.2. The examples of knots we have encountered so far are all alternating, as in definition 0.14. The diagram of the knot 8_{19} in figure 1.12 is not alternating. In fact, the knot 8_{19} has no alternating diagram.

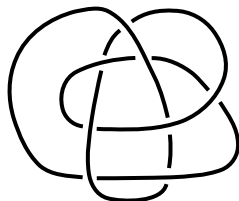


FIGURE 1.12. The knot 8_{19} , which has no alternating diagram.

Determine the polyhedral decomposition for the given diagram of the knot 8_{19} . Note: as above, many ideal vertices are obtained by shrinking overstrands to a point. However, you will have to use, for example, figure 1.3 to determine what happens between two understrands.

EXERCISE 1.3. Recall that the *valence* of a vertex in a graph is the number of edges that meet that vertex. The valence of an ideal vertex is defined similarly.

- (a) If a knot diagram is alternating, we obtain a very special ideal polyhedron. In particular, all ideal vertices will have the same valence. What is it? Show that the ideal vertices for an alternating knot all have this valence.
- (b) What are the possible valences of ideal vertices in general, i.e. for non-alternating knots? For which $n \geq 0 \in \mathbb{Z}$ is there a knot diagram whose polyhedral decomposition yields an ideal vertex of valence n ? Explain your answer, with (portions of) knot diagrams.

EXERCISE 1.4. In the polyhedral decomposition for alternating knots, the polyhedra are given by simply labeling each ball with the projection graph of the knot and declaring each vertex to be ideal.

- (1) Prove this statement for any alternating knot. That is, prove that the decomposition gives polyhedra whose edges match the projection graph of the diagram.
- (2) Show that for non-alternating knots, this is false. That is, the decomposition does not give polyhedra whose edges match the projection graph of the diagram.

EXERCISE 1.5. A graph admits a *checkerboard coloring* if all the complementary regions can be colored either white or shaded, with white faces meeting shaded faces across the edges. Any 4-valent graph can be checkerboard colored, particularly projection graphs of knot diagrams.

In the case of an alternating knot, faces are identified from the top polyhedron to the identical face on the bottom polyhedron, and the identification is by a *gear rotation*: white faces on the top are rotated once counter-clockwise and then glued to the corresponding face on the bottom; shaded faces on the top are rotated once clockwise and then glued. This is

shown for the figure-8 knot in figure 1.13. Prove that for the decomposition of any alternating knot, faces are identified by a gear rotation.

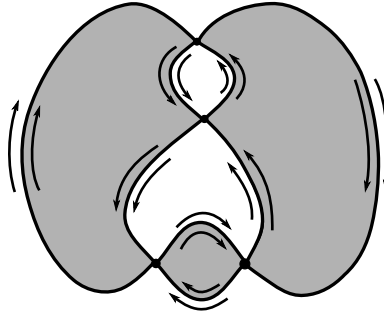


FIGURE 1.13. Checkerboard coloring and “gear rotation” for the figure-8 knot.

EXERCISE 1.6. The diagrams we have encountered so far are all reduced, as in definition 0.6, but we can follow the above procedure for non-reduced diagrams. For example, we can obtain a polyhedral decomposition for diagrams which contain a nugatory crossing.

Show that the polyhedral decomposition of a knot diagram will contain a monogon, i.e. a face whose boundary is a single edge and a single vertex, if and only if the diagram has a simple nugatory crossing.

EXERCISE 1.7. Recall that a bigon is a region of a graph bounded by exactly two edges and exactly two vertices. Note that when a bigon appears in our polyhedral decomposition, the two edges of the bigon must be isotopic to each other. Hence, we sometimes will remove bigon faces from the polyhedral decomposition, identifying their two edges.

Let bigons be bygone. — William Menasco

For the figure-8 knot, sketch the two polyhedra we get when bigon faces are removed. How many edges are there in this new, bigon-free decomposition? The resulting polyhedra are well known solids in this case. What are they?

For each of the polyhedra obtained in exercise 1.1, sketch the resulting polyhedra with bigons removed.

EXERCISE 1.8. Suppose we start with an alternating knot diagram with at least two crossings, and do the polyhedral decomposition above, collapsing bigons at the last step. What are possible valences of vertices? Sketch the diagram of a single alternating knot that has all possible valences of ideal vertices in its polyhedral decomposition.

What valences of vertices can you get if you don't require the diagram to be alternating but collapse bigons? Can you find 1-valent vertices? For any $n > 4 \in \mathbb{Z}$, can you find n -valent vertices?

CHAPTER 2

Calculating in Hyperbolic Space

We will need to manipulate objects in 2 and 3-dimensional hyperbolic space. This chapter provides a very brief introduction to the tools that will be needed in the future, the objects that will be studied (lines, triangles, tetrahedra, metric properties), and examples of calculations that will appear.

We will use terminology and calculations from standard elementary Riemannian geometry. The reader who is not as comfortable with Riemannian geometry might find it helpful to follow along in the first few chapters of an introductory Riemannian geometry text, such as do Carmo [dC92, Chapter 1]. We will not provide all the details to all the statements given. The idea is that we want to begin calculating on knot complements and other 3-manifolds immediately, without getting lost early in details. Thus our aim is to provide just enough information here to start calculating in future chapters. Many more details and results can be found in other books, including full books on hyperbolic geometry. Anderson gives a very nice introduction to 2-dimensional hyperbolic geometry [And05]. More details in all dimensions appear in Ratcliffe [Rat06]. The book by Marden includes more on groups of isometries of hyperbolic space, including results on infinite volume hyperbolic 3-manifolds [Mar07]. An introduction to hyperbolic geometry that includes a discussion of its visualization is also given by Thurston [Thu97].

2.1. Hyperbolic geometry in dimension two

We start with hyperbolic 2-space, \mathbb{H}^2 .

There are several models of hyperbolic space. Here, we will work with the upper half plane model. In this model, hyperbolic 2-space \mathbb{H}^2 is defined to be the set of points in the upper half plane:

$$\mathbb{H}^2 = \{x + iy \in \mathbb{C} \mid y > 0\},$$

equipped with the metric whose first fundamental form is given by

$$ds^2 = \frac{dx^2 + dy^2}{y^2}.$$

That is, start with the usual Euclidean metric on \mathbb{R}^2 , whose first fundamental form is $dx^2 + dy^2$. To obtain the metric on the hyperbolic plane, rescale the usual Euclidean metric by $1/y$, where y is height in the plane.

Note that a point in \mathbb{H}^2 can either be thought of as a complex number $x + iy \in \mathbb{C}$ or as a point $(x, y) \in \mathbb{R}^2$. Both perspectives are useful: \mathbb{R}^2 leads more easily to coordinates and calculations, and \mathbb{C} works seamlessly with our definition of isometries below. Changing perspectives does not affect our results, so we will regularly switch between the two without comment.

Our first task is to explore the meaning of the hyperbolic metric, and how it affects measurements.

2.1.1. Hyperbolic 2-space and Riemannian geometry. In this subsection, we briefly review how the metric and the space \mathbb{H}^2 described above fit into a more general picture of Riemannian geometry. We also describe tools from Riemannian geometry we will use to do calculations. If you are not yet familiar with Riemannian geometry, feel free to skim this section, noting equations (2.1), (2.2), and (2.3). This section was primarily written for a student who has seen some Riemannian geometry, but may have difficulty applying abstract concepts of that field to the specific metric of hyperbolic geometry. In the author's experience, a few key equations will be enough to get started.

In Riemannian geometry, a *Riemannian metric* on a manifold M is defined to be a correspondence associating to each point $p \in M$ an inner product $\langle \cdot, \cdot \rangle_p$ on the tangent space $T_p M$. This inner product gives us a way of measuring the lengths of vectors tangent to M at p , as well as computing areas, angles between curves, etc. The *first fundamental form* is defined by $\langle v, v \rangle_p$ for $v \in T_p M$.

In our case, the Riemannian manifold we consider is \mathbb{H}^2 , and we have natural local coordinates on the manifold given by $x + iy \in \mathbb{C}$, or $(x, y) \in \mathbb{R}^2$, for $y > 0$. We may use these coordinates to describe the Riemannian metric. In particular, at the point $(x, y) \in \mathbb{H}^2$, a tangent vector $v \in T_{(x,y)}\mathbb{H}^2$ can also be described by coordinates $v = v_x \frac{\partial}{\partial x} + v_y \frac{\partial}{\partial y}$, and we write it as a vector

$$v = \begin{pmatrix} v_x \\ v_y \end{pmatrix}.$$

Then the metric on \mathbb{H}^2 is given by a matrix

$$\langle v, w \rangle = (v_x, v_y) \begin{pmatrix} 1/y^2 & 0 \\ 0 & 1/y^2 \end{pmatrix} \begin{pmatrix} w_x \\ w_y \end{pmatrix}.$$

One of the simplest geometric measurements we can compute using the definition of the metric is the arc length of a curve. If $\gamma(t)$ is a (differentiable) curve in \mathbb{H}^2 , for $t \in [a, b]$, then we obtain a tangent vector $\gamma'(t)$ at each point of $\gamma(t)$ in \mathbb{H}^2 , called the velocity vector. The *arc length* of γ for $t \in [a, b]$ is

defined to be

$$|\gamma| = \int_a^b \sqrt{\langle \gamma'(s), \gamma'(s) \rangle} ds.$$

When considering \mathbb{H}^2 , we will have coordinates $\gamma(t) = (\gamma_x(t), \gamma_y(t))$, and $\gamma'(t) = (\gamma'_x(t), \gamma'_y(t))^T$. Thus the arc length will be

$$(2.1) \quad |\gamma| = \int_a^b \sqrt{(\gamma'_x(s))^2 + (\gamma'_y(s))^2} \frac{1}{\gamma_y(s)} ds.$$

We will use this formula to compute examples in the next subsection.

Another piece of geometric information we can compute with a metric is the volume of a region, which we typically call “area” in two dimensions. In the most general setting, if $R \subset M$ is contained in a coordinate neighborhood of the Riemannian manifold M , with coordinates (x_1, \dots, x_n) and metric given by the matrix g_{ij} in these coordinates, then we can compute the volume of R to be

$$(2.2) \quad \text{vol}(R) = \int_R d \text{vol} = \int_R \sqrt{\det(g_{ij})} dx_1 \dots dx_n.$$

The form $d \text{vol}$ is the *volume form*. Thus in our setting, with $M = \mathbb{H}^2$ and metric as above,

$$(2.3) \quad \text{area}(R) = \int_R \frac{1}{y^2} dx dy.$$

2.1.2. Computing arc lengths and areas. Now we will use the formulas obtained above to do calculations, in order to better understand the hyperbolic space \mathbb{H}^2 .

EXAMPLE 2.1. Fix a height $h > 0$, and consider first a horizontal line segment between points $(0, h) = ih$ and $(1, h) = 1 + ih$ in \mathbb{H}^2 . We may parameterize the line segment by $\gamma(t) = (t, h)$, for $t \in [0, 1]$. Using equation (2.1), we find the arc length of γ is $|\gamma| = 1/h$. Note that because h is fixed, the arc length of γ is just its usual Euclidean length rescaled by $1/h$. Thus when $h = 1$, the length of γ is 1. When h becomes large, the arc length becomes very small. In other words, points with the same height become very close together as their heights increase. On the other hand, as h approaches 0, the length of γ approaches infinity. In fact, points near the real line $\mathbb{R} = \{(x, 0) \in \mathbb{R}^2\}$ can be very far apart.

EXAMPLE 2.2. Consider now a vertical line between points (x, a) and (x, b) , for x, a, b fixed in \mathbb{R} , $0 < a < b$. Such a line can be parameterized by $\zeta(t) = (x, t)$ for $t \in [a, b]$. So $\zeta'(t) = (0, 1)$. Thus its arc length is given by

$$|\zeta| = \int_a^b \sqrt{0 + 1} \frac{1}{s} ds = \log \left(\frac{b}{a} \right).$$

If we set $b = 1$ and let a approach 0, note that the arc length of ζ gets arbitrarily large, approaching infinity. Similarly setting $a = 1$ and letting b approach infinity gives arbitrarily long lengths.

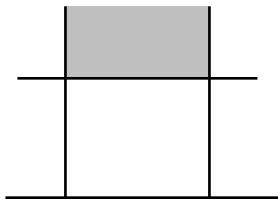


FIGURE 2.1. The region of example 2.4

The real line $\mathbb{R} = \{(x, 0) \in \mathbb{R}^2\}$ along with the point at infinity ∞ play an important role in the geometry of \mathbb{H}^2 , although these points are not contained in \mathbb{H}^2 .

DEFINITION 2.3. We call $\mathbb{R} \cup \{\infty\}$ the *boundary at infinity* for \mathbb{H}^2 . Note it is homeomorphic to a circle S^1 , and hence is sometimes called the *circle at infinity*. It is denoted by S_∞^1 , $\partial\mathbb{H}^2$, and sometimes $\partial_\infty\mathbb{H}^2$.

Areas behave quite differently in hyperbolic space than in Euclidean space.

EXAMPLE 2.4. In this example, we will compute the area of the region R of \mathbb{H}^2 that is the intersection of the half-plane lying to the left of the line $x = 1$, the half-plane to the right of the line $x = 0$, and the plane lying above $y = 1$. The region R is shown in figure 2.1.

Using equation (2.3), we see that the area of the region is given by

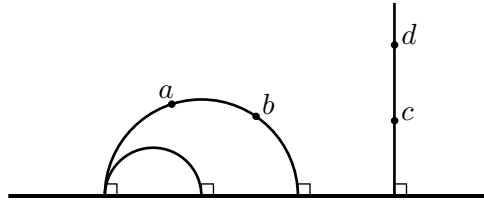
$$\begin{aligned} \text{area}(R) &= \int_R \frac{1}{y^2} dx dy \\ &= \int_0^1 \int_1^\infty \frac{1}{y^2} dy dx \\ &= \int_0^1 1 dx = 1 \end{aligned}$$

This example shows that regions with infinite Euclidean area may have finite hyperbolic area.

2.1.3. Geodesics and isometries. Recall that a *geodesic* between points p and q is a length minimizing curve between those points. An *infinite geodesic* is a curve γ from \mathbb{R} to a Riemannian manifold such that for any $s < t \in \mathbb{R}$, the curve $\gamma([s, t])$ minimizes the distance between $\gamma(s)$ and $\gamma(t)$.

THEOREM 2.5. *The infinite geodesics in \mathbb{H}^2 consist of vertical straight lines and semi-circles with center on the real line.* \square

Note these are exactly the circles and lines in the upper half plane that meet S_∞^1 at right angles. See figure 2.2. Observe that between any two points in the upper half plane, there is a unique vertical line or semi-circle between them. Thus a geodesic between points p and q in \mathbb{H}^2 is a segment

FIGURE 2.2. Some geodesics and points in \mathbb{H}^2 .

of a semi-circle or a vertical straight line. An infinite geodesic can also be viewed as the unique semi-circle or vertical straight line between two points on the boundary at infinity of \mathbb{H}^2 . We will typically drop the word “infinite” to describe geodesics between points on the boundary at infinity. Thus we use the same word “geodesic” to describe both infinite or bounded arcs, depending on context.

The proof of theorem 2.5 is left as an exercise in Riemannian geometry. The simplest way to prove the theorem uses coordinates and a bit more Riemannian geometry than we have reviewed so far. The interested reader can work through the details. The fact that these are the geodesics of \mathbb{H}^2 is all we will need going forward.

An *isometry* between Riemannian manifolds M and N is a diffeomorphism $f: M \rightarrow N$ such that

$$\langle v, w \rangle_p = \langle df_p(v), df_p(w) \rangle_{f(p)} \quad \text{for all } p \in M, v, w \in T_p M.$$

Isometries preserve lengths, angles, and other geometric information. We are most interested in orientation preserving isometries from hyperbolic space to itself, i.e. diffeomorphisms $\phi: \mathbb{H}^2 \rightarrow \mathbb{H}^2$ that preserve the metric and orientation on \mathbb{H}^2 . All such isometries form a group acting on \mathbb{H}^2 . We will assume the following theorem; see also exercise 2.2.

THEOREM 2.6. *The full group of isometries of \mathbb{H}^2 is generated by reflections in geodesics in \mathbb{H}^2 .*

The group of orientation preserving isometries of \mathbb{H}^2 is the group of linear fractional transformations

$$z \mapsto \frac{az + b}{cz + d},$$

where $a, b, c, d \in \mathbb{R}$, and $ad - bc > 0$. □

By taking the quotient of a , b , c , and d by $\sqrt{ad - bc}$, the linear fractional transformation is equivalent to an element of $\text{PSL}(2, \mathbb{R})$, the group of projective 2 by 2 matrices with real coefficients and determinant 1. That is, we may view $A \in \text{PSL}(2, \mathbb{R})$ as given by a matrix

$$A = \pm \begin{pmatrix} a & b \\ c & d \end{pmatrix},$$

where $a, b, c, d \in \mathbb{R}$ and $ad - bc = 1$. The sign in front reflects the fact that it is *projective*; it is well-defined only up to multiplication by $\pm \text{Id}$. On the other hand, A acts on \mathbb{H}^2 via

$$Az = \frac{az + b}{cz + d}.$$

Note the action is unaffected when we multiply $a, b, c,$ and d by the same real constant, thus it is necessary to take projective matrices.

Linear fractional transformations take circles and lines to circles and lines, so they map geodesics to geodesics. For more information on these transformations, see for example [Ahl78, pp 76–89].

The following lemma is very useful.

LEMMA 2.7. *Given any three distinct points $z_1, z_2,$ and z_3 in $\partial\mathbb{H}^2$, there exists an orientation preserving isometry of \mathbb{H}^2 taking z_3 to ∞ , and taking $\{z_1, z_2\}$ to $\{0, 1\}$. It follows that there exists an isometry of \mathbb{H}^2 taking any three distinct points on $\partial\mathbb{H}^2$ to any other three distinct points, with appropriate orientation.*

PROOF. This is a standard fact of linear fractional transformations. We need to take some care to preserve orientation. If necessary, switch z_1 and z_2 so that the sequence z_1, z_2, z_3 runs in counterclockwise order around $\partial\mathbb{H}^2 \cong S^1$.

If none of $z_1, z_2,$ and z_3 are infinity, then a linear fractional transformation sending z_1 to 1, z_2 to 0, and z_3 to ∞ is given by

$$z \mapsto \frac{z - z_2}{z - z_3} \frac{z_1 - z_3}{z_1 - z_2}.$$

Note that the determinant of this transformation is

$$(z_1 - z_3)(z_1 - z_2)(z_2 - z_3).$$

Because the sequence z_1, z_2, z_3 is in counterclockwise order, this is positive. Thus it gives the desired orientation preserving isometry.

If $z_1 = \infty, z_2 = \infty,$ or $z_3 = \infty$, then the isometry is given by

$$z \mapsto \frac{z - z_2}{z - z_3}, \quad z \mapsto \frac{z_1 - z_3}{z - z_3}, \quad z \mapsto \frac{z - z_2}{z_1 - z_2}$$

respectively. One can check that again, because we ensured the sequence z_1, z_2, z_3 is in counterclockwise order, the determinant of each transformation is positive. \square

Many metric calculations in \mathbb{H}^2 can be simplified greatly by applying an appropriate isometry, including the use of lemma 2.7. For example, the following lemma is easily proved using an isometry.

LEMMA 2.8. *Two distinct geodesics ℓ_1 and ℓ_2 in \mathbb{H}^2 either*

- (1) *intersect in a single point in the interior of \mathbb{H}^2 ,*
- (2) *intersect in a single point on the boundary $\partial\mathbb{H}^2$, or*
- (3) *are completely disjoint in $\mathbb{H}^2 \cup \partial\mathbb{H}^2$.*

In the third case, there is a unique geodesic ℓ_3 that is perpendicular to both ℓ_1 and ℓ_2 .

PROOF. We may apply an isometry g of \mathbb{H}^2 , taking endpoints of ℓ_1 to 0 and ∞ , and taking one of the endpoints of ℓ_2 to 1. The image of the second endpoint of ℓ_2 under g is then some point w in $\partial\mathbb{H}^2 = \mathbb{R} \cup \{\infty\}$. Note that $g(\ell_1)$ is the vertical line from 0 to ∞ in \mathbb{H}^2 . The point w determines the image of $g(\ell_2)$.

If $w = 0$ or if $w = \infty$, then we are in the second case, and $g(\ell_2)$ is a semi-circle with endpoints 0 and 1, or a vertical line from 1 to ∞ .

If $w \in \mathbb{R}$ is less than zero, then we are in the first case. The two endpoints of $g(\ell_2)$ are separated by the line $g(\ell_1)$, so the geodesics must meet.

Finally, if $w \in \mathbb{R}$ is greater than zero, then we are in the third case, and the geodesics are disjoint. One way to see that there is a unique geodesic perpendicular to both is to apply another isometry h , taking \sqrt{w} to 0 and $-\sqrt{w}$ to ∞ . That is, let $h: \mathbb{H}^2 \rightarrow \mathbb{H}^2$ be given by

$$h(z) = \frac{z - \sqrt{w}}{z + \sqrt{w}}.$$

Note that $h(0) = -1$, $h(\infty) = 1$, so $h(g(\ell_1))$ is the geodesic that is a semi-circle with endpoints at -1 and 1 . Also,

$$h(1) = \frac{1 - \sqrt{w}}{1 + \sqrt{w}} \quad \text{and} \quad h(w) = \frac{w - \sqrt{w}}{w + \sqrt{w}} = -\frac{1 - \sqrt{w}}{1 + \sqrt{w}}.$$

So $h(g(\ell_2))$ is the geodesic that is a semi-circle with endpoints $h(1)$ and $-h(1)$. Thus images of both geodesics are semi-circles with center at 0. The geodesic from 0 to ∞ is therefore perpendicular to both, and it is the unique such geodesic. Set ℓ_3 to be the image of the line from 0 to ∞ under the composition $g^{-1} \circ h^{-1}$. \square

In the previous proof, knowing which isometry h to apply in the last step required a calculation. However, once that isometry was applied, the existence and uniqueness of the geodesic ℓ_3 was clear.

Computing lengths of geodesics is also simplified by applying isometries.

EXAMPLE 2.9. Length computation.

Suppose you wish to compute the length of a segment, or the distance between two points in \mathbb{H}^2 . One strategy for doing this is to apply an isometry taking the two points to a simpler picture. For example, in figure 2.2, we may find an isometry taking the geodesic containing points a and b to the vertical geodesic from 0 to ∞ . Then under this isometry, the points a and b map to points of the form $(0, t_1)$ and $(0, t_2)$.

In example 2.2, we already computed the length of the vertical segment between $(0, t_1)$ and $(0, t_2)$; its length is $\log(t_1/t_2)$ (assuming here that $t_2 < t_1$, otherwise take the negative of the log). This gives the distance between a and b .

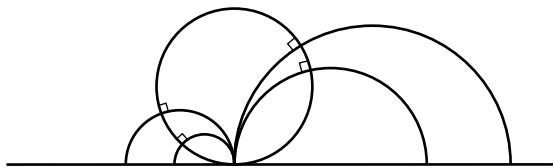


FIGURE 2.3. A horocycle

2.1.4. Triangles and horocycles.

DEFINITION 2.10. An *ideal triangle* in \mathbb{H}^2 is a triangle with three geodesic edges, with all three vertices on $\partial\mathbb{H}^2$.

There is an isometry of \mathbb{H}^2 taking any ideal triangle to the ideal triangle with vertices 0 , 1 , and ∞ , by lemma 2.7. Hence all ideal triangles in \mathbb{H}^2 are isometric. In fact, we will see that they all have finite area. Thus all ideal triangles have the same area!

DEFINITION 2.11. A *horocycle* centered at an ideal point $p \in \partial\mathbb{H}^2$ is defined as a curve perpendicular to all geodesics through p . When p is a point on $\mathbb{R} \subset \partial\mathbb{H}^2 = \mathbb{R} \cup \{\infty\}$, a horocycle is a Euclidean circle tangent to p , as in figure 2.3. When p is the point ∞ , a horocycle at p is a line parallel to \mathbb{R} . That is, in this case the horocycle consists of points of the form $\{(x, y) \mid y = c\}$ where $c > 0$ is constant.

DEFINITION 2.12. A *horoball* is the region of \mathbb{H}^2 interior to a horocycle.

Note a horoball will either be a Euclidean disk tangent to $\mathbb{R} \subset \partial\mathbb{H}^2$ or a region consisting of points of the form $\{(x, y) \mid y > c\}$.

In example 2.4, we computed the area of a portion of a horoball, and we observed it was finite. Using this, we can show that the area of an ideal triangle is finite.

LEMMA 2.13. *The area of an ideal triangle is finite.*

PROOF. Given any ideal triangle in \mathbb{H}^2 , we may apply an isometry taking its vertices to 0 , 1 , and ∞ . Let T denote this ideal triangle. Consider the intersection of T with the horoball about infinity of height 1 . This is the region R of example 2.4.

Note that the isometries

$$z \mapsto \frac{z-1}{z} \quad \text{and} \quad z \mapsto \frac{-1}{z-1}$$

take the horoball about infinity to horoballs of Euclidean diameter 1 centered at 1 and at 0 , respectively, and take T to T . Thus the intersections of T with these horoballs also have areas 1 .

Finally, note that the complement of these horoballs in T is a closed and bounded region B , lying below the line $y = 1$, above the horocycle of Euclidean diameter 1 centered at 0 , and above the horocycle of Euclidean

diameter 1 centered at 1. The region B lies in the rectangle $[0, 1] \times [\frac{1}{2}, 1]$. It follows that the area of B is at most the area of the rectangle, which is finite.

Thus the area of T is 3 plus the area of B , which is finite. \square

From the lemma, we see that the area of an ideal triangle is larger than 3. The exercises lead you through a calculation showing that the area of an ideal triangle is in fact π .

2.2. Hyperbolic geometry in dimension three

Hyperbolic 3-space is defined as follows:

$$\mathbb{H}^3 = \{(x + iy, t) \in \mathbb{C} \times \mathbb{R} \mid t > 0\},$$

under the metric with first fundamental form

$$(2.4) \quad ds^2 = \frac{dx^2 + dy^2 + dt^2}{t^2}.$$

We have the following theorems, which we will assume. Their proofs can be found in texts on hyperbolic geometry.

THEOREM 2.14. *The geodesics in \mathbb{H}^3 consist of vertical lines and semi-circles orthogonal to the boundary $\partial\mathbb{H}^3 = \mathbb{C} \cup \{\infty\}$. Totally geodesic planes are vertical planes and hemispheres centered on \mathbb{C} .* \square

THEOREM 2.15. *The full group of isometries of \mathbb{H}^3 is generated by reflections in geodesic planes.*

The group of orientation preserving isometries of \mathbb{H}^3 is $\mathrm{PSL}(2, \mathbb{C})$. Its action on the boundary $\partial\mathbb{H}^3 = \mathbb{C} \cup \{\infty\}$ is the usual action of $\mathrm{PSL}(2, \mathbb{C})$ on $\mathbb{C} \cup \{\infty\}$, via Möbius transformation. \square

An element $A \in \mathrm{PSL}(2, \mathbb{C})$ can be represented by a matrix, up to multiplication by $\pm \mathrm{Id}$. Theorem 2.15 states that if

$$A = \pm \begin{pmatrix} a & b \\ c & d \end{pmatrix} \in \mathrm{PSL}(2, \mathbb{C}),$$

then the action of A on $\partial\mathbb{H}^3$ is given by

$$A(z) = \frac{az + b}{cz + d}, \text{ for } z \in \partial\mathbb{H}^3.$$

The action of an element of $\mathrm{PSL}(2, \mathbb{C})$ extends to the interior of hyperbolic 3-space, and there is a unique way to extend. Marden works through it carefully in [Mar07, Chapter 1]. However, we will not need the formula, and it is complicated, so we omit it here.

THEOREM 2.16. *Apart from the identity, any element of $\mathrm{PSL}(2, \mathbb{C})$ is exactly one of the following:*

- (1) elliptic, which has two fixed points on $\partial\mathbb{H}^3$ and rotates about the geodesic axis between them in \mathbb{H}^3 , fixing the axis pointwise,
- (2) parabolic, which has a single fixed point on $\partial\mathbb{H}^3$,

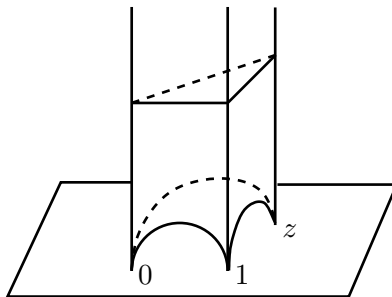


FIGURE 2.4. Ideal tetrahedron

- (3) loxodromic, which has two fixed points on $\partial\mathbb{H}^3$, and dilates and rotates about the axis between them.

For example, the element $\begin{pmatrix} \exp(i\theta) & 0 \\ 0 & \exp(-i\theta) \end{pmatrix} \in \mathrm{PSL}(2, \mathbb{C})$ is elliptic: it fixes the points 0 and ∞ , and the axis between them, and rotates about that axis by angle 2θ .

The element $\begin{pmatrix} 1 & 1 \\ 0 & 1 \end{pmatrix} \in \mathrm{PSL}(2, \mathbb{C})$ is parabolic. It fixes the point ∞ only. Its action on $\partial\mathbb{H}^3$ is $z \mapsto z + 1$, which extends to Euclidean translation by 1 in the interior of hyperbolic 3-space.

Finally, the element $\begin{pmatrix} \rho & 0 \\ 0 & \rho^{-1} \end{pmatrix}$ is loxodromic whenever ρ is a complex number with $|\rho| > 1$. It fixes the points 0 and ∞ in $\partial\mathbb{H}^3$, but translates along the axis between them, and rotates and translates points in the interior of \mathbb{H}^3 that do not lie on the axis.

In fact, after conjugating by an appropriate element of $\mathrm{PSL}(2, \mathbb{C})$, any element of $\mathrm{PSL}(2, \mathbb{C})$ actually becomes one of these three examples. This is stated as lemma 5.2 in chapter 5. As a warm up for that theorem and theorem 2.16, exercise 2.4 works through a similar classification for isometries of \mathbb{H}^2 .

DEFINITION 2.17. An *ideal tetrahedron* is a tetrahedron in \mathbb{H}^3 with all four vertices on $\partial\mathbb{H}^3$, and with geodesic edges and faces.

Since there exists a Möbius transformation taking any three points to 0, 1, and ∞ in $\mathbb{C} \cup \{\infty\}$, we may assume our tetrahedron has vertices at 0, 1, and ∞ , and at some point $z \in \mathbb{C} \setminus \{0, 1\}$. So any ideal tetrahedron is parameterized by z . See figure 2.4.

The value of z tells us about the geometry of the ideal tetrahedron. For example, the argument of z is the dihedral angle between the vertical planes through 0, 1, ∞ and through 0, z , ∞ .

The modulus of z also has geometric meaning. Consider the hyperbolic geodesic through $z \in \mathbb{C}$ that meets the vertical line from 0 to ∞ in a right angle at a point p_1 . Consider also the geodesic through $1 \in \mathbb{C}$ that meets

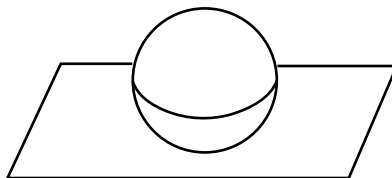


FIGURE 2.5. Horosphere

the vertical line from 0 to ∞ at a right angle at point p_2 . The hyperbolic distance between p_1 and p_2 is exactly $|\log |z||$ (exercise 2.7). Hence

$$\log z = (\text{signed dist between altitudes}) + i(\text{dihedral angle}).$$

DEFINITION 2.18. A *horosphere* about ∞ in $\partial\mathbb{H}^3$ is a plane parallel to \mathbb{C} , consisting of points $\{(x + iy, c) \in \mathbb{C} \times \mathbb{R}\}$ where $c > 0$ is constant. Note for any $c > 0$, this plane is perpendicular to all geodesics through ∞ . When we apply an isometry that takes ∞ to some $p \in \mathbb{C}$, note a horosphere is taken to a Euclidean sphere tangent to p . By definition, this is a horosphere about p . A *horoball* is the region interior to a horosphere.

The metric on \mathbb{H}^3 induces a metric on a horosphere. For a horosphere $\{(x + iy, c) \in \mathbb{C} \times \mathbb{R}\}$ about ∞ , the metric is just the Euclidean metric, rescaled by $1/c$. We may apply an isometry to any horosphere, taking it to one about ∞ . Thus the induced metric on any horosphere will always be Euclidean. Hence when we intersect horospheres about 0, 1, ∞ and z with an ideal tetrahedron through those points, we obtain four Euclidean triangles. These four triangles are similar (exercise 2.11).

2.3. Exercises

EXERCISE 2.1 (Requires geometry). Prove theorem 2.5, that is, show that vertical lines and semi-circles are geodesics, without using isometries of \mathbb{H}^2 . One way to solve this problem is to use Riemannian geometry, such as calculations in coordinates on \mathbb{H}^2 . Break the problem into two steps.

- (1) Prove that vertical lines $L(t) = (x, t)$, $t > 0$, are geodesics in \mathbb{H}^2 .
- (2) Prove that semi-circles $C(t) = (x + r \cos(t), r \sin(t))$, $t \in (0, \pi)$ are geodesics in \mathbb{H}^2 .

EXERCISE 2.2 (Requires some geometry). Suppose C is a geodesic in \mathbb{H}^2 that is a Euclidean semi-circle with center $a \in \mathbb{R}$ and radius R . Then the *reflection through C* takes z to $R^2/(\bar{z} - \bar{a}) + a$, where \bar{z} denotes complex conjugation.

Prove the reflection through C is an isometry of \mathbb{H}^2 that fixes C pointwise. Note this is an orientation reversing isometry.

A similar result holds for reflection through a vertical line. Find a description for the reflection through a vertical line, and prove it is an isometry.

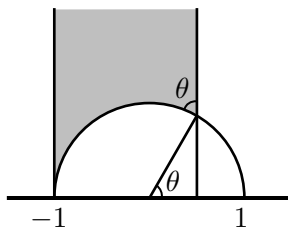


FIGURE 2.6. 2/3-ideal triangle.

EXERCISE 2.3 (Requires geometry). Prove any isometry of \mathbb{H}^2 is the product of reflections in hyperbolic geodesics.

EXERCISE 2.4. Work through the classification of isometries of \mathbb{H}^2 as elliptic, parabolic, or loxodromic. (E.g. Thurston [Thu79, page 67]).

EXERCISE 2.5. Lemma 2.7 shows there exists an orientation preserving isometry of \mathbb{H}^2 taking any three points of $\partial\mathbb{H}^2$ to any other three points, provided we are careful with orientation. Prove a similar statement for \mathbb{H}^3 : Given distinct b, c and d in $\mathbb{C} \cup \{\infty\}$, prove there exists an orientation preserving isometry of \mathbb{H}^3 taking b to 1, c to 0, and d to ∞ . Write it down as a matrix in $\text{PSL}(2, \mathbb{C})$. Note in \mathbb{H}^3 we no longer have to worry about orientation.

EXERCISE 2.6. Prove the following analogue of lemma 2.8 in \mathbb{H}^3 . Show two distinct geodesics l_1 and l_2 either intersect in a single point in the interior of \mathbb{H}^3 , intersect in a single point on $\partial\mathbb{H}^3$, or are completely disjoint in $\mathbb{H}^3 \cup \partial\mathbb{H}^3$. In the third case, show there exists a unique geodesic that is perpendicular to both l_1 and l_2 .

EXERCISE 2.7 (Cross ratios). Given $a \in \mathbb{C}$, the image of a under the isometry of exercise 2.5 is said to be the *cross ratio* of a, b, c, d , and is denoted $\lambda(a, b; c, d)$.

Let x be the point on the geodesic in \mathbb{H}^3 between c and d such that the geodesic from a to x is perpendicular to that between c and d . Let y be the point on the geodesic between c and d such that the geodesic from b to y is perpendicular to that between c and d . Prove the hyperbolic distance between x and y is equal to $|\log |\lambda(a, b; c, d)||$.

EXERCISE 2.8 (Areas of ideal triangles). Prove that the area of an ideal hyperbolic triangle is π . (E.g. use calculus.)

EXERCISE 2.9 (Areas of 2/3-ideal triangles). A *2/3-ideal triangle* is a triangle with two vertices on the boundary at infinity $\partial\mathbb{H}^2$, and the third in the interior of \mathbb{H}^2 such that the interior angle at the third vertex is θ .

- (a) Show that all 2/3-ideal triangles of angle θ are congruent to the triangle shown in figure 2.6, with one ideal vertex at infinity, one at $-1 \in \partial\mathbb{H}^2 = \mathbb{R} \cup \{\infty\}$, and the third in the interior of \mathbb{H}^2 with edges making angle θ .

- (b) Define a function $A: (0, \pi) \rightarrow \mathbb{R}$ by: $A(\theta)$ is the area of the $2/3$ -ideal triangle with interior angle $\pi - \theta$. Show that

$$A(\theta_1 + \theta_2) = A(\theta_1) + A(\theta_2),$$

when this is defined. (Hint: Figure 2.7 may be useful.)

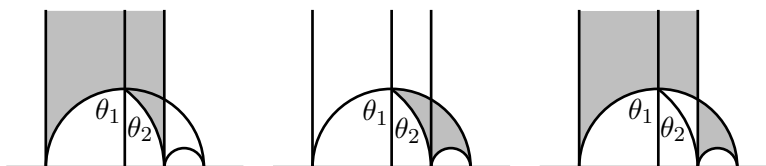


FIGURE 2.7. Areas of triangles.

- (c) It follows that A is \mathbb{Q} -linear. Since A is continuous, it must be \mathbb{R} -linear. Show $A(\theta) = \theta$.

EXERCISE 2.10. (Areas of general triangles.) Using the previous two problems, show that the area of a triangle with interior angles α , β , and γ is equal to $\pi - \alpha - \beta - \gamma$. Note an ideal vertex has interior angle 0.

EXERCISE 2.11. (Ideal tetrahedra and dihedral angles.) The dihedral angles on a tetrahedron are labeled A , B , C , D , E , and F in figure 2.8. Using linear algebra, prove that opposite dihedral angles agree. That is, show $A = E$, $B = F$, and $C = D$.

EXERCISE 2.12. (Ideal tetrahedra and cross ratios.) Orient an ideal tetrahedron with vertices a, b, c, d . When we apply a Möbius transformation taking b, c, d to $1, 0, \infty$, respectively, the point a goes to the cross ratio $\lambda(a, b; c, d)$. Label the edge from c to d by the complex number $\lambda = \lambda(a, b; c, d)$. We may do this for each edge of the tetrahedron, labeling by a different cross ratio. (Notice you need to keep track of orientation.) Find all labels on the edges of the tetrahedra in terms of λ .

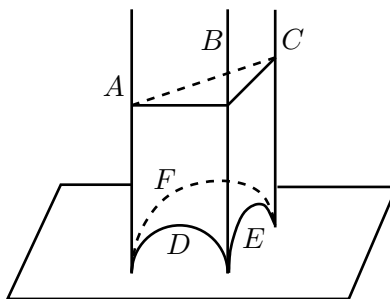


FIGURE 2.8. Dihedral angles of an ideal tetrahedron.

EXERCISE 2.13. (Volume of a region in a horoball) Let R be the region in \mathbb{H}^3 given by $A \times [1, \infty)$, where A is some region contained in the horosphere about ∞ of height 1, i.e. $A \subset \{(x + iy, 1)\}$. Prove that $\text{vol}(R) = \text{area}(A)/2$.

CHAPTER 3

Geometric Structures on Manifolds

In this chapter, we give our first examples of hyperbolic manifolds, combining ideas from the previous two chapters.

3.1. Geometric structures

3.1.1. Introductory example: The torus. A geometric structure you are likely familiar with is a 2-dimensional Euclidean structure on a torus. Given any parallelogram, we obtain a torus by gluing the top and bottom sides of the parallelogram, and the right and left sides, as shown in figure 3.1.

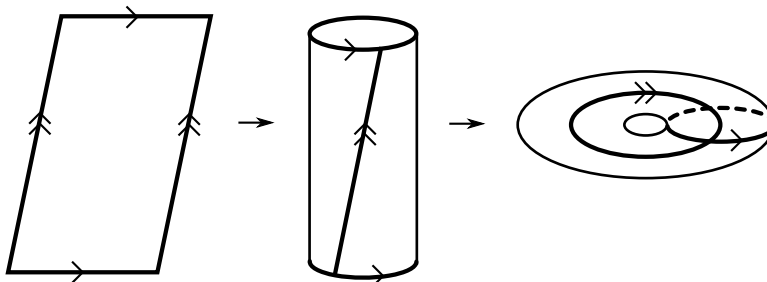


FIGURE 3.1. A parallelogram glued to a torus

The universal cover of the torus is obtained by gluing copies of the parallelogram to itself in \mathbb{R}^2 . We may glue infinitely many copies in two directions, and we obtain a tiling of the plane \mathbb{R}^2 by parallelograms, as in figure 3.2. These parallelograms define a lattice in \mathbb{R}^2 , and covering transformations of the universal cover \mathbb{R}^2 of the torus are given by Euclidean translations by points of the lattice. That is, if the parallelogram is determined by vectors \vec{v} and \vec{w} along its sides, then any covering transformation is of the form $a\vec{v} + b\vec{w}$ for $a, b \in \mathbb{Z}$. This construction works for any choice of parallelogram.

Now modify this construction by choosing a more general quadrilateral instead of a parallelogram. We can still identify opposite sides in an orientation preserving manner, so when we glue we still get an object homeomorphic

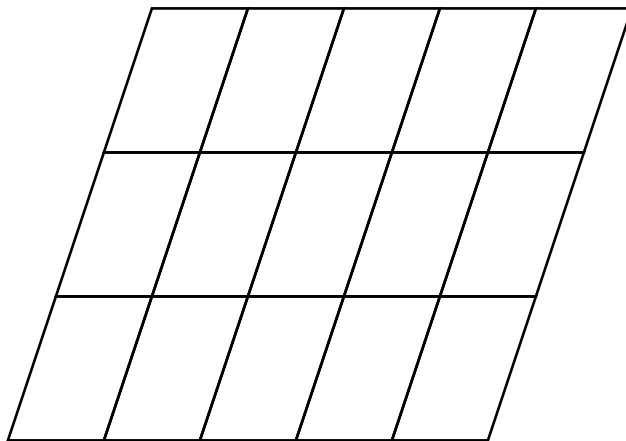


FIGURE 3.2. The universal cover of a Euclidean torus.

to a torus. However, the quadrilateral no longer determines a tiling of \mathbb{R}^2 , nor a lattice. Indeed, when we glue copies of the quadrilateral to itself, as we did when constructing the universal cover above, we have to shrink, expand, and rotate the quadrilateral to glue copies, and the result is not a tiling of the plane. See figure 3.3.

These examples of the torus can be generalized to different surfaces and manifolds. The torus was created by gluing quadrilaterals. More generally, we will glue different types of polygons, including ideal polygons, and in 3-dimensions, polyhedra.

DEFINITION 3.1. Let M be a 2-manifold. A *topological polygonal decomposition* of M is a combinatorial way of gluing polygons so that the result is homeomorphic to M .

We allow ideal polygons, i.e. those with one or more ideal vertex. Additionally, by *gluing* we mean an identification that takes faces to faces, edges to edges, and vertices to vertices.

Both constructions of the torus above give examples of topological polygonal decompositions of the torus.

DEFINITION 3.2. A *geometric polygonal decomposition* of M is a topological polygonal decomposition along with a metric on each polygon such that gluing is by isometry and the result of the gluing is a smooth manifold with a complete metric.

Recall that a metric space is *complete* if every Cauchy sequence converges; and recall that a *Cauchy sequence* is a sequence $\{x_i\}_{i=1}^{\infty}$ such that for each $\epsilon > 0$, there exists a positive integer N such that $d(x_i, x_j) < \epsilon$ if $i, j \geq N$.

The first construction of the torus gives a complete Euclidean metric on the torus, by pulling back the Euclidean metric on the parallelogram.

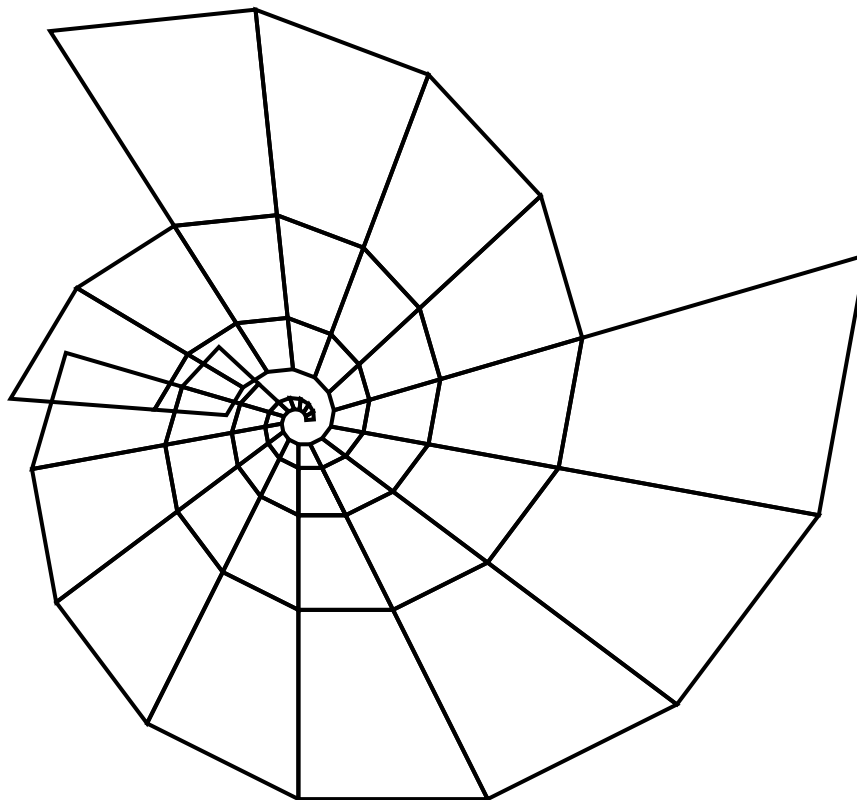


FIGURE 3.3. When we construct a torus from a quadrilateral that is not a parallelogram, generally a single point is omitted from the plane.

Because gluings of the sides of the parallelogram are by Euclidean isometries, this will be well-defined. The second construction of the torus does not give a complete Euclidean metric, or any Euclidean metric: gluings of the quadrilaterals are by affine transformations (rotation, translation, scale), not isometries of the Euclidean plane, so we cannot pull back a well-defined metric. Note also that toward the center of figure 3.3, the quadrilaterals are becoming arbitrarily small. In fact, there is a point in the figure that is disjoint from all quadrilaterals (see exercise 3.8).

We will also be studying polygonal decompositions of manifolds and their generalization to three dimensions: polyhedral decompositions. More generally, we can discuss geometric structures on manifolds.

3.1.2. Geometric structures on manifolds.

DEFINITION 3.3. Let X be a manifold, and G a group acting on X . We say a manifold M has a (G, X) -structure if for every point $x \in M$, there exists a *chart* (U, ϕ) , that is, a neighborhood $U \subset M$ of x and a homeomorphism $\phi: U \rightarrow \phi(U) \subset X$. We also sometimes refer to the map ϕ

as a chart when U is understood. Charts satisfy the following: if two charts (U, ϕ) and (V, ψ) overlap, then the *transition map* or *coordinate change map*

$$\gamma = \phi \circ \psi^{-1}: \psi(U \cap V) \rightarrow \phi(U \cap V)$$

is an element of G .

In the examples we encounter here, X will be simply connected, and G a group of *real analytic diffeomorphisms* acting transitively on X . The reason we need real analytic diffeomorphisms is that they are uniquely determined by their restriction to any open set. This is true, for example, of isometries of Euclidean space, and isometries of hyperbolic space. While we present the results in this full generality, the reader who is unfamiliar with real analytic diffeomorphisms can read with Euclidean or hyperbolic isometries in mind.

Our manifold X will typically admit a known metric as well, and G will be the group of isometries of X . It will follow that M inherits a metric from X (exercise 3.2). We will say that M has a *geometric structure*.

EXAMPLE 3.4 (Euclidean torus). Let X be 2-dimensional Euclidean space, \mathbb{E}^2 . Let G be isometries of Euclidean space $\text{Isom}(\mathbb{E}^2)$. The torus admits an $(\text{Isom}(\mathbb{E}^2), \mathbb{E}^2)$ -structure, also called a *Euclidean structure*.

To help us understand the definition, let's look at some charts and transition maps for this example.

We know the universal cover of the torus is given by tiling the plane \mathbb{R}^2 with parallelograms. For simplicity, we will work with the example in which each parallelogram is a square, and one square has vertices $(0,0)$, $(1,0)$, $(1,1)$, and $(0,1)$ in \mathbb{R}^2 . Call this square the *basic square*.

Now pick any point p on the torus. This will lift to a collection of points on \mathbb{R}^2 , one for each copy of the unit square. Take a disk of radius $1/4$ around each lift. These all project under the covering map to an open neighborhood U of p in the torus. Therefore we have the following charts: (U, ϕ) is a chart, where ϕ maps U into the disk of radius $1/4$ centered around the lift \widehat{p}_0 of p in the basic square. Another chart is (U, ψ) , where ψ maps U into the disk of radius $1/4$ about the lift \widehat{p}_1 of p in some other square. Such a lift is given by a translation of \widehat{p}_0 by a vector $(m, n) \in \mathbb{Z} \times \mathbb{Z}$, in the lattice determined by the basic square. Thus $\phi \circ \psi^{-1}$ will be a Euclidean translation by integral values in the x and y direction. These are Euclidean isometries.

More generally, let q be a point such that a lift \widehat{q}_0 of q has distance less than $1/2$ to \widehat{p}_0 in the basic square. Thus a disk of radius $1/4$ about \widehat{p}_0 overlaps with a disk of radius $1/4$ about \widehat{q}_0 . These disks project to give open neighborhoods U and V of p and q respectively in the torus. Since these neighborhoods overlap, we need to ensure that any corresponding charts differ by a Euclidean isometry in the region of overlap. Obtain charts by mapping U to your favorite disk of radius $1/4$ about a lift of p in \mathbb{R}^2 . Map V to your favorite disk of radius $1/4$ about a lift of q in \mathbb{R}^2 ; see figure 3.4 for an example. Again, regardless of the choice of ϕ and ψ , the overlap

$$\phi \circ \psi^{-1}: \psi(U \cap V) \rightarrow \phi(U \cap V)$$

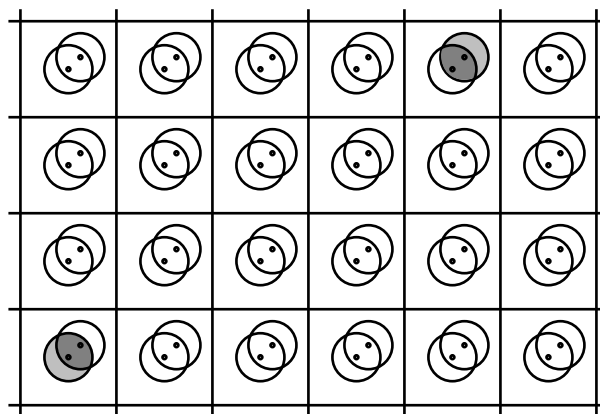


FIGURE 3.4. Euclidean structure on a torus: Transition maps are Euclidean translations.

will be a Euclidean translation of the intersection of the two disks by some $(n, m) \in \mathbb{Z} \times \mathbb{Z}$ corresponding to the choice of lifts. Again see figure 3.4.

This idea extends to arbitrary neighborhoods U and V : transition maps will always be translations by $(n, m) \in \mathbb{Z} \times \mathbb{Z}$. Therefore, we conclude that the torus obtained by gluing sides of the square with vertices $(0, 0)$, $(0, 1)$, $(1, 0)$ and $(1, 1)$ admits an $(\text{Isom}(\mathbb{E}^2), \mathbb{E}^2)$ -structure, where \mathbb{E}^2 denotes \mathbb{R}^2 with the standard Euclidean metric.

EXAMPLE 3.5 (The affine torus). Again let $X = \mathbb{R}^2$, but this time let G be the affine group acting on \mathbb{R}^2 . That is, G consists of invertible affine transformations, i.e. linear transformations followed by a translation:

$$x \mapsto Ax + b.$$

The torus of figure 3.3 admits a (G, \mathbb{R}^2) -structure. This can be seen in a manner similar to that in the previous example. Charts will differ by a scaling, rotation, then translation.

In practice, we rarely use charts to show manifolds have a particular (G, X) -structure. Instead, as in the two previous examples, we build manifolds by starting with an existing manifold X and taking the quotient by the action of a group, or by gluing together polygons.

3.1.3. Hyperbolic surfaces. Let $X = \mathbb{H}^2$, and let $G = \text{Isom}(\mathbb{H}^2)$, the group of isometries of \mathbb{H}^2 . When a 2-manifold admits an $(\text{Isom}(\mathbb{H}^2), \mathbb{H}^2)$ -structure, we say the manifold admits a *hyperbolic structure*, or is hyperbolic. More generally, an n -manifold that admits an $(\text{Isom}(\mathbb{H}^n), \mathbb{H}^n)$ -structure admits a *hyperbolic structure*, or is hyperbolic.

We will look at some examples of hyperbolic 2-manifolds obtained from geometric polygonal decompositions. To do so, we start with a collection of hyperbolic polygons in \mathbb{H}^2 , for example, a collection of triangles. We allow

vertices to either be finite or ideal, i.e. in the interior of \mathbb{H}^2 or on $\partial_\infty \mathbb{H}^2$, respectively. In any case, we will always assume each polygon is convex, and edges are segments of geodesics in \mathbb{H}^2 . Now, to each edge, associate exactly one other edge. Just as in the case of the torus, glue polygons along associated edges by an isometry of \mathbb{H}^2 .

When does the result of this gluing give a manifold that admits a hyperbolic structure? We obtain a hyperbolic structure exactly when each point in the result has a neighborhood U and a homeomorphism into \mathbb{H}^2 so that transition maps are in $\text{Isom}(\mathbb{H}^2)$. The following lemma gives a condition that will guarantee this.

LEMMA 3.6. *A gluing of hyperbolic polygons yields a 2-manifold with a hyperbolic structure, with structure agreeing with that in the interior of the polygons, if and only if each point in the gluing has a neighborhood (in the quotient topology) isometric to a disk in \mathbb{H}^2 .*

More generally, a gluing of n -dimensional hyperbolic polyhedra yields a hyperbolic n -manifold, with hyperbolic structure agreeing with that in the interior of the polyhedra, if and only if each point has a neighborhood (in the quotient topology) isometric to a ball in \mathbb{H}^n , with the isometry the identity in the interior of polyhedra.

Here by a *gluing* of hyperbolic polyhedra, we mean a collection of geodesic polyhedra embedded in \mathbb{H}^n , along with identifications on faces, called gluing maps or face-pairings, which are given by an isometry on each face. The quotient space of the polyhedra with identifications given by the gluing maps is the gluing.

Additionally, we say that the hyperbolic structure agrees with the structure in the interior of the polyhedra if, for any point in the interior of the polyhedron, a ball U containing that point, lying in the interior of the polyhedron, along with the identity map from U to $U \subset \mathbb{H}^3$, provides a chart in the hyperbolic structure.

PROOF OF LEMMA 3.6. We will prove the more general statement. Suppose first that a gluing of hyperbolic polyhedra M yields an n -manifold with hyperbolic structure, agreeing with the hyperbolic structure in the interior of the polyhedra. Then every point x in M has a neighborhood U and a chart $\phi: U \rightarrow \phi(U) \subset \mathbb{H}^n$ such that transition maps are isometries of \mathbb{H}^n . By restricting ϕ to a subset of U , we may assume $\phi(U)$ is a ball in \mathbb{H}^n . The neighborhood U is open in the quotient topology on the gluing. Thus it is made up of portions of open neighborhoods meeting the polyhedra in \mathbb{H}^n , identified by gluing isometries. In the interior of a polyhedron P , ϕ composed with the identity map on $U \cap P$ is an isometry of \mathbb{H}^n . Thus we may view $U \cap P$ as the intersection of a hyperbolic ball with P . Since gluing maps are isometries, they identify faces of $U \cap P$ into a hyperbolic ball, and ϕ must be an isometry of U into a ball in \mathbb{H}^n .

Now suppose that under the quotient topology, every point of M has a neighborhood isometric to a ball of \mathbb{H}^n , with isometry the identity for

points in the interior of a polyhedron. Then this isometry gives a chart $\phi: U \rightarrow \phi(U) \subset \mathbb{H}^n$. If (U, ϕ) and (V, ψ) are charts and $U \cap V \neq \emptyset$, then $\phi \circ \psi^{-1}: \psi(U \cap V) \rightarrow \phi(U \cap V)$ is the composition of isometries, hence an isometry, so M has an $(\text{Isom}(\mathbb{H}^n), \mathbb{H}^n)$ -structure. Because charts in the interior of polyhedra are identity maps, the hyperbolic structure agrees with that on the polyhedra. \square

When does each point in a gluing of hyperbolic polygons have a neighborhood isometric to a disk in the hyperbolic plane? Let x be a point in the gluing, and consider its lifts to the polygons. There are three cases.

- (1) If x lifts to a point \hat{x} in the interior of one of the polygons, then that lift is unique. In this case, for small enough $\epsilon > 0$, there is a disk about \hat{x} of radius ϵ embedded in the interior of the polygon in \mathbb{H}^2 . This projects under the quotient map to a disk about x isometric to a disk in \mathbb{H}^2 .
- (2) If x lifts to a point on an edge of a polygon, then it has two lifts, \hat{x}_0 and \hat{x}_1 , on two different edges that are glued to each other by the gluing map. A neighborhood of x in the quotient topology lifts to give a “half-neighborhood” of \hat{x}_0 glued to a corresponding “half-neighborhood” of \hat{x}_1 . Each contains a half-disk in \mathbb{H}^2 , and we may scale the disks so that they glue to a disk under the gluing map. Thus in this case as well, x has a neighborhood isometric to a disk in \mathbb{H}^2 .
- (3) If x lifts to a finite vertex of a polygon, then it may have several lifts, possibly including several vertices of the collection of polygons. In this case, we need to be more careful. The following lemma gives a condition that will guarantee we have an isometry to a hyperbolic disk in this case as well.

LEMMA 3.7. *A gluing of hyperbolic polygons gives a 2-manifold with a hyperbolic structure if and only if for each finite vertex v of the polygons, the sum of interior angles at each vertex glued to v is 2π .*

PROOF. This is an immediate consequence of lemma 3.6 and the observation that around a vertex, portions of the polygons meet in a cycle, with total angle around the finite vertex equal to the sum of interior angles of the polyhedron at that vertex. We need to check that each finite vertex has a neighborhood isometric to a neighborhood in \mathbb{H}^2 . This will hold if and only if the sum of interior angles is 2π . \square

3.2. Complete structures

Given a gluing of hyperbolic polygons, suppose the angle sum at each finite vertex is 2π , so that we have a hyperbolic structure by lemma 3.7. Does it necessarily follow that we have a geometric polygonal decomposition?

Recall from definition 3.2 that for a geometric polygonal decomposition, we need a geometric structure on each polygon so that the result of the gluing

is a smooth manifold with a complete metric. Our hyperbolic structure gives a smooth manifold with a metric. However, in the presence of ideal vertices, the metric may not be complete.

It will be easier to discuss criteria for completeness using the language of *developing maps* and *holonomy*. Our exposition of these terms is based on that of Thurston [Thu97].

3.2.1. Developing map and holonomy. The developing map, which we define in this subsection, encodes information on the (G, X) -structure of a manifold. It is a local homeomorphism into X . When a manifold has a polygonal decomposition, say by polygons in $X = \mathbb{R}^2$ or \mathbb{H}^2 , the developing map “develops” the gluing information on the polygons by attaching copies of the polygons along edges in the space X , as we did for the torus in Figures 3.2 and 3.3.

More generally, a developing map can be defined for any manifold M with a (G, X) -structure, assuming as before that X is a manifold and G is a group of real analytic diffeomorphisms acting transitively on X . Any chart (U, ϕ) gives a homeomorphism of U onto $\phi(U) \subset X$. To define the developing map, we wish to extend this map.

Suppose (V, ψ) is another chart, and $y \in U \cap V$. Then

$$\gamma = \phi \circ \psi^{-1}: \psi(U \cap V) \rightarrow \phi(U \cap V)$$

is an element of G acting on $\psi(U \cap V)$. By setting $y \mapsto \gamma$, we obtain a map from $U \cap V$ to G . Because G is a group of real analytic diffeomorphisms, the element γ is uniquely determined in a neighborhood of $\psi(y)$. This implies that the map $y \mapsto \gamma$ is locally constant: we obtain the same element γ for all x in a neighborhood of y in $U \cap V$. We let $\gamma(y)$ denote this element of G . Then we may define a map $\Phi: U \cup V \rightarrow X$ by

$$\Phi(x) = \begin{cases} \phi(x) & \text{if } x \in U \\ \gamma(y) \cdot \psi(x) & \text{if } x \in V \end{cases}$$

Note that if $U \cap V$ is connected, then Φ is a well-defined homeomorphism, since for $x \in U \cap V$, we have $\phi(x) = \gamma(y) \cdot \psi(x)$. Thus in this case, Φ is an extension of ϕ . However, note that we may run into trouble when $U \cap V$ is not connected, as follows. If x is in a component disjoint from that containing y , then $\phi(x)$ may not equal $\gamma(y) \cdot \psi(x)$. This is illustrated in the following example.

EXAMPLE 3.8. Consider the Euclidean torus obtained by gluing sides of a square with vertices $(0, 0)$, $(1, 0)$, $(0, 1)$, and $(1, 1)$ in \mathbb{R}^2 . Suppose the union of two simply connected neighborhoods U and V forms a neighborhood of a longitude for the torus, as in figure 3.5, such that $U \cap V$ has two components. Suppose y lies in one component of $U \cap V$. There exist charts (U, ϕ) and (V, ψ) sending y to the interior of the basic square in \mathbb{R}^2 . Then the transition map $\gamma(y)$ is the identity element of G in this case, since $\phi(U)$ and $\psi(V)$ overlap in the component of $U \cap V$ containing y . However, the map Φ defined above

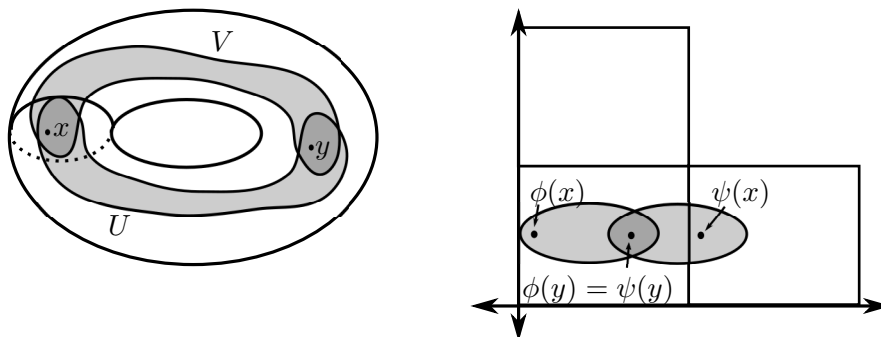


FIGURE 3.5. Neighborhoods U and V on the torus have two components of intersection, one containing x and one containing y . The map ϕ cannot be extended over V because it will not be well-defined at x

is not well-defined, for if x lies in the other component of $U \cap V$, $\phi(x)$ lies in the basic square, but $\gamma(y) \cdot \psi(x) = \psi(x)$ lies in the square with vertices $(1, 0)$, $(2, 0)$, $(1, 1)$, and $(1, 2)$.

Similarly, as we attempt to extend Φ by considering other coordinate neighborhoods overlapping U and V , the natural extensions using transition maps such as $\gamma(y)$ again may not be well-defined.

To overcome this problem, we use the universal cover of M . Recall from algebraic topology that the universal cover \widetilde{M} of M can be defined to be the space of homotopy classes of paths in M that start at a fixed basepoint x_0 . See, for example [Mun00, Theorem 82.1] or [Hat02, page 64]. Let $\alpha: [0, 1] \rightarrow M$ be a path representing a point $[\alpha] \in \widetilde{M}$, and let the chart (U_0, ϕ_0) contain the basepoint x_0 .

Now find $0 = t_0 < t_1 < \dots < t_n = 1$ and charts (U_i, ϕ_i) such that $\alpha([t_i, t_{i+1}])$ is contained in U_i for $i = 0, 1, \dots, n-1$. Denote the points $\alpha(t_i)$ by $x_i \in M$. We extend ϕ_0 to all of α as follows. First, note that each x_i , for $i = 1, \dots, n-1$, is contained in a connected component of the intersection of two charts, $x_i \in U_{i-1} \cap U_i$. Then the transition map $\gamma_{i-1,i} = \phi_{i-1} \circ \phi_i^{-1}$ gives an element $\gamma_{i-1,i}(x_i)$ in G that is well-defined on the entire connected component. Thus at the first step, we may extend ϕ_0 to a function from $[0, t_2]$ to X by defining $\Phi_1: [0, t_2] \rightarrow X$ to be the function:

$$\Phi_1(t) = \begin{cases} \phi_0(\alpha(t)) & \text{if } t \in [0, t_1] \\ \gamma_{0,1}(x_1) \cdot \phi_1(\alpha(t)) & \text{if } t \in [t_1, t_2] \end{cases}$$

This will be well-defined on all of $[0, t_2]$, since $\phi_0(\alpha(t_1)) = \gamma_{0,1}(x_1) \cdot \phi_1(\alpha(t_1))$.

Extend inductively to $\Phi_i: [0, t_{i+1}] \rightarrow X$ by setting:

$$\Phi_i(t) = \begin{cases} \Phi_{i-1}(t) & \text{if } t \in [0, t_i] \\ \gamma_{0,1}(x_1) \gamma_{1,2}(x_2) \dots \gamma_{(i-1),i}(x_i) \cdot \phi_i(\alpha(t)) & \text{if } t \in [t_i, t_{i+1}] \end{cases}$$

Again this is well-defined, for we know $\phi_{i-1}(\alpha(t_i)) = \gamma_{(i-1),i}(x_i) \cdot \phi_i(\alpha(t_i))$. Thus by induction, at the point t_i ,

$$\begin{aligned}\Phi_{i-1}(t_i) &= \gamma_{0,1}(x_1)\gamma_{1,2}(x_2) \cdots \gamma_{(i-2),(i-1)}(x_{i-1}) \cdot \phi_{i-1}(\alpha(t_i)) \\ &= \gamma_{0,1}(x_1)\gamma_{1,2}(x_2) \cdots \gamma_{(i-1),i}(x_i) \cdot \phi_i(\alpha(t_i)).\end{aligned}$$

After the $(n-1)$ -st step, we have a map $\Phi_{n-1}: [0, 1] \rightarrow X$. In fact, note that the definition of Φ_{n-1} actually provides a map $\Phi_{[\alpha]}: U \rightarrow X$, for some small neighborhood U of $\alpha(1)$, defined by

$$\Phi_{[\alpha]}(x) = \gamma_{0,1}(x_1)\gamma_{1,2}(x_2) \cdots \gamma_{(n-2),(n-1)}(x_n) \cdot \phi_{n-1}(x).$$

The function $\Phi_{[\alpha]}$ defined in this manner, with fixed initial chart (U_0, ϕ_0) and fixed basepoint x_0 , is an example of a function defined by *analytic continuation*. It is well known that analytic continuation gives a well-defined function, independent of choice of the charts $(U_1, \phi_1), \dots, (U_{n-1}, \phi_{n-1})$, independent of the choice of points t_1, \dots, t_{n-1} , and independent of the choice of path α in the homotopy class $[\alpha] \in \widetilde{M}$. For our particular application, we will leave this as an exercise (exercise 3.4).

DEFINITION 3.9. The *developing map* $D: \widetilde{M} \rightarrow X$ is the map

$$D([\alpha]) = \Phi_n(1) = \gamma_{0,1}(x_1)\gamma_{1,2}(x_2) \cdots \gamma_{(n-2),(n-1)}(x_{n-1}) \cdot \phi_{n-1}(\alpha(1)),$$

with notation given above.

PROPOSITION 3.10. *The developing map $D: \widetilde{M} \rightarrow X$ satisfies the following properties.*

- (1) *For fixed basepoint x_0 and initial chart (U_0, ϕ_0) , with $x_0 \in U_0$, the map D is well-defined, independent of all other choices used to define it, including charts, points in the intersection of chart neighborhoods, and independent of choice of α in the homotopy class of $[\alpha]$.*
- (2) *D is a local diffeomorphism.*
- (3) *If we define a new map in the same way as D , except beginning with a new choice of basepoint and initial chart, the resulting map is equal to the composition of D with an element of G .*

PROOF. Showing the map is well-defined, part (1), is a standard exercise in analytic continuation, and uses heavily the fact that G is analytic. We leave it as exercise 3.4. We also leave part (3) as an exercise. Part (2) follows from part (1), the fact that each $\gamma_{i,(i+1)}(x_i)$ is a diffeomorphism and ϕ_n is a local diffeomorphism on M , and the topology on \widetilde{M} . \square

Now consider the case that $[\alpha] \in \widetilde{M}$ is an element of the fundamental group of M . That is, $[\alpha]$ is a homotopy class of loops starting and ending at x_0 . Analytic continuation along a loop gives a function $\Phi_{[\alpha]}$ whose domain is a neighborhood of the basepoint of the loop; this is a new chart defined in a neighborhood of the basepoint. Since ϕ_0 and $\Phi_{[\alpha]}$ are both charts defined

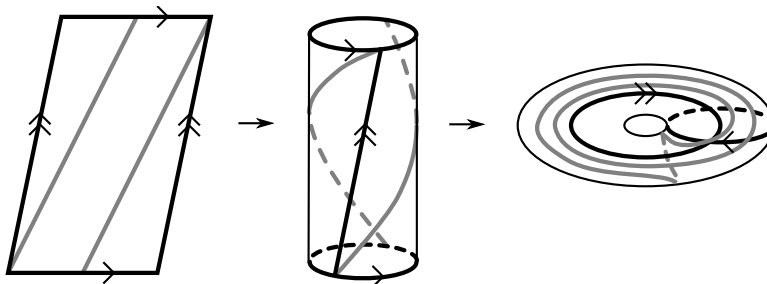


FIGURE 3.6. A nontrivial curve γ (gray) on the torus. Meridian and longitude curves are shown in black.

in a neighborhood of the basepoint, these maps must differ by an element of G . Let $g_{[\alpha]} \in G$ be the element such that $\Phi_{[\alpha]} = g_{[\alpha]}\phi_0$.

Let $T_{[\alpha]}$ denote the covering transformation of \widetilde{M} that corresponds to $[\alpha]$. It follows that

$$D \circ T_{[\alpha]} = g_{[\alpha]} \circ D.$$

Note also that for $[\alpha], [\beta] \in \widetilde{M}$,

$$D \circ T_{[\alpha]} \circ T_{[\beta]} = (g_{[\alpha]} \circ D) \circ T_{[\beta]} = g_{[\alpha]} \circ g_{[\beta]} \circ D.$$

It follows that the map $\rho: \pi_1(M) \rightarrow G$ defined by $\rho([\alpha]) = g_{[\alpha]}$ is a group homomorphism.

DEFINITION 3.11. The element $g_{[\alpha]}$ is the *holonomy* of $[\alpha]$. The group homomorphism ρ is called the *holonomy* of M . Its image is the *holonomy group* of M .

Note that ρ depends on the choices from the construction of D . When D changes, ρ changes by conjugation in G (exercise).

EXAMPLE 3.12. Pick a point x on the torus, say x lies at the intersection of a choice of meridian and longitude curves for the torus, and consider a nontrivial curve γ based at x . An example of a nontrivial curve γ on the torus is shown in figure 3.6.

Now consider a Euclidean structure on the torus. There exists a chart mapping x onto the Euclidean plane. We can take our chart to be an open parallelogram about x , where boundaries of the parallelogram glue in the usual way to form the torus. As the curve γ passes over a meridian or longitude, in the image of the developing map we must glue a new parallelogram to the appropriate side of the parallelogram we just left. See figure 3.7, left, for an example. The tiling of the plane by parallelograms is the image of the developing map, or the developing image of the Euclidean torus.

As for the affine torus, example 3.5, each time a curve crosses a meridian or longitude we attach a rescaled, rotated, translated copy of our quadrilateral to the appropriate edge. Figure 3.7 right shows an example. Figure 3.3 shows (part of) the developing image of the affine torus.

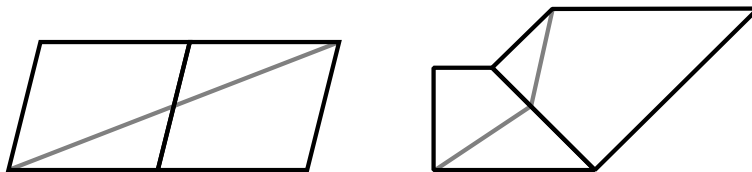


FIGURE 3.7. Left to right: developing a Euclidean torus, developing an affine torus.

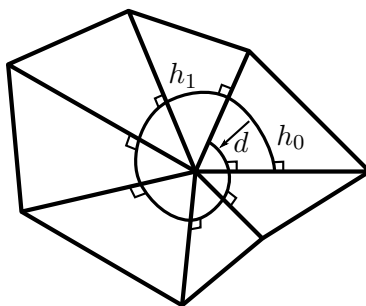


FIGURE 3.8. Extending a horocycle: view inside the manifold.

3.2.2. Completeness of polygonal gluings. Now we return to the question of determining when a gluing of hyperbolic polygons gives a complete hyperbolic structure. We know there will be a hyperbolic structure provided the angle sum around finite vertices is 2π (lemma 3.7). The question of whether the structure is complete or not depends on what happens near ideal vertices.

Let M be an oriented hyperbolic surface obtained by gluing *ideal* hyperbolic polygons. An *ideal vertex* of M is an equivalence class of ideal vertices of the polygons, identified by the gluing.

Let v be an ideal vertex of M . Then v is identified to some ideal vertex v_0 of a polygon P_0 . Let h_0 be a horocycle centered at v_0 on P_0 , and extend h_0 counterclockwise around v_0 . The horocycle h_0 will meet an edge e_0 of P_0 , which is glued to an edge of some polygon P_1 meeting ideal vertex v_1 identified to v . Note h_0 meets e_0 at a right angle. It extends to a unique horocycle h_1 about v_1 in P_1 . Continue extending the horocycle in this manner, obtaining horocycles h_2, h_3, \dots . Since we only have a finite number of polygons with a finite number of vertices, eventually we return to the vertex v_0 of P_0 , obtaining a horocycle h_n about that ideal vertex. Note h_n may not agree with the initial horocycle h_0 . See figure 3.8.

DEFINITION 3.13. Let $d(v)$ denote the signed hyperbolic distance between h_0 and h_n on P_0 . See figure 3.8. The sign is taken such that if h_n is closer to v_0 than h_0 , then $d(v)$ is positive. This is the direction shown in the figure.

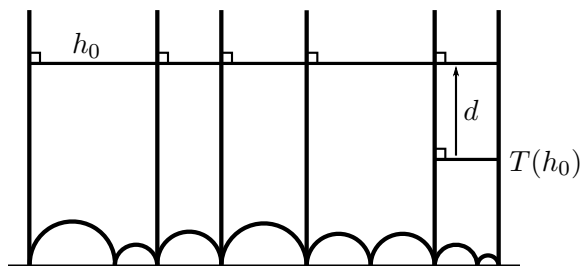


FIGURE 3.9. Extending a horocycle.

LEMMA 3.14. *The value $d(v)$ does not depend on the initial choice of horocycle h_0 , nor on the initial choice of v_0 in the equivalence class of v .*

PROOF. Exercise. \square

It may be easier to compute $d(v)$ if we look at polygons in \mathbb{H}^2 , using terminology of developing map and holonomy.

Fix an ideal vertex on one of the polygons P . Put P in \mathbb{H}^2 with v at infinity. Now take h_0 to be a horocycle centered at infinity intersected with P . Follow h_0 to the right. When it meets the edge of P , a new polygon is glued. The developing map instructs us how to embed that new polygon as a polygon in \mathbb{H}^2 , with one edge the vertical geodesic which is the edge of P . Continue along this horocycle, placing polygons in \mathbb{H}^2 according to their developing image. Eventually the horocycle will meet P again with v at infinity. When this happens, the developing map will instruct us to glue a copy of P to the given edge. This copy of P will be isometric to the original copy of P , where the isometry is the holonomy of the closed path which encircles the ideal vertex v once in the counterclockwise direction. This holonomy isometry, call it T , takes the horocycle h_0 on our original copy of P to a horocycle $T(h_0)$, and $T(h_0)$ will be of distance $d(v)$ from the extended horocycle that began with h_0 . See figure 3.9.

PROPOSITION 3.15. *Let S be a surface with hyperbolic structure obtained by gluing hyperbolic polygons. Then the metric on S is complete if and only if $d(v) = 0$ for each ideal vertex v .*

Before we prove this proposition, let's look at an example.

EXAMPLE 3.16 (Complete 3-punctured sphere). A topological polygonal decomposition for the 3-punctured sphere consists of two ideal triangles. See figure 3.10.

Let's try to construct a geometric polygonal decomposition by building the developing image. We can put one of the ideal triangles in \mathbb{H}^2 as the triangle with vertices at $0, 1, \infty$. If we glue the other triangle immediately to the right, we have two vertices at 1 and at ∞ , but the third can go to any point x , where $x > 1$. See figure 3.11. These two triangles on the left, labeled A and B , give a fundamental region for the 3-punctured sphere.

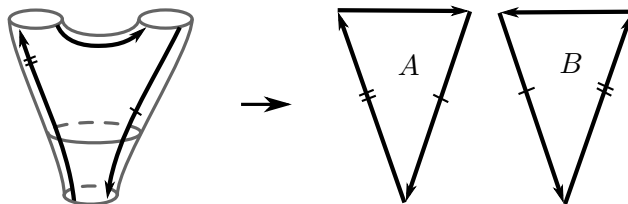


FIGURE 3.10. Topological polygonal decomposition for the 3-punctured sphere.

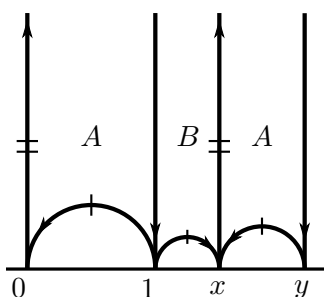


FIGURE 3.11. We may choose any $x > 1$, $y > x$ when finding a hyperbolic structure.

The developing image will be created by gluing additional copies of these two triangles to edges in the figure by holonomy isometries.

We may choose the position of the next copy of the triangle A glued to the right, putting its vertex at the point y as in figure 3.11. After this choice, notice we cannot choose where the next vertex of B to the right will go. This is because the choice y determines an isometry of \mathbb{H}^2 taking the triangle A on the left to the triangle labeled A on the right. This isometry is exactly the holonomy element corresponding to the closed curve running once around the vertex at infinity. The same isometry, which has been determined with the choice of y , must take B in the middle to the next triangle glued to the right in our figure. In fact, now that we know this holonomy element, we may apply it and its inverse successively to the triangles of figure 3.11, and we obtain the entire developing image of all triangles adjacent to infinity.

Recall that we want our hyperbolic structure to be complete. By proposition 3.15, we need to look at horocycles. Pick a collection of horocycles about the vertices 0 , 1 , and ∞ . Each of these horocycles extends to give a new horocycle about another copy of A . Each copy of A is obtained by applying a holonomy isometry to the original triangle with vertices at 0 , 1 , and ∞ . We want the horocycles obtained under these holonomy isometries to agree with the horocycles obtained by extending the original horocycles. This is the condition for completeness.

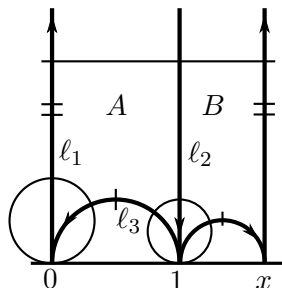


FIGURE 3.12. Lengths between horocycles

Here is one way to determine complete structures. Let ℓ_1 denote the distance in \mathbb{H}^2 between the horocycle at infinity and the horocycle at 0. See figure 3.12. The holonomy element ψ , corresponding to the group element fixing the ideal vertex at infinity, is an isometry of \mathbb{H}^2 , hence it preserves distances. Thus, under this isometry, the distance between the image of the horocycle at infinity and the horocycle at $\psi(0) = x$ must also be ℓ_1 . If the structure is complete, then the horocycle about infinity is preserved by ψ . Thus the horocycle at x must have the same (Euclidean) diameter as the horocycle at 0.

Now consider the length of the edge between horocycles at 0 and 1, labeled ℓ_3 in figure 3.12. There is another holonomy isometry ϕ mapping the geodesic edge between 0 and 1 to one between x and 1, corresponding to the group element encircling the ideal vertex at 1. Again completeness implies that the horocycle at 1 is fixed by ϕ . The horocycle at 0 maps to the horocycle centered at x , and again because ϕ is an isometry, the distance between horocycles centered at 1 and x must still be ℓ_3 . We already determined the fact that the horocycle at x has the same (Euclidean) diameter as the one at 0. The only possible way that the distance ℓ_3 will also be preserved is if $x = 2$, and the picture is symmetric across the edge from 1 to infinity.

Note at this point that the holonomy ψ is completely determined: It fixes ∞ , takes 0 to 2, and maps a point ih on a horocycle about infinity to the point $2 + ih$. This is the translation $\psi(z) = z + 2$. Similarly, the holonomy ϕ is also completely determined, as it fixes 1, maps 0 to 2 and takes a point on a horocycle on the edge of length ℓ_3 to a determined point on the edge from x to 1. Because the fundamental group of the 3-punctured sphere is generated by the two loops corresponding to ψ and ϕ , this determines the complete structure. We have therefore shown:

PROPOSITION 3.17. *There is a unique complete hyperbolic structure on the 3-punctured sphere. A fundamental region for the structure is given by two ideal triangles with vertices 0, 1, and ∞ and 1, 2, and ∞ , respectively.*

□

EXAMPLE 3.18 (Incomplete structure on 3-punctured sphere). What if we choose a different value for x besides $x = 2$? Say we let $x = 3/2$. To

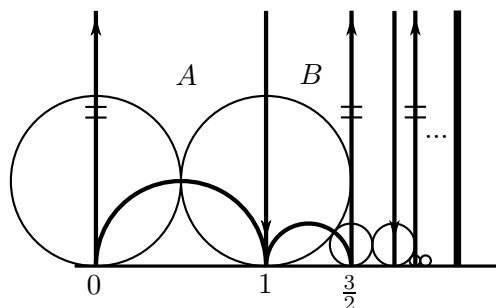


FIGURE 3.13. Part of developing image of an incomplete structure on a 3-punctured sphere.

simplify things, let's keep the length of the edge between horocycles at 0 and 1 constant as we extend horocycles. Choose horocycles at 0 and 1 of (Euclidean) radius $1/2$, so that these horocycles are tangent along the edge between 0 and 1, hence the distance between horocycles is 0. This distance will remain equal to 0 under each holonomy element, so there will be a horocycle at $x = 3/2$ tangent to the horocycle about 1, to preserve distance 0. This determines where the image of the triangle A must go under the holonomy fixing infinity: its third vertex (called y in figure 3.11) must have a horocycle about it of the same (Euclidean) size as the horocycle at $3/2$. This determines the holonomy isometry about the vertex at infinity. Apply this holonomy isometry successively, and we obtain a pattern of triangles as in figure 3.13.

Notice that the edges of the triangles approach a limit — the thick line shown on the far right of the figure. Notice also that this line is not part of the developing image of the 3-punctured sphere.

This hyperbolic structure is incomplete: for any horocycle about infinity in \mathbb{H}^2 , the sequence of points at the intersection of the horocycle and the edges of the developing images of ideal triangles projects to a Cauchy sequence that does not converge. Alternately, the value $d(v)$ is nonzero for v the ideal vertex lifting to the point at infinity.

An incomplete metric space may be completed by adjoining points corresponding to limits of Cauchy sequences, and giving the resulting space the metric topology. In our case, the completion of this incomplete 3-punctured sphere is obtained by attaching a geodesic segment — the projection of the thick line in figure 3.13. Each point of the thick geodesic on the right of figure 3.13 corresponds to the limiting point of the Cauchy sequence given by a horocycle about infinity at the appropriate height. Note that in the quotient, however, we attach a closed curve of length $d(v)$, since points on that thick geodesic lying on horospheres of distance $d(v)$ apart will be identified.

Note that horocycles about infinity run straight into this thick geodesic, meeting it at right angles. On the other hand, these horocycles meet infinitely many edges of ideal triangles on their way into the geodesic, and none

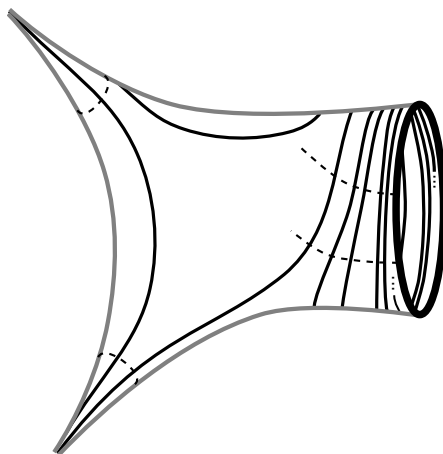


FIGURE 3.14. The completion of an incomplete structure on a 3-punctured sphere. Attach a geodesic of length $d(v)$. Ideal edges spin arbitrarily close to the attached geodesic without meeting it. Horocycles (dashed) run directly into the geodesic. (This example has two complete cusped ends and one incomplete end.)

of these ideal edges meets the geodesic. It follows that the ideal edges of the two triangles A and B become arbitrarily close to the geodesic attached in the completion, without ever meeting it. Geometrically, it appears that the edges of the ideal triangles spin around the geodesic infinitely many times, while horocycles run directly into it. See figure 3.14.

PROOF OF PROPOSITION 3.15. Let S be a surface obtained by gluing hyperbolic polygons.

Suppose first that $d(v)$ is nonzero. Then take a sequence of points on a horocycle about v , one point for each intersection of the horocycle with an ideal edge. This gives a Cauchy sequence that does not converge. Therefore, the metric is not complete.

Now suppose $d(v) = 0$ for each ideal vertex v . Then some horocycle closes up around each ideal vertex, so we may remove the interior horoball from each polygon. After this removal, the remainder is a compact manifold with boundary. For any $t > 0$, let S_t be the compact manifold obtained by removing interiors of horocycles of distance t from our original choice of horocycle. Then the compact subsets S_t of S satisfy $\bigcup_{t \in \mathbb{R}^+} S_t = S$ and S_{t+a} contains a neighborhood of radius a about S_t . Any Cauchy sequence must be contained in some S_t for sufficiently large t . Hence by compactness of S_t , the Cauchy sequence must converge. \square

3.3. Developing map and completeness

Here is a better condition for completeness that works in all dimensions and all geometries.

THEOREM 3.19. *Let M be an n -manifold with a (G, X) -structure, where G acts transitively on X , and X admits a complete G -invariant metric. Then the metric on M inherited from X is complete if and only if the developing map $D: \widetilde{M} \rightarrow X$ is a covering map.*

PROOF. Suppose first that the developing map $D: \widetilde{M} \rightarrow X$ is a covering map. Let $\{x_n\}_{n=1}^\infty$ be a Cauchy sequence in M . For n large enough, x_n will be contained in an ϵ -ball in M that is evenly covered in \widetilde{M} . Thus the sequence lifts to a Cauchy sequence $\{\tilde{x}_n\}$ in \widetilde{M} . Since D is a local isometry, $\{D(\tilde{x}_n)\}$ is a Cauchy sequence in X . Finally since X is complete, $\{D(\tilde{x}_n)\}$ converges to $y \in X$. Now, because D is a covering map, there is a neighborhood U of y that is evenly covered by D . Lift this to a neighborhood \tilde{U} of \widetilde{M} containing infinitely many points of the sequence $\{\tilde{x}_n\}$. The lift of y in this neighborhood, call it \tilde{y} , must be a limit point of $\{\tilde{x}_n\}$. Then the projection of \tilde{y} to M is a limit point of the sequence $\{x_n\}$, so M is complete.

For the converse, we appeal to a proof by Thurston [Thu97, Proposition 3.4.15]. Suppose M is complete. To show $D: \widetilde{M} \rightarrow X$ is a covering map, we show that any path α_t in X lifts to a path $\tilde{\alpha}_t$ in \widetilde{M} . Since D is a local homeomorphism, this implies that D is a covering map.

First, if M is complete, then \widetilde{M} must also be complete, where the metric \widetilde{M} is the lift of the metric on M , as follows. The projection to M of any Cauchy sequence gives a Cauchy sequence in M , with limit point x . Then x has a compact neighborhood which is evenly covered in \widetilde{M} , hence there is a compact neighborhood in \widetilde{M} containing all but finitely many points of the Cauchy sequence and also containing a lift of x . Thus the sequence converges in \widetilde{M} .

Let α_t be a path in X . Because D is a local homeomorphism, we may lift α_t to a path $\tilde{\alpha}_t$ in \widetilde{M} for $t \in [0, t_0)$, some $t_0 > 0$. By completeness of \widetilde{M} , the lifting extends to $[0, t_0]$. But because D is a local homeomorphism, a lifting to $[0, t_0]$ extends to $[0, t_0 + \epsilon)$. Hence the lifting extends to all of α_t and D is a covering map. \square

COROLLARY 3.20. *If X is simply connected, and M is a manifold with a (G, X) -structure as in theorem 3.19, then M is complete if and only if the developing map is an isometry of X .*

PROOF. The developing map is a local isometry by construction. Theorem 3.19 shows that M is complete if and only if the developing map is a covering map. Since X and \widetilde{M} are simply connected, the developing map is a covering map if and only if it is a covering isomorphism. A covering isomorphism that is a local isometry must be an isometry. \square

3.4. Exercises

EXERCISE 3.1. We have seen that Euclidean structures on a torus are determined by a parallelogram.

- (a) Show that by applying translation and rotation isometries of \mathbb{E}^2 , we may assume that the parallelogram has vertices $(0, 0)$, $(x_1, 0)$, (x_2, y) , and $(x_1 + x_2, y)$ where $x_1 > 0$ and $y > 0$.
- (b) Show that up to rescaling, a parallelogram has vertices $(0, 0)$, $(1, 0)$, (x, y) , and $(x + 1, y)$ for some $(x, y) \in \mathbb{R}^2$ with $y > 0$.

EXERCISE 3.2. If X is a metric space, and G is a group of isometries acting transitively on X , and M is a manifold admitting a (G, X) -structure, show that M inherits a metric from X . That is, explain how to define a metric on M from that on X , and show that the metric is well-defined.

EXERCISE 3.3. (Induced structures [Thu97, Exercise 3.1.5]). Let N be a topological space and M a manifold with a (G, X) -structure, and suppose $\pi: N \rightarrow M$ is a local homeomorphism. Prove N has a (G, X) -structure that is preserved by π . As a corollary, show that any covering space of M admits a (G, X) -structure.

EXERCISE 3.4 (Analytic continuation). Prove item (1) of proposition 3.10. That is, prove the following.

- (a) Suppose $\alpha: [0, 1] \rightarrow M$ is a path. Let (U_i, ϕ_i) and (V_j, ψ_j) be two choices of charts that cover $\alpha([0, 1])$. Let

$$0 = t_0 < t_1 < \cdots < t_n = 1 \text{ and } 0 = s_0 < s_1 < \cdots < s_m = 1$$

be points in $[0, 1]$ such that $\alpha([t_i, t_{i+1}]) \subset U_i$ and $\alpha([s_j, s_{j+1}]) \subset V_j$. Define inductively extensions $\Phi_i(t)$ and $\Psi_j(t)$ as in the definition of the developing map. Finally, let $X \subset [0, 1]$ be the set of points on which $\Phi_i(t) = \Psi_j(t)$. Prove that $X = [0, 1]$.

(Hint: You will need to use the fact that G is analytic. One reference for analytic continuation is [Con78, Chapter IX].)

- (b) Suppose α and β are homotopic paths with the same endpoints. By part (a), there are well-defined functions $D(\alpha)$ and $D(\beta)$, defined separately on α and on β as in definition 3.9. Prove that $D(\alpha) = D(\beta)$. This proves that the definition of D is independent of choice α in the homotopy class of $[\alpha] \in \widetilde{M}$.

(Again you will use the fact that G is analytic; see for example [Con78, Chapter IX].)

EXERCISE 3.5. Prove item (3) of proposition 3.10. Show that if we define a new map in the same way as D , except we change the basepoint x_0 or the initial chart (U_0, ϕ_0) , then the resulting map is equal to the composition of D with an element of G .

EXERCISE 3.6. Let T be the affine torus obtained by identifying the sides of the trapezoid with vertices $(0, 0)$, $(1, 0)$, $(0, 1)$, and $(1/2, 1)$.

- (a) Compute the holonomy elements of T corresponding to meridian and longitude (i.e. the loop running along the horizontal edge of the trapezoid and the loop running along the vertical edge of the trapezoid). What is the holonomy group of T ?
- (b) For basepoint $(0, 0)$ and initial chart chosen so that the trapezoid is mapped by the identity into \mathbb{R}^2 , compute explicitly the developing images of various curves, including the following:
- The curve running twice along the meridian (based at $(0, 0)$).
 - The curve running twice along the longitude.
 - The curve running twice along the meridian and three times along the longitude.

EXERCISE 3.7. Let T be the affine torus of exercise 3.6, obtained by identifying sides of the trapezoid with vertices $(0, 0)$, $(1, 0)$, $(0, 1)$, and $(1/2, 1)$, and let \tilde{T} denote its universal cover. Prove that the developing image $D(\tilde{T}) \subset \mathbb{R}^2$ misses exactly one point.

EXERCISE 3.8. Generalize exercise 3.7: Let T be any affine torus. Prove that either the developing map $D: \tilde{T} \rightarrow \mathbb{R}^2$ is a covering map, and T is a Euclidean torus, or the image of the developing map misses a single point in \mathbb{R}^2 .

EXERCISE 3.9. Fix an example of your favorite quadrilateral that is not a parallelogram, and let T be the torus obtained by identifying sides. Use a computer to create a picture such as figure 3.3 for your quadrilateral.

EXERCISE 3.10. Prove lemma 3.14, that $d(v)$ is independent of initial choice of horocycle, and independent of choice of v_0 in the equivalence class of v .

EXERCISE 3.11. Prove the holonomy group of the complete structure on a 3-punctured sphere is generated by

$$\begin{pmatrix} 1 & 2 \\ 0 & 1 \end{pmatrix} \quad \text{and} \quad \begin{pmatrix} 1 & 0 \\ 2 & 1 \end{pmatrix}.$$

EXERCISE 3.12. How many incomplete hyperbolic structures are there on a 3-punctured sphere? How can they be parameterized? Give a geometric interpretation of this parameterization. That is, relate the parameterization to the developing image of the associated hyperbolic structure.

EXERCISE 3.13. A torus with 1 puncture has a topological polygonal decomposition consisting of two triangles.

- (a) Find a complete hyperbolic structure on the 1-punctured torus and prove your structure is complete.
- (b) Find all complete hyperbolic structures on the 1-punctured torus. How are they parameterized?

EXERCISE 3.14. A sphere with 4 punctures has a topological polygonal decomposition consisting of four triangles. Repeat exercise 3.13 for the 4-punctured sphere.

CHAPTER 4

Hyperbolic Structures and Triangulations

In chapter 3, we learned that hyperbolic structures lead to developing maps and holonomy, and that the developing map is a covering map if and only if the hyperbolic structure is complete.

In this chapter, we wish to compute explicit complete hyperbolic structures on 3-manifolds, again with our primary examples being knot complements. One of the most straightforward ways to find a hyperbolic structure is to first triangulate the manifold, or subdivide it into tetrahedra, and then to put a hyperbolic structure on each tetrahedron, ensuring the tetrahedra glue to give a $(\mathrm{PSL}(2, \mathbb{C}), \mathbb{H}^3)$ -structure whose developing map is complete. This method of computing hyperbolic structures has been studied by many, and in particular was implemented on the computer by J. Weeks as part of his 1985 PhD thesis [Wee85]. Here we will describe the conditions required to obtain a complete hyperbolic structure via triangulations, and as usual, work through examples.

4.1. Geometric triangulations

In chapter 3, we defined topological and geometric polygonal decompositions of 2-manifolds. We can extend these notions to 3-manifolds by considering decompositions into ideal polyhedra. In chapter 1, we obtained topological ideal polyhedral decompositions for knot complements. For many applications, including those later in this chapter, it simplifies matters greatly to consider decompositions into ideal tetrahedra.

DEFINITION 4.1. Let M be a 3-manifold. A *topological ideal triangulation* of M is a combinatorial way of gluing truncated tetrahedra (ideal tetrahedra) so that the result is homeomorphic to M . Truncated parts will correspond to the boundary of M . As before, a gluing should take faces to faces, edges to edges, etc.

EXAMPLE 4.2. The figure-8 knot has a topological ideal triangulation consisting of two ideal tetrahedra, as we saw in exercise 1.7 in chapter 1.

For a given knot complement, it is relatively easy to find topological ideal triangulations. For example, starting with any polyhedral decomposition, choose an ideal vertex v and cone to that vertex: i.e. add edges between v

and all other ideal vertices, between any two edges meeting v add an ideal triangle (adding an additional edge opposite v if necessary), and between three triangles meeting v add an ideal tetrahedron. Split off the resulting tetrahedra. This reduces the collection of polyhedra to a collection with at least one fewer ideal vertex. Hence after repeating a finite number of times, we are left with a collection of topological tetrahedra.

4.1.1. An extended example: the 6_1 knot. We work out an example for the 6_1 knot carefully. We will see how to decompose the complement into five tetrahedra. (In fact, the complement of the 6_1 knot can be decomposed into four tetrahedra, but we won't bother simplifying further here.)

We start with a polyhedral decomposition of the 6_1 knot. We use the decomposition obtained using the methods of chapter 1. The result is shown in figure 4.1, with the knot on the left, the top polyhedron in the center, and the bottom polyhedron on the right. Recall all polyhedra are viewed from the outside; that is the ball of the polyhedron is behind the projection plane in each figure. In this example, oriented edges are labeled 1 through 6.

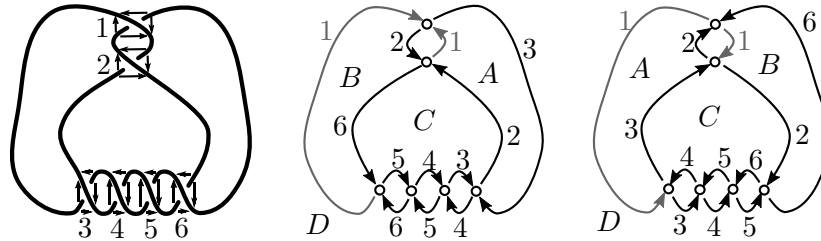


FIGURE 4.1. Left to right: The 6_1 knot, the top polyhedron, the bottom polyhedron

Collapse all bigons, identifying edges 1 and 2, and 3 through 6. New edges and orientations are shown in figure 4.2.

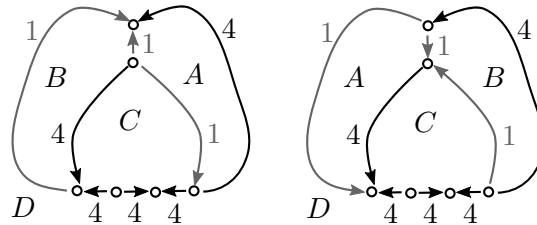


FIGURE 4.2. Polyhedra for 6_1 knot with bigons collapsed

We cone the top polyhedron to the vertex in the center. This subdivides faces C and D into triangles, shown in figure 4.3 in both top and bottom polyhedra.

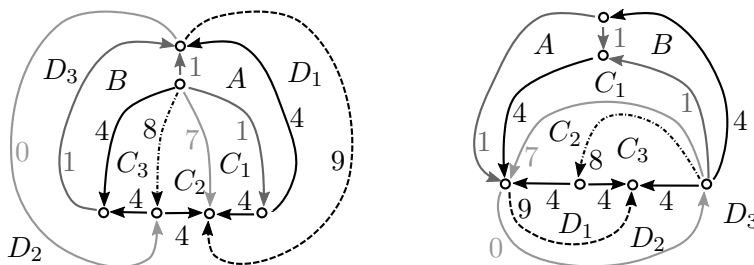


FIGURE 4.3. A subdivision of faces C and D in the top polyhedron (left) leads to a subdivision of the bottom (right)

Continuing the subdivision in the top polyhedron, two edges meeting in the center vertex bound an ideal triangle; three triangles bound a tetrahedron. Thus edges labeled 1, 7, 9 bound an ideal triangle E_1 ; edges labeled 1, 8, 0 bound an ideal triangle E_2 . Triangles A, C_1, D_1 , and E_1 bound an ideal tetrahedron, as do triangles B, C_3, D_3 , and E_2 . When we split off these tetrahedra a single tetrahedron remains. All tetrahedra making up the top polyhedron are shown in figure 4.4.

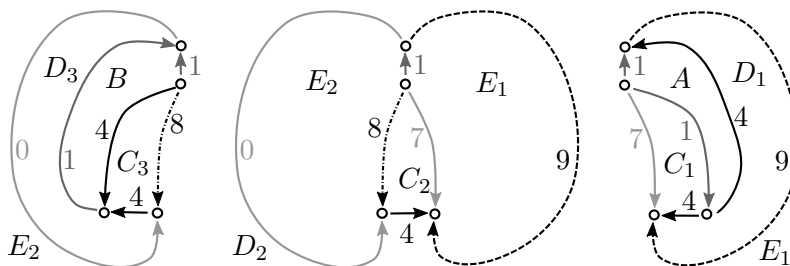


FIGURE 4.4. The top polyhedron splits into the three tetrahedra shown

Now we split the bottom polyhedron into tetrahedra. However, first, observe in figure 4.3 that edges labeled 7 and 0 in the bottom polyhedron run between the same two ideal vertices. Thus these two edges should be flattened and identified in the bottom polyhedron. While we could do that now in one step, we believe it is more geometrically clear how to flatten and identify if we first cut off ideal tetrahedra from the bottom polyhedron.

So first, note there will be an ideal triangle E_3 with edges labeled 4, 7, and 1, and this cuts off an ideal tetrahedron with sides A, B, C_1, E_3 . Similarly there is an ideal triangle E_4 with edges 7, 9, and 4, cutting off an ideal tetrahedron with sides C_2, C_3, E_4 , and D_1 . These two tetrahedra, as well as the remnant of the bottom polyhedron, are shown in figure 4.5.

Notice that the object on the right of figure 4.5 is not a tetrahedron: edges labeled 7 and 0 in that polyhedron form a bigon, which collapses to a single edge which we label 7. When we do the collapse, the faces E_4 and

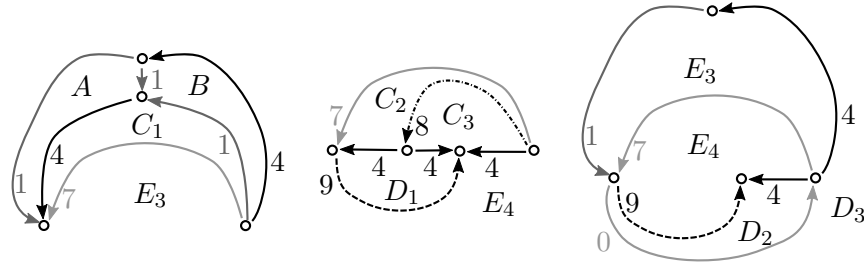
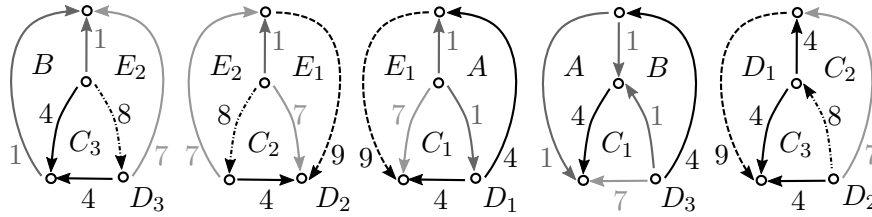


FIGURE 4.5. Splitting off two tetrahedra in the bottom polyhedron

FIGURE 4.6. Five tetrahedra which glue to give the complement of the 6_1 knot

D_2 collapse to a single triangle, which we will label D_2 . The faces E_3 and D_3 also collapse to a single triangle, which we will label D_3 .

When we have finished, we have five tetrahedra that glue to give the complement of the 6_1 knot. All five tetrahedra with their edges and faces labeled are shown in figure 4.6.

4.1.2. Geometric ideal triangulations.

DEFINITION 4.3. A *geometric ideal triangulation* of M is a topological ideal triangulation such that each tetrahedron has a (positively oriented) hyperbolic structure, and the result of gluing is a smooth manifold with a complete metric. We also call such a triangulation a *geometric triangulation* for short.

As of the writing of this book, it is still an open question as to whether every 3-manifold that admits a complete hyperbolic structure actually admits a geometric ideal triangulation. It is known that every cusped hyperbolic 3-manifold can be decomposed into convex ideal polyhedra [EP88]: we will go through this in chapter 14. However, subdividing this decomposition into tetrahedra may create degenerate tetrahedra — actual topological tetrahedra (as opposed to the object on the right of figure 4.5), but tetrahedra that are flat in the hyperbolic structure on M . There are known examples of generalized spaces with singularities that do not admit geometric triangulations [Cho04].

4.2. Edge gluing equations

In chapter 3, we saw that a gluing of hyperbolic polygons has a hyperbolic structure if and only if the angle sum around each finite vertex is 2π (lemma 3.7). There are similar conditions for a gluing of hyperbolic tetrahedra. We now need to consider gluing around an edge.

Let T be an ideal tetrahedron embedded in \mathbb{H}^3 . Any ideal tetrahedron has six edges. If we select any one, say e , we may choose an isometry of \mathbb{H}^3 taking the endpoints of e to 0 and ∞ , and sending a third vertex to $1 \in \mathbb{C} \subset \partial_\infty \mathbb{H}^3$. This choice uniquely determines the isometry. The fourth vertex of T will be mapped to some $z' \in \mathbb{C}$. We may assume that z' has positive imaginary part, for if not, apply an isometry of \mathbb{H}^3 rotating around the geodesic from 0 to ∞ and rescaling so that z' maps to 1. In this case, the image of 1 under this isometry will be a complex number with positive imaginary part.

DEFINITION 4.4. For an ideal tetrahedron T embedded in \mathbb{H}^3 , and edge e of that tetrahedron, define the number $z(e)$ in \mathbb{C} to be the complex number with positive imaginary part obtained by applying the unique isometry of \mathbb{H}^3 that takes the vertices of e to 0 and ∞ , takes another vertex to 1, and takes the final vertex of T to $z(e)$. This is called the *edge invariant* of e .

REMARK 4.5. Note that it is possible to map an ideal tetrahedron to \mathbb{H}^3 so that three vertices map to 0, ∞ , and 1, and the fourth maps to a point on the real line. In this case, the tetrahedron produced does not have a hyperbolic structure. If the fourth vertex is not 0 or 1, it is said to be *flat*. If the fourth vertex is 0 or 1, it is *degenerate*. Similarly, a fourth vertex mapped to infinity is a degenerate tetrahedron. An ideal triangulation of a hyperbolic 3-manifold with flat or degenerate tetrahedra is not a geometric ideal triangulation. When looking for geometric triangulations, we must rule out such tetrahedra. Similarly, for geometric triangulations, all edge invariants of all tetrahedra must have positive imaginary part. This ensures the tetrahedra are *positively oriented*. Finally, the procedure above always chooses an edge invariant with positive imaginary part. However, when we glue many tetrahedra together, at times it is impossible to simultaneously choose all edge invariants to have positive imaginary part; some may have negative imaginary part. Such a tetrahedron is a *negatively oriented* tetrahedron.

Edge invariants of an ideal tetrahedron determine each other, in the following way.

LEMMA 4.6. *Let T be an ideal tetrahedron with edge e_1 , mapped so that vertices of T lie at ∞ , 0, 1, and $z(e_1)$ (so endpoints of e_1 lie at 0 and ∞). Then T has the following additional edge invariants.*

- The edge e'_1 opposite e_1 , with vertices 1 and $z(e_1)$, has edge invariant $z(e'_1) = z(e_1)$.

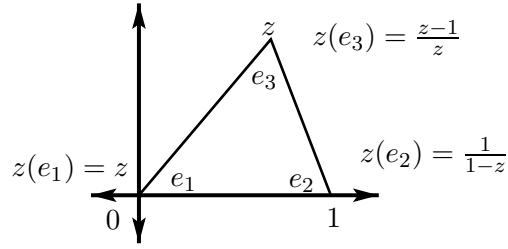


FIGURE 4.7. Edge invariants

- The edge e_2 with vertices ∞ and 1 has edge invariant

$$z(e_2) = \frac{1}{1 - z(e_1)}.$$

- The edge e_3 with vertices ∞ and $z(e_1)$ has edge invariant

$$z(e_3) = \frac{z(e_1) - 1}{z(e_1)}.$$

Thus we have the following relationships for these edge invariants.

$$z(e_1)z(e_2)z(e_3) = -1, \quad \text{and} \quad 1 - z(e_1) + z(e_1)z(e_3) = 0$$

PROOF. The proof is obtained by considering isometries of \mathbb{H}^3 that move the different edges of T onto the geodesic from 0 to ∞ . For ease of notation, we set $z = z(e_1)$.

For the first part, we label one more edge. Let e'_3 be the edge of T opposite e_3 . So e'_3 has endpoints 0 and 1. Note there is a geodesic γ in \mathbb{H}^3 that meets the edges e_3 and e'_3 orthogonally. An elliptic isometry rotating about γ by angle π maps 0 to 1 and 1 to 0, and maps ∞ to z and z to ∞ , thus it preserves T . It takes the edge e'_1 with endpoints 1 and z to an edge with endpoints 0 and ∞ . Hence $z(e'_1) = z$.

To determine $z(e_2)$, we apply a Möbius transformation fixing ∞ , taking 1 to 0, and taking z to 1. This transformation is given by

$$w \mapsto \frac{w - 1}{z - 1}.$$

It sends 0 to $-1/(z - 1)$. Thus $z(e_2) = 1/(1 - z)$.

As for the edge e_3 running from z to ∞ , to determine its edge invariant we apply a Möbius transformation fixing ∞ , sending z to 0, and sending 0 to 1. This is given by

$$w \mapsto \frac{w - z}{-z}.$$

It sends 1 to $(1 - z)/(-z)$. Thus $z(e_3) = (z - 1)/z$. \square

The three edge invariants of a tetrahedron are shown in figure 4.7.

Now consider a gluing of ideal tetrahedra. Fix an edge e of the gluing, and let T_1 be a tetrahedron which has edge e_1 glued to e . Put T_1 in \mathbb{H}^3

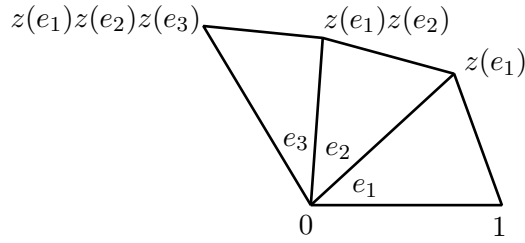


FIGURE 4.8. Vertices of attached triangles.

with the edge e_1 running from 0 to ∞ , with a third vertex at 1 , and the fourth vertex at $z(e_1)$, where $z(e_1)$ has positive imaginary part. The gluing identifies each face of T_1 with another face. Let F_1 denote the face of T_1 with vertices 0 , $z(e_1)$, and ∞ . This is glued to a face F'_1 in some tetrahedron T_2 , where the edge e_2 in T_2 glues to e .

Now, we could put T_2 in \mathbb{H}^3 with vertices at 0 , ∞ , 1 , and $z(e_2)$, but since we're gluing to T_1 , we want the face F'_1 to have vertices 0 , ∞ , and $z(e_1)$ rather than vertices 0 , ∞ , and 1 . Thus to do the gluing, we apply an isometry of \mathbb{H}^3 fixing 0 and ∞ , mapping 1 to $z(e_1)$. This takes the fourth vertex of T_2 to $z(e_1)z(e_2)$.

Continue attaching tetrahedra counterclockwise around e . The next tetrahedron attached will have vertices 0 , ∞ , $z(e_1)z(e_2)$, and $z(e_1)z(e_2)z(e_3)$ in \mathbb{C} . See figure 4.8. Eventually one of the tetrahedra will be glued to T_1 again. The fourth vertex of the final tetrahedron will be at the point $z(e_1)z(e_2) \cdots z(e_n)$.

THEOREM 4.7 (Edge gluing equations). *Let M^3 admit a topological ideal triangulation such that each ideal tetrahedron has a hyperbolic structure. The hyperbolic structures on the ideal tetrahedra induce a hyperbolic structure on the gluing, M , if and only if for each edge e ,*

$$\prod z(e_i) = 1 \quad \text{and} \quad \sum \arg(z(e_i)) = 2\pi,$$

where the product and sum are over all edges that glue to e .

PROOF. The hyperbolic structure on the tetrahedra induces a hyperbolic structure on M if and only if every point in M has a neighborhood isometric to a ball in \mathbb{H}^3 , by lemma 3.6. Consider a point on an edge. If it has a neighborhood isometric to a ball in \mathbb{H}^3 then the sum of the dihedral angles around the edge must be 2π . See figure 4.9. This sum of dihedral angles is $\sum \arg(z(e_i))$. Moreover there must be no nontrivial translation as we move around the edge. Since the last face of the last triangle glues to the triangle with vertices 0 , 1 , and ∞ , this condition requires that $\prod z(e_i) = 1$.

Conversely, if we have $\prod z(e_i) = 1$ and $\sum \arg(z(e_i)) = 2\pi$, then any point on the edge under the gluing has a ball neighborhood isometric to a ball in \mathbb{H}^3 . \square

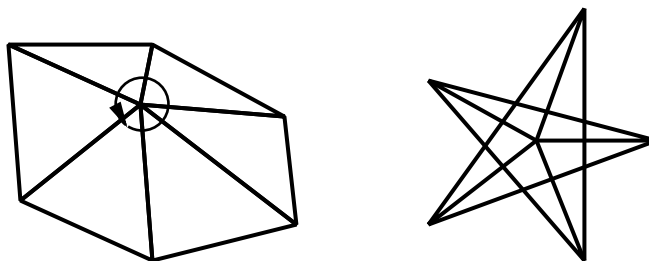


FIGURE 4.9. Left: Angle sum must be 2π . Right: An example of why this condition is important.

The equations $\prod z(e_i) = 1$ (and restrictions $\sum \arg(z(e_i)) = 2\pi$) are called the *edge gluing equations*. We have one for each edge. However, since by lemma 4.6 the three edge invariants of a tetrahedron are all determined by a single edge invariant, one ideal tetrahedron contributes at most one unknown to the gluing equations.

EXAMPLE 4.8 (Edge gluing equations for the figure-8 knot). The figure-8 knot decomposes into two ideal tetrahedra. Choose the two tetrahedra to be *regular*. That is, all dihedral angles are $\pi/3$. We claim that this gives a hyperbolic structure on the figure-8 knot complement.

We wish to find all such structures.

Thurston worked through this example in detail in his notes; we recall his work here [Thu79, pages 50–52].

Figure 4.10 shows the two tetrahedra in the decomposition of the figure-8 knot complement, which we obtained in chapter 1. These tetrahedra come from the two ideal polyhedra that glue to give the figure-8 knot complement that we discussed in detail in chapter 1; see figure 1.8 and figure 1.10. The tetrahedra differ from those in chapter 1 in the following ways. First, we have collapsed the bigons. This gives two remaining edge classes, which we label with one tick mark and with two tick marks. Second, in figure 1.8, we viewed the top ideal polyhedron from the inside; that is, the ball of the polyhedron lay above the plane of projection. To be more consistent in viewing both top and bottom polyhedron, we have rotated our perspective such that now both tetrahedra are viewed from the outside.

For each tetrahedron, we label each edge with a complex number z_i or w_i , to denote the edge invariant associated with that edge. Note that opposite edges in a tetrahedron have the same edge invariant. We also have relationships between z_1 , z_2 , and z_3 as in lemma 4.6, and similarly for w_1 , w_2 , and w_3 .

There are two edge classes in the tetrahedra in figure 4.10, labeled with one or two tick marks on the edge. We obtain the edge gluing equations by taking the product of edge invariants for all edges identified with each edge class.

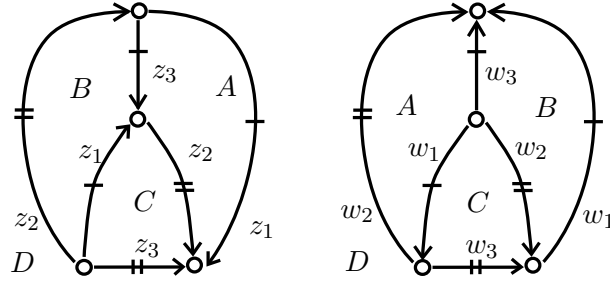


FIGURE 4.10. The ideal tetrahedra of the figure-8 knot complement.

For the edge with one tick mark, we obtain the edge gluing equation

$$z_1^2 z_3 w_1^2 w_3 = 1.$$

For the edge with two tick marks,

$$z_2^2 z_3 w_2^2 w_3 = 1.$$

We set $z_1 = z$ and $w_1 = w$. From lemma 4.6, the first edge gluing equation gives

$$z^2 \left(\frac{z-1}{z} \right) w^2 \left(\frac{w-1}{w} \right) = 1,$$

or

$$(4.1) \quad z(z-1)w(w-1) = 1.$$

Solving for z in terms of w :

$$z = \frac{1 \pm \sqrt{1 + 4/(w(w-1))}}{2}.$$

We need the imaginary parts of z and w to be strictly greater than 0. For each value of w , there is at most one solution for z with positive imaginary part. The solution exists provided that the discriminant $1 + 4/(w(w-1))$ is not positive real. Thus solutions are parameterized by the region of \mathbb{C} shown in figure 4.11 (see also exercise 4.6).

Notice that

$$z = w = \sqrt[3]{-1} = \frac{1}{2} + \frac{\sqrt{3}}{2}i$$

is one solution to the equations. We will see that this gives a complete hyperbolic structure on the complement of the figure-8 knot.

4.3. Completeness equations

Suppose now that M is a 3-manifold with torus boundary. In much of this section, we will assume that M admits a topological ideal triangulation, and moreover we have a solution to the edge gluing equations for this triangulation, thus M admits a hyperbolic structure. We need to consider cusps of the manifold to determine whether this is a complete structure or not.

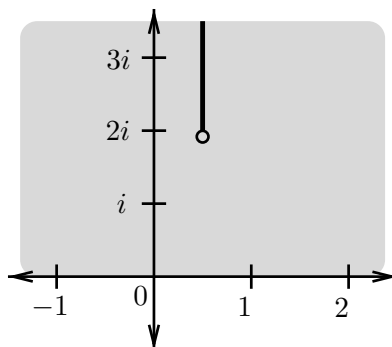


FIGURE 4.11. Solutions to edge gluing equations for the figure-8 knot complement are parameterized by the above region.

DEFINITION 4.9. Let M be a 3-manifold with torus boundary. Define a *cuspidal neighborhood* of M to be a neighborhood of ∂M homeomorphic to the product of a torus and an interval, $T^2 \times I$. Define a *cuspidal torus* to be a torus component of ∂M , or the boundary of a cusp.

A hyperbolic structure on M induces an affine structure on the boundary of any cusp of M .

THEOREM 4.10. *Let M be a 3-manifold with torus boundary and hyperbolic structure, i.e. with $(\text{Isom}(\mathbb{H}^3), \mathbb{H}^3)$ -structure. Then the structure on M is complete if and only if for each cusp of M , the induced structure on the boundary of the cusp is a Euclidean structure on the torus.*

PROOF. Exercise 4.7. Hint: the proof is very similar to that of the analogous result in two dimensions, proposition 3.15. \square

DEFINITION 4.11. Let M have a topological ideal triangulation. If we truncate the vertices of each ideal tetrahedron, we obtain a collection of triangles, each of which lies on the boundary of a cusp. Edges of each triangle inherit a gluing from the gluing of faces of the ideal tetrahedra. This gives a triangulation of each boundary torus, which we call a *cuspidal triangulation*.

An example for the figure-8 knot is shown in figure 4.12. The truncated ideal vertices give eight triangles, with labels a through h . These glue together on the boundary of the cusp to give a triangulation of the torus as shown. Note that the corner of each triangle is labeled with the edge invariant of the tetrahedron corresponding to the edge meeting that corner.

Figure 4.12 shows a fundamental region of the cuspidal triangulation. By tracing through gluings of cuspidal triangles, we may obtain the full developing image of the cuspidal torus. Theorem 4.10 states that the original manifold is complete if and only if the cuspidal tori are Euclidean, which will hold if and

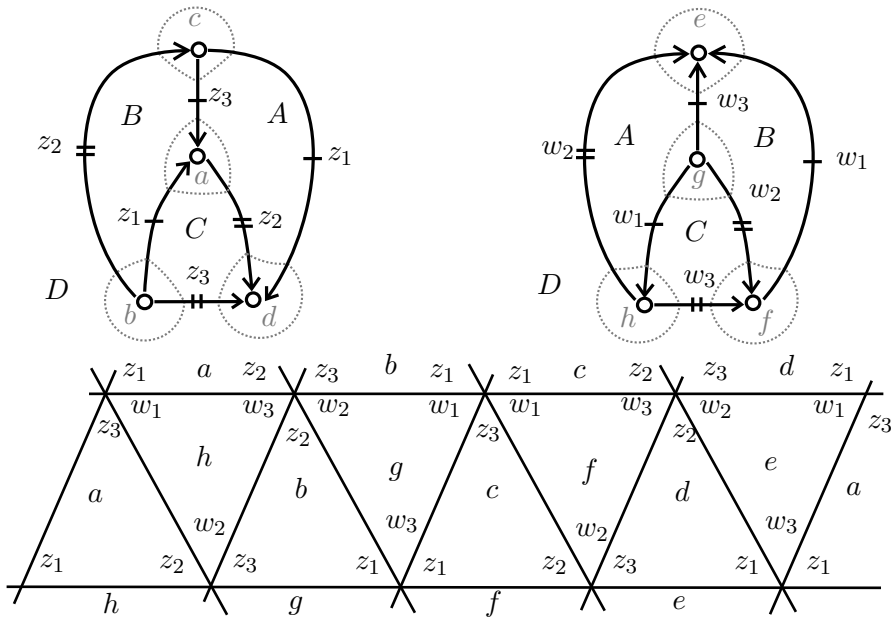


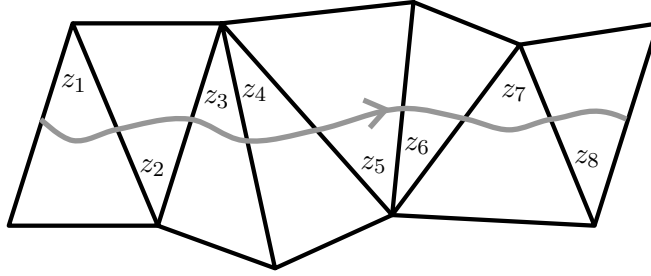
FIGURE 4.12. Finding the cusp triangulation of the figure-8 knot complement

only if the holonomy maps for each element of $\pi_1(T)$ on each cusp torus T are pure Euclidean translations, without rotation or scale.

We can determine if holonomy maps are Euclidean translations directly from the cusp triangulation. Start with a triangle Δ whose vertices we may assume lie at 0, 1, and $z(e_1)$ in the complex plane \mathbb{C} . Let $\alpha \in \pi_1(T)$. Then the holonomy $\rho(\alpha)$ takes Δ to a new triangle, which appears in the developing image. The holonomy $\rho(\alpha)$ will be a Euclidean translation if and only if the triangle side from 0 to 1 of Δ is mapped to the side of a triangle of length 1 pointing in the same direction, without rotation (or scale). To determine whether this holds, we may follow the side of the triangle in the developing image, and obtain exactly its rotation and scale by considering the edge invariants that adjust its length and direction as it is adjusted in the cusp triangulation, as in figure 4.8. This can be described efficiently in the following way.

DEFINITION 4.12. Suppose M has a topological ideal triangulation, and let T be the boundary torus of a cusp of M . Let $[\alpha] \in \pi_1(T)$, so α is a loop on T in the homotopy class of $[\alpha]$. We associate a complex number $H(\alpha)$ to α as follows.

First, orient the loop α on T . The loop α can be homotoped to run through any triangle of the cusp triangulation of T monotonically, i.e. in such a way that it cuts off a single corner of each triangle it enters. Denote the edge invariants of the corners cut off by α by z_1, z_2, \dots, z_n . Further associate to each corner a value $\epsilon_i = \pm 1$: if the i -th corner cut off by α lies

FIGURE 4.13. Example for determining $H([\alpha])$

to the left of α , set $\epsilon_i = +1$. If the corner lies to the right of α , set $\epsilon_i = -1$. Finally, set the value of $H(\alpha)$ to be

$$(4.2) \quad H(\alpha) = \prod_{i=1}^n z_i^{\epsilon_i}$$

EXAMPLE 4.13. An example cusp is shown in figure 4.13. For this example, the value of $H(\alpha)$ is given by

$$H(\alpha) = z_1 z_2^{-1} z_3 z_4 z_5^{-1} z_6^{-1} z_7 z_8^{-1}.$$

We will see that H is independent of homotopy class of α (exercise 4.11). For this reason, we sometimes denote the complex number by $H([\alpha])$, or evaluate it on a homotopy class rather than a curve.

EXAMPLE 4.14. For the figure-8 knot, there is a closed curve on the cusp torus running from the left side of the triangle labeled a on the left of figure 4.12 to the left side of the triangle labeled a on the right of that figure. Call this curve α . Then we can compute:

$$H(\alpha) = z_3 w_2^{-1} z_2 w_3^{-1} z_3 w_2^{-1} z_2 w_3^{-1} = \left(\frac{z_2 z_3}{w_2 w_3} \right)^2$$

Another closed curve runs from the base of the triangle labeled a on the left of figure 4.12 to the top of the triangle labeled h , also on the left of that figure. Call this curve β . Then we have:

$$H(\beta) = z_2^{-1} w_1 = \frac{w_1}{z_2}.$$

PROPOSITION 4.15 (Completeness equations). *Let T be the torus boundary of a cusp neighborhood of M , where M admits a topological ideal triangulation, and the ideal tetrahedra admit hyperbolic structures that satisfy the edge gluing equations (theorem 4.7). Let α and β generate $\pi_1(T)$. If $H(\alpha) = H(\beta) = 1$, then the ideal triangulation is a geometric ideal triangulation, i.e. the hyperbolic structure on M induced by the hyperbolic structure on the tetrahedra will be a complete structure.*

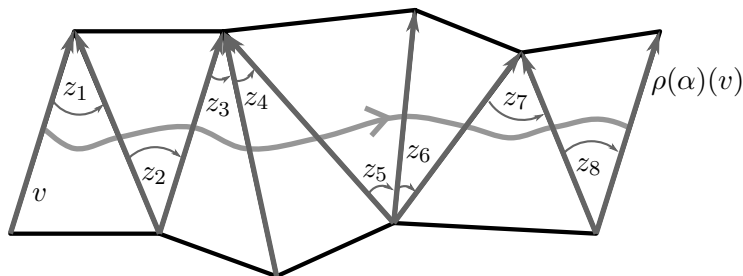


FIGURE 4.14. A path of vectors in the proof of proposition 4.15

The equations $H(\alpha) = 1$ and $H(\beta) = 1$ are called the *completeness equations*.

PROOF OF PROPOSITION 4.15. By theorem 4.10, it suffices to show that the induced structure on T is Euclidean. To do so, it suffices to show that the holonomy elements $\rho(\alpha)$ and $\rho(\beta)$ are pure translations, with no rotation and scale. Thus we will show $\rho(\alpha)$ and $\rho(\beta)$ do not rotate or scale.

To show this, let Δ be a triangle met by the curve α used in defining the complex number $H(\alpha)$, and suppose α meets a side e_1 of Δ . Let v be a vector with length equal to the length of e_1 , pointing in the direction of e_1 such that the oriented curve α and the vector v are oriented according to the right hand rule. This is true of the vector v shown on the far left of figure 4.14.

The holonomy $\rho(\alpha)$ is Euclidean if and only if the image of v under $\rho(\alpha)$ still has length v , and points in the same direction as v . We determine the effect of holonomy by considering what happens to v in each triangle of the cusp triangulation.

We may rotate v around a vertex of the triangle Δ meeting e_1 , and scale, so that the result lines up with a second edge e_2 of the triangle, having the same length and direction as e_2 . We know exactly how the rotation and scale is determined when the vertex of the triangle is labeled with edge invariant z_1 : if we rotate in a counterclockwise direction, v is adjusted by multiplication by z_1 , as in figure 4.8. If we rotate in a clockwise direction, v is adjusted by multiplication by $1/z_1$.

Now, our path α cuts off exactly one corner of each triangle it meets. This defines a path of edges of triangles, namely, starting with v , at each step we have a vector lying on the side of a triangle where α enters that triangle. In this triangle, rotate through the corner cut off by α to produce a new vector pointing in the direction of the side where α exits. An example path of such vectors is shown in figure 4.14. When α returns to the initial triangle Δ , the final vector of this path will be parallel to the image of v under $\rho(\alpha)$. Then $\rho(\alpha)$ will be a Euclidean transformation if and only if the final vector in the path has length and direction identical to that of v .

On the other hand, the final length and direction of the vector $\rho(\alpha)v$ is given by the product of edge invariants at the corners of each triangle in the path of edges, with edge invariant either multiplied or divided depending on whether the rotation is in the counterclockwise or clockwise direction, respectively. This is exactly the complex number $H(\alpha)$. Thus $\rho(\alpha)$ is Euclidean if and only if $H(\alpha) = 1$.

The same argument applies to $H(\beta)$ and $\rho(\beta)$. Since the holonomy group of the cusp is generated by $\rho(\alpha)$ and $\rho(\beta)$, the cusp will be Euclidean if and only if $H(\alpha) = H(\beta) = 1$. \square

EXAMPLE 4.16. Returning to the example of the figure-8 knot, in example 4.14, we found that completeness equations are given by

$$H(\alpha) = \left(\frac{z_2 z_3}{w_2 w_3} \right)^2 \quad \text{and} \quad H(\beta) = \frac{w_1}{z_2}.$$

Lemma 4.6 implies that these can be rewritten in terms of variables z and w alone, as

$$H(\alpha) = \left(\frac{1}{1-z} \cdot \frac{z-1}{z} \cdot \frac{1-w}{1} \cdot \frac{w}{w-1} \right)^2 = \left(\frac{w}{z} \right)^2$$

and

$$(4.3) \quad H(\beta) = w(1-z)$$

If the hyperbolic structure is complete, then by proposition 4.15, $H(\alpha) = H(\beta) = 1$, so $z = w$.

From equation (4.3), $z(z-1) = -1$. Hence the only possibility is $z = w = \frac{1}{2} + i\frac{\sqrt{3}}{2}$.

4.4. Computing hyperbolic structures

Given a triangulation of a 3-manifold M with torus boundary, we may determine a complete hyperbolic structure on M by solving the edge gluing and completeness equations. However, note this amounts to solving a complicated system of nonlinear equations. Consequently, it is difficult to use these to find exact hyperbolic structures on infinite families of manifolds.

However in practice, topological triangulations, edge gluing equations, and completeness equations can be found very efficiently by computer for specific, finite examples. The resulting nonlinear system of equations can then be solved numerically. The first software to find hyperbolic structures on knots and 3-manifolds was the program SnapPea, written by Weeks [Wee85] (see also [Wee05]). This program has allowed researchers to run experiments on large classes of hyperbolic 3-manifolds, making observations and testing conjectures, and has been influential in a great deal of results on hyperbolic structures on knots and 3-manifolds. The SnapPea kernel is now part of a program maintained by Culler, Dunfield, Goerner, and others, reincarnated as SnapPy, and available for free download [CDGW16]. This

new program includes much additional functionality, and still remains an excellent tool for research in hyperbolic knot theory.

One issue in the past with finding a hyperbolic structure via SnapPea (SnapPy) is that it would only give a numerical approximation to a hyperbolic structure, and there was no guarantee that the manifold would be actually provably hyperbolic. This has been addressed in a few ways. The program Snap [CGHN00] deduces exact solutions from the numerical approximations, which can be used to prove hyperbolicity. In another direction, Moser used analytic techniques to prove that a solution to edge gluing and completeness equations exists in a small neighborhood of an approximate solution [Mos09]. In [HIK⁺16], interval arithmetic is used to prove hyperbolic structures exist when a structure is computed numerically. Thus using these tools, we can often prove that if SnapPy computes a hyperbolic structure on a knot complement, then the knot is indeed hyperbolic.

4.5. Exercises

EXERCISE 4.1. Write down the edge gluing equations (not completeness equations) for the 6_1 knot, using the ideal tetrahedra of example 4.1.1. Make appropriate substitutions such that your equations contain exactly one variable per tetrahedron.

EXERCISE 4.2. Notice that for both the figure-8 knot complement and for the 6_1 knot, we had exactly the same number of edges as tetrahedra in the ideal triangulation.

- (a) Prove that this will always be true. That is, prove that if M is any 3-manifold with (possibly empty) boundary consisting of tori, then for any topological ideal triangulation of M , the number of edges of the triangulation will always equal the number of tetrahedra.
- (b) Since we have one unknown per ideal tetrahedra, part (a) implies that the number of gluing equations will equal the number of unknowns. However, in fact the gluing equations are always redundant. Prove this fact.

EXERCISE 4.3. In chapter 1, we found a polyhedral decomposition of the 5_2 knot complement (without bigons). Split this into a topological ideal triangulation of the knot complement.

EXERCISE 4.4. Using the ideal tetrahedra of exercise 4.3, or otherwise, write down all edge invariants and all edge gluing equations, one variable per tetrahedron.

EXERCISE 4.5. Find a topological ideal triangulation of the 6_3 knot, edge invariants, and edge gluing equations.

EXERCISE 4.6. Check that figure 4.11 does indeed parameterize the space of hyperbolic structures on the figure-8 knot complement. What is the equation of the vertical ray shown in that picture?

EXERCISE 4.7. Prove theorem 4.10: the hyperbolic structure on M is complete if and only if for each cusp of M , the induced structure on the boundary of the cusp is a Euclidean structure on the torus.

EXERCISE 4.8. For the topological triangulation of the 5_2 knot of exercise 4.3:

- Find the triangulation of the cusp. Label a fundamental domain, and meridian and longitude.
- Write down completeness equations.

EXERCISE 4.9. Find the cusp triangulation for the complement of the 6_1 knot from example 4.1.1.

EXERCISE 4.10. Find completeness equations for the 6_1 or 6_3 knot.

EXERCISE 4.11. Suppose M admits an ideal triangulation that satisfies the edge gluing equations.

- In definition 4.12, we claimed that for any closed curve α in a torus boundary component of ∂M , we could homotope α in such a way that it cuts off a single corner of each triangle that it meets. Prove this.
- Show that $H([\alpha])$ is independent of the choice of α in the homotopy class of $[\alpha]$. In particular, if α is homotoped to run through different triangles, the value of $H([\alpha])$ is unchanged.

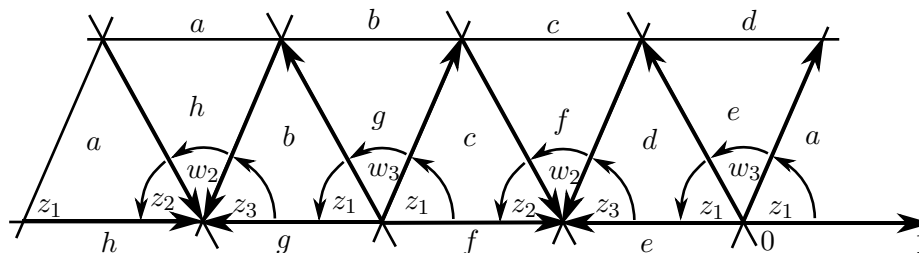


FIGURE 4.15. Path of vectors going from e_1 , the oriented edge from 0 to 1, to $\rho(-\alpha)(e_1)$

EXERCISE 4.12. In Thurston's 1979 notes [Thu79], he computed completeness equations for the figure-8 knot using a method similar to our proof of proposition 4.15. Namely, he found a path of vectors from an edge on a triangle Δ to the same edge on $\rho(-\alpha)(\Delta)$ and $\rho(\beta)(\Delta)$. His path of vectors for $\rho(\beta)$ agrees with ours. His path of vectors for $\rho(-\alpha)$ is different from our path for $\rho(\alpha)$, and is shown in figure 4.15.

- Prove that the completeness equation obtained from Thurston's path of vectors is equivalent to our completeness equation.

- (b) More generally, prove that if we replace our path of vectors used to construct the complex number $H([\alpha])$ by any other path of vectors obtained by rotating around vertices of the cusp triangulation, with same starting and ending vectors, then the equation we obtain from multiplying (and dividing) by edge invariants corresponding to the path of vectors gives a completeness equation that is equivalent to $H([\alpha]) = 1$.

EXERCISE 4.13. What breaks down when you try to find triangulations and edge gluing equations for non-hyperbolic knots and links, such as the trefoil or the $(2, 4)$ -torus link?

EXERCISE 4.14. Use the computer program SnapPy to determine which of the knots with seven or fewer crossings admit a hyperbolic structure [CDGW16]. For those that do admit a hyperbolic structure, use SnapPy to find the cusp triangulation of the knot. Obtain a screen shot of this information, which should include cusp triangles as well as a fundamental parallelogram for the cusp.

Discrete Groups and the Thick–Thin Decomposition

Suppose we have a complete hyperbolic structure on an orientable 3-manifold M . Then the developing map $D: \widetilde{M} \rightarrow \mathbb{H}^3$ is a covering map, by theorem 3.19. Since \widetilde{M} and \mathbb{H}^3 are both simply connected, it follows that the developing map is an isometry. Thus we may view \mathbb{H}^3 as the universal cover of M . The covering transformations are then the elements of the holonomy group $\rho(\pi_1(M)) = \Gamma \leq \mathrm{PSL}(2, \mathbb{C})$. Hence M is homeomorphic to the quotient $M \cong \mathbb{H}^3/\Gamma$.

Subgroups Γ of $\mathrm{PSL}(2, \mathbb{C})$ can have very nice properties, and have been investigated for many decades. In this chapter, we discuss some classical results in the area and their consequences for hyperbolic 3-manifolds. Some of our discussion follows closely work of Jørgensen and Marden; we recommend the book [Mar07] for more details, generalizations, and consequences.

5.1. Discrete subgroups of hyperbolic isometries

5.1.1. Isometries and subgroups. In theorem 2.16 we classified elements of $\mathrm{PSL}(2, \mathbb{C})$ as elliptic, parabolic, or loxodromic depending on their fixed points. One of the first things we need is an extension of that theorem.

Before we give the extension, recall that we can view an element of $\mathrm{PSL}(2, \mathbb{C})$ as a matrix

$$A = \begin{pmatrix} a & b \\ c & d \end{pmatrix}, \text{ with } a, b, c, d \in \mathbb{C} \text{ and } ad - bc = 1,$$

and the matrix is well-defined up to multiplication by $\pm \mathrm{Id}$. In this chapter, we will frequently write an isometry of \mathbb{H}^3 as a 2 by 2 matrix with determinant 1, omitting and ignoring the \pm sign. The sign very rarely affects our arguments, but the reader should be aware that we are suppressing it, for example in the following definition.

DEFINITION 5.1. We say $A \in \mathrm{PSL}(2, \mathbb{C})$ is *conjugate* to $B \in \mathrm{PSL}(2, \mathbb{C})$ if there exists $U \in \mathrm{PSL}(2, \mathbb{C})$ such that $A = UBU^{-1}$. The *trace* of A is the trace of its normalized matrix:

$$\mathrm{tr} \begin{pmatrix} a & b \\ c & d \end{pmatrix} = a + d.$$

Jessica S. Purcell, Hyperbolic Knot Theory

Note there is a sign ambiguity in our definition of trace; again this will not affect our arguments. Note also that conjugate elements have the same trace.

LEMMA 5.2. For $A \in \mathrm{PSL}(2, \mathbb{C})$,

- A is parabolic if and only if $\mathrm{tr}(A) = \pm 2$, and if and only if A is conjugate to

$$z \mapsto z + 1.$$

- A is elliptic if and only if $\mathrm{tr}(A) \in (-2, 2) \subset \mathbb{R} \subset \mathbb{C}$, and if and only if A is conjugate to

$$z \mapsto e^{2i\theta} z, \quad \text{with } 2\theta \neq 2\pi n \text{ for any } n \in \mathbb{Z}.$$

- A is loxodromic if and only if $\mathrm{tr}(A) \in \mathbb{C} - [-2, 2]$, and if and only if A is conjugate to

$$z \mapsto \zeta^2 z, \quad \text{with } |\zeta| > 1.$$

PROOF. Exercise 5.2 □

DEFINITION 5.3. A subgroup of $\mathrm{PSL}(2, \mathbb{C})$ is said to be *discrete* if it contains no sequence of distinct elements converging to the identity element. A discrete subgroup of $\mathrm{PSL}(2, \mathbb{C})$ is often called a *Kleinian group*.

An example of a discrete group is a subgroup generated by a single loxodromic element, or a single parabolic element. These are the simplest such groups. They are so simple that they are examples of what are called *elementary groups*; see definition 5.11. Examples of discrete groups in general can be quite complicated. In proposition 5.10, we will prove that the holonomy group of any complete hyperbolic 3-manifold is always a discrete group. Meanwhile, consider the example of the figure-8 knot complement.

EXAMPLE 5.4. Let K be the figure-8 knot, and give $S^3 - K$ its complete hyperbolic structure by gluing two regular ideal tetrahedra, with face-pairings as in figure 4.10. We will find generators of the holonomy group, which is a discrete subgroup of $\mathrm{PSL}(2, \mathbb{C})$, as we will see in proposition 5.10. These are obtained by face-pairing isometries, as follows.

Place the two ideal tetrahedra in \mathbb{H}^3 , putting ideal vertices for one tetrahedron at $0, 1, \omega$, and ∞ , where $\omega = \frac{1}{2} + i\frac{\sqrt{3}}{2}$, and putting the ideal vertices of the other tetrahedron at $1, \omega, \omega + 1$, and ∞ . This glues the faces labeled A along the ideal triangle with vertices $1, \omega$, and ∞ , to obtain one connected fundamental region for the knot complement, shown in figure 5.1.

The manifold $S^3 - K$ is obtained by gluing the remaining faces labeled B, C , and D . These gluings, or face-pairings, correspond to holonomy isometries, which we will denote by T_B, T_C , and T_D , respectively. A calculation (exercise 5.3) shows that the gluing isometries are given by:

$$(5.1) \quad T_B = \frac{i}{\sqrt{\omega}} \begin{pmatrix} 1 & 1 \\ 1 & -\omega^2 \end{pmatrix}, \quad T_C = \begin{pmatrix} 1 & \omega \\ 0 & 1 \end{pmatrix}, \quad T_D = \begin{pmatrix} 2 & -1 \\ 1 & 0 \end{pmatrix}.$$

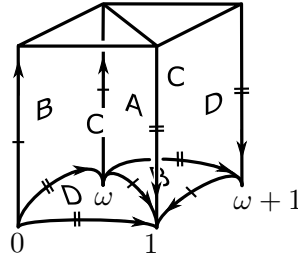


FIGURE 5.1. A connected fundamental region for the figure-8 knot complement

These three gluing isometries generate the holonomy group for $S^3 - K$. In fact, T_B can be written as a (somewhat complicated) product involving T_C and T_D and their inverses.

Riley was the first to prove that $S^3 - K$ has a hyperbolic structure [Ril75]. He did so by taking a presentation of the fundamental group of $S^3 - K$ with two generators, and finding an explicit representation of the fundamental group into $\mathrm{PSL}(2, \mathbb{C})$. Exercises 5.4, 5.5, and 5.6 explore this work a little further.

We finish this section with one quick condition equivalent to a group being discrete.

LEMMA 5.5. *A subgroup $G \leq \mathrm{PSL}(2, \mathbb{C})$ is discrete if and only if it does not contain an infinite sequence of distinct elements that converges to some element $A \in \mathrm{PSL}(2, \mathbb{C})$.*

PROOF. One implication is trivial: If G is not discrete, by definition it contains an infinite sequence of distinct elements converging to the identity in $\mathrm{PSL}(2, \mathbb{C})$.

For the other direction, suppose $\{A_n\} \subset G$ is an infinite sequence of distinct elements of G converging to $A \in \mathrm{PSL}(2, \mathbb{C})$. Consider $\{A_{n+1}A_n^{-1}\} \subset G$. Note the sequence converges to the identity. To show G is not discrete, it remains to show that $\{A_{n+1}A_n^{-1}\}$ contains infinitely many distinct elements. Suppose not. Then $A_{n+1} = CA_n$ for some fixed $C \in G$ and some subsequence. Since $A_{n+1}A_n^{-1} \rightarrow \mathrm{Id}$, we must have $C = \mathrm{Id}$, and thus $A_{n+1} = A_n$. This contradicts the fact that $\{A_n\}$ is a sequence of distinct elements. Thus G is not discrete. \square

5.1.2. Sequences of isometries. We can learn a lot about subgroups of $\mathrm{PSL}(2, \mathbb{C})$ by considering sequences of group elements. For example, note that the definition of a discrete group involves sequences. We also have the following result, which will be used later in the chapter.

LEMMA 5.6. *Let $\{A_n\}$ be a sequence of elements of $\mathrm{PSL}(2, \mathbb{C})$. Then either a subsequence of $\{A_n\}$ converges to some $A \in \mathrm{PSL}(2, \mathbb{C})$, or there exists a point $q \in \partial\mathbb{H}^3$ such that for all $x \in \mathbb{H}^3$, the sequence $\{A_n(x)\}$ has a subsequence converging to q .*

PROOF. Let p_n, q_n denote the fixed points of A_n ; note we could have $p_n = q_n$. Then $\{p_n\}$ and $\{q_n\}$ are sequences in $\partial\mathbb{H}^3 \cong S^2$, which is compact, so they have convergent subsequences. Replace A_n, p_n, q_n by a subsequence such that $p_n \rightarrow p$ and $q_n \rightarrow q$. Again note that p could equal q .

Case 1. Suppose $p \neq q$. Then for large enough n , $p_n \neq q_n$. Consider an isometry R_n of \mathbb{H}^3 mapping p_n to 0 and q_n to ∞ . Furthermore, for concreteness, fix a point $y \in \partial\mathbb{H}^3$, independent of n that is disjoint from the sequences $\{p_n\}, \{q_n\}$ and from p and q . We may take R_n to map y to 1.

If we view R_n as a sequence of matrices for example, we see that R_n converges to the hyperbolic isometry $R \in \mathrm{PSL}(2, \mathbb{C})$ taking p to 0, q to ∞ , and y to 1. Consider $B_n = R_n A_n R_n^{-1}$. This is an isometry in $\mathrm{PSL}(2, \mathbb{C})$ fixing 0 and ∞ . Hence it has the form $B_n(z) = a_n z$ for $a_n \in \mathbb{C}$. If $\{|a_n|\}$ has a bounded subsequence, then some subsequence a_n converges to $a \in \mathbb{C}$. Hence there is a subsequence B_n with $B_n \rightarrow B$, where B is the hyperbolic isometry $B(z) = az$. This is an element of $\mathrm{PSL}(2, \mathbb{C})$. It follows that $A_n = R_n^{-1} B_n R_n$ converges to $A = R^{-1} B R \in \mathrm{PSL}(2, \mathbb{C})$.

If $|a_n| \rightarrow \infty$, then for any $z \in \partial\mathbb{H}^3$, $B_n(z) \rightarrow \infty$. Thus for any point $x \in \mathbb{H}^3$, $B_n(x) \rightarrow \infty$. It follows that for all $x \in \mathbb{H}^3$, $A_n(x) = R_n^{-1} B_n R_n(x)$ converges to $q \in \partial\mathbb{H}^3$.

Case 2. Now suppose $p = q$. Then again we will conjugate A_n by an isometry R_n taking q_n to infinity. For concreteness, choose y_1 and y_2 disjoint from $\{p_n\}, \{q_n\}$, and q . Let R_n be the isometry taking y_1 to 1, y_2 to 0, and q_n to ∞ . Then R_n converges to the isometry R taking y_1, y_2 , and q to 1, 0, and ∞ , respectively. Finally let $B_n = R_n A_n R_n^{-1}$. Note B_n fixes ∞ , hence it is of the form $B_n = a_n z + b_n$ for $a_n, b_n \in \mathbb{C}$. If $a_n = 1$, B_n is parabolic and has unique fixed point ∞ . Otherwise, the other fixed point of B_n is $b_n/(1 - a_n)$.

If $\{|b_n|\}$ has a bounded subsequence, then some subsequence $b_n \rightarrow b$. In that case, either $a_n = 1$ for large n , or since p_n, q_n converge to $p = q$, the fixed point $b_n/(1 - a_n)$ converges to ∞ . Thus a_n converges to 1. In any case, $B_n(z)$ converges to $B(z) = z + b$. This is an element of $\mathrm{PSL}(2, \mathbb{C})$. It follows that $A_n = R_n^{-1} B_n R_n$ converges to $R^{-1} B R \in \mathrm{PSL}(2, \mathbb{C})$.

If $\{|b_n|\}$ has no bounded subsequence, then $b_n \rightarrow \infty$. We know that the fixed point $b_n/(1 - a_n)$ converges to ∞ because it is a fixed point of B_n , so $(1 - a_n)/b_n \rightarrow 0$. Rewrite B_n to have the form

$$B_n(z) = b_n \left(\frac{(a_n - 1)z}{b_n} + 1 \right) + z.$$

Then as $n \rightarrow \infty$, $B_n(z) \rightarrow \infty$ for all $z \in \partial\mathbb{H}^3$. Thus $B_n(x) \rightarrow \infty$ for all $x \in \mathbb{H}^3$. It follows that $A_n(x) = R_n^{-1} B_n R_n(x)$ converges to q for all $x \in \mathbb{H}^3$. \square

5.1.3. Action of groups of isometries. We return to the problem of showing that holonomy groups of complete hyperbolic 3-manifolds are discrete. We will show this by considering the action of these groups on \mathbb{H}^3 .

DEFINITION 5.7. The action of a group $G \leq \mathrm{PSL}(2, \mathbb{C})$ on \mathbb{H}^3 is *properly discontinuous* if for every closed ball $B \subset \mathbb{H}^3$, the set $\{\gamma \in G \mid \gamma(B) \cap B \neq \emptyset\}$ is a finite set.

DEFINITION 5.8. The action of a group $G \leq \mathrm{PSL}(2, \mathbb{C})$ is *free* if the identity element of G is the only element to have a fixed point in \mathbb{H}^3 .

Note that parabolics and loxodromics have fixed points on $\partial\mathbb{H}^3$, but not in the interior of \mathbb{H}^3 . However, elliptics have fixed points in the interior of \mathbb{H}^3 . Thus the action of G is free if and only if G contains no elliptics.

LEMMA 5.9. *A subgroup of $\mathrm{PSL}(2, \mathbb{C})$ is discrete if and only if its action on \mathbb{H}^3 is properly discontinuous.*

PROOF. Suppose G is a subgroup of $\mathrm{PSL}(2, \mathbb{C})$ that is not discrete, so there exists a sequence $\{A_n\}$ in G with $A_n \rightarrow \mathrm{Id}$. Then for all $x \in \mathbb{H}^3$, the hyperbolic distance $d(x, A_n x) \rightarrow 0$. Let B be any closed ball about x with radius $R > 0$. For n such that $d(x, A_n x) < R$, the set

$$\{A \in G \mid A(B) \cap B \neq \emptyset\}$$

contains A_n . Since this is true for infinitely many A_n , the action is not properly discontinuous.

Now suppose that for $G \leq \mathrm{PSL}(2, \mathbb{C})$, there exists a closed ball B of radius R such that the set $\{A \in G \mid A(B) \cap B \neq \emptyset\}$ is infinite. Let $\{A_n\}$ be a sequence of distinct elements in this set. Note that for $x \in B$, the hyperbolic distance $d(x, A_n x)$ is bounded by $4R$, for all n . Thus $\{A_n x\}$ has no subsequence converging to a point on $\partial\mathbb{H}^3$. Lemma 5.6 implies that $\{A_n\}$ has a subsequence converging to $A \in \mathrm{PSL}(2, \mathbb{C})$. Then lemma 5.5 implies G is not discrete. \square

We are now ready to prove the main result in this section, namely that a complete hyperbolic 3-manifold has a discrete holonomy group, and conversely a discrete subgroup of $\mathrm{PSL}(2, \mathbb{C})$ that acts freely gives rise to a complete hyperbolic 3-manifold.

PROPOSITION 5.10. *The action of a group $G \leq \mathrm{PSL}(2, \mathbb{C})$ on \mathbb{H}^3 is free and properly discontinuous if and only if \mathbb{H}^3/G is a 3-manifold with a complete hyperbolic structure and with covering projection $\mathbb{H}^3 \rightarrow \mathbb{H}^3/G$.*

PROOF. Suppose the action of G on \mathbb{H}^3 is free and properly discontinuous. Let $x \in \mathbb{H}^3/G$, and let $\tilde{x} \in \mathbb{H}^3$ be a point that projects to x under the map $\mathbb{H}^3 \rightarrow \mathbb{H}^3/G$. Because the action of G is properly discontinuous, there is a closed ball B_x that intersects only finitely many of its translates. Because the action is free, we may shrink B_x until all its translates are disjoint. Then the interior of B_x maps isometrically to a neighborhood of x in \mathbb{H}^3/G , so \mathbb{H}^3/G is a hyperbolic manifold. Moreover, this neighborhood is evenly covered (by translates of the interior of B_x), and so the quotient map is a covering projection.

Conversely, suppose \mathbb{H}^3/G is a hyperbolic manifold and $p: \mathbb{H}^3 \rightarrow \mathbb{H}^3/G$ is a covering projection. For any $x \in \mathbb{H}^3$, the action of G permutes the preimages $\{p^{-1}p(x)\}$. Only the identity of G fixes x , so the action is free.

Let $B \subset \mathbb{H}^3$ be a closed ball. Consider the compact set $B \times B$. For any $(x, y) \in B \times B$, we claim there exist neighborhoods U_{xy} of x and V_{xy} of y such that $g(U_{xy}) \cap V_{xy} \neq \emptyset$ for at most one $g \in G$. To see this, if y is not in the orbit of x , then $p(x)$ and $p(y)$ have disjoint neighborhoods in \mathbb{H}^3/G . Shrink these neighborhoods to be evenly covered, and let U_{xy} and V_{xy} be neighborhoods of x and y respectively homeomorphic to the disjoint neighborhoods of $p(x)$ and $p(y)$. For any $g \in G$, $g(U_{xy}) \cap V_{xy} = \emptyset$ in this case. On the other hand, if $y = g_1(x)$ for some $g_1 \in G$, then take U_{xy} to be homeomorphic to an evenly covered neighborhood of $p(x) = p(y)$ in \mathbb{H}^3/G , and let $V_{xy} = g_1(U_{xy})$. Then $g(U_{xy}) \cap V_{xy} \neq \emptyset$ only when $g = g_1$.

Now $B \times B$ is compact, and the set $\{U_{xy} \times V_{xy}\}_{(x,y) \in B \times B}$ forms an open cover. Thus there is a finite subcover $\{U_1 \times V_1, \dots, U_n \times V_n\}$, where $U_i \times V_i$ has the property that $g(U_i) \cap V_i \neq \emptyset$ only when $g = g_i \in G$.

If $\gamma \in G$ is a group element such that there exists $x \in \gamma(B) \cap B$, then consider $(\gamma^{-1}(x), x) \in B \times B$. There must be some $U_i \times V_i$ containing $(\gamma^{-1}(x), x)$. Since $x \in \gamma(U_i) \cap V_i$, it follows that $\gamma = g_i$. Thus γ must be one of the elements g_1, \dots, g_n associated to the finite covering. It follows that the action is properly discontinuous. \square

Proposition 5.10 implies that if \mathbb{H}^3/G is a hyperbolic 3-manifold, then G contains no elliptics. For this reason, we will exclude elliptic elements from discrete groups G whenever possible to simplify our proofs in the rest of the chapter. In fact, many results below also hold for discrete groups that contain elliptics. Details can be found, for example, in Marden [Mar07].

5.2. Elementary groups

DEFINITION 5.11. A subgroup $G \leq \text{PSL}(2, \mathbb{C})$ is *elementary* if one of the following holds.

- (1) The union of all fixed points on $\partial\mathbb{H}^3$ of all nontrivial elements of G is a single point on $\partial\mathbb{H}^3$.
- (2) The union of all fixed points on $\partial\mathbb{H}^3$ of all nontrivial elements of G consists of exactly two points on $\partial\mathbb{H}^3$.
- (3) There exists $x \in \mathbb{H}^3$ such that for all $g \in G$, $g(x) = x$.

The group is *nonelementary* if it is not elementary.

Elementary groups will be important subgroups of the discrete groups we study. Because of that, we will need to know more about their form.

PROPOSITION 5.12. *Let G be a discrete nontrivial elementary subgroup of $\text{PSL}(2, \mathbb{C})$ without elliptics. Then either*

- (1) *the union of fixed points of nontrivial elements of G is a single point on $\partial\mathbb{H}^3$, G is isomorphic to \mathbb{Z} or $\mathbb{Z} \times \mathbb{Z}$, and G is generated by parabolics (fixing the same point on $\partial\mathbb{H}^3$), or*

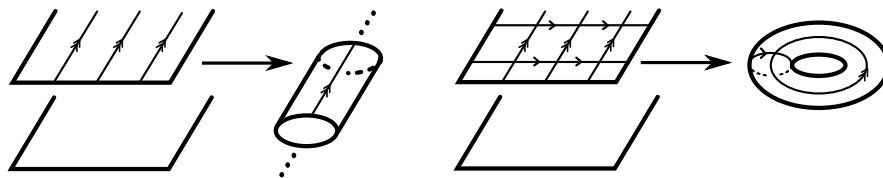


FIGURE 5.2. Left: The quotient of horosphere ∂C under the group \mathbb{Z} generated by a single parabolic gives a cylinder, or annulus. Right: The quotient of ∂C under $\mathbb{Z} \times \mathbb{Z}$ is a torus

- (2) *the union of fixed points of nontrivial elements of G consists of two points on $\partial\mathbb{H}^3$, G is isomorphic to \mathbb{Z} , and G is generated by a single loxodromic leaving invariant the line between the fixed points.*

PROOF. If the union of all fixed points of nontrivial elements of G consists of a single point on $\partial\mathbb{H}^3$, then G must contain only parabolics fixing that point. Conjugate so that the fixed point is ∞ in \mathbb{H}^3 . Then G fixes a horosphere about ∞ , which is isometric to the Euclidean plane P . The group G acts on P by Euclidean translations. Since G is discrete, G must be generated by either one translation, in which case $G \cong \mathbb{Z}$, or two linearly independent translations, in which case $G \cong \mathbb{Z} \times \mathbb{Z}$.

If the union of all fixed points of nontrivial elements of G consists of two points, then G contains only loxodromics fixing the axis between them. The group G acts on the axis; the fact that the group is discrete means that there is some finite minimal translation distance τ under this group action. Let $A \in G$ realize the minimal translation distance, i.e. $d(x, Ax) = \tau$ for x on the axis. We claim $G = \langle A \rangle$. First, we show all $C \in G$ translate by distance $n\tau$ for some $n \in \mathbb{Z}$, for if some $C \in G$ has translation distance that is not a multiple of τ , then $C(x)$ lies between $A^n(x)$ and $A^{n+1}(x)$ for any x on the axis. But then $CA^{-n} \in G$ translates $A^n(x)$ a distance strictly less than τ , which is a contradiction. Thus all $C \in G$ translate along the axis a distance equal to a multiple of τ . Now suppose $C \in G$ translates by $n\tau$ for some integer n . Then CA^{-n} fixes the axis pointwise. Because G contains no elliptics, $C = A^n$. So G is cyclic generated by A . \square

Consider the first case of proposition 5.12.

DEFINITION 5.13. Suppose G is an infinite elementary discrete group in $\mathrm{PSL}(2, \mathbb{C})$ fixing a single point on $\partial\mathbb{H}^3$. We may conjugate G so that fixed point is the point at infinity. Let H be the closed horoball of height 1:

$$H = \{(x, y, z) \mid z \geq 1\}.$$

Proposition 5.12 tells us that G is isomorphic to \mathbb{Z} or $\mathbb{Z} \times \mathbb{Z}$.

If $G \cong \mathbb{Z}$, the quotient of the horoball H/G is homeomorphic to the space $A \times [1, \infty)$, where A is an annulus, or cylinder; see figure 5.2. We say that H/G is a *rank-1 cusp*.

If $G \cong \mathbb{Z} \times \mathbb{Z}$, the quotient of the horoball H/G is homeomorphic to $T \times [1, \infty)$, where T is a Euclidean torus; see figure 5.2, right. We say that H/G is a *rank-2 cusp*.

Proposition 5.12 has an immediate corollary giving information about $\mathbb{Z} \times \mathbb{Z}$ subgroups of discrete groups, which will be used in later chapters.

COROLLARY 5.14 ($\mathbb{Z} \times \mathbb{Z}$ subgroups). *Suppose a discrete group G without elliptics has a subgroup isomorphic to $\mathbb{Z} \times \mathbb{Z}$. Then the subgroup is generated by two parabolic elements fixing the same point on the boundary at infinity $\partial\mathbb{H}^3$ of \mathbb{H}^3 .*

PROOF. Let A and B denote the generators of the subgroup of G isomorphic to $\mathbb{Z} \times \mathbb{Z}$. Since A and B commute, they must have the same fixed points on the boundary at infinity $\partial\mathbb{H}^3$ of \mathbb{H}^3 (exercise 5.11). Thus $H \cong \langle A, B \rangle$ is an elementary discrete group isomorphic to $\mathbb{Z} \times \mathbb{Z}$. By proposition 5.12, H must be generated by parabolics fixing the same point on $\partial\mathbb{H}^3$. \square

Discrete elementary groups are often defined in terms of the set of accumulation points of the group on $\partial\mathbb{H}^3$; for example this is the definition in [Thu79]. We review that definition here as well.

DEFINITION 5.15. Let $G \leq \mathrm{PSL}(2, \mathbb{C})$ be a discrete group, and let $x \in \mathbb{H}^3$ be any point. The *limit set* $\Lambda(G)$ is defined to be the set of accumulation points on $\partial\mathbb{H}^3$ of the orbit $G(x)$.

LEMMA 5.16. *The limit set $\Lambda(G)$ is well-defined, independent of choice of x in definition 5.15.*

PROOF. Suppose $\{A_n\} \subset G$ is a sequence such that $A_n(x)$ converges to a point $p \in \Lambda(G) \subset \partial\mathbb{H}^3$. Let $y \in \mathbb{H}^3$. Then the distance between x and y is a constant, equal to the distance between $A_n(x)$ and $A_n(y)$ for all n . Thus as $n \rightarrow \infty$, $A_n(x)$ and $A_n(y)$ lie a bounded distance apart, but $A_n(x)$ approaches p . This is possible only if $A_n(y)$ approaches the same point p on $\partial\mathbb{H}^3$. \square

Consider a few examples of groups G and limit sets $\Lambda(G)$. If G is generated by a single loxodromic element g , then its limit set $\Lambda(G)$ consists of the two fixed points of g on $\partial\mathbb{H}^3$: one is an accumulation point for $g^n(x)$, and the other for $g^{-n}(x)$. If G is generated by a single parabolic element, then $\Lambda(G)$ consists of a single point. If G contains both a loxodromic element g and a parabolic element h , then $\Lambda(G)$ contains the fixed points of g on $\partial\mathbb{H}^3$, as well as the fixed points of $h^n \circ g$ for all n ; this is a countably infinite set. Finally, if G is the identity group, consisting only of the identity element, then $\Lambda(G)$ is empty.

The following is often given as the definition of an elementary discrete subgroup of $\mathrm{PSL}(2, \mathbb{C})$.

LEMMA 5.17. *A discrete subgroup $G \leq \mathrm{PSL}(2, \mathbb{C})$ with no elliptics is elementary if and only if $\Lambda(G)$ consists of 0, 1, or 2 points.* \square

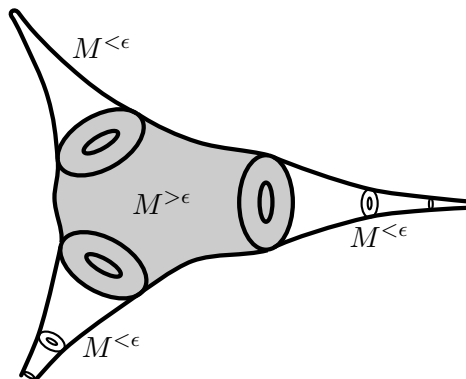


FIGURE 5.3. A schematic picture of a hyperbolic 3-manifold M , with $M^{<\epsilon}$ a collection of cusps and tubes

5.3. Thick and thin parts

We are now ready to put together facts about elementary and nonelementary discrete groups to prove a remarkable result on the geometry and topology of hyperbolic 3-manifolds, namely that any such manifold decomposes into a thick part and completely classified thin parts. To state the result precisely, we give a few definitions.

DEFINITION 5.18. Suppose M is a complete hyperbolic 3-manifold and $x \in M$. The *injectivity radius* of x , denoted $\text{injrads}(x)$, is defined to be the supremal radius r such that a metric r -ball around x is embedded.

DEFINITION 5.19. Let M be a complete hyperbolic 3-manifold, and let $\epsilon > 0$. Define the ϵ -thin part of M , denoted $M^{<\epsilon}$ to be

$$M^{<\epsilon} = \{x \in M \mid \text{injrads}(x) < \epsilon/2\}.$$

Similarly, the ϵ -thick part, denoted $M^{>\epsilon}$ is defined to be

$$M^{>\epsilon} = \{x \in M \mid \text{injrads}(x) > \epsilon/2\}.$$

We also have closed versions $M^{\geq\epsilon}$ and $M^{\leq\epsilon}$ defined in the obvious way.

THEOREM 5.20 (Structure of thin part). *There exists a universal constant $\epsilon_3 > 0$ such that for $0 < \epsilon \leq \epsilon_3$, the ϵ -thin part of any complete, orientable, hyperbolic 3-manifold M consists of tubes around short geodesics, rank-1 cusps, and/or rank-2 cusps.*

A cartoon illustrating theorem 5.20 is given in figure 5.3.

DEFINITION 5.21. The supremum of all constants ϵ_3 satisfying theorem 5.20 is called the *Margulis constant*. More generally, given a complete hyperbolic 3-manifold M , a number $\epsilon > 0$ is said to be a *Margulis number* for M if $M^{<\epsilon}$ satisfies the conclusions of theorem 5.20, i.e. $M^{<\epsilon}$ consists of tubes around short geodesics, rank-1, and/or rank-2 cusps. The Margulis

constant is therefore the infimum over all complete hyperbolic 3-manifolds M of the supremum of all Margulis numbers for M .

As of the writing of this book, the optimal Margulis constant is still unknown, although there are bounds on its value. R. Meyerhoff gave what is currently the best lower bound on ϵ_3 in [Mey87, Section 9], that it is at least 0.104. As for an upper bound, M. Culler has discovered a closed hyperbolic 3-manifold with Margulis number less than 0.616 using SnapPea [Wee05].

We save the proof of theorem 5.20 until the end of this section. We will see that it is a consequence of a well-known theorem concerning the structure of discrete groups of isometries, commonly called the Margulis lemma, which appears in a paper of Kařdan and Margulis [KM68]. The actual Margulis lemma is very general, concerning discrete groups acting on symmetric spaces. We restrict to the case of discrete subgroups of $\mathrm{PSL}(2, \mathbb{C})$ acting freely on hyperbolic space. The consequence we will need is the following.

THEOREM 5.22 (Universal Elementary Neighborhoods). *There is a universal constant $\epsilon_3 > 0$ such that for all $x \in \mathbb{H}^3$, and for any discrete group $G \leq \mathrm{PSL}(2, \mathbb{C})$ without elliptics, if H denotes the subgroup of G generated by all elements of G that translate x distance less than ϵ_3 , then H is elementary.*

We will give a proof of theorem 5.22 in section 5.5. Before that, a few remarks are in order. First, the Margulis lemma holds when we allow elliptics; this appears in Wang [Wan69] in the full generality of the theorem of Kařdan and Margulis. Second, the form of theorem 5.22 above, concerning discrete subgroups of $\mathrm{PSL}(2, \mathbb{C})$, is due to Jørgensen and Marden, only their result is more general in that it also includes elliptics. Their proof appears in [Mar07], and is the basis for the proof that we include below in subsection 5.5.1.

However, before we discuss the proof, we show how theorem 5.22 implies theorem 5.20 (Structure of thin part). First, we need to relate translation distance to injectivity radius.

LEMMA 5.23. *Let M be a complete, orientable, hyperbolic 3-manifold with $M \cong \mathbb{H}^3/\Gamma$ for a discrete group $\Gamma \leq \mathrm{PSL}(2, \mathbb{C})$. For any $x \in M$ with lift $\tilde{x} \in \mathbb{H}^3$,*

$$\mathrm{injrad}(x) = \frac{1}{2} \inf_{A \neq \mathrm{Id} \in \Gamma} \{d(\tilde{x}, A\tilde{x})\}.$$

Moreover, this is realized. That is, there exists nontrivial $A \in \Gamma$ such that $2 \mathrm{injrad}(x) = d(\tilde{x}, A\tilde{x})$.

PROOF. A metric r -ball is embedded at x if and only if for all $A \neq \mathrm{Id} \in \Gamma$, the metric r -ball $B(r, \tilde{x})$ is disjoint from the metric r -ball $A(B(r, \tilde{x})) = B(r, A\tilde{x})$. This holds if and only if the translation distance $d(\tilde{x}, A\tilde{x})$ is at least $2r$ for all A .

Now suppose $\text{inrad}(x) = b$. Then a metric b -ball is embedded, but for any $\epsilon > 0$, a metric $b + \epsilon$ -ball is not embedded. Thus for each $\epsilon > 0$, there is $A_\epsilon \in \Gamma$ such that $d(\tilde{x}, A_\epsilon(\tilde{x})) < 2(b + \epsilon)$. If the set $\{A_\epsilon\}$ contains infinitely many distinct elements, then we obtain a sequence $\{A_n\}$ such that $A_n(\tilde{x})$ is of bounded distance from \tilde{x} . By lemma 5.6, $A_n \rightarrow A \in \text{PSL}(2, \mathbb{C})$, implying Γ is not discrete by lemma 5.5. This is a contradiction. Thus $\{A_\epsilon\}$ is a finite set. Let $A \in \Gamma$ be such that $d(\tilde{x}, A\tilde{x})$ is minimal. This A satisfies the conclusion of the lemma. \square

We are now ready to complete the proof of theorem 5.20, assuming theorem 5.22.

PROOF OF THEOREM 5.20 (STRUCTURE OF THIN PART). Take $\epsilon_3 > 0$ as in theorem 5.22. Let $M \cong \mathbb{H}^3/\Gamma$ be a complete, orientable, hyperbolic 3-manifold, so $\Gamma \leq \text{PSL}(2, \mathbb{C})$ is a discrete subgroup with no elliptics.

For $\epsilon \leq \epsilon_3$, if $x \in M^{<\epsilon}$, then by definition $\text{inrad}(x) < \epsilon/2$. By lemma 5.23, it follows that there exists $A \neq \text{Id} \in \Gamma$ such that $d(\tilde{x}, A\tilde{x}) < \epsilon$ for any lift \tilde{x} of x . But theorem 5.22 implies that the subgroup Γ_ϵ of Γ generated by all $A \in \Gamma$ such that $d(\tilde{x}, A\tilde{x}) < \epsilon$ is elementary. Since Γ_ϵ contains $A \neq \text{Id}$, proposition 5.12 implies that Γ_ϵ either fixes a single point $\zeta \in \partial\mathbb{H}^3$ and is generated by parabolics fixing ζ , or Γ_ϵ is generated by a single loxodromic preserving an axis $\ell \subset \mathbb{H}^3$.

Suppose first that Γ_ϵ fixes a single point $\zeta \in \partial\mathbb{H}^3$. Then Γ_ϵ is generated by one or two parabolics (proposition 5.12), and \tilde{x} lies on a horosphere H about ζ that is fixed by Γ_ϵ . Suppose \tilde{y} lies in the horoball bounded by H . Then the height of \tilde{y} is at least C : \tilde{y} has coordinates $(a + bi, t)$ with $t \geq C$. A generator A of Γ_ϵ takes \tilde{y} to a point with the same height t . A calculation in this case (exercise 5.14) shows that

$$\epsilon > d(\tilde{x}, A\tilde{x}) \geq d(\tilde{y}, A\tilde{y}),$$

and it follows that in the quotient \mathbb{H}^3/Γ , the point \tilde{y} maps to $M^{<\epsilon}$. Since this is true for every point in the horoball bounded by H , $M^{<\epsilon}$ contains the quotient of a horoball under the elementary group Γ_ϵ ; this is a rank-1 or rank-2 cusp.

Now suppose that H is generated by a single loxodromic A preserving the axis ℓ . Let R denote the distance from \tilde{x} to the axis ℓ , and let T_R denote the set of points in \mathbb{H}^3 of distance R from the axis ℓ . Then T_R bounds a tube consisting of all points in \mathbb{H}^3 of distance at most R from ℓ . If \tilde{y} is any point within this tube, then one can calculate (exercise 5.15) that $d(\tilde{y}, A\tilde{y}) \leq d(\tilde{x}, A\tilde{x}) < \epsilon$, so $M^{<\epsilon}$ contains the quotient of a tube about ℓ under the elementary group $\langle A \rangle$. This is a tube around a short geodesic. \square

5.4. Hyperbolic manifolds with finite volume

In chapter 4 we gave a method that will allow us to compute (complete) hyperbolic structures on many 3-manifolds, including many knot complements. Once we have a hyperbolic structure on a 3-manifold, we have

equipped the manifold with a Riemannian metric with very nice properties, for example the metric can be described in local coordinates by equation (2.4).

One of the simplest invariants we can compute from a hyperbolic metric is the volume of the underlying manifold. This gives a good measure of the “size” of the manifold. In chapter 13, we will discuss volumes in some detail, including how to compute volumes of hyperbolic 3-manifolds including knot and link complements. Meanwhile, we give an application of the thick–thin decomposition of hyperbolic 3-manifolds to classifying those with finite volume.

THEOREM 5.24. *A hyperbolic 3-manifold M has finite volume if and only if M is closed (compact without boundary), or M is homeomorphic to the interior of a compact manifold \overline{M} with torus boundary components.*

PROOF. If M is closed then a fundamental domain for M in its universal cover \mathbb{H}^3 is a compact set, hence has finite volume. If M is the interior of a manifold with torus boundary, then each such boundary component will be realized as a cusp in the complete hyperbolic structure on M . The complement of the cusps of M in M is compact, hence has finite volume. We now show that each cusp has finite volume.

Consider the universal cover \mathbb{H}^3 . For any cusp C , we may apply an isometry to \mathbb{H}^3 so that the point at infinity projects to that cusp, and a horoball of height 1 projects to an embedded horoball neighborhood of the cusp. On the horosphere of height 1, some parallelogram A will be a fundamental region for the torus of the cusp, since the structure is complete (theorem 4.10). Then the volume of the cusp is given by

$$\int_C d \text{vol} = \int_{t=1}^{\infty} \int_A d \text{vol} = \int_{t=1}^{\infty} \int_A \frac{dx dy dt}{t^3} = \frac{1}{2} \text{area}(A).$$

(See exercise 2.13.) Thus every cusp has finite volume. Since the volume of M is the sum of the volumes of the compact region with cusps removed, as well as a finite number of finite-volume cusps, the manifold M has finite volume.

To prove the converse, we use theorem 5.20. Suppose M is a complete hyperbolic manifold with finite volume. Fix $\epsilon > 0$ less than the universal constant ϵ_3 of theorem 5.20, and consider $M^{<\epsilon}$ and $M^{\geq\epsilon}$. By theorem 5.20, $M^{<\epsilon}$ consists of cusps and tubes. Note that a rank-1 cusp has infinite volume, hence since M has finite volume, $M^{<\epsilon}$ consists of rank-2 cusps and tubes, each of which has finite volume. On the other hand, $M^{\geq\epsilon}$ has finite volume. Moreover, any point in $M^{\geq\epsilon}$ is contained in an embedded ball of radius at least $\frac{1}{2}\epsilon$. If two points in $M^{\geq\epsilon}$ have distance at least ϵ , then the balls of radius $\frac{1}{2}\epsilon$ about each are disjointly embedded in $M^{\geq\epsilon}$. Thus a collection of points with pairwise distance at least ϵ in $M^{\geq\epsilon}$ leads to a pairwise disjoint collection of $\epsilon/2$ -balls. Because M has finite volume there can only be finitely many of these. Starting with any such collection of points, we may complete

the collection to a maximal collection of points of $M^{\geq\epsilon}$ of distance at least ϵ ; there are finitely many of these and the $\epsilon/2$ -balls around each are embedded. Then the closed ϵ -balls about the collection must contain $M^{\geq\epsilon}$. The union of these balls is a compact set, and $M^{\geq\epsilon}$ is a closed subset. Hence $M^{\geq\epsilon}$ is compact.

Now the union of $M^{\geq\epsilon}$ and any tubes of $M^{<\epsilon}$ is the union of compact sets, hence compact. This is a manifold with boundary homeomorphic to a finite collection of tori corresponding to the finite number of cusps of $M^{<\epsilon}$. Attach a closed collar neighborhood of each torus boundary component, and call the result N ; each collar neighborhood is homeomorphic to $T^2 \times [0, 1]$, where T^2 is a torus. Then by construction, the manifold M is homeomorphic to the interior of N . \square

By theorem 5.24, the complement of any knot or link in S^3 with a hyperbolic structure must have finite hyperbolic volume.

5.5. Universal elementary neighborhoods

In this section, we give a proof of theorem 5.22, on the existence of universal elementary neighborhoods.

In fact, we split this section into two subsections. The first gives a proof of theorem 5.22 that is elementary, in the sense that it uses only the machinery of subgroups of $\mathrm{PSL}(2, \mathbb{C})$ developed in this chapter. However, it is also quite technical, requiring calculations that, upon first glance, may seem mysterious and arbitrary. Nevertheless, by the end of subsection 5.5.1, the proof of theorem 5.22 is complete.

The second subsection is an attempt to put theorem 5.22 into a wider mathematical context. Although we have presented a proof that uses only the tools of $\mathrm{PSL}(2, \mathbb{C})$, related theorems hold for much more general Lie groups. The technical calculations of subsection 5.5.1 can be seen as instances of more general, and in some sense simpler, mathematical phenomena, put into a broader context.

5.5.1. A technical proof in $\mathrm{PSL}(2, \mathbb{C})$. We now give a complete proof of theorem 5.22, restricting to the setting of $\mathrm{PSL}(2, \mathbb{C})$.

We need a few more tools before we begin. Namely, proposition 5.12 classifies elementary discrete groups without elliptics. We also need the following result giving more information on *nonelementary* discrete groups without elliptics.

LEMMA 5.25. *If G is a nonelementary discrete subgroup of $\mathrm{PSL}(2, \mathbb{C})$ that contains no elliptics, then the following hold.*

- (1) G is infinite.
- (2) For any nontrivial $A \in G$, there exists a loxodromic $B \in G$ that has no common fixed points with A .
- (3) If $B \in G$ is loxodromic, then there is no nontrivial $C \in G$ that has exactly one fixed point in common with B .

- (4) G contains two loxodromic elements with no fixed points in common.

PROOF. The group G must be nontrivial; since it contains no elliptics it must contain a loxodromic or parabolic. Such an element has infinite order, so G is infinite, proving (1).

Next we show (3). Suppose B is loxodromic, and C has exactly one fixed point in common with B ; we will show that the group generated by B and C is indiscrete, contradicting the fact that G is discrete. Conjugate the group. Lemma 5.2 implies we may assume $B = \begin{pmatrix} \rho & 0 \\ 0 & 1/\rho \end{pmatrix}$, and since C has exactly one fixed point in common with B , it has the form $C = \begin{pmatrix} a & b \\ 0 & 1/a \end{pmatrix}$ where $b \neq 0$. Then

$$B^n C B^{-n} C^{-1} = \begin{pmatrix} 1 & ab(\rho^{2n} - 1) \\ 0 & 1 \end{pmatrix}.$$

If $|\rho| < 1$, let $n \rightarrow \infty$. If $|\rho| > 1$, let $n \rightarrow -\infty$. In either case, $B^n C B^{-n} C^{-1}$ approaches the parabolic $\begin{pmatrix} 1 & -ab \\ 0 & 1 \end{pmatrix}$. Lemma 5.5 now implies that the subgroup generated by B and C is not discrete, therefore G is not discrete.

Now we show (2). There are two cases depending on whether A is parabolic or loxodromic. Note that if we can show the result for a conjugate group UGU^{-1} for $U \in \mathrm{PSL}(2, \mathbb{C})$, then the result holds for G , so in both cases we will replace G by a conjugate group at the first step.

Case 1. Suppose A is parabolic. Then by lemma 5.2, A is conjugate to $z \mapsto z + 1$, so we may assume $A = \begin{pmatrix} 1 & 1 \\ 0 & 1 \end{pmatrix}$ and A fixes ∞ . Because G is nonelementary, there exists $C \in G$ that does not fix ∞ . If C is loxodromic, we are done. If not, C must be parabolic, and $C = \begin{pmatrix} a & b \\ c & d \end{pmatrix}$ with $c \neq 0$. Note that $A^n C$ cannot fix ∞ for any integer n , and $\mathrm{tr}(A^n C) = a + nc + d = nc \pm 2$. For $|n|$ sufficiently large, this cannot be in $[-2, 2]$, so $A^n C$ is the desired loxodromic by lemma 5.2.

Case 2. Suppose A is loxodromic. Then after conjugating, lemma 5.2 implies we may assume $A = \begin{pmatrix} \rho & 0 \\ 0 & \rho^{-1} \end{pmatrix}$ with $|\rho| > 1$, so A fixes 0 and ∞ . Because G is nonelementary and discrete, (3) implies there is $C = \begin{pmatrix} a & b \\ c & d \end{pmatrix} \in G$ that does not fix either 0 or ∞ (so $b, c \neq 0$). If C happens to be loxodromic, we are done. If not, C is parabolic, so $a + d = \pm 2$. Then $A^n C$ also has distinct fixed points from those of A for any integer n , and $\mathrm{tr}(A^n C) = a\rho^n + d\rho^{-n}$. For $|n|$ large, this lies outside $[-2, 2]$, hence $A^n C$ is loxodromic by lemma 5.2. This concludes the proof of (2).

Finally, to prove part (4), we use part (2). Suppose $A \in G$ is not the identity. Then (2) implies there is a loxodromic $B \in G$ with distinct fixed

points from A . If A is also loxodromic, we are done. Otherwise, apply (2) to B , to obtain a loxodromic C with no fixed points in common with B . Then B and C are the desired loxodromics. \square

The following theorem, on convergence of nonelementary discrete groups, is due to Jørgensen and Klein [JK82], using previous work of Jørgensen [Jør76].

THEOREM 5.26 (Jørgensen and Klein, 1982). *Let*

$$G_n = \langle A_{1,n}, A_{2,n}, \dots, A_{r,n} \rangle$$

be a sequence of r -generator, nonelementary, discrete subgroups of $\mathrm{PSL}(2, \mathbb{C})$ such that $A_k = \lim_{n \rightarrow \infty} A_{k,n}$ exists and is an element of $\mathrm{PSL}(2, \mathbb{C})$ for each k . Then $G = \langle A_1, A_2, \dots, A_r \rangle$ is also nonelementary and discrete. Moreover, for sufficiently large n , the map $A_k \rightarrow A_{k,n}$ for each k extends to a homomorphism from G to G_n .

The proof of theorem 5.26 follows from an analysis of various properties of elements of $\mathrm{PSL}(2, \mathbb{C})$ and discrete subgroups. Its proof is not unlike many of the other results proved in this chapter. However, its proof would lead us a little further afield than we wish to go, into technicalities of $\mathrm{PSL}(2, \mathbb{C})$. The full proof can be found in the original papers; Marden also gives an exposition closely following the original proof in [Mar07]. We will refer the interested reader to those references.

Meanwhile, we don't actually need the full strength of theorem 5.26; we only need the following immediate consequence.

COROLLARY 5.27. *Suppose $\{\langle A_n, B_n \rangle\}$ is a sequence of nonelementary discrete subgroups of $\mathrm{PSL}(2, \mathbb{C})$ such that $\lim A_n = A$ and $\lim B_n = B$ in $\mathrm{PSL}(2, \mathbb{C})$. Then $\langle A, B \rangle$ is a nonelementary discrete subgroup of $\mathrm{PSL}(2, \mathbb{C})$.* \square

PROOF OF THEOREM 5.22. First we establish some notation. For fixed $x \in \mathbb{H}^3$ and $A \in \mathrm{PSL}(2, \mathbb{C})$, let $d(x, Ax)$ denote the distance in \mathbb{H}^3 between x and Ax . For fixed $r > 0$, let $G(r, x)$ denote the set

$$G(r, x) = \{A \in G \mid d(x, Ax) < r\}.$$

The group generated by $G(r, x)$ will be denoted by $\langle G(r, x) \rangle$.

Our goal is to show that there exists $r > 0$ such that for all discrete G and for all x , the group $\langle G(r, x) \rangle$ is elementary.

As a first step, we show that if we fix a discrete group G with no elliptics and fix x , then there exists $r > 0$ such that the group $\langle G(r, x) \rangle$ is elementary. For suppose this is not the case. Then for a sequence $r_n \rightarrow 0$, each $\langle G(r_n, x) \rangle$ is nonelementary. It follows that there exists a sequence of distinct $A_n \in G(r_n, x)$ with $d(x, A_n x) < r_n$. But then lemma 5.6 implies that A_n must converge to some $A \in \mathrm{PSL}(2, \mathbb{C})$. Using lemma 5.5, we see that this contradicts the fact that G is a discrete group. So for $r > 0$ sufficiently small, $\langle G(r, x) \rangle$ is elementary, and it follows that $G(r, x)$ contains finitely

many elements. By choosing $r > 0$ smaller than the translation distance of each of these elements, we find that $G(r, x)$ contains only the identity element. Note that the identity group is elementary.

Now we will prove the more general result, that there is a universal $r > 0$, independent of G and x , such that $\langle G(r, x) \rangle$ is always elementary. Again suppose not. Then there is a sequence $r_n \rightarrow 0$, a sequence of discrete groups $G_n \leq \mathrm{PSL}(2, \mathbb{C})$ without elliptics, and a sequence of points $x_n \in \mathbb{H}^3$ such that $\langle G_n(r_n, x_n) \rangle$ is not elementary.

We will simplify the argument by replacing x_n with a fixed x for all n : choose any $x \in \mathbb{H}^3$, and let $R_n \in \mathrm{PSL}(2, \mathbb{C})$ be an isometry mapping x_n to x . Consider the group $R_n G_n R_n^{-1}$. Note that $A \in G_n(r_n, x_n)$ if and only if $R_n A R_n^{-1}$ is in $R_n G_n R_n^{-1}(r_n, x)$, and so $\langle R_n G_n R_n^{-1}(r_n, x) \rangle$ is nonelementary. Thus if we replace G_n by $R_n G_n R_n^{-1}$, we may work with a single fixed value of x . So we assume there is a fixed x and sequences $r_n \rightarrow 0$ and G_n so that $\langle G_n(r_n, x) \rangle$ is nonelementary.

Now fix n . Our next goal is to find A_n and B_n in $G_n(r_n, x)$ such that $\langle A_n, B_n \rangle$ is nonelementary. Since $\langle G_n(r_n, x) \rangle$ is nonelementary, lemma 5.25 implies that there exist loxodromics S_n and T_n with no common fixed points in $\langle G_n(r_n, x) \rangle$, and certainly they generate a nonelementary group. However, we need to take some care to ensure that A_n and B_n are actually in $G_n(r_n, x)$. To do this, we use the first part of this proof: consider the groups $\langle G_n(\rho, x) \rangle$ as ρ ranges between 0 and r_n . We have observed that for some $\rho_n < r_n$, the group $\langle G_n(\rho_n, x) \rangle$ will consist only of the identity element. As ρ increases, the sets $G_n(\rho, x)$ will be nested. There will be some value $0 < \mu_n \leq r_n$ such that $\langle G_n(\rho, x) \rangle$ is elementary for $\rho < \mu_n$ but $\langle G_n(\mu_n, x) \rangle$ is nonelementary. We may assume $\mu_n = r_n$.

Moreover, there is some $\tau_n < r_n$ such that for $\tau_n \leq \rho < r_n$, the groups $\langle G_n(\rho, x) \rangle$ are all elementary and isomorphic, equal to the group $\langle G_n(\tau_n, x) \rangle$.

Suppose that the elementary group $\langle G_n(\tau_n, x) \rangle$ is infinite with two fixed points on $\partial\mathbb{H}^3$. Then proposition 5.12 implies that it contains a loxodromic $A_n \in G_n(\tau_n, x)$ fixing a line ℓ . Since $\langle G_n(r_n, x) \rangle$ is not elementary, $G_n(r_n, x)$ must contain a loxodromic B_n that does not fix ℓ . Then A_n and B_n are loxodromics in $G_n(r_n, x)$ with no common fixed points. So $\langle A_n, B_n \rangle$ is not elementary.

Now suppose that the elementary group $\langle G_n(\tau_n, x) \rangle$ fixes a single point $\zeta \in \partial\mathbb{H}^3$. Then $G_n(\tau_n, x)$ contains a parabolic A_n . Since $\langle G_n(r_n, x) \rangle$ is not elementary, $G_n(r_n, x)$ contains some B_n that does not fix ζ . So again A_n and B_n are elements of $G_n(r_n, x)$ with no common fixed points, and $\langle A_n, B_n \rangle$ is not elementary.

Finally suppose that the elementary group $\langle G_n(\tau_n, x) \rangle$ consists only of the identity element. Since $\langle G_n(r_n, x) \rangle$ is nonelementary with no elliptics, the generating set $G_n(r_n, x)$ must contain two elements A_n and B_n with no common fixed point. Thus $\langle A_n, B_n \rangle$ is not elementary.

In all cases, we have a nonelementary subgroup with two generators, $\langle A_n, B_n \rangle$, and $A_n, B_n \in G_n(r_n, x)$. Note that $A_n(x) \rightarrow x$ and $B_n(x) \rightarrow x$,

so lemma 5.6 implies there are subsequences of $\{A_n\}$ and $\{B_n\}$ converging to $A \in \mathrm{PSL}(2, \mathbb{C})$ and $B \in \mathrm{PSL}(2, \mathbb{C})$, respectively. Then corollary 5.27 implies that $\langle A, B \rangle$ is nonelementary.

On the other hand, $A_n, B_n \in G_n(r_n, x)$, so as $n \rightarrow \infty$, A_n and B_n must converge to elements of $\mathrm{PSL}(2, \mathbb{C})$ fixing x . Thus $\langle A, B \rangle$ fixes x , hence it is elementary by definition. This contradiction finishes the proof. \square

5.5.2. A sketch of a broader result in Lie groups. The Universal Elementary Neighborhoods theorem, theorem 5.22, which we proved using properties of $\mathrm{PSL}(2, \mathbb{C})$ in the previous subsection, actually follows quickly from a broader result in Lie groups due to Každan and Margulis [KM68]. We will not go into many details on Lie groups here, but we do include a sketch of some of the ideas.

DEFINITION 5.28. Let G be a group with subgroups H and K . The group $[H, K]$ is defined to be the subgroup of G generated by elements $[h, k] = hkh^{-1}k^{-1}$ for all $h \in H$ and $k \in K$.

The m -th commutator G^m of G is defined recursively by $G^1 = [G, G]$, and $G^{m+1} = [G, G^m]$, for $m \geq 1$.

A group is *nilpotent* if for some integer m , $G^m = \{1\}$.

The following is due to Zassenhaus, proved in 1937 [Zas37].

THEOREM 5.29 (Zassenhaus Theorem). *Let G be a Lie group. Then there is a neighborhood of the identity $U_Z \subset G$ such that for each discrete subgroup $\Gamma \leq G$, the group generated by $\Gamma \cap U_Z$ is nilpotent.*

PROOF SKETCH. The derivative of the commutator map $[\cdot, \cdot]: G \times G \rightarrow G$ at $(1, 1)$ can be shown to be identically 0, so $[\cdot, \cdot]$ is a strict contraction in a neighborhood U of the identity, in both variables. Thus for $\gamma_1, \dots, \gamma_m \in \Gamma \cap U$, the iterated commutator

$$y_m = [\gamma_1, [\gamma_2, [\dots [\gamma_{m-1}, \gamma_m] \dots]]]$$

must lie in U and must satisfy $\lim_{m \rightarrow \infty} y_m = 1$. Because Γ is a discrete group, there exists an integer N such that for $n \geq N$, $y_N = 1$. Then the group is nilpotent. \square

This in turn implies a more general result on Lie groups, proved in [KM68]. Before we state the theorem, we say a few words about the general setting in which the theorem applies.

Let G be a Lie group, and K a maximal compact subgroup of G . We may give G a left-invariant Riemannian metric that is also right-invariant under K . Then the space G/K becomes a Riemannian manifold with G acting on X on the left by isometries of X . We say $X = G/K$ is the *homogeneous space associated with G* .

For example, in the setting of \mathbb{H}^3 , we may take G to be the group of isometries of \mathbb{H}^3 , and K the subgroup fixing a point $x \in \mathbb{H}^3$. This is isomorphic to the compact Lie group $O(2)$. Then the quotient G/K is \mathbb{H}^3 ,

with its usual metric and action of G by isometries. We will apply the theorem in this setting.

THEOREM 5.30 (Kazhdan–Margulis Theorem). *Let X be the homogeneous space associated with a Lie group G . There exists a constant $\eta = \eta(X)$ satisfying the following. Let $x \in X$, and let Γ be any discrete group generated by elements $\{g_1, \dots, g_\ell\} \subset G$ such that $d(x, g_j(x)) \leq \eta$ for all j . Then there exists a subgroup Γ' of Γ of finite index such that Γ' is nilpotent.*

A proof of this version of the Margulis Lemma can be found in [Kap01]. See also [BGS85] for a version that applies to Riemannian manifolds with negative sectional curvature, or [BP92] for another proof when $X = \mathbb{H}^n$.

PROOF SKETCH. The proof begins by taking a Zassenhaus neighborhood U_Z of $1 \in G$ from theorem 5.29. There exists $\epsilon > 0$ depending only on X such that the ball of radius ϵ around $1 \in G$ is contained in U_Z : $B_\epsilon(1) \subset U_Z$.

Next, because X is homogeneous, we may assume x is the projection of $1 \in G$ to $X = G/K$, removing the dependence of the argument upon x .

The value of η is determined from ϵ as follows. Because K is compact, there is an $\epsilon/10$ -dense subset of K consisting of a finite number of elements; say N elements. Choose η such that whenever $\{g_1, \dots, g_\ell\}$ satisfy $d(x, g_j(x)) \leq \eta$, any word $w = w(g_1, \dots, g_\ell)$ in the g_j of length at most N satisfies $d(x, wx) \leq \epsilon/5$.

For this value of η , whenever such $\{g_1, \dots, g_\ell\}$ generate a discrete group Γ , the group $\Gamma \cap B_\epsilon(1) = \Gamma'$ is nilpotent, by theorem 5.29. The choice of η allows one to show that Γ' also has finite index in Γ . \square

Assuming the Kazhdan–Margulis theorem, theorem 5.30, we obtain a quick proof of theorem 5.22, the Universal Elementary Neighborhoods theorem, which we now explain.

Recall that the *center* of a group is the subgroup of all elements that commute with every other element.

LEMMA 5.31. *A non-trivial nilpotent group has non-trivial center.*

PROOF. Suppose G is nilpotent, with $G^n = [G, G^{n-1}] = 1$ but $G^{n-1} \neq 1$. Then $[G, G^{n-1}] = 1$ if and only if for every $x \in G^{n-1}$ and every $g \in G$, the product $x^{-1}g^{-1}xg = 1$, which holds if and only if $xg = gx$. Thus G^{n-1} lies in the center of G , and is nontrivial. \square

COROLLARY 5.32. *A nilpotent subgroup G of $\mathrm{PSL}(2, \mathbb{C})$ without elliptics must satisfy one of the following:*

- $G = \{1\}$
- $G - \{1\}$ consists of loxodromic elements with the same fixed points at infinity.
- $G - \{1\}$ consists of parabolic elements with the same fixed point at infinity.

PROOF. By lemma 5.31, if G is nontrivial then there is a nontrivial element $g \in G$ that commutes with every other element of G . By exercise 5.11, every element in G must have the same fixed points as g . The cases follow depending on whether g is loxodromic or parabolic. \square

PROOF OF THEOREM 5.22 ASSUMING THEOREM 5.30. Let G be a discrete subgroup of $\mathrm{PSL}(2, \mathbb{C})$ without elliptics, let $x \in \mathbb{H}^3$, and let η be the constant from the Každan–Margulis Theorem, theorem 5.30. If H denotes the subgroup of G generated by elements of G that translate x distance less than η , then there exists a nilpotent subgroup H' of H such that H/H' is finite. By corollary 5.32, H' has one of three forms.

If H' is trivial, then H is a finite group. Since there are no elliptics in G , H must also be trivial, and so H is elementary.

Since H' is a finite index subgroup of H , for any $h \in H$ there exists an integer m such that $h^m \in H'$. Then h^m has the same fixed points as H' , and hence h has the same fixed points as H' . Thus either $H' - \{1\}$ consists of loxodromic elements with two fixed points at infinity, and all elements of H have the same fixed points at infinity, or $H' - \{1\}$ consists of parabolics with one point at infinity, and all elements of H have the same fixed point at infinity. In either case, H is elementary. \square

5.6. Exercises

EXERCISE 5.1. Is a subgroup of $\mathrm{PSL}(2, \mathbb{C})$ generated by a single elliptic element always discrete? Prove it is discrete, or give a counterexample.

EXERCISE 5.2. Prove lemma 5.2, giving more properties of parabolic, elliptic, and loxodromics in $\mathrm{PSL}(2, \mathbb{C})$.

EXERCISE 5.3. Prove that the gluing isometries for the figure-8 knot complement are the elements of $\mathrm{PSL}(2, \mathbb{C})$ given in equation (5.1).

EXERCISE 5.4. R. Riley gave a presentation of the fundamental group of the figure-8 knot complement in [Ril75]:

$$\pi_1(S^3 - K) = \langle a, b \mid yay^{-1} = b \rangle,$$

where $y = a^{-1}bab^{-1}$. He let

$$A = \begin{pmatrix} 1 & 1 \\ 0 & 1 \end{pmatrix}, \quad B = \begin{pmatrix} 1 & 0 \\ -\sigma & 1 \end{pmatrix},$$

where σ is a primitive cube root of unity, and let

$$\rho: \pi_1(S^3 - K) \rightarrow \langle A, B \rangle \leq \mathrm{PSL}(2, \mathbb{C})$$

be the representation $\rho(a) = A$, $\rho(b) = B$. Prove the representation ρ gives an isomorphism of groups.

EXERCISE 5.5. Let A and B in $\mathrm{PSL}(2, \mathbb{C})$ be as in exercise 5.4. Find an explicit element $U = \begin{pmatrix} a & b \\ c & d \end{pmatrix}$ of $\mathrm{PSL}(2, \mathbb{C})$ such that Riley's A and B are

conjugate via U to our isometries T_C and T_D^{-1} , respectively. That is, find U such that

$$A = UT_CU^{-1}, \quad B = UT_D^{-1}U^{-1}.$$

Even better: U can be written as a composition of a parabolic fixing infinity T , followed by a rotation R : $U = RT$. Find T and R .

EXERCISE 5.6. Note that Riley's isometries A and B of exercise 5.4 do not give face-pairings of the fundamental domain in figure 5.1. Find a fundamental domain for the figure-8 knot such that A and B are face-pairing isometries.

Hint: exercise 5.5 might be helpful.

EXERCISE 5.7. If a group G acts on Euclidean space \mathbb{R}^n or hyperbolic space \mathbb{H}^n , extend the definitions of properly discontinuous and free actions in the obvious way.

Show directly by definitions that each of the following groups G acts freely and properly discontinuously on the given space X .

- (1) $X = \mathbb{R}^2$, G is generated by two translations $\phi: \mathbb{R}^2 \rightarrow \mathbb{R}^2$ and $\psi: \mathbb{R}^2 \rightarrow \mathbb{R}^2$ given by $\phi(x, y) = (x + t, y)$ and $\psi(x, y) = (x, y + s)$ for $s, t \in \mathbb{R}$.
- (2) $X = \mathbb{H}^2$, G is the holonomy group of the (complete) 3-punctured sphere.
- (3) $X = \mathbb{H}^3$, G is generated by face-pairing isometries of an ideal polyhedron such that the face identifications give a complete hyperbolic 3-manifold.

EXERCISE 5.8. Show that the following give finite elementary groups.

- (1) Cyclic groups fixing an axis in \mathbb{H}^3 .
- (2) Orientation preserving symmetries of an ideal platonic solid (tetrahedron, octahedron/cube, icosahedron/dodecahedron).
- (3) Dihedral groups preserving an ideal polygon with n sides inscribed in a plane in \mathbb{H}^3 .

EXERCISE 5.9. Show that the finite groups in exercise 5.8 are the only finite elementary groups.

EXERCISE 5.10. Let G be a subgroup of $\mathrm{PSL}(2, \mathbb{C})$. Show that the following are equivalent.

- (1) G is discrete.
- (2) G has no limit points in the interior of \mathbb{H}^3 . That is, for any $x \in \mathbb{H}^3$, there is no $y \in \mathbb{H}^3$ and no sequence of distinct elements $\{A_n\}$ in G such that $A_n(y) = x$.

EXERCISE 5.11. Let A and B in $\mathrm{PSL}(2, \mathbb{C})$ be distinct from the identity. Prove that the following are equivalent.

- (a) A and B commute.

- (b) Either A and B have the same fixed points, or A and B have order 2 and each interchanges the fixed points of the other.
- (c) Either A and B are parabolic with the same fixed point at infinity, or the axes of A and B coincide, or A and B have order 2 and their axes intersect orthogonally in \mathbb{H}^3 .

EXERCISE 5.12. Suppose that A and B in $\mathrm{PSL}(2, \mathbb{C})$ are loxodromics with exactly one fixed point in common. Show that $\langle A, B \rangle$ is not discrete.

EXERCISE 5.13. State and prove a version of theorem 5.20, the structure of the thin part, for hyperbolic 2-manifolds.

EXERCISE 5.14. Suppose A is a parabolic fixing the point ζ and p is a point in \mathbb{H}^3 such that $d(p, A(p)) < \epsilon$. After applying an isometry, we may assume that $\zeta = \infty$, that $A = \begin{pmatrix} 1 & \alpha \\ 0 & 1 \end{pmatrix}$ for some $\alpha \in \mathbb{C}$, and p lies on a horosphere H_C that is a Euclidean plane of constant height $t = C$ for some $C > 0$:

$$H_C = \{(x + yi, C) \mid C > 0\}.$$

- (a) Prove that if a point q lies inside the horoball bounded by H_C on a horosphere H_t of height $t \geq C$, then the Euclidean distance from q to $A(q)$ measured along H_t is at most the Euclidean distance from p to $A(p)$ measured along H .
- (b) Prove that the hyperbolic distances, measured in \mathbb{H}^3 , satisfy

$$\epsilon > d(p, A(p)) \geq d(q, A(q)).$$

EXERCISE 5.15. Suppose A is a loxodromic fixing an axis ℓ , and p is a point in \mathbb{H}^3 such that $d(p, A(p)) < \epsilon$.

- (1) Prove that the distance from any $q \in \mathbb{H}^3$ to ℓ is the same as the distance from $A(q)$ to ℓ .
- (2) We can use cylindrical coordinates in \mathbb{H}^3 about the geodesic ℓ . Let r denote the distance from ℓ , θ the rotation about ℓ (measured modulo 2π), and ζ the translation distance along ℓ . Finally, let $\widehat{\mathbb{H}}^3$ denote the cover of \mathbb{H}^3 in which θ is no longer measured modulo 2π , but is a real number.

Using these coordinates, it can be shown that the distance d between points p_1 and p_2 in $\widehat{\mathbb{H}}^3$ with cylindrical coordinates (r_1, θ_1, ζ_1) and (r_2, θ_2, ζ_2) with $|\theta_1 - \theta_2| < \pi$ is given by

$$\cosh d = \cosh(\zeta_1 - \zeta_2) \cosh r_1 \cosh r_2 - \cos(\theta_1 - \theta_2) \sinh r_1 \sinh r_2.$$

(See [GMM01, Lemma 2.1])

Using this formula, prove that if $x, y \in \mathbb{H}^3$ are points such that $d(y, \ell) \leq d(x, \ell)$, then

$$d(y, A(y)) \leq d(x, A(x)).$$

CHAPTER 6

Completion and Dehn Filling

In chapter 3 we considered some incomplete structures on hyperbolic 2-manifolds, particularly the 3-punctured sphere, example 3.18. In this chapter, we examine incomplete hyperbolic structures on 3-manifolds with torus boundary, and their completions.

6.1. Mostow–Prasad rigidity

We begin by stating a few important results on complete hyperbolic structures on manifolds to set up some context for the rest of the chapter.

Many surfaces admit infinitely many complete hyperbolic structures. For example, in exercises 3.13 and 3.14 you found 2-parameter families of complete hyperbolic structures on the 1-punctured torus and 4-punctured sphere. This flexibility is only possible in two dimensions. In higher dimensions, there is only *one* complete structure on a finite volume hyperbolic manifold, up to isometry. This result was proved in the case M is a closed manifold by Mostow [Mos73], and extended to the case of open manifolds with finite volume by Prasad [Pra73]. Recall that by theorem 5.24, an open hyperbolic 3-manifold has finite volume if and only if it is the interior of a manifold with torus boundary components.

THEOREM 6.1 (Mostow–Prasad rigidity). *If M_1^n and M_2^n are complete hyperbolic n -manifolds with finite volume and $n \geq 3$, then any isomorphism of fundamental groups $\phi: \pi_1(M_1) \rightarrow \pi_1(M_2)$ is realized by a unique isometry.*

We will not include the proof in this book, as it leads us a little further away from knots and links than we wish to stray. However, the proof of the theorem can be found in the original papers, or in books on hyperbolic geometry including [BP92] and [Rat06].

Recall also Gordon and Luecke’s knot complement theorem, theorem 0.4 from chapter 0, which states that knots with homeomorphic complement are equivalent.

Knots with homeomorphic complements have isomorphic fundamental group. By theorem 6.1, Mostow–Prasad rigidity, any complete hyperbolic structure on the knot complement is the *only* complete hyperbolic structure.

So the complete hyperbolic structure on a knot complement distinguishes any two knots. This is one reason hyperbolic geometry gives many very nice knot invariants!

6.2. Completion of incomplete structures

What about incomplete structures on a manifold M with torus boundary? There are many of these. For the figure-8 knot complement, for example, we found a 1-complex parameter family of incomplete structures, parameterized by $w \in \mathbb{C}$ as in figure 4.11. If we take the *completion* of a hyperbolic structure on a 3-manifold, we obtain surprising topological results.

As a warm up, recall completions of incomplete structure on 2-manifolds. In chapter 3, we saw an example of an incomplete structure on a hyperbolic 3-punctured sphere. Recall that in the developing map for an incomplete structure, ideal polygons approached a limiting line. By selecting a point on a horocycle about infinity, approaching this line, we obtained a Cauchy sequence that did not converge. See figure 3.13. Adjoining a point where each horocycle met the limiting line, we obtained the completion. The completion was given by attaching a geodesic of length $d(v)$, as in figure 3.14.

Now consider an incomplete structure on a 3-manifold M such that M is the interior of a compact manifold with torus boundary. Let C be a cusp torus of M . Then the torus C inherits an affine structure from the hyperbolic structure on M , and because the structure on M is not complete, the affine structure is not Euclidean (theorem 4.10).

Let α and β generate $\pi_1(C) \cong \mathbb{Z} \times \mathbb{Z}$. Corresponding to α and β are two holonomy isometries $\rho(\alpha)$ and $\rho(\beta)$. To simplify notation, we will drop the ρ , abusing notation slightly, and simply refer to these isometries as α and β . Assume the action of α and β does not induce a Euclidean structure on C , so the hyperbolic structure on M is not complete. To form its completion, we remove a small neighborhood $N(C)$ of C , take the completion of $N(C)$, and then reattach this neighborhood to M . Thus to analyze the completion of M , we analyze the completion of neighborhoods of cusp tori.

PROPOSITION 6.2. *The completion of $N(C)$ is obtained by adjoining some portion of a geodesic to $N(C)$.*

PROOF. Consider the developing map for the affine torus C . The image will miss a single point (exercise 3.8), for example as in figure 3.3. This image is obtained by considering the action of α and β restricted to a horosphere. More precisely, if C has a fundamental domain that is a quadrilateral, then we build its developing image by starting with a copy of that quadrilateral on \mathbb{C} , which we identify with a horosphere about infinity, and attaching copies of the quadrilateral according to instructions given by the holonomy isometries corresponding to α and β , acting on the fixed horosphere.

If we shift the original choice of horosphere up, we will see the same image of the developing map. In particular, the developing map will still miss a single point, with the same complex value for each choice of horosphere.

These missed points form a vertical geodesic in \mathbb{H}^3 . We may apply an isometry so that this vertical geodesic runs from 0 to ∞ in \mathbb{H}^3 . Notice that the developing image of the neighborhood $N(C)$ is obtained by taking developing images of C on all horospheres about ∞ above some fixed initial height. Thus the developing image $N(C)$ misses the single geodesic from 0 to ∞ in \mathbb{H}^3 . Hence the completion of $N(C)$ is obtained by adjoining some portion of this geodesic to $N(C)$. \square

As in the case of incomplete 2-manifolds, the length of the portion of adjoined geodesic of proposition 6.2 will be determined by considering the action of the holonomy. Considering this action leads to the following result on the topology of the completion.

PROPOSITION 6.3. *Let $N(C)$ be the neighborhood of a cusp torus C of an incomplete hyperbolic manifold, so $N(C)$ is homeomorphic to $C \times (0, 1)$. Then the completion of $N(C)$ is either homeomorphic to the 1-point compactification of $N(C)$ obtained by crushing $C \times \{1\}$ to a point, or it is homeomorphic to the solid torus obtained by attaching a solid torus to $C \times \{1\}$.*

PROOF. As in the proof of proposition 6.2, consider the developing image of $N(C)$ and assume it misses the geodesic from 0 to ∞ . Note the group $\langle \alpha, \beta \rangle$ acts on the geodesic from 0 to ∞ . Since points in our completion should be identified to their images under the holonomy action, we should identify each point z on the geodesic from 0 to ∞ with $\langle \alpha, \beta \rangle \cdot z$. There are two cases.

Case 1. The image of z under the action of α and β is dense in the line from 0 to ∞ . In this case, the completion is the 1-point compactification. It is not a manifold (exercise 6.5).

Case 2. The image of z is a discrete set of points on the line, each of some distance $d(C)$ apart. In this case the completion is obtained by adjoining a geodesic circle of length $d(C)$ to $N(C)$. Denote the completion by $\overline{N(C)}$. We wish to understand the topology of $\overline{N(C)}$.

We may obtain a manifold homeomorphic to $N(C)$ by removing a small, closed tubular neighborhood of the geodesic circle adjoined to form $\overline{N(C)}$. Notice that a tubular neighborhood of a circle is a solid torus, with the geodesic at its core. Thus we obtain a manifold homeomorphic to $\overline{N(C)}$ by attaching a solid torus to the torus $C \times \{1\}$ of $N(C)$ \square

DEFINITION 6.4. Let M be a manifold with torus boundary component T . Let s be an isotopy class of simple closed curves on T ; s is called a *slope*. The manifold obtained from M by attaching a solid torus to T so that s bounds a disk in the resulting manifold is called the *Dehn filling of M along s* and is denoted $M(s)$.

A cartoon describing Dehn filling is shown in figure 6.1.

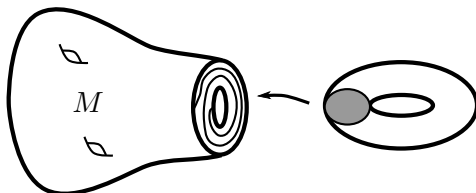


FIGURE 6.1. A cartoon describing Dehn filling. After filling, the curve shown on the torus boundary component of M will bound a disk.

By proposition 6.3, the space obtained by taking the completion of an incomplete hyperbolic structure on M either fails to be a manifold, or is homeomorphic to a Dehn filling of M .

Dehn filling is a very important topological procedure in 3-manifold topology, due to work of Wallace and Lickorish in the 1960s. Independently, they showed the following theorem [Wal60, Lic62]. A nice, highly readable proof can be found in the book [Rol90].

THEOREM 6.5 (Fundamental theorem of Wallace and Lickorish). *Let M be a closed, orientable 3-manifold. Then M is obtained by Dehn filling the complement of a link in S^3 .* \square

Theorem 6.5 gives a topological result on manifolds. By considering completions of hyperbolic 3-manifolds, we can make Dehn filling a geometric procedure.

DEFINITION 6.6. Consider the geodesic running from 0 to ∞ in \mathbb{H}^3 . We may write points in \mathbb{H}^3 in cylindrical coordinates (r, θ, ζ) where r is the distance from this geodesic, θ is a rotation angle around the geodesic, measured modulo 2π , and ζ , the height, is translation distance in the direction of the geodesic. In these coordinates, the metric is given by

$$dr^2 + \sinh^2 r d\theta^2 + \cosh^2 r d\zeta^2,$$

with θ measured modulo 2π .

Now fix $\alpha > 0$. Adjust the metric so θ is measured modulo α . Then a neighborhood of a point on the geodesic from 0 to ∞ is called a *hyperbolic cone* with *cone angle* α . Note the definition makes sense when $\alpha > 2\pi$. A cross section perpendicular to the geodesic is a 2-dimensional cone with cone angle α .

A 3-dimensional *hyperbolic cone manifold* is a manifold M in which each point x either has a neighborhood isometric to a ball in \mathbb{H}^3 , or has a neighborhood isometric to a hyperbolic cone.

In a hyperbolic cone manifold, the set of points that only have neighborhoods of the second kind form a geodesic link in M called the *singular locus*. The hyperbolic metric on M is smooth everywhere except at points on the singular locus.

PROPOSITION 6.7. *When the completion \overline{M} of M is topologically equivalent to attaching a solid torus, obtained by Dehn filling, it has the structure of a cone manifold. The singular locus Σ is the geodesic (link) attached in the completion.*

PROOF. As before, let C be a cusp torus of M with neighborhood $N(C)$, whose developing image misses the geodesic from 0 to ∞ in \mathbb{H}^3 . Let $\zeta \in \pi_1(C)$ generate the kernel of the action of $\pi_1(C) \cong \langle \alpha, \beta \rangle$ on the line from 0 to ∞ . The isometry ζ will be a rotation about this line by some angle α . Then a perpendicular cross section of the circle added to $\overline{N(C)}$ to form the completion will be a 2-dimensional hyperbolic cone, of cone angle α . Thus a neighborhood of a point on the completion is isometric to a hyperbolic cone.

Thus when we attach $\overline{N(C)}$ to M , the result \overline{M} is a hyperbolic cone manifold with singular locus along the attached geodesic. \square

There is one very important case of proposition 6.7. When the cone angle at the singular locus of \overline{M} is actually 2π , then the hyperbolic structure on \overline{M} is smooth everywhere. Thus \overline{M} is a hyperbolic manifold. We conclude:

COROLLARY 6.8. *When the holonomy $\rho(\pi_1(C))$ acts on the geodesic omitted from the developing image of $N(C)$ by a fixed translation, and when the generator $\zeta \in \pi_1(C)$ of the kernel has holonomy a rotation by 2π , then the completion of M is a complete hyperbolic manifold, homeomorphic to the Dehn filled manifold $M(\zeta)$.* \square

6.3. Hyperbolic Dehn filling space

We re-interpret the above section in the language of complex lengths of isometries of \mathbb{H}^3 .

Anytime M admits a hyperbolic structure, consider a cusp torus C for M . The fundamental group of the torus is isomorphic to $\mathbb{Z} \times \mathbb{Z}$, generated by some α and β .

REMARK 6.9. When M is a knot complement, $M \cong S^3 \setminus N(K)$, we often choose α to be the *meridian*, i.e. the curve on $\partial N(K)$ bounding a disk in $N(K) \subset S^3$, and β to be the *standard longitude*, i.e. the curve on $\partial N(K)$ that is homologous to 0 in $S^3 \setminus N(K)$.

Consider the holonomy elements of α and β . These are some isometries of \mathbb{H}^3 . As above, we will continue to abuse notation and denote the holonomy isometries corresponding to α and β by α and β .

Recall the classification of isometries of \mathbb{H}^3 , from lemma 5.2. Any isometry is one of three types: parabolic, elliptic, or loxodromic. Since α and β generate $\mathbb{Z} \times \mathbb{Z}$, they must commute. This is possible only if α and β are parabolic, fixing the same point on the boundary at infinity, or if α and β share the same axis (exercise 5.11).

If α and β are parabolic, fixing a point at infinity, then they must fix an entire horosphere about infinity. Conjugating to put their fixed point at ∞ in $\partial\mathbb{H}^3$, they are of the form $\alpha(z) = z + a$, $\beta(z) = z + b$. Hence they restrict to Euclidean isometries on the horosphere, and the hyperbolic structure is complete.

Now suppose α and β are not parabolic. In this case, because α and β commute but are not parabolic, they share an axis, and are both given by rotation and/or dilation along this axis. The hyperbolic structure is not complete, and the axis must be exactly the geodesic whose points are omitted from the developing image of C for each horosphere.

DEFINITION 6.10. Suppose the interior of M has a hyperbolic structure, and C is a cusp torus of M , with $N(C)$, homeomorphic to $T^2 \times I$, a neighborhood of C . Let $\alpha, \beta \in \pi_1(C)$ be generators. Suppose the interior of M has a hyperbolic structure, and the holonomy elements corresponding to α and β are not parabolic, so they share an axis. Fix a direction on the axis of α and β . Any element γ of $\pi_1(C)$ translates some signed distance d along the axis, and rotates by total angle $\theta \in \mathbb{R}$, where the sign of θ is given by the right hand rule. Let $\mathcal{L}(\gamma) = d + i\theta$. The value $\mathcal{L}(\gamma)$ is called the *complex length* of γ . This defines a function \mathcal{L} from $\pi_1(C) = H_1(C; \mathbb{Z})$ to \mathbb{C} .

Notice that if $\gamma = p\alpha + q\beta$, then $\mathcal{L}(\gamma) = p\mathcal{L}(\alpha) + q\mathcal{L}(\beta)$, so \mathcal{L} is a linear map. We may extend it canonically to a linear map $\mathcal{L}: H_1(C; \mathbb{R}) \rightarrow \mathbb{C}$. The value $\mathcal{L}(c)$ for any $c \in H_1(C; \mathbb{R}) \cong \mathbb{R}^2$ will be called the complex length of c .

Suppose that the complex length of a simple closed curve γ on C equals $2\pi i$. Then in the completion of M , γ will bound a smooth hyperbolic disk. This implies that the completion of M is a manifold homeomorphic to the Dehn filled manifold $M(\gamma)$, and that $M(\gamma)$ admits a complete hyperbolic structure.

Suppose instead that the complex length of a closed curve γ on C equals $\theta i \neq 2\pi i$. Then in the completion of M , γ will bound a hyperbolic cone, with cone angle θ . The completion of M is still homeomorphic to the Dehn filled manifold $M(\gamma)$. However, the metric on $M(\gamma)$ inherited from the completion of M is not smooth. The core of the added solid torus is the singular locus, with cone angle θ .

For an incomplete structure, there will be a unique element $c \in H_1(C; \mathbb{R})$ so that $\mathcal{L}(c) = 2\pi i$.

DEFINITION 6.11. We say $c \in H_1(C; \mathbb{R})$ such that $\mathcal{L}(c) = 2\pi i$ is the *Dehn filling coefficient* of the boundary component C .

When c is of the form (p, q) , with p and q relatively prime integers, it corresponds to a simple closed curve and the completion is smooth.

We have been looking at a fixed incomplete hyperbolic structure on M , and examining possible completions for this fixed structure. Now we turn our attention to a topological manifold X , homeomorphic to M , and consider all possible hyperbolic structures on X .

DEFINITION 6.12. Let X be a 3-manifold with cusp torus C . The subset of $H_1(C; \mathbb{R})$ consisting of Dehn filling coefficients of hyperbolic structures on X is called the *hyperbolic Dehn filling space* for X .

If X admits a complete hyperbolic structure, then we let ∞ correspond to the complete hyperbolic structure on X .

THEOREM 6.13 (Thurston’s hyperbolic Dehn filling theorem). *Let X be a 3-manifold homeomorphic to the interior of a compact manifold with boundary a single torus T , such that X admits a complete hyperbolic structure. Then hyperbolic Dehn filling space for X always contains an open neighborhood of ∞ in $\mathbb{R}^2 \cup \{\infty\} \cong H_1(T; \mathbb{R}) \cup \{\infty\}$.*

More generally, if X is the interior of a compact manifold with torus boundary components T_1, \dots, T_n , and X admits a complete hyperbolic structure, then the hyperbolic Dehn filling space for X contains an open neighborhood of ∞ for each T_i .

Theorem 6.13 is an important result, and the result, its proofs, and its extensions continue to have useful consequences. The first proof of theorem 6.13 was sketched in Thurston’s 1979 notes [Thu79], and uses results on holonomy representations. A proof in the case that X admits a geometric triangulation was given in [NZ85], presented with expanded details in [BP92]. This proof was extended to the case of more general hyperbolic 3-manifolds by Petronio and Porti [PP00]. Martelli puts these proofs together to give a complete exposition in his recent book [Mar16]. Additionally, precise universal bounds on the size of the open neighborhood of infinity provided by the theorem were given by Hodgson and Kerckhoff [HK05], about 25 years after theorem 6.13 was proved. All the proofs require work.

In chapters 8 and 13 we will give full proofs of related results that are weaker than what is claimed in theorem 6.13. Here, we provide only a short sketch of the argument that goes into the proof of theorem 6.13, and then focus on applications.

PROOF SKETCH OF THEOREM 6.13. Suppose first that X is homeomorphic to the interior of a compact manifold with a single torus boundary component T , and X admits a complete hyperbolic structure.

Because X is hyperbolic, there is a holonomy representation

$$\rho: \pi_1(X) \rightarrow \mathrm{PSL}(2, \mathbb{C})$$

whose image is a discrete group. The fundamental group of the cusp torus $\pi_1(T)$ has image generated by two parabolics $\rho(\alpha)$ and $\rho(\beta)$, which we may assume fix the point at infinity in \mathbb{H}^3 .

Now Thurston shows that there exists a one-complex parameter family of deformations of the holonomy representation [Thu79, Theorem 5.6].

Each small deformation of the complete hyperbolic structure taking $\rho(\alpha)$ to a loxodromic must take $\rho(\beta)$ to a loxodromic with the same fixed points.

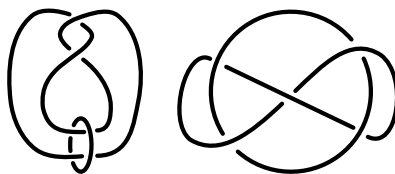


FIGURE 6.2. Two diagrams of the Whitehead link.

As in the discussion above, this extends to an incomplete hyperbolic structure, with Dehn filling coefficient some complex number $d + i\theta = z$, and where $z = \infty$ corresponds to the complete hyperbolic structure on X .

To complete the proof, one shows that z varies continuously over a neighborhood of infinity.

When there are $k > 1$ cusps, the proof is similar. In this case, there is a k -complex parameter family of deformations, with completions giving Dehn filling coefficients $d_1 + i\theta_1, \dots, d_k + i\theta_k$. Again one shows that these vary in a neighborhood of (∞, \dots, ∞) . \square

COROLLARY 6.14. *Let X be a manifold with a single torus boundary component such that the interior of X admits a complete hyperbolic metric. Then there are at most finitely many Dehn fillings of X which do not admit a complete hyperbolic metric.* \square

COROLLARY 6.15. *Let X be a manifold with n torus boundary components T_1, \dots, T_n . For each T_i , exclude finitely many Dehn fillings. The remaining Dehn fillings yield a manifold with a complete hyperbolic structure.* \square

Corollaries 6.14 and 6.15 follow immediately from theorem 6.13.

Notice that corollary 6.15 does not rule out the fact that a manifold with more than one torus boundary component may have infinitely many non-hyperbolic Dehn fillings, as in the following example.

EXAMPLE 6.16. The Whitehead link is the link shown in figure 6.2. We will see that it admits a complete hyperbolic structure (proposition 7.4).

If we erase one of the link components, that action can be seen as attaching a solid torus to the link complement in a trivial way. This is called *trivial Dehn filling*. For this example, perform trivial Dehn filling on the component that clasps itself in figure 6.2, leaving a single unknotted component, a trivial knot in S^3 . Its complement is a solid torus.

DEFINITION 6.17. A *lens space* is the 3-manifold obtained by gluing together two solid tori along their common torus boundary components.

Thus any Dehn filling of a trivial knot in S^3 is a lens space.

THEOREM 6.18. *A lens space cannot admit a hyperbolic structure.*

PROOF. Exercise 6.7. \square

There are infinitely many Dehn fillings on the trivial knot in S^3 that produce lens spaces. Thus there are infinitely many non-hyperbolic Dehn fillings of the Whitehead link complement.

The fundamental theorem of Wallace and Lickorish, theorem 6.5, implies that any closed orientable 3-manifold is obtained by Dehn filling a link complement in S^3 . In fact we may take that link complement to be hyperbolic, due to work of Myers [Mye93]. Thus the hyperbolic Dehn filling theorem implies that in some sense, “almost all” 3-manifolds are hyperbolic.

There are still many unanswered questions about hyperbolic Dehn filling space. As of the writing of this book, the following questions are all unknown.

QUESTION 6.19. What is the topology of hyperbolic Dehn filling space? For example, is it connected? Is it path connected? That is, if a finite volume manifold $M(s)$ admits a complete hyperbolic structure, and if M also admits a complete hyperbolic structure, is there necessarily a deformation of the hyperbolic structure running from the complete structure on M to the complete structure on $M(s)$?

Stronger: If $M(s)$ admits a complete hyperbolic structure, and M admits a complete hyperbolic structure, can we deform the hyperbolic structure on M through cone manifolds with cone angles increasing monotonically from 0 (at the complete structure on M) to 2π (at the complete structure on $M(s)$)?

As of the writing of this book, we do not even know if hyperbolic Dehn filling space is connected for the simplest of examples — the figure-8 knot complement. The following example is discussed in [CHK00].

EXAMPLE 6.20 (Dehn filling space for the figure-8 knot). Thurston identified part of the boundary of the neighborhood about infinity separating hyperbolic Dehn fillings from non-hyperbolic ones. This is done on pages 58 through 61 of his notes [Thu79]. To determine these boundaries, he considers what is happening to the two hyperbolic structures on the tetrahedra as the values of their edge invariants approach the boundaries given by the gluing equations (the boundaries of the region in figure 4.11). When both tetrahedra degenerate, the hyperbolic structure collapses and the limiting manifold is not hyperbolic.

However, when only one tetrahedron degenerates, we still have a hyperbolic structure for a little while. In this case, we will be gluing a positively oriented tetrahedron to a negatively oriented one. We can make sense of this by cutting the negatively oriented tetrahedron into pieces and subtracting them from the positively oriented one, leaving a polyhedron P . Faces of P may then be identified to give a hyperbolic structure. No one knows exactly where this stops working, although Hodgson’s 1986 PhD thesis [Hod86] gives evidence that the boundary should be as shown in figure 6.3.

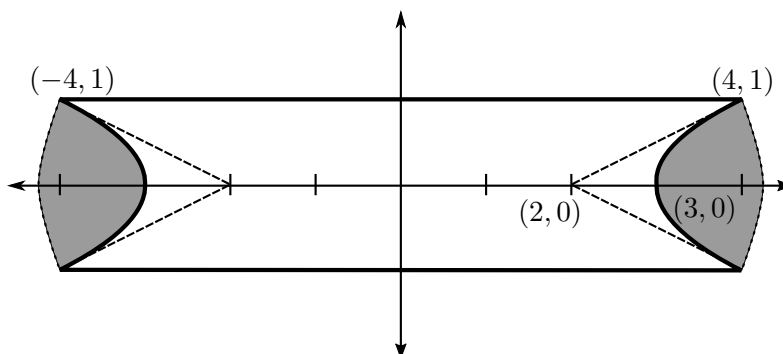


FIGURE 6.3. Hyperbolic Dehn filling space for the figure-8 knot complement is known to include the unshaded region exterior to the dark curve shown, is conjectured to contain the two shaded regions, and is conjectured to contain no other points. Figure modified from [CHK00]

In exercise 6.1, you are asked to study how tetrahedra degenerate in the figure-8 knot complement.

QUESTION 6.21. What is the hyperbolic Dehn filling space for the figure-8 knot complement?

DEFINITION 6.22. Dehn fillings that do not yield a hyperbolic manifold are called *exceptional*.

There are many interesting problems on exceptional Dehn fillings. We include an example, that as of the writing of this book is open.

It is known (and you can prove as an exercise) that no hyperbolic manifold can contain an embedded 2-sphere that does not bound a 3-ball. A manifold that contains such a 2-sphere is called *reducible*. If you start with a hyperbolic 3-manifold, perform Dehn filling, and obtain a reducible manifold, the Dehn filling is called *reducible*.

CONJECTURE 6.23 (The cabling conjecture). *No hyperbolic knot complement admits a reducible Dehn filling.*

The original wording of the cabling conjecture is that only cables of knots admit reducible Dehn fillings. The conjecture listed as conjecture 6.23 is the remaining case to prove.

6.3.1. Triangulations and Dehn filling. When X is a hyperbolic 3-manifold that admits an ideal triangulation, then Dehn filling of X can frequently be performed by adjusting the edge invariants, as in definition 4.4, of the ideal tetrahedra making up X . That is, given a triangulation of a 3-manifold X with torus boundary, we may solve a non-linear system of equations in the tetrahedra's edge parameters to find a hyperbolic structure

on a Dehn filling of X . To do so, use the edge gluing equations of chapter 4, but not the completeness equations.

Carefully, let μ and λ be generators of $H_1(\partial X)$, with associated completeness equations $H([\mu]) = H([\lambda]) = 1$, with $H([\mu]) = \prod_j z_{i_j}$ as in definition 4.12, and similarly for $H([\lambda])$.

Let $s = p\mu + q\lambda \in H_1(\partial X)$ be the slope of the Dehn filling. To find a complete hyperbolic structure on $X(s)$, we solve the system of equations consisting of edge gluing equations and the *Dehn filling equation*

$$(6.1) \quad p \log H([\mu]) + q \log H([\lambda]) = 2\pi i.$$

Note a solution to these equations will produce an incomplete hyperbolic structure on X , with Dehn filling coefficient $(p, q) \in H_1(\partial X; \mathbb{R})$. In fact, this process is valid for any $(p, q) \in \mathbb{R} \oplus \mathbb{R} \cong H_1(\partial X; \mathbb{R})$, not just relatively prime integers.

The system of edge gluing equations along with equation (6.1) may not have a solution. If it does have a solution, it may not be the case that all tetrahedron parameters have positive imaginary part. For such a solution, the corresponding tetrahedra are not all positively oriented; some are negatively oriented as well.

In practice, it is possible to implement this process by computer, to find solutions to gluing and Dehn filling equations numerically, and this has been implemented in SnapPy [CDGW16]. Indeed, in 2009, Schleimer and Segerman investigated hyperbolic Dehn filling space for thousands of manifolds, using SnapPy [SS09]. Graphically, they identified regions of hyperbolic Dehn filling space for which SnapPy computed positively oriented tetrahedra, negatively oriented tetrahedra, and degenerate tetrahedra, as well as regions for which no solution was found.

Schleimer and Segerman's computed space for the figure-8 knot is shown in figure 6.4. Green regions are those for which the computer found a solution with all positively oriented tetrahedra. Blue regions are those for which the computer only found solutions with some negatively oriented tetrahedra. In the white regions, the computer failed to recognize a solution. The gray region around the origin is where no solution was found. The shading in green and blue regions corresponds to volume; lines in those regions are level sets of volume. It is difficult to see in the printed version, but there is also a thin red line between green and white regions. Red indicates that all tetrahedra are flat and non-degenerate, i.e. the cross-ratio of the four ideal points for each tetrahedron is real, but bounded away from 0, 1, and ∞ . Any point where at least one tetrahedron is degenerate, i.e. its cross-ratio is near 0, 1, or ∞ , would be shaded purple.

Note that the green and blue regions away from the origin in figure 6.4 match the conjectured picture for Dehn filling space in figure 6.3. The blue and green regions in the interior are conjectured to be noise, and not to correspond to actual hyperbolic structures.

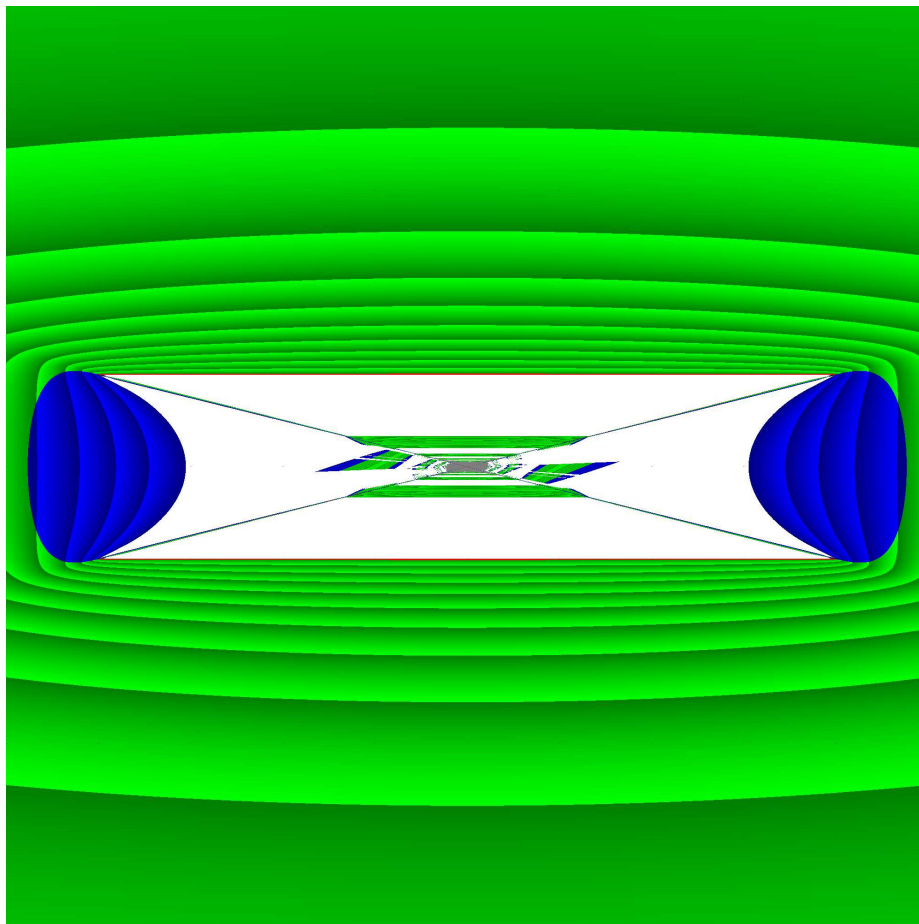


FIGURE 6.4. Computer generated picture of hyperbolic Dehn filling space for the figure-8 knot complement, generated by Schleimer and Segerman. Compare with the conjectural picture of the space, figure 6.3

In addition, we include Schleimer and Segerman's images of hyperbolic Dehn filling space for the 5_2 knot, and for the 6_3 knot, in figure 6.5 and figure 6.6, respectively. The color scheme is the same as for the figure-8 knot, above. The triangulation used in these cases is known as the *canonical triangulation*, which will be defined in chapter 10. Using different triangulations can lead to different regions of negatively oriented triangles. However, the boundary between hyperbolic and non-hyperbolic structures (green or blue versus white regions) seems to be independent of choice of triangulation. These figures and many more can be found on Segerman's website [SS09].

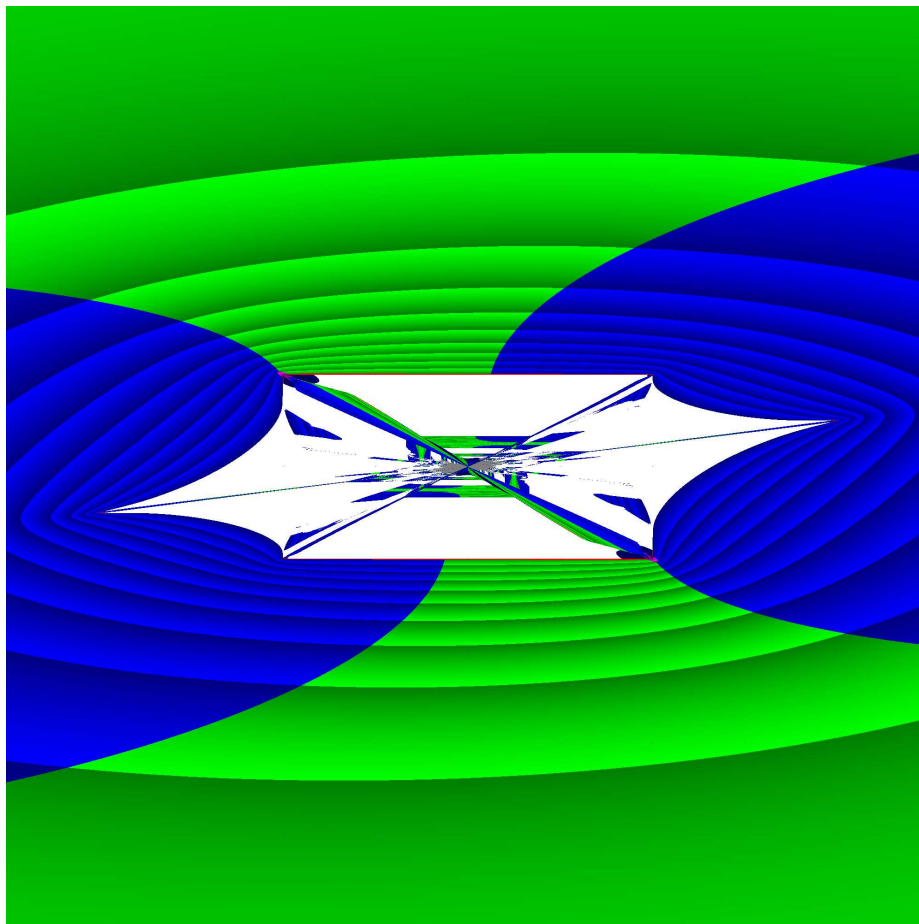


FIGURE 6.5. Computer generated picture of hyperbolic Dehn filling space for the 5_2 knot complement, generated by Schleimer and Segerman

6.4. A brief summary of geometric convergence

Theorem 6.13, the hyperbolic Dehn filling theorem, actually gives information on convergence of geometry of spaces. The 3-manifolds obtained by hyperbolic Dehn filling on a complete hyperbolic manifold M are “close” geometrically to M . This statement can be made precise, and often explicit, which is very useful: if we can bound geometric quantities for M , then the fact that (certain) Dehn fillings are geometrically close often translates into a bound on the same geometric quantities for Dehn fillings.

In this section, we define convergence of spaces and state a stronger version of the hyperbolic Dehn filling theorem that includes such convergence. We also survey briefly a few results and consequences of these results.

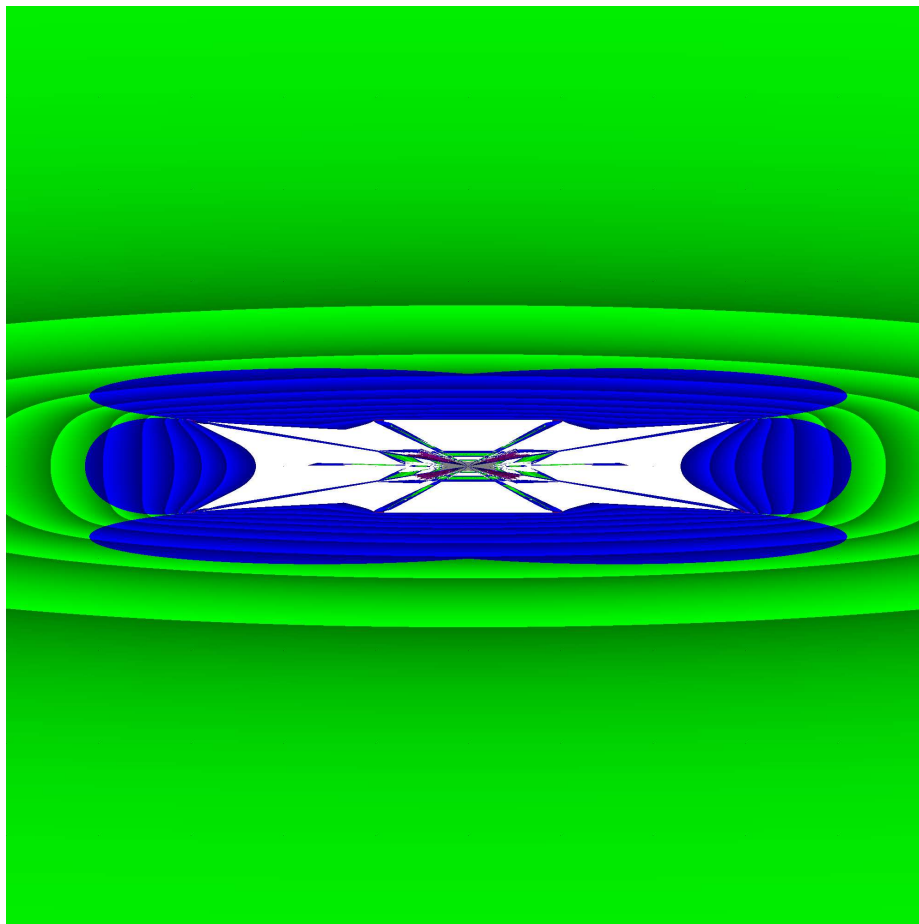


FIGURE 6.6. Computer generated picture of hyperbolic Dehn filling space for the 6_3 knot complement, generated by Schleimer and Segerman

6.4.1. Convergence of spaces. Given two abstract metric spaces, we need a way to measure distance between them, and to describe when a sequence of spaces converges to another space. Convergence of metric spaces has been studied by Gromov [Gro99]. In the case of hyperbolic spaces, [CEG06], [BP92, Chapter E], [Kap01, Chapter 8], and [CHK00, Chapter 6] give further details and examples.

There are actually several different definitions of geometric convergence of metric spaces in the literature on hyperbolic 3-manifolds and cone manifolds, which can be confusing. However, many are equivalent; see for example [CEG06, Theorem 3.2.9] and [Kap01, Theorem 8.11]. We give one definition here, as well as some examples that motivate other equivalent definitions.

One way of measuring “distance” between spaces is via quasi-isometries.

DEFINITION 6.24. Let X and Y be metric spaces with distance functions d_X and d_Y , respectively. For $K > 1$ and $c > 0$, a bijection $f: X \rightarrow Y$ is a (K, c) -quasi-isometric embedding if for all distinct points $x, y \in X$,

$$\frac{1}{K}d_X(x, y) - c \leq d_Y(f(x), f(y)) \leq Kd_X(x, y) + c.$$

Let $f: X \rightarrow Y$ be a (K, c) -quasi-isometric embedding. We say f is a (K, c) -quasi-isometry if there also exists a map $\bar{f}: Y \rightarrow X$ that is a (K, c) -quasi-isometric embedding as well as an *approximate inverse*:

$$\text{for all } x \in X \text{ and } y \in Y, d_X(\bar{f} \circ f(x), x) \leq c \text{ and } d_Y(f \circ \bar{f}(y), y) \leq c.$$

DEFINITION 6.25. Let $\{X_n\}$ be a sequence of metric spaces, each with a basepoint $x_n \in X_n$. Let X be a metric space with basepoint $x \in X$. Let $B_r(x_n)$ denote the set of points in X_n with distance at most r from x_n . Similarly, let $B_r(x)$ denote the set of points in X with distance at most r from x .

We say that the sequence (X_n, x_n) converges to the metric space (X, x) in the *quasi-isometric topology* (or *Gromov–Hausdorff topology* or *geometric topology*) if the following holds.

Suppose that for all $\epsilon > 0$ and all $r > 0$ there exists an integer N such that if $n > N$, then there exists a $(1 + 1/n, \epsilon)$ -quasi-isometry

$$f_n: B_r(x_n) \rightarrow B_r(x).$$

In this case, we also say that the space X is a *geometric limit* of the sequence X_n . The spaces X_n *converge geometrically* to X .

In other words, the spaces X_n with basepoints x_n converge in the quasi-isometric topology, or converge geometrically, if there are better and better quasi-isometries between larger and larger closed and bounded sets about the basepoints. The maps f_n are becoming closer and closer to actual isometries on larger and larger compact sets.

Notice that a basepoint, and compact sets around basepoints, feature prominently in the definition. The choice of basepoint does affect geometric limits, as the following example shows.

EXAMPLE 6.26 (A 2-dimensional geometric limit). Suppose S is a compact surface with genus three. Let $\gamma \subset S$ be a simple closed curve such that cutting S along γ yields two components: a genus one surface with one boundary component and a genus two surface with one boundary component. Let X_n be the metric space obtained by giving S a hyperbolic metric in which γ has length $1/n$. Let x_n be a basepoint that lies on the genus one side of γ in X_n and let y_n be a basepoint that lies on the genus two side. See figure 6.7.

Then (X_n, x_n) has a geometric limit (X, x) such that X is homeomorphic to a torus with one cusp, as shown on the left of figure 6.7. However, (X_n, y_n) has a geometric limit (Y, y) where Y is homeomorphic to a genus two surface

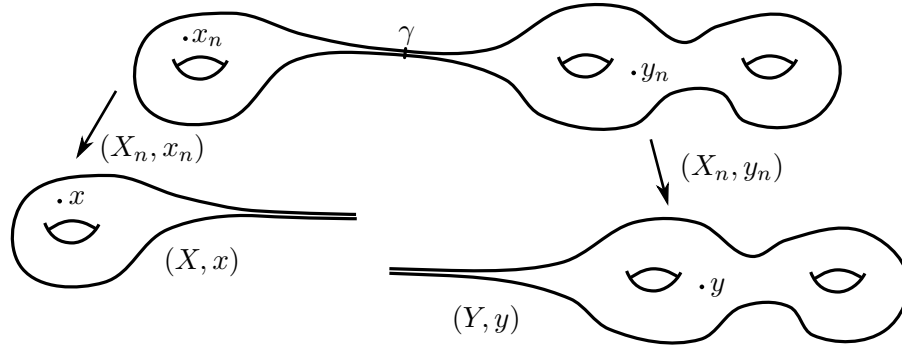


FIGURE 6.7. Changing the basepoint from x_n to y_n can change the homeomorphism type of a geometric limit.

with one cusp, as shown on the right of figure 6.7. Thus changing the basepoint can change the homeomorphism type of a geometric limit.

The following gives a 3-dimensional example of geometric convergence.

EXAMPLE 6.27 (Geometric convergence of ideal tetrahedra). Consider a sequence of ideal tetrahedra T_n in \mathbb{H}^3 with vertices at $0, 1, \infty$, and z_n , where z_n is converging to some $z_\infty \in \mathbb{C}$ with $\Im(z_\infty) > 0$. For n sufficiently large, there will be a point $p \in \mathbb{H}^3$ in the interior of all tetrahedra T_n and in the ideal tetrahedron T_∞ with vertices at $0, 1, \infty$, and z_∞ . For fixed $R > 0$, consider the compact set given by taking the intersection of T_n with a closed ball $B_R(p) \subset \mathbb{H}^3$. For large n , there will be better and better quasi-isometries from the balls $B_R(p) \cap T_n$ to $B_R(p) \cap T_\infty$. It follows that the ideal tetrahedra (T_n, p) converge geometrically to the ideal tetrahedron (T_∞, p) .

EXAMPLE 6.28 (Polyhedral convergence). More generally, suppose M is a complete hyperbolic 3-manifold obtained by gluing faces of an ideal polyhedron (possibly with infinite volume) in \mathbb{H}^3 , and suppose M_n is another complete hyperbolic 3-manifold obtained by face-pairings of slightly deformed polyhedra, with face-pairings of M_n pairing the same (combinatorial) faces as those of M . Suppose also that the polyhedra making up M_n converge geometrically to those making up M as $n \rightarrow \infty$, with appropriate basepoints. Then with the same basepoints, (M_n, x_n) converges to (M, x) in the quasi-isometric topology. This is made precise in [Mar07]; convergence of spaces in this manner is called *polyhedral convergence*.

Finally, taking the example one step farther, note that face-pairings are isometries in $\mathrm{PSL}(2, \mathbb{C})$, generating a discrete group G_n when M_n is hyperbolic. If M is also hyperbolic, with face-pairings generating the discrete group G , we say that the sequence of groups G_n converges to G *geometrically*. These notions of convergence can be shown to be equivalent to convergence in the quasi-isometric topology; for example see [Kap01, theorem 8.11].

Our main reason for defining geometric convergence is that it allows us to restate a much stronger version of Thurston's hyperbolic Dehn filling theorem, theorem 6.13, as follows.

THEOREM 6.29 (Hyperbolic Dehn filling with geometric convergence). *Let M admit a complete hyperbolic structure with fixed horoball neighborhood of a cusp C . Let s_n be a sequence of slopes on ∂C such that the length of a geodesic representative of s_n , measured in the induced Euclidean metric on ∂C , approaches infinity. Then for large enough n , the Dehn filled manifolds $M(s_n)$ are hyperbolic and approach M as a geometric limit.*

Similarly, if M has multiple cusps, then Dehn filled manifolds along slopes with lengths approaching infinity approach M as a geometric limit.

PROOF IDEA. In the proof sketch of Thurston's hyperbolic Dehn filling theorem, theorem 6.13, we noted that incomplete hyperbolic structures on M can be obtained by one-complex parameter families of deformations of the complete hyperbolic structure. These deformations are continuous maps in the quasi-isometric topology. \square

6.4.2. Some consequences of geometric convergence. The fact that M is a geometric limit in theorem 6.29 implies that geometric properties of Dehn fillings of M converge to those of M . For example, the thick parts of a cusped finite-volume manifold and its high Dehn fillings will be quasi-isometric. A geodesic in the cusped manifold will map to curves that will eventually be isotopic to geodesics in the filled manifolds, with lengths approaching the length of the original. Unfortunately, theorem 6.29 does not give any information on how high the Dehn fillings need to be in order to guarantee concrete bounds on geometry change. However, since the theorem appeared, there has been progress in making it more concrete.

For example, the volume of a finite volume hyperbolic 3-manifold M is one of its most useful geometric properties. If 3-manifolds M_n converge to M as a geometric limit, then their volumes converge:

$$\lim_{n \rightarrow \infty} \text{vol}(M_n) \rightarrow \text{vol}(M).$$

Much more can be said on volumes and Dehn filling. As a first step, the following theorem is also due to Thurston, and appears in the same notes in which he outlined the proof of theorem 6.29, as [Thu79, theorem 6.5.6].

THEOREM 6.30 (Volume under Dehn filling). *If M is hyperbolic with cusp C , and s is a slope on ∂C such that $M(s)$ is hyperbolic, then*

$$\text{vol}(M) > \text{vol}(M(s)).$$

Similarly if M has multiple cusps C_1, \dots, C_n and slopes s_1, \dots, s_n , one on each C_j , such that $M(s_1, \dots, s_n)$ is hyperbolic, then

$$\text{vol}(M) > \text{vol}(M(s_1, \dots, s_n)).$$

While theorem 6.29 implies that volumes of $M(s)$ approach volumes of M , theorem 6.30 implies that volume strictly decreases under Dehn filling for any slope giving a hyperbolic manifold. The slope need not be in the neighborhood of infinity provided by theorem 6.13; the volume decreases regardless.

The full proof of theorem 6.30 can be found in [Thu79]. In this book, we will give a full proof of a slightly weaker result in chapter 9, so we will delay the discussion of the proof ideas until then.

For volumes, even more can be said, and there have been concrete results bounding the change in volume under Dehn filling by Neumann and Zagier [NZ85] and by Hodgson and Kerckhoff [HK05], among others. We state one additional result along these lines here.

Note that if M has a complete hyperbolic structure with cusp C , then ∂C has a Euclidean structure, and any slope $s \subset \partial C$ is isotopic to a geodesic with well-defined Euclidean length $\ell_{\partial C}(s)$. Provided the length of s is at least 2π , a lower bound on volume under Dehn filling can also be obtained. We will prove the following theorem in chapter 13.

THEOREM 6.31 ([FKP08]). *Suppose M is a hyperbolic manifold with cusps C_1, \dots, C_n and slopes s_1, \dots, s_n , one on each ∂C_i , such that the minimal length slope $\ell_{\min} = \min\{\ell_{\partial C_j}(s_j)\}$ has length at least 2π . Then the Dehn filled manifold $M(s_1, \dots, s_n)$ is hyperbolic with volume satisfying*

$$\text{vol}(M(s_1, \dots, s_n)) \geq \left(1 - \left(\frac{2\pi}{\ell_{\min}}\right)^2\right)^{3/2} \text{vol}(M).$$

6.5. Exercises

EXERCISE 6.1. (Incomplete structures on the figure-8 knot) Thurston's notes contain a figure showing all parameterizations of hyperbolic structures on the figure-8 knot [Thu79, page 52]. For any w in this region, formula 4.3.2 in the notes gives us a corresponding z so that if two tetrahedra with edge invariants z and w are glued, we obtain a (possibly incomplete) hyperbolic structure on the figure-8 knot.

Analyze what happens to the tetrahedra corresponding to z and to w as w approaches a point on the boundary of this region.

More specifically, if w approaches certain points on the boundary of this region, tetrahedra corresponding to both z and w start to become degenerate. Which points are these? Prove that the two tetrahedra are becoming degenerate in this case.

As w approaches other values on the boundary, only one of the tetrahedra degenerates. Which points are these? Prove that only one tetrahedron is degenerating in this case.

EXERCISE 6.2. We have seen that the completion of an incomplete hyperbolic 3-manifold is no longer homeomorphic to the original hyperbolic 3-manifold. Is this true for completions of incomplete structures on the

3-punctured sphere? What surface do we obtain when we complete an incomplete hyperbolic structure on a 3-punctured sphere? Prove it.

EXERCISE 6.3. Suppose M is a closed manifold with a complete hyperbolic structure. Prove that $\pi_1(M)$ cannot contain a $\mathbb{Z} \times \mathbb{Z}$ subgroup. Conclude that M cannot contain an embedded torus T such that $\pi_1(T)$ injects into $\pi_1(M)$. [Such a torus is called *incompressible*. A Dehn filling resulting in a closed manifold with an embedded incompressible torus is another example of an exceptional filling.]

EXERCISE 6.4. Let M be an orientable 3-manifold with a decomposition into ideal polyhedra, each with a hyperbolic structure, such that the polyhedra induce a hyperbolic structure on M . Let v be an ideal vertex of M , i.e. an equivalence class of ideal vertices of the polyhedra, where vertices are equivalent if and only if they are identified under the gluing of the polyhedra.

Recall that $\text{link}(v)$ is defined to be the boundary of a neighborhood of v in M .

- (a) Prove $\text{link}(v)$ always inherits a similarity structure from the hyperbolic structure on M . Here a similarity structure is a $(\text{Sim}(\mathbb{E}^2), \mathbb{E}^2)$ -structure, where $\text{Sim}(\mathbb{E}^2)$ is a subgroup of the group of affine transformations consisting of elements of the form $x \mapsto Ax + b$, where A is a linear map that rotates and/or scales only. Thus $\text{Sim}(\mathbb{E}^2)$ is formed by rotations, scalings, and translations.
- (b) Prove that the only closed, orientable surface which admits a similarity structure is a torus. It follows that $\text{link}(v)$ is always homeomorphic to a torus when M is an orientable manifold with hyperbolic structure (even incomplete).

EXERCISE 6.5. Let M be an orientable 3-manifold that admits an incomplete hyperbolic structure with completion given by attaching the one-point compactification of a cusp neighborhood $N(C)$. Prove that the completion is not a manifold.

EXERCISE 6.6. Prove that a reducible manifold cannot be hyperbolic. That is, it admits no complete hyperbolic structure.

EXERCISE 6.7. Prove that a lens space cannot admit a complete hyperbolic structure.

EXERCISE 6.8. (On complex length of A in $\text{PSL}(2, \mathbb{C})$)

- (a) Suppose $A \in \text{PSL}(2, \mathbb{C})$ has axis the geodesic from 0 to ∞ . Then the matrix of A may be parameterized by a single complex number λ . What is the form of this matrix?
- (b) Denote the trace of a matrix A by $\text{tr}(A)$, and its complex length by $\mathcal{L}(A)$. Prove that $\text{tr}(A) = 2 \cosh(\mathcal{L}(A)/2)$.

EXERCISE 6.9. By computer, investigate the hyperbolic Dehn filling space obtained by filling a single component of the Whitehead link. Identify regions for which the result has a decomposition into positively oriented tetrahedra, negatively oriented tetrahedra, etc.

EXERCISE 6.10. (Algebraic versus geometric convergence) The purpose of this exercise is to work through a basic example of Thurston [Thu79] showing a difference between algebraic and geometric convergence of discrete groups. Let $A_n \in \text{PSL}(2, \mathbb{C})$ have matrix representation

$$A_n = \begin{pmatrix} \exp(w_n) & n \sinh(w_n) \\ 0 & \exp(-w_n) \end{pmatrix} \quad \text{where} \quad w_n = \frac{1}{n^2} + i\frac{\pi}{n}.$$

- (1) Show that the matrices A_n converge to the matrix $A = \begin{pmatrix} 1 & i\pi \\ 0 & 1 \end{pmatrix}$; thus the group $\langle A_n \rangle$ converges algebraically to the group $\langle A \rangle$.
- (2) Show that $\langle A_n \rangle$ does not converge geometrically to the group $\langle A \rangle$, by finding a subsequence A_{n_j} converging to an element of $\text{PSL}(2, \mathbb{C})$ that does not lie in $\langle A \rangle$.

Part 2

Tools, Techniques, and Families of Examples

CHAPTER 7

Twist Knots and Augmented Links

In this chapter, we study a class of knots that have some of the simplest hyperbolic geometry, namely twist knots. This class includes the figure-8 knot, the 5_2 knot, and the 6_1 knot that we have encountered so far. We also generalize to give examples of knots and links whose geometry is relatively explicit. This will equip us with many examples.

From now on, we say a knot or link in S^3 is *hyperbolic* if its complement $S^3 - K$ admits a complete hyperbolic structure. Similarly, a *hyperbolic 3-manifold* is a 3-manifold that admits a complete hyperbolic structure. Note that the completeness of the hyperbolic structure is implied in this terminology.

7.1. Twist knots and Dehn fillings

Recall the definition of twist knots from chapter 0.



FIGURE 7.1. A twist region of a diagram

A twist region is a string of bigon regions in the diagram graph of a knot diagram, with the bigons arranged end-to-end at their vertices, as in figure 7.1. Recall also that a twist region is maximal in the sense that there are no additional bigon regions meeting the vertices on either end. A single crossing adjacent to no bigons is also a twist region. Recall also that twist regions are required to be alternating.

The *twist knot* $J(2, n)$, defined in definition 0.12, is the knot with a diagram consisting of exactly two twist regions, one of which contains two crossings, and the other containing $n \in \mathbb{Z}$ crossings. The direction of crossing depends on the sign of n .

Twist knots $J(2, 2)$, $J(2, 3)$, $J(2, 4)$, and $J(2, 5)$ are shown again in figure 7.2.

DEFINITION 7.1. The *Whitehead link* is the link shown in figure 7.3. Note the two links shown are isotopic.

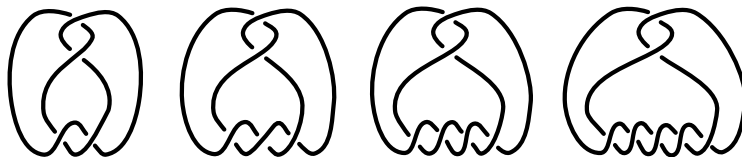


FIGURE 7.2. Twist knots $J(2, 2)$ (the figure-8 knot), $J(2, 3)$ (the 5_2 knot), $J(2, 4)$ (the 6_1 or Stevedore knot), and $J(2, 5)$

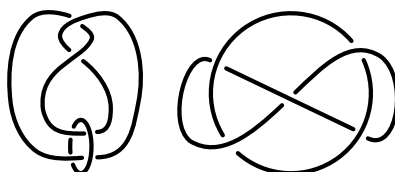


FIGURE 7.3. Two diagrams of the Whitehead link.

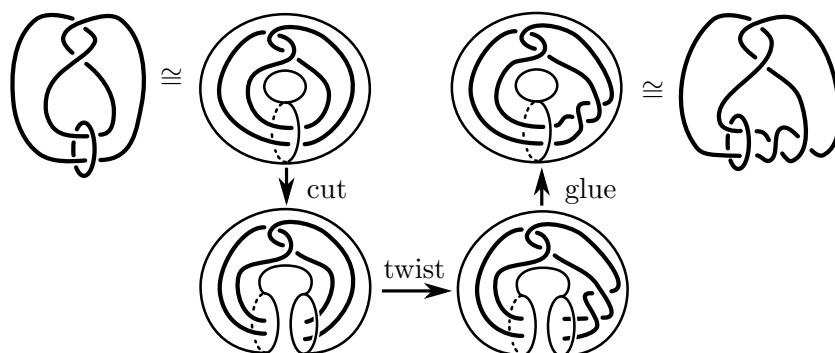


FIGURE 7.4. The Whitehead link complement is homeomorphic to a knot in a solid torus, which we cut, twist, and reglue. The result is homeomorphic to the complement of $J(2, 2) \cup U$

We will show in proposition 7.4 that the complement of the Whitehead link is hyperbolic.

PROPOSITION 7.2. *The complement of the twist knot $J(2, n)$ is obtained by Dehn filling the hyperbolic manifold isometric to the complement of the Whitehead link.*

PROOF. The proof uses topological properties of the sphere S^3 and the solid torus. Recall first that the sphere S^3 is the union of two solid tori whose cores are linked exactly once, but each core alone is unknotted.

The diagram of the Whitehead link on the left of figure 7.3 has a component at the bottom that is unknotted and does not cross itself. The complement of this component in S^3 is a solid torus. Note then that the other component is a knot in a solid torus, as shown on the left of figure 7.4.

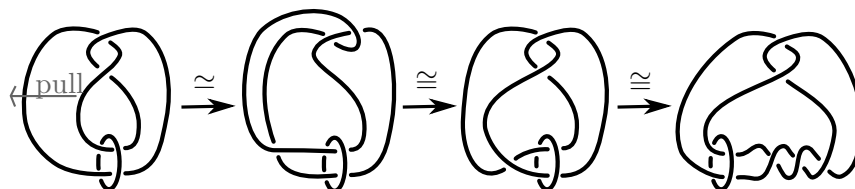


FIGURE 7.5. A sequence of homeomorphisms of the Whitehead link complement

Now we apply a homeomorphism to the solid torus, which we view as $S^1 \times D^2$. There is a homeomorphism given by slicing along a disk $\{x\} \times D^2$ of the solid torus, rotating one full time, then gluing back together. This homeomorphism is shown in the center of figure 7.4.

The homeomorphism replaces the original link in the solid torus by a link with two additional crossings. By applying the homeomorphism repeatedly, we see that the complement of the Whitehead link is homeomorphic to the complement of the link with any even number of crossings encircled by the unknotted component. In particular, it is homeomorphic to the complement of the link $J(2, 2k) \cup U$, where U is a single unknotted component. By the Mostow–Prasad rigidity theorem (theorem 6.1), these link complements have isometric hyperbolic structures.

To obtain the knot $J(2, 2k)$, attach a solid torus to $S^3 - (J(2, 2k) \cup U)$, filling in U in a trivial way to give $S^3 - J(2, 2k)$. Thus $J(2, 2k)$ is obtained from a manifold isometric to the complement of the Whitehead link by Dehn filling.

So far our proof only works for $J(2, n)$ with n even. Now we consider the case of the knot $J(2, 2k + 1)$, with odd second component. We may isotope the Whitehead link, starting with the diagram on the left of figure 7.3, to reverse the two crossings at the top, and insert a crossing encircled by the unknotted component at the bottom. This is shown in figure 7.5, left.

Following that figure, we may then reflect the diagram in the plane of projection, reversing all the crossings. This is a homeomorphism of the knot complement, hence an isometry. Now just as in the even case, we may insert any even number of crossings into the two strands encircled by the unknotted component. To obtain $J(2, 2k + 1)$, simply Dehn fill the unknotted component in the obvious way. \square

COROLLARY 7.3. *The complement of the Whitehead link is a geometric limit of $S^3 - J(2, n)$.*

PROOF. Because they are obtained by Dehn filling the complement of the Whitehead link, all but finitely many link complements $S^3 - J(2, n)$ lie in any given neighborhood of infinity in the Dehn surgery space for a cusp of the complement of the Whitehead link. Theorem 6.29 implies that the Whitehead link is therefore a geometric limit of these manifolds. \square

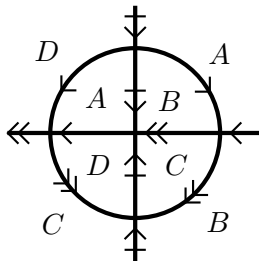


FIGURE 7.6. Shown is the boundary of an ideal octahedron (one vertex at infinity). Pairing faces as shown gives the complement of the Whitehead link.

In order to study the geometry of twist knots, we study the geometry of the geometric limit, the Whitehead link complement.

PROPOSITION 7.4. *The complete hyperbolic structure on the complement of the Whitehead link is obtained by gluing faces of a regular ideal octahedron, with the face pairings as shown in figure 7.6.*

A *regular ideal octahedron* is the ideal octahedron in \mathbb{H}^3 with all dihedral angles equal to $\pi/2$.

PROOF. The fact that the Whitehead link complement is obtained by face pairings of an ideal octahedron can be readily seen by applying the methods of chapter 1 to the diagram of the Whitehead link on the right of figure 7.3. After collapsing bigons, we obtain two ideal polyhedra with four triangular faces and one quadrilateral face. Glue the quadrilaterals to obtain an ideal octahedron. The form is shown in figure 7.6. We leave the details for exercise 7.2.

In a regular ideal octahedron, all dihedral angles are $\pi/2$, so horospheres intersect a neighborhood of each ideal vertex in a square. We need to check that the face pairings give a hyperbolic structure in this case. Note first that every point in the interior of an octahedron and in the interior of a face of the octahedron has a neighborhood isometric to a ball in \mathbb{H}^3 . We need to show that each point on an edge also has such a neighborhood, and then lemma 3.6 will imply that the gluing is a manifold with a (possibly incomplete) hyperbolic structure.

Note first that each of the edges (there are three) is glued four times. Thus the total angle around each edge will be $4\pi/2 = 2\pi$. This is not quite enough to show that each point on an edge has a neighborhood isometric to a ball in \mathbb{H}^3 , because composing the gluings around an edge may introduce nontrivial translation or scale. To show that this does not happen, consider each end of an ideal edge within a cusp. Any horosphere intersects a neighborhood of an ideal vertex of the regular ideal octahedron in a Euclidean square. Under the developing map, squares can only patch together in squares to give a tiling of the universal cover of each cusp by Euclidean

squares. There are four squares meeting around a vertex in the cusp corresponding to one of our ideal edges. Note that the squares cannot be scaled or sheared. It follows that edges glue up without shearing singularities, and the structure is hyperbolic.

To show that the structure is complete, we use theorem 4.10: the structure is complete if and only if for each cusp, the induced structure on the boundary is Euclidean. But as already noted, each cusp is tiled by Euclidean squares corresponding to intersections of a horosphere with an ideal vertex of the regular ideal octahedron. Under the developing map, squares can only patch together to give a Euclidean structure: there will be no rotation or scale. Thus the hyperbolic structure must be complete. \square

In chapter 9, we will obtain a formula to calculate the volume of a regular hyperbolic ideal octahedron. For now, we state that the volume is a constant $v_{\text{oct}} = 3.66\dots$

COROLLARY 7.5. *The volume of a hyperbolic twist knot is universally bounded*

$$\text{vol}(S^3 - J(2, n)) < v_{\text{oct}},$$

and as $n \rightarrow \infty$, $\text{vol}(S^3 - J(2, n)) \rightarrow v_{\text{oct}}$.

PROOF. The Dehn filling bound follows immediately from Thurston's theorem on volume change under Dehn filling, theorem 6.30. The convergence follows from theorem 6.29. \square

We have not yet discussed which twist knots are hyperbolic. We have seen that the figure-8 knot is hyperbolic, and similar methods can be used to show each of the knots in figure 0.10 are hyperbolic. More generally, we will see in chapter 11 (or by other methods in chapter 10) that all twist knots $J(2, n)$ with $n \geq 2$ or $n \leq -3$ are hyperbolic. When $n = 1$ or -2 , the standard diagram of $J(2, n)$ can be easily reduced to a diagram with only a single twist region, which is not hyperbolic, and when $n = -1$ its diagram can be easily reduced to that of the unknot, which is also not hyperbolic. All other twist knots are hyperbolic.

7.2. Double twist knots and the Borromean rings

The results of the previous section generalize immediately to knots and links with exactly two twist regions, but with any number of crossings in either twist region.

DEFINITION 7.6. The *double twist knot or link* $J(k, \ell)$ is the knot or link with a diagram consisting of exactly two twist regions, one of which contains k crossings, and the other contains ℓ crossings, for $k, \ell \in \mathbb{Z}$. See figure 7.7. Note that $J(k, \ell)$ is a knot if and only if at least one of k, ℓ is even; otherwise it is a link with two components.

Just as for twist knots, double twist knots are obtained by Dehn filling a simple link complement.

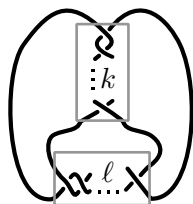


FIGURE 7.7. A double twist knot or link has two twist regions, one with k crossings and one with l crossings

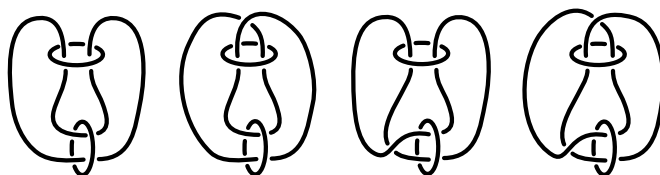


FIGURE 7.8. Complements of $J(k, \ell)$ are obtained by Dehn filling one of these four links. The link on the left is known as the Borromean rings.

PROPOSITION 7.7. *The complement of the link $J(k, \ell)$ is obtained by Dehn filling the complement of one of the four links shown in figure 7.8, depending on the parity of k and ℓ .*

PROOF. The proof is nearly identical to that of proposition 7.2, except now it is done in two steps, since there are two unknotted components. Apply a homeomorphism of a solid torus as in figure 7.5 two times. The details are left to the reader. \square

The link on the left of figure 7.8 is equivalent to a link more famously known as the *Borromean rings*; its more common diagram is shown in figure 7.18. We will call the other links of figure 7.8 the *Borromean twisted sisters*, and say the links are in the *Borromean family*. In fact, the middle two links are equivalent.

PROPOSITION 7.8. *The complements of the Borromean rings and the Borromean twisted sisters all admit complete hyperbolic structures obtained by gluing two regular ideal octahedra.*

PROOF. Because the Borromean rings has a diagram that is alternating, its complement can be split into ideal polyhedra using the methods of chapter 1. However, we present a new way to decompose the complements of links of the Borromean family that we will generalize below.

View the diagrams of figure 7.8 in three dimensions. The two link components in each diagram that will be Dehn filled to produce $J(k, \ell)$ should be viewed as lying perpendicular to the plane of the paper, which is the plane of projection $S^2 \subset S^3$. The other link component(s) should be viewed

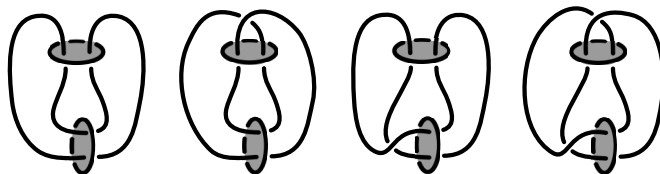


FIGURE 7.9. Shaded 2-punctured disks.

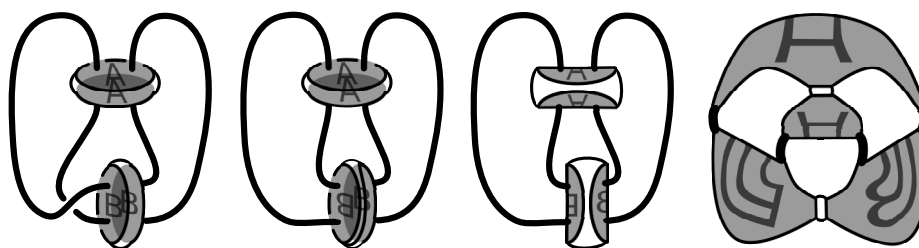


FIGURE 7.10. Left: slice 2-punctured disks up the middle (obtain parallel 2-punctured disks, shown here pulled apart). Middle left: Untwist single crossings. Middle right: Cut along plane of projection. Right: collapse remnants of the link to ideal vertices.

as lying in the plane of projection except at crossings; when the component crosses itself it dips briefly above or below the plane of projection, then returns to the plane.

The components lying perpendicular to the plane of projection are unknotted, and each bounds a 2-punctured disk, shown as shaded in figure 7.9.

As the first step of the decomposition, slice each of these disks up the middle, replacing a single 2-punctured disk with two parallel copies of the 2-punctured disk. This move is shown on the left of figure 7.10.

Now if a 2-punctured disk is adjacent to a crossing in the plane of projection, the next step is to rotate that 2-punctured disk 180° to unwind the crossing, as in the middle left of figure 7.10. Note this rotation pulls the diagram along with it on one side, but the rotation is only performed on the 2-punctured disk adjacent to the crossing, not on the parallel 2-punctured disk. After this step, all crossings in the plane of projection have been removed.

Next, cut along the plane of projection, splitting the complement into two identical pieces as in the middle right of figure 7.10.

Finally, for each piece, collapse remnants of the link to ideal vertices, as on the right of figure 7.10. We claim the result in that figure is topologically an octahedron. To see this, note it has two ideal vertices colored white, coming from crossing circles, and four ideal vertices colored black, coming from the component of the link on the plane of projection. There are four shaded faces that all have three edges, hence all shaded faces are triangles.

There are four white faces, including the one running through the point at infinity in the plane of projection, and each of these white faces also has three edges, so each is a triangle. Thus the result is an ideal octahedron. Recall that there is actually another octahedron coming from our decomposition: the other octahedron comes from the region below the plane of projection after slicing along that plane. So the link complements in the Borromean family all decompose into two ideal octahedra.

Note that the face pairings of the two ideal octahedra that give back the original link complement will be different for the different links; they can be found by tracing backwards through the decomposition process above. To undo the step of cutting along the plane of projection, we glue matching white faces of the opposite octahedra together in pairs. To undo the step of slicing along 2-punctured disks, we glue remaining shaded triangles in pairs; however there are two options depending on whether or not we untwisted a crossing. If both parallel 2-punctured disks were adjacent to no crossings, then corresponding shaded triangles on the same ideal octahedron are glued across an ideal vertex (one of the white vertices of figure 7.10). If there was an adjacent crossing, then a shaded triangle on one octahedron is glued to the opposite shaded triangle on the other octahedron across the (white) ideal vertex.

Finally, to see that these link complements all admit a complete hyperbolic structure, we give each of the two octahedra the geometry of a hyperbolic regular ideal octahedron, then argue as in the proof of proposition 7.4. We check: each edge of the decomposition comes from the intersection of a 2-punctured disk with the plane of projection, and each edge class in the manifold is obtained by gluing four such edges. Thus the total angle around each edge will be $4(\pi/2) = 2\pi$. Again horospheres meet ideal vertices in Euclidean squares, and so the developing image cannot scale, shear, or rotate these squares. Thus edges glue without shearing singularities, and cusps are Euclidean. Hence the result is a complete hyperbolic structure. \square

COROLLARY 7.9. *The volume of a double twist knot satisfies*

$$\text{vol}(J(k, \ell)) < 2v_{\text{oct}},$$

where $v_{\text{oct}} = 3.66\dots$ is the volume of a regular ideal octahedron.

7.3. Augmenting and highly twisted knots

The above procedure can be generalized.

DEFINITION 7.10. For any twist region of any link diagram, a new link is obtained by adding a single unknotted link component to the diagram, encircling the two strands of the link component. The link is said to be *augmented*. The added link component is called a *crossing circle*. We will refer to the original link components as *knot strands*.

When a crossing circle is added to each twist region of the diagram, the link is said to be *fully augmented*.

The complement of an augmented link is homeomorphic to the complement of the link with any even number of crossings added to or removed from the twist region, by the same argument illustrated in figure 7.4. Thus the complement of a fully augmented link is homeomorphic to the complement of the fully augmented link with one or zero crossings adjacent to each crossing circle. When there is one crossing adjacent to a crossing circle, we say the crossing circle is adjacent to a *half-twist*.

The four links of figure 7.8 are examples of fully augmented links. The decomposition of proposition 7.8 goes through more generally for all fully augmented links. This decomposition appears in the appendix to [Lac04] by Agol and D. Thurston. These links have very beautiful geometric properties, explored further in [FP07], [Pur07], [Pur08], and in the survey article [Pur11]. Some of these results are included below, modeled off the exposition in [Pur11].

THEOREM 7.11. *Let L be any fully augmented link, and assume we have applied a homeomorphism to $S^3 - L$ so that L has one or zero crossings adjacent to each crossing circle. Then the link complement $S^3 - L$ decomposes into two identical ideal polyhedra with the following properties.*

- (1) *Faces of the polyhedra can be checkerboard colored. White faces correspond to regions of the plane of projection. Shaded faces are all triangles, and come from 2-punctured disks bounded by crossing circles, which we call crossing disks.*
- (2) *Ideal vertices are all 4-valent (before gluing).*
- (3) *Gluing the polyhedra identifies exactly four edges to a single edge class in the link complement.*

PROOF. The decomposition is obtained very similarly to that in the proof of proposition 7.8. First, each crossing circle bounds a 2-punctured disk, which we shade. After applying a homeomorphism removing all pairs of crossings in each twist region, we may assume that the shaded disk is either adjacent to no crossings, or adjacent to a single crossing (half-twist).

Slice along the 2-punctured disks, splitting each into two parallel 2-punctured disks. Next, apply a 180° rotation to those 2-punctured disks adjacent to a crossing, unwinding the crossing. Then slice along the plane of projection, splitting the complement into two identical pieces. Finally, shrink remnants of the link to ideal vertices. We check that each item of the theorem holds.

First, note faces are already checkerboard colored, with shaded faces coming from 2-punctured disks and white faces coming from the plane of projection. Note that edges of the decomposition come from intersections of white and shaded faces. There are exactly three edges bordering each shaded face, so each shaded face is a triangle.

Ideal vertices of the polyhedra come from remnants of the link. For those ideal vertices coming from a component of the link in the plane of projection, the ideal vertex will be adjacent to two edges coming from the 2-punctured

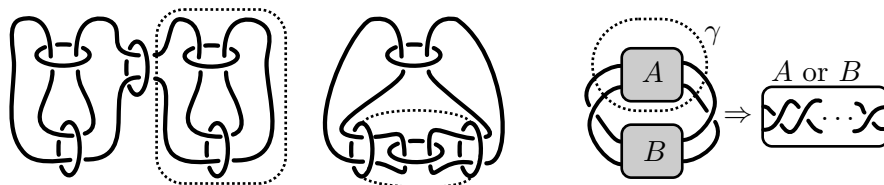


FIGURE 7.11. Left: a fully augmented link with a diagram that is not prime, with dotted lines indicating the closed curve contradicting the definition of prime. Middle: a fully augmented link that is not reduced, with parallel crossing circles indicated by the dotted lines. Removing one of the parallel crossing circles will give a reduced link. Right: The diagram is twist-reduced if one of the regions A or B consists only of bigons in a twist region.

disk on one of its ends, and two edges coming from the 2-punctured disk on its other end. Thus it is 4-valent. An ideal vertex coming from a crossing circle is also adjacent to four edges: two from each point where the link component meets the plane of projection.

Finally, note that each edge class contains four edges: two in each polyhedron lying on the parallel copies of the 2-punctured disk. \square

Just as with the family of Borromean rings, we can show that many of these links are hyperbolic, but not all. For example, if a fully augmented link has only one crossing circle, then the polyhedral decomposition of theorem 7.11 will have white bigon regions, and collapsing these will collapse the entire polyhedron to a triangle (exercise). Similarly, if there are parallel crossing circles then there will be white bigon faces. We wish to rule these out.

DEFINITION 7.12. A fully augmented link is called *reduced* if the following hold.

- (1) Its diagram is connected.
- (2) Its diagram is *prime*, i.e. any closed curve meeting the diagram twice bounds a region on one side with no crossings.
- (3) None of its crossing circles are parallel. That is, there are no closed curves in the diagram running over exactly two crossing circles and meeting exactly two white faces on either side of the two crossing circles. See figure 7.11.

Reduced fully augmented links come from adding crossing circles to links with reduced diagrams as in the sense of the following definition.

DEFINITION 7.13. A diagram is *twist-reduced* if whenever a simple closed curve γ meets the diagram exactly twice in two crossings, running from one side of each crossing to the opposite side, then the curve γ bounds a

portion of the diagram containing a string of bigons arranged end-to-end. See figure 7.11, right.

Note that if a diagram is not twist-reduced, then there exists a curve γ meeting the diagram in exactly two crossings, with those crossings not separated by a string of bigons. Because the two crossings are not separated by bigons, they lie in different twist regions. Augmenting the two twist regions results in two parallel crossing circles. Thus a diagram that is not twist-reduced has an associated fully augmented link that is not reduced.

We will encounter twist-reduced diagrams again, for example in definition 11.10. Meanwhile, the following gives a way of building large numbers of reduced fully augmented links.

LEMMA 7.14. *Let K be a link with a connected, prime, twist-reduced diagram. Then the fully augmented link obtained from K by adding crossing circles to each twist region gives a reduced fully augmented link.*

PROOF. Adding crossing circles to twist regions of a diagram does not change whether it is prime or connected. If the resulting fully augmented link is not reduced, there must be two parallel crossing circles. Thus in the original K , there are two distinct twist regions in the diagram with the property that when crossing circles are added around them, the crossing circles are parallel. Then an isotopy of one of the crossing circles to the other traces out two arcs on the plane of projection disjoint from K . Straightening these, and drawing arcs across K over the crossing circle defines a closed curve in the diagram whose boundary meets the diagram exactly twice, once in each of the two distinct twist regions. Isotope slightly to give a curve in K contradicting the definition of a twist-reduced diagram. \square

LEMMA 7.15. *Suppose a fully augmented link is reduced and contains at least two crossing circles. Then the polyhedra in the decomposition of theorem 7.11 admit a hyperbolic structure in which all dihedral angles are $\pi/2$.*

The proof of the lemma uses circle packings.

DEFINITION 7.16. A *circle packing* is a connected collection of circles with disjoint interiors. The *intersection graph* of a circle packing is the graph with a vertex at the center of each circle, and an edge between vertices whenever the corresponding circles are tangent.

Figure 7.12 shows an example of a circle packing and most of its intersection graph on the left — the vertex of the intersection graph in the unbounded region has been omitted.

THEOREM 7.17 (Circle packing theorem). *Let G be a finite planar graph that is simple, meaning G has no loops and no multiple edges between a pair of vertices. Then G is (isotopic to) the intersection graph of a circle packing on S^2 . If G is a triangulation of S^2 , then the circle packing is unique up to Möbius transformation.*

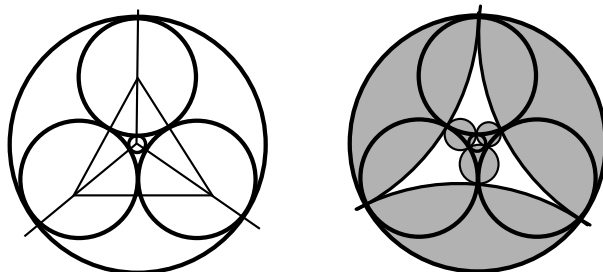


FIGURE 7.12. Left: A circle packing and its intersection graph. Right: Gray circles meeting white circles of a circle packing

Theorem 7.17 is also known as the Koebe–Andreev–Thurston theorem. It was first proved by Koebe [Koe36]. We will use it here without giving its proof, as the proof is somewhat unrelated to the topic at hand.

PROOF OF LEMMA 7.15. Consider a polyhedron P from theorem 7.11 for a reduced fully augmented link with at least two crossing circles. Edges and vertices of the polyhedron form a graph Γ on S^2 . Form a new graph G on S^2 by taking a vertex for each white face of Γ , and an edge between vertices of G if two white faces are adjacent across an ideal vertex of Γ .

If we superimpose G on P , then notice that each region of G will contain exactly one shaded triangular face of P . Thus G is a triangulation of S^2 . We show that G has no loops and no multiple edges.

Suppose first that G has a loop. Then the edge of G forming the loop can be superimposed on P to run from a white face, through an ideal vertex of P , then back to the same white face. White faces correspond to regions of the diagram, and ideal vertices correspond to remnants of the link. Thus there is a closed curve γ on the link diagram that runs from a region back to itself crossing over a single component of the link diagram. Because the link diagram consists of closed curves, this is possible only if the curve γ runs along a crossing circle from one white region back to the same white region. Pushing off the crossing circle slightly, this contradicts the fact that the diagram is prime.

Now suppose that the graph G has a multi-edge. Then there is a pair of white faces W_1 and W_2 of P and a pair of ideal vertices v_1 and v_2 such that v_1 and v_2 are both adjacent to W_1 and W_2 . Form a loop in P running from W_1 through v_1 to W_2 , then back through v_2 to W_1 . This loop corresponds to a loop γ in the diagram meeting the regions on the plane of projection corresponding to W_1 and W_2 and meeting two distinct link components between those regions. If the link components came from components on the plane of projection, then this contradicts the fact that the diagram is prime. If the link components came from crossing circles, then it contradicts the fact that the diagram is reduced. If one link component lies in the plane

of projection and the other is a crossing circle, then we may slide slightly off the crossing circle to obtain a loop meeting exactly three components in the plane of projection. This is impossible for a closed curve and closed link components.

It follows that G is a finite, simple, planar graph that is a triangulation of S^2 . The circle packing theorem, theorem 7.17, implies that there is a unique circle packing of S^2 with G as its intersection graph. View S^2 as the boundary at infinity of \mathbb{H}^3 . The circle packing of G is then a circle packing on $\partial\mathbb{H}^3$. Each Euclidean circle on $\partial\mathbb{H}^3$ is the boundary of a plane in \mathbb{H}^3 . Color these planes *white*.

Because the intersection graph of the circle packing is a triangulation, regions complementary to the circle packing meet exactly three circles from the packing. There is a unique Euclidean circle running through the three points of tangency of the circle packing. Again this defines a geodesic plane in \mathbb{H}^3 . This plane will intersect the white planes at right angles. Color this plane *gray*. See figure 7.12.

For each white plane, remove from \mathbb{H}^3 the region bounded by that plane that is disjoint from the other white planes. Similarly for each gray plane. The result is a right-angled hyperbolic ideal polyhedron that is isomorphic to P , proving the lemma. \square

THEOREM 7.18. *The complement of a reduced fully augmented link with at least two crossing circles admits a complete hyperbolic structure, which is obtained by putting a right-angled structure on each of the polyhedra of theorem 7.11.*

PROOF. By lemma 7.15, there exists a right-angled ideal hyperbolic polyhedron with the combinatorics of one of the polyhedron of theorem 7.11. We give each of the polyhedra of theorem 7.11 the hyperbolic structure of this right-angled hyperbolic polyhedron, and glue by corresponding face-pairing isometries to obtain the fully augmented link.

To show this admits a complete hyperbolic structure, we need to show the angle around each edge is 2π , that there is no shearing around edges, and that the cusps are all Euclidean. Because each edge class contains four edges, and each edge has dihedral angle $\pi/2$, the angle sum around each edge is 2π .

Now consider cusps. Any horosphere meets an ideal vertex of the right-angled polyhedron in a rectangle. The developing image of a cusp is obtained by gluing these rectangles according to the gluing isometries on the faces. Note that a white face is glued by a reflection to the identical white face on the opposite polyhedron, so gluing across white sides of a rectangle does not scale or rotate. But then the gluing across shaded faces cannot scale or rotate either. Hence the developing image of each cusp is a tiling of the plane by Euclidean rectangles. Thus around each vertex there cannot be shearing, and the structure on the cusp must be Euclidean. So this gives the complete hyperbolic structure on the fully augmented link. \square

COROLLARY 7.19. *In a reduced fully augmented link with at least two crossing circles, each shaded 2-punctured disk bounded by a crossing circle is a totally geodesic surface embedded in the link complement. The white surface, obtained by gluing together regions corresponding to regions on the plane of projection (white faces), is also a totally geodesic surface embedded in the hyperbolic link complement. Moreover, these shaded 2-punctured disks and white surfaces meet at right angles whenever they intersect.*

PROOF. In the polyhedral decomposition, these surfaces become white and shaded faces, which are straightened to portions of geodesic planes to obtain the hyperbolic structure. Thus we know that these surfaces are *pleated*, i.e. they decompose into ideal polygons, each of which is totally geodesic. In general pleated surfaces are bent along the edges bounding each polygon, so they are not necessarily totally geodesic. However, in this case, white faces meet shaded faces at angle $\pi/2$, thus in the gluing, white faces glue to white faces with angle π , i.e. no bending, and similarly for shaded faces. It follows that these surfaces are totally geodesic. \square

7.4. Cusps of fully augmented links

For many applications in later chapters, it will be useful to know more explicit information about the geometry of fully augmented links, particularly the geometry of their *cusps*. Recall from theorem 4.10 that each cusp admits a Euclidean structure. In this section, we will determine properties of that Euclidean structure for fully augmented links. The exposition is similar to that in [FP07].

Consider the universal cover of the complement of a hyperbolic fully augmented link. By corollary 7.19, the universal cover will contain the lift of embedded totally geodesic white surfaces, which will be a collection of disjoint totally geodesic planes that we color white in \mathbb{H}^3 . It will also contain the lifts of embedded totally geodesic shaded 2-punctured disks bounded by crossing circles. These will also be totally geodesic planes in \mathbb{H}^3 and we call them *shaded*. The white planes and shaded planes meet at right angles in \mathbb{H}^3 . They cut out all the translates of the two ideal polyhedra of theorem 7.11 under the developing map.

Apply an isometry so that the boundary \tilde{T} of a neighborhood of the point at infinity in \mathbb{H}^3 projects under the covering map to a cusp torus T of the fully augmented link. Because each link component meets both white and shaded surfaces, in the universal cover we will see vertical planes corresponding to white and shaded surfaces running into the point at infinity, meeting \tilde{T} in a rectangular lattice.

If we forget the fact that the edges of the lattice have lengths, but consider each rectangle on \tilde{T} as a topological object with two opposite shaded sides and two opposite white sides, then we obtain the following.

LEMMA 7.20. *Let T be a cusp torus of a fully augmented link, with universal cover \tilde{T} tiled by rectangles coming from white and shaded surfaces.*

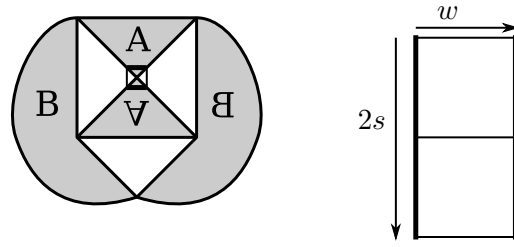


FIGURE 7.13. A fundamental region for a crossing circle.

Let s denote a step along a shaded surface between two white surfaces, and let w denote a step along a white surface between two shaded ones. Then a fundamental domain for T is given as follows.

- If T comes from a crossing circle without a half-twist, then it has meridian w and longitude $2s$.
- If T comes from a crossing circle with a half-twist, it has meridian $w \pm s$ (depending on the direction of the twist) and longitude $2s$.
- If T comes from a knot strand, i.e. a component that is not a crossing circle, then it has meridian $2s$ and longitude $nw + ks$, where n is the number of twist regions met by the strand, with multiplicity, and k is some integer.

PROOF. From the construction of the polyhedral decomposition of $S^3 - L$, each crossing circle gives rise to an ideal vertex of each polyhedron. Thus a fundamental domain for a crossing circle consists of two rectangles, given by neighborhoods of the corresponding 4-valent ideal vertices.

In the case that there are no half-twists, the shaded faces adjacent to the ideal vertex are glued to each other. Thus an arc running along a white face has its endpoints glued into a meridian, and thus the meridian in this case is w . As for the longitude, a white face on one polyhedron is glued to a white face on the other. Thus a longitude steps along two shaded sides, one on one polyhedron and one on the other, before closing up. See figure 7.13.

For a knot strand K meeting no half-twists, there will be one ideal vertex of one polyhedron, hence one rectangular vertex neighborhood, for each portion of K between adjacent crossing circles. These rectangles are glued end to end along shaded faces coming from the crossing disks to complete a longitude. Thus there will be n such rectangles, and a longitude is given by n steps along white faces, or nw . There will be n identical rectangles glued end to end in the other polyhedron. These two blocks of n rectangles will be glued along their white faces to form a $2 \times n$ block, making up the fundamental domain of K . A meridian is given by two steps along shaded faces. See figure 7.14.

If there are half-twists, then the gluing changes along shaded faces at half-twists. A shaded triangle on one polyhedron will be glued to the opposite shaded triangle on the other polyhedron. This introduces shearing into the

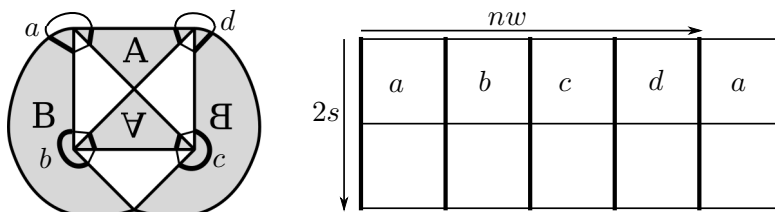


FIGURE 7.14. A fundamental region for a knot strand with no half twists.

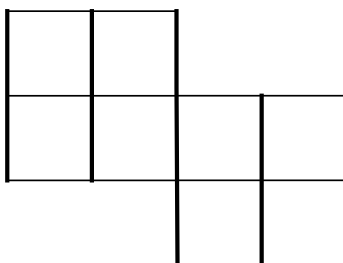


FIGURE 7.15. Adding a half twist shifts the gluing along the shaded faces, shearing the fundamental domain.

fundamental domain, as in figure 7.15. Since the shearing only occurs as shaded faces are glued, it does not affect the longitude of a crossing circle or the meridian of a knot strand: these are both $2s$. However, it will adjust a meridian of a crossing circle by adding $\pm s$, and it will adjust the longitude of a knot strand by adding $\pm s$ for each half-twist. Thus the longitude of a knot strand becomes $nw + ks$ for some integer k . \square

Lemma 7.20 is purely topological. We now wish to give geometric information on the rectangles forming the cusps. To do so, we need to find more explicit embedded cusp neighborhoods of the cusps of a fully augmented link. An embedded cusp neighborhood lifts to a disjoint collection of horoballs in the universal cover \mathbb{H}^3 , one for each ideal vertex of each translate of the ideal polyhedra under the developing map. We will find an embedded cusp neighborhood by finding a collection of embedded horoballs about ideal vertices of the polyhedra forming a fully augmented link.

DEFINITION 7.21. Let $T \subset \mathbb{H}^3$ be an ideal triangle. For each edge e of T , define the *midpoint* m of e to be the point such that the geodesic from m to the opposite ideal vertex is perpendicular to e . Note this point is unique. See figure 7.16.

For each edge e of the ideal polyhedral decomposition of a fully augmented link, define its *midpoint* to be the midpoint of that edge on one of the two ideal triangles adjacent to the edge. Note that since the two polyhedra are symmetric by a reflection in the white faces, both triangles adjacent to e have the same midpoint, so the midpoint of each edge is well-defined.

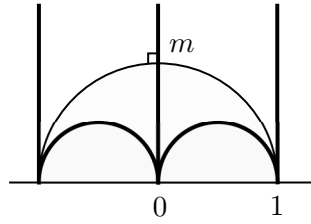


FIGURE 7.16. When an ideal triangle in \mathbb{H}^2 has vertices at 0, 1, and ∞ , one of its midpoints will lie in \mathbb{H}^2 at height 1.

LEMMA 7.22. *Let L be a hyperbolic fully augmented link, with decomposition into ideal polyhedra P_1 and P_2 . For each ideal vertex of P_i , there is a unique horoball meeting the midpoint of each edge through that ideal vertex. The collection of all such horoballs, intersected with P_i and P_j , glue to give an embedded cusp neighborhood of all the cusps of $S^3 - L$.*

PROOF. Place P_i in \mathbb{H}^3 so that the ideal vertex of interest lies at infinity, and so that one of the two shaded faces meeting the ideal vertex has its ideal vertices at 0, 1, and ∞ in \mathbb{H}^3 . Note that the edges of that shaded face have midpoints at height 1, as in figure 7.16. Because the polyhedron is right-angled, the other shaded face will have ideal points at some points ci , $1 + ci$, and ∞ for some $c \in \mathbb{R}$. Thus again the midpoints of these edges lie at height 1. Then the horoball of height 1 about infinity meets the midpoint of each edge through the ideal vertex.

The above discussion applies to any vertex of any polyhedron, and so this proves the first statement of the lemma. However, to show that these horoballs glue to give an embedded cusp neighborhood, we need to show that under the developing map, these horoballs have disjoint embedded interiors in \mathbb{H}^3 .

Develop in a neighborhood of infinity. Since white faces are glued by reflection, the developing map takes P_i to a reflected copy of P_i , where the reflection is through the vertical plane determined by a white face meeting infinity. Note that the reflection isometry takes points at height 1 to points at height 1. Similarly, because the polyhedra are right angled, developing by gluing shaded faces produces shaded faces of the same width, and thus midpoints are height 1. Thus a horoball of height 1 through infinity will meet the midpoints of all edges through infinity under the developing image.

We claim that this horoball cannot meet any white faces besides those that have an ideal vertex at infinity. Consider a white face that does not meet infinity. It lies in a hemisphere with boundary a circle C on \mathbb{C} . Because the white surface is embedded in the fully augmented link complement, the lifts of this surface are disjointly embedded in \mathbb{H}^3 . Thus the boundary circles of all lifts of white faces meet only at points of tangency corresponding to ideal vertices. Thus the circle C meets the boundaries of the vertical planes containing white faces meeting ∞ only in points of tangency. The vertical

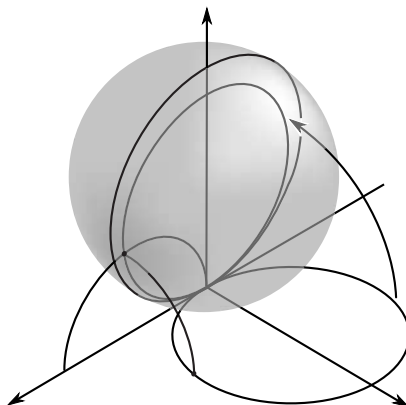


FIGURE 7.17. If H is centered at a point p on a vertical white plane, and has diameter greater than 1, then it must contain the midpoint of an edge through p .

planes have boundary on \mathbb{C} a collection of parallel vertical lines, and these lines must be exactly distance 1 apart. Then the diameter of C can be at most 1. It follows that the height of the hemisphere containing a white face that does not run through infinity must be at most $1/2$; therefore the horoball at height $1/2$ cannot meet it.

By an isometry, the previous argument applies to any ideal vertex. Thus we have proved that the horoballs through the midpoints of ideal vertices of P_i only meet white faces that run through the center of the horoball at infinity.

Suppose, by way of contradiction, that under the developing map one of these horoballs H centered at a point p in \mathbb{C} has diameter strictly greater than 1, so that the collection of interiors of horoballs will not be embedded. Then p must lie on the boundary of one of the vertical white planes, else H intersects a vertical white plane in a compact region, giving a contradiction.

So p is an ideal vertex of a polyhedron meeting a white face on a vertical plane V , and some other white plane W . The boundary ∂W is a circle on \mathbb{C} of diameter at most 1, as we have seen above. The vertex p also meets two shaded faces, and at least one of these, call it S , is not a vertical plane. Then $S \cap V$ is an ideal edge of a polyhedron, and it must have a midpoint. The midpoint is obtained by taking a perpendicular from a point on ∂W to the semicircle $S \cap V$ on the vertical plane V . The set of all points obtained by dropping a perpendicular from ∂W to V is a circle of diameter equal to the diameter of ∂W on the plane V ; see figure 7.17. But H has diameter greater than 1, so this entire circle lies inside of H . This contradicts the fact that H does not contain any of the midpoints of edges through p .

Thus when we expand all horoballs to the midpoints of their adjacent edges, all those centered at points on \mathbb{C} have diameter at most 1, while that at infinity has height exactly 1, so their interiors are embedded. Since the

above discussion applies to any ideal vertex of any polyhedron, we conclude that under the developing map, interiors of all such horoballs are embedded, and thus the quotient under the covering map gives an embedded horoball neighborhood of each cusp of $S^3 - L$. \square

COROLLARY 7.23. *Let L be a hyperbolic fully augmented link. There exists an embedded horoball neighborhood of the cusps of $S^3 - L$ such that, when measured in the induced Euclidean metric on the boundary of each cusp, the sides of the steps s and w (of lemma 7.20) have lengths $\ell(s) = 1$ and $\ell(w) \geq 1$.*

PROOF. If we place the ideal vertices of a shaded triangle at 0, 1, and ∞ , then the midpoints of the edges from 0 to ∞ and from 1 to ∞ are of height 1. Thus the horoball neighborhood through these points is at height 1, and distance along the boundary of this horoball is just Euclidean distance. Since the shaded triangle meets this plane in a line segment from 0 to 1, the length of the step s is $\ell(s) = 1$.

To find w , we note that there will be horoballs of diameter 1 centered at all the corners of the rectangle containing the step w . Two of these will be centered at 0 and 1, the other two at some ci and $1 + ci$ in \mathbb{C} , for some $c = \ell(w)$. Because the four horoballs are disjoint, we must have $\ell(w) \geq 1$. \square

The above results lead to consequences on slope lengths of Dehn fillings.

THEOREM 7.24. *Let L be a hyperbolic fully augmented link. Let C_1, \dots, C_k be crossing circles of L . Let s_j be a slope on $N(C_j)$ such that Dehn filling along s_j replaces the crossing circle C_j by a twist region with n_j crossings (with n_j even if and only if C_j is not adjacent to a half-twist). Then there is an embedded horoball neighborhood of all cusps of $S^3 - L$ such that on the boundary of each cusp, the length of s_j is at least $\ell(s_j) \geq \sqrt{n_j^2 + 1}$.*

PROOF. The slope of the Dehn filling that replaces a crossing circle with $2a_j$ crossings runs over one meridian and a_j longitudes.

If $n_j = 2a_j$ is even, then C_j meets no half-twist. Then lemma 7.20 implies that the slope s_j will have the form $w + 2a_j s$ or $w - 2a_j s$. Because w and s run in orthogonal directions, and each has length at least one by corollary 7.23, the length of $w \pm 2a_j s$ is at least $\sqrt{1 + (2a_j)^2} = \sqrt{1 + n_j^2}$, as claimed.

If $n_j = 2a_j + 1$ is odd, then C_j meets a half-twist, and lemma 7.20 implies that s_j has the form $w \pm s + 2a_j s$ or $w \pm s - 2a_j s$, with the signs the same: $s_j = w \pm (2a_j + 1)s$. Again because w and s are orthogonal, corollary 7.23 implies the length of s_j is at least $\sqrt{1 + (2a_j + 1)^2} = \sqrt{1 + n_j^2}$. \square

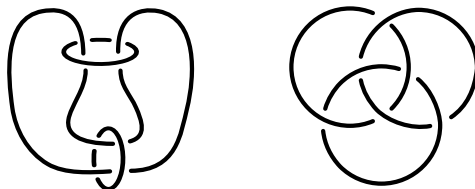


FIGURE 7.18. Two different diagrams of the Borromean rings.

7.5. Exercises

EXERCISE 7.1. In this exercise, you investigate the two diagrams of the Whitehead link shown in figure 7.3.

- (1) Show by a sequence of diagrams that the two links in that figure are isotopic.
- (2) Use SnapPy [CDGW16] to show that the two link complements are isometric. The check using SnapPy is not mathematically rigorous, but in this case the link has a special property: it is *arithmetic*. We will not define an arithmetic link here (we won't use the definition elsewhere), but a consequence of arithmeticity is that the program Snap [CGHN00] can be used to give a mathematically rigorous certification that the two links shown are isometric.

EXERCISE 7.2. Use the methods of chapter 1 to prove that the complement of a Whitehead link can be decomposed into two ideal pyramids with a square base, which in turn can be glued to an ideal octahedron.

EXERCISE 7.3. Shown on the left of figure 7.18 is the diagram of a link which we claim is the Borromean rings. Shown on the right is a more familiar diagram of the Borromean rings. There are several different ways to prove the complements of these hyperbolic manifolds are isometric.

- (1) Show by a sequence of diagram moves that the links are isotopic. Why does this suffice to show the complements are isometric?
- (2) Find a hyperbolic structure on each by hand, and show by hand that the manifolds are isometric. This will take some work, and sounds tedious. The exercise here is to think about why this will be tedious: list the steps involved.
- (3) Use computational tools. Use SnapPy [CDGW16] to show they are isometric. As in exercise 7.1, these links are arithmetic, so you can check using Snap [CGHN00] that the link complements are isometric, which gives a mathematically rigorous certification.

EXERCISE 7.4. The (p, q, r) -pretzel link. As p, q, r go to infinity, find geometric limits of pretzel links. Find a universal upper bound on their volumes.

EXERCISE 7.5. (Topology of the solid torus) A solid torus V is homeomorphic to $S^1 \times D^2$, where a specified homeomorphism $h: S^1 \times D^2 \rightarrow V$ is called a *framing*.

- (a) A non-trivial simple closed curve in ∂V is called a *meridian* if it bounds a disk in V . Prove that if μ is a meridian, then for some framing $h: S^1 \times D^2 \rightarrow V$, $\mu = h(\{1\} \times \partial D^2)$.
- (b) A non-trivial simple closed curve λ in ∂V is called a *longitude* if it represents a generator of $\pi_1(V) \cong \mathbb{Z}$. Prove that if λ is a longitude, then for some framing $h: S^1 \times D^2 \rightarrow V$, $\lambda = h(S^1 \times \{1\})$.
- (c) Prove that there are infinitely many ambient isotopy classes of longitudes in a solid torus.

EXERCISE 7.6. For the Whitehead link, find slopes of Dehn filling giving the twist knot $J(2, n)$ for n even. Write them as $p\mu + q\lambda$, for relatively prime integers p and q , where μ is a meridian and λ is the longitude that bounds a disk in S^3 . This is called the *standard longitude*.

Repeat for n odd, using the isometric link.

EXERCISE 7.7. Using the meridian and standard longitude as a basis for two boundary components of the exterior of the Borromean rings (i.e. take a longitude on each component that bounds a disk in S^3), find the slopes of the Dehn fillings of the Borromean rings that give $J(2k, 2\ell)$.

Repeat for $J(2k, 2\ell + 1)$ and $J(2k + 1, 2\ell + 1)$.

EXERCISE 7.8. The simplest fully augmented link has a single crossing circle; it comes from augmenting a knot with only one twist region. Show that when we apply the decomposition of this chapter to the fully augmented link with only one crossing circle, the result is not a decomposition into two ideal polyhedra. What does the decomposition give?

EXERCISE 7.9. Prove a result analogous to theorem 7.24 for knot strand cusps. If K_i is a knot strand cusp of a hyperbolic fully augmented link, and s_i is a slope on K_i that represents a nontrivial filling (i.e. s_i is not a meridian), then the length of s_i is at least m_i , where m_i denotes the number of crossing disks that K_i intersects, counted with multiplicity.

EXERCISE 7.10. In chapter 10 we will consider a class of links called *two-bridge links* which have twist regions arranged in two rows, illustrated in figure 10.2. Show that the complement of the fully augmented link coming from a 2-bridge link can be obtained by gluing a collection of regular ideal octahedra. How many regular ideal octahedra?

CHAPTER 8

Essential Surfaces

We have already encountered hyperbolic surfaces embedded in hyperbolic 3-manifolds, for example the 3-punctured spheres that bound “shaded surfaces” in fully augmented links. In this chapter, we explore surfaces more carefully. We will see that many results can be deduced about the geometry of 3-manifolds from the topology of the surfaces they contain.

8.1. Incompressible surfaces

This section gives many of the definitions needed to describe surfaces in 3-manifolds. These are topological in nature, and are standard in 3-manifold topology. Good references are [Hem04], [Hat07], and [Sch14].

REMARK 8.1. Whenever we step from geometric arguments to topological ones, we typically need to take some care to discuss whether our objects will be merely continuous, or piecewise linear, or smooth, because the topology of manifolds, maps, etc. can behave very differently under different assumptions. We will assume throughout that our manifolds and maps are smooth, i.e. in the C^∞ category, unless otherwise stated. This allows us to assume basic results on differentiable manifolds:

- Submanifolds have *tubular neighborhoods*. That is, for any submanifold S embedded in a manifold M of codimension k , there exists an open neighborhood of S embedded in M diffeomorphic to $S \times D^k$. Thus a link L embedded in S^3 lies in a tube $L \times D^2$ embedded in S^3 with L at its core. A surface S lies in a thickened surface $S \times D^1 = S \times I$. A tubular neighborhood is also sometimes called a *regular neighborhood*.
- An isotopy of a submanifold can be extended to an isotopy of the ambient manifold, i.e. to an ambient isotopy.
- Submanifolds can be perturbed to intersect transversely.

More information on these results can be found in a standard text on differential topology.

Our submanifolds will typically be surfaces, and throughout, these will almost always be *properly* embedded in the ambient 3-manifold, where a *proper* embedding is one in which the boundary of the surface is mapped

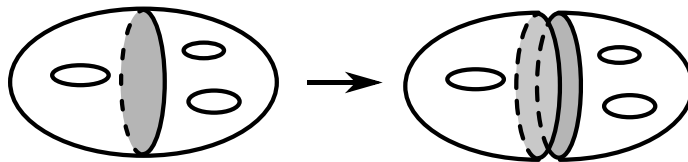


FIGURE 8.1. A compressible surface can be surgered along a disk, replaced with a simpler surface or surfaces

by the embedding to the boundary of the 3-manifold: $S \cap \partial M = \partial S$ where the intersection is transverse. Additionally, we will assume throughout that the ambient 3-manifold is orientable; this is the case for knot complements in S^3 , for example.

DEFINITION 8.2. Let F be a connected surface properly embedded in a 3-manifold. An embedded disk $D \subset M$ with $\partial D \subset F$ is said to be a *compression disk* for F if ∂D does not bound a disk on F . A surface that admits a compression disk is *compressible*. If the surface contains no compression disk, and is not the sphere S^2 , projective plane P^2 , or disk D^2 , then we say it is *incompressible*.

Compressible surfaces can be simplified, as follows. Suppose S is a surface properly embedded in a 3-manifold M , and D is a disk embedded in M with ∂D contained in S . Let $\nu(D)$ be a thickened D : i.e. $\nu(D)$ is homeomorphic to $D \times I$, with $(\partial D) \times I$ a regular neighborhood of ∂D in S , and $\nu(D)$ embedded in a tubular neighborhood of D in M . We may form a new (possibly disconnected) properly embedded surface from S and D by the following procedure: remove $\partial\nu(D) \cap S$ from S and attach the two parallel disks $\partial\nu(D) - (\partial\nu(D) \cap S)$ to S . See figure 8.1. (Technically, as a final last step we need to smooth corners, to remain in the C^∞ category. Such a smoothing is easily done, and we will assume it is done without comment for related constructions.)

DEFINITION 8.3. The process of replacing S by attaching the two disks $\partial\nu(D) - (\partial\nu(D) \cap S)$ to curves $S - (\partial\nu(D) \cap S)$ is called *surgery* of S along D . Usually, we use the verb to describe the procedure: *surger* S along D .

An incompressible surface admits no compression disk. That means that if D is a disk embedded in the ambient 3-manifold with $\partial D \subset S$, then ∂D also bounds a disk $E \subset S$. Thus in this case, if we surger S along D we obtain two surfaces: one diffeomorphic to S , and one diffeomorphic to a 2-sphere ($D \cup E$). Often in our applications the 2-sphere bounds a ball and contracts to a point. Thus surgery on an incompressible surface does nothing to simplify the surface.

EXAMPLE 8.4. As an example of an incompressible surface, consider the torus T marked by dashed lines embedded in the knot complement shown in figure 8.2. On its outside, this torus bounds a manifold homeomorphic to the figure-8 knot complement.

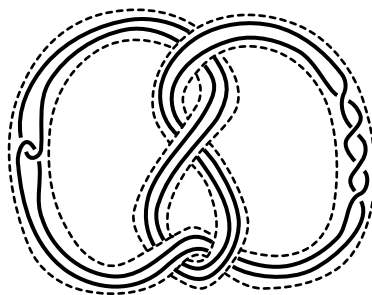


FIGURE 8.2. The torus shown (dotted lines) bounds the figure-8 knot complement on one side, the Whitehead link on the other, hence is incompressible.

We claim there cannot be a compression disk on the outside, in the complement of the figure-8 knot. For suppose D is such a disk. Surger the torus T along D . The result is a sphere S embedded in S^3 . Any sphere in S^3 bounds two balls, one on either side. One ball bounded by S must contain the figure-8 knot and the compression disk D . The other is a ball contained in the figure-8 knot complement, disjoint from $D \times I$. If we undo the surgery along D , we glue this ball along two disks, $D \times \{0\}$ and $D \times \{1\}$, yielding a solid torus. This implies that the figure-8 knot complement is homeomorphic to a solid torus, which is the unknot complement. But this is a contradiction, for example because the figure-8 knot is hyperbolic.

So if the torus T of figure 8.2 is compressible, then a compression disk must lie on the inside of the torus. But the inside of the torus is homeomorphic to a solid torus in S^3 containing a knot complement. In fact, the inside is homeomorphic to the complement of the Whitehead link, the knot in the solid torus shown in figure 7.4. Again if there were an embedded compression disk for the torus on this side, surgering would give a sphere embedded in the Whitehead link complement, bounding two balls in S^3 . A similar argument to that above would imply that one of the components of the Whitehead link lies in a ball in a solid torus in the link complement. But then the two link components are unlinked, which is a contradiction: the Whitehead link is nontrivially linked.

Thus the torus in figure 8.2 is incompressible.

DEFINITION 8.5. An embedded surface F in a 3-manifold M is said to be *boundary parallel* if it can be isotoped into the boundary of M .

DEFINITION 8.6. A *satellite knot* is a knot whose complement contains an incompressible torus that is not boundary parallel.

Equivalently, a satellite knot can be formed as follows. Start with a knot K' in a solid torus V , with K' chosen so that it is not contained in a ball in V , and K' not isotopic to the core of the solid torus. Let K'' be a nontrivial knot in S^3 . Form the satellite knot (complement) by removing a tubular neighborhood of K'' and replacing it with $V - K'$ in a trivial way (that is,

attach V so that the meridian curve of K'' still bounds a disk in V). The knot K'' is called the *companion knot*. The satellite knot lies in a regular neighborhood of the companion.

For orientable surfaces in orientable 3-manifolds, incompressibility is equivalent to the fundamental group injecting in the 3-manifold.

LEMMA 8.7. *An orientable surface in an orientable 3-manifold is incompressible if and only if it is π_1 -injective, i.e. if the fundamental group of the surface injects into the fundamental group of the 3-manifold under the homomorphism induced by inclusion.*

A nonorientable surface S is π_1 -injective if and only if the boundary of a regular neighborhood of S is an orientable incompressible surface.

PROOF. Exercise 8.3 and exercise 8.4. □

There is an additional notion of incompressibility for properly embedded surfaces with boundary.

DEFINITION 8.8. Let F be a surface with boundary properly embedded in a 3-manifold M . A *boundary compression disk* for F is a disk D with ∂D consisting of two arcs, $\partial D = \alpha \cup \beta$, such that $\alpha = D \cap F \subset F$ and $\beta = D \cap \partial M \subset \partial M$, and such that there is no arc γ of ∂F such that $\gamma \cup \alpha$ bounds a disk on F .

If F admits a boundary compression disk it is *boundary compressible*, otherwise it is *boundary incompressible*.

We will give an example of a class of knots that always contains a boundary incompressible surface. First we define the class of knots.

DEFINITION 8.9. Let (p, q) be relatively prime integers. Then the pair $(p, q) \in \mathbb{Z} \times \mathbb{Z} \cong H_1(T^2; \mathbb{Z})$ defines a nontrivial simple closed curve on a torus. View the torus T as the boundary of a neighborhood of an unknot in S^3 . Notice that there is one compression disk to the inside of T ; its boundary is a meridian m for the unknot. There is also a compression disk to the outside of T ; its boundary is a longitude ℓ of the unknot. We choose a basis so that the curve (p, q) has minimal representative intersecting m a total of $|p|$ times, and ℓ a total of $|q|$ times, with the signs of p, q determining the direction (right or left handed screw motion).

A *torus knot*, or (p, q) -*torus knot*, is the knot in S^3 given by the (p, q) curve on the unknotted torus T in S^3 . It is frequently denoted by $T(p, q)$. Figure 8.3 shows an example.

EXAMPLE 8.10. Suppose $T(p, q) = K$ is a torus knot with $|p|, |q| \geq 2$. The surface $T - K$ is an annulus; we will denote the annulus by F . We show that F is boundary incompressible in $S^3 - K$.

For suppose there is a boundary compression disk D for F . Since $F \cup K$ is the torus T , the disk D lies to one side of T . Because T is an unknotted torus in S^3 , the disk D is either (freely) homotopic to a disk with boundary

FIGURE 8.3. The torus knot $T(2, 3)$

m or to one with boundary ℓ . By definition, $T(p, q)$ has intersection number $|p|$ with m and $|q|$ with ℓ . On the other hand, a boundary compression disk intersects F in exactly one arc, and K in exactly one arc. This is impossible when $|p|, |q| \geq 2$.

We now fold all our definitions into one.

DEFINITION 8.11. A surface F properly embedded in a 3-manifold M is *essential* if one of the following holds.

- (1) F is a 2-sphere that does not bound a 3-ball.
- (2) F is a disk and either $\partial F \subset \partial M$ does not bound a disk on ∂M , or $\partial F \subset \partial M$ does bound a disk E on ∂M , but $E \cup F$ does not bound a 3-ball.
- (3) F is not a disk or sphere, and is incompressible, boundary incompressible, and not boundary parallel.

DEFINITION 8.12. A 3-manifold is said to be:

- *irreducible* if it contains no essential 2-sphere,
- *boundary irreducible* if it contains no essential disk,
- *atoroidal* if it contains no essential torus, and
- *anannular* if it contains no essential annulus.

THEOREM 8.13. *A manifold that contains an embedded essential torus cannot be hyperbolic.*

The proof of this theorem was part of an exercise in chapter 6, but we will go through the argument here.

PROOF. Suppose M contains an essential torus. By lemma 8.7, the fundamental group of M contains a $\mathbb{Z} \times \mathbb{Z}$ subgroup. Corollary 5.14 implies that the subgroup is generated by two parabolic elements fixing the same point on the boundary of \mathbb{H}^3 at infinity. But then the thick–thin decomposition (theorem 5.20 structure of thin part) implies that the torus is parallel to a cusp torus, hence it is boundary parallel. This contradicts the definition of essential. \square

COROLLARY 8.14. *A satellite knot complement does not admit a hyperbolic structure.* \square

THEOREM 8.15. *Suppose M is a 3-manifold with torus boundary components whose interior has a complete finite volume hyperbolic metric. Then M cannot contain an essential annulus.*

PROOF. Suppose not. Suppose M is hyperbolic, and A is an essential annulus in M . Consider the core curve γ of A . Note γ is isotopic to ∂A , hence γ is isotopic into ∂M . Under the hyperbolic structure on the interior of M , torus boundary components become cusps. Thus in the hyperbolic structure, γ is isotopic into a cusp, so is isotopic to closed curves of arbitrarily small length. Then the loop γ corresponds to a covering transformation of $\mathbb{H}^3 \rightarrow M$ that is parabolic. But then both boundary components of ∂A correspond to the same parabolic element. Thus the annulus has boundary components given by the same curve in the same cusp. This is possible only if the annulus is boundary parallel. \square

COROLLARY 8.16. *A torus knot complement does not admit a hyperbolic structure.*

PROOF. Consider the curve $T(p, q)$ embedded on an unknotted torus $T \subset S^3$. If $(p, q) \in \{(\pm 1, q) \mid q \in \mathbb{Z}\} \cup \{(p, \pm 1) \mid p \in \mathbb{Z}\}$ then $T(p, q)$ is the unknot in S^3 , which does not have hyperbolic complement. Otherwise the annulus $T - T(p, q)$ is incompressible (exercise 8.5). We showed in example 8.10 that it is boundary incompressible. A similar argument shows it cannot be boundary parallel. So it is essential. Thus a torus knot is not hyperbolic. \square

Theorems 8.13 and 8.15 give surfaces which preclude a knot from being hyperbolic. In fact, an even stronger result is known.

THEOREM 8.17 (Thurston, Hyperbolization). *A knot complement admits a complete hyperbolic structure if and only if it is not a satellite knot or a torus knot.*

More generally, a compact 3-manifold with nonempty torus boundary has interior admitting a complete hyperbolic structure if and only if it is irreducible, boundary irreducible, atoroidal, and anannular. \square

Theorem 8.17 follows from the geometrization theorem for Haken manifolds, which is a very deep result; see [Thu82]. The proof requires a book of its own (e.g. [Kap01]), and we will not include it here. However we will use the theorem to show many knot and link complements are hyperbolic.

Note that theorem 8.17 turns the geometric problem of determining whether a manifold admits a hyperbolic structure into a topological problem of finding surfaces in 3-manifolds, or proving such surfaces cannot exist. It has been applied to show many knots and 3-manifolds admit a hyperbolic structure, although unfortunately it does not give much information on such a structure, beyond the fact that it exists. We will see some results along these lines in the rest of this chapter.

8.2. Torus decomposition, Seifert fibering, and geometrization

While we are most interested in hyperbolic spaces and hyperbolic geometry, we will also need to identify non-hyperbolic spaces as we encounter

them in knot theory. Theorem 8.17 gives us a characterization of hyperbolic knots, but we also have the tools now to study non-hyperbolic knots. This section gives a brief overview of the terminology and results that we will need.

DEFINITION 8.18. Let p and q be relatively prime integers. A *Seifert fibered solid torus* of type (p, q) is a solid torus $S^1 \times D^2$ constructed as the union of disjoint circles, as follows. Begin with a solid cylinder $D^2 \times [0, 1]$, fibered by intervals $\{x\} \times [0, 1]$. Glue the disk $D^2 \times \{0\}$ to $D^2 \times \{1\}$ by a $2\pi p/q$ rotation. The fiber $\{0\} \times [0, 1]$ in $D^2 \times [0, 1]$ becomes a circle; this is called the *exceptional fiber*. Every other fiber $\{x\} \times [0, 1]$ is glued to q segments to form a circle. These are called *normal fibers*. If $q = 1$, the Seifert fibered solid torus is called a *regularly fibered solid torus*.

DEFINITION 8.19. A *Seifert fibered space* is an orientable 3-manifold M that is the union of pairwise disjoint circles, called *fibers*, such that every fiber has neighborhood diffeomorphic to a fibered solid torus, preserving fibers.

EXAMPLE 8.20. The 3-sphere S^3 is the union of two solid tori V and W . For relatively prime integers (p, q) , give V the fibering of a Seifert fibered solid torus of type (p, q) , and give W the fibering of a Seifert fibered solid torus of type (q, p) . Then when we glue ∂V to ∂W to form S^3 , the fibers on the boundaries are identified. Thus S^3 is Seifert fibered.

EXAMPLE 8.21 (Torus knot complements). The complement of a (p, q) -torus knot (definition 8.9) is Seifert fibered, as follows. Take the Seifert fibering of S^3 of the previous example. A regular fiber on ∂V is a (p, q) -torus knot. Thus when we remove a fibered solid torus neighborhood of this regular fiber, the result is a Seifert fibered space homeomorphic to the exterior of a torus knot, $S^3 - N(T(p, q))$.

A Seifert fibered space is never hyperbolic. The following theorem follows from work of many people, including work of Casson and Jungreis [CJ94] and Gabai [Gab92].

THEOREM 8.22 (Characterization of Seifert fibered spaces). *A compact orientable irreducible 3-manifold M with infinite fundamental group is a Seifert fibered space if and only if $\pi_1(M)$ contains a normal infinite cyclic subgroup.* \square

For further information on Seifert fibered spaces, see [Sch14], [Hat07], or [Sco83].

The following theorem applies to manifolds that admit an embedded essential torus. It was proved by Jaco, Shalen [JS79], and Johannson [Joh79].

THEOREM 8.23 (JSJ decomposition). *For any compact irreducible, boundary irreducible 3-manifold M , there exists a (possibly empty) finite collection*

\mathcal{T} of disjoint essential tori such that each component of the 3-manifold obtained by cutting M along \mathcal{T} is either atoroidal or Seifert fibered. Moreover, a minimal such collection \mathcal{T} is unique up to isotopy. \square

DEFINITION 8.24. The minimal collection of tori \mathcal{T} as in theorem 8.23 is called the *JSJ-decomposition* of M , or sometimes the *torus decomposition* of M . The union of the Seifert fibered pieces of M cut along \mathcal{T} is called the *characteristic submanifold* of M .

In example 8.4, the torus decomposition consists of the single essential torus shown in figure 8.2. Cutting along it splits the 3-manifold into two hyperbolic pieces, hence the characteristic submanifold is empty.

Thurston's hyperbolization theorem implies if the JSJ-decomposition of M is nontrivial, then atoroidal components of M cut along \mathcal{T} are hyperbolic. More generally, even in the closed case we now know the following theorem.

THEOREM 8.25 (Geometrization of closed 3-manifolds). *Let M be a closed, orientable, irreducible 3-manifold.*

- (1) *If $\pi_1(M)$ is finite, then M is spherical; i.e. M is homeomorphic to S^3/Γ where Γ is a finite subgroup of $O(4)$ acting on S^3 without fixed points.*
- (2) *If $\pi_1(M)$ is infinite and contains a $\mathbb{Z} \times \mathbb{Z}$ subgroup, then M is either Seifert fibered or contains an incompressible torus (so is not hyperbolic).*
- (3) *If $\pi_1(M)$ is infinite and contains no $\mathbb{Z} \times \mathbb{Z}$ subgroup, then M is hyperbolic.* \square

The second part of the theorem follows from work of Casson and Jungreis [CJ94] and Gabai [Gab92]. The first and third parts were proved by Perelman [Per02], [Per03].

8.3. Normal surfaces, angled polyhedra, and hyperbolicity

In this section, we will use theorem 8.17 to prove that many manifolds are hyperbolic. We will be considering 3-manifolds that admit an ideal polyhedral decomposition, for example a decomposition into ideal tetrahedra, but also more general ideal polyhedra as in chapter 1 and chapter 7. We will see that we need only consider surfaces that intersect the polyhedra in simple ways: in disks with well-behaved boundaries.

8.3.1. Normal surfaces. To describe nice positions of embedded surfaces in polyhedra, we give the following definition.

DEFINITION 8.26. Let P be an ideal polyhedron. Truncate the ideal vertices of P , so they become *boundary faces*, and denote the truncated polyhedron by \overline{P} . The edges between (regular) faces and boundary faces are called *boundary edges*. See figure 8.4, left.

Let D be a disk embedded in \overline{P} with $\partial D \subset \partial \overline{P}$. We say that D is *normal* if it satisfies the following conditions.

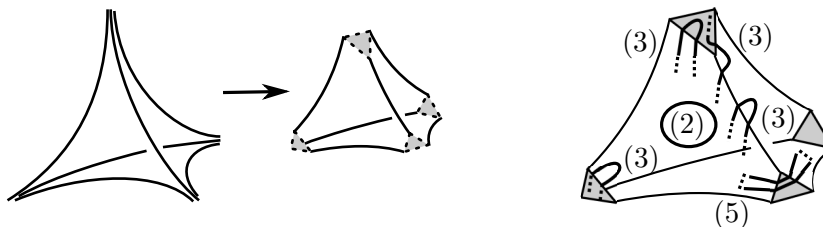


FIGURE 8.4. Left: truncating an ideal polyhedron. Boundary faces are shaded, boundary edges dashed, (regular) faces are white, and (regular) edges are solid black. Right: examples of curves that cannot be the boundary of a normal disk, along with the number of the property of definition 8.26 that they violate

- (1) ∂D meets the faces, boundary faces, edges, and boundary edges of \overline{P} transversely.
- (2) ∂D does not lie entirely on a single face or boundary face of \overline{P} .
- (3) Any arc of intersection of ∂D with a face of \overline{P} does not have both endpoints on the same edge, or on the same boundary edge, or on an adjacent edge and boundary edge. Similarly, any arc of intersection of ∂D with a boundary face does not have both endpoints on the same boundary edge.
- (4) ∂D meets any edge at most once.
- (5) ∂D meets any boundary face at most once.

Figure 8.4 illustrates some of these conditions.

DEFINITION 8.27. A surface is in *normal form*, with respect to a polyhedral decomposition, or is *normal*, for short, if it intersects the (truncated) polyhedra in a collection of normal disks.

Normal surfaces in 3-manifolds are well-studied objects, and the following theorem is classical, dating back to work of Kneser in the late 1920s [Kne29], and Haken and Schubert in the 1960s [Hak61, Sch61], and many others since then.

THEOREM 8.28. *Suppose M admits an ideal polyhedral decomposition.*

If M contains an essential 2-sphere, then it contains one in normal form.

If M is irreducible and M contains an essential disk, then it contains one in normal form.

If M is irreducible and boundary irreducible, and contains an essential surface, then that surface can be isotoped in M to meet the polyhedra in normal form.

PROOF. Let S be an essential surface in M . We may isotope S so that it intersects faces, boundary faces, edges, and boundary edges of the truncated polyhedra of M transversely. Let f denote the number of times S meets a

face or boundary face, and let e denote the number of times S meets an edge or boundary edge. The pair (f, e) is called the *complexity* of S in M , and we order it lexicographically. We will adjust S to remove intersections with the polyhedra that violate normality while reducing its complexity. Since the complexity is finite, it follows that a finite number of adjustments give the result.

First we claim we can adjust S so that it meets the polyhedra only in disks, lowering the complexity. If S is a sphere, this is done by replacing S . If M is irreducible, then this is done by isotopy of S . The argument is similar to arguments below and so we leave it as exercise 8.6.

We now assume that the components of intersection of S with a truncated polyhedron P are all disks. Suppose that $\partial(S \cap P)$ contains a simple closed curve of intersection contained entirely in a face or boundary face. Then there must be an innermost such curve γ , and γ bounds a disk E inside that face disjoint from S .

If S is a 2-sphere, then surger S along E , obtaining two 2-spheres, S' and S'' , which we push slightly to be disjoint from a neighborhood of E . Thus S' and S'' have strictly fewer intersections with ∂P . Either S' or S'' must still be essential, else S could not be essential, so say S'' is essential. Replace S with S'' . Then S'' has strictly smaller complexity than S . Repeating a finite number of times, we may assume S does not meet faces or boundary faces of P in closed curves in this case.

If M is irreducible and S is a disk, then as before surger along E . This gives two surfaces, a disk S' and a sphere S'' , both of strictly smaller complexity than S . Because M is irreducible, the sphere S'' bounds a ball, and we may isotope S through that ball to the disk S' . Repeat for each closed curve of intersection of S with faces, removing all such intersections.

If M is irreducible and boundary irreducible, then S is not a sphere or disk. Because S is essential, γ bounds a disk E' in S . Then the sphere $E \cup E'$ must bound a ball by irreducibility. Isotope S through this ball, removing the intersection γ and reducing complexity. Repeating finitely many times eliminates all closed curves of intersection of S with faces of P .

Now suppose an arc of intersection of S with a face or boundary face of P has both its endpoints on the same edge or boundary edge, or on an edge and adjacent boundary edge. Then there must be an outermost such arc α , bounding a disk E on that face or boundary face, with E disjoint from S . In the case that the face is a boundary face, or the endpoints of S do not both lie on a boundary edge, we may slide S through a neighborhood of E to isotope across the edge, decreasing complexity.

When the arc α lies on a regular face, and both endpoints of α lie on boundary edges, then we have to take more care since we cannot isotope the surface S past the boundary edge without changing its topology. In this case, we know S is a surface with boundary, so not a sphere, so we are in the case that M is irreducible. If S is a disk, surger along E and push off

the face slightly, obtaining two disks with lower complexity. One of them must be essential, since S is essential. Replace S with this essential disk.

If S is not a disk, then M is irreducible and boundary irreducible. Since S is essential, E is not a boundary compression disk for S , thus α bounds a disk E' on S . Then $E \cup E'$ is a disk with boundary on ∂M . Because M is boundary irreducible, it must be parallel to a disk E'' on ∂M . Then $E \cup E' \cup E''$ is a sphere, so bounds a ball, and we may isotope S through this ball to remove the intersection α , strictly decreasing complexity.

Finally, we need to show for each polyhedron P , any disk of $S \cap P$ has boundary meeting each edge of P at most once, and meeting each boundary face of P at most once. We leave these as exercises 8.7 and 8.8. \square

8.3.2. Angle structures and combinatorial area. We are interested in 3-manifolds that are hyperbolic. If a 3-manifold admits a decomposition into ideal tetrahedra, recall from theorem 4.7 (edge gluing equations) and definition 4.12 (completeness equations) that a complete hyperbolic structure satisfies a system of nonlinear equations. If we take the log of the edge gluing equations, the complex product becomes a sum of real and imaginary parts:

$$\log \left(\prod z(e_j) \right) = \sum (\log |z(e_j)| + i \operatorname{Arg} z(e_j)) = 2\pi i.$$

The imaginary parts encode relations on dihedral angles of the tetrahedra. If we ignore the real part, then finding solutions to the imaginary parts involves finding dihedral angles that satisfy a system of linear equations. Thus by considering dihedral angles alone, we reduce a complicated nonlinear problem to a linear problem. This can significantly simplify computations.

DEFINITION 8.29. An *angle structure* on an ideal triangulation T of a manifold M is a collection of (interior) dihedral angles, one for each edge of each tetrahedron, satisfying the following conditions.

- (0) Opposite edges of the tetrahedron have the same angle.
- (1) Dihedral angles lie in $(0, \pi)$.
- (2) The sum of angles around any ideal vertex of any tetrahedron is π .
- (3) The sum of angles around any edge class of M is 2π .

The set of all angle structures for triangulation T is denoted by $\mathcal{A}(T)$.

Conditions (0) and (1) are required for nonsingular tetrahedra. Condition (2) ensures that a triangular cross-section of any ideal vertex of any tetrahedron is actually a Euclidean triangle. Finally, condition (3) is the imaginary part of the edge gluing equations. Note we have not included the completeness equations. For many results, we don't need them!

An angle structure on an ideal tetrahedron uniquely determines the shape of that tetrahedron. If it has assigned dihedral angles α, β, γ in clockwise order, then there is a unique hyperbolic tetrahedron with those dihedral angles, and its edge invariant corresponding to the edge with angle

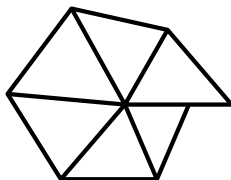


FIGURE 8.5. Angle structures typically have shearing singularities.

α can be shown to be

$$(8.1) \quad z(\alpha) = \frac{\sin \gamma}{\sin \beta} e^{i\alpha}.$$

Thus if a triangulation has an angle structure (not all do), we can think of the manifold as being built of hyperbolic tetrahedra.

Note that because we have discarded the completeness equations, an angle structure typically will not give a complete hyperbolic structure. In fact, because we have discarded the nonlinear part of the edge gluing equations, an angle structure typically won't even give a hyperbolic structure. There will likely be shearing singularities around each edge, as in figure 8.5.

Even so, much useful information can be extracted from angle structures, which we will see in later chapters. In this chapter, we will show that if an angle structure exists on a triangulation of a manifold, then the manifold admits (some) hyperbolic structure.

The idea of an angled triangulation can be generalized to ideal polyhedra as well. First, we need to assign to each edge a dihedral angle, which is a number lying in the range $(0, \pi)$. Once that has been done, we can measure a combinatorial area of normal disks embedded in the polyhedra, as follows.

DEFINITION 8.30. Let D be a normal disk in a (truncated) ideal polyhedral decomposition of M , such that each ideal edge of M has been assigned an interior dihedral angle in the range $(0, \pi)$. Let $\alpha_1, \dots, \alpha_n$ be the angles assigned to the ideal edges met by ∂D . Then the *combinatorial area* of D is defined as:

$$a(D) = \sum_{i=1}^n (\pi - \alpha_i) - 2\pi + \pi |\partial D \cap \partial M|.$$

Here $|\partial D \cap \partial M|$ indicates the number of components of intersection of ∂D with boundary faces.

If S is a surface in normal form, the *combinatorial area* of S is defined to be the sum of combinatorial areas of the normal disks making up S .

Note in the case D is contained in a hyperbolic plane, meeting each edge of the polyhedron orthogonally, the combinatorial area of D agrees with the actual hyperbolic area (exercise 8.9).

We can now generalize the idea of an angle structure on a triangulation to an angle structure on an ideal polyhedral decomposition.

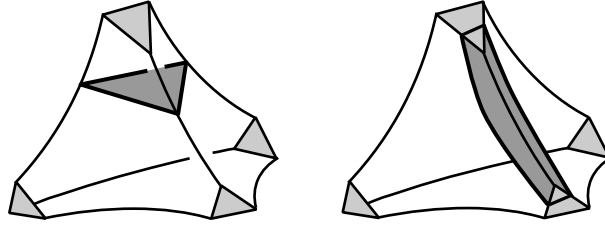


FIGURE 8.6. Normal disks: a vertex triangle and a boundary bigon

DEFINITION 8.31. An *angled polyhedral structure* on a 3-manifold M is a decomposition of M into ideal polyhedra, along with a collection of (interior) dihedral angles, one for each edge of each polyhedra, that satisfy the following conditions.

- (1) Each dihedral angle lies in the range $(0, \pi)$.
- (2) Every normal disk has non-negative combinatorial area.
- (3) Interior angles around an edge sum to 2π .

EXAMPLE 8.32. An angle structure on an ideal triangulation of M is an example of an angled polyhedral structure. To show this, suppose we have an angle structure on a triangulation of M . Then by definition 8.29, the dihedral angles are in the correct range, and interior angles around edges must sum to 2π to satisfy the definition of an angle structure. So we need only consider normal disks, and show that each has non-negative combinatorial area. Two examples of normal disks are shown in figure 8.6.

The triangle in the figure has combinatorial area

$$a(D) = (\pi - \alpha) + (\pi - \beta) + (\pi - \gamma) - 2\pi = \pi - (\alpha + \beta + \gamma) = 0,$$

since α, β, γ encircle an ideal vertex of a tetrahedron. We call this normal disk a *vertex triangle*.

The other normal disk shown also has zero combinatorial area:

$$a(D) = 0 - 2\pi + \pi \cdot 2.$$

This disk is called a *boundary bigon*.

LEMMA 8.33. *Let M be a triangulated 3-manifold with an angle structure. Then the combinatorial area of any normal disk D in an ideal tetrahedron of M is non-negative. It is zero if and only if D is a vertex triangle or a boundary bigon.*

PROOF. As we have seen above, the combinatorial areas of boundary bigons and vertex triangles are zero.

If D is a normal disk that meets at least two boundary faces, its combinatorial area is at least the sum $\sum(\pi - \alpha_i)$, and any term $(\pi - \alpha_i)$ is positive, so $a(D) \geq 0$ in this case.

If D meets exactly one boundary face, then because ∂D cannot meet edges adjacent to a boundary edge, it must meet an opposite edge in each of

the triangles on either side of the boundary face. These cannot be opposite edges in the tetrahedron. Hence the combinatorial area is

$$a(D) \geq \pi - \alpha + \pi - \beta - 2\pi + \pi = \pi - \alpha - \beta = \gamma > 0,$$

where here we let α , β , and γ denote the angles of an ideal tetrahedron with $\alpha + \beta + \gamma = \pi$. Thus if D meets just one boundary face, $a(D)$ is strictly positive.

If D meets no boundary faces, then it is either a vertex triangle or a quad separating two opposite edges. In the first case, the combinatorial area is zero. In the second, the combinatorial area is

$$a(D) = 2(\pi - \alpha) + 2(\pi - \beta) - 2\pi = 2(\pi - \alpha - \beta) = 2\gamma > 0.$$

In all cases, the combinatorial area is non-negative. \square

Thus we have shown:

THEOREM 8.34. *An angle structure on an ideal triangulation of M is an angled polyhedral structure.* \square

LEMMA 8.35 (Gauss–Bonnet). *A normal surface S in an angled polyhedral structure satisfies*

$$a(S) = -2\pi\chi(S).$$

PROOF. Recall that $\chi(S)$, the Euler characteristic of S , is given by $\chi(S) = v - e + f$, where v is the number of vertices in a polygonal decomposition of S , e is the number of edges, and f is the number of faces. In our case, the intersection of S with the polyhedra determines a polygonal decomposition. Then f is the number of normal disks, or intersections of S with interiors of the polyhedra. The value e is the number of intersections of S with faces of the polyhedra, and v is the number of intersections of S with ideal edges of the polyhedra. Intersections of S with boundary edges and boundary faces do not affect Euler characteristic at all.

By definition,

$$\begin{aligned} a(S) &= \sum_D a(D) = \sum_D \left(\sum_i (\pi - \alpha_i) + \pi |\partial D \cap \partial M| - 2\pi \right) \\ &= \pi \sum_D \left(\left(\sum_i 1 \right) + |\partial D \cap \partial M| \right) - \sum_D \sum_i \alpha_i - \sum_D 2\pi, \end{aligned}$$

where the sum is over normal disks $D \subset S$. Note that the last term in the sum is $-2\pi f$, since we add -2π for each normal disk of intersection in $S \cap P$.

The term $\sum_D \sum_i \alpha_i$ gives the sum of all interior angles met by the surface S . This is $2\pi v$.

Finally, we claim that $(\sum_i 1 + |\partial D \cap \partial M|)$ counts the number of edges in faces (not boundary faces) in the normal disk D . To see this, orient ∂D and give each edge the corresponding direction. Its initial endpoint is either on an ideal edge of the polyhedron or a boundary edge. The sum counts all the

initial endpoints of edges of ∂D on faces, without counting initial endpoints of edges on boundary faces. Denote this by

$$\left(\sum_i 1 + |\partial D \cap \partial M| \right) = e(D).$$

Now take the sum $\sum_D e(D)$. The sum over all normal disks counts each edge exactly twice, so its value is $2e$. Thus $\pi \sum_D (\sum_i 1 + |\partial D \cap \partial M|) = 2\pi e$.

Putting it together, we find

$$a(S) = 2\pi e - 2\pi v - 2\pi f = -2\pi\chi(S). \quad \square$$

8.3.3. Hyperbolicity.

THEOREM 8.36. *Let M be a manifold admitting an angled polyhedral structure. Then M is irreducible and boundary irreducible, and its boundary consists of tori.*

Moreover, if the angled polyhedral structure is actually an angle structure on a triangulation of M , then M is atoroidal and anannular. Hence any manifold admitting an angle structure is hyperbolic.

PROOF. Suppose S is an essential sphere in M . By theorem 8.28, we can put S into normal form with respect to the polyhedral decomposition of M , and obtain a combinatorial area for S . By definition of an angled polyhedral structure, each normal disk of S has non-negative combinatorial area, so $a(S)$ is non-negative. But lemma 8.35 implies $a(S) = -4\pi$. This contradiction proves that M is irreducible. A similar argument shows that S cannot be an essential disk, so M is boundary irreducible.

Now consider the boundary components of M . These are obtained by gluing boundary faces. Pushing in slightly, we find that ∂M is parallel to a normal surface made up of boundary parallel disks. By the definition of an angle structure, definition 8.29, and the definition of combinatorial area, definition 8.30, it follows that each such disk has combinatorial area zero. So ∂M has combinatorial area zero. Because ∂M consists of closed surfaces in an orientable manifold, it must be a disjoint union of tori.

Now suppose the angled polyhedral structure is an angle structure on a triangulation of M , and suppose S is an essential torus. Then S can be put into normal form by theorem 8.28, and lemma 8.35 implies that $a(S) = 0$, so each normal disk of S has zero combinatorial area. Then lemma 8.33 implies that each normal disk is a vertex triangle or a boundary bigon. Since S is a closed surface embedded in M , it does not meet boundary faces of M , hence each normal disk is a vertex triangle. But vertex triangles join to form the boundary of M , hence a component of ∂M is a torus, and S is parallel to ∂M . This contradicts the fact that S is essential.

Finally, suppose S is an essential annulus in the manifold M with a triangulation and angle structure. Then again $a(S) = 0$, so S is made up of vertex triangles and boundary bigons. There must be at least one boundary bigon. This must be glued to another boundary bigon, since the

edges on the face of the tetrahedron run between boundary edges. Then S is made up entirely of boundary bigons. The only possibility is that the boundary bigons encircle a single edge of the triangulation of M . This is not incompressible. So S is anannular.

The fact that M is hyperbolic now follows from theorem 8.17. \square

8.4. Pleated surfaces and a 6-theorem

When a 3-manifold admits a hyperbolic structure, then that structure can often be used to induce a hyperbolic structure on a properly embedded essential surface with punctures. If the surface is totally geodesic inside the 3-manifold, such as for the white and shaded surfaces in a fully augmented link, corollary 7.19, then the induced hyperbolic structure on the surface is unique. But usually a properly embedded surface is not totally geodesic. In this case, frequently we may still straighten the surface.

DEFINITION 8.37. An embedded surface S in a 3-manifold M is *homotopically boundary incompressible*, or *homotopically ∂ -incompressible*, if for any properly embedded arc α in S that is not homotopic rel endpoints into ∂S , the arc α in M is not homotopic rel endpoints into ∂M . That is, a nontrivial arc in S remains nontrivial in M . (This is also sometimes called *algebraically ∂ -incompressible*.)

Notice that a homotopically ∂ -incompressible surface is boundary incompressible. However, now arcs may be immersed and a homotopy gives a singular disk.

LEMMA 8.38. *Let S be a surface with non-empty boundary properly embedded in a 3-manifold M whose interior admits a complete hyperbolic structure. Suppose S is homotopically ∂ -incompressible. Then the ideal edges of any ideal triangulation of S can be homotoped to be geodesics in M . Similarly, each ideal triangle can be homotoped to be totally geodesic in M .*

PROOF. Any edge of an ideal triangulation on S is homotopically non-trivial on S . Because S is homotopically ∂ -incompressible, each edge must also be homotopically non-trivial in M . Thus it lifts to an arc with distinct endpoints in the universal cover \mathbb{H}^3 of M . Such an arc is homotopic to a unique geodesic in \mathbb{H}^3 . The image of this geodesic (and the homotopy) under the covering map gives the desired geodesic (and homotopy) in M .

Now for any ideal triangle of S , the edges of the triangle are homotopic to geodesics in M . Lift one edge to be a geodesic in \mathbb{H}^3 . Because the interior of the triangle is homotopically trivial in S and in M , it lifts to the interior of a triangle in \mathbb{H}^3 , and thus we may choose lifts of the other two edges of the triangle such that the three bound a unique totally geodesic triangle, homotopic to a lift of S , in \mathbb{H}^3 . The image of this triangle (and homotopy) under the covering map gives the desired totally geodesic triangle in M . \square

We often refer to the homotopy of lemma 8.38 as *straightening*. After straightening edges and triangles in lemma 8.38, note that the surface will

typically be bent along the geodesic ideal edges. In addition, note that the homotopy is not at all guaranteed to leave the surface embedded. Thus after such a straightening the surface is frequently only immersed, not embedded. However, the process still can give significant geometric information.

DEFINITION 8.39. A *pleated surface* in a hyperbolic 3-manifold M is a pair (S, φ) consisting of a surface S with complete hyperbolic structure, and a local isometry $\varphi: S \rightarrow \varphi(S) \subset M$ such that each point in S lies in a geodesic mapped by φ to a geodesic. When (S, φ) is a pleated surfaces, will also sometimes say that the image $\varphi(S) \subset M$ is pleated.

PROPOSITION 8.40. *A homotopically ∂ -incompressible surface (with non-empty boundary) properly embedded in a hyperbolic 3-manifold can be pleated. That is, it is homotopic to the image of a local isometry $\varphi: S \rightarrow \varphi(S)$ coming from a pleated surface.*

PROOF. This follows almost immediately from lemma 8.38; we only need to describe the hyperbolic structure on S . The straightening process of lemma 8.38 maps each ideal triangle of S to a hyperbolic ideal triangle. We define a hyperbolic structure on S by taking isometric ideal triangles in S and attaching them along edges such that the map from S into the homotopic surface in M is an isometry. Thus the hyperbolic structure on S can be viewed as pulling the triangles of S out of M and lining them up, without bending, in \mathbb{H}^2 . This gives a fundamental domain for S . The surface is obtained by applying isometric gluing maps on edges. \square

Let M be a compact 3-manifold with a torus boundary component T such that the interior of M admits a complete hyperbolic structure. Then recall that in the complete hyperbolic structure, the boundary of any embedded horoball neighborhood of the cusp corresponding to T inherits a Euclidean structure (theorem 4.10).

DEFINITION 8.41. Recall that an isotopy class of simple closed curves on the torus T is a *slope*. In a Euclidean metric on T , any slope can be isotoped to a geodesic. The *slope length* of s is defined to be the length of such a geodesic, denoted $\ell(s)$.

For M a compact 3-manifold with torus boundary components and hyperbolic interior, a fixed choice of cusp neighborhoods gives a fixed Euclidean structure on each torus boundary component. The slope length of s is measured in this fixed Euclidean structure.

Hyperbolic geometry and pleated surfaces can be used to give a proof of the following theorem.

THEOREM 8.42 (A 6-theorem). *Suppose M is a compact manifold with torus boundary components, such that the interior of M admits a complete hyperbolic structure. Let s_1, \dots, s_n be slopes on distinct boundary components of M such that each slope length $\ell(s_i)$ is strictly larger than 6 on a*

collection of disjoint embedded horospherical tori for M . Then the manifold $M(s_1, \dots, s_n)$ obtained by Dehn filling M along slopes s_1, \dots, s_n is irreducible, boundary irreducible, anannular, and atoroidal.

Theorem 8.42 is a 6-theorem, but not exactly *the* 6-theorem. The 6-theorem, proved independently and simultaneously by Agol [Ago00] and Lackenby [Lac00], is stronger. Their theorem states that if slope lengths are at least six, then the Dehn filled manifold cannot be reducible, toroidal, Seifert fibered or have finite fundamental group. The geometrization theorem implies such a manifold must be hyperbolic. When the Dehn filling gives a closed manifold, our 6-theorem, in theorem 8.42, does not rule out Seifert fibered or finite fillings. However, in the case that the manifold we obtain after Dehn filling still has boundary, it will be hyperbolic by Thurston's hyperbolization theorem, theorem 8.17. Also, our proof uses a little less machinery, while still giving a nice introduction to the geometric arguments involved. We highly recommend reading the original papers [Ago00] and [Lac00].

Our proof of theorem 8.42 will follow three simple steps. First, assuming that $M(s)$ is reducible, boundary reducible, annular, or toroidal, we show that there is a punctured 2-sphere or punctured torus S embedded in M that is essential, with boundary components on ∂M tracing out slopes s_i . Second, because S is essential, it can be pleated, and it inherits a hyperbolic metric and cusp neighborhoods from the metric on M and its embedded horocusps. Third, arguments in hyperbolic geometry show that the slope lengths are at most six.

LEMMA 8.43. *Let M, s_1, \dots, s_n be as in the statement of theorem 8.42. Suppose $M(s_1, \dots, s_n)$ contains an embedded essential sphere, disk, annulus, or torus. Then M contains an essential, homotopically ∂ -incompressible punctured sphere or torus S , with ∂S some subset of the slopes s_1, \dots, s_n . Moreover, if S is a punctured sphere then it has at least three punctures.*

PROOF. Let T be an embedded essential sphere, disk, annulus, or torus in $M(s_1, \dots, s_n)$. Note that $M \subset M(s_1, \dots, s_n)$. If T is embedded in M , then it cannot be essential in M because M is hyperbolic. But if T is compressible or boundary compressible in M , then a compression disk for T is embedded in $M \subset M(s_1, \dots, s_n)$, hence is a compression disk for T in $M(s_1, \dots, s_n)$, contradicting the fact that T is essential. Similarly, if T is boundary parallel in M then it is compressible in $M(s_1, \dots, s_n)$. So T cannot be embedded in M ; it must meet the solid tori attached to M to form $M(s_1, \dots, s_n)$. We may assume it meets the cores of the added solid tori transversely, else we could isotope the surface to lie in M , which would be a contradiction. Thus when we drill these cores from $M(s_1, \dots, s_n)$, the surface S given by removing neighborhoods of the cores from T is a surface with boundary whose boundary components come from the set of slopes $\{s_1, \dots, s_n\}$. Note S is a punctured sphere or punctured torus.

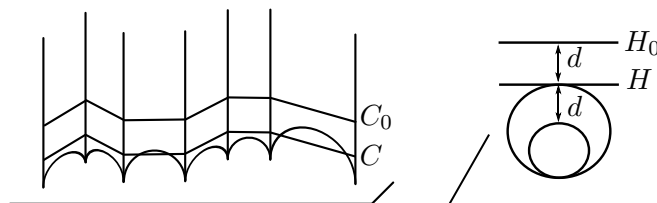


FIGURE 8.7. Left: Choose C_0 to meet only tips of triangles.
Right: Distances between horoballs

Now, S cannot be compressible in M , else a compression disk is a compression disk for T in $M(s_1, \dots, s_n)$. Any boundary compression disk D must have boundary consisting of an arc α in S and an arc β running along a boundary component of M . Using D , we may isotope T through D to the core of a solid torus in $M(s_1, \dots, s_n)$, and then slightly past, removing two intersections of T with cores of filled solid tori. So after repeating this move finitely many times, we may assume S is boundary incompressible. Note also that S cannot be boundary parallel, or T is compressible. So S is essential.

To show S is homotopically ∂ -incompressible, apply a proof similar to that of lemma 8.7 to show that if S is not homotopically ∂ -incompressible, then the boundary of a regular neighborhood of S is boundary compressible. The same argument as above implies that intersections of S with cores of solid tori can be removed in this case.

Finally, if S is a punctured sphere, then it must have at least three punctures else it will be an essential disk or annulus in M , but the hyperbolicity of M rules out such surfaces. \square

The following lemma is from [FS14], and uses arguments of [Ago00].

LEMMA 8.44. *Suppose M is an orientable hyperbolic 3-manifold with a cusp, and horoball neighborhood C about the cusp. Suppose $f: S \rightarrow M$ is a pleating of a punctured surface S , with n punctures of S mapping to C . Suppose finally that for each puncture of S , a loop about the puncture is represented by a geodesic of length λ on ∂C in M . Then in the hyperbolic metric on S given by the pleating, the preimage $f^{-1}(C) \subset S$ contains horospherical cusp neighborhoods R_1, \dots, R_n of the n punctures of S , with disjoint interiors, such that*

$$\ell(\partial R_i) = \text{area}(R_i) \geq \lambda \quad \text{for each } i.$$

PROOF. The pleating of S gives S an ideal triangulation. Start with a cusp neighborhood $C_0 \subset C$ such that f maps all ideal edges of the triangulation to geodesic rays running into the cusp. That is, C_0 does not intersect any edge of the triangulation in a compact arc. See figure 8.7, left. Then $f(S) \cap C_0$ consists of tips of triangles, and $f^{-1}(C_0)$ is a collection of embedded cusps R_1^0, \dots, R_n^0 in S .

Lift M to the universal cover \mathbb{H}^3 . The cusps C and C_0 both lift to collections of disjoint horoballs. Because C_0 is contained in C , for each horoball lift H of C , there is a horoball lift H_0 of C_0 contained in H . Let d denote the hyperbolic distance between H_0 and H . Note that since C is embedded, the distance from H_0 to any other lift of C_0 must be at least $2d$. See figure 8.7, right. Projecting back to M , a geodesic between H_0 and any other lift of C_0 projects to a geodesic from C_0 to C_0 of length at least $2d$. Pulling back to S , the distance from R_i^0 to any other R_j^0 is at least $2d$. Let R_1, \dots, R_n be cusps in S of distance d from R_1^0, \dots, R_n^0 . They must be embedded.

We now show that the lengths $\ell(\partial R_i)$ are at least λ for all i . Let γ_0 be a Euclidean geodesic on ∂C_0 representing $f(\partial R_i^0)$. Since pleating may decrease distance, $\ell(\gamma_0) \leq \ell(\partial R_i^0)$. Moreover, letting γ be the loop on ∂C homotopic to γ_0 , we have $\lambda = \ell(\gamma) = e^{-d}\ell(\gamma_0)$, because γ and γ_0 lie on cusp boundaries of hyperbolic distance d apart. Moreover, $\ell(\partial R_i) = e^{-d}\ell(\partial R_i^0)$. Putting this together,

$$\lambda \leq \ell(\gamma) = e^{-d}\ell(\gamma_0) \leq e^{-d}\ell(\partial R_i^0) = e^{-d} \cdot e^d \ell(\partial R_i) = \ell(\partial R_i).$$

Finally, we need to show that $f(R_i)$ is contained in C . We know $f(R_i^0)$ is contained in C_0 . By construction, $f(R_i)$ is contained in a d -neighborhood of C_0 . But a d -neighborhood of C_0 is the cusp C . Thus $f(R_i)$ lies in C . \square

Now we present a result from [Bör78].

THEOREM 8.45 (Böröczky cusp density theorem). *Let S be a hyperbolic surface with cusps, and let H be an embedded horoball neighborhood for the cusps of S . Then*

$$\text{area}(H) \leq \frac{3}{\pi} \text{area}(S).$$

PROOF. Given S and H , we claim there exists an ideal triangulation of S such that for T any triangle, H meets T only in connected neighborhoods of its ideal vertices in noncompact sets. For example this will hold for a subdivision of the canonical decomposition of S with respect to H , which is defined in chapter 14. We will assume such a decomposition exists.

Map T isometrically to the triangle $T' \subset \mathbb{H}^2$ with ideal vertices at 0, 1, and ∞ . The image of H determines horoballs H_0 , H_1 , and H_∞ about 0, 1, ∞ , respectively. The area of $H \cap T$ in S is given by the sum

$$(8.2) \quad \text{area}(H \cap T) = \text{area}(H_0 \cap T') + \text{area}(H_1 \cap T') + \text{area}(H_\infty \cap T'),$$

and the area of H is given by the sum of all such areas over all triangles T . Since the area of S is just π times the number of triangles, to maximize the cusp density $\text{area}(H)/\text{area}(S)$ we need to maximize the cusp density within ideal triangles, or maximize the sum of equation (8.2) within each triangle.

So consider the triangle $T' \subset \mathbb{H}^2$ with vertices at 0, 1, and ∞ , and with horoballs H_∞ about ∞ of height h_∞ , H_0 about 0 of diameter h_0 , and H_1 about 1 of diameter h_1 . By the observation that (open) horoballs do not

meet edges of the triangulation in intervals with compact closure, we know that h_0 and h_1 are at most 2, and h_∞ is at least $1/2$. These give constraints on h_0 , h_1 , and h_∞ . We also have constraints coming from the fact that H_0 , H_1 , and H_∞ are disjoint.

If one of H_0 , H_1 , or H_∞ is not tangent to one of the other two, then we may expand it, increasing cusp area, until either it is as large as possible given our constraints, or it is tangent to one of the other horoballs. If one of the H_i is as large as possible, but still not tangent to the other horoballs, then the other two horoballs are much smaller than our constraints, and we may expand them until they are tangent to H_i . In any case, we may assume that the cusp area is maximized when each horoball is tangent to one other horoball; because there are three, it follows that one horoball, without loss of generality H_∞ , is tangent to the other two.

Now we may compute the cusp area directly. Since H_0 and H_1 are tangent to H_∞ , they have diameters $h_0 = h_1 = h_\infty$, and H_∞ has height H_∞ . Then the areas of the cusps satisfy (exercise 8.10):

$$\text{area}(H_\infty \cap T') = \frac{1}{h_\infty}, \quad \text{area}(H_0 \cap T') = \text{area}(H_1 \cap T') = h_\infty,$$

so

$$\text{area}(H \cap T') = \frac{1}{h_\infty} + 2h_\infty.$$

We maximize this equation for h_∞ subject to constraints: h_∞ is at least $1/2$, and H_1 and H_0 are disjoint, so h_∞ is at most 1. We find that the function has a critical point at $\sqrt{2}$, but that it reaches its maximum value when $h_\infty = 1/2$ and when $h_\infty = 1$, and the maximum is 3.

Now let n be the number of triangles in S . Then

$$\frac{\text{area}(H)}{\text{area}(S)} \leq \frac{3 \cdot n}{\pi \cdot n} = \frac{3}{\pi}. \quad \square$$

PROOF OF THEOREM 8.42, A 6-THEOREM. Suppose by way of contradiction that $M(s_1, \dots, s_n)$ is reducible, boundary reducible, annular, or toroidal. Then lemma 8.43 implies M contains an embedded essential punctured 2-sphere or torus, whose boundary components on ∂M are parallel to slopes s_1, \dots, s_n .

By proposition 8.40, S may be pleated. By lemma 8.44, the pleating induces horoball neighborhoods R_1, \dots, R_m of cusps of S for which

$$\ell(\partial R_i) = \text{area}(R_i) \geq \ell(s_j),$$

where $f(\partial R_i)$ is the slope s_j . Let H denote the union of the horoball neighborhoods R_i .

Now theorem 8.45 and the Gauss–Bonnet theorem imply

$$(8.3) \quad \sum_i \ell(s_{j_i}) \leq \sum_i \ell(\partial R_i) = \text{area}(H) \leq \frac{3}{\pi} \text{area}(S) = \frac{3}{\pi} \cdot 2\pi |\chi(S)| = 6|\chi(S)|.$$

On the other hand, each $\ell(s_{j_i}) > 6$, and there are m of these, where m is the number of boundary components of S . If S is a punctured sphere, $|\chi(S)| = m - 2$ and equation (8.3) implies $6m < 6(m - 2)$, which is a contradiction. If S is a punctured torus, equation (8.3) implies $6m < 6m$, again a contradiction. \square

Our 6-theorem has immediate consequences to determining when certain knots and links are hyperbolic.

DEFINITION 8.46. For an integer $c > 0$, we say a knot or link is *c-highly twisted* if it admits a diagram in which every twist region has at least c crossings. If c is understood from the context, we also say such a knot or link is *highly twisted*.

The following theorem was first proved in [FP07].

THEOREM 8.47 (Hyperbolicity of highly twisted links). *Let $K \subset S^3$ be a link with a prime, twist-reduced diagram, as in definition 7.13. Assume that K has at least two twist regions. If every twist region of the diagram contains at least six crossings, then the complement of K is hyperbolic.*

PROOF. By lemma 7.14, when we add crossing circles to every twist region of K , we obtain a fully augmented link L ; K now forms the knot strands of this link. Remove all crossings of the knot strands except possibly single crossings in twist regions. Then K is obtained from L by performing Dehn filling along slopes s_j on crossing circles C_j that replace the crossing circle with a twist region with at least six crossings.

By theorem 7.24, each slope s_j has length at least $\sqrt{(6)^2 + 1} = \sqrt{37} > 6$. Thus by our 6-Theorem, theorem 8.42, the link complement L obtained by the Dehn filling is irreducible, boundary irreducible, anannular, and atoroidal. By Thurston's hyperbolization theorem, theorem 8.17, it is hyperbolic. \square

The full 6-theorem can be used to identify knots in S^3 .

COROLLARY 8.48. *Suppose M is a hyperbolic 3-manifold with a single cusp. Then M is the complement of a knot in S^3 if and only if there exists a slope s on the cusp of M of length at most six such that $M(s)$ is homeomorphic to S^3 .*

PROOF. A manifold with a torus boundary component is the complement of a knot in S^3 if and only if a Dehn filling gives S^3 . The full 6-theorem of Agol and Lackenby implies such a slope on a horocusp of a hyperbolic 3-manifold must have length at most six. \square

Since only finitely many slopes on a fixed hyperbolic 3-manifold have length at most six, to determine whether a hyperbolic 3-manifold is a knot in S^3 , it suffices to check finitely many Dehn fillings, and then to identify whether or not the filled manifold is S^3 .

8.5. Exercises

EXERCISE 8.1. Prove that the unknot is the only knot K in S^3 such that $S^3 - N(K)$ admits a properly embedded compression disk for $\partial N(K)$.

EXERCISE 8.2. Prove that the paragraph starting with “Equivalently” in definition 8.6 is indeed an equivalent definition of a satellite knot. You may assume Alexander’s theorem from 3-manifold topology that states that an embedded torus in S^3 bounds a solid torus on at least one side.

EXERCISE 8.3. Prove lemma 8.7. For one direction, you may use the *loop theorem*, which is a classical result in 3-manifold topology:

THEOREM 8.49 (Loop theorem [Pap57]). *If N is a 3-manifold with boundary, and there is a map $f: D^2 \rightarrow N$ such that the loop $f(\partial D^2) \subset \partial N$ is homotopically nontrivial in ∂N , then there is an embedding with the same property.*

EXERCISE 8.4. Prove that a nonorientable surface S properly embedded in a 3-manifold M is π_1 -injective if and only if \tilde{S} , the boundary of a regular neighborhood of S in M , is an orientable incompressible surface.

- EXERCISE 8.5. (1) Prove that a (p, q) -torus knot $T(p, q)$ is nontrivial if $|p|, |q| \geq 2$.
- (2) Let T denote the torus in S^3 on which the torus knot $T(p, q)$ lies, and let A denote the annulus $T - T(p, q)$. Prove A is incompressible if $|p|, |q| \geq 2$.

Hint for both parts: Seifert–Van Kampen theorem.

EXERCISE 8.6. Suppose M is a 3-manifold with an ideal polyhedral decomposition and S a properly embedded essential surface in M with complexity as in the proof of theorem 8.28.

- (1) Prove that if S is an embedded essential sphere, then we may replace S with an embedded essential sphere S' meeting each polyhedron in disks such that the complexity of S' is at most that of S .
- (2) Prove that if M is irreducible and S is an essential surface properly embedded in M , then S can be isotoped to meet polyhedra only in disks, reducing (or at worst fixing) complexity.

EXERCISE 8.7. Suppose M is a 3-manifold with an ideal polyhedral decomposition, and S is an essential surface properly embedded in M . Suppose there is a disk D of intersection of S with a polyhedron P such that ∂D meets an edge of P more than once. Prove S can be isotoped to remove at least two intersections with that edge.

EXERCISE 8.8. Suppose M is a 3-manifold with an ideal polyhedral decomposition, and S is an essential surface with boundary properly embedded in M . Suppose there is a disk D of intersection of S with a polyhedron such

that ∂D meets a boundary face more than once. Then if S is a disk, prove it can be replaced by an essential disk meeting the boundary face fewer times. If S is not a disk and M is irreducible and boundary irreducible, prove S can be isotoped to meet the boundary face fewer times.

EXERCISE 8.9. Prove that if D is a hyperbolic polygon, then its hyperbolic area is

$$\text{area}(D) = \sum (\pi - \alpha_i) - 2\pi + \pi v,$$

where α_i is the angle of the i -th finite vertex, and v is the number of ideal vertices of D .

EXERCISE 8.10. Consider the ideal triangle Δ with vertices at 0, 1, and ∞ , and horoballs H_∞ about ∞ of height h_∞ , H_0 about 0 of diameter h_0 , and H_1 about 1 of diameter h_1 . Prove that the areas of $H_i \cap \Delta$ satisfy

$$\text{area}(H_\infty \cap \Delta) = \frac{1}{h_\infty}, \quad \text{area}(H_0 \cap \Delta) = h_0, \quad \text{and} \quad \text{area}(H_1 \cap \Delta) = h_1,$$

so the total cusp area of Δ is $1/h_\infty + h_0 + h_1$.

EXERCISE 8.11. Let S be a hyperbolic surface with a cusp, with horoball cusp neighborhood C . Show that the length of the boundary of C is equal to the area of C .

EXERCISE 8.12. Let T' be the ideal triangle in \mathbb{H}^2 with vertices at 0, 1, and ∞ , with horoballs H_∞ about ∞ of height h_∞ , H_0 about 0 of diameter h_0 , and H_1 about 1 of diameter h_1 . Show that

$$\text{area}(H_\infty \cap T') = \frac{1}{h_\infty}, \quad \text{area}(H_0 \cap T') = h_0, \quad \text{area}(H_1 \cap T') = h_1.$$

CHAPTER 9

Volume and Angle Structures

Those hyperbolic 3-manifolds that admit a triangulation by positively oriented geometric tetrahedra exhibit many additional nice properties. The existence of such a triangulation often gives a simpler way to prove many results in hyperbolic geometry. We present some of the techniques and consequences in this chapter.

In the theory of knots and links, these tools have been applied to great effect to an infinite class of knots and links called 2-bridge links, which we will describe (and triangulate) in the next chapter.

9.1. Hyperbolic volume of ideal tetrahedra

Ideal tetrahedra are building blocks of many complete hyperbolic manifolds. In this section, we will calculate volumes of ideal tetrahedra.

Recall that a hyperbolic ideal tetrahedron is completely determined by $z \in \mathbb{C}$ with positive imaginary part, as in definition 4.4. It is also determined by three dihedral angles, as the following lemma shows.

LEMMA 9.1. *Let α, β, γ be angles in $(0, \pi)$ such that $\alpha + \beta + \gamma = \pi$. Then $\alpha, \beta,$ and γ determine a unique hyperbolic ideal tetrahedron up to isometry of \mathbb{H}^3 . Conversely, any hyperbolic tetrahedron determines unique $\{\alpha, \beta, \gamma\} \subset (0, \pi)$ with $\alpha + \beta + \gamma = \pi$.*

PROOF. First we prove the converse. Given an ideal tetrahedron with ideal vertices on $\partial\mathbb{H}^3$ at $0, 1, \infty,$ and $z,$ note that a horosphere about ∞ intersects the tetrahedron in a Euclidean triangle. Let α, β, γ denote the interior angles of the triangle; these are dihedral angles of the tetrahedron. Each angle α, β, γ lies in $(0, \pi),$ and the sum $\alpha + \beta + \gamma = \pi,$ as desired. Exercise 2.11 shows that taking a different collection of vertices to $0, 1,$ and ∞ will give the same dihedral angles $\alpha, \beta, \gamma,$ so these three angles are uniquely determined by the tetrahedron.

Now, suppose $\alpha, \beta,$ and γ in $(0, \pi)$ are given, with $\alpha + \beta + \gamma = \pi.$ Then these three numbers determine a Euclidean triangle, uniquely up to scale, with interior angles $\alpha, \beta, \gamma.$ View the triangle as lying in $\mathbb{C};$ we may adjust such a triangle so that it has vertices at $0, 1,$ and some $z \in \mathbb{C}$ with positive imaginary part. This determines a tetrahedron with edge parameter $z.$ If we

rotate and scale the triangle so that different vertices map to 0 and 1, this corresponds to mapping different ideal vertices of the tetrahedron to 0 and 1. The parameter z will be adjusted as in lemma 4.6, but the tetrahedron will be the same up to isometry. \square

Lemmas 9.1 and 4.6 give two different ways of uniquely describing an ideal tetrahedron, either by a single complex number z or by a triple of angles α, β, γ with $\alpha + \beta + \gamma = \pi$. We will compute volumes of an ideal tetrahedron, and we choose to compute volumes using a parameterization by angles rather than edge parameter, although computations can be done either way. (See exercises.)

DEFINITION 9.2. The *Lobachevsky function* $\Lambda(\theta)$ is the function defined by

$$\Lambda(\theta) = - \int_0^\theta \log |2 \sin u| \, du.$$

THEOREM 9.3. *Suppose $\alpha, \beta,$ and γ are angle measures strictly between 0 and π , and suppose $\alpha + \beta + \gamma = \pi$, so they determine a hyperbolic ideal tetrahedron $\Delta(\alpha, \beta, \gamma)$. Then the volume $\text{vol}(\Delta(\alpha, \beta, \gamma))$ is equal to*

$$\text{vol}(\Delta(\alpha, \beta, \gamma)) = \Lambda(\alpha) + \Lambda(\beta) + \Lambda(\gamma),$$

where Λ is the Lobachevsky function of definition 9.2.

EXAMPLE 9.4. The figure-8 knot complement has complete hyperbolic structure built of two regular ideal tetrahedra. Therefore the volume of the figure-8 knot complement is $6\Lambda(\pi/3)$, which can be numerically calculated to be approximately 2.0299.

Our proof of theorem 9.3 follows that given by Milnor in [Mil82] and also in [Thu79, Chapter 7]. Milnor, in turn, credits Lobachevsky for several of his calculations.

First, we need a lemma concerning the Lobachevsky function.

LEMMA 9.5. *The Lobachevsky function $\Lambda(u)$ satisfies:*

- (1) *It is well-defined and continuous on \mathbb{R} (even though the defining integral is improper).*
- (2) *$\Lambda(-\theta) = -\Lambda(\theta)$, i.e. $\Lambda(\theta)$ is odd.*
- (3) *$\Lambda(\theta)$ is periodic of period π .*
- (4) *It satisfies the expression $\Lambda(2\theta) = 2\Lambda(\theta) + 2\Lambda(\theta + \pi/2)$.*

PROOF. To prove the lemma, we will relate the Lobachevsky function to the well-known *dilogarithm function*

$$(9.1) \quad \psi(z) = \sum_{n=1}^{\infty} z^n/n^2 \quad \text{for } |z| \leq 1.$$

For more information on the dilogarithm, see for example [Zag07]. Note that for $|z| < 1$, the derivative of $\psi(z)$ satisfies

$$\psi'(z) = \sum_{n=1}^{\infty} \frac{z^{n-1}}{n} = \frac{1}{z} \left(\sum_{n=1}^{\infty} \frac{z^n}{n} \right).$$

The sum on the right hand side is a well-known Taylor series:

$$-\log(1-z) = \sum_{n=1}^{\infty} \frac{z^n}{n} \quad \text{for } |z| < 1.$$

Thus the analytic continuation of $\psi(z)$ is given by

$$(9.2) \quad \psi(z) = - \int_0^z \frac{\log(1-u)}{u} du \quad \text{for } z \in \mathbb{C} - [1, \infty).$$

For $0 < u < \pi$, consider $\psi(e^{2iu}) - \psi(1)$. Although the integral formula equation (9.2) above is not defined at $z = 1$, the summation of equation (9.1) is defined and continuous at $z = 1$ (in fact, $\psi(1) = \pi^2/6$), so we may write

$$\psi(e^{2iu}) - \psi(1) = - \int_1^{e^{2iu}} \frac{\log(1-w)}{w} dw.$$

Substitute $w = e^{2i\theta}$ into this expression to obtain

$$\begin{aligned} \psi(e^{2iu}) - \psi(1) &= - \int_{\theta=0}^u \log(1 - e^{2i\theta}) (2i) d\theta \\ &= - \int_0^u \log \left(-2ie^{i\theta} \left(\frac{e^{i\theta} - e^{-i\theta}}{2i} \right) \right) (2i) d\theta \\ &= - \int_0^u 2i(\log(-i) + \log(e^{i\theta}) + \log(2 \sin \theta)) d\theta \\ &= - \int_0^u (\pi - 2\theta + 2i \log(2 \sin \theta)) d\theta. \end{aligned}$$

Take the imaginary parts of both sides of the above equation. Note $\psi(1)$ is real, hence

$$\Im(\psi(e^{2iu}) - \psi(1)) = \Im(\psi(e^{2iu})) = \Im \left(\sum_{n=1}^{\infty} \frac{e^{2inu}}{n^2} \right) = \sum_{n=1}^{\infty} \frac{\sin(2nu)}{n^2}.$$

On the other side, this equals

$$\Im(\psi(e^{2iu}) - \psi(1)) = 2 \int_0^u -\log(2 \sin \theta) d\theta = 2\Lambda(u).$$

Thus for $0 \leq u \leq \pi$, we have the uniformly convergent Fourier series for $\Lambda(u)$ given by

$$(9.3) \quad \Lambda(u) = \frac{1}{2} \sum_{n=1}^{\infty} \frac{\sin(2nu)}{n^2} \quad \text{for } 0 \leq u \leq \pi.$$

This shows $\Lambda(u)$ is well-defined and continuous for $0 \leq u \leq \pi$. It also shows that $\Lambda(u)$ can be defined on $-\pi \leq u \leq 0$, and it is an odd function on this range. Finally, it shows that $\Lambda(0) = \Lambda(\pi) = 0$.

Notice now that the derivative $d\Lambda(\theta)/d\theta = -2 \log |2 \sin \theta|$ is periodic of period π . Then for $\theta > \pi$,

$$\begin{aligned} \Lambda(\theta) &= \int_0^\theta \Lambda'(u) du = \int_0^\pi \Lambda'(u) du + \int_\pi^\theta \Lambda'(u) du \\ &= \Lambda(\pi) + \int_0^{\theta-\pi} \Lambda'(u) du = \Lambda(\theta - \pi), \end{aligned}$$

by the periodicity of Λ' , and the fact that $\Lambda(\pi) = 0$. This shows that Λ is well-defined and continuous for $\theta \geq 0$; a similar result implies it is well-defined and continuous for $\theta \leq 0$, and it will be odd everywhere.

It only remains to show the last item of the lemma. To do so, begin with the identity

$$2 \sin(2\theta) = 4 \sin \theta \cos \theta = (2 \sin \theta)(2 \sin(\theta + \pi/2)).$$

Then note that

$$\begin{aligned} \Lambda(2\theta) &= \int_0^{2\theta} -\log |2 \sin u| du \\ &= 2 \int_0^\theta -\log |2 \sin(2w)| dw \quad (\text{letting } w = u/2) \\ &= 2 \int_0^\theta -\log |2 \sin w| dw + 2 \int_0^\theta -\log |2 \sin(w + \pi/2)| dw \\ &= 2\Lambda(\theta) + 2 \int_{\pi/2}^{\theta+\pi/2} -\log |2 \sin v| dv \\ &= 2\Lambda(\theta) + 2\Lambda(\theta + \pi/2) - 2\Lambda(\pi/2). \end{aligned}$$

Finally, note that if we substitute $u = \pi/2$ into equation (9.3), we obtain $\Lambda(\pi/2) = 0$. This finishes the proof of the lemma. \square

REMARK 9.6. Item (4) of lemma 9.5 is a special case of more general identities known as the *Kubert identities*, which have the following form. For any nonzero integer n ,

$$\Lambda(n\theta) = \sum_{k=0}^{n-1} n\Lambda(\theta + k\pi/n).$$

You are asked to prove these identities in the exercises.

To prove theorem 9.3, we will subdivide our ideal tetrahedron into six 3-dimensional simplices, each simplex with some finite and some infinite vertices. Such a simplex will be described by a region in \mathbb{H}^3 . To obtain the volume, we integrate the hyperbolic volume form $d \text{vol} = dx dy dz / z^3$ over the region describing the simplex, and then sum the six results.

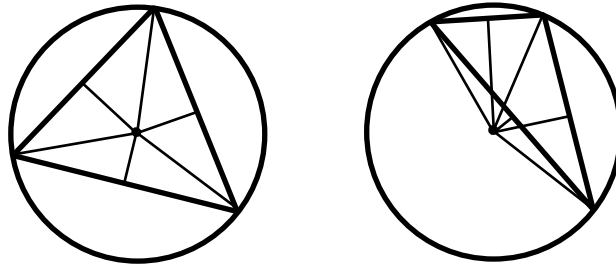


FIGURE 9.1. Left is a tetrahedron for which the point $(0, 0)$ lies in the interior of the triangle on \mathbb{C} , right is one for which it is exterior. Both show subdivisions into six triangles.

More carefully, given an ideal tetrahedron in \mathbb{H}^3 , we have been viewing the tetrahedron as having vertices 0 , 1 , ∞ , and z . The three points 0 , 1 , and z determine a Euclidean circle on \mathbb{C} , which is the boundary of a Euclidean hemisphere, giving a hyperbolic plane in \mathbb{H}^3 . To this picture, apply a hyperbolic isometry that takes the circle on \mathbb{C} through 0 , 1 , z to the unit circle in \mathbb{C} , taking 0 , 1 , z to some points p , q , r on $S^1 \subset \mathbb{C}$.

Now, drop a perpendicular from ∞ to the hemisphere; this will be a vertical ray from $(0, 0, 1) \in \mathbb{H}^3$ to ∞ . There will be two cases to consider: the case that the point $(0, 0) \in \mathbb{C}$ is interior to the triangle determined by p , q , r , and the case that the point $(0, 0)$ is exterior to that triangle. The cases are shown in figure 9.1.

Consider first the case that the point $(0, 0)$ is interior to the triangle determined by p , q , and r . Then the ray from $(0, 0, 1)$ to ∞ lies interior to the tetrahedron. Now, on the hemisphere whose boundary is the unit circle, draw perpendicular arcs from $(0, 0, 1)$ to each edge of the tetrahedron lying on that hemisphere. Also draw arcs from $(0, 0, 1)$ to the vertices of the tetrahedron, as shown in figure 9.1. Now cone to ∞ . This divides the original tetrahedron up into six simplices. Similarly, if $(0, 0)$ is not interior to the triangle determined by p , q , and r , it still makes sense to draw the same arcs and rays, as in figure 9.1, right. However, in this case the six simplices obtained overlap each other. In either case, we have the following result.

LEMMA 9.7. *Each of the six simplices obtained as above has the following properties, illustrated in figure 9.2.*

- (1) *It has two finite vertices and two ideal vertices.*
- (2) *Three of its dihedral angles are $\pi/2$, the other dihedral angles are ζ , ζ , and $\pi/2 - \zeta$ for some $\zeta \in (0, \pi/2)$.*

PROOF. Note that by construction, the two ideal vertices are at ∞ and one of p , q , r , i.e. one of the vertices of the original ideal tetrahedron. The other vertices are at $(0, 0, 1)$, and some point on the unit hemisphere where

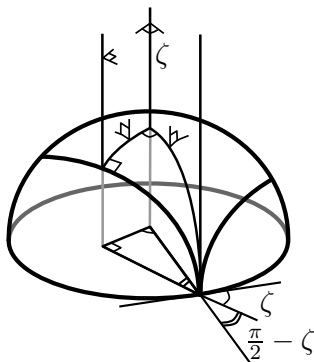


FIGURE 9.2. One of the six simplices obtained from subdividing an ideal tetrahedron

an arc from $(0, 0, 1)$ meets an edge of the original tetrahedron in a right angle.

Consider the dihedral angles of the faces meeting infinity. Each of these is a cone (to ∞) over an edge on the unit hemisphere. The dihedral angles agree with the dihedral angles of the vertical projection of the simplex to \mathbb{C} , which is the triangle T shown in figure 9.1; these angles are $\pi/2$, ζ , and $\pi/2 - \zeta$ for some $\zeta \in (0, \pi/2)$. The fourth face of the tetrahedron lies on the hemisphere. It meets both vertical faces through $(0, 0, 1)$ in right angles. The final face is a subset of a vertical plane whose boundary on \mathbb{C} is a line L containing a side of the projection triangle T . The angle this vertical plane meets with the unit hemisphere is obtained by measuring the angles between the line L and a tangent to the unit circle at the points where these intersect. Notice this angle is complementary to $\pi/2 - \zeta$, hence is ζ . \square

A simplex with the form of lemma 9.7 is called an *orthoscheme*, named by Schläfli in the 1950s [Sch50, Sch53]. Around that time, he computed volumes of orthoschemes.

LEMMA 9.8. *Let $S(\zeta)$ denote a simplex obtained as above, with properties of lemma 9.7. That is, $S(\zeta)$ has two finite vertices and two ideal vertices, three dihedral angles of $\pi/2$, and other dihedral angles ζ , ζ , and $\pi/2 - \zeta$ for $\zeta \in (0, \pi/2)$. Then the volume of $S(\zeta)$ is*

$$\text{vol}(S(\zeta)) = \frac{1}{2}\Lambda(\zeta).$$

PROOF. The proof is a computation.

Apply an isometry to \mathbb{H}^3 so that one ideal vertex of $S(\zeta)$ lies at ∞ , the other on the unit circle, with one of the finite vertices at $(0, 0, 1)$; this is the same position of the simplex in the proof of lemma 9.7 above. When we project vertically to \mathbb{C} , we obtain a triangle T with one vertex at 0, one on the unit circle, and the last some $v \in \mathbb{C}$. The angle at v is $\pi/2$, and the other two angles are ζ and $\pi/2 - \zeta$. By applying a Möbius transformation

that rotates and reflects (but does not affect volume), we may assume v is the point $\cos(\zeta) \in \mathbb{R} \subset \mathbb{C}$, and the third point, on the unit circle, is the point $\cos(\zeta) + i \sin(\zeta)$.

Now the triangle T is described by the region

$$0 \leq x \leq \cos(\zeta) \quad \text{and} \quad 0 \leq y \leq x \tan(\zeta).$$

Then $\text{vol}(S(\zeta))$ is given by

$$\text{vol}(S(\zeta)) = \int_T \int_{z \geq \sqrt{1-x^2-y^2}} d \text{vol} = \int_0^{\cos(\zeta)} \int_0^{x \tan(\zeta)} \int_{\sqrt{1-x^2-y^2}}^{\infty} \frac{dz \, dy \, dx}{z^3}$$

Integrating with respect to z , we obtain

$$\text{vol}(S(\zeta)) = \int_0^{\cos(\zeta)} \int_0^{x \tan(\zeta)} \frac{dx \, dy}{2(1-x^2-y^2)},$$

which we rewrite

$$\text{vol}(S(\zeta)) = \int_0^{\cos(\zeta)} \int_0^{x \tan(\zeta)} \frac{dx \, dy}{2((\sqrt{1-x^2})^2 - y^2)},$$

and integrate with respect to y :

$$\begin{aligned} \text{vol}(S(\zeta)) &= \int_0^{\cos(\zeta)} \frac{1}{4\sqrt{1-x^2}} \log \left(\frac{\sqrt{1-x^2} + x \tan \zeta}{\sqrt{1-x^2} - x \tan \zeta} \right) dx \\ &= \int_0^{\cos(\zeta)} \frac{1}{4\sqrt{1-x^2}} \log \left(\frac{\sqrt{1-x^2} \cos(\zeta) + x \sin(\zeta)}{\sqrt{1-x^2} \cos(\zeta) - x \sin(\zeta)} \right) dx. \end{aligned}$$

Using the substitution $x = \cos(\theta)$, the integral becomes

$$\begin{aligned} \text{vol}(S(\zeta)) &= \int_{\pi/2}^{\zeta} \frac{1}{4} \log \left(\frac{\sin \theta \cos \zeta + \cos \theta \sin \zeta}{\sin \theta \cos \zeta - \cos \theta \sin \zeta} \right) (-d\theta) \\ &= -\frac{1}{4} \left(\int_{\pi/2}^{\zeta} \log \left(\frac{2 \sin(\theta + \zeta)}{2 \sin(\theta - \zeta)} \right) d\theta \right) \\ &= \frac{1}{4} \left(\int_{\pi/2}^{\zeta} -\log(2 \sin(\theta + \zeta)) d\theta - \int_{\pi/2}^{\zeta} -\log(2 \sin(\theta - \zeta)) d\theta \right) \\ &= \frac{1}{4} \left(\int_{\pi/2+\zeta}^{2\zeta} -\log(2 \sin(u)) du - \int_{\pi/2-\zeta}^0 -\log(2 \sin(u)) du \right) \\ &= \frac{1}{4} (\Lambda(2\zeta) - \Lambda(\pi/2 + \zeta) + \Lambda(\pi/2 - \zeta)). \end{aligned}$$

To finish, we use lemma 9.5. Since $\Lambda(\theta)$ is periodic of period π , note that $\Lambda(\pi/2 - \zeta) = \Lambda(-\pi/2 - \zeta)$. Since Λ is an odd function, $\Lambda(-\pi/2 - \zeta) = -\Lambda(\pi/2 + \zeta)$. Finally, since $\Lambda(2\zeta) = 2\Lambda(\zeta) + 2\Lambda(\zeta + \pi/2)$, the above becomes

$$\text{vol}(S(\zeta)) = \frac{1}{4} (2\Lambda(\zeta) + 2\Lambda(\zeta + \pi/2) - 2\Lambda(\pi/2 + \zeta)) = \frac{1}{2} \Lambda(\zeta). \quad \square$$

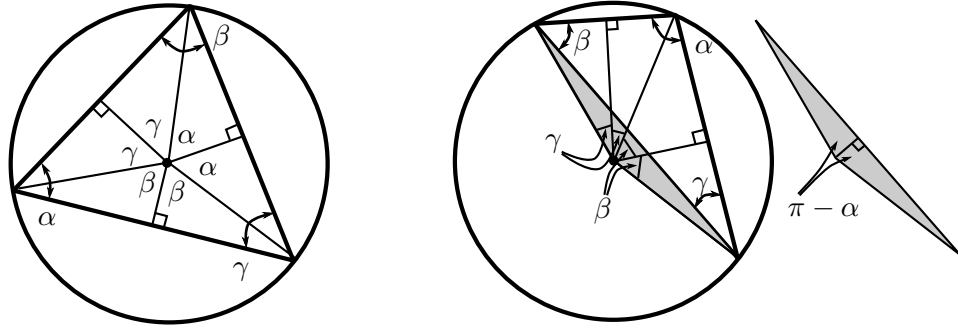


FIGURE 9.3. Left: angles of subsimplices when perpendicular ray lies interior to the tetrahedron. Right: angles when it is exterior

PROOF OF THEOREM 9.3. For an ideal tetrahedron with dihedral angles α , β , and γ , place the tetrahedron in \mathbb{H}^3 with vertices at ∞ , and at p, q, r all on the unit circle in \mathbb{C} . As above, drop a perpendicular ray to the unit hemisphere.

Case 1. Suppose first that the ray lies in the interior of the ideal tetrahedron. Then subdivide the tetrahedron into six simplices as before. Each of the simplices has the properties of lemma 9.7, and is determined by some $\zeta \in (0, \pi/2)$. By lemma 9.8, its volume is determined by ζ as well, so it remains to calculate ζ for each of the six simplices making up the ideal tetrahedron. Project vertically to the complex plane \mathbb{C} ; the angles determining the simplex can then be easily computed using Euclidean geometry. In particular, there are two with angle α , two with angle β , and two with angle γ . See the left of figure 9.3.

Then the volume of the tetrahedron $\Delta(\alpha, \beta, \gamma)$ is

$$\begin{aligned} \text{vol}(\Delta(\alpha, \beta, \gamma)) &= 2 \text{vol}(S(\alpha)) + 2 \text{vol}(S(\beta)) + 2 \text{vol}(S(\gamma)) \\ &= \Lambda(\alpha) + \Lambda(\beta) + \Lambda(\gamma) \end{aligned}$$

Case 2. Now suppose that the ray from ∞ to the point $(0, 0, 1)$ lies outside of the ideal tetrahedron. We may still draw perpendicular lines from $(0, 0, 1)$ to the edges of the ideal tetrahedron on the unit hemisphere, and lines from $(0, 0, 1)$ to vertices of the ideal tetrahedron; the right of figure 9.3 shows the projection to \mathbb{C} and the corresponding angles. Note that we may still cone to ∞ , obtaining six simplices with the properties of lemma 9.7, only now they overlap. However, by adding and subtracting volumes of overlapping simplices, we still will obtain the volume of the ideal tetrahedron. In particular, we have the following.

$$\begin{aligned} \text{vol}(\Delta(\alpha, \beta, \gamma)) &= 2 \text{vol}(S(\gamma)) + 2 \text{vol}(S(\beta)) - 2 \text{vol}(S(\pi - \alpha)) \\ &= \Lambda(\gamma) + \Lambda(\beta) - \Lambda(\pi - \alpha) \end{aligned}$$

Since Λ is an odd function and has period π , $-\Lambda(\pi - \alpha) = \Lambda(\alpha)$. Hence $\text{vol}(\Delta(\alpha, \beta, \gamma)) = \Lambda(\alpha) + \Lambda(\beta) + \Lambda(\gamma)$ in this case as well. \square

The formula for volume of a tetrahedron has the following useful consequences.

THEOREM 9.9. *Let \mathcal{A} be the set of possible angles on a tetrahedron:*

$$\mathcal{A} = \{(\alpha, \beta, \gamma) \in (0, \pi)^3 \mid \alpha + \beta + \gamma = \pi\}.$$

Then the function $\text{vol}: \mathcal{A} \rightarrow \mathbb{R}$ given by

$$\text{vol}(\alpha, \beta, \gamma) = \Lambda(\alpha) + \Lambda(\beta) + \Lambda(\gamma)$$

is strictly concave down on \mathcal{A} . Moreover, we can compute its first two derivatives. For $a = (a_1, a_2, a_3) \in \mathcal{A}$ a point and $w = (w_1, w_2, w_3) \in T_a \mathcal{A}$ a nonzero tangent vector, the first two derivatives of vol in the direction of w satisfy

$$\frac{\partial \text{vol}}{\partial w} = \sum_{i=1}^3 -w_i \log \sin a_i, \quad \frac{\partial^2 \text{vol}}{\partial w^2} < 0.$$

PROOF. First, note that since w is a tangent vector to \mathcal{A} , and the sum of the three coordinates of each point in \mathcal{A} is π , it follows that $w_1 + w_2 + w_3 = 0$.

Next, by theorem 9.3, the directional derivative of vol at a in the direction of w is given by

$$\begin{aligned} \frac{\partial \text{vol}}{\partial w} &= \sum_{i=1}^3 -w_i \log |2 \sin a_i| \\ &= \sum_{i=1}^3 w_i (-\log 2) + \sum_{i=1}^3 -w_i \log |\sin a_i| \\ &= 0 + \sum_{i=1}^3 -w_i \log \sin a_i. \end{aligned}$$

The last line holds since $w_1 + w_2 + w_3 = 0$ and since $a_i \in (0, \pi)$, hence $\sin a_i > 0$.

For the second derivative, we know $a_1 + a_2 + a_3 = \pi$, so at least two of a_1, a_2, a_3 are strictly less than $\pi/2$. Without loss of generality, say a_1 and a_2 are less than $\pi/2$.

Then the second derivative is

$$\frac{\partial^2 \text{vol}}{\partial w^2} = \sum_{i=1}^3 -w_i^2 \cot a_i.$$

Since $a_3 = \pi - a_1 - a_2$ and $w_3 = -w_1 - w_2$, we may write

$$w_3^2 \cot a_3 = (w_1 + w_2)^2 \cot(\pi - a_1 - a_2) = -(w_1 + w_2)^2 \frac{\cot a_1 \cot a_2 - 1}{\cot a_1 + \cot a_2},$$

where the last equality is an exercise in trig identities.

Then we obtain

$$\begin{aligned} -\frac{\partial^2 \text{vol}}{\partial w^2} &= w_1^2 \cot a_1 + w_2^2 \cot a_2 - (w_1 + w_2)^2 \frac{\cot a_1 \cot a_2 - 1}{\cot a_1 + \cot a_2} \\ &= \frac{(w_1 + w_2)^2 + (w_1 \cot a_1 - w_2 \cot a_2)^2}{\cot a_1 + \cot a_2}. \end{aligned}$$

The denominator of the last fraction is positive, because $a_1, a_2 \in (0, \pi/2)$. The numerator is the sum of squares, hence at least zero. In fact, if it equals zero, then we have $w_1 = -w_2$ and $\cot a_1 = -\cot a_2$. But $a_1, a_2 \in (0, \pi/2)$, so this is impossible. Thus numerator and denominator are strictly positive, and so $\partial^2 \text{vol} / \partial w^2$ is strictly negative, hence strictly concave down. \square

THEOREM 9.10. *The regular ideal tetrahedron, with dihedral angles $\alpha = \beta = \gamma = \pi/3$, maximizes volume over all ideal tetrahedra.*

PROOF. Because vol is continuous, we know it obtains a maximum on the cube $[0, \pi]^3$. First we consider the boundary of that cube, and we show the maximum cannot occur there. If any angle is π , then $\alpha + \beta + \gamma = \pi$ implies the other two angles are 0. Thus to show the maximum does not occur on the boundary of the cube, it suffices to show the maximum does not occur when one of the angles is zero. So suppose $\alpha = 0$. Since $\Lambda(0) = \Lambda(\pi) = 0$ by equation (9.3), and since $\Lambda(\beta) + \Lambda(\pi - \beta) = \Lambda(\beta) + \Lambda(-\beta) = 0$ by lemma 9.5, the volume in this case will be 0. So the maximum does not occur on the boundary.

Thus we seek a maximum in the interior. We maximize $\text{vol}(\alpha, \beta, \gamma) = \Lambda(\alpha) + \Lambda(\beta) + \Lambda(\gamma)$ subject to the constraint $\pi = \alpha + \beta + \gamma =: f(\alpha, \beta, \gamma)$. The theory of Lagrange multipliers tells us that at the maximum, there is a scalar λ such that

$$\nabla \text{vol} = \lambda \nabla f, \quad \text{or}$$

$$\log \sin \alpha = \log \sin \beta = \log \sin \gamma = \lambda.$$

This will be satisfied when $\sin \alpha = \sin \beta = \sin \gamma$. Since $\alpha, \beta, \gamma \in (0, \pi)$, and $\alpha + \beta + \gamma = \pi$, it follows that $\alpha = \beta = \gamma = \pi/3$, and the tetrahedron is regular. \square

9.2. Angle structures and the volume functional

Note that in theorem 9.3, we showed that the volume of an ideal tetrahedron can be computed given only its dihedral angles. A dihedral angle can be obtained by taking the imaginary part of the log of a tetrahedron's edge invariant. Thus the imaginary parts alone of the edge invariants allow us to assign a volume to the structure. These are exactly the angles of an angle structure.

Recall from definition 8.29 that we defined an angle structure on an ideal triangulation \mathcal{T} of a manifold M to be a collection of (interior) dihedral angles satisfying:

- (0) Opposite edges of a tetrahedron have the same angle.

- (1) Dihedral angles lie in $(0, \pi)$.
- (2) The sum of angles around any ideal vertex of any tetrahedron is π .
- (3) The sum of angles around any edge class of M is 2π .

The set of all angle structures for a triangulation \mathcal{T} is denoted by $\mathcal{A}(\mathcal{T})$. For M is an orientable 3-manifold with boundary consisting of tori, and \mathcal{T} a triangulation of M , we will study the set of angle structures $\mathcal{A}(\mathcal{T})$.

PROPOSITION 9.11. *Let \mathcal{T} be an ideal triangulation of a 3-manifold M consisting of n tetrahedra, and as usual denote the set of angle structures by $\mathcal{A}(\mathcal{T})$. If $\mathcal{A}(\mathcal{T})$ is nonempty, then it is a convex, finite-sided, bounded polytope in $(0, \pi)^{3n} \subset \mathbb{R}^{3n}$.*

PROOF. For each tetrahedron of \mathcal{T} , an angle structure selects three dihedral angles lying in $(0, \pi)$. Thus $\mathcal{A}(\mathcal{T})$ is a subset of $(0, \pi)^{3n}$. The equations coming from conditions (2) and (3) are linear equations whose solution set is an affine subspace of \mathbb{R}^{3n} . When we intersect the solution space with the cube $(0, \pi)^{3n}$, we obtain a bounded, convex, finite-sided polytope. \square

There is no guarantee that $\mathcal{A}(\mathcal{T})$ is nonempty. However, proposition 9.11 implies that if it is nonempty, then we may view a point of $\mathcal{A}(\mathcal{T})$ as a point in $(0, \pi)^{3n}$. We write $a \in \mathcal{A}(\mathcal{T})$ as $a = (a_1, \dots, a_{3n})$.

DEFINITION 9.12. The *volume functional* $\mathcal{V}: \mathcal{A}(\mathcal{T}) \rightarrow \mathbb{R}$ is defined by

$$\mathcal{V}(a_1, \dots, a_{3n}) = \sum_{i=1}^{3n} \Lambda(a_i).$$

Thus $\mathcal{V}(a)$ is the sum of volumes of hyperbolic tetrahedra associated with the angle structure a .

A reason angle structures are so useful comes from the following two theorems.

THEOREM 9.13 (Volume and angle structures). *Let M be an orientable 3-manifold with boundary consisting of tori, with ideal triangulation \mathcal{T} . If a point $A \in \mathcal{A}(\mathcal{T})$ is a critical point for the volume functional \mathcal{V} then the ideal hyperbolic tetrahedra obtained from the angle structure A give M a complete hyperbolic structure.*

The converse is also true:

THEOREM 9.14. *If M is finite volume hyperbolic 3-manifold with boundary consisting of tori such that M admits a positively oriented hyperbolic ideal triangulation \mathcal{T} , then the angle structure $A \in \mathcal{A}(\mathcal{T})$ giving the angles of \mathcal{T} for the complete hyperbolic structure is the unique global maximum of the volume functional \mathcal{V} on $\mathcal{A}(\mathcal{T})$.*

The two theorems are attributed to Casson and Rivin, and follow from proofs in [Riv94]. The first direct proof of the results are written in Chan's honors thesis [Cha02], using work of Neumann and Zagier [NZ85]. A very

nice self-contained exposition and proof of both theorems is given in [FG11]. We will follow the ideas of Futer and Guéritaud to show theorem 9.13 in section 9.3.

To prove the converse, we will follow a simple proof of Chan using the Schläfli formula for the variation of volumes of ideal tetrahedra. Chan credits his proof to unpublished ideas of Schlenker.

9.3. Leading–trailing deformations

LEMMA 9.15. *Let M be an orientable 3-manifold with boundary consisting of tori, with ideal triangulation \mathcal{T} consisting of n tetrahedra. Then the volume functional $\mathcal{V}: \mathcal{A}(\mathcal{T}) \rightarrow \mathbb{R}$ is strictly concave down on $\mathcal{A}(\mathcal{T})$. For $a = (a_1, \dots, a_{3n}) \in \mathcal{A}(\mathcal{T})$ and $w = (w_1, \dots, w_{3n}) \in T_a\mathcal{A}(\mathcal{T})$ a non-zero tangent vector, the first two directional derivatives of \mathcal{V} satisfy*

$$\frac{\partial \mathcal{V}}{\partial w} = \sum_{i=1}^{3n} -w_i \log \sin a_i \quad \text{and} \quad \frac{\partial^2 \mathcal{V}}{\partial w^2} < 0.$$

PROOF. Because the volume functional \mathcal{V} is the sum of volumes of ideal tetrahedra, the formulas for derivatives follow by linearity from theorem 9.9. Because the second derivative is strictly negative, the volume functional is strictly concave down. \square

We will need to take derivatives in carefully specified directions. To that end, we now define a vector $w = (w_1, \dots, w_{3n}) \in \mathbb{R}^{3n}$ and show that w lies in $T_a\mathcal{A}(\mathcal{T})$. Again the ideas follow from [FG11].

DEFINITION 9.16. Let C be a cusp of M with a cusp triangulation corresponding to the ideal tetrahedra of \mathcal{T} . Let ζ be an oriented closed curve on C , isotoped to run monotonically through the cusp triangulation, as in definition 4.12. Let ζ_1, \dots, ζ_k be the oriented segments of ζ in distinct triangles. For the segment ζ_i in triangle t_i , define the *leading corner* of t_i to be the corner of the triangle that is opposite the edge where ζ_i enters t_i , and define the *trailing corner* to be the corner opposite the edge where ζ_i exits.

Each corner of the triangle t_i is given a dihedral angle a_j in an angle structure, thus corresponds to a coordinate of $\mathcal{A}(\mathcal{T}) \subset \mathbb{R}^{3n}$. Similarly for any $a \in \mathcal{A}(\mathcal{T})$, each corner of t_i corresponds to a coordinate of the tangent space $T_a\mathcal{A}(\mathcal{T}) \subset \mathbb{R}^{3n}$.

We define a vector $w(\zeta_i) \in \mathbb{R}^{3n}$ by setting the coordinate corresponding to the leading corner of t_i equal to $+1$, and the coordinate corresponding to the trailing corner of t_i equal to -1 . Set all other coordinates equal to zero. The *leading–trailing deformation* corresponding to ζ is defined to be the vector $w(\zeta) = \sum_i w(\zeta_i)$.

An example is shown in figure 9.4.

LEMMA 9.17. *Let σ be a curve encircling a vertex of the cusp triangulation on cusp C . Let μ be an embedded curve isotopic to a generator of the*

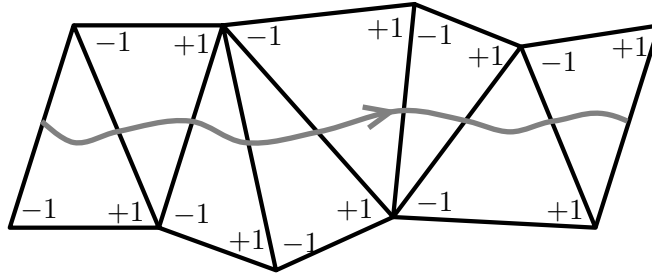


FIGURE 9.4. For the oriented curve ζ shown, leading corners are marked with $+1$ and trailing corners with -1

holonomy group of the cusp torus. Then the corresponding leading-trailing deformation vectors $w(\sigma)$ and $w(\mu)$ both lie in the tangent space $T_a\mathcal{A}(\mathcal{T})$, for any $a \in \mathcal{A}(\mathcal{T})$.

PROOF. The space $\mathcal{A}(\mathcal{T})$ is a submanifold of \mathbb{R}^3 cut out by linear equations corresponding to (2) and (3) of definition 8.29, namely that angles at each ideal vertex of a tetrahedron sum to π , and angles about an edge of M sum to 2π . Let $f_i(a) = a_i + a_{i+1} + a_{i+2}$ be the sum of angles of the i -th tetrahedron, and let $g_e(a) = \sum a_{e_i}$ be the sum of angles about the edge e . So $\mathcal{A}(\mathcal{T}) \subset (0, \pi)^{3n}$ is the space cut out by all equations $f_i = \pi$ and $g_e = 2\pi$. Thus to see that $w(\zeta)$ is a tangent vector to $\mathcal{A}(\mathcal{T})$ at a point a , we need to show that the vector is orthogonal to the gradient vectors ∇f_i and ∇g_e at a , for all i and all e .

Note ∇f_i is the vector $(0, \dots, 0, 1, 1, 1, 0, \dots, 0)$, with 0s away from the i^{th} tetrahedron t_i and 1s in the three positions corresponding to the angles of t_i . There are four cusp triangles coming from this tetrahedron, corresponding to its four ideal vertices. Suppose ζ is a curve in the cusp triangulation of C . If no segment of ζ runs through a triangle of t_i , then $w(\zeta)$ has only 0s in the position corresponding to the 1s of ∇f_i , hence $\nabla f_i \cdot w(\zeta) = 0$ in this case. So suppose that some segment ζ_j of ζ runs through a triangle of t_i . Then one corner of the triangle is a leading corner for ζ_j , and one is a trailing corner, so $w(\zeta_j)$ has one 0, one $+1$, and one -1 in the three positions corresponding to angles of t_i . Hence $\nabla f_i \cdot w(\zeta_j) = 0$. By linearity, $\nabla f_i \cdot w(\zeta) = 0$.

So it remains to show that for each edge e , $\nabla g_e \cdot w(\zeta) = 0$, where ζ is one of the curves σ or μ in the hypothesis of the lemma. Note that ∇g_e is a vector $(\epsilon_1, \dots, \epsilon_{3n})$, where ϵ_j is one of the integers 0, 1, or 2, counting the number of times a dihedral angle of a tetrahedron occurs in the gluing equation g_e . We will consider the segments of ζ one at a time. Note that any segment ζ_j of ζ contributes 0, $+1$, and -1 to opposite edges of exactly one tetrahedron t_j , as illustrated in figure 9.5, left.

If the edge e is not identified to any of the edges of the tetrahedron t_j , then $\nabla g_e \cdot w(\zeta_j) = 0$. Similarly, if e is identified only to one or both of

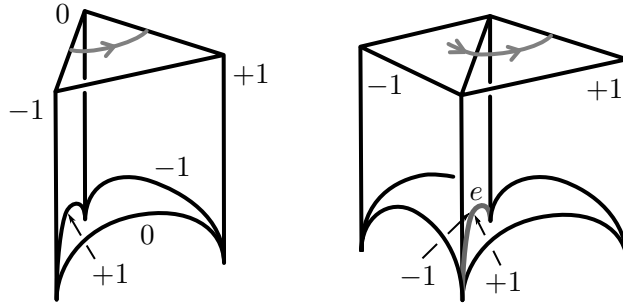


FIGURE 9.5. Left: Effect of $w(\sigma_j)$ on the edges of a tetrahedron. Right: If the lower edge is identified to e , then the contribution of $+1$ from $w(\zeta_j)$ to e cancels with the -1 contribution from $w(\zeta_{j-1})$.

the edges for which $w(\zeta_j)$ contributes a 0, then although the corresponding coordinate of ∇g_e will be 1 or 2, the dot product $\nabla g_e \cdot w(\zeta_j)$ will still be 0.

If e is identified to one or both of the edges labeled with a $+1$ by $w(\zeta_j)$, then there will be a contribution of $+1$ or $+2$ (respectively) to $\nabla g_e \cdot w(\zeta_j)$ coming from these labels. We will show that in this case, there exists one or two (respectively) segments of ζ each contributing -1 , so that the positive contributions cancel.

Suppose first that e is identified to the non-vertical edge of t_j labeled $+1$. Then consider the segment ζ_{j-1} . This lies in a tetrahedron t_{j-1} glued to t_j along a face containing the edge identified to e . In the cusp triangulation, ζ_{j-1} exits its cusp triangle at this face. Thus the opposite corner of the cusp triangle is a trailing corner, and is assigned a -1 . This trailing corner corresponds to an edge opposite e . So e picks up a -1 from $w(\zeta_{j-1})$. See figure 9.5, right. Hence the $+1$ contribution of $w(\zeta_j)$ is canceled in this case with this -1 from $w(\zeta_{j-1})$.

Now suppose e is identified to the vertical edge of t_j labeled $+1$. Let $\zeta_j, \zeta_{j+1}, \dots, \zeta_{j+r}$ be a maximal collection of segments in cusp triangles adjacent to e . Note if $\zeta = \sigma$ encircles a vertex, that vertex will not correspond to the endpoint of e . Then $r = 1$, i.e. there are just two segments of ζ adjacent to e . If $\zeta = \mu$ is a generator of cusp homology, then $r \geq 1$. Because we are assuming ζ is embedded and meets each edge of the cusp triangulation at most once, we know $\zeta_j, \dots, \zeta_{j+r}$ do not encircle e completely in this case. See figure 9.6.

In both cases $\zeta = \sigma$ and $\zeta = \mu$, for segments ζ_{j+k} with $0 < k < r$, note $w(\zeta_{j+k})$ contributes only 0s to the edge e . Since the segment after ζ_{j+r} is no longer adjacent to the vertical edge e , it follows that $w(\zeta_{j+r})$ contributes -1 to e . Then the $+1$ contribution from $w(\zeta_j)$ cancels with the -1 contribution from $w(\zeta_{j+r})$.

Finally, it could be the case that e is identified to both edges labeled $+1$ by $w(\zeta_j)$, so that ∇g_e has a 2 in that coordinate and $\nabla g_e \cdot w(\zeta_j)$ picks up a

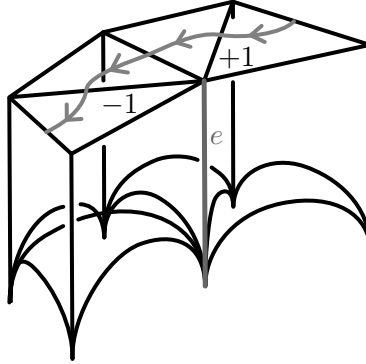


FIGURE 9.6. If $w(\zeta_j)$ contributes $+1$ to a vertical edge meeting e , there is a maximal collection of segments running through cusp triangles adjacent to e .

$+2$ from these two edges. But in this case, combining both arguments above implies that one of the $+1$ contributions is canceled by a -1 coming from $w(\zeta_{j-1})$ and one by a -1 coming from $w(\zeta_{j+r})$ for appropriate r . Thus both are canceled.

We have shown that for each j , each $+1$ contribution of $w(\zeta_j)$ to $\nabla g_e \cdot w(\zeta_j)$ is canceled by a -1 contribution from some $w(\zeta_k)$. Provided none of the -1 contributions from $w(\zeta_k)$ are repeated for distinct j , this shows that $\nabla g_e \cdot w(\zeta) \leq 0$. The fact that these contributions are not repeated follows from the uniqueness of the choice of ζ_{j-1} and ζ_{j+r} .

A similar argument implies $\nabla g_e \cdot w(\zeta) \geq 0$. Thus $\nabla g_e \cdot w(\zeta) = 0$, as desired. \square

LEMMA 9.18. *Let ζ be one of the curves σ or μ of lemma 9.17, and let $w(\zeta) \in T_a\mathcal{A}(\mathcal{T})$ be the corresponding leading-trailing deformation vector. Let $H(\zeta)$ be the complex number associated to the curve ζ given in definition 4.12 (completeness equations). Then*

$$\frac{\partial \mathcal{V}}{\partial w(\zeta)} = \Re(\log H(\zeta)).$$

PROOF. Let ζ_1, \dots, ζ_k denote segments of ζ in cusp triangles t_1, \dots, t_k , respectively. Label the dihedral angles of triangle t_i by $\alpha_i, \beta_i, \gamma_i$, in clockwise order, so that α_i is the angle cut off by t_i . By definition 4.12,

$$\Re(\log H(\zeta)) = \sum_i \epsilon_i \Re(\log |z(\alpha_i)|),$$

where $z(\alpha_i)$ is the edge invariant associated with the edge labeled α_i , and $\epsilon_i = +1$ if α_i is to the left of ζ_i and $\epsilon_i = -1$ if α_i is to the right of ζ_i .

On the other hand, comparing figure 4.13 and figure 9.4, we see that when α_i is to the left of ζ_i , the vector $w(\zeta_i)$ has a $+1$ in the position corresponding to β_i and a -1 in the position corresponding to γ_i , and when α_i is to the right of ζ_i , the vector $w(\zeta_i)$ has a -1 in the position corresponding to

β_i and a +1 in the position corresponding to γ_i . Then lemma 9.15 implies that

$$\begin{aligned} \frac{\partial \mathcal{V}}{\partial w} &= \sum_{j=1}^{3n} -w_j \log \sin a_j \\ &= \sum_i -\epsilon_i \log \sin \beta_i + \epsilon_i \log \sin \gamma_i \\ &= \sum_i \epsilon_i \log \left(\frac{\sin \gamma_i}{\sin \beta_i} \right) \\ &= \sum_i \epsilon_i \Re(\log |z(\alpha_i)|), \quad \text{by equation (8.1)} \end{aligned}$$

This is what we needed to show. \square

We now have the tools we need to prove theorem 9.13, to show that a critical point $a \in \mathcal{A}(\mathcal{T})$ of the volume functional corresponds to a complete hyperbolic structure on the manifold M .

PROOF OF THEOREM 9.13. Suppose $a \in \mathcal{A}(\mathcal{T})$ is a critical point of the volume functional \mathcal{V} . Then a assigns a dihedral angle to each tetrahedron of \mathcal{T} , giving each ideal tetrahedron a unique hyperbolic structure. By theorem 4.7, gluing these tetrahedra will give a hyperbolic structure on M if and only if the edge gluing equations are satisfied for each edge. By theorem 4.10, the hyperbolic structure will be complete if and only if the induced geometric structure on each cusp torus is a Euclidean structure, and we obtain a Euclidean structure when the completeness equations are satisfied by proposition 4.15.

Consider first the edge gluing equations. Notice that any angle structure gives hyperbolic ideal tetrahedra satisfying the imaginary part of the gluing equations, so we need to show that our tetrahedra satisfy the real part. Fix an edge of the triangulation, and let σ be a curve on a cusp torus encircling an endpoint of that edge. The real part of the gluing equation corresponding to this edge will be satisfied if and only if $\Re(\log H(\sigma)) = 0$. But lemma 9.18 implies that $\Re(\log H(\sigma)) = \frac{\partial \mathcal{V}}{\partial w(\sigma)}$, and this is zero because our angle structure is a critical point of the volume functional. So the gluing equations hold.

As for the completeness equations, for any cusp torus C , and μ_1 and μ_2 generators of the first homology group of C , the completeness equations require that $H(\mu_1) = H(\mu_2) = 1$. By lemma 9.18, we know

$$\Re \log(H(\mu_i)) = \frac{\partial \mathcal{V}}{\partial w(\mu_i)} = 0,$$

since a is a critical point. Thus the real part of each of these completeness equations is satisfied.

Consider the developing image of a fundamental domain for the cusp torus C . Because we know the angles given by a satisfy the gluing equations,

the structure on C is at least an affine structure on the torus. Therefore the developing image of the fundamental domain is a quadrilateral in \mathbb{C} . Since the real parts of the completeness equations for μ_1 and μ_2 are both satisfied, it follows that the holonomy elements corresponding to μ_1 and μ_2 do not scale either side of the fundamental domain. But then the holonomy elements cannot effect a non-trivial rotation either; a quadrilateral in \mathbb{C} whose opposite sides are the same length is a parallelogram. Thus the developing image of a fundamental domain is a parallelogram, the holonomy elements corresponding to μ_1 and μ_2 must be pure translations, and the cusp torus admits a Euclidean structure. So the completeness equations hold. \square

Theorem 9.13 gives us a way of proving not only that a 3-manifold M is hyperbolic, but also that it admits a positively oriented geometric triangulation. To use the theorem, first, fix a triangulation \mathcal{T} . Then show the space of angle structures $\mathcal{A}(\mathcal{T})$ is nonempty. Finally, show that the volume functional achieves its maximum in the interior of $\overline{\mathcal{A}(\mathcal{T})}$. The last step can often be accomplished by considering angle structures on the boundary $\overline{\mathcal{A}(\mathcal{T})} - \mathcal{A}(\mathcal{T})$ and proving such structures cannot maximize volume. We will follow exactly this procedure for 2-bridge knots in chapter 10.

The following proposition is a useful tool for examining the maximum of the volume functional on the boundary $\overline{\mathcal{A}(\mathcal{T})} - \mathcal{A}(\mathcal{T})$.

PROPOSITION 9.19. *Suppose an angle structure $a \in \overline{\mathcal{A}(\mathcal{T})}$ maximizes the volume functional \mathcal{V} . Suppose that for some tetrahedron Δ_i , one of the three angles of Δ_i in the angle structure a is 0. Then two of the angles are 0 and the third is π .*

PROOF. Suppose instead that one angle, say a_i is 0, but the other two angles of Δ_i are nonzero: $a_{i+1} \neq 0$ and $a_{i+2} \neq 0$. We will find a path through $\mathcal{A}(\mathcal{T})$ with endpoint the angle structure a , and we will show that the derivative of this path is positive, and in fact unbounded, as it approaches the endpoint corresponding to a . It will follow that a cannot be a maximum, which contradicts our assumption on a .

The space of angle structures $\mathcal{A}(\mathcal{T})$ is a bounded open convex subset of \mathbb{R}^{3n} . Its tangent space can be extended to its boundary. We may choose a tangent vector w in $T_a \overline{\mathcal{A}(\mathcal{T})}$ pointing into the interior of $\mathcal{A}(\mathcal{T})$, and take the path corresponding to geodesic flow in the direction of this tangent vector. Theorem 9.9 implies that the derivative of the volume functional along this path is the sum of terms of the form $\sum_{i=1}^{3n} -w_i \log \sin(a_i)$.

Consider the contribution from Δ_i . The terms

$$w_{i+1} \log \sin(a_{i+1}) \text{ and } w_{i+2} \log \sin(a_{i+2})$$

are bounded, since a_{i+1} and a_{i+2} are bounded away from zero. But as the path approaches the angle structure a , the term coming from $-w_i \log \sin(a_i)$ approaches positive infinity. Thus such a point cannot be a maximum. \square

9.4. The Schläfli formula

In this short section, we prove theorem 9.14, the converse to theorem 9.13. Our proof uses the Schläfli formula for ideal tetrahedra, which can be stated as follows.

THEOREM 9.20 (Schläfli's formula for ideal tetrahedra). *Let P be an ideal tetrahedron. Let H_1, \dots, H_n be a collection of horospheres centered on the ideal vertices of P . For each edge e_{ij} , running between the i -th to the j -th ideal vertices of P , let $\ell(e_{ij})$ denote the signed distance between H_i and H_j (that is, $\ell(e_{i,j})$ is defined to be negative if $H_i \cap H_j \neq \emptyset$). Finally, let θ_{ij} denote the dihedral angle along edge $e_{i,j}$. Then the variation in the volume of P satisfies*

$$(9.4) \quad d\mathcal{V}(P) = -\frac{1}{2} \sum_{i,j} \ell(e_{ij}) d\theta_{i,j}.$$

Schläfli's formula was originally proved for finite spherical simplices by Schläfli in the 1850s. It has been extended in many directions, including to finite and ideal polyhedra in spaces of constant curvature. A proof of a formula that contains the result in theorem 9.20 can be found in [Mil94]; see also [Riv94]. These sources note that the right hand side of equation (9.4) is independent of the choice of horospheres.

Using this, we can finish the proof.

PROOF OF THEOREM 9.14. Choose a horosphere about each cusp in the complete hyperbolic structure on M . Because the hyperbolic structure is complete, this choice gives a well-defined horosphere about each ideal vertex of each ideal tetrahedron in the positively oriented hyperbolic ideal triangulation \mathcal{T} . Thus for each tetrahedron, we may use this choice to define the edge lengths $\ell(e_{ij})$ of theorem 9.20.

Now note that because the total angle around each edge is a constant 2π , the contributions to the variation of the volume coming from each simplex add to zero for each edge. Thus the right hand side of equation (9.4) is zero. It follows that the complete structure is a critical point for the volume functional.

On the other hand, since the volume functional is strictly concave down on \mathcal{A} , theorem 9.9, it must follow that the complete structure is the unique global maximum. \square

9.5. Consequences

Theorem 9.13 and its converse have a number of important immediate consequences. We leave many proofs as exercises.

COROLLARY 9.21 (Lower volume bounds, angle structures). *Suppose M has ideal triangulation \mathcal{T} such that the volume functional $\mathcal{V}: \mathcal{A}(\mathcal{T}) \rightarrow \mathbb{R}$ has*

a critical point $p \in \mathcal{A}(\mathcal{T})$. Then for any other point $q \in \overline{\mathcal{A}(\mathcal{T})}$, the volume functional satisfies

$$\mathcal{V}(q) \leq \text{vol}(M),$$

with equality if and only if $q = p$, i.e. q also gives the complete hyperbolic metric on M .

PROOF. By lemma 9.15, the volume functional is strictly concave down on $\overline{\mathcal{A}(\mathcal{T})}$, and so for any point $q \in \overline{\mathcal{A}(\mathcal{T})}$, $\mathcal{V}(q)$ is at most the maximum value of the volume functional, which is the value $\mathcal{V}(p)$ by hypothesis, and with equality if and only if $q = p$. By theorem 9.13, $\text{vol}(M) = \mathcal{V}(p)$. \square

More is conjectured to be true. Corollary 9.21 only gives a bound when there is a known critical point of the volume functional in the interior of the space of angle structures. If the maximum of the volume functional occurs on the boundary, it still seems to be the case in practice that the maximum is bounded by the volume of the complete hyperbolic structure. However, the following conjecture is currently still open.

CONJECTURE 9.22 (Casson's conjecture). *Let M be a cusped hyperbolic 3-manifold, and let \mathcal{T} be any ideal triangulation of M . If the space of angle structures $\mathcal{A}(\mathcal{T})$ is nonempty, then the maximum value for the volume functional on $\overline{\mathcal{A}(\mathcal{T})}$ is at most the volume of the complete hyperbolic structure on M .*

We may use angle structures to find hyperbolic Dehn fillings of triangulated 3-manifolds as well. Recall from chapter 6 that the (p, q) Dehn filling on a triangulated manifold satisfies equation (6.1):

$$p \log H(\mu) + q \log H(\lambda) = 2\pi i.$$

THEOREM 9.23 (Angle structures and Dehn fillings). *Let M be a manifold with torus boundary components T_1, \dots, T_n , with generators μ_j, λ_j of $\pi_1(T_j)$ for each j . For each j , let (p_j, q_j) denote a pair of relatively prime integers. Let $\mathcal{A}_{(p_1, q_1), \dots, (p_n, q_n)} \subset \mathcal{A}$ be the set of all angle structures that satisfy the imaginary part of the Dehn filling equations:*

$$\Im(p_j \log H(\mu_j) + q_j \log H(\lambda_j)) = 2\pi.$$

Then a critical point of the volume functional \mathcal{V} on $\mathcal{A}_{(p_1, q_1), \dots, (p_n, q_n)}$ gives the complete hyperbolic structure on the Dehn filling $M((p_1, q_1), \dots, (p_n, q_n))$ of M .

PROOF. As in the proof of theorem 9.13, we will have a complete hyperbolic structure on the Dehn filling if and only if each edge gluing equation is satisfied and additionally each Dehn filling equation

$$p_j \log H(\mu_j) + q_j \log H(\lambda_j) = 2\pi i$$

is satisfied.

The proof that edge gluing equations are satisfied follows exactly as in the proof of theorem 9.13. As for the Dehn filling equations, the imaginary

part of each equation is satisfied by the given constraint on the space of angle structures. By lemma 9.18, the real part satisfies

$$\Re(p_j \log(H(\mu_j)) + q_j \log(H(\lambda_j))) = p_j \frac{\partial \mathcal{V}}{\partial w(\mu_j)} + q_j \frac{\partial \mathcal{V}}{\partial w(\lambda_j)} = 0,$$

because this is a critical point for the volume functional. Thus each Dehn filling equation is satisfied. \square

Corollary 9.21 and theorem 6.13 imply the following (weaker) version of Thurston's theorem on volume change under Dehn filling, theorem 6.30.

COROLLARY 9.24. *Let M be as in theorem 9.23. If s is a slope in the neighborhood of ∞ provided by Thurston's hyperbolic Dehn filling theorem, theorem 6.13, then the volume of $M(s)$ is strictly smaller than the volume of M .*

PROOF. Exercise 9.9. \square

We also have the tools to prove a rigidity theorem originally due to Weil. The following follows from Mostow–Prasad rigidity, theorem 6.1, but was first proved over a decade before that theorem, and can now be proved easily using angle structures.

COROLLARY 9.25 (Weil rigidity theorem). *Suppose M is a 3-manifold with boundary consisting of tori, and suppose the interior of M admits a complete hyperbolic metric. Then the metric is locally rigid, i.e. there is no local deformation of the metric through complete hyperbolic structures.*

PROOF. Exercise 9.10. \square

9.6. Exercises

EXERCISE 9.1. Find a formula for volume of a tetrahedron with ideal vertices 0 , 1 , ∞ and z in terms of z alone.

EXERCISE 9.2. Give a proof that the figures of figure 9.3 are correct. That is, given a Euclidean triangle with vertices on the unit circle, and angles α , β , and γ , prove that the angles around the origin are given as shown in the figure.

EXERCISE 9.3. Prove the Kubert identities for the Lobachevsky function:

$$\Lambda(n\theta) = \sum_{k=0}^{n-1} n\Lambda(\theta + k\pi/n).$$

Hint: cyclotomic identities:

$$2 \sin(n\theta) = \prod_{k=0}^{n-1} 2 \sin\left(\theta + \frac{k\pi}{n}\right).$$

EXERCISE 9.4. Find an explicit convex polytope describing the set of angle structures on the complement of the figure-8 knot.

EXERCISE 9.5. Find an explicit convex polytope describing the set of angle structures on the complement of the 5_2 knot.

EXERCISE 9.6. Suppose an ideal tetrahedron has dihedral angles α , β , γ in clockwise order. Prove equation (8.1): that the edge invariant of the tetrahedron assigned to the edge with angle α is

$$z(\alpha) = \frac{\sin(\gamma)}{\sin(\beta)} e^{i\alpha}.$$

EXERCISE 9.7. An ideal octahedron can be obtained by gluing two identical ideal pyramids over an ideal quadrilateral base along the ideal quadrilateral. We triangulate this by running an edge from the ideal point opposite the quadrilateral on one pyramid, through the quadrilateral, to the ideal point opposite the quadrilateral on the other pyramid, and then we stellar subdivide. Using angle structures on this collection of ideal tetrahedra, prove that the maximal volume ideal hyperbolic octahedron is the regular one: the one for which the quadrilateral base is a square.

EXERCISE 9.8. Generalize exercise 9.7 to the ideal object obtained by gluing two ideal pyramids over an ideal n -gon base. Using stellar subdivision and angle structures, prove that the volume of the ideal double pyramid with base an n -gon is maximized when the n -gon is regular.

EXERCISE 9.9. Prove that volume decreases locally under Dehn filling, corollary 9.24.

EXERCISE 9.10. Prove the Weil rigidity theorem, corollary 9.25. First prove it for manifolds admitting an angle structure. Extend to all manifolds using the following theorem of Luo, Schleimer, and Tillmann, which can be found in [LST08]. (You may assume the theorem for the exercise.)

THEOREM 9.26 (Geometric triangulations exist virtually). *Let M be a 3-manifold with boundary consisting of tori, such that the interior of M admits a complete hyperbolic structure. Then M has a finite cover N such that N decomposes into positively oriented ideal tetrahedra.*

Two-Bridge Knots and Links

In this chapter we will study in detail a class of knots and links that has particularly nice geometry, namely the class of 2-bridge knots and links. The key property of these links that we will explore is the fact that they admit a geometric triangulation that can be read off of a diagram, or an algebraic description of the link. In this chapter, we will define 2-bridge knots and links, describe their triangulations, and mention some of their geometric properties and consequences.

10.1. Rational tangles and 2-bridge links

In 1956, H. Schubert showed that the class of 2-bridge knots and links are classified by a rational number, and any continued fraction expansion of this number gives a diagram of the knot [Sch56]. In this section, we work through the description of 2-bridge knots and links via rational numbers. Additional references are [BZ85] and [Mur96].

First, we define tangles.

DEFINITION 10.1. A *tangle* is a 1-manifold properly embedded in a 3-ball B . That is, it is a collection of arcs with endpoints on ∂B and interiors disjointly embedded in the interior of B , possibly along with a collection of simple closed curves. For our purposes, we will consider only tangles consisting of two arcs, thus with four endpoints embedded on the boundary of a ball.

The simplest tangle is a rational tangle.

DEFINITION 10.2. A *rational tangle* is a tangle obtained by embedding two disjoint arcs on the surface of a 4-punctured sphere (pillowcase), and then pushing the interiors slightly into the 3-ball bounded by the 4-punctured sphere.

The tangles are called rational because they can be defined by a rational number, as follows. Recall that a rational number can be described by a

continued fraction:

$$\frac{p}{q} = [a_n, a_{n-1}, \dots, a_1] = a_n + \frac{1}{a_{n-1} + \frac{1}{\dots + \frac{1}{a_1}}}.$$

Now, given a continued fraction $[a_n, \dots, a_1]$, we will form a rational tangle. Start by labeling the four points on the pillowcase NW, NE, SW, and SE. If n is even, connect NE to SE and NW to SW by attaching two arcs as in figure 10.1(a). Perform a homeomorphism of B^3 that rotates the points NW and NE $|a_1|$ times, creating a vertical band of $|a_1|$ crossings in the two arcs. If $a_1 > 0$, rotate in a counterclockwise direction, so that the overcrossings of the result have positive slope. This is called a *positive crossing*. If $a_1 < 0$ rotate in a clockwise direction, so that overcrossings have negative slope, forming a *negative crossing*. In figure 10.1(b), three positive crossings have been added. After twisting, relabel the points NW, NE, SW, and SE to match their original orientation. Next, apply a homeomorphism of B^3 that rotates NE and SE $|a_2|$ times, adding crossings in a horizontal band. Again these crossings will be positive if $a_2 > 0$, and negative if $a_2 < 0$. Repeat this process for each a_i . When finished, we obtain a rational tangle. An example is shown in figure 10.1.

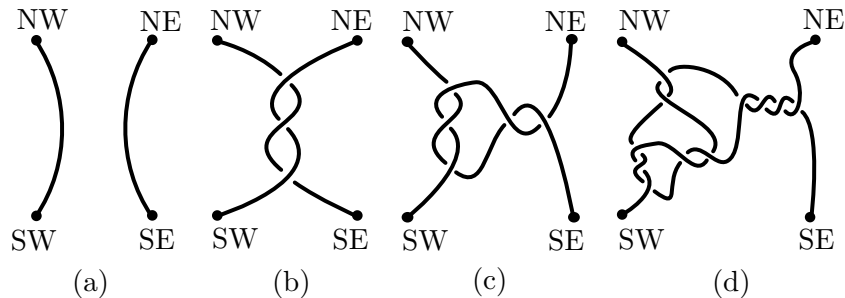


FIGURE 10.1. Building a rational tangle from the continued fraction $[4, -2, -2, 3]$.

If n is odd, start with two arcs connecting NW to NE and SW to SE. In this case we add a horizontal band of crossings first, and then continue as before, alternating between horizontal and vertical bands for each a_i .

Any rational tangle may be built by this process. As a convention, we require that the left-most term a_n in the continued fraction expansion corresponds to a horizontal band of crossings. If we build a rational tangle ending with a vertical band, as in figure 10.1(b), then we insert a 0 into the corresponding continued fraction, representing a horizontal band of 0 crossings. For example, the continued fraction corresponding to the tangle in figure 10.1(b) is $[0, 3]$. This convention ensures that any continued fraction completely specifies a single rational tangle. There are two trivial rational

tangles, namely $0 = [0]$, with untwisted strands connecting NW to NE and SW to SE, and $\infty = [0, 0] = 0 + \frac{1}{0}$, with untwisted strands connecting NW to SW and NE to SE. The tangle ∞ is shown in figure 10.1(a).

PROPOSITION 10.3 ([**Con70**]). *Equivalence classes of rational tangles are in one-to-one correspondence with the set $\mathbb{Q} \cup \infty$. In particular, tangles $T(a_n, \dots, a_1)$ and $T(b_m, \dots, b_1)$ are equivalent if and only if the continued fractions $[a_n, \dots, a_1]$ and $[b_m, \dots, b_1]$ are equal.* \square

Proposition 10.3 allows us to put all our tangles into nice form.

COROLLARY 10.4. *For any rational tangle, there exists an equivalent tangle $T(a_n, \dots, a_1)$ for which $a_i \neq 0$ for $1 \leq i < n$, and either all $a_i \geq 0$ or all $a_i \leq 0$.*

PROOF. This follows immediately from exercise 10.2. \square

Thus we will assume that positive tangles have only positive crossings, and negative tangles have only negative crossings. In either case, this will make the tangle diagram alternating.

DEFINITION 10.5. The *numerator closure* $\text{num}(T)$ of a rational tangle T is formed by connecting NW to NE and SW to SE by simple arcs with no crossings. The *denominator closure* $\text{denom}(T)$ is formed by connecting NW to SW and NE to SE by simple arcs with no crossings.

DEFINITION 10.6. A *2-bridge knot or link* is the denominator closure of a rational tangle.

Notice that the denominator closure of the tangle $T(a_n, a_{n-1}, \dots, a_1)$ is always equivalent to the denominator closure of the tangle $T(0, a_{n-1}, \dots, a_1)$, since a_n corresponds to horizontal crossings that can simply be unwound after forming the denominator closure. Thus when we consider 2-bridge knots, we may assume that in our rational tangle, $a_n = 0$.

DEFINITION 10.7. The 2-bridge knot or link that is the denominator closure of the tangle $T(a_n, a_{n-1}, \dots, a_1)$ (and $T(0, a_{n-1}, \dots, a_1)$) is denoted by $K[a_{n-1}, \dots, a_1]$.

The above discussion of twisting and taking denominator closure gives a nice correspondence between diagrams of 2-bridge knots and continued fraction expansions of rational numbers p/q with $|p/q| \leq 1$. This is summarized in the following lemma.

LEMMA 10.8. *Suppose $[0, a_{n-1}, \dots, a_1]$ is a continued fraction with either $a_i > 0$ for all i or $a_i < 0$ for all i . Then the diagram of $K[a_{n-1}, \dots, a_1]$ contains $n - 1$ twist regions, arranged left to right. The twist region on the far left contains $|a_1|$ crossings, with sign opposite that of a_1 when n is even, the next twist region to the right contains $|a_2|$ crossings, with sign opposite that of a_2 when n is odd, and so on, with the i -th twist region from the left containing $|a_i|$ crossings, with sign the same as a_i if i and n are both even*

or both odd, and opposite sign of a_i if one of i and n is even and the other odd. Twist regions connect as illustrated in figure 10.2.

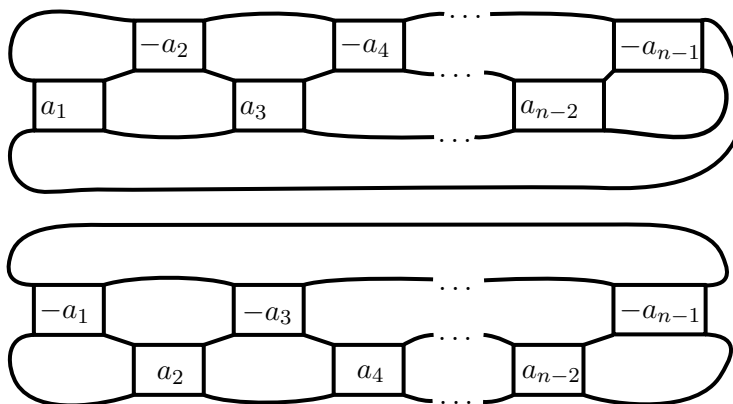


FIGURE 10.2. The diagram of $K[a_{n-1}, \dots, a_1]$. Top: n odd; bottom: n even. Box labeled $\pm a_i$ denotes a (horizontal) twist region with $|a_i|$ crossings, with sign of the crossings equal to that of $\pm a_i$.

PROOF. The tangle $T(0, a_{n-1}, \dots, a_1)$ is obtained by forming horizontal or vertical bands of $|a_i|$ crossings, for $i = 1, \dots, n - 1$. Thus the diagram of the denominator closure has $n - 1$ twist regions with the numbers of crossings as claimed. To put it into the form of figure 10.2, isotope the diagram by rotating vertical twist regions to be horizontal. Note that the rotation changes the sign of the crossing. Thus when n is even, this rotates twist regions with odd index i to be horizontal, and thus sign becomes opposite that of a_i , for even n and odd i . When n is odd, this rotates twist regions with even index to be horizontal, again with sign opposite that of a_i , for odd n and even i . \square

LEMMA 10.9. For a 2-bridge knot or link $K[a_{n-1}, \dots, a_1]$, we may always assume $|a_1| \geq 2$ and $|a_{n-1}| \geq 2$.

PROOF. Exercise. One way to see this is to consider the form of a 2-bridge knot or link with $|a_1| = 1$ or $|a_{n-1}| = 1$, and show that the corresponding twist region can be subsumed into another twist region. \square

For the rest of this chapter, we will assume the conclusions of corollary 10.4 and lemma 10.9, namely that if $K[a_{n-1}, \dots, a_1]$ is a 2-bridge knot or link, then either $a_i > 0$ for all i or $a_i < 0$ for all i , and $|a_{n-1}| \geq 2$ and $|a_1| \geq 2$.

10.2. Triangulations of 2-bridge links

We now describe a way to triangulate 2-bridge link complements that was first observed by Sakuma and Weeks [SW95]. A description was also given by Futer in the appendix of [Gu 06b]; we base our exposition here off of the latter paper.

Consider again our construction of a rational tangle. We started with two strands in a 4-punctured sphere, or pillowcase. To form each crossing, we either rotate the points NE and NW or the points NE and SE. In the former case, we call the crossing a *vertical* crossing, and in the latter a *horizontal* crossing. For all but the first crossing in a tangle, adding a crossing can be seen as stacking a region $S^2 \times I$ to the outside of a pre-existing tangle, where $S^2 \times I$ contains four strands, two of them forming a crossing. Positive vertical and horizontal crossings in $S^2 \times I$ are shown in figure 10.3, negative ones will be in the opposite direction. If we drill the four strands from $S^2 \times I$, the region becomes $S \times I$, where S is a 4-punctured sphere.

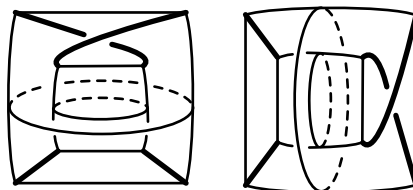


FIGURE 10.3. Vertical (left) and horizontal (right) blocks of the form $S \times I$. The 4-punctured spheres on the outside and inside correspond to $S \times \{1\}$ and $S \times \{0\}$, respectively

LEMMA 10.10. *Let $K := K[a_{n-1}, \dots, a_1]$ be a 2-bridge link and let C denote the number of crossings of K ; so $C = |a_1| + \dots + |a_{n-1}|$. Assume either $a_i < 0$ for all i or $a_i > 0$ for all i , and $|a_1| \geq 2$ and $|a_{n-1}| \geq 2$. Let N be the manifold obtained from the complement $S^3 - K$ by removing a ball neighborhood of the first and last crossings, and let S denote the 4-punctured sphere. Then N is homeomorphic to $S \times [a, b]$, obtained from stacking $C - 2$ copies of $S \times I$ end to end, with each copy of $S \times I$ corresponding to either a horizontal or vertical crossing.*

- *If n is even, the first $a_1 - 1$ copies of $S \times I$ are vertical, followed by a_2 horizontal copies, a_3 vertical, etc, finishing with $a_{n-1} - 1$ vertical copies of $S \times I$.*
- *If n is odd, the first $a_1 - 1$ copies of $S \times I$ are horizontal, followed by a_2 vertical copies, a_3 horizontal, etc, finishing with $a_{n-1} - 1$ vertical copies.*

The i -th copy of $S \times I$ is glued along $S \times \{1\}$ to $S \times \{0\}$ on the $(i + 1)$ -st copy, $i = 2, 3, \dots, C - 1$. \square

An example of lemma 10.10 is shown in figure 10.4.

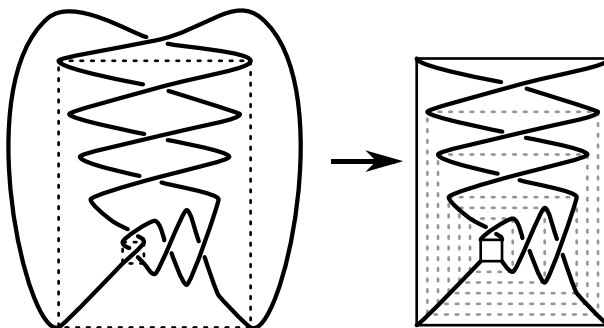


FIGURE 10.4. On the left is $K[4, 2, 2]$. On the right, remove neighborhoods of inside and outside crossings to obtain a manifold homeomorphic to $S \times [a, b]$. Each crossing is contained in a block $S \times I$ of the form of figure 10.3

We will obtain a triangulation of a 2-bridge link complement by first finding a triangulation of the manifold N in lemma 10.10. To do so, we will consider each of the blocks $S \times I$ separately, and then consider how they fit together.

Denote the blocks of lemma 10.10 by $S_2 \times I, S_3 \times I, \dots, S_{C-1} \times I$, where $S_i \times I$ corresponds to the i -th crossing of the tangle. In the description below, we will consider the case that all crossings are positive, i.e. $a_j > 0$ for all j , so that if the i -th crossing is vertical, then $S_i \times I$ has the form of the left of figure 10.3, and if it is horizontal, then $S_i \times I$ has the form of the right. The case of all negative crossings will be similar.

In $S_i \times I$, the 4-punctured sphere S_i is embedded at any level $S_i \times \{t\}$. We will focus in particular on $S_i \times \{0\}$ and $S_i \times \{1\}$.

LEMMA 10.11. *There is an ideal triangulation of S_i such that when we isotope the triangulation to $S_i \times \{1\}$, edges are horizontal (from NE to NW and from SE to SW), vertical (from SW to NW and from SE to NE), and diagonal, and when we isotope the triangulation to $S_i \times \{0\}$, edges are still horizontal, vertical, and diagonal, but the diagonals are opposite those of $S_i \times \{1\}$.*

PROOF. First consider the outside, $S_i \times \{1\}$. Draw vertical and horizontal ideal edges on $S_i \times \{1\}$; that is, draw horizontal edges from NE to NW and from SE to SW, and draw vertical edges from SE to NE and from SW to NW. Now isotope from $S_i \times \{1\}$ through $S_i \times \{t\}$ inside to $S_i \times \{0\}$, and track these ideal edges through the isotopy.

In the case that $S_i \times I$ has a vertical crossing, as on the left of figure 10.3, notice that the isotopy takes the horizontal edges in $S_i \times \{1\}$ to horizontal edges in $S_i \times \{0\}$, but it takes vertical edges in $S_i \times \{1\}$ to diagonal edges in $S_i \times \{0\}$, as shown on the left of figure 10.5. Now consider the vertical edges in $S_i \times \{0\}$, i.e. the ideal edges running from SE to NE and SW to NW on the inside of the block. When we isotope $S_i \times \{0\}$ to $S_i \times \{1\}$, notice that

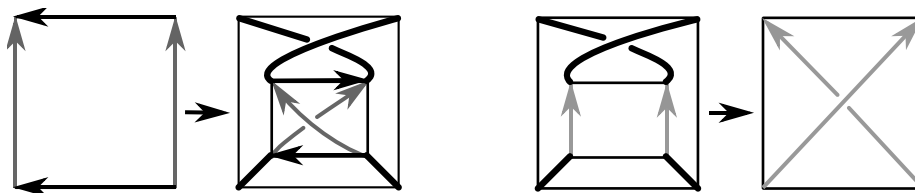


FIGURE 10.5. Effect on ideal edges of isotopies between $S_i \times \{1\}$ and $S_i \times \{0\}$.

these edges become diagonal edges on $S_i \times \{1\}$, as shown on the right of figure 10.5. Notice that these diagonals are exactly opposite the diagonals on the inside on the left of the figure; see also figure 10.6.

When $S_i \times I$ has a horizontal crossing, as on the right of figure 10.3, the vertical ideal edges in $S_i \times \{1\}$ are isotopic to vertical edges in $S_i \times \{0\}$. Horizontal edges on $S_i \times \{1\}$ isotope to diagonal edges on $S_i \times \{0\}$, and horizontal edges on $S_i \times \{0\}$ isotope to diagonal edges on $S_i \times \{1\}$. Again the diagonal edges have opposite slopes on the inside and outside.

In either case, add all horizontal and vertical edges to S_i on $S_i \times \{1\}$ and add all horizontal and vertical edges to S_i on $S_i \times \{0\}$. Since either horizontal or vertical edges are duplicated, we add six ideal edges total. This is the triangulation claimed in the lemma. \square

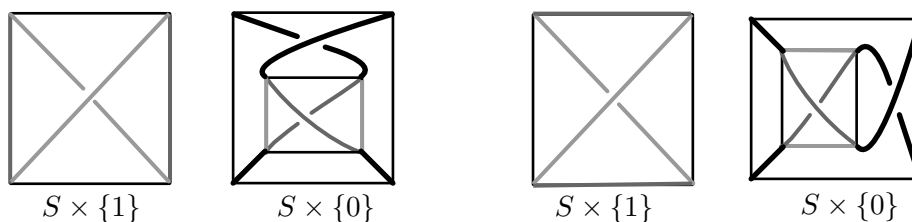


FIGURE 10.6. Triangulation of $S_i \times \{1\}$ and $S_i \times \{0\}$, shown for both horizontal and vertical (positive) crossings.

The triangulation of $S_i \times \{1\}$ and $S_i \times \{0\}$ for both vertical and horizontal crossings is shown in figure 10.6. (We have removed the arrows from the edges as we will not need to work with directed edges, and keeping track of direction will unnecessarily complicate the discussion.) Note the ideal edges cut $S_i \times \{1\}$ into four ideal triangles: two on the front and two on the back. Similarly, these ideal triangles can be isotoped to the inside $S_i \times \{0\}$, giving two triangles on the front and two on the back, although notice that the isotopy does not take both triangles in the front of $S_i \times \{1\}$ to triangles in the front of $S_i \times \{0\}$.

So far we only have ideal triangles on surfaces S_i , and no ideal tetrahedra. The ideal tetrahedra are obtained when we put blocks $S_{i-1} \times I$ and $S_i \times I$ together, and we now describe how this works.

LEMMA 10.12. *With S_{i-1} and S_i triangulated as in lemma 10.11, gluing $S_{i-1} \times I$ to $S_i \times I$ by identifying $S_{i-1} \times \{1\}$ and $S_i \times \{0\}$ gives rise to two ideal tetrahedra, each with two faces on S_{i-1} and two on S_i .*

PROOF. Consider the triangulations of $S_{i-1} \times \{1\}$ and $S_i \times \{0\}$, shown in figure 10.6. Notice that the diagonal edges of $S_{i-1} \times \{1\}$ are exactly opposite the diagonal edges of $S_i \times \{0\}$, and so these edges do not match up. The horizontal and vertical edges on $S_{i-1} \times \{1\}$ and $S_i \times \{0\}$ can be identified, but the diagonal edges cannot. To keep these edges embedded, we view the diagonals of $S_{i-1} \times \{1\}$ as inside of the diagonals of $S_i \times \{0\}$, as shown in figure 10.7.

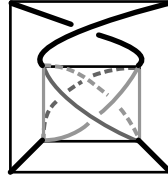


FIGURE 10.7. When blocks are glued, diagonals of the triangulated surfaces S_i and S_{i-1} are as shown.

With horizontal and vertical edges identified, notice that the interior of the region between $S_{i-1} \times \{1\}$ and $S_i \times \{0\}$ lies in two components: one on the front of the figure, and one on the back. Each of these components is bounded by four triangular faces, six ideal edges, and four ideal vertices; each is an ideal tetrahedron as desired. \square

By lemma 10.12, when we glue $S_i \times I$ to $S_{i+1} \times I$, we obtain two additional tetrahedra, and these will be attached along S_i to the two tetrahedra from $S_i \times I$ and $S_{i-1} \times I$. Thus as we run from $S_2 \times I$ out to $S_{C-1} \times I$, we obtain pairs of tetrahedra for each gluing of blocks, and these are glued inside to outside to form a triangulation of $N \cong S \times [a, b]$.

Now, at this stage, we have a triangulation of N , but there will be four triangular faces on the very inside corresponding to S_2 that are unglued, and four triangular faces on the very outside corresponding to S_{C-1} that are unglued. To complete the description of the triangulation of the 2-bridge link complement, we need to describe what happens at the outermost and innermost crossings, e.g. on the left of figure 10.4.

PROPOSITION 10.13. *Let $K := K[a_{n-1}, \dots, a_1]$ be a 2-bridge link with at least two twist regions, with either $a_i > 0$ for all $1 \leq i \leq n-1$, or $a_i < 0$ for all i . Assume $|a_1| \geq 2$ and $|a_{n-1}| \geq 2$. Let $C = |a_1| + \dots + |a_{n-1}|$ denote the number of crossings of K . Then $S^3 - K$ has a decomposition into $2(C-3)$ ideal tetrahedra denoted by T_i^1, T_i^2 , for $i = 2, \dots, C-2$.*

- For $2 \leq i \leq C-2$, the tetrahedra T_i^1 and T_i^2 each have two faces on S_i and two on S_{i+1} .
- The two faces of T_2^1 on S_2 glue to the two faces of T_2^2 on S_2 .

- Similarly, the two faces of T_{C-2}^1 on S_{C-1} glue to the two faces of T_{C-2}^2 on S_{C-1} .

PROOF. The tetrahedra come from the triangulation of N . By the previous lemmas, there are two tetrahedra for each pair of adjacent crossings, omitting the first and last, thus $2(C-3)$ tetrahedra. By lemma 10.12, each tetrahedron in each pair has two faces on S_i and two on S_{i+1} , where $S_i \times I$ and $S_{i+1} \times I$ are blocks corresponding to the two adjacent crossings. We label the tetrahedra $T_2^1, T_2^2, T_3^1, T_3^2, \dots, T_{C-2}^1, T_{C-2}^2$, so that the first item is satisfied.

It remains to show that the innermost and outermost tetrahedra, T_2^1, T_2^2 and T_{C-2}^1, T_{C-2}^2 , glue as claimed. We will focus on the outermost tetrahedra here. The innermost case is similar, but we leave its description to the reader.

For the outermost crossing, recall that we may assume our 2-bridge knot is the denominator closure of a tangle $T(a_n, a_{n-1}, \dots, a_1)$ with $a_n = 0$. Thus the outermost crossing will be vertical, not horizontal. Hence we restrict to pictures with a single vertical crossing on the outside.

The outermost 4-punctured sphere S_{C-1} will be triangulated as shown on the left of figure 10.8. Notice that when we add the outside crossing as shown, vertical edges and horizontal edges all become isotopic and hence are identified, by isotopies swinging the endpoints around the strand of the crossing. One such isotopy is indicated by the small arrow on the left of figure 10.8.

The diagonal edges are not identified to horizontal or vertical edges. When we follow the isotopy of figure 10.8, the diagonal edge in the front wraps once around a strand of the knot, as shown on the right of figure 10.8. Thus the triangle in the upper left corner of S_{C-1} maps under the isotopy to a triangle with two of its edges identified, looping around a strand of the 2-bridge knot.

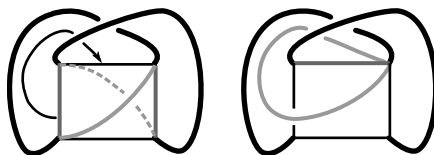


FIGURE 10.8. Identifying triangles of the outermost 4-punctured sphere

Now consider the triangle in front in the lower right corner. We will isotope the triangle by dragging its vertex on the SE corner around the strand of the knot to the NW corner. If we perform this isotopy while holding the diagonal fixed, note that the lower left triangle flips around backwards to be identified to the upper right triangle in the front. Thus the two triangles on the front of $S_{C-1} \times \{1\}$ will be identified under isotopy. Similarly for the two back triangles.

Thus inserting the outermost crossing identifies the four outside triangular faces of the outermost tetrahedra in pairs.

The tetrahedra T_{C-2}^1 and T_{C-2}^2 have triangular faces on S_{C-1} , shown in figure 10.7. One of these, say T_{C-2}^1 , will lie in front in that figure and one will lie in back.

However, note that in figure 10.7, we have isotoped the surface S_{C-1} to be in the position of $S_{C-1} \times \{0\}$, while in figure 10.8, when we glue faces of S_{C-1} , we have isotoped S_{C-1} to be in the position of $S_{C-1} \times \{1\}$. Isotoping from $S_{C-1} \times \{0\}$ to $S_{C-1} \times \{1\}$ will move the faces of T_{C-2}^1 and T_{C-2}^2 . In particular, the face of T_{C-2}^1 lying on the upper right of figure 10.7 will be moved by isotopy to lie in the back on the upper right, and the face of T_{C-2}^1 lying in the lower left will be moved by isotopy to lie in front, in the lower right. See figure 10.9.

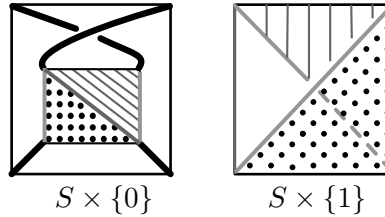


FIGURE 10.9. Locations of faces of T_{C-2}^1 under isotopy from $S \times \{0\}$ to $S \times \{1\}$

Thus the identification of triangles on the outside identifies faces of T_{C-2}^1 to faces of T_{C-2}^2 . \square

10.2.1. The cusp triangulation. Now we consider the view of the tetrahedra from a cusp. Consider first the manifold N with ball neighborhoods of the first and last crossings removed. The manifold N is homeomorphic to the product of a 4-punctured sphere and a closed interval. Note that in N , there are four distinct cusps, corresponding to the product of I and the four distinct punctures of the 4-punctured sphere. Note that each cusp meets each 4-punctured sphere S_i , and that a curve on S_i running around the puncture forms a meridian. Finally, note that between each S_i and S_{i+1} lie two tetrahedra, as in figure 10.7. Each tetrahedron has exactly one ideal vertex on each of the four cusps. Thus the cusp triangulation of N consists of four disjoint cusp neighborhoods. Each cusp neighborhood meets each S_i , in the same order, and each cusp neighborhood meets each tetrahedron in the decomposition in the same order. Thus the four cusp triangulations look identical at this stage, at least combinatorially. We will create one of these four cusps.

In order to see the pattern of tetrahedra in one of these cusps, note that there will be a stack of triangles in each cusp, each triangle corresponding to the tip of a tetrahedron. By proposition 10.13, the triangles will be

sandwiched between 4-punctured spheres S_i and S_{i+1} , with the bottom of the stack of triangles bounded by S_2 and the top by S_{C-1} . (Recall that the 4-punctured sphere S_i actually lies in a block $S_i \times I$, so when we refer to S_i in the following it may be helpful to recall that we are referring to a surface isotopic to $S_i \times \{t\}$ for appropriate t .)

When we run along a meridian of the cusp on S_i , we stay on edges of the cusp triangulation. Moreover, note that we pass over exactly three ideal edges; see the left of figure 10.10. Thus in the cusp triangulation, running along such a meridian on the surface S_i will correspond to running over three edges of triangles. This is shown in figure 10.10 for S_i . The vertical dotted lines indicate boundaries of a fundamental region for the cusp torus; in this case running from one dotted line to the other corresponds to a meridian.

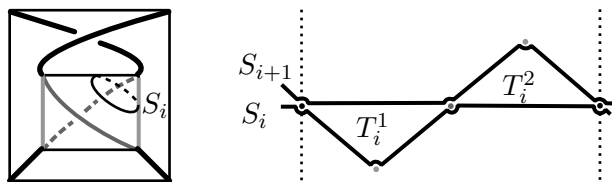


FIGURE 10.10. Form of two meridians running over S_i and S_{i+1}

When the i -th, $(i + 1)$ -st, and $(i + 2)$ -nd blocks are all vertical crossings, note that the surfaces S_i , S_{i+1} , and S_{i+2} will all share an edge; a horizontal edge in figure 10.6. Similarly adjacent horizontal crossings also lead to surfaces sharing an edge.

NOTATION 10.14. In the cusp triangulation we see 4-punctured spheres S_2, \dots, S_{C-1} . Give the label R to each 4-punctured sphere S_i corresponding to a block $S_i \times I$ containing a horizontal crossing. Give the label L to each corresponding to a block containing a vertical crossing. A tetrahedron that lies between layers labeled R and L is called a *hinge tetrahedron*.

The labels R and L are given for historical reasons; they refer to moves to the right and left for a path in the Farey graph given by the rational number of our tangle. We won't delve into the history of this notation here, but we will use this notation for ease of reference with other literature. For more information see [Gué06b].

EXAMPLE 10.15. A cusp triangulation for an example N is shown in figure 10.11. That figure follows some standard conventions. Because we have many surfaces S_i , we connect edges of S_i to form a single connected jagged line, identifiable as one surface in the cusp, and put a little space between multiple such surfaces at a vertex they share. We also put vertices of the triangles in two columns (in a fundamental domain). Finally, we shade the hinge layers.

Note in the figure as we move inside to out, we move from the bottom of the cusp triangulation to the top. Tetrahedron T_2^1 lies between surfaces S_2

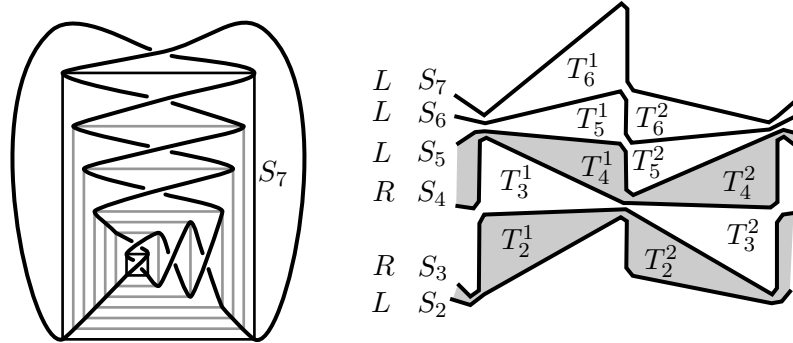


FIGURE 10.11. On the right is shown the cusp triangulation of one of the four cusps of N on the left

associated with the second innermost crossing (vertical, L) and S_3 associated with the third innermost crossing (horizontal, R). It is a hinge tetrahedron. Tetrahedron T_3^1 lies between S_3 and S_4 , both of which are associated with horizontal crossings, R . Note there is an ideal edge shared by all three surfaces S_2 , S_3 , and S_4 , and this corresponds to a shared vertex of T_2^1 and T_3^1 in the cusp triangulation (in the center).

Now we determine what happens to cusps when we put in the innermost and outermost crossings. At the outermost crossing, note that the cusp corresponding to the vertex SE becomes identified with the cusp corresponding to the vertex NW, and similarly for SW and NE. Thus the four identical cusp triangulations we have obtained so far will be glued. Recall that the gluing is along triangle faces of S_{C-1} in the case of the outermost crossing. The faces of T_{C-2}^1 are glued to faces of T_{C-2}^2 . The result is a “folding” of triangles. See figure 10.12. We call this a *hairpin turn*.

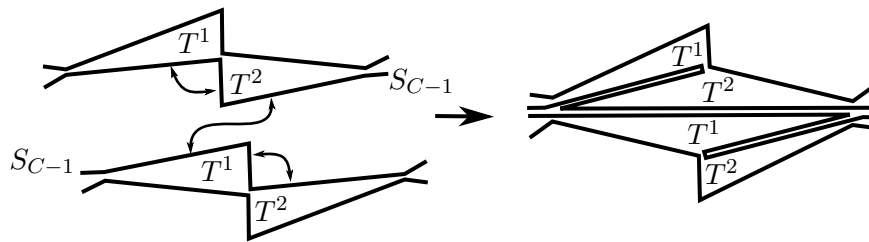


FIGURE 10.12. Gluing tetrahedra across S_{C-1} yields a hairpin turn

If K is a knot, if we follow a longitude of the cusp, starting at one of the corners of S_2 , we will see 4-punctured spheres S_2, S_3, \dots, S_{C-2} , then a hairpin turn on S_{C-1} corresponding to the outside crossing as in figure 10.12. Continuing, we will pass $S_{C-2}, S_{C-3}, \dots, S_3$, then another hairpin turn on S_2 corresponding to the inside crossing, then S_3, \dots, S_{C-1} and a hairpin

turn, and finally S_{C-2}, \dots, S_3 and the original S_2 with a hairpin turn. A hairpin turn appears in the cusp triangulation as a single edge stretching across a meridian, adjacent to two triangles whose third vertex is 3-valent.

We summarize:

PROPOSITION 10.16. *Let $K := K[a_{n-1}, \dots, a_1]$ be a 2-bridge knot with at least two twist regions, such that either $a_i > 0$ for all i , or $a_i < 0$ for all i , and $|a_1| \geq 2$ and $|a_{n-1}| \geq 2$. Let $C = |a_1| + \dots + |a_{n-1}|$ denote the number of crossings of K . The cusp triangulation of K has the following properties.*

- *It is made of four pieces, each piece bookended by hairpin turns corresponding to 4-punctured spheres S_2 and S_{C-1} . Between lies a sequence of 4-punctured spheres S_3, \dots, S_{C-2} . We call the 4-punctured spheres zig-zags.*
- *The first and third pieces are identical; the second and fourth are also identical and given by rotating the first piece 180° about a point in the center of the edge of the final hairpin turn (and swapping some labels T_i^1 as T_i^2). Thus the second and fourth pieces follow the first in reverse.*
- *When running in a longitudinal direction, the first piece begins with $|a_{n-1}| - 1$ zig-zags labeled L ; the first of these is S_{C-1} , the hairpin turn corresponding to the outside crossing of the knot. These zig-zags are followed by $|a_{n-2}|$ zig-zags labeled R , then $|a_{n-3}|$ labeled L , and so on. If n is even, finish with $|a_1| - 1$ zig-zags labeled L , the last of which is the final hairpin turn, corresponding to S_2 at the inside crossing. If n is odd, the final $|a_1| - 1$ zig-zags are labeled R .*
- *A meridian follows a single segment of the zig-zag in a hairpin turn, or three segments of any other zig-zag.*

Note we see each S_i exactly four times, including seeing S_2 twice for each of the two hairpin turns in the cusp triangulation corresponding to the inside crossing, and seeing S_{C-1} twice for each hairpin turn corresponding to the outside crossing.

An example sketched by SnapPy ([CDGW16]) is shown in figure 10.13.

10.3. Positively oriented tetrahedra

The triangulation described in the last section has nice geometry. In particular, when the 2-bridge link has at least two twist regions, we can find angle structures on the triangulation. These can be used to prove that the 2-bridge link is hyperbolic (corollary 10.20), and to show that in the complete hyperbolic structure on the link complement, the tetrahedra are all geometric. Thus we will obtain our first infinite class of knots and links with known geometric triangulations.

The main theorem of the next two sections is theorem 10.17, below. It was originally proved by Futer in the appendix to [Gué06b].

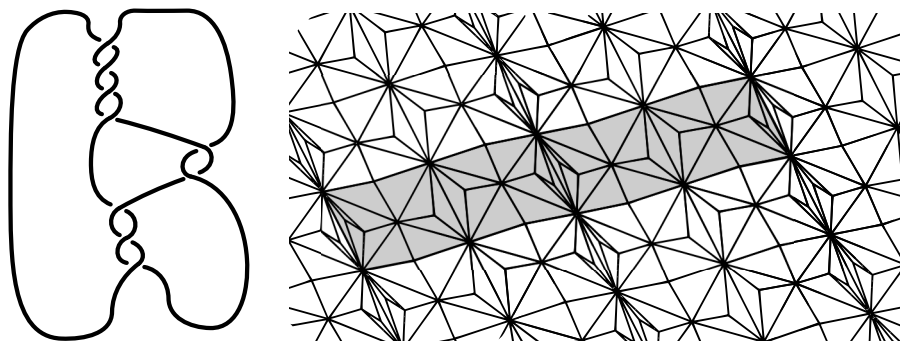


FIGURE 10.13. An example of a 2-bridge knot and its cusp triangulation from SnapPy. The shaded region shows a fundamental domain for the cusp torus, stretching from one hairpin turn through three others back to the same hairpin turn.

THEOREM 10.17. *Let K be a 2-bridge knot or link with a reduced alternating diagram with at least two twist regions. Let \mathcal{T} be the triangulation of $S^3 - K$ as described above. Then $S^3 - K$ is hyperbolic, and in the complete hyperbolic structure on $S^3 - K$, all tetrahedra of \mathcal{T} are positively oriented.*

The proof of theorem 10.17 uses angle structures on \mathcal{T} , as in definition 8.29, and is done in two steps. First, the space of angle structures $\mathcal{A}(\mathcal{T})$ is shown to be non-empty. In theorem 8.36, we showed that the existence of an angle structure is enough to conclude that the manifold admits a hyperbolic structure. We conclude that these 2-bridge link complements are hyperbolic.

Second, in the next section, we show that the volume functional cannot achieve its maximum on the boundary of $\mathcal{A}(\mathcal{T})$. This is all that is needed: because the volume functional is strictly concave down on $\mathcal{A}(\mathcal{T})$ (lemma 9.15), it achieves a maximum in the interior of $\mathcal{A}(\mathcal{T})$. By theorem 9.13, the maximum corresponds to the complete hyperbolic structure, and at that structure, all angles are strictly positive, meaning all tetrahedra are geometric — positively oriented.

PROPOSITION 10.18. *Let \mathcal{T} be the triangulation of a 2-bridge knot or link complement with at least two twist regions, as described above. Then the space of angle structures $\mathcal{A}(\mathcal{T})$ is nonempty.*

The proof of the proposition is not hard, but requires additional notation. First, we need to label the angles of each of the tetrahedra constructed in the previous section. Remember that the tetrahedra were constructed in pairs, and the pairs of tetrahedra lie between two 4-punctured spheres of the manifold $N = S \times [a, b]$, as in figure 10.7. In order to show some angle structure exists, we will first assume that the angles on each of these pairs of tetrahedra agree. Let z_i denote the angle on the outside diagonal edges of tetrahedra T_i^1 and T_i^2 . Because opposite edges have the same angle, z_i is also

the angle on the inside diagonal edge. Denote the angle at the horizontal edges by x_i and the angle at vertical edges by y_i . We may add these angles to the cusp triangulation. The cusp triangulation was obtained by adding layers of zig-zagging 4-punctured spheres. Each 4-punctured sphere shares two edges with the previous 4-punctured sphere, and has one new edge. In the cusp triangulation, this forms a sequence of triangles in which two vertices are shared, but one new vertex is added. The new vertex corresponds to the diagonal edge, so is labeled z_i . Note that angles labeled x_i are glued together, as are angles labeled y_i . Finally, we have oriented tetrahedra so that angles read x_i, y_i, z_i in clockwise order around a cusp triangle. This completely determines the labeling on all the cusp triangles of $N = S \times [a, b]$. An example is shown in figure 10.14.

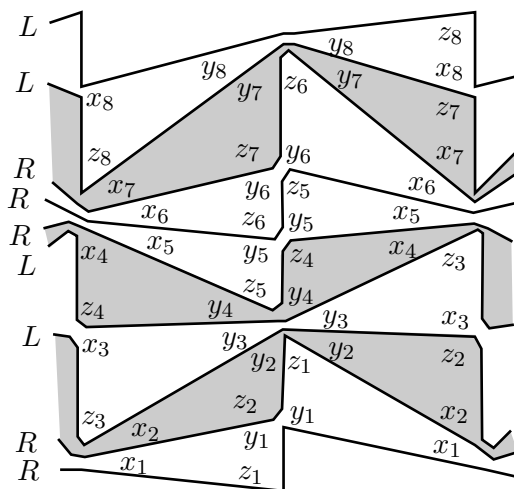


FIGURE 10.14. Labels on the cusp triangulation of $N = S \times [a, b]$ for an example

In the example, a 4-punctured sphere corresponding to a horizontal crossing is labeled R , and one corresponding to a vertical crossing is labeled L , as in notation 10.14.

Now (x_i, y_i, z_i) give us labels for angles of all the tetrahedra on the 2-bridge link complement. We will need $x_i + y_i + z_i = \pi$ for each i to satisfy condition (8.29) of the definition of an angle structure, definition 8.29. We also need sums of angles around edge classes to be 2π .

Away from hairpin turns, the edge gluings of $S^3 - K$ agree with those of $N = S \times [a, b]$, so we will first consider angle sums around edges of N , simplifying these conditions to a system of equations in terms of the z_i alone, then deal with hairpin turns later. There will be four cases depending on whether the i -th tetrahedron lies between two horizontal crossings, two vertical crossings, a horizontal followed by a vertical crossing, or a vertical followed by a horizontal crossing. These cases are denoted by RR, LL, RL , and LR , respectively.

The labels for two consecutive LL 4-punctured spheres are shown in figure 10.15. Note in this case, there is a 4-valent vertex in the cusp triangulation (or 4-valent ideal edge in the decomposition into tetrahedra). In order for the angle sum around this edge to be 2π , we need $2x_i + z_{i+1} + z_{i-1} = 2\pi$, or $x_i = \frac{1}{2}(2\pi - z_{i-1} - z_{i+1})$. Then in order for $x_i + y_i + z_i = \pi$, we need $y_i = \frac{1}{2}(z_{i-1} - 2z_i + z_{i+1})$.

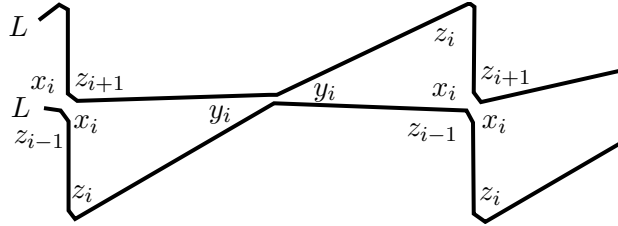


FIGURE 10.15. Labels in the LL case

A similar picture occurs in the RR case. Again there is a 4-valent vertex, and reading the labels around that vertex we find that we need the formulas $y_i = \frac{1}{2}(2\pi - z_{i-1} - z_{i+1})$, and $x_i = \frac{1}{2}(z_{i-1} - 2z_i + z_{i+1})$.

In the LR and RL cases, there is not a single edge all of whose labels we can read off the diagram. In these cases, we find restrictions by considering *pleating angles*. Pleating angles α_1 , α_2 , and α_3 are the angles determining the bending of the pleated 4-punctured sphere. They are shown for 4-punctured spheres labeled L and R in figure 10.16.

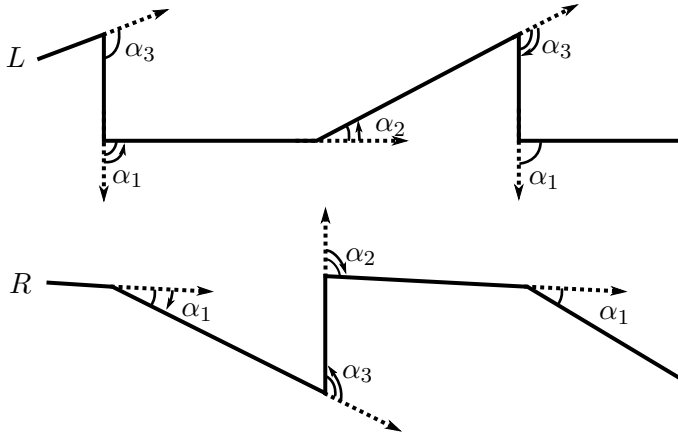


FIGURE 10.16. Pleating angles for 4-punctured spheres

LEMMA 10.19. *If the angle structure gives a Euclidean structure on the cusp, then it will be the case that pleating angles as in figure 10.16 satisfy $\alpha_1 + \alpha_2 - \alpha_3 = 0$.*

PROOF. Exercise. □

| <i>LL</i> | | <i>RR</i> | |
|-----------|--|--|--|
| x_i | $\frac{1}{2}(2\pi - z_{i-1} - z_{i+1})$ | $\frac{1}{2}(z_{i-1} - 2z_i + z_{i+1})$ | |
| y_i | $\frac{1}{2}(z_{i-1} - 2z_i + z_{i+1})$ | $\frac{1}{2}(2\pi - z_{i-1} - z_{i+1})$ | |
| z_i | z_i | z_i | |
| <i>LR</i> | | <i>RL</i> | |
| x_i | $\frac{1}{2}(\pi - z_{i-1} - z_i + z_{i+1})$ | $\frac{1}{2}(\pi + z_{i-1} - z_i - z_{i+1})$ | |
| y_i | $\frac{1}{2}(\pi + z_{i-1} - z_i - z_{i+1})$ | $\frac{1}{2}(\pi - z_{i-1} - z_i + z_{i+1})$ | |
| z_i | z_i | z_i | |

TABLE 10.1. Label conditions in terms of the z_i

To find an angle structure, we will assume this pleating condition holds in the *LR* and *RL* case.

The *LR* labels are shown in figure 10.17. Note that the pleating angles for the 4-punctured sphere at the bottom of the diagram are $\alpha_1 = \pi - z_i$, $\alpha_2 = \pi - (2y_i + z_{i+1})$, and $\alpha_3 = \pi - z_{i-1}$. Thus the condition $\alpha_1 + \alpha_2 - \alpha_3 = 0$ implies $y_i = \frac{1}{2}(\pi + z_{i-1} - z_i - z_{i+1})$. The pleating angles on the 4-punctured sphere on the top of the diagram in figure 10.17 are $\alpha_1 = \pi - (2x_i + z_{i-1})$, $\alpha_2 = \pi - z_i$, and $\alpha_3 = \pi - z_{i+1}$. Thus the pleating condition for this 4-punctured sphere gives $x_i = \frac{1}{2}(\pi - z_{i-1} - z_i + z_{i+1})$. Conditions can be obtained in a similar manner in the *RL* case.

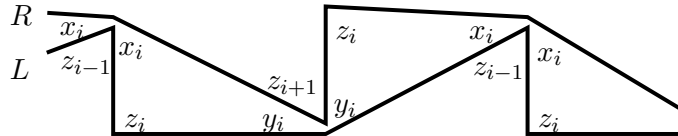


FIGURE 10.17. Labels in the *LR* case

In summary, away from hairpin turns, labels must satisfy the conditions given in table 10.1.

Notice this allows us to express x_i and y_i in terms of z_{i-1} , z_i , and z_{i+1} alone. Note also that the sum of the angles $x_i + y_i + z_i = \pi$ in each case.

Finally, we claim that with the conditions in table 10.1, the angle sum around each edge in N is 2π . To see this, note first that we have constructed the angles so that the sum is 2π around 4-valent edges. We now check the remaining edges. The angle sum around one such edge will be

$$z_{j-1} + 2x_j + \sum_{i=j+1}^{k-1} 2x_i + 2x_k + z_{k+1},$$

where j and k are indices of hinge tetrahedra, with j between *LR* and k between *RL*, and $j < k$, and all 4-punctured spheres labeled *R* between

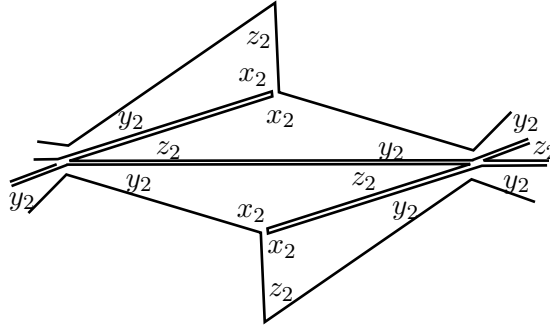


FIGURE 10.18. Labels from a hairpin turn

them; refer to figure 10.14. By the formulas in the tables, this is

$$z_{j-1} + \pi - z_{j-1} - z_j + z_{j+1} + \sum_{i=j+1}^{k-1} (z_{i-1} - 2z_i + z_{i+1}) + \pi + z_{k-1} - z_k - z_{k+1} + z_{k+1}.$$

This is a telescoping sum; all terms cancel except 2π , as desired.

The angle sum around another such edge will be

$$z_{j-1} + 2y_j + \sum_{i=j+1}^{k-1} 2y_i + 2y_k + z_{k+1},$$

where j and k are hinge indices, with j between RL and k between LR , and $j < k$, and all 4-punctured spheres are labeled L between them. Again check that everything cancels except 2π .

We still need to consider the hairpin turns. With the gluing that comes from a hairpin turn, labels are as shown in figure 10.18, for the LL case. The cases RR , LR , RL are similar (exercise).

If we set $z_1 = 0$, the interior angle in which the 4-punctured sphere S_2 is bent at the hairpin turn, then all the equations in table 10.1 hold, depending on whether the hairpin turn occurs in the case LL , RR , LR , or RL . It remains only to check the edge equations. For the edge at the sharp bend, the equation will be identical to one of the previous equations, only now with angle $z_1 = 0$ included. The sum is still 2π . As for the final edges, in the case S_2 is R , these contribute $2z_2 + 4x_2 + \dots$, where the remainder of terms depends on whether the hairpin turn occurs at a hinge or not. In either case, the sum is 2π . Similarly when S_2 is L , and similarly for the outside hairpin turn that occurs at the 4-punctured sphere S_{C-1} .

We are now ready to show the space of angle structures is nonempty.

PROOF OF PROPOSITION 10.18. We show the space of angle structures is nonempty by showing there is a choice of $(z_1, z_2, \dots, z_{C-2}, z_{C-1})$ with $z_1 = z_{C-1} = 0$, all other $z_i \in (0, \pi)$, and $x_i, y_i \in (0, \pi)$. For this to hold, the

equations in table 10.1 tell us that:

$$(10.1) \quad \begin{cases} 2z_i < z_{i-1} + z_{i+1} & \text{if } i \text{ is not a hinge (} LL \text{ or } RR) \\ |z_{i+1} - z_{i-1}| < \pi - z_i & \text{if } i \text{ is a hinge index (} LR \text{ or } RL) \end{cases}$$

The first equation is called the *convexity equation*. The second is the *hinge equation*.

We find a point with all $z_i \in (0, \pi)$ that satisfies convexity and hinge equations. Namely, let $z_1 = z_{C-1} = 0$. For each hinge index i , let $z_i = \pi/3$. Between hinge indices, choose a sequence to satisfy the convexity equations. For example, if j, k are consecutive hinge indices with $j < k$, then for all $j \leq i \leq k$, take

$$z_i = \frac{\pi}{3} - \frac{2(i-j)(k-i)}{(k-j)^2}.$$

Then the sequence $(z_1, z_2, \dots, z_{C-2}, z_{C-1})$ satisfies all required conditions. Letting x_i and y_j be as in the tables, this gives an angle structure. \square

COROLLARY 10.20. *Let $K[a_{n-1}, \dots, a_1]$ be a 2-bridge knot or link with $a_i > 0$ for all i , or $a_i < 0$ for all i , and $|a_1| \geq 2$ and $|a_{n-1}| \geq 2$. Assume also that $n \geq 3$, so there are at least two twist regions in the diagram of K given by the denominator closure of the rational tangle $T(0, a_{n-1}, \dots, a_1)$. Then $S^3 - K$ is hyperbolic.*

PROOF. The link complement $S^3 - K$ admits a triangulation as in proposition 10.13. Then proposition 10.18 implies the set of angle structures on this triangulation is nonempty. By theorem 8.36 in chapter 8, any manifold admitting an angle structure must also admit a hyperbolic structure. \square

Corollary 10.20 is a special case of a stronger theorem due to Menasco determining when any alternating knot or link is hyperbolic [Men84]. We will return to that theorem in chapter 11.

REMARK 10.21. Corollary 10.20 will also follow from theorem 10.17, which we will finish proving in the next section, by an appeal to theorem 9.13 (volume and angle structures). While the proof of corollary 10.20 given above appears short, in fact recall that the proof of theorem 8.36 requires the difficult hyperbolization theorem of Thurston, theorem 8.17, whose proof is beyond the scope of this book. By contrast, finishing the proof of theorem 10.17 requires only calculus and some calculations, and we go through it in the next section. Moreover, when finished, we will additionally know that the hyperbolic structure on 2-bridge links arises from a geometric triangulation of the link complements, and that triangulation can be explicitly described. Thus a proof of corollary 10.20 using the calculations in the next section is in many ways a “better” proof, worth finishing.

10.4. Maximum in interior

In this section we conclude the proof of theorem 10.17, by proving the following.

PROPOSITION 10.22. *For the 2-bridge links of proposition 10.18, the volume functional $\mathcal{V}: \mathcal{A}(\mathcal{T}) \rightarrow \mathbb{R}$ cannot have a maximum on the boundary of the space of angle structures.*

REMARK 10.23 (Summary of proof). The proof is given by a series of lemmas and calculations, and is quite technical. However, the idea of the proof is straightforward. First, we show that we can use the conditions on angle structures obtained in table 10.1; this is done in lemma 10.24. We then assume the maximum occurs on the boundary. Using the conditions of table 10.1, we find restrictions on the tetrahedra that arise; this is done in lemma 10.25. Finally, we show that in all cases that remain there is a path from the purported maximum on the boundary of the space of angle structures to the interior for which the directional derivative of \mathcal{V} is strictly increasing. This contradicts the fact that the boundary point is a maximum.

We note that the technical arguments required for the proof of proposition 10.22 are used only in this section, and are not required for other chapters of the book.

Let K be a 2-bridge knot or link as in proposition 10.18. To obtain angle structures on $S^3 - K$, we made some simplifying assumptions in the proof of proposition 10.18. Namely, when constructing the triangulation \mathcal{T} , we had two tetrahedra T_i^1 and T_i^2 at each level, and we assumed that the angles on the two tetrahedra agreed. This led to the calculations of the previous section.

LEMMA 10.24. *The maximum of the volume functional $\mathcal{V}: \mathcal{A}(\mathcal{T}) \rightarrow \mathbb{R}$ must occur at a point for which the angles (x_i^1, y_i^1, z_i^1) of T_i^1 agree with those (x_i^2, y_i^2, z_i^2) of T_i^2 , for all i , where T_i^1 and T_i^2 are the two tetrahedra constructed at the i -th level.*

PROOF. Suppose the volume is maximized at an angle structure A for which angles of T_i^1 and T_i^2 do not agree. Because of the symmetry of the construction of \mathcal{T} , note that we obtain a new angle structure A' by swapping angles of T_i^1 with the corresponding angles of T_i^2 , for all tetrahedra of A . Note that since A and A' contain isometric ideal tetrahedra, $\mathcal{V}(A) = \mathcal{V}(A')$. Then A and A' are distinct angle structures, and the volume is maximized on both.

By theorem 9.9, the volume functional is strictly concave down on $\mathcal{A}(\mathcal{T})$. Thus if the volume obtains its maximum in the interior, then that maximum is unique, and the fact that $\mathcal{V}(A) = \mathcal{V}(A')$ gives an immediate contradiction in this case. If A lies on the boundary, then A' also lies on the boundary. Because $\mathcal{A}(\mathcal{T})$ is convex (proposition 9.11), the line between A and A' lies in $\mathcal{A}(\mathcal{T})$. But then along this line, the second directional derivative in the direction of the line is strictly negative, which implies the maximum cannot occur at the endpoints. This is a contradiction. \square

By lemma 10.24, we may assume angles of T_i^1 and T_i^2 agree. Thus we may use the conditions on angles in table 10.1 that we calculated in the previous section to prove proposition 10.22.

Now assume that the maximum of \mathcal{V} does occur on the boundary of the space of angle structures $\mathcal{A}(\mathcal{T})$. Then there will be a flat tetrahedron (or more accurately, a pair of flat tetrahedra). We will slowly narrow in on what type of tetrahedron it is, and where it occurs in the triangulation.

Note we will switch notation slightly. Rather than referring to the two tetrahedra between S_i and S_{i+1} as T_i^1 and T_i^2 , we will simply refer to such a tetrahedron by Δ_i . Because the angles of T_i^1 and T_i^2 can be assumed to agree by lemma 10.24, this will simplify our notation.

LEMMA 10.25. *Suppose the maximum of the volume functional occurs on the boundary of $\mathcal{A}(\mathcal{T})$.*

- (1) *Then there exists a flat tetrahedron in the triangulation of the 2-bridge link.*
- (2) *The flat tetrahedron is not adjacent to any other flat tetrahedra.*
- (3) *The flat tetrahedron is not adjacent to a hairpin turn.*
- (4) *The flat tetrahedron occurs at a hinge, and satisfies $z_i = \pi$, and for the two adjacent tetrahedra, $z_{i-1} = z_{i+1}$.*
- (5) *If some tetrahedron Δ_i is type LL or RR , then Δ_{i-1} and Δ_{i+1} cannot both be flat.*

PROOF. By proposition 9.19, if the volume takes its maximum at an angle structure for which a tetrahedron has an angle equal to 0, then it must have two angles equal to 0 and one equal to π . This is a flat tetrahedron. Because we are assuming the maximum is on the boundary, there must be a flat tetrahedron in the triangulation, say tetrahedron Δ_i is flat, where $2 \leq i \leq C - 2$. This proves item (1).

There are three cases for the angles, namely (x_i, y_i, z_i) can equal $(0, 0, \pi)$, $(0, \pi, 0)$, or $(\pi, 0, 0)$. There are also four possibilities for the tetrahedron: type LL , RR , LR , or RL . The equations of table 10.1 give us angles of adjacent tetrahedra in all cases, and an analysis of these will lead to the conclusions of the lemma.

Case $(x_i, y_i, z_i) = (0, 0, \pi)$.

LL, RR: Equations of table 10.1 imply

$$0 = \frac{1}{2}(2\pi - z_{i-1} - z_{i+1}), \text{ which implies } z_{i-1} = z_{i+1} = \pi.$$

In this case, both adjacent tetrahedra must be flat.

LR, RL: Equations of table 10.1 imply

$$0 = \frac{1}{2}(z_{i+1} - z_{i-1}), \text{ or } z_{i-1} = z_{i+1}.$$

Note in this case, it is not necessarily true that both adjacent tetrahedra are flat, but if one is flat then so is the other.

Case $(x_i, y_i, z_i) = (0, \pi, 0)$. .

LL: $0 = \frac{1}{2}(2\pi - z_{i-1} - z_{i+1})$ implies $z_{i-1} = z_{i+1} = \pi$.

RR: $0 = \frac{1}{2}(z_{i-1} + z_{i+1})$ implies $z_{i-1} = z_{i+1} = 0$.

LR: $0 = \frac{1}{2}(\pi - z_{i-1} + z_{i+1})$ implies $\pi + z_{i+1} = z_{i-1}$. Since angles lie in $[0, \pi]$, it follows that $z_{i+1} = 0$ and $z_{i-1} = \pi$.

RL: Similar to the last case, $z_{i+1} = \pi$ and $z_{i-1} = 0$.

For all types of tetrahedra in this case, the two tetrahedra adjacent to Δ_i are flat.

Case $(x_i, y_i, z_i) = (\pi, 0, 0)$.

LL: Equations of table 10.1 imply $z_{i-1} = z_{i+1} = 0$.

RR: $z_{i-1} = z_{i+1} = \pi$.

LR: $z_{i-1} = 0, z_{i+1} = \pi$.

RL: $z_{i+1} = 0, z_{i-1} = \pi$.

Again this shows that the two adjacent tetrahedra are both flat in this case.

In all cases, if two adjacent tetrahedra are flat, then the next adjacent tetrahedron is also flat. It follows that if there are two adjacent flat tetrahedra, then all tetrahedra are flat, and the structure has zero volume, which cannot be a maximum for the volume. Thus we cannot have two adjacent flat tetrahedra. This proves item (2).

Moreover, the only case that does not immediately imply multiple adjacent flat tetrahedron is the first case, with $z_i = \pi$, for the hinge tetrahedra *RL* or *LR*, and the calculation above gives the relationship $z_{i-1} = z_{i+1}$, proving item (4).

If the tetrahedron is adjacent to a hairpin turn, then $i = 2$ or $i = C - 2$, and $z_i = \pi$. We also have $z_1 = 0$ and $z_{C-1} = 0$, hence in either case the equations above imply that a next adjacent tetrahedron, corresponding to z_3 or z_{C-3} , is flat, and thus all tetrahedra are flat, contradicting item (2). This proves (3).

Now suppose Δ_{i-1} and Δ_{i+1} are flat. By the previous work, we know $z_{i-1} = z_{i+1} = \pi$. If Δ_i is type *LL*, the equations of table 10.1 imply $x_i = \frac{1}{2}(2\pi - \pi - \pi) = 0$, so Δ_i is flat. Similarly if Δ_i is of type *RR*, then $y_i = 0$ and Δ_i is flat. But then we have three adjacent flat tetrahedra, contradicting item (2). This proves item (5). \square

We now know that any flat tetrahedron occurring in a maximum for \mathcal{V} on the boundary has a very particular form. To finish the proof of proposition 10.22, we will show that the maximum cannot occur in the remaining cases. For the argument, we will find a path through the space of angle structures starting at the purported maximum for \mathcal{V} on the boundary, and then show that the derivative at time 0 in the direction of this path is strictly positive. This will contradict the fact that the point is a maximum.

The paths we consider adjust the angles of the flat tetrahedron Δ_i by

$$(x_i(\epsilon), y_i(\epsilon), z_i(\epsilon)) = ((1 + \lambda)\epsilon, (1 - \lambda)\epsilon, \pi - 2\epsilon),$$

where $\epsilon \rightarrow 0$ and λ will be a carefully chosen constant. In such a path, we will leave as many angles unchanged away from the i -th tetrahedron as possible. However, the equations in table 10.1 imply that many angles of adjacent tetrahedra must change with ϵ as well.

Recall from lemma 9.15 that the derivative of the volume functional in the direction of a vector $w = (w_1, \dots, w_n)$ at a point $a = (a_1, \dots, a_n)$ is

$$\frac{\partial \mathcal{V}}{\partial w} = \sum_{i=1}^{3n} -w_i \log \sin a_i.$$

The terms of the sum are grouped into threes, with each group corresponding to a single tetrahedron, with derivative coming from theorem 9.9.

LEMMA 10.26. *Let $\gamma(t)$ be a path through $\overline{\mathcal{A}(\mathcal{T})}$ with the angles of the i -th tetrahedron Δ_i in $\gamma(t)$ satisfying $(x_i, y_i, z_i) = ((1 + \lambda)t, (1 - \lambda)t, \pi - 2t)$. Then the derivative of the volume of Δ_i along this path at $t = 0$ satisfies*

$$\left. \frac{d \text{vol}(\Delta_i)}{dt} \right|_{t=0} = \log \left(\frac{4}{1 - \lambda^2} \left(\frac{1 - \lambda}{1 + \lambda} \right)^\lambda \right).$$

PROOF. By theorem 9.9, the derivative in the direction of $\gamma'(0) = w = ((1 + \lambda), (1 - \lambda), -2)$ is

$$\begin{aligned} \frac{\partial \text{vol}}{\partial w} &= \lim_{t \rightarrow 0} \left[-(1 + \lambda) \log \sin((1 + \lambda)t) - (1 - \lambda) \log \sin((1 - \lambda)t) \right. \\ &\quad \left. + 2 \log \sin(\pi - 2t) \right]. \end{aligned}$$

Using the Taylor expansion $\sin(At) = At$ near $t = 0$, this becomes

$$\begin{aligned} \frac{\partial \text{vol}}{\partial w} &\lim_{t \rightarrow 0} \left[-(1 + \lambda) \log((1 + \lambda)t) - (1 - \lambda) \log((1 - \lambda)t) + 2 \log(2t) \right] \\ &= \log \left(\frac{4}{(1 + \lambda)(1 - \lambda)} \left(\frac{1 - \lambda}{1 + \lambda} \right)^\lambda \right) \quad \square \end{aligned}$$

We denote the location of a flat tetrahedron by a vertical line:

$$\dots LL|RR \dots$$

By lemma 10.25, a vertical line can only appear at a hinge: $L|R$ or $R|L$; at least two letters lie between consecutive vertical lines; and patterns $L|RR|L$ and $R|LL|R$ cannot occur. The remaining cases are $LR|LR$ and $RL|RL$, which we deal with simultaneously; $RR|LR$ and $LL|RL$ and their reversals $RL|RR$ and $LR|LL$; and $RR|LL$ and $LL|RR$.

In all cases, we find a path $\gamma(t)$ through $\mathcal{A}(\mathcal{T})$ with $\gamma(0)$ a point on the boundary with the flat tetrahedron specified in the given case.

Case $LR|LR$ and $RL|RL$: Begin with the $LR|LR$ case. Let Δ_i denote the flat tetrahedron, with $(x_i, y_i, z_i) = (0, 0, \pi)$. We take a path $\gamma(t)$ to satisfy $(x_i(t), y_i(t), z_i(t)) = (t, t, \pi - 2t)$, i.e. $\lambda = 0$ in lemma 10.26, and we will keep as many other angles constant as possible. The formulas in table 10.1 imply that angles of tetrahedra Δ_{i-1} and Δ_{i+1} must also vary, as in the following table. In the table, we let $z_{i-1} = z_{i+1} = w$ (required by lemma 10.25(4)), and we let $u = z_{i-2}$, $v = z_{i+2}$.

| Angle | Δ_{i-1} | Δ_i | Δ_{i+1} |
|-------|----------------------------------|------------|----------------------------------|
| x | $\frac{1}{2}(2\pi - u - w - 2t)$ | t | $\frac{1}{2}(2t - w + v)$ |
| y | $\frac{1}{2}(u - w + 2t)$ | t | $\frac{1}{2}(2\pi - 2t - w - v)$ |
| z | w | $\pi - 2t$ | w |

Thus the derivative vector to the path at time $t = 0$ is

$$\gamma'(t) = (0, \dots, 0, \underbrace{-1, 1, 0}_{\Delta_{i-1}}, \underbrace{1, 1, -2}_{\Delta_i}, \underbrace{1, -1, 0}_{\Delta_{i+1}}, \dots, 0).$$

Hence the derivative of the volume functional in the direction of the path is given by

$$\begin{aligned} \left. \frac{d\mathcal{V}}{dt} \right|_{t=0} &= \log \sin \left(\frac{1}{2}(2\pi - u - w) \right) - \log \sin \left(\frac{1}{2}(u - w) \right) + \log 4 \\ &\quad - \log \sin \left(\frac{1}{2}(v - w) \right) + \log \sin \left(\frac{1}{2}(2\pi - v - w) \right) \\ &= \log \left(\frac{4 \sin(u/2 - w/2) \sin(v/2 - w/2)}{\sin(u/2 + w/2) \sin(v/2 + w/2)} \right) > 0. \end{aligned}$$

Note this is strictly positive, hence the volume functional cannot have a maximum at this boundary point. The calculation is similar for $RL|RL$.

Remaining cases: We will first take care of cases $RR|LR$ and $RR|LL$.

As in the previous case, we will take a path such that the flat tetrahedron Δ_i changes. This time, we will find a fixed λ such that angles of Δ_i satisfy $(x_i, y_i, z_i) = ((1 - \lambda)t, (1 + \lambda)t, \pi - 2t)$ for $t \in [0, \epsilon]$, for some $\epsilon > 0$. At time $t = 0$, we require $z_{i-1} = z_{i+1} = w$, a constant. Set $z_{i-2} = u$ and $z_{i+2} = v$, also constant. Additionally, adjust z_{i-1} so that at time t , $z_{i-1} = w - 2\lambda t$. In the argument below, we will assume that $i - 2 \neq 1$, so there is a tetrahedron Δ_{i-2} . We also need to consider the case $i - 2 = 1$; we will do this at the very end of the proof. Assuming $i - 2 \neq 1$, the angles that are modified are shown in the tables below for the cases $RR|LR$ and $RR|LL$.

| Angle | R | R | L | R |
|-------|---------------------------------|-------------------------|------------------|---------------------------|
| | Δ_{i-2} | Δ_{i-1} | Δ_i | Δ_{i+1} |
| x | $A + \frac{1}{2}w - \lambda t$ | $x_{i-1}(t, \lambda)$ | $(1 + \lambda)t$ | $x_{i+1}(t, \lambda)$ |
| y | $A' - \frac{1}{2}w + \lambda t$ | $\frac{1}{2}(\pi - 2t)$ | $(1 - \lambda)t$ | $\frac{1}{2}(2t - w + v)$ |
| z | u | $w - 2\lambda t$ | $\pi - 2t$ | w |

| Angle | Δ_{i-2} | R Δ_{i-1} | R Δ_i | L Δ_{i+1} |
|-------|---------------------------------|-------------------------|-------------------|-----------------------------|
| x | $A + \frac{1}{2}w - \lambda t$ | $x_{i-1}(t, \lambda)$ | $(1 + \lambda)t$ | $\frac{1}{2}(\pi + 2t - v)$ |
| y | $A' - \frac{1}{2}w + \lambda t$ | $\frac{1}{2}(\pi - 2t)$ | $(1 - \lambda)t$ | $y'_{i+1}(t, \lambda)$ |
| z | u | $w - 2\lambda t$ | $\pi - 2t$ | w |

Here A and A' are constants, $x_{i-1}(t, \lambda) = \frac{1}{2}(u - 2w + 4\lambda t + \pi - 2t)$, $x_{i+1}(t, \lambda) = \frac{1}{2}(2\pi - 2t - w - v)$, and $y'_{i+1}(t, \lambda) = \frac{1}{2}(\pi - 2t - 2w + v)$.

If $i > 3$, we may use the table to compute the derivative in the direction of the path, and find in the case $RR|LR$, $d\mathcal{V}/dt|_{t=0}$ equals:

$$(10.2) \quad \left. \frac{d\mathcal{V}}{dt} \right|_{t=0} = \log \left(\frac{4 \sin(\frac{v}{2} + \frac{w}{2}) \sin x_{i-1}}{1 - \lambda^2 \sin(\frac{v}{2} - \frac{w}{2}) \sin y_{i-1}} \left(\frac{1 - \lambda}{1 + \lambda} \cdot \frac{\sin x_{i-2} \sin^2 z_{i-1}}{\sin y_{i-2} \sin^2 x_{i-1}} \right)^\lambda \right).$$

And in the case $RR|LL$, $d\mathcal{V}/dt|_{t=0}$ equals:

$$(10.3) \quad \left. \frac{d\mathcal{V}}{dt} \right|_{t=0} = \log \left(\frac{4 \sin x_{i-1} \sin y_{i+1}}{1 - \lambda^2 \sin y_{i-1} \sin x_{i+1}} \left(\frac{1 - \lambda}{1 + \lambda} \cdot \frac{\sin x_{i-2} \sin^2 z_{i-1}}{\sin y_{i-2} \sin^2 x_{i-1}} \right)^\lambda \right).$$

LEMMA 10.27. *Let X, Y be positive constants, and let*

$$f(\lambda) = \log \left(\frac{4}{1 - \lambda^2} X \left(\frac{1 - \lambda}{1 + \lambda} Y \right)^\lambda \right).$$

Then f has a critical point at $\lambda = (Y - 1)/(Y + 1)$, and f takes the value $\log(X(Y + 1)^2/Y)$ at this point.

PROOF. Calculus. □

Now apply lemma 10.27 to equation (10.2) and equation (10.3), choosing λ to be the value given by that lemma at time $t = 0$. For this value of λ , we obtain the following:

The derivative $d\mathcal{V}/dt|_{t=0}$ in the case $RR|LR$ equals:

$$(10.4) \quad \begin{aligned} & \log \left(\frac{\sin(\frac{v}{2} + \frac{w}{2}) \sin x_{i-1}}{\sin(\frac{v}{2} - \frac{w}{2}) \sin y_{i-1}} \left(1 + \frac{\sin x_{i-2} \sin^2 z_{i-1}}{\sin y_{i-2} \sin^2 x_{i-1}} \right)^2 \frac{\sin y_{i-2} \sin^2 x_{i-1}}{\sin x_{i-2} \sin^2 z_{i-1}} \right) \\ & \geq \log \left(\frac{\sin x_{i-1}}{\sin y_{i-1}} \left(1 + \frac{\sin x_{i-2} \sin^2 z_{i-1}}{\sin y_{i-2} \sin^2 x_{i-1}} \right)^2 \frac{\sin y_{i-2} \sin^2 x_{i-1}}{\sin x_{i-2} \sin^2 z_{i-1}} \right). \end{aligned}$$

The derivative $d\mathcal{V}/dt|_{t=0}$ in the case $RR|LL$ equals:

$$(10.5) \quad \log \left(\frac{\sin x_{i-1} \sin y_{i+1}}{\sin y_{i-1} \sin x_{i+1}} \left(1 + \frac{\sin x_{i-2} \sin^2 z_{i-1}}{\sin y_{i-2} \sin^2 x_{i-1}} \right)^2 \frac{\sin y_{i-2} \sin^2 x_{i-1}}{\sin x_{i-2} \sin^2 z_{i-1}} \right).$$

A similar calculation holds in the $LL|RL$ case. By swapping the indices $i-1, i+1$, and $i-2, i+2$, the same argument shows the derivative is strictly positive in the $RL|RR$ and $LR|LL$ cases, provided $i+2$ is not the index of a hairpin turn.

We now finish the $RR|LL$ case.

LEMMA 10.30. *In the $RR|LL$ case, with P', Q' , and T' as in figure 10.19, $P'/T' = T/P$, and $\sin(y_{i+1})/\sin(x_{i+1}) = P'/Q'$.*

PROOF. By lemma 10.25, item (5), there is no flat tetrahedron either directly before or directly after the sequence $RR|LL$, so the angles of Δ_{i-2} , Δ_{i-1} , Δ_{i+1} , and Δ_{i+2} are all positive. Thus the parameter w can vary freely in an open interval when $t = 0$. Since the volume is maximized, the derivative with respect to w satisfies

$$\left. \frac{d\mathcal{V}}{dw} \right|_{t=0} = \log \left(\sqrt{\frac{\sin x_{i-2}}{\sin y_{i-2}}} \cdot \frac{\sin z_{i-1}}{\sin x_{i-1}} \cdot \frac{\sin z_{i+1}}{\sin y_{i+1}} \cdot \sqrt{\frac{\sin y_{i+2}}{\sin x_{i+2}}} \right) = 0.$$

Thus

$$\frac{\sin y_{i-2} \sin^2 x_{i-1}}{\sin x_{i-2} \sin^2 z_{i-1}} \cdot \frac{\sin^2 y_{i+1} \sin x_{i+2}}{\sin^2 z_{i+1} \sin y_{i+2}} = 1.$$

Using an expanded version of figure 10.19, one can check (exercise) that

$$\frac{\sin y_{i-2} \sin^2 x_{i-1}}{\sin x_{i-2} \sin^2 z_{i-1}} = \frac{P}{T}, \quad \text{and} \quad \frac{\sin^2 y_{i+1} \sin x_{i+2}}{\sin^2 z_{i+1} \sin y_{i+2}} = \frac{P'}{T'}.$$

This shows $P'/T' = T/P$.

Similarly using figure 10.19, one can check that $\sin(y_{i+1})/\sin(x_{i+1}) = P'/Q'$. \square

By lemma 10.30 and equation (10.5), we find that in the $RR|LL$ case,

$$\begin{aligned} \left. \frac{d\mathcal{V}}{dt} \right|_{t=0} &= \log \left(\frac{P}{Q} \frac{P'}{Q'} \left(1 + \frac{T}{P} \right)^2 \frac{P}{T} \right) \\ &= \log \left(\frac{P}{Q} \left(1 + \frac{T}{P} \right) \frac{P'}{Q'} \left(1 + \frac{P'}{T'} \right) \frac{T'}{P'} \right) \\ &= \log \left(\frac{P+T}{Q} \cdot \frac{P'+T'}{Q'} \right) \\ &> \log(1) = 0. \end{aligned}$$

A similar calculation takes care of the $LL|RR$ case.

So far, we have argued only for $i > 3$. It remains to consider what happens when $i = 3$. In this case, $i-2 = 1$ is the index of a hairpin turn, and the terms $\sin y_1/\sin x_1$ disappear from the computations of $d\mathcal{V}/dt$ in equation (10.2) and equation (10.3). We have a result similar to lemma 10.29: R^aL is a tessellated Euclidean triangle, and lengths still behave as in lemma 10.29 to give the same result; see [Gué06b, Lemma 1.5].

This concludes the proof of proposition 10.22. \square

We now assemble the pieces to obtain the stronger result, theorem 10.17.

PROOF OF THEOREM 10.17. Let K be a knot or link with a reduced alternating diagram with at least two twist regions. Let \mathcal{T} be the triangulation of $S^3 - K$ described in this chapter. By proposition 10.18, the space of angle structures $\mathcal{A}(\mathcal{T})$ is nonempty. By proposition 10.22, the volume functional $\mathcal{V}: \mathcal{A}(\mathcal{T}) \rightarrow \mathbb{R}$ cannot have a maximum on the boundary of the space of angle structures. It follows that the maximum of \mathcal{V} is on the interior of the space of angle structures. Let $A \in \mathcal{A}(\mathcal{T})$ denote this critical point. Thus by theorem 9.13 (volume and angle structures), the ideal hyperbolic tetrahedra obtained from the angle structure A give $S^3 - K$ a complete hyperbolic structure. Note since A lies in the interior, the ideal hyperbolic tetrahedra it determines are all positively oriented, as claimed. \square

10.5. Exercises

EXERCISE 10.1. Sketch rational tangles and diagrams of 2-bridge links associated to the following continued fractions: $[3, 2]$, $[0, 3, 2]$, $[1, 3, 2]$.

EXERCISE 10.2. Continued fractions. Show every rational number has a continued fraction expansion $p/q = [a_n, a_{n-1}, \dots, a_1]$ such that if $i < n$, then $a_i \neq 0$, and such that if $p/q > 0$, then each $a_i \geq 0$, while if $p/q < 0$, then each $a_i \leq 0$.

EXERCISE 10.3. Prove lemma 10.9. That is, show that if $K[a_{n-1}, \dots, a_1]$ is a 2-bridge knot or link, then we may assume that $|a_{n-1}| \geq 2$ and $|a_1| \geq 2$.

EXERCISE 10.4. Work through the identification of tetrahedra at the innermost crossing. Prove that faces of the innermost tetrahedra are glued in pairs, two triangles of one tetrahedron glued to triangles of the opposite tetrahedron. Why is there no need to consider both horizontal and vertical crossings for the innermost crossing?

EXERCISE 10.5. In proposition 10.13, we require at least two twist regions. Show that this requirement is necessary by showing that the construction fails to give a triangulation of a knot or link with just one twist region. What breaks down?

EXERCISE 10.6. This exercise asks you to consider hairpin turns.

- (1) Prove if $|a_{n-1}| \geq 3$, there is a 3-valent vertex of the cusp triangulation.
- (2) Prove all vertices aside from possibly a single vertex in a hairpin turn must have valence at least four.
- (3) If $|a_{n-1}| = 2$, prove the vertex corresponding to the outside hairpin turn may have arbitrarily high valence.

EXERCISE 10.7. Use the methods of this chapter to find the form of the cusp triangulation for the twist knot $J(2, n)$. How many tetrahedra are in its decomposition?

EXERCISE 10.8. Find the form of the cusp triangulation for $J(k, \ell)$, where one of k, ℓ is even. How many tetrahedra are in its decomposition?

EXERCISE 10.9. Find the form of the cusp triangulation of a 2-bridge knot with exactly three twist regions.

EXERCISE 10.10. Prove lemma 10.19: that pleating angles as in figure 10.16 satisfy $\alpha_1 + \alpha_2 - \alpha_3 = 0$ when the cusp is Euclidean.

EXERCISE 10.11. Determine the labels of the hairpin turns of the form RR, LR, RL , similar to figure 10.18.

EXERCISE 10.12. In the cases $RR|LR$ and $RR|LL$, compute the derivative $d\mathcal{V}/dt|_{t=0}$ and check that it agrees with the formulas given in equation (10.2) or equation (10.3).

EXERCISE 10.13. Give the proof of lemma 10.29.

EXERCISE 10.14. Work through the geometric details of lemma 10.30. First, sketch the zigzag labeled L at the top of figure 10.19, along with angles at its corners, and show that:

$$\frac{\sin y_{i-2} \sin^2 x_{i-1}}{\sin x_{i-2} \sin^2 z_{i-1}} = \frac{P}{T}, \quad \text{and} \quad \frac{\sin^2 y_{i+1} \sin x_{i+2}}{\sin^2 z_{i+1} \sin y_{i+2}} = \frac{P'}{T'}.$$

Also show $\sin(y_{i+1})/\sin(x_{i+1}) = P'/Q'$.

EXERCISE 10.15. Go carefully through the proof of cases $RR|LR$ and $RR|LL$ when the index of the flat tetrahedron is $i = 3$.

Alternating Knots and Links

Alternating knots and links need their own chapter, because there is a wealth of geometric information coming from them. Of all knots, alternating knots seem to have hyperbolic geometry most closely related to their diagrams. As of the writing of this book, there are many open conjectures concerning how the geometry and diagrams interact.

An *alternating knot or link* has a diagram with an orientation such that when following the knot in the direction of the orientation, the crossings alternate between over and under, all the way along the diagram. Alternating knots account for large numbers of knots with small crossing numbers, but they are less prevalent among knots with higher crossing numbers. Indeed, the proportion of alternating knots and links among all prime n -crossing knots and links is known to approach zero exponentially as n approaches infinity [ST98, Thi98]. The first non-alternating knot in the knot tables has eight crossings. Note that it takes some work to prove that a knot is non-alternating: one must show that among all possible knot diagrams, there is no alternating diagram. In this chapter, we won't consider the question of whether a knot with a non-alternating diagram actually is alternating. Instead we will assume we have an alternating knot diagram, and consider what this implies for the geometry of the knot complement.

One main result of the chapter is a proof of a theorem originally due to Menasco that identifies when alternating knots and links are hyperbolic [Men84]. We also define checkerboard surfaces of these links, and show they are essential.

11.1. Alternating diagrams and hyperbolicity

Since we are interested in hyperbolic knots and links, we will consider only *connected diagrams* of knots and links throughout; that is, the underlying 4-valent diagram graph is connected. For note that if a diagram is not connected, it contains an obvious essential 2-sphere, namely one separating two diagram components. Since a hyperbolic knot or link complement can contain no essential 2-sphere, we restrict to connected diagrams.

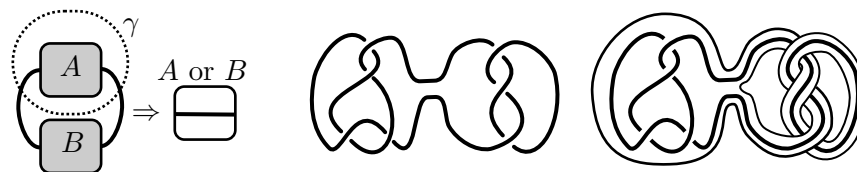


FIGURE 11.1. Left: a prime diagram. Middle: a diagram that is not prime. Right: a swallow–follow torus

We also wish to work with diagrams that have been simplified in obvious ways. For example, we wish to untwist all reducible crossings, like those shown in figure 0.3 in chapter 1.

We also wish to work with prime diagrams, also defined in chapter 1. We recall the definition again.

DEFINITION 11.1. A diagram is *prime* if, for every simple closed curve γ in the plane of projection, if γ meets the knot exactly twice transversely away from crossings, then γ bounds a region of the diagram with no crossings. See figure 11.1, left.

Figure 11.1, middle, shows an example of a diagram that is not prime: a curve running through the center of the diagram meets the knot exactly twice, with crossings on both sides. It is constructed of two simpler knots via the following procedure, which we also defined in chapter 0; see figure 0.6.

DEFINITION 11.2. Given two knots K_1 and K_2 in S^3 , form their *knot sum* or *connected sum* as follows. For each knot $K_i \subset S^3$, take a ball B_i in S^3 such that $B_i \cap K_i$ is a single unknotted arc, with K_i meeting ∂B_i transversely in two points. That is, (B_i, K_i) is homeomorphic to the product of an interval and a disk with a single marked point.

Now, remove B_i from $S^3 - K_i$. The result is homeomorphic to an arc in a ball. Glue $(S^3 - K_1) - B_1$ to $(S^3 - K_2) - B_2$ via a homeomorphism taking $(\partial B_1, \partial B_1 \cap K_1)$ to $(\partial B_2, \partial B_2 \cap K_2)$. (Here the notation means that ∂B_1 is mapped to ∂B_2 in such a way that the two points $\partial B_1 \cap K_1$ are mapped to the two points $\partial B_2 \cap K_2$.)

DEFINITION 11.3. A knot or link is said to be *prime* if it cannot be expressed as a connected sum of knots.

The knot in the middle of figure 11.1 is a connected sum. Again from the point of view of hyperbolic geometry, knots that are not prime are not interesting, since they always contain an incompressible torus called a *swallow–follow torus*. The torus is built by taking the boundary of one of the balls $\partial B_1 - N(K_1)$ in the construction of the connected sum, and then attaching a tube from one component of $N(K_1)$ on ∂B_1 to the other, following K_2 . This forms a torus which “swallows” K_1 , then “follows” K_2 . The right side of figure 11.1 shows a swallow–follow torus for the given example.

Notice that prime diagrams and prime knots are not the same thing in general. Every knot, whether or not it is prime, admits a diagram that is not prime: simply insert a nugatory crossing. In general, if a knot admits a prime diagram, it still may not be a prime knot.

Recall the definitions of meridian and longitude of a knot or link.

DEFINITION 11.4. A curve on the boundary of a neighborhood of a knot or link in S^3 that bounds a disk inside the neighborhood of the link is called a *meridian*.

For a knot, a *longitude* is a curve on the boundary of a neighborhood of the knot that intersects a meridian exactly once. The *standard longitude* is the longitude that is homologous to zero in $H_1(S^3 - K)$.

More generally, a *standard longitude* of a component K_1 of a link is the longitude that is trivial in $H_1(S^3 - K_1)$.

LEMMA 11.5. *Let K be a knot in S^3 . Then K is a connected sum of nontrivial knots if and only if $S^3 - N(K)$ contains an essential annulus that meets the boundary of the neighborhood $N(K)$ in two simple meridians.*

We call such an annulus an *essential meridional annulus*.

PROOF. Suppose first that $S^3 - N(K)$ contains an essential annulus with boundary two meridians of $N(K)$. Cut S^3 along the sphere obtained from the union of this annulus and two disks bounded by the meridians. This separates S^3 into two balls B_1 and B_2 , each containing an arc of K . Form new knots K_1 and K_2 by attaching to each $(\partial B_i, B_i \cap K)$ a ball with an unknotted arc. By construction, K is the connected sum of K_1 and K_2 .

Now suppose that K is a connected sum of nontrivial knots. Then $S^3 - N(K)$ is obtained from nontrivial knots K_1 and K_2 by removing 3-balls B_1 and B_2 from $S^3 - N(K_1)$ and $S^3 - N(K_2)$, respectively, each meeting $\partial N(K_i)$ transversely in two simple meridians. The result has boundary an annulus $A \cong B_i - N(K_i)$, and these annuli are glued to form $S^3 - N(K)$. We claim A is the essential annulus required. It meets $N(K)$ in meridians, as required. If it is compressible, then a disk D with boundary isotopic to the essential core curve of A lies inside $(S^3 - K_i) - B_i$ for one of $i = 1, 2$. Slice ∂B_i along ∂D to obtain a disk E_i meeting K_i exactly once. Attach to E_i the disk D . This is a sphere meeting K_i exactly once. But K_i is a closed curve in S^3 , hence it meets any sphere an even number of times. This contradiction proves that A is incompressible.

Now suppose that there is a boundary compression disk D for A . An arc of ∂D must run from one (meridian) boundary component of A to the other along A . The other arc of ∂D must run along K , either along K_1 or K_2 , say K_1 . But then D can be used to isotope K_1 through B_1 to ∂B_1 , contradicting the fact that K_1 is nontrivial.

Finally, A cannot be boundary parallel, else one side $(S^3 - K_i) - B_i$ is homeomorphic to an unknotted arc in the ball B_i , again contradicting the fact that K_i is nontrivial. This concludes the proof that a connected

sum of knots contains an essential annulus with boundary two meridians of $N(K)$. \square

11.1.1. Polyhedral decomposition, revisited. We know from the above discussion that alternating diagrams that are not connected and not prime cannot have hyperbolic complement. More generally, we need to determine which alternating diagrams lead to essential spheres, disks, tori, and annuli in the complement to rule out hyperbolicity. Our main tool will be a polyhedral decomposition of the link complement.

Recall that in chapter 1 we worked through a decomposition of the figure-8 knot complement into two ideal polyhedra. This was extended in the exercises. In particular, following the methods of that chapter, the exercises outline a proof of the following theorem.

THEOREM 11.6. *Let L be an alternating link. Then the complement of L can be obtained by gluing two ideal polyhedra that satisfying:*

- (1) *The polyhedra are obtained by labeling the boundary of two balls with the projection graph of the alternating diagram of L , and declaring each vertex to be ideal. On one ball, the outside boundary is labeled with the diagram, on the other the inside.*
- (2) *Ideal vertices are 4-valent, corresponding to overcrossings in one polyhedron, undercrossings in the other.*
- (3) *Ideal edges correspond to crossing arcs in the diagram, and each edge class contains four ideal edges of the two polyhedra.*
- (4) *Faces correspond to regions of the diagram, and are checkerboard colored, white and shaded.*
- (5) *Each face on one polyhedron is glued to the identical face on the opposite polyhedron. The gluing rotates the face by one edge in the clockwise direction for white faces, and rotates by one edge in the counterclockwise direction for shaded faces.* \square

The theorem is illustrated in figure 11.2.

In the exercises of chapter 1, we collapsed bigons to a single edge. We will actually keep bigons around in this chapter, as they make certain arguments simpler.

11.1.2. Angled polyhedra and alternating links.

PROPOSITION 11.7. *Let K be a knot or link with a connected, prime, alternating diagram. If we assign a dihedral angle of $\pi/2$ to each ideal edge of the polyhedral decomposition of $S^3 - K$ of theorem 11.6, then we obtain an angled polyhedral structure, as in definition 8.31.*

PROOF. We need to check that the polyhedra with interior dihedral angles $\pi/2$ satisfy the three conditions of definition 8.31. The first condition is immediate: $\pi/2$ lies in $(0, \pi)$. The third condition is also straightforward: each ideal edge of the ideal polyhedral decomposition appears exactly four times in the decomposition, hence interior angles sum to 2π .

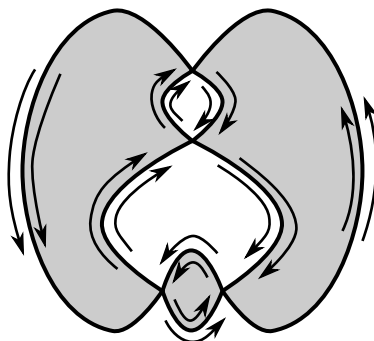


FIGURE 11.2. Ideal polyhedral decomposition of an alternating link (the figure-8 knot). Shown is one ideal polyhedron. The other is identical (with head on the opposite side) and gluing of faces is by a rotation in each face as shown

The second condition takes the most work. We need to show that every normal disk has non-negative combinatorial area. Recall the combinatorial area of a normal disk D is defined to be

$$a(D) = \sum_{i=1}^n (\pi - \alpha_i) - 2\pi + \pi|\partial D \cap \partial M|,$$

where $\alpha_1, \dots, \alpha_n$ are the dihedral angles met by ∂D , and $|\partial D \cap \partial M|$ is the number of times ∂D meets a boundary face. In our case, each $\alpha_i = \pi/2$, so the sum is

$$a(D) = \frac{\pi}{2}|\partial D \cap e(M)| - 2\pi + \pi|\partial D \cap \partial M|,$$

where $|\partial D \cap e(M)|$ is the number of times ∂D meets an ideal edge (not a boundary edge).

Notice that if ∂D meets at least four ideal edges, or at least two boundary faces, then the combinatorial area of D is non-negative. The only possible ways it could be negative is if ∂D meets three or fewer edges and no boundary faces, or if it meets one boundary face and at most one edge. We rule these out.

First, suppose ∂D meets exactly one boundary face. The endpoints of the arc of ∂D on the boundary face must be on distinct boundary edges, by definition of a normal disk. So ∂D runs through at least two distinct regular faces of the polyhedron, and so ∂D must meet an edge of the polyhedron to connect into a closed curve. If ∂D meets only one edge, then it cannot meet an edge adjacent to the boundary face, by definition of normal. So ∂D encloses boundary faces on both sides. See figure 11.3. But recall that the graph of the polyhedron is exactly the diagram graph of K , and boundary faces correspond to crossings of K . Then ∂D gives a simple closed curve in the diagram of K meeting a single crossing and a single strand of the link. We may slide ∂D off the crossing slightly so that it meets one more strand of the link near this crossing. Then ∂D is a closed curve in the link

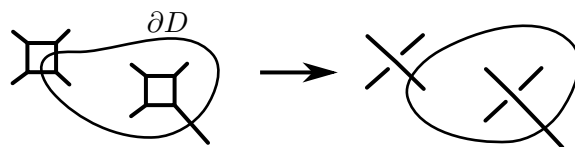


FIGURE 11.3. If ∂D meets just one edge and one boundary face, it determines a simple closed curve in the diagram of K as shown

diagram meeting the diagram exactly twice transversely away from crossings, enclosing crossings on either side. This contradicts the fact that the diagram is prime.

Now suppose ∂D meets no boundary faces, but has negative combinatorial area. Then ∂D meets fewer than four edges, but more than zero edges by definition of normal. Because edges correspond to strands of the link, and the link consists of closed curves, it follows that ∂D meets exactly two ideal edges. Transferring ∂D to the diagram, it becomes a closed curve meeting the diagram exactly twice. But then because K has a prime diagram, there are no crossings on one side of ∂D . Transferring back to the polyhedron, this means an arc of ∂D meets the same edge of the polyhedron two times. This contradicts the definition of normal. \square

COROLLARY 11.8. *Let K be a knot or link with a connected, prime, alternating diagram. Then $S^3 - K$ is irreducible and boundary irreducible.*

PROOF. For such a knot or link, $S^3 - K$ admits an angled polyhedral structure by proposition 11.7. Then the result follows from the first part of theorem 8.36. \square

In fact, we may say more. The following is proved in [Men84], using Thurston's theorem 8.17; we also give a proof here.

THEOREM 11.9. *A knot with a connected prime alternating diagram is either a $(2, q)$ -torus knot or it is hyperbolic.*

We have already shown alternating knots have complements that are irreducible and boundary irreducible. To prove theorem 11.9 we need to consider essential annuli and tori, and we do so in the next subsections.

11.1.3. Alternating knots and essential annuli. There are alternating knots that contain essential annuli, namely the $(2, q)$ -torus knots. However, all other alternating knots are anannular. In this section, we prove that fact. In Menasco's original proof classifying hyperbolic alternating knots, he proves knots are anannular by appealing to an algebraic result of Simon [Sim73]. We take a more direct approach here, giving a geometric proof of this fact using the angled polyhedral structure of the previous subsection.

First, we need more terminology to describe $(2, q)$ -torus knots. The following definition is definition 7.13, repeated here for convenience.

DEFINITION 11.10. A diagram is *twist-reduced* if, whenever γ is a simple closed curve on the plane of projection meeting the diagram exactly twice in two crossings, running from one side of the crossing to the opposite side, the curve γ bounds a string of bigons on one side. See figure 11.4, left.

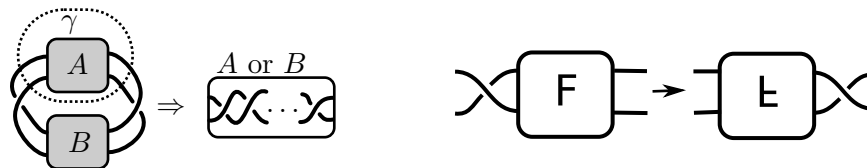


FIGURE 11.4. Left: A twist-reduced diagram. Right: A flype

DEFINITION 11.11. Let γ be a simple closed curve meeting the diagram of K transversely exactly four times in knot strands, with two intersections adjacent to a crossing on the outside of γ . A *flype* is a move on the diagram that rotates the region inside γ by 180° , moving the crossing outside γ to lie between the opposite two strands. See figure 11.4, right.

LEMMA 11.12. *Every knot or link K has a twist-reduced diagram.*

Moreover, if a diagram of K is connected, prime, and alternating, then there is a twist-reduced diagram of K that is connected, prime, and alternating.

PROOF. Start with a diagram of a knot or link. It has a finite number of twist regions, and a finite number of crossings in each twist region. Suppose the diagram is not twist reduced. Then there is a curve meeting the diagram exactly four times adjacent to two distinct twist regions. Slide the curve so that all crossings of both twist regions are on the outside of the curve, say with one twist region on the left and one on the right. Perform a sequence of flypes. Each flype will remove a crossing in the twist region on the left, and either add or remove a crossing in the twist region on the right (depending on the direction of crossings on the right and the direction of the flype). Continue until there are no crossings on the left. When finished, the diagram has one fewer twist region and at most the same number of crossings as before. Repeat, strictly reducing the number of twist regions. Since the number of twist regions is finite, the process will terminate in a twist-reduced diagram.

Finally, note that the process of flyping takes a connected diagram to a connected diagram. It also takes a prime diagram to a prime diagram and an alternating diagram to an alternating diagram (exercise 11.2). Thus if the original diagram of a link is connected, prime, and alternating, then the twist-reduced diagram, obtained by performing flypes, is also connected, prime, and alternating. \square

DEFINITION 11.13. The *twist-number* of a knot diagram is the number of twist regions in a twist-reduced diagram.

EXAMPLE 11.14. A $(2, q)$ -torus knot has twist-number 1. Any knot with a prime alternating diagram that is not a $(2, q)$ -torus knot has twist number at least 2. In particular, the figure-8 knot shown in figure 1.1 has twist number 2. More generally, any twist knot $J(k, \ell)$ has twist number 2.

We are now ready to consider essential annuli.

LEMMA 11.15. *Suppose K is a knot or link with a connected prime alternating diagram, with $S^3 - N(K)$ given its (truncated ideal) polyhedral decomposition. Suppose S is an essential annulus embedded in $S^3 - N(K)$. Then when S is isotoped into normal form, it contains at least one normal disk D meeting a boundary face, and ∂D either meets exactly two boundary faces and no edges, or ∂D meets exactly one boundary face and exactly two edges.*

PROOF. When we put S into normal form, lemma 8.35 implies the combinatorial area of S is 0. Because each normal disk of S has non-negative combinatorial area, in fact each normal disk of S must have combinatorial area 0. Because S is a surface with boundary, there is at least one normal disk of S that meets a boundary face; this is D . Now, considering the formula for the combinatorial area of D , there are only two possibilities: ∂D either meets exactly two boundary faces and no edges, or ∂D meets one boundary face and exactly two edges. \square

LEMMA 11.16. *If K has a prime alternating diagram, and S is an embedded normal annulus properly embedded in the truncated polyhedral decomposition of $S^3 - N(K)$, containing at least one normal disk D_2 whose boundary meets exactly one boundary face and exactly two edges of the polyhedra, then:*

- (1) *S contains a subannulus S' for which all normal disks meet exactly one boundary face and two edges.*
- (2) *K is a $(2, q)$ -torus link with two components, and there is an annulus Σ bounded by the two components of the link that is obtained by gluing bigon faces of the polyhedral decomposition.*
- (3) *A component of ∂S and $\partial S'$ runs along at least one longitude of the link, so ∂S is not a meridian.*
- (4) *The other component of $\partial S'$ runs along the core of the annulus Σ .*

PROOF. Let S , K , and D_2 be as in the statement of the lemma. The disk D_2 is glued to normal disks D_1 and D_3 in the opposite polyhedron. The gluing maps a side of D_2 in a face to a side of D_1 , and the gluing map on a face rotates the side either clockwise or counterclockwise. Without loss of generality, say clockwise. Thus a side of D_2 running from a boundary face to an edge is glued to a side of D_1 running from a boundary face to an edge, although rotated. Similarly for a side of D_2 . See figure 11.5, left. Since D_1 and D_3 also have combinatorial area 0, they must each meet one boundary

face and exactly two edges. Repeat for disks meeting D_1 and D_3 . Eventually this string of disks will glue up. Thus if there is one normal disk meeting a single boundary face and two edges, then there is a cycle of normal disks meet a single boundary face and two edges, gluing to form a subannulus S' of S as claimed.

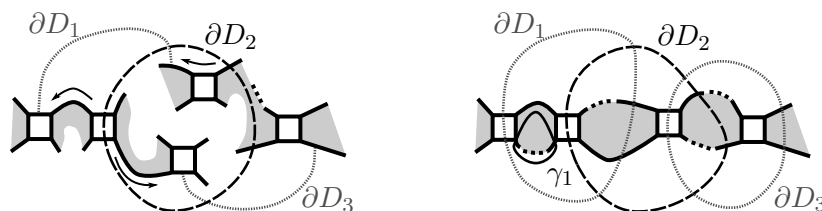


FIGURE 11.5. Curve ∂D_2 must be glued to arcs of ∂D_1 and ∂D_3 as shown on the left. Since ∂D_1 and ∂D_3 are disjoint, the only possibility for ∂D_1 is that shown on the right. Then there is a curve γ_1 meeting the diagram exactly twice; it must bound an unknotted strand, forming a bigon.

Sketch ∂D_2 onto the boundary of the polyhedron, which has the combinatorics of the diagram graph. We will add to this picture ∂D_1 and ∂D_3 by superimposing, as in figure 11.5. By what we know of the gluing maps, an arc of ∂D_1 must have its endpoints rotated once clockwise from an arc of ∂D_2 , as shown on the left of figure 11.5, and similarly for an arc of ∂D_3 .

Because D_1 and D_3 are disjoint, ∂D_1 must lie to one side of the arc of ∂D_3 shown in figure 11.5, and thus ∂D_1 and ∂D_3 close up as shown on the right of that figure. Now inside of ∂D_1 , we may draw a curve γ_1 running through the shaded face between boundary faces met by ∂D_1 and ∂D_2 , and through a single white face as in figure 11.5. This gives a curve meeting the diagram exactly twice. Because the diagram is prime, γ_1 bounds an arc of the diagram with no crossings on one side. Thus that shaded face is a simple bigon. (Similar arguments show that other dotted lines in figure 11.5, right, are also single edges, but we will not use this.)

Repeating this argument with D_1 replacing D_2 , and so on, we find that S' is made up of disks bounding a closed chain of bigons. Thus the diagram of K contains a single twist region, and K is a $(2, q)$ -torus knot or link. To see it is a link, note that disks D_i for i odd must all be disjoint, and disks D_i for i even must also be disjoint. If there are an odd number of bigons in the chain, this will be impossible. So there are an even number of bigons, K is a 2-component link, and the surface Σ made up of the bigons lies between the strands of K and is an annulus.

Now note that ∂D_1 and ∂D_2 together meet both ideal vertices on either side of a bigon face in the polyhedral decomposition. One of D_1, D_2 lies in one polyhedron, and one in the other. But then some ∂D_i will meet each ideal vertex in the diagram graph. It follows that ∂S meets each ideal vertex

in each polyhedron at least once. This implies that ∂S runs along at least one longitude.

Finally, the arc of ∂D_i lying in a shaded face is a simple arc through the bigon. Thus it runs from one crossing arc bounding the bigon to the other. When we glue all the disks D_i , the boundary of S' traces the core of the annulus Σ . \square

LEMMA 11.17. *Suppose K is a knot or link with a connected, twist-reduced, prime, alternating diagram. Suppose S is an essential annulus in normal form in the polyhedral decomposition of $S^3 - K$ such that S contains a normal disk whose boundary meets exactly two boundary faces and no ideal edges of the polyhedra. Then all normal disks of S meet exactly two boundary faces, and the diagram of K is that of a $(2, q)$ -torus knot or link. Further, ∂S runs along at least one longitude of the knot or link, so ∂S is not a meridian.*

PROOF. Suppose D_2 is a normal disk of S such that ∂D_2 meets exactly two boundary faces and no edges. Then the fact that the diagram is prime and twist-reduced implies that D_2 is either a boundary bigon or ∂D_2 encircles a portion of a twist region in the diagram.

Suppose first that all normal disks of S that meet boundary faces are boundary bigons. Then by considering how such disks must glue, note that there can only be four disks, and they must encircle a single edge of the polyhedral decomposition. Thus S is an annulus encircling a crossing circle. This contradicts the fact that S is essential.

Now suppose all normal disks encircle portions of twist regions. Because these match up to form an annulus, the diagram of K must consist only of a single twist region, and the knot is a $(2, q)$ -torus knot or link. As in the proof of lemma 11.16, trace the boundary of S in this case. Superimpose onto a single polyhedron to obtain a string of boundaries of normal squares, with every other normal square coming from the same polyhedron. Because normal squares in a polyhedron are disjoint, this forces each square to bound either a single bigon, or a pair of adjacent bigons; see exercise 11.4. Then ∂S meets every ideal vertex at least once, so ∂S is not a meridian.

So finally suppose normal disks of S consist both of curves encircling twist regions and boundary bigons. There must be a disk D_2 that is a boundary bigon adjacent to a disk D_1 encircling a portion of a twist region. Superimpose ∂D_1 and ∂D_2 on a single polyhedron. By following the gluing maps, we find ∂D_1 bounds a single bigon face of the polyhedron, and ∂D_2 bounds an edge sharing the same boundary face (ideal vertex) with the bigon. See figure 11.6, left.

There is another normal disk D_3 attached to D_2 , in the opposite polyhedron from that containing D_2 . Because D_1 and D_3 are disjoint, D_3 must be a boundary bigon of the form shown in figure 11.6. Then D_4 cannot be a boundary bigon, for if it is, D_4 is not glued to D_1 (its side is in the wrong region), thus D_4 is glued to another disk D_5 . Because D_5 and D_1

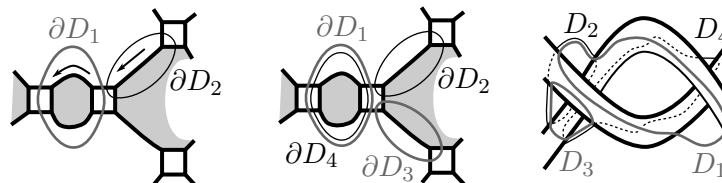


FIGURE 11.6. Left: Boundary bigon adjacent to a disk encircling a portion of twist region must have the form shown on the left. Middle: two next disks must have the form shown. Right: sketch the disks in the 3-dimensional knot complement

are disjoint, D_5 must be a boundary bigon, and then some D_6 will also be a boundary bigon contained inside D_2 , and so on, and there will be infinitely many boundary bigons spiraling around the same edge class. This is impossible. So D_4 bounds a portion of twist region, and ∂D_4 is parallel to ∂D_1 when superimposed (although recall that the disk D_1 lies in the opposite polyhedron from D_4). The disks D_1 through D_4 are shown superimposed on the same polyhedron in figure 11.6, middle, and in the link complement in figure 11.6, right.

We claim the annulus S can be isotoped so that these four disks become two normal boundary bigons, and all other normal disks of S are unchanged. The isotopy is by sliding past a crossing of the twist region where the boundary bigons cause the annulus to double back on itself. The isotopy is shown in figure 11.7.

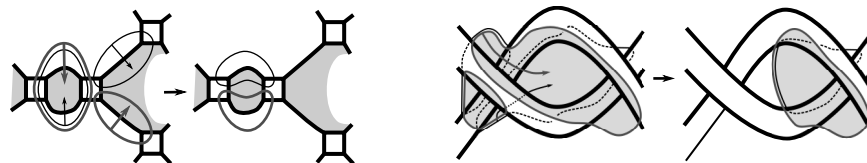


FIGURE 11.7. An isotopy of S removes normal disks bounding portions of twist region. Shown on the left is the effect of the isotopy in the diagram graph. Shown on the right is the result of the isotopy in the link complement

Repeating this move a finite number of times, we remove all disks bounding twist regions, and S is made up only of boundary bigons. This is a contradiction. \square

PROPOSITION 11.18. *If K is a knot or link with a connected, twist-reduced, prime, alternating diagram, and K is not a $(2, q)$ -torus knot or link, then K is anannular.*

If K is a $(2, q)$ -torus knot or link, then any essential annulus in $S^3 - K$ has boundary tracing out at least one longitude. Thus there is no essential meridional annulus.

PROOF. Suppose $S^3 - N(K)$ contains an embedded essential annulus S . We may isotope it into normal form, and by lemma 11.15 each normal disk making up S either meets one boundary face and two ideal edges, or two boundary faces and no ideal edges. In the former case, lemma 11.16 implies K is a $(2, q)$ -torus link and S is not meridional. In the latter case, lemma 11.17 implies K is a $(2, q)$ -torus knot or link and S is not meridional. \square

COROLLARY 11.19. *If K has a connected prime alternating diagram, then K is a prime link.*

PROOF. By lemma 11.5, the link K is not prime if and only if $S^3 - N(K)$ contains an essential meridional annulus. By lemma 11.12, K has a diagram that is connected, prime, alternating, and twist-reduced. Then proposition 11.18 implies that $S^3 - N(K)$ cannot contain an essential meridional annulus. So K is prime. \square

11.1.4. Closed surfaces and alternating knots. Our goal is still to prove theorem 11.9, that a knot with a connected, prime, alternating diagram is either a $(2, q)$ -torus knot or is hyperbolic. We now consider closed essential surfaces embedded in $S^3 - K$.

LEMMA 11.20. *Suppose S is a closed essential surface embedded in the complement of a knot or link K with a prime, connected, alternating diagram. Then S contains a closed curve that encircles a meridian of K at a crossing.*

PROOF. Put S into normal form with respect to the polyhedral decomposition of $S^3 - K$. Let D be an innermost normal disk in the polyhedron; that is, D cuts off a portion of a polyhedron that contains no other normal disks of S . Now, because S is a closed surface, D must meet a regular (i.e. not boundary) face F of the polyhedron. Moreover, normality implies an arc of ∂D meets F on two distinct edges e_1 and e_2 bordering F . These edges correspond to crossing arcs. Recall from the construction of the polyhedra (e.g. in chapter 1) that each such edge is identified to an edge on the opposite side of an ideal vertex in the polyhedron. Because the diagram is alternating, the two edges that are identified to e_1 and e_2 must lie on opposite sides of D ; see figure 11.8.

Because D meets edges e_1 and e_2 , another normal disk of S in the same polyhedron must meet the opposite edges identified to e_1 and e_2 , and thus there is an arc of a normal disk of S on either side of D . In figure 11.8, these are shown as dashed arcs. But D was chosen to be innermost, so one of those arcs must also belong to D . Then D contains an arc running from one crossing arc on one side of an ideal vertex back to the identified crossing arc on the other side of the ideal vertex. This arc glues up in S to be a closed curve encircling a meridian at the crossing. \square

COROLLARY 11.21. *If K is a knot or link with a prime alternating diagram, then its complement is atoroidal.*

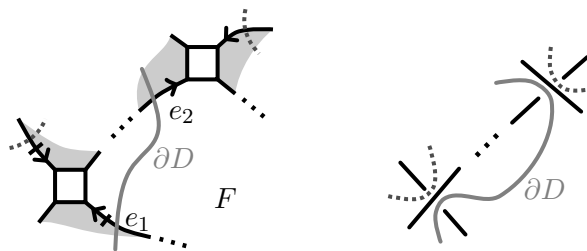


FIGURE 11.8. Crossing arcs identified to edges meeting ∂D lie on opposite sides of D . This is shown on the left in the polyhedron, and on the right in the diagram of the knot.

PROOF. Suppose S is an essential torus in $S^3 - K$. Then S contains a closed curve encircling a meridian at a crossing, by lemma 11.20. This closed curve bounds a disk in S^3 that meets the knot exactly once in a meridian at a crossing. Surger along this disk and push both ends away from the crossing. We obtain a sphere S' that meets the knot exactly twice in two meridians, with a crossing on the outside. Then $S' - N(K) := A$ is a meridional annulus. Because the link is prime, by corollary 11.19, the annulus A cannot be essential. It follows that A is boundary parallel, and thus the original torus S is boundary parallel, not essential. \square

PROOF OF THEOREM 11.9. Corollary 11.8 implies that a knot or link K with a prime alternating diagram is irreducible and boundary irreducible. Corollary 11.21 implies that it is atoroidal. By proposition 11.18, if it is not a $(2, q)$ -torus knot, then it is also anannular. The fact that $S^3 - K$ is hyperbolic then follows from Thurston's theorem 8.17. \square

11.2. Checkerboard surfaces

Recall that the diagram graph of a knot or link is a 4-valent graph embedded in the plane of projection. We may checkerboard color the regions of the graph, white and shaded. This checkerboard coloring may be used to define two surfaces embedded in any link complement.

DEFINITION 11.22. Let K be a knot or link. Consider all the shaded regions in the checkerboard coloring of the complement of the diagram graph of K . By removing a neighborhood of each vertex, these can be embedded as disks in the link complement, with boundary lying on the knot and along crossing arcs. At each crossing, attach a *twisted band* between crossing arcs on opposite sides of the crossing; see figure 11.9. Note the twisting is in the same direction as the crossing. The result is a surface embedded in $S^3 - N(K)$, with boundary on $N(K)$. This is called the *shaded checkerboard surface*. The *white checkerboard surface* is obtained similarly, using the opposite regions of the checkerboard coloring.

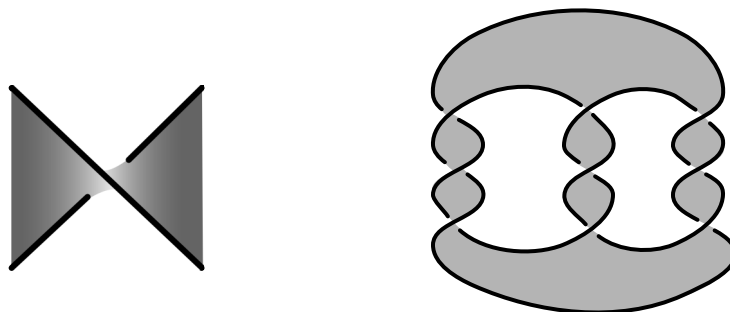


FIGURE 11.9. A twisted band is shown on the left, and a checkerboard surface on the right.

The main result of this section will be to show that if K is alternating, then checkerboard surfaces are essential. Our main tool again will be the checkerboard polyhedral decomposition of an alternating link.

For an alternating knot or link, the checkerboard surfaces are closely related to the polyhedral decomposition of theorem 11.6. In that theorem, we obtained two polyhedra with checkerboard colored faces that glue to give the link complement. The shaded checkerboard surface is obtained from the shaded faces of the polyhedra, the white checkerboard surface from the white faces.

DEFINITION 11.23. Let Σ be a properly embedded surface in a compact manifold M with torus boundary components. Let $N(\Sigma)$ be a regular neighborhood of Σ . The manifold *cut along Σ* is the manifold

$$M \setminus \setminus \Sigma := M - N(\Sigma).$$

The boundary of $M \setminus \setminus \Sigma$ is a union of two subsurfaces. One of these is the surface $\partial(N(\Sigma)) \subset \partial(M \setminus \setminus \Sigma)$; it is homeomorphic to the double cover $\tilde{\Sigma}$ of Σ . The other is the remnant of ∂M , consisting of $\partial M - (\partial M \cap N(\Sigma))$, containing annuli and tori. The latter surface is called the *parabolic locus* of $M \setminus \setminus \Sigma$.

DEFINITION 11.24. A *bounded polyhedral decomposition* of a manifold $M \setminus \setminus \Sigma$ is a decomposition of $M \setminus \setminus \Sigma$ into truncated ideal polyhedra with interior and boundary faces, as well as *surface faces*, which are unglued, and which come from $\tilde{\Sigma} \subset \partial(M \setminus \setminus \Sigma)$. As in definition 8.26, boundary edges are still defined to lie between boundary faces and other faces, *interior edges* lie between pairs of interior faces, and *surface edges* lie between surface faces and interior faces. We do not allow two surface faces to be adjacent along an edge. Moreover, under the gluing, each edge class either contains no surface edges, or it contains exactly two surface edges.

Our main example of a bounded polyhedral decomposition comes from checkerboard surfaces and alternating knots.

LEMMA 11.25. *Suppose $M = S^3 - N(K)$ is the exterior of an alternating knot or link K , and suppose Σ is the shaded checkerboard surface. Then the cut manifold $M \setminus \Sigma$ has a bounded polyhedral decomposition into the two checkerboard colored polyhedra of theorem 11.6. Surface faces are shaded faces; boundary faces glue to form the parabolic locus of $M \setminus \Sigma$. A similar statement holds for the white checkerboard surface.*

PROOF. The decomposition is just as before, only in the gluing of the two polyhedra, leave the shaded faces unglued. \square

There is a theorem for normal surfaces in bounded polyhedral decompositions that is completely analogous to theorem 8.28, for normal surfaces in ideal polyhedral decompositions.

THEOREM 11.26. *Let $M \setminus \Sigma$ have a bounded polyhedral decomposition.*

- (1) *If M is reducible, then M contains a normal 2-sphere.*
- (2) *If M is irreducible and boundary reducible, then M contains a normal disk.*
- (3) *If M is irreducible and boundary irreducible, then any essential surface in M can be isotoped into normal form.*

PROOF. The proof is nearly identical to that of theorem 8.28, except we can no longer isotope an essential surface S through surface faces, as they are now part of the boundary of $M \setminus \Sigma$. We modify the proof of theorem 8.28 where required to avoid such moves. Note that the proofs of the first two parts of the theorem require surgering, not isotoping, and so their arguments go through unchanged. So suppose M is irreducible and boundary irreducible, and S is essential.

First, if a component of ∂S lies entirely in a surface face and bounds a disk in that face, then since S is incompressible, that curve bounds a disk in S as well, hence S has a disk component, parallel into a surface face, contradicting the fact that it is essential.

If an arc of intersection of S with a face has both its endpoints on the same surface edge, and the arc lies in an interior face, then the arc and the edge bound a disc D with one arc of ∂D on S and one arc on a surface face. Because S is essential, it is boundary incompressible; it follows that the arc of intersection can be pushed off. A similar argument implies that an arc of intersection of S with an interior face that has one endpoint on a boundary edge and one on a surface edge can be pushed off. For all other arcs of intersection with endpoints on one edge, or an edge and adjacent boundary edges, the argument follows just as before. \square

As in the case of polyhedral decompositions, we may put angled structures on bounded polyhedral decomposition and assign to normal disks and normal surfaces a combinatorial area, exactly as in definition 8.30.

DEFINITION 11.27. A *bounded angled polyhedral structure* is a decomposition of $M \setminus \Sigma$ into ideal polyhedra, glued along interior faces, along with

a collection of dihedral angles, one for each (surface or interior) edge, that satisfy the following.

- (1) Each dihedral angle lies in the range $(0, \pi)$.
- (2) Each normal disk in a polyhedron has nonnegative combinatorial area.
- (3) Under the gluing, dihedral angles sum to 2π around an edge class meeting no surface edges. They sum to π if they meet surface edges.

PROPOSITION 11.28. *Suppose $M = S^3 - N(K)$ is the exterior of an alternating knot or link K , and Σ is the shaded checkerboard surface. Then the cut manifold $M \setminus \Sigma$ has a bounded angled polyhedral structure.*

PROOF. As in proposition 11.7, label each ideal edge of the checkerboard polyhedra by $\pi/2 \in (0, \pi)$. Then the proof of proposition 11.7 carries through to show that every normal disk has non-negative combinatorial area. We only need to check that dihedral angles sum to π at surface edges. Note that because each ideal edge is adjacent to both white and shaded faces, in fact each ideal edge is a surface edge. Because we no longer glue shaded faces, each edge class contains exactly two surface edges. Thus the sum of dihedral angles at each edge is $\pi/2 + \pi/2 = \pi$, as required. \square

LEMMA 11.29 (Bounded Gauss–Bonnet). *Let S be a surface properly embedded in $M \setminus \Sigma$, in normal form with respect to a bounded angled polyhedral structure on $M \setminus \Sigma$. Let p denote the number of times ∂S intersects a boundary edge adjacent to a surface face. Then*

$$a(S) = -2\pi\chi(S) + \frac{\pi}{2}p.$$

PROOF. Exercise. \square

DEFINITION 11.30. Let S be a surface properly embedded in a compact 3-manifold M with boundary. We say S is *boundary π_1 -injective* if whenever $\alpha \subset S$ is an arc properly embedded in S that is not homotopic rel endpoints to ∂S in S , then α is not homotopic rel endpoints to ∂M inside M .

We say the surface S is *π_1 -essential* if it is π_1 -injective, boundary π_1 -injective, and not parallel into ∂M .

Note that boundary π_1 -injective is stronger than boundary incompressible, and π_1 -essential is stronger than essential. For checkerboard surfaces, we have this stronger result.

THEOREM 11.31. *Let K be a link with a connected, prime, reduced alternating diagram, and let Σ be one of its checkerboard surfaces. Then Σ is π_1 -injective and boundary π_1 -injective, hence it is π_1 -essential.*

PROOF. We claim first that Σ is π_1 -injective and boundary π_1 -injective if and only if the surface $\tilde{\Sigma} = \partial N(\Sigma)$ is incompressible and boundary incompressible. The proof uses the loop theorem; we leave it as an exercise.

Now we claim that if D is a compression disk for $\tilde{\Sigma}$ in $S^3 - N(K)$, then we may assume D is properly embedded in $(S^3 - N(K)) \setminus \Sigma$. This is because $\tilde{\Sigma}$ separates $S^3 - N(K)$ into $N(\Sigma)$ and $(S^3 - N(K)) \setminus \Sigma$. An innermost disk argument implies that D can be isotoped to be disjoint $\tilde{\Sigma}$ in its interior, so D either lies in $(S^3 - N(K)) \setminus \Sigma$, as desired, or in the product $N(\Sigma)$. If D is in the product, then an isotopy mapping $N(\Sigma)$ to Σ takes the disk D to a disk parallel to Σ , hence parallel to $\tilde{\Sigma}$, contradicting the fact that it is a compression disk for $\tilde{\Sigma}$.

Thus D is an essential disk in $(S^3 - N(K)) \setminus \Sigma$ with boundary completely contained in $\tilde{\Sigma}$. Put D into normal form with respect to the bounded polyhedral decomposition of $(S^3 - N(K)) \setminus \Sigma$. Because ∂D meets no boundary faces, lemma 11.29, the bounded Gauss–Bonnet lemma, implies that $a(D) = -2\pi$. But each normal disk making up D has nonnegative combinatorial area, by proposition 11.28. This is a contradiction.

Now suppose that D is a boundary compression disk for $\tilde{\Sigma}$. An innermost disk and outermost arc argument implies that D is isotopic to a disk with interior disjoint from $\tilde{\Sigma}$, and again this disk must lie in $(S^3 - N(K)) \setminus \Sigma$. Put the disk into normal form. One arc of ∂D lies on $\tilde{\Sigma}$ and one arc lies on boundary faces. Note this arc begins and ends on boundary edges adjacent to a surface face, but if it meets any other boundary edges in its interior they must be adjacent to interior edges. Then the bounded Gauss–Bonnet lemma, lemma 11.29 implies that $a(D) = -2\pi + \pi = -\pi$. Again this contradicts the fact that normal disks have nonnegative combinatorial area.

So Σ is π_1 -injective and boundary π_1 -injective. Because it has boundary on $N(K)$ it cannot be boundary parallel. So it is π_1 -essential. \square

By theorem 11.31, every alternating knot contains a pair of π_1 -essential checkerboard surfaces. The converse is also true: independently, Howie [How17] and Greene [Gre17] showed that if a 3-manifold contains a pair of essential surfaces satisfying certain conditions required of checkerboard surfaces, then the 3-manifold is the complement of an alternating knot in S^3 and the surfaces are isotopic to checkerboard surfaces.

In addition to being π_1 -essential, checkerboard surfaces of a hyperbolic alternating knot also exhibit other nice geometric properties. We discuss these in the next chapter.

11.3. Exercises

EXERCISE 11.1. Give a proof that a knot or link with a connected, prime, alternating diagram is a prime link.

One way to prove this is to note that essential meridional annuli can be put into normal form while ensuring boundary components of the annuli stay well-behaved, and then analyzing the number and form of normal disks that could possibly arise.

EXERCISE 11.2. (Flypes and alternating diagrams)

- (1) Prove that a flype takes a prime diagram to a prime diagram.
- (2) Prove that a flype takes an alternating diagram to an alternating diagram.

EXERCISE 11.3. Prove the following result, which will be used in chapter 12.

PROPOSITION 11.32. *Let K be a knot or link with a connected, prime, alternating diagram. Then in the polyhedral decomposition of the link complement, there can be no bigon in normal form. That is, there is no normal disk embedded in a polyhedron that meets exactly two interior edges.*

EXERCISE 11.4. Work through the details of the proof of lemma 11.17: Suppose K is a knot or link with a connected, twist-reduced, prime, alternating diagram. Suppose S is an essential annulus in normal form with respect to the polyhedral decomposition. Suppose some normal disk making up D_2 meets exactly two boundary faces, but runs through opposite sides of those boundary faces.

- (a) Show that ∂D_2 encircles a twist region of the diagram.
- (b) Assume that ∂D_2 runs through exactly two boundary faces and exactly two white faces. One arc of ∂D_2 in a white face is glued to the side of a normal disk D_2 , and the other arc of ∂D_2 in a white face is glued to the side of a normal disk D_3 . Following the example of figure 11.5 left, sketch the images of these arcs of ∂D_1 and ∂D_3 superimposed on the same polyhedron containing ∂D_2 .
- (c) Prove that ∂D_1 and ∂D_3 must each encircle a string of adjacent bigons.
- (d) Prove that in fact, ∂D_1 , ∂D_2 , and ∂D_3 either all encircle a single bigon each, or they all encircle a pair of bigons each. Sketch these curves superimposed on the same polyhedron.

EXERCISE 11.5. Prove lemma 11.29, the bounded Gauss–Bonnet theorem.

EXERCISE 11.6. Prove that a properly embedded surface S in a compact 3-manifold M is π_1 -injective if and only if the surface $\tilde{S} = \partial N(S)$ is incompressible.

EXERCISE 11.7. Prove that a properly embedded surface S in a compact 3-manifold M is boundary π_1 -injective if and only if the surface $\tilde{S} = \partial N(S)$ is boundary incompressible.

The Geometry of Embedded Surfaces

In this chapter, we discuss the geometry of essential surfaces embedded in hyperbolic 3-manifolds.

In the first section, we show that specific surfaces embedded in hyperbolic 3-manifolds always admit isometries. This allows us to cut along such surfaces and reglue, obtaining new manifolds whose geometry can be understood from the geometry of the original. The most straightforward instance of this uses the 3-punctured sphere, and was discovered by Adams [Ada85], building on work of Wielenberg [Wie81]. Ruberman discovered a similar result for 4-punctured spheres and related surfaces [Rub87]. Both techniques are still frequently used to build examples of hyperbolic knots and links with particular geometric properties (for example volume: [Bur16], [AKC⁺17], short geodesics: [Mil17], cusp shapes: [DP19]).

We then return to more general essential surfaces, and discuss a geometric classification of such surfaces as quasifuchsian (or Fuchsian), accidental, or virtual fibered. We illustrate the behavior of such surfaces using examples from knot complements, especially alternating knots. We show that for hyperbolic alternating links, their checkerboard surfaces are always quasifuchsian.

12.1. Belted sums and mutations

This section describes two techniques for building distinct links with related hyperbolic structures; for example they have the same volume. The techniques both arose in the 1980s by cutting along an embedded surface in a hyperbolic 3-manifold and regluing via isometry.

12.1.1. 3-punctured spheres and belted sums. Suppose M is a hyperbolic 3-manifold that contains an embedded incompressible 3-punctured sphere S . We have seen examples of this: in chapter 7, each crossing circles of a reduced fully augmented link bounds an embedded essential 3-punctured sphere. In corollary 7.19 we noted that these 3-punctured spheres are always totally geodesic in fully augmented links. We now generalize this.

THEOREM 12.1. *Let M be a 3-manifold admitting a complete, finite volume hyperbolic structure, so M is the interior of a compact manifold \bar{M}*

with torus boundary. Let S be a π_1 -injective (equivalently, incompressible) 3-punctured sphere properly embedded in \overline{M} . Then S is isotopic to a properly embedded 3-punctured sphere that is totally geodesic in the hyperbolic structure on M .

PROOF. Let α , β , and $\gamma = \alpha \cdot \beta$ be generators of $\pi_1(S)$ that encircle the three punctures of S . Because M admits a complete hyperbolic structure, there is a representation $\rho: \pi_1(M) \rightarrow \mathrm{PSL}(2, \mathbb{C})$ taking α , β , and γ to parabolic elements. We may conjugate to adjust the images of three points at infinity; we conjugate so that the fixed point of $\rho(\alpha)$ is ∞ , so that $\rho(\alpha)$ translates $0 \in \mathbb{C}$ to $2 \in \mathbb{C}$, and so that the fixed point of $\rho(\beta)$ is 0. Then the three parabolics have the form

$$\rho(\alpha) = \begin{pmatrix} 1 & 2 \\ 0 & 1 \end{pmatrix}, \quad \rho(\beta) = \begin{pmatrix} 1 & 0 \\ z & 1 \end{pmatrix}, \quad \text{and } \rho(\alpha \cdot \beta) = \begin{pmatrix} 1 + 2z & 2 \\ z & 1 \end{pmatrix}.$$

Because $\rho(\alpha \cdot \beta)$ is parabolic, its trace is $2 + 2z = \pm 2$, so $z = 0$ or $z = -2$. If $z = 0$, $\rho(\beta)$ is the identity, contradicting the fact that S is π_1 -injective. Thus $z = -2$.

Now note that both $\rho(\alpha)$ and $\rho(\beta)$ (and hence $\rho(\alpha \cdot \beta)$) preserve the real line $\mathbb{R} \subset \mathbb{C} \subset \partial_\infty \mathbb{H}^3$. Hence $\rho(\pi_1(S))$ preserves the vertical plane P in \mathbb{H}^3 whose boundary is the real line. Thus under the covering map $p: \mathbb{H}^3 \rightarrow \mathbb{H}^3 / \rho(\pi_1(M)) = M$, the plane P maps to a totally geodesic surface homeomorphic to S in M .

It remains to show that $p(P)$ is embedded in M , and S is isotopic to the embedded totally geodesic surface $p(P)$. To do so, consider $p^{-1}(S)$. This is a disjoint union of embedded, possibly non-geodesic planes in \mathbb{H}^3 . One lift \tilde{S} is fixed by $\rho(\alpha)$, $\rho(\beta)$, and $\rho(\gamma)$ above. It follows that \tilde{S} and P have the same limit set; recall limit set is defined in definition 5.15. Then for any $\gamma \in \pi_1(M)$, $\rho(\gamma)(P)$ has the same limit set as $\rho(\gamma)(\tilde{S})$. Because S is embedded, translates of \tilde{S} are disjoint, and it follows that translates of P are disjoint embedded planes in \mathbb{H}^3 . Then $p(P)$ is an embedded surface in M , an isotopy from \tilde{S} to P projects to an isotopy from S to $p(P)$ in M , and S is isotopic to a properly embedded totally geodesic 3-punctured sphere. \square

COROLLARY 12.2. *Let M and M' be hyperbolic 3-manifolds containing essential embedded 3-punctured spheres S and S' , respectively. Then $M \setminus \setminus S$ and $M' \setminus \setminus S'$ are hyperbolic 3-manifolds, each with two totally geodesic 3-punctured sphere boundary components. Moreover:*

- (1) *Any manifold M'' obtained by identifying 3-punctured sphere boundary components of $M \setminus \setminus S$ to those of $M' \setminus \setminus S'$ will be hyperbolic, containing embedded essential 3-punctured spheres, and $M \setminus \setminus S$ and $M' \setminus \setminus S'$ embed isometrically in M'' . In particular, $\mathrm{vol}(M'') = \mathrm{vol}(M) + \mathrm{vol}(M')$.*

- (2) Any manifold M''' obtained by identifying the 3-punctured sphere boundary components of $M \setminus S$ via homeomorphism will be hyperbolic, containing an embedded essential 3-punctured sphere, and $\text{vol}(M''') = \text{vol}(M)$.

PROOF. Because S and S' are isotopic to totally geodesic hyperbolic surfaces, we obtain $M \setminus S$ and $M' \setminus S'$, respectively, by removing a collection of half spaces from \mathbb{H}^3 corresponding to lifts of S and S' , and then taking the quotient. Note that the geometry of $M \setminus S$ and $M' \setminus S'$ therefore agree with geometry of M and M' , respectively, away from S and S' . In particular, $\text{vol}(M \setminus S) = \text{vol}(M)$ and $\text{vol}(M' \setminus S') = \text{vol}(M')$. Moreover, $M \setminus S$ and $M' \setminus S'$ have totally geodesic 3-punctured sphere boundary.

By proposition 3.17, there is a unique hyperbolic structure on a 3-punctured sphere. Therefore, any gluing of 3-punctured spheres can be obtained by isometry. So M'' is obtained by gluing $M \setminus S$ to $M' \setminus S'$ by isometry. Thus $M \setminus S$ and $M' \setminus S'$ isometrically embed in M'' , and the volume of M'' is equal to $\text{vol}(M) + \text{vol}(M')$.

Similarly, $M \setminus S$ isometrically embeds in M''' and $\text{vol}(M''') = \text{vol}(M)$. \square

Theorem 12.1 and corollary 12.2 were used by Adams to construct explicit examples of links in S^3 with additive volumes.

DEFINITION 12.3. A *belted tangle* is a link in S^3 with one link component unknotted in S^3 , bounding a disk meeting other components of the link exactly two times; see figure 12.1, left.

The *belted sum* of two belted tangles is the belted tangle obtained by tangle addition as in figure 12.1, right.

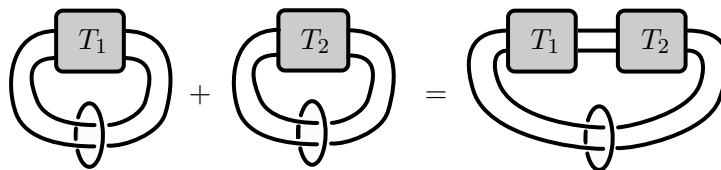


FIGURE 12.1. A belted tangle is a link with an unknotted component bounding an embedded 2-punctured disk; two are shown on the left. On the right, a belted sum is obtained from two belted tangles via the tangle addition shown.

COROLLARY 12.4. If L_1 and L_2 are belted tangles that are hyperbolic, then their belted sum L is a hyperbolic link with volume satisfying $\text{vol}(L) = \text{vol}(L_1) + \text{vol}(L_2)$.

PROOF. Note that $S^3 - L_1$ and $S^3 - L_2$ each contain an embedded 3-punctured sphere, namely the 2-punctured disk whose boundary is on the unknotted component of the link. Because these two link complements are

hyperbolic, the 3-punctured sphere must be incompressible in both cases (easy exercise). The result then follows from corollary 12.2. \square

12.1.2. 4-punctured spheres and mutation. Note that to prove corollary 12.4, we glued isometric 3-punctured spheres. Unfortunately, the 3-punctured sphere is the only hyperbolic surface with a unique hyperbolic structure. All others have infinitely many hyperbolic structures, and so a gluing homeomorphism will not necessarily give an isometry, and volume will not necessarily be additive. However, in certain cases we may still cut and glue along an essential surface and still ensure that geometry is well behaved. One way to do this is a process called *mutation*, which applies to 4-punctured spheres.

This section gives a condition on the diagrams of two knots and links that will guarantee that the geometries of their complements are similar; in particular they will have the same hyperbolic volume. This was first discovered by Ruberman [Rub87], who proved the result using minimal surfaces. Because the full proof requires more background on minimal surfaces than we wish to include here, we will refer to his paper for the complete result. However, we will provide full details in the special case that an embedded essential 4-punctured sphere is isotopic to an embedded pleated 4-punctured sphere isometric to the boundary of an ideal tetrahedron.

DEFINITION 12.5. A *Conway sphere* is a 4-punctured sphere obtained from the diagram of a knot or link K as follows. Let γ be a simple closed curve in the plane of projection of the diagram of K that meets the diagram exactly four times, transversely in edges of the diagram. Let \bar{S} be the sphere embedded in $S^3 - K$ obtained by attaching two disks to γ , one on either side of the plane of projection. Let S denote the corresponding 4-punctured sphere in $S^3 - K$. In the case that S is essential, we say that it is a *Conway sphere* for K .

We will put geometric structures on Conway spheres, and cut and reglue via isometry of the spheres. Note that a hyperbolic ideal tetrahedron has boundary a pleated 4-punctured sphere. This gives us a special case of a hyperbolic structure on a 4-punctured sphere and an isometry preserving it.

LEMMA 12.6. *Let T be a hyperbolic ideal tetrahedron. For each pair of opposite edges, there is an axis in \mathbb{H}^3 meeting the two edges orthogonally. Rotation by π about such an axis is an isometry of the ideal tetrahedron.*

PROOF. Rotation by π through an axis is an isometry of \mathbb{H}^3 that maps the tetrahedron back to itself. \square

COROLLARY 12.7. *Let S be a pleated 4-punctured sphere with hyperbolic structure identical to the boundary of an ideal hyperbolic tetrahedron. Then any of the three rotations of lemma 12.6 gives an isometry of S .*

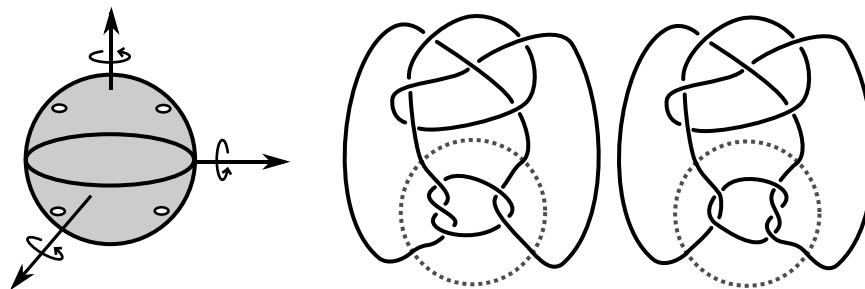


FIGURE 12.2. Mutation cuts along a Conway sphere, performs one of the involutions shown on the left, and then reglues. Shown on the right is an example of two distinct knots related by mutation.

DEFINITION 12.8. A *mutation* of a knot or link is obtained by cutting along a Conway sphere, rotating by π along one of three axes shown in figure 12.2, and then regluing.

THEOREM 12.9. Let K be a hyperbolic knot or link admitting an embedded essential Conway sphere. Let K^μ be any mutation of K . Then K^μ is hyperbolic, and $\text{vol}(K) = \text{vol}(K^\mu)$.

PROOF. Let S be the essential Conway sphere, and pleat S . If the pleating is embedded, isometric to the boundary of an ideal tetrahedron, then we may cut along the pleated surface to obtain two hyperbolic manifolds whose boundaries are isometric pleated 4-punctured spheres, and isometric to the boundary of a hyperbolic ideal tetrahedron. By corollary 12.7, rotation by π through an axis orthogonal to opposite edges of the tetrahedron gives an isometry of the pleated surface S . Thus we may apply this isometry to one of the pieces and reglue, to obtain a complete hyperbolic manifold with an embedded essential Conway sphere, and volume equal to the volume of $S^3 - K$. Note this is exactly a mutation.

In the case that the pleating is not embedded, then Ruberman shows that S is still isotopic to an embedded 4-punctured sphere that is a minimal surface with respect to the hyperbolic metric, and that mutation is an isometry of this minimal surface [Rub87]. Thus the same argument applies to show the volumes agree. \square

12.2. Fuchsian, quasifuchsian, and accidental surfaces

We now return to more general essential surfaces embedded in a hyperbolic 3-manifold.

Let M be hyperbolic, such that M is the interior of a compact 3-manifold \overline{M} with boundary. Since M is hyperbolic, we know there is a discrete, faithful representation $\rho: \pi_1(M) \rightarrow \text{PSL}(2, \mathbb{C})$ (proposition 5.10). If S is a surface properly embedded in M , then the restriction of ρ to $\pi_1(S)$ will

be a discrete subgroup of $\mathrm{PSL}(2, \mathbb{C})$. We will consider properties of this subgroup.

Let $\Gamma \leq \mathrm{PSL}(2, \mathbb{C})$ be a discrete group. Recall from definition 5.15 that the limit set of Γ is the set of accumulation points on $\partial\mathbb{H}^3$ of the orbit $\Gamma(x)$ for any point $x \in \mathbb{H}^3$.

DEFINITION 12.10. A discrete group $\Gamma \leq \mathrm{PSL}(2, \mathbb{C})$ is said to be *Fuchsian* if its limit set is a geometric circle on $\partial\mathbb{H}^3$. If its limit set is a Jordan curve and no element of Γ interchanges the complementary components of the limit set, then Γ is said to be *quasifuchsian*.

EXAMPLE 12.11. Let $\Gamma \leq \mathrm{PSL}(2, \mathbb{R})$ be the image of a discrete faithful representation of the fundamental group of a hyperbolic surface S that is either closed or punctured without boundary. Then the limit set of Γ in \mathbb{H}^2 is all of $\partial\mathbb{H}^2$. Now view $\Gamma \leq \mathrm{PSL}(2, \mathbb{R}) \leq \mathrm{PSL}(2, \mathbb{C})$ as acting on a hyperplane H in \mathbb{H}^3 . When we extend the action of Γ to all of \mathbb{H}^3 , the limit set is the geometric circle that is the boundary of the hyperplane ∂H . Thus Γ is Fuchsian.

Now adjust the representation very slightly, to $\Gamma_\epsilon \leq \mathrm{PSL}(2, \mathbb{C})$. The limit set also adjusts slightly. If Γ_ϵ is no longer a subgroup of $\mathrm{PSL}(2, \mathbb{R})$, then its limit set is no longer a geometric circle. However, it will be a topological circle. Thus Γ_ϵ is quasifuchsian. An example is shown in figure 12.3; this figure first appeared in [Thu82].

The examples of figure 12.3 were created by computer. Adjusting deformations of Fuchsian group by computer leads to beautiful fractal images. See, for example, [MSW02]. Software to visualize limit sets has also been developed by Wada [Wad16]. Yamashita has written a note to help users create their own software [Yam12]. As a first step for the interested reader, we suggest working through Yamashita's example in exercise 12.3. For further work, the book [MSW02] includes direction on creating and exploring limit sets by computer.

DEFINITION 12.12. Let M be a hyperbolic 3-manifold and $S \subset M$ a properly embedded essential surface. Let $\rho: \pi_1(M) \rightarrow \mathrm{PSL}(2, \mathbb{C})$ be a discrete, faithful representation. The surface S is *totally geodesic*, if, under the induced representation, the image $\rho(\pi_1(S)) \leq \mathrm{PSL}(2, \mathbb{C})$ is Fuchsian. Sometimes a totally geodesic surface is also called *Fuchsian*. The surface S is *quasifuchsian* if $\rho(\pi_1(S)) \leq \mathrm{PSL}(2, \mathbb{C})$ is quasifuchsian.

DEFINITION 12.13. Let S be a surface properly embedded in M . A nontrivial loop γ that is not freely homotopic into ∂S in S is called an *accidental parabolic* if $\rho(\gamma)$ is parabolic in $\mathrm{PSL}(2, \mathbb{C})$. The surface S is said to be *accidental* if it contains an accidental parabolic.

THEOREM 12.14. *If S is a totally geodesic or quasifuchsian surface properly embedded in the hyperbolic 3-manifold M , then S is not accidental.*

PROOF. If S is a totally geodesic surface, then any closed curve γ in S that is not freely homotopic into ∂S must be freely homotopic to a closed

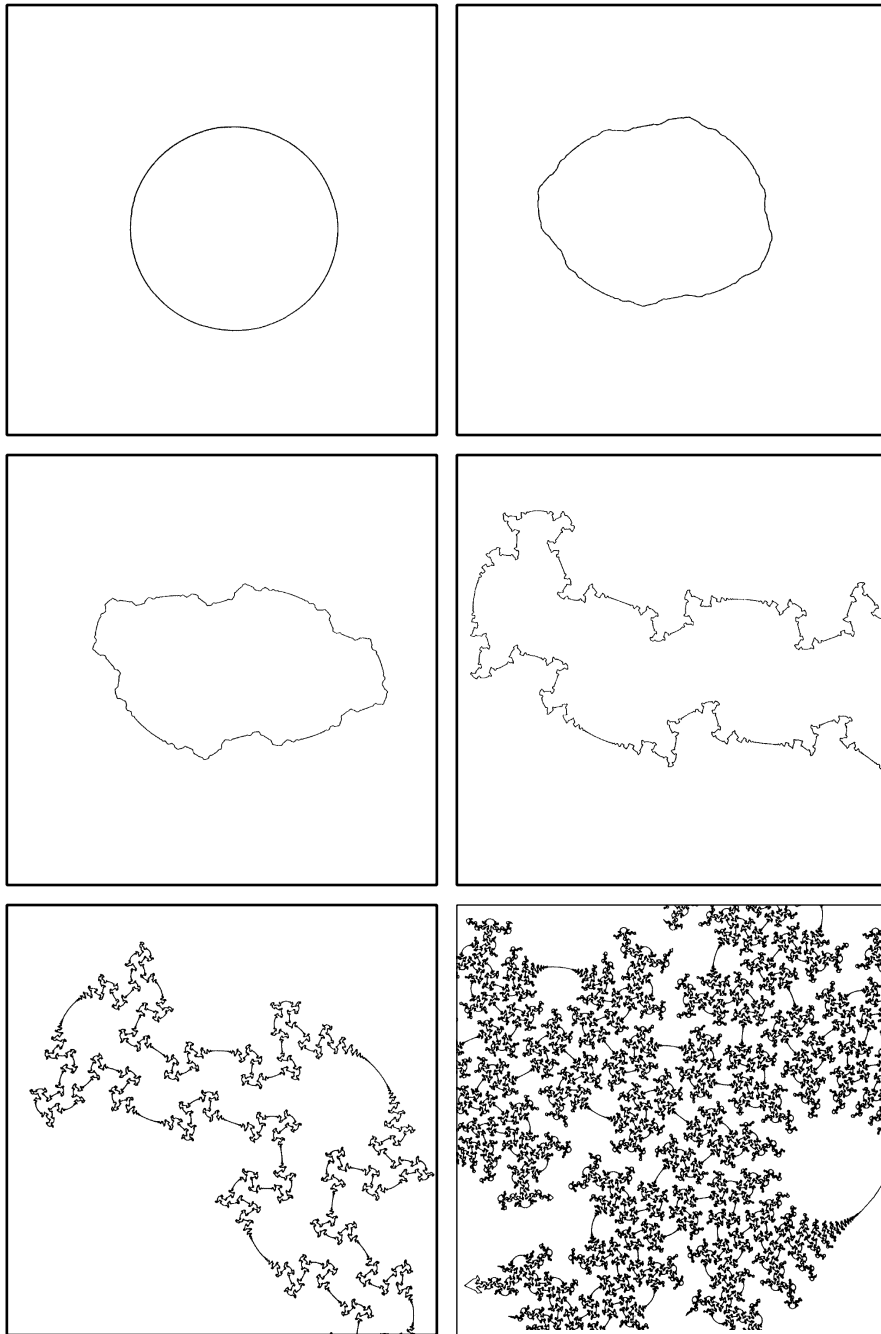


FIGURE 12.3. The limit set of a Fuchsian group, and various limit sets of quasifuchsian groups obtained by deforming the Fuchsian group slightly. Figures are from [Thu82].

geodesic in S . In turn, this closed geodesic in S is a closed geodesic in M . Thus $\rho(\gamma)$ has a geodesic axis, and cannot be parabolic. Thus S has no accidental parabolics in this case.

If S is quasifuchsian, the same argument does not immediately apply. However, it is known that a quasifuchsian group cannot contain an accidental parabolic element. See Chapter IX, proposition D.17 of [Mas88]. Thus S is not accidental. \square

COROLLARY 12.15. *Let K be a knot or link with a prime, connected, alternating diagram, and suppose K is not a $(2, q)$ -torus knot. Then the hyperbolic manifold $S^3 - K$ contains no closed embedded totally geodesic surface.*

PROOF. Suppose S is a closed, embedded, totally geodesic surface in the link complement $S^3 - K$. By lemma 11.20, any closed essential surface contains a closed curve that encircles a meridian of K . In particular, S must contain a closed curve γ encircling a meridian. But then γ is freely isotopic to a meridian of K , meaning γ is an accidental parabolic. This contradicts theorem 12.14. \square

In [MR92], Menasco and Reid were the first to observe corollary 12.15. Based on their observation, they made the following conjecture, which is still open at the time of writing this book.

CONJECTURE 12.16 (Menasco–Reid conjecture). *Let K be a knot in S^3 such that $S^3 - K$ is hyperbolic. Then $S^3 - K$ admits no closed, embedded, totally geodesic surface.*

Since the conjecture was proposed in the 1990s, evidence has developed both for and against the Menasco–Reid conjecture. As evidence for the conjecture, Menasco and Reid showed that in addition to alternating knots, additional classes of hyperbolic knots cannot contain a closed embedded totally geodesic surface (closed 3-braids and tunnel number one knots) [MR92]. Since then, even more classes of knots and links have been shown to contain no closed, embedded, totally geodesic surfaces; a summary of such results can be found in the survey [Ada05].

On the other hand, conjecture 12.16 is known to be false for link complements, shown first in [MR92]. Leininger showed that there exists a sequence of hyperbolic knots whose complements contain closed embedded essential surfaces with principal curvatures converging to zero [Lei06]; if the principal curvatures were known to be zero the surfaces would be totally geodesic. DeBlois showed that conjecture 12.16 does not hold for knots in rational homology spheres [DeB06]. And Adams and Schoenfeld showed that conjecture 12.16 is false if surfaces are allowed to have punctures [AS05]. For example, they showed that the checkerboard surface of certain pretzel knots, such as the surface shown in figure 11.9, is totally geodesic.

Most of the evidence in support of conjecture 12.16 is obtained by showing that any closed surface properly embedded in a particular type of knot

complement must contain an accidental parabolic, similar to lemma 11.20. Thus there is interest in finding examples of essential surfaces without accidental parabolics.

If we consider surfaces with (parabolic) boundary, we already have most of the tools in place to prove the following.

THEOREM 12.17. *Let K be a link with a connected, prime, reduced alternating diagram, and let Σ be one of its checkerboard surfaces. Then Σ is not accidental.*

Before we prove the theorem, we need a definition and a lemma.

DEFINITION 12.18. Let M be a hyperbolic 3-manifold, such that M is the interior of a compact 3-manifold \overline{M} with boundary. The *parabolic locus* P of M consists of tori and annuli in $\partial\overline{M}$ such that each simple curve in P lifts to a parabolic element of $\pi_1(M) \leq \mathrm{PSL}(2, \mathbb{C})$.

LEMMA 12.19. *Suppose S is a π_1 -essential surface properly embedded in an irreducible, boundary irreducible 3-manifold M , and suppose S is accidental. Then there is an essential annulus A embedded in $M \setminus S$ with one boundary component on the parabolic locus P of M and one boundary component an essential closed curve on \tilde{S} .*

The proof of the lemma uses the annulus theorem of Jaco [Jac80, Theorem VIII.13] stated below. Briefly, it ensures we can replace an immersion of an annulus into a compact 3-manifold with an embedding. For a proof of the annulus theorem, see [Jac80]. Compare to theorem 8.49, the loop theorem.

THEOREM 12.20 (Annulus theorem). *Let M be a compact, irreducible 3-manifold with incompressible boundary. Suppose $f: (A, \partial A) \rightarrow (M, \partial M)$ is a proper map, i.e. f takes ∂A to ∂M . Suppose also that f is nondegenerate, i.e. that f cannot be homotoped to the boundary of M . Then there exists an embedding $g: (A, \partial A) \rightarrow (M, \partial M)$ that is nondegenerate. Furthermore, if the restriction of f to ∂A is an embedding, then g may be chosen so that its restriction to ∂A is the same embedding.*

PROOF OF LEMMA 12.19. If S is accidental, then there exists a nontrivial closed curve on S that is freely homotopic into ∂M through M . Note if S is nonorientable, then \tilde{S} , the boundary of a regular neighborhood of S , is also accidental, with accidental parabolic a double cover of the curve on S . So we may assume there is a nontrivial closed curve γ on \tilde{S} that is freely homotopic into ∂M through M . The free homotopy defines a map of an annulus A' into M ; one boundary component of A' lies on γ and one on ∂M . Adjust A' so all intersections with \tilde{S} are transversal, and move the component of A' on \tilde{S} in a bicollar of S to be disjoint from \tilde{S} .

Now consider intersections of the interior of A' with \tilde{S} . Consider first a closed curve of intersection that bounds a disk on A' . Since \tilde{S} is incompressible (because S is π_1 -essential), an innermost such curve also bounds a

disk in \tilde{S} . Since M is irreducible, the union of the disk on A' and that on \tilde{S} bounds a ball in M , and we may isotope A' through the ball to remove the intersection. Thus we may assume there are no closed curves of intersection that bound disks on A' . Suppose there is an arc of intersection $A' \cap \tilde{S}$ with both endpoints on ∂M . This arc co-bounds a disk on A' along with an arc on $\partial A' \subset \partial M$. Because \tilde{S} is boundary incompressible and M is boundary irreducible, an innermost such arc may be isotoped away. So we assume there are no such arcs of intersection. Finally, because we have isotoped A' away from \tilde{S} in a bicollar of the curve $\gamma \subset \tilde{S}$, there are no arcs of intersection $A' \cap \tilde{S}$ with an endpoint on \tilde{S} . Thus there are no arcs of intersection of $A' \cap \tilde{S}$. The only remaining possibility is that $A' \cap \tilde{S}$ is a collection of essential closed curves on A' .

Apply a homotopy to minimize the number of closed curves of intersection. There is a sub-annulus $A'' \subset A'$ that is outermost: it has one boundary component on ∂M and one on \tilde{S} and interior disjoint from \tilde{S} . Thus we may consider A'' as an immersion of an annulus into $M \setminus \tilde{S}$. It is nondegenerate, else we could have reduced the number of closed curves of intersection of A' . Now we apply theorem 12.20, the annulus theorem. There exists a nondegenerate embedding of an annulus A into $M \setminus \tilde{S}$ with one boundary component on \tilde{S} and one on the parabolic locus ∂M . To finish the proof, we need to show that the embedding lies in $M \setminus S$.

Note that $M \setminus \tilde{S}$ consists of two components, one homeomorphic to $M \setminus S$ and one to a regular neighborhood of S . The regular neighborhood of S only meets ∂M in a neighborhood of ∂S . Since ∂A has a component on ∂M , if A is embedded in the neighborhood of S , it has a component running parallel to ∂S on ∂M . But then the retraction of A to S defines a free homotopy of the closed curve $\partial A \cap S$ to ∂S , contradicting the definition of accidental. Thus A is embedded in the component of $M \setminus \tilde{S}$ that is homeomorphic to $M \setminus S$. \square

PROOF OF THEOREM 12.17. Let Σ be a checkerboard surface, and suppose by way of contradiction that it is accidental. Then by lemma 12.19, there exists an essential annulus A embedded in $(S^3 - N(K)) \setminus \Sigma$ with one boundary component on $\tilde{\Sigma}$ and one on $N(K)$.

Consider the bounded polyhedral decomposition of $(S^3 - N(K)) \setminus \Sigma$ (lemma 11.25). By theorem 11.26, we may take A to be in normal form with respect to the polyhedra. Note that because components of ∂A lie entirely in \tilde{S} and in $\partial N(K)$, respectively, there are no arcs of ∂A intersecting a boundary edge adjacent to a surface face. Thus by lemma 11.29, the combinatorial area of A is 0. It follows that each normal disk of A has combinatorial area 0. This is possible only if the disk has one of three forms: each normal disk either meets exactly two boundary faces and no edges, or it meets exactly one boundary face and exactly two edges, or it meets exactly four edges. Because one component of ∂A lies on $\partial N(K)$,

there must be a normal disk meeting a boundary face. If the normal disk meets two boundary faces, then there is an arc of intersection of A with a white face that runs from the boundary component of ∂A on ∂M back to the same boundary component, cutting off a disk in A . Because the white checkerboard surface is boundary incompressible, such an arc bounds a disk on the white checkerboard surface. By normality, the disk cannot be contained in a single white face: the arc would run from one boundary edge back to the same edge. But an innermost intersection with a shaded face would give a crossing arc cutting off a boundary compression disk for the link. This is also impossible in a reduced diagram. So we may assume that there is a normal disk of A meeting exactly one boundary face and exactly two edges of the polyhedron. On A , such an arc runs from the component $\partial A \cap \partial M$ of ∂A to $A \cap S$, which is the other component of ∂A .

Then lemma 11.16 implies that all normal disks of A have this form, and that K is a $(2, q)$ -torus link. The surface S is the annulus lying between the two strands of the link. Moreover, the boundary component γ of ∂A on \tilde{S} must run along the core of the annulus S . It follows that γ is boundary parallel. But then γ is not accidental. This is a contradiction. \square

12.3. Fibers and semifibers

Consider again the limit set of a group $\rho(\pi_1(S))$ where S is a surface embedded in a hyperbolic 3-manifold M and $\rho: \pi_1(M) \rightarrow \mathrm{PSL}(2, \mathbb{C})$ is the holonomy representation. Figure 12.3 shows the limit set of Fuchsian and quasifuchsian examples. There is an additional option: the limit set of a discrete group isomorphic to $\pi_1(S)$ might be a space-filling curve. In this section, we will analyze surfaces with this property. First we present two topological definitions.

DEFINITION 12.21. Let S be a surface properly embedded in a 3-manifold M . We say S is a *fiber* if M can be written as a fiber bundle over S^1 , with fiber the surface S . Equivalently, there is a homeomorphism $f: S \rightarrow S$ such that M is the mapping torus

$$M \cong (S \times [0, 1]) / (0, x) \sim (1, f(x)).$$

DEFINITION 12.22. An *I-bundle* is a 3-manifold homeomorphic to $S \times I$, where S is a surface, possibly with boundary. The *vertical boundary* is $\partial S \times I$; note it is a collection of annuli. The *horizontal boundary* consists of $S \times \partial I$. If S is orientable, this consists of the disjoint union of $S \times \{0\}$ and $S \times \{1\}$. If S is nonorientable, we say that the *I-bundle* is *twisted*, and the horizontal boundary is homeomorphic to the oriented double cover of S . We often denote a twisted *I-bundle* by $S \tilde{\times} I$. See exercise 12.4.

DEFINITION 12.23. A surface S properly embedded in a 3-manifold M is a *semifiber* if it is either a fiber, or if S is the boundary of an *I-bundle* $S' \times I$ over a nonorientable surface S' , and M is obtained by gluing two

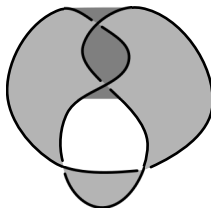


FIGURE 12.4. The Seifert surface of the figure-8 knot complement.

copies of this I -bundle by the identity on S . In the latter case, sometimes S is called a *strict semifiber*.

A strict semifiber is an example of a *virtual fiber*, defined below. See exercise 12.5.

DEFINITION 12.24. A surface S properly embedded in a 3-manifold M is called a *virtual fiber* if there is a finite index cover of M in which S lifts to a fiber.

The following is due to Thurston [**Thu79**] and Bonahon [**Bon86**]. See also [**CEG06**].

THEOREM 12.25. *Let S be an essential surface in a hyperbolic 3-manifold M . Then S has exactly one of three forms:*

- (1) S is Fuchsian or quasifuchsian,
- (2) S is accidental, or
- (3) S is a virtual fiber.

The proof of the theorem is obtained by analyzing surfaces that are not accidental, and whose limit set is not a circle or topological circle.

EXAMPLE 12.26. The figure-8 knot complement contains a surface that is a fiber, namely the punctured torus shown in figure 12.4.

A portion of the limit set of this surface was computed by S. Schleimer, following W. Thurston, and is shown in figure 12.5. Its lift to the universal cover, given a pleating, is shown in figure 12.6, due to S. Schleimer and H. Segerman.

Another view of the surface is shown in figure 12.7, due to D. Bachman, S. Schleimer, and H. Segerman. Note that in figure 12.6, the cusps of the surface have been cut off to show a larger view of the pleating. On the other hand, figure 12.7 gives a better view of the surface near infinity, without cusps cut off.

We will be dealing only with embedded surfaces. In the case a surface is embedded, the virtual fiber case of the trichotomy reduces to a simpler situation.

LEMMA 12.27. *Suppose S is a properly embedded surface in a 3-manifold M . Then S is a virtual fiber if and only if S is a semifiber.*

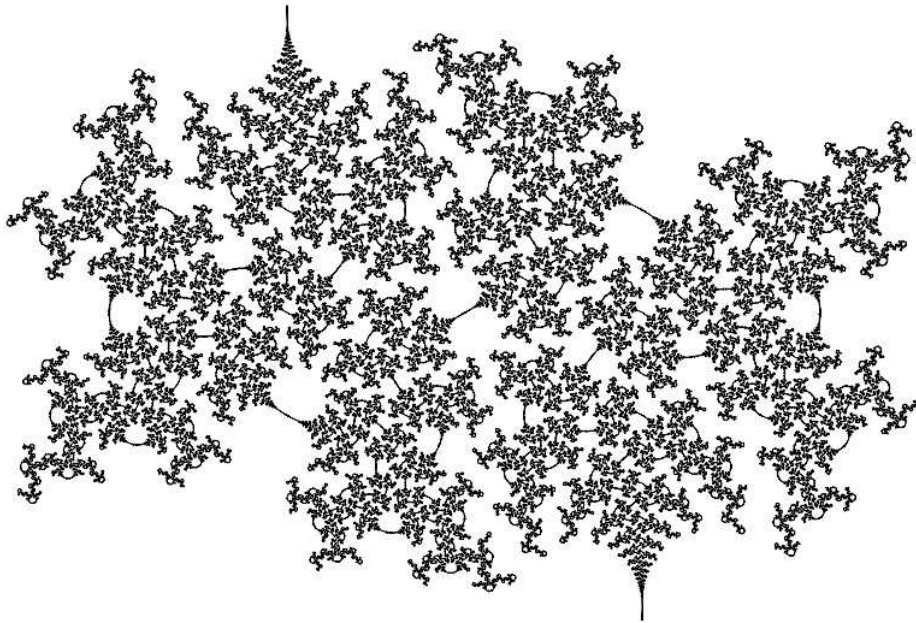


FIGURE 12.5. The limit set of the Seifert surface of the figure-8 knot complement, created by S. Schleimer.

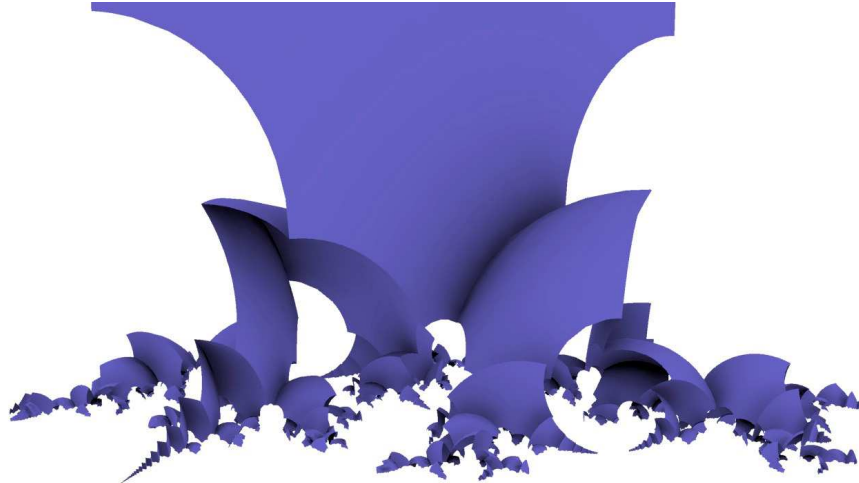


FIGURE 12.6. The lift of the figure-8 knot Seifert surface to the universal cover \mathbb{H}^3 , with a pleating. Created by S. Schleimer and H. Segerman.

PROOF. Exercise 12.7. □

As an additional example of a fibered surface in a link complement, consider the checkerboard surfaces of the $(2, q)$ -torus knot or link.

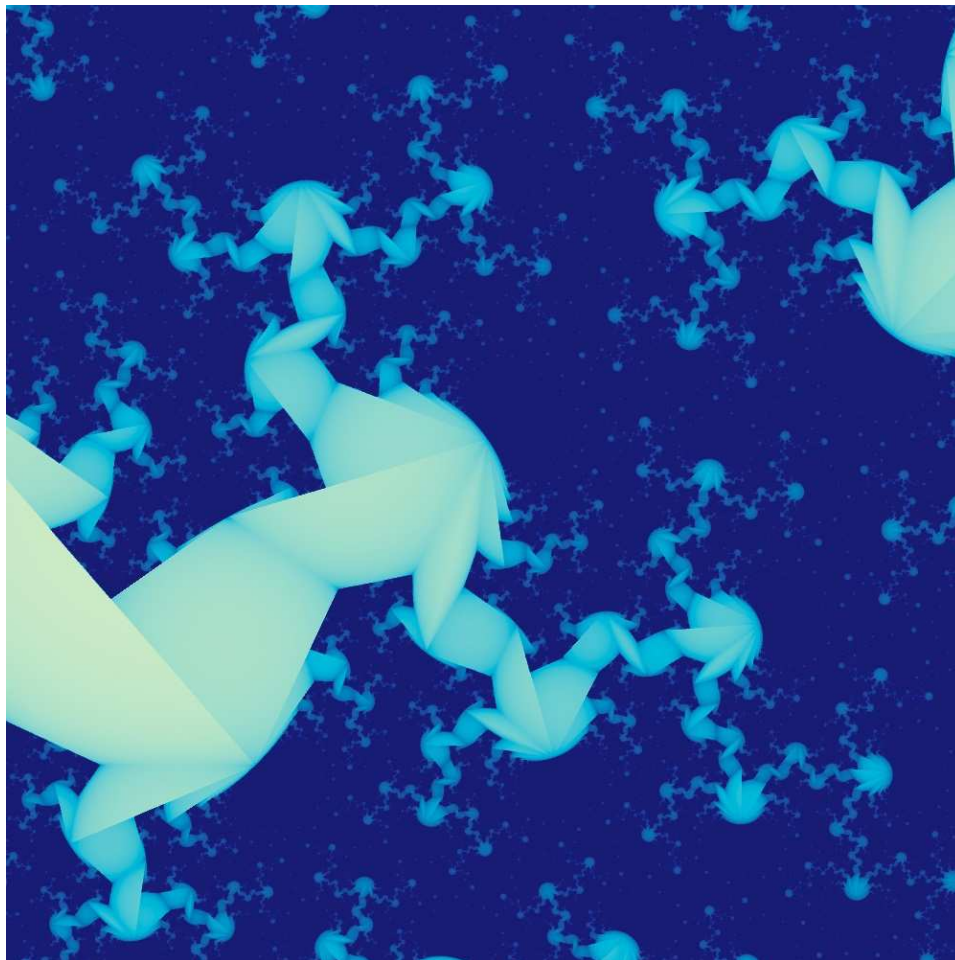


FIGURE 12.7. More of the lift of the figure-8 knot Seifert surface to \mathbb{H}^3 , without cusps cut off. Created by D. Bachman, S. Schleimer and H. Segerman.

LEMMA 12.28. *One of the checkerboard surfaces of a standard diagram of a $(2, q)$ -torus knot or link is a fiber.*

PROOF. One of the checkerboard surfaces is an annulus or Möbius band running between the two strands of the link. Let that be the white checkerboard surface. We will show the shaded surface Σ is a fiber. Note that Σ is orientable, as it is built of two disks with a sequence of (singly) twisted bands between them. Thus the cut manifold $(S^3 - N(K)) \setminus \Sigma$ has boundary consisting of parabolic locus and $\tilde{\Sigma}$, which is two copies of Σ in the orientable case. The surface Σ is a semifiber if and only if the cut manifold $(S^3 - N(K)) \setminus \Sigma$ is an I -bundle:

$$(S^3 - N(K)) \setminus \Sigma \cong \Sigma \times I.$$

Consider the polyhedral decomposition of the cut manifold in this case. The two polyhedra consist of a chain of adjacent white bigons along with two shaded disks, one inside and one outside the chain of bigons. Note each of these polyhedra is an I -bundle over the shaded face, of the form $D \times I$ where D is a shaded disk. White bigon faces are of the form $\alpha_i \times I$, where α_i is an arc with endpoints on edges of the polyhedron (shaded faces). The parabolic locus consists of boundary squares, which are also products $\text{arc} \times I$, parallel to $\alpha_i \times I$ on their sides meeting white faces, with endpoints of arcs on shaded faces.

To obtain $(S^3 - N(K)) \setminus \Sigma$, glue white faces. The gluing takes each bigon face $\alpha_i \times I$ to another bigon face $\alpha_j \times I$, matching the I -bundle structure. Thus $(S^3 - N(K)) \setminus \Sigma$ is an I -bundle. So Σ is a semifiber.

To see that Σ is actually a fiber, note that the gluing of the two polyhedra along white faces matches $D_1 \times \{0\}$ in one polyhedron to $D_2 \times \{0\}$ in the other, and $D_1 \times \{1\}$ to $D_2 \times \{1\}$ in the other. Thus the boundary of the I -bundle has two components, so it is not an I -bundle over a nonorientable surface, and cannot be a strict semifiber. \square

THEOREM 12.29. *Let K be a knot or link with a connected, twist-reduced, prime, alternating diagram, and let Σ be an associated checkerboard surface. Then Σ is a semifiber if and only if K is a $(2, q)$ -torus link and Σ is the checkerboard surface of lemma 12.28 that is a fiber.*

Before proving the theorem, we give a lemma. Its proof is very similar to Lemma 4.17 of [FKP13]; see also [HP17].

LEMMA 12.30. *Let K be a knot or link as in the statement of theorem 12.29, and let Σ be its shaded checkerboard surface. Let B be an I -bundle embedded in $M_\Sigma = (S^3 - N(K)) \setminus \Sigma$, with horizontal boundary on $\tilde{\Sigma}$, and suppose the vertical boundary of B is essential. Let W be a white face of the polyhedral decomposition of the cut manifold. Then $B \cap W$ is isotopic in M_Σ to a collection of product rectangles $\alpha \times I$, where $\alpha \times \{0\}$ and $\alpha \times \{1\}$ are arcs of ideal edges on the boundary of W .*

PROOF. First suppose $B = Q \times I$ is a product I -bundle over an orientable base. Consider a component of $\partial(B \cap W)$. If it lies entirely in the interior of W , then it lies in the vertical boundary $V = \partial Q \times I$. The intersection $V \cap W$ then contains a closed curve component; an innermost one bounds a disk in W . Since the vertical boundary is essential, we may isotope B to remove such intersections. So assume each component of $\partial(B \cap W)$ meets $\tilde{\Sigma}$. Note that it follows that each component of $B \cap W$ is a disk.

Note $W \cap \tilde{\Sigma}$ consists of ideal edges on the boundary of the face W . It follows that the boundary of each component of $B \cap W$ consists of arcs $\alpha_1, \beta_1, \dots, \alpha_n, \beta_n$ with α_i an arc in an ideal edge of $W \cap \tilde{\Sigma}$ and β_i in the vertical boundary of B , in the interior of W . We may assume that each arc β_i runs between distinct ideal edges, else isotope B through the disk bounded by β_i and an ideal edge to remove β_i , and merge α_i and α_{i+1} .

We may assume that β_i runs from $Q \times \{0\}$ to $Q \times \{1\}$, for if not, then $\beta_i \subset W$ is an arc from $\partial Q \times \{1\}$ to $\partial Q \times \{1\}$, say, in an annulus component of $\partial Q \times I$. Such an arc bounds a disk in $\partial Q \times I$. This disk has boundary consisting of the arc β_i in W and an arc on $\partial Q \times \{1\} \subset \tilde{\Sigma}$. If the disk were essential, it would give a contradiction to proposition 11.32. So it is inessential, and we may isotope B to remove β_i , merging α_i and α_{i+1} .

Finally we show that $n = 2$, i.e. that each component of $B \cap W$ is a quadrilateral with arcs $\alpha_1, \beta_1, \alpha_2, \beta_2$. For if not, there is an arc $\gamma \subset W$ with endpoints on α_1 and α_3 . By sliding along the disk W , we may isotope B so γ lies in $B \cap W$. Then note that γ lies in $Q \times I$ with endpoints on $Q \times \{1\}$. It must be parallel vertically to an arc $\delta \subset Q \times \{1\} \subset \tilde{\Sigma}$. This gives another disk with boundary consisting of an arc on W and an arc on $\tilde{\Sigma}$. Either the disk contradicts proposition 11.32, or α_1 and α_3 lie on the same ideal edge in the boundary of W . But then β_1 and β_2 are arcs running from α_2 on one ideal edge on the boundary of W to the same ideal edge on the boundary of W containing α_1 and α_3 . The only way that the boundary of this component of $B \cap W$ bounds a disk in W is if $n = 3$, and β_3 runs from an endpoint of α_1 to an endpoint of α_3 . But then β_3 runs from $Q \times \{1\}$ to $Q \times \{1\}$, which we ruled out in the previous paragraph. So $n = 2$ and $B \cap W$ is a product rectangle $\alpha_1 \times I$.

Next suppose B is a twisted I -bundle $B = Q \tilde{\times} I$ where Q is non-orientable. Let $\gamma_1, \dots, \gamma_m$ be a maximal collection of orientation reversing closed curves on Q . Let $A_i \subset B$ be the I -bundle over γ_i . Each A_i is a Möbius band. The bundle $B_0 = B \setminus (\cup_i A_i)$ is then a product bundle $B_0 = Q_0 \times I$ where $Q_0 = Q \setminus (\cup_i \gamma_i)$ is an orientable surface. Our work above then implies that $B_0 \cap W$ is a product rectangle for each white region W . To obtain $B \cap W$, we attach the vertical boundary of such a product rectangle to the vertical boundary of a product rectangle of A_i . This procedure respects the product structure of all rectangles, hence the result is a product rectangle. \square

PROOF OF THEOREM 12.29. One direction is lemma 12.28: If the link diagram is the standard diagram of a $(2, q)$ -torus link, then a checkerboard surface is a fiber.

Conversely, if the checkerboard surface Σ is a semifiber, then $M_\Sigma = (S^3 - N(K)) \setminus \Sigma$ is an I -bundle. In this case, lemma 12.30 implies M_Σ intersects each white face W in a product rectangle of the form $\alpha \times I$, where $\alpha \times \{0\}$ and $\alpha \times \{1\}$ lie on ideal edges of W . Since $W \subset M_\Sigma$, the face W is a product rectangle, with exactly two ideal edges $\alpha \times \{0\}$ and $\alpha \times \{1\}$. Thus W is a bigon. So every white face is a bigon. Thus the diagram of K is a chain of bigons lined up end to end. This is a $(2, q)$ -torus link. The white checkerboard surface is obtained by gluing sides of those bigons, and so forms the annulus or Möbius band between the link components. The shaded checkerboard surface must therefore be the fiber of lemma 12.28. \square

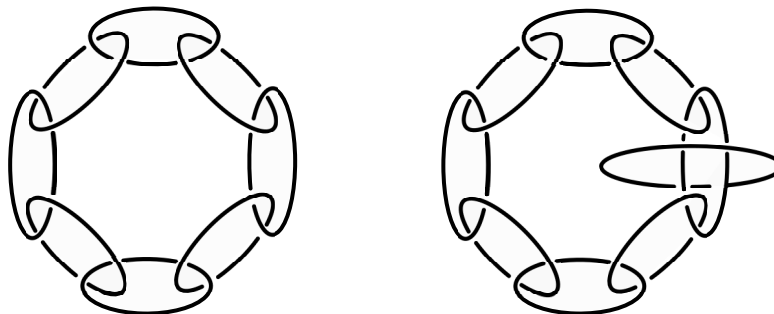


FIGURE 12.8. Left: The minimally twisted chain link with eight link components. Right: the augmented minimally twisted chain link.

COROLLARY 12.31. *Let K be a knot or link with a connected, twist-reduced, prime, alternating diagram, and let Σ be an associated checkerboard surface. If K is hyperbolic, then Σ is quasifuchsian.*

PROOF. If K is hyperbolic, it cannot be a $(2, q)$ -torus link. Then theorem 12.29 implies that Σ cannot be a semifiber. Because Σ is an embedded surface, lemma 12.27 implies that Σ is not a virtual fiber. Theorem 12.17 implies that Σ is not accidental. By theorem 12.25, it must be quasifuchsian. \square

12.4. Exercises

EXERCISE 12.1. (Easy) Show that the 3-punctured sphere bounded by the crossing circle in a hyperbolic belted tangle must be incompressible.

EXERCISE 12.2. A chain link is a link that has the form of a circular chain, as in figure 12.8, left. Note that the link components of the chain can be twisted. We define the minimally twisted chain link with an even number of components to be the chain link with every other link component lying flat in the plane of projection, and alternate link components to be perpendicular to the plane of projection.

A minimally twisted chain link may be augmented by adding a crossing circle encircling the circular chain, as in figure 12.8, right.

- (1) Using belted sums and the volume of the Whitehead link, find the volume of any augmented minimally twisted chain link with an even number of chain components.
- (2) Find a belted tangle T such that repeatedly taking belted sums of T with the Whitehead link gives the augmented minimally twisted chain link with an odd number of chain components. What is the volume of the augmented minimally twisted chain link with an odd number of chain components?

EXERCISE 12.3. Following Yamashita's instructions, create a python program that allows us to visualize the limit set as hyperbolic structures are

varied on a punctured torus. Print an example with a Fuchsian limit set, and three examples of quasifuchsian limit sets. See [Yam12].

EXERCISE 12.4. Suppose S' is a closed nonorientable surface. Consider $S' \times I$ (also frequently denoted $S' \tilde{\times} I$). Prove that its boundary is a closed orientable surface S homeomorphic to the oriented double cover of S' .

EXERCISE 12.5. Prove that a strict semifiber is a virtual fiber.

EXERCISE 12.6. Prove that a nonorientable surface can never be a fiber in a link complement $S^3 - L$. That is, there are no strict semifibers for links in S^3 .

EXERCISE 12.7. Prove lemma 12.27: that a properly embedded surface that is a virtual fiber in a 3-manifold must be a semifiber.

Part 3

Hyperbolic Knot Invariants

Estimating Volume

We have seen that hyperbolic 3-manifolds have finite volume if and only if they are compact or the interior of a compact manifold with finitely many torus boundary components (theorem 5.24). However, it is not completely straightforward to estimate volumes of large classes of manifolds, including knot complements. There are many open questions concerning the relationship of volume of a hyperbolic manifold to other invariants, such as knot invariants. In this chapter, we discuss different ways to estimate volumes of hyperbolic 3-manifolds that are defined topologically or combinatorially, such as knot complements.

13.1. Summary of bounds encountered so far

13.1.1. Upper bounds. It is usually an easier problem to give upper bounds on the volume of a hyperbolic 3-manifold than lower bounds, although there are exceptions, especially when sharp upper bounds are needed. Here we review two methods we have already encountered that can give upper bounds on volume.

13.1.1.1. *Volume bounds from polyhedra.* Recall from theorem 9.10 that the maximal volume tetrahedron is the regular ideal tetrahedron. Its volume is the value $3\Lambda(\pi/3) := v_{\text{tet}} = 1.0149\dots$. In various chapters, we have found decompositions of several different knot and link complements into ideal tetrahedra. The volume of such a knot or link is therefore bounded by v_{tet} times the number of tetrahedra in its decomposition.

For example, this can be used to show the following theorem, originally proved by Agol and D. Thurston in the appendix to [Lac04].

THEOREM 13.1. *A fully augmented link L with $t(L)$ crossing circles has volume at most $10v_{\text{tet}}(t(L) - 1)$.*

PROOF. In chapter 7, we saw that a fully augmented link has a decomposition into two right angled ideal polyhedra P_1 and P_2 , with white and shaded faces, where shaded faces are ideal triangles coming from 2-punctured disks bounded by crossing circles, and white faces come from the plane of projection.

For the polyhedron P_1 , add a finite vertex v_1 in the interior and cone to the faces of the polyhedra. Do the same for P_2 , adding vertex v_2 and

coning. Each shaded triangle in ∂P_1 gives rise to a tetrahedron. There are two shaded triangles per crossing circle in each of the two polyhedra, so $4t(L)$ tetrahedra arise in this way.

The white faces are coned to pyramids. Glue a pair of pyramids in P_1 and P_2 together across a matching white face, and perform stellar subdivision. That is, add an edge running from the finite vertex in one polyhedron through the center of the face to the finite vertex in the other polyhedron, then add triangles around the edge to divide the pyramids into tetrahedra. If the face has d edges, it is subdivided into d tetrahedra. Note each crossing circle contributes six edges to each polyhedron. Thus the total number of edges of the white faces will be $6t(L)$, and thus the white faces contribute $6t(L)$ tetrahedra to the decomposition.

This gives us $10t(L)$ tetrahedra, but these have finite vertices. We can improve the bound by choosing an ideal vertex w_1 in P_1 , and collapsing the edge from w_1 to v_1 . Similarly, choose the corresponding vertex w_2 in P_2 , and collapse the edge from w_2 to v_2 . Now simplify the triangulation by collapsing monogons to vertices, bigons to a single edge, and parallel triangles to a single triangle. Note that all tetrahedra adjacent to w_1 and w_2 are collapsed to triangles under this procedure. We count the number of these.

The ideal vertex w_1 is adjacent to two shaded triangles and two white faces. The white faces each have at least three edges, and so give rise to at least three tetrahedra to be collapsed, running between the two polyhedra. Thus there are at least six such tetrahedra arising from white faces. Each shaded face gives rise to one tetrahedron to be collapsed in each P_i , or four total. Thus there is an ideal triangulation with at most $10t(L) - 10$ tetrahedra.

Now apply theorem 9.10. The volume of each of the $10t(L) - 10$ tetrahedra is at most v_{tet} . Thus the volume of the fully augmented link is at most $10v_{\text{tet}}(t(L) - 1)$. \square

The bound of theorem 13.1 is *asymptotically sharp*, in the sense that there is a sequence of fully augmented links whose volumes approach the upper bound; this is proved in the first part of exercise 13.1.

13.1.1.2. *Dehn filling.* Recall Thurston's theorem on volume change under Dehn filling, theorem 6.30: If M is hyperbolic with cusps C_1, \dots, C_n , and s_1, \dots, s_n are slopes, one on each ∂C_j , such that $M(s_1, \dots, s_n)$ is hyperbolic, then

$$\text{vol}(M) > \text{vol}(M(s_1, \dots, s_n)).$$

This result can be combined with the previous to give an upper bound on the volume of knots in terms of the twist number, first observed in [Lac04].

THEOREM 13.2. *Suppose K is a knot or link with a prime, twist-reduced diagram with twist number $\text{tw}(K) \geq 2$. Then $S^3 - K$ is hyperbolic, and the*

volume of $S^3 - K$ satisfies

$$\text{vol}(S^3 - K) < 10v_{\text{tet}}(\text{tw}(K) - 1).$$

Again the bound of theorem 13.2 is asymptotically sharp; this is proved in the second part of exercise 13.1.

PROOF OF THEOREM 13.2. Because the diagram of K is prime and twist-reduced, when we fully augment K by adding a crossing circle to each twist region, and then remove pairs of crossings to form a fully augmented link, the resulting link L is hyperbolic; see lemma 7.14 and lemma 7.15. It will have $t(L) = \text{tw}(K)$ crossing circles. By theorem 13.1, the volume of the fully augmented link is at most $10v_{\text{tet}}(\text{tw}(K) - 1)$.

Now, we obtain $S^3 - K$ from $S^3 - L$ by Dehn filling the crossing circles, filling the i -th one along a slope $1/n_i$ where n_i is an integer such that $2n_i$ crossings were removed at that twist region to go from the diagram of K to that of L . By Thurston's theorem on volume change under Dehn filling, theorem 6.30,

$$\text{vol}(S^3 - K) < \text{vol}(S^3 - L) \leq 10v_{\text{tet}}(\text{tw}(K) - 1). \quad \square$$

13.1.2. Lower bounds via angle structures. In addition to previously obtaining results that lead to upper bounds on volume, we have also built the tools to give lower bounds on hyperbolic volume in special cases, in particular when the manifold admits an angle structure. Recall theorem 9.13: if the maximum of the volume functional over the set of all angle structures on a manifold M occurs in the interior of the set of angle structures, then that angle structure gives the unique complete hyperbolic metric on M . We have the following corollary.

COROLLARY 13.3. *Suppose M is an orientable 3-manifold with boundary consisting of tori, with an ideal triangulation \mathcal{T} . Suppose that the set of angle structures $\mathcal{A}(\mathcal{T})$ is nonempty, and that the volume functional takes its maximum on the interior of the set of all angle structures $\mathcal{A}(\mathcal{T})$. Let A be any structure in the closure of $\mathcal{A}(\mathcal{T})$. Then M is hyperbolic, and $\text{vol}(M) \geq \mathcal{V}(A)$.*

PROOF. The fact that M is hyperbolic is a consequence of theorem 8.36. The volume functional is strictly concave down by theorem 9.9, and is uniquely maximized at the complete hyperbolic structure in the interior by theorem 9.13 and theorem 9.14. Thus any structure in the closure of $\mathcal{A}(\mathcal{T})$ gives a volume at most that of M . \square

Corollary 13.3 was used by Futer and Guéritaud to obtain bounds on the volumes of 2-bridge knots in terms of their continued fraction decompositions [Gué06b]. They proved the following.

THEOREM 13.4. *Let K be a reduced alternating diagram of a hyperbolic 2-bridge link K with $\text{tw}(K)$ twist regions. Then*

$$\text{vol}(S^3 - K) > 2v_{\text{tet}}\text{tw}(K) - 2.7066.$$

Moreover, the lower bound is asymptotically sharp.

PROOF. We may suppose that the diagram of K is determined by a continued fraction $[0, a_{n-1}, \dots, a_1]$, where $\text{tw}(K) = n - 1$, as in definition 10.7. The link complement has a geometric triangulation discussed in chapter 10, determined by real numbers $(z_1, z_2, \dots, z_{C-2}, z_{C-1})$, where C is the crossing number of the diagram of K ; see the proof of proposition 10.18. We will choose explicit values of the z_i that give a structure in the boundary of the space of angle structures. By corollary 13.3 the volume of the result gives a lower bound on the actual hyperbolic volume.

First assume that $\text{tw}(K) \geq 3$, so $n \geq 2$. We let $z_1 = z_{C-1} = 0$, and we will choose $z_i = \pi/3$ for indices i such that $a_1 \leq i \leq C - a_{n-1}$.

These choices satisfy the hinge equation of equation (10.1): $|z_{i+1} - z_{i-1}| = 0 < \pi - z_i = 2\pi/3$, for appropriate i . They do not satisfy the strict inequality of the convexity equation of equation (10.1), but only satisfy the weak inequality: $2z_i \leq z_{i-1} + z_{i+1}$. When $a_1 < i < C - a_{n-1}$, these will assign values to x_i and y_i using table 10.1. Note the angles will take values of $\pi/3$ in the hinge case, but $2\pi/3$ and 0 in the non-hinge case, and thus there will be flat tetrahedra. However, our choices so far give rise to a structure on the boundary of $\mathcal{A}(\mathcal{T})$, which will be sufficient for our purposes. Each hinge index contributes volume v_{tet} to the structure, while non-hinges contribute nothing to volume. Note hinges occur between twist regions; there are $\text{tw}(K) - 3$ hinge indices between a_1 and $C - a_{n-1}$.

We cannot choose $z_i = \pi/3$ for all the indices in the first and last fans, else even the weak inequality of the convexity equations (10.1) will not be satisfied near $i = 1$ or $i = C - 1$. Instead, in the first and last fans, interpolate between 0 and $\pi/3$ in a way that satisfies the weak versions of equation (10.1). Then again angles x_i and y_i will be determined by table 10.1. At the hinge indices $i = a_1$ or $i = C - a_{n-1}$, the angles will be:

$$\frac{\pi}{2} - z_{i-1}, \quad \frac{\pi}{6} + z_{i-1}, \quad \frac{\pi}{3}.$$

The volume defined by these angles is smallest when $z_{i-1} = 0$, which occurs when the three angles are $\pi/2$, $\pi/6$, $\pi/3$, and the volume is $0.84578\dots$. Thus the four tetrahedra $T_{a_1}^1$, $T_{a_1}^2$, $T_{C-a_{n-1}}^1$, and $T_{C-a_{n-1}}^2$ each have volume at least 0.84578 , and the volume of this structure satisfies

$$\mathcal{V} > 2v_{\text{tet}}(\text{tw}(K) - 3) + 4(0.84578) > 2v_{\text{tet}}\text{tw}(K) - 2.7066.$$

Finally, check that when $\text{tw}(K) = 2$, $\mathcal{V} > 2(0.84578)$ still satisfies the theorem. \square

13.2. Negatively curved metrics and Dehn filling

We now turn our attention to a new technique for bounding volume from below that has not arisen in previous chapters. This bound comes from differential geometric methods, in particular from finding volumes of hyperbolic

manifolds under families of metrics, and showing that the hyperbolic metric maximizes volume among such a family.

A hyperbolic manifold has constant sectional curvature equal to -1 . The metrics we will consider will have negative sectional curvature, not necessarily constant. If a 3-manifold admits such a metric, it actually follows from the Geometrization theorem that the manifold also admits a hyperbolic metric; see theorem 13.5. However, the proof of that fact gives no information on how the hyperbolic metric relates to the negatively curved one. Often we can build an explicit negatively curved metric, and we will use this metric to make conclusions about the hyperbolic geometry of the manifold. This section presents a number of results along these lines, particularly relating to volume.

THEOREM 13.5. *Suppose M is a compact orientable 3-manifold whose interior admits a Riemannian metric with negative sectional curvature. Then M admits a hyperbolic metric.*

PROOF. Because sectional curvature is negative, the Cartan–Hadamard theorem implies that the universal cover of M is homeomorphic to \mathbb{R}^3 (see for example [GHL04, Theorem 3.87]). It follows that the fundamental group of M is infinite. It also follows that M is irreducible, for any sphere in M lifts to a sphere in \mathbb{R}^3 , which bounds a ball. Then the image of the sphere in M bounds the image of that ball in M , which is a ball.

In the case that M is closed, because M has strictly negative curvature, it is known that every abelian subgroup of its fundamental group is cyclic [Pre43]. Thus there is no $\mathbb{Z} \times \mathbb{Z}$ subgroup of its fundamental group. So in this case, M is irreducible, with $\pi_1(M)$ infinite, containing no $\mathbb{Z} \times \mathbb{Z}$ subgroup. By the Geometrization Theorem, theorem 8.25, M admits a hyperbolic structure.

In the case that M has boundary, there may be a $\mathbb{Z} \times \mathbb{Z}$ subgroup of $\pi_1(M)$, but the fact that the curvature is strictly negative in the interior implies that the subgroup is peripheral, hence M is atoroidal [BGS85]. If M is a Seifert fibered space with infinite fundamental group, then $\pi_1(M)$ contains a cyclic normal subgroup (theorem 8.22). But again, a complete negatively curved finite volume Riemannian manifold cannot have a cyclic normal subgroup [BGS85]. It follows that M is hyperbolic. \square

Notice that the proof of theorem 13.5 gives no information on the relationship between the negatively curved metric and the hyperbolic metric. For example, we can make no conclusions about the difference in volumes of the manifolds. In the closed case, work of Besson, Courtois, and Gallot [BCG95] can be used to bound the volume of a manifold under one negatively curved metric in terms of the volume of another. This was extended to the finite volume case by Boland, Connell, and Souto [BCS05]. In 3-dimensions, a special case of their work is the following theorem.

THEOREM 13.6. *Let σ and σ' be two complete, finite volume Riemannian metrics on the same 3-manifold N . Suppose the Ricci curvature of σ satisfies $\text{Ric}_\sigma \geq -2\sigma$, and suppose the sectional curvatures of σ' lie in the interval $[-a, -1]$ for some constant $a \geq 1$. Then*

$$\text{vol}(N, \sigma) \geq \text{vol}(N, \sigma'),$$

with equality if and only if both metrics are hyperbolic. \square

Our goal in this section is to bound the change in volume of a hyperbolic manifold under Dehn filling by constructing a negatively curved metric on the Dehn filling of a hyperbolic manifold, and then applying theorem 13.6. This volume estimate was first obtained in [FKP08]. Along the way we will obtain additional important consequences, for example the 2π -theorem [BH96].

13.2.1. Negatively curved metrics on a solid torus. We will construct metrics in this subsection, and use them to bound volume. The arguments here require a little more familiarity with Riemannian geometry than the rest of the book so far. However, these arguments are only needed in this section and will not be required elsewhere in the book. Thus a reader disinclined to work carefully through the calculations in Riemannian geometry at this time may accept the statements of the main results here and skip ahead to their applications in subsection 13.2.2.

The metrics we construct will have constant sectional curvatures away from a collection of solid tori, namely those we glue to perform Dehn filling. Within a solid torus, we will use cylindrical coordinates.

DEFINITION 13.7. Let V be a solid torus, and let \tilde{V} be its universal cover. The *cylindrical coordinates* on \tilde{V} are given by (r, μ, λ) , where $r \leq 0$ is the radial distance measured outward from ∂V , $0 \leq \mu \leq 1$ is measured around each meridional circle, and $-\infty < \lambda < \infty$ is measured in the longitudinal direction, orthogonal to μ . Normalize the coordinates so that the generator of the deck transformation group on \tilde{V} changes the λ coordinate by 1. These coordinates descend to *cylindrical coordinates* on V , where $r \leq 0$ is radial distance measured outward from ∂V , $0 \leq \mu \leq 1$ is in the meridional direction, and $0 \leq \lambda \leq 1$ is measured orthogonal to μ .

LEMMA 13.8. *Let (r, μ, λ) be cylindrical coordinates on a solid torus or its universal cover. Then a metric of the form*

$$(13.1) \quad ds^2 = dr^2 + f(r)^2 d\mu^2 + g(r)^2 d\lambda^2,$$

where $f: \mathbb{R} \rightarrow \mathbb{R}$ and $g: \mathbb{R} \rightarrow \mathbb{R}$ are smooth functions of r , satisfies the property that all sectional curvatures are convex combinations of

$$-\frac{f''}{f}, \quad -\frac{g''}{g}, \quad -\frac{f'g'}{fg}.$$

Moreover, the metric is nonsingular if $f'(r_0) = 2\pi$, where $r_0 < 0$ is the root of f nearest 0 (if it exists).

PROOF. The proof will be a standard calculation from Riemannian geometry, following [BH96].

For notational convenience, set $r = x_1$, $\mu = x_2$, $\lambda = x_3$. Our Riemannian metric can be written in coordinates as

$$(g_{ij}) = \begin{pmatrix} 1 & 0 & 0 \\ 0 & f(r)^2 & 0 \\ 0 & 0 & g(r)^2 \end{pmatrix} \quad \text{and} \quad (g^{ij}) = \begin{pmatrix} 1 & 0 & 0 \\ 0 & f(r)^{-2} & 0 \\ 0 & 0 & g(r)^{-2} \end{pmatrix}$$

The Christoffel symbols $\Gamma_{ij}^k = \sum_{\ell} \Gamma_{ij\ell} g^{\ell k}$ can be computed using

$$\Gamma_{ijk} = \frac{1}{2} \left(\frac{\partial g_{jk}}{\partial x_i} + \frac{\partial g_{ik}}{\partial x_j} - \frac{\partial g_{ij}}{\partial x_k} \right).$$

Most of the 27 Γ_{ijk} are zero; the non-zero ones are $\Gamma_{122} = f \cdot f'$, $\Gamma_{133} = g \cdot g'$, $\Gamma_{212} = f \cdot f'$, $\Gamma_{221} = -f \cdot f'$, $\Gamma_{313} = g \cdot g'$, and $\Gamma_{331} = -g \cdot g'$. We then obtain the connection $\nabla_{\partial/\partial x_i}(\partial/\partial x_j) = \sum_k \Gamma_{ij}^k \cdot \partial/\partial x_k$ as follows.

| $\nabla_{\partial/\partial x_i}(\partial/\partial x_j)$ | | j | | |
|---|---|------------------------------------|---|---|
| | | 1 | 2 | 3 |
| i | 1 | 0 | $f'/f \cdot \partial/\partial x_2$ | $g'/g \cdot \partial/\partial x_3$ |
| | 2 | $f'/f \cdot \partial/\partial x_2$ | $-f \cdot f' \cdot \partial/\partial x_1$ | 0 |
| | 3 | $g'/g \cdot \partial/\partial x_3$ | 0 | $-f \cdot f' \cdot \partial/\partial x_1$ |

The Riemannian curvature tensor is given by

$$R(X, Y, Z) = \nabla_Y \nabla_X Z - \nabla_X \nabla_Y Z + \nabla_{[X, Y]} Z,$$

and the sectional curvatures

$$K(X, Y) = -\frac{\langle R(X, Y, X), Y \rangle}{|X|^2 |Y|^2 - \langle X, Y \rangle^2}$$

are all convex combinations of the three sectional curvatures

$$K_{ij} = K(\partial/\partial x_i, \partial/\partial x_j)$$

for $\{i, j\} \subset \{1, 2, 3\}$. We compute

$$\begin{aligned} K_{12} &= -\frac{\langle R(\partial/\partial x_1, \partial/\partial x_2, \partial/\partial x_1), \partial/\partial x_2 \rangle}{\langle \partial/\partial x_1, \partial/\partial x_1 \rangle \langle \partial/\partial x_2, \partial/\partial x_2 \rangle - \langle \partial/\partial x_1, \partial/\partial x_2 \rangle^2} \\ &= -\frac{\langle \nabla_{\partial/\partial x_1} \cdot \nabla_{\partial/\partial x_2}(\partial/\partial x_1) - \nabla_{\partial/\partial x_2} \cdot \nabla_{\partial/\partial x_1}(\partial/\partial x_1), \partial/\partial x_2 \rangle}{1 \cdot f^2 - 0^2} \\ &= -\frac{\langle \nabla_{\partial/\partial x_1}(f'/f \cdot \partial/\partial x_2), \partial/\partial x_2 \rangle}{f^2} \\ &= -\frac{f''/f \cdot \langle \partial/\partial x_2, \partial/\partial x_2 \rangle}{f^2} \\ &= -f''/f. \end{aligned}$$

A symmetric calculation shows $K_{13} = -g''/g$. Finally

$$\begin{aligned} K_{23} &= -\frac{\langle \nabla_{\partial/\partial x_2} \cdot \nabla_{\partial/\partial x_3} (\partial/\partial x_2) - \nabla_{\partial/\partial x_3} \cdot \nabla_{\partial/\partial x_2} (\partial/\partial x_2), \partial/\partial x_3 \rangle}{f^2 \cdot g^2} \\ &= -\frac{\langle -\nabla_{\partial/\partial x_3} (-f' \cdot f \cdot \partial/\partial x_1), \partial/\partial x_3 \rangle}{f^2 \cdot g^2} \\ &= -\frac{f' \cdot f \cdot g'/g \langle \partial/\partial x_3, \partial/\partial x_3 \rangle}{f^2} \\ &= -\frac{f' \cdot g'}{f \cdot g}. \end{aligned}$$

Finally, to ensure the metric is nonsingular, it must have a cone angle of 2π along the core, i.e. at the point $r = r_0 < 0$ nearest 0 such that $f(r_0) = 0$. If $f(r_0) = 0$, then

$$f'(r_0) = \lim_{r \rightarrow r_0} \frac{1}{r - r_0} \int_0^1 f(r) d\mu$$

gives the cone angle along the core circle of the solid torus. Thus we must ensure that $f'(r_0) = 2\pi$. \square

LEMMA 13.9. *Suppose V is a solid torus with a prescribed Euclidean metric on ∂V such that a Euclidean geodesic representing a meridian has length $\ell_1 > 2\pi$. Then there exists a smooth Riemannian metric on V that is hyperbolic on a collar neighborhood of ∂V , has negative sectional curvature elsewhere, and the restriction of the metric to ∂V gives the prescribed Euclidean metric.*

PROOF. Let \tilde{V} denote the universal cover of V . We will assign a metric to \tilde{V} that has the form of equation (13.1). The functions f and g must satisfy a number of properties.

To obtain the prescribed Euclidean metric, we must have $f(0) = \ell_1$ and $g(0) = \ell_2$ where $\ell_2 = \text{area}(V)/\ell_1$. Then the deck transformation group on \tilde{V} is generated by

$$(r, \mu, \lambda) \mapsto (r, \mu + \theta, \lambda + 1),$$

where $\theta \in [0, 1)$ is appropriately chosen so that the fundamental domain of ∂V has the correct shape. The metric on \tilde{V} descends to give a smooth metric on V .

In order for the metric to be hyperbolic near ∂V , f and g must give sectional curvatures equal to -1 near $r = 0$. This will hold if $f(r) = \ell_1 e^r$ and $g(r) = \ell_2 e^r$ near $r = 0$. To ensure it is nonsingular, we need to ensure $f'(r_0) = 2\pi$ where r_0 is the negative root of f nearest 0.

To finish the proof of the lemma, we need to show that there exist functions f and g satisfying the above properties. For purposes of this lemma, it suffices to choose r_0 such that $-\ell_1/2\pi < r_0 < -1$ and define f and g near $r = r_0$ by $f(r) = 2\pi \sinh(r - r_0)$ and $g(r) = b \cosh(r - r_0)$,

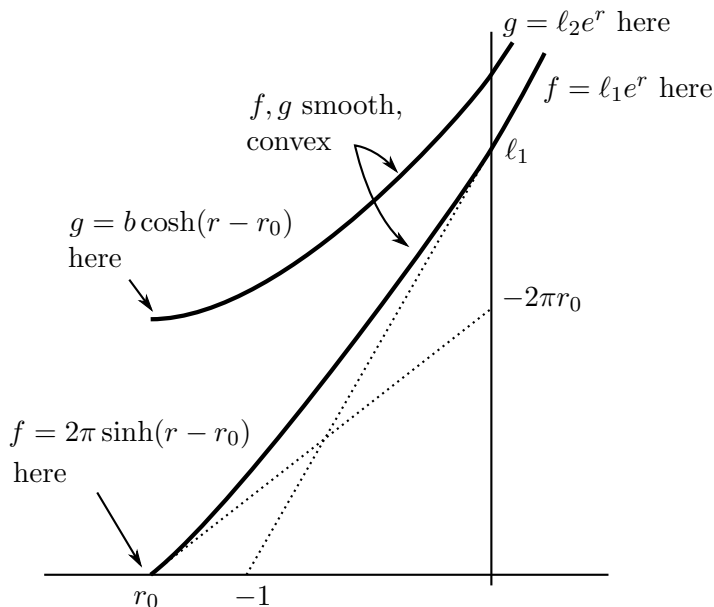


FIGURE 13.1. Extending f and g to be strictly convex, increasing, positive, smooth functions on $r_0 < r < 0$

for $0 < b < \ell_2$. Note that f and g give a metric of constant curvature -1 near r_0 , and that $f'(r_0) = 2\pi$, so the metric will be nonsingular. To see that definitions of f and g can be extended, note that the tangent line to f at $r = r_0$ runs through the points $(r_0, 0)$ and $(0, -2\pi r_0)$, and the tangent line to f at $r = 0$ runs through points $(0, \ell_1)$ and $(-1, 0)$. Because $-2\pi r_0 < \ell_1$ and $r_0 < -1$, the function f can be extended to be strictly convex, increasing, positive and smooth on $r_0 < r < 0$; see figure 13.1. Similarly, $g'(r_0) = 0 < \ell_2 = g'(0)$, and $0 < b = g(r_0) < \ell_2 = g(0)$, so g can be extended to be strictly convex, increasing, positive and smooth on $r_0 < r < 0$. This gives the desired negatively curved metric. \square

THEOREM 13.10 (2π -Theorem). *Suppose M is a hyperbolic 3-manifold with disjoint embedded cusps C_1, \dots, C_n and slopes s_j on C_j such that a geodesic representative of each s_j on ∂C_j has length strictly greater than 2π in the induced Euclidean metric. Then the Dehn filled manifold $M(s_1, \dots, s_n)$ admits a metric of negative curvature. Thus it is hyperbolic.*

PROOF. Remove the cusps C_1, \dots, C_n . By lemma 13.9, there exists a negatively curved metric on a solid torus V_j such that the Euclidean metric on ∂V_j agrees with that of ∂C_j , and such that the metric is hyperbolic on a collar neighborhood of ∂V_j . Then put a metric on $M(s_1, \dots, s_n)$ by taking the hyperbolic metric on $M - (\bigcup_{i=1}^n C_i)$, and gluing in solid tori with the metric from lemma 13.9. \square

Note that there is flexibility in choosing the metric of lemma 13.9. For example, the value of b in the proof can be anything in a range of values. If we take a little more care to determine the metric, we can obtain bounds on additional geometric information. For example, we can determine the curvature more explicitly, using the following lemma, and bound the volume of the negatively curved solid torus, as in lemma 13.12.

LEMMA 13.11. *Let $k(r)$ be a smooth, increasing function that lies in $[0, 1]$ for all r . Define f and g to be solutions to the differential equations $f''/f = k$ and $(f'g')/(fg) = k$, subject to initial conditions $f(0) = f'(0) = \ell_1$ and $g(0) = \ell_2$. Then the function g satisfies $g''/g = k + (f/f')k'$.*

PROOF. To check the formula for g''/g , note $g'/g = kf/f'$, and differentiate both sides of this equation.

$$\frac{g''}{g} - \left(\frac{g'}{g}\right)^2 = k \left(1 + \frac{f''}{f} \left(\frac{f}{f'}\right)^2\right) + \frac{f}{f'}k'.$$

Using the fact that $g'/g = kf/f'$ and $f''/f = k$, this simplifies to the desired equation:

$$\frac{g''}{g} = k + \frac{f}{f'}k'. \quad \square$$

LEMMA 13.12. *Let $\ell_1 > 2\pi$, let k be a constant function $k(r) = t \in (0, 1)$, and let f and g be defined by the differential equations in lemma 13.11. Let V be a solid torus with metric of equation (13.1). Then:*

(1) *Letting $r_0 = -\operatorname{arctanh}(\sqrt{t})/\sqrt{t}$, f and g have the form:*

$$\begin{aligned} f(r) &= \frac{\ell_1\sqrt{1-t}}{\sqrt{t}} \sinh(\sqrt{t}(r-r_0)) \\ g(r) &= \ell_2\sqrt{1-t} \cosh(\sqrt{t}(r-r_0)) \end{aligned}$$

(2) *At r_0 , $f(r_0) = 0$ and $f'(r_0) = \ell_1\sqrt{1-t}$. Thus the solid torus V has a nonsingular metric of negative curvature $-t$ when $t = 1 - (2\pi/\ell_1)^2$.*

(3) *For any $t \in (0, 1)$, the volume of the (possibly singular) solid torus V with metric $ds^2 = dr^2 + f(r)^2d\mu^2 + g(r)^2d\lambda^2$ is given by*

$$\operatorname{vol}(V) = \int_{r_0}^0 f(r)g(r)dr = \frac{\ell_1\ell_2}{2}.$$

PROOF. By lemma 13.11 and lemma 13.8, the metric will have negative sectional curvature. We need to show the additional properties. The proof is a series of calculations. First, solving the differential equation $f''/f = t$, the function f has the form

$$f(r) = c_1e^{\sqrt{t}r} + c_2e^{-\sqrt{t}r}.$$

Given initial conditions $f(0) = f'(0) = \ell_1$, we find

$$\begin{aligned} f(r) &= \frac{\ell_1}{2} \left(1 + \frac{1}{\sqrt{t}} \right) e^{\sqrt{t}r} + \frac{\ell_1}{2} \left(1 - \frac{1}{\sqrt{t}} \right) e^{-\sqrt{t}r} \\ &= \ell_1 \left(\cosh(r\sqrt{t}) + \frac{1}{\sqrt{t}} \sinh(r\sqrt{t}) \right) \\ &= \frac{\ell_1 \sqrt{1-t}}{\sqrt{t}} \sinh(\sqrt{t}(r-r_0)), \end{aligned}$$

where $r_0 = -\operatorname{arctanh}(\sqrt{t})/\sqrt{t}$, as claimed. Note that

$$f'(r) = \ell_1 \sqrt{1-t} \cosh(\sqrt{t}(r-r_0)),$$

so when $r = r_0$, we have $f(r_0) = 0$ and $f'(r_0) = \ell_1 \sqrt{1-t}$. Thus $f'(r_0) = 2\pi$ if $t = 1 - (2\pi/\ell_1)^2$, and the metric will be nonsingular in this case.

As for g , we may solve $g'/g = tf'/f = \sqrt{t} \tanh(\sqrt{t}(r-r_0))$ by integration, to obtain

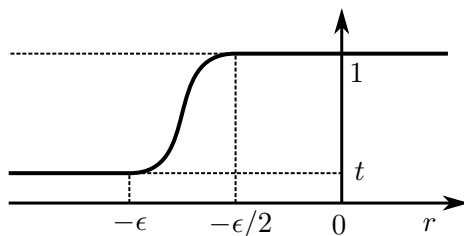
$$g(r) = c_2 \cosh(\sqrt{t}(r-r_0)) = \ell_2 \sqrt{1-t} \cosh(\sqrt{t}(r-r_0)),$$

using the initial condition $g(0) = \ell_2$ to determine the constant c_2 .

Finally we compute the volume of a solid torus V with metric as in equation (13.1).

$$\begin{aligned} \operatorname{vol}(V) &= \int_{r_0}^0 f(r)g(r) dr \\ &= \int_{r_0}^0 \frac{\ell_1 \ell_2 (1-t)}{\sqrt{t}} \sinh(\sqrt{t}(r-r_0)) \cosh(\sqrt{t}(r-r_0)) \\ &= \left[\frac{\ell_1 \ell_2 (1-t)}{2t} \sinh^2(\sqrt{t}(r-r_0)) \right]_{r=r_0}^0 \\ &= \frac{\ell_1 \ell_2 (1-t)}{2t} \sinh^2(\operatorname{arctanh}(\sqrt{t})) \\ &= \frac{\ell_1 \ell_2 (1-t)}{2t} \cdot \frac{t}{1-t} \\ &= \frac{\ell_1 \ell_2}{2}. \quad \square \end{aligned}$$

Now we would like to use the metric on the solid torus V obtained from lemma 13.12, along with theorem 13.6, to bound the volume of Dehn filled manifolds. However, at this point we have a problem. Although we have constructed a nonsingular Riemannian metric on the solid torus with nice curvature and volume, note that the metric does not give a hyperbolic metric, with sectional curvatures -1 , on a collar neighborhood of the boundary of V . Thus we cannot glue the metric of lemma 13.12 to the metric of the cusped manifold with horoball neighborhoods removed to obtain a negatively curved metric on the Dehn filled manifold, as we did in theorem 13.10. The way

FIGURE 13.2. Graph of $k_{t,\epsilon}(r)$.

to fix this problem is to do a little deeper analysis, which is done in the following lemma.

LEMMA 13.13. *Suppose V is a solid torus with a prescribed Euclidean metric on ∂V , such that a Euclidean geodesic representing a meridian has length $\ell_1 > 2\pi$. Let $\zeta \in (0, 1)$ be a constant. Then there exists a smooth, negatively curved Riemannian metric on V that satisfies the following properties.*

- (1) *The metric is hyperbolic on a collar neighborhood of ∂V , and its restriction to ∂V gives the prescribed Euclidean metric.*
- (2) *The sectional curvatures are bounded above by $-\zeta(1 - (2\pi/\ell_1)^2)$.*
- (3) *The volume of V in this metric is at least $\frac{1}{2}\zeta \text{area}(\partial V)$.*

PROOF. We use the ideas of lemma 13.11 and lemma 13.12 to define f and g by differential equations. However, we do not choose $k(r)$ to be constant. We need $k(r) = 1$ near $r = 0$ to obtain the appropriate curvature estimates on the boundary of V . We have seen in lemma 13.12 that we may obtain nice volume and curvature results when $k(r) = t$ for some $t \in (0, 1)$ for $r < 0$. So we define k to be a smooth bump function, depending on r , t , and $\epsilon > 0$, as follows. If $r \leq -\epsilon$, set $k_{t,\epsilon}(r) = t$. If $r \geq -\epsilon/2$, set $k_{t,\epsilon}(r) = 1$. For r between $-\epsilon$ and $-\epsilon/2$, the function $k_{t,\epsilon}(r)$ is smooth and strictly increasing. See figure 13.2 for a typical graph.

Then k is continuous in the three variables t, ϵ, r . We also define $k_{t,0}(r)$ to be the step function

$$k_{t,0}(r) = \lim_{\epsilon \rightarrow 0^+} k_{t,\epsilon}(r) = \begin{cases} t & \text{if } r < 0, \\ 1 & \text{if } r \geq 0. \end{cases}$$

Now for $\epsilon \geq 0$ and $t \in (0, 1)$, define $f_{t,\epsilon}$ and $g_{t,\epsilon}$ by the differential equations

$$\frac{f''_{t,\epsilon}(r)}{f_{t,\epsilon}(r)} = k_{t,\epsilon}(r), \quad \frac{g'_{t,\epsilon}(r)}{g_{t,\epsilon}(r)} = k_{t,\epsilon}(r) \frac{f'_{t,\epsilon}(r)}{f_{t,\epsilon}(r)}.$$

The family of functions $f_{t,\epsilon}(r)$ and $g_{t,\epsilon}(r)$ can be shown to have a number of nice properties. Away from $\epsilon = 0$, these mostly follow by standard facts in differential equation. As $\epsilon \rightarrow 0^+$, a little more analysis is required, which

we will omit here. For full details see [FKP08]. In particular, the following hold.

Nonsingularity: For all $t \in (0, 1)$ and $\epsilon \geq 0$, $f_{r,\epsilon}(r)$ has a unique root $r_0(t, \epsilon)$. The function $f'_{t,\epsilon}(r_0(t, \epsilon))$ is continuous in t and ϵ , and strictly decreasing in both variables. For every t between 0 and $1 - (2\pi/\ell_1)^2 < 1$, there is a unique value $\epsilon(t) > 0$ such that $f'_{t,\epsilon(t)}(r_0(t, \epsilon(t))) = 2\pi$. This gives a nonsingular metric for every t . Moreover, as $t \rightarrow 1 - (2\pi/\ell_1)^2$, $\epsilon(t) \rightarrow 0$.

Now let $t \in (0, 1)$ and define $\tau(t)$ to be the nonsingular Riemannian metric given by the functions $f_t(r) = f_{t,\epsilon(t)}(r)$ and $g_t(r) = g_{t,\epsilon(t)}(r)$.

Sectional curvatures: The metric $\tau(t)$ has all sectional curvatures bounded above by $-t$. This follows from lemma 13.11, along with the fact that the function $f_t(r)$ is positive and increasing. Thus $f_t(r)/f'_t(r)$ is positive. Moreover, $k'_{t,\epsilon(t)}(r)$ is positive, since $k_{t,\epsilon(t)}(r)$ is increasing with r . Thus lemma 13.11 implies that $g''_t(r)/g_t(r)$ is least $k_{t,\epsilon(t)}(r) \geq t$. By definition, $f''_t(r)/f_t(r)$ and $(f'_t(r)g'_t(r))/(f_t(r)g_t(r))$ are equal to $k_{t,\epsilon(t)}(r) \geq t$. So all sectional curvatures are bounded above by $-t$.

Volumes: Recall we have fixed $\zeta > 0$. For notational purposes, define t_0 to be $t_0 = 1 - (2\pi/\ell_1)^2$. Let t lie in the interval $(\zeta t_0, t_0)$. Then for the metric $\tau(t)$, we have

$$\lim_{t \rightarrow t_0} \text{vol}(V, \tau(t)) = \frac{\ell_1 \ell_2}{2} = \frac{1}{2} \text{area } \partial V.$$

This follows from the fact that f_t and g_t converge uniformly to $f_{t_0,0}$ and $g_{t_0,0}$ as $t \rightarrow t_0$. Moreover, $r_0(t, \epsilon(t))$ converges to $r_0(t_0, 0)$. Then the limit must be the limit of the differential equation in the case k is constant, which we computed in lemma 13.12. In particular, we have

$$\lim_{t \rightarrow t_0} \text{vol}(V, \tau(t)) = \text{vol}(V, t_0) = \frac{\ell_1 \ell_2}{2}.$$

To finish the proof of the lemma, select $t \in (\zeta t_0, t_0)$ near enough to t_0 so that $\text{vol}(V, \tau(t)) \geq \frac{1}{2}\zeta \text{area}(\partial V)$. For this metric, sectional curvatures are bounded above by $-t \leq -\zeta t_0 = -\zeta(1 - (2\pi/\ell_1)^2)$. Finally, the metric is nonsingular, and by choice of bump function and initial conditions, on a collar neighborhood of ∂V it is hyperbolic, with metric agreeing with the prescribed metric on ∂V . □

We are now ready to prove the main result of this section.

THEOREM 13.14 (Volume change under Dehn filling). *Let M be a complete, finite volume hyperbolic manifold with cusps. Suppose C_1, \dots, C_n are disjoint embedded cusps with slopes s_j on C_j such that a geodesic representative of s_j on ∂C_j has length strictly greater than 2π . Denote the minimal*

slope length by ℓ_{\min} . Then the Dehn filled manifold $M(s_1, \dots, s_n)$ is a hyperbolic manifold with

$$\text{vol}(M(s_1, \dots, s_n)) \geq \left(1 - \left(\frac{2\pi}{\ell_{\min}}\right)^2\right)^{3/2} \text{vol}(M).$$

PROOF. Fix an arbitrary constant $\zeta \in (0, 1)$. Replace each cusp C_j by a solid torus V_j whose meridian is s_j . By lemma 13.13, the smooth Riemannian metric τ_j on V_j agrees with the hyperbolic metric on ∂C_j , so this gives a smooth Riemannian metric τ on $M(s_1, \dots, s_n)$. Additionally, for each j , sectional curvatures on V_j are at most $-\zeta(1 - (2\pi/\ell_{\min})^2)$, and the volume of V_j is at least $\zeta \text{area}(\partial V_j)/2 = \zeta \text{vol}(C_j)$ where $\text{vol}(C_j)$ is the cusp volume in the hyperbolic metric. Note that sectional curvatures in V_j are also bounded below by some constant, since V_j is compact.

Thus the metric τ on $M(s_1, \dots, s_n)$ has sectional curvatures bounded above by $-\zeta(1 - (2\pi/\ell_{\min})^2)$ and bounded below by some constant. Moreover

$$\begin{aligned} \text{vol}(M(s_1, \dots, s_n)) &\geq \text{vol}(M - \cup_{j=1}^n C_j) + \zeta \sum \text{vol}(C_j) \\ &\geq \zeta \text{vol}(M). \end{aligned}$$

Rescale the metric to obtain a metric with sectional curvatures bounded above by -1 . To do this, replace τ by $\sigma = \sqrt{\zeta(1 - (2\pi/\ell_{\min})^2)}\tau$. Note this multiplies all sectional curvatures by $(\zeta(1 - (2\pi/\ell_{\min})^2))^{-1}$. The volume is rescaled by a factor of $(\zeta(1 - (2\pi/\ell_{\min})^2))^{3/2}$. Thus under the metric σ , sectional curvatures of $M(s_1, \dots, s_n)$ lie in $[-a, 1]$ for some $a \geq 1$, and $\text{vol}(M(s_1, \dots, s_n), \sigma) \geq \zeta^{5/2}(1 - (2\pi/\ell_{\min})^2)^{3/2} \text{vol}(M)$.

Now let S denote the set of all metrics on $M(s_1, \dots, s_n)$ whose sectional curvatures lie in the interval $[-a, -1]$. Since ζ is arbitrary, by the above work the supremum of volumes of $M(s_1, \dots, s_n)$ over all metrics in S satisfies:

$$\sup_{\sigma \in S} \text{vol}(M(s_1, \dots, s_n), \sigma) \geq \left(1 - \left(\frac{2\pi}{\ell_{\min}}\right)^2\right)^{3/2} \text{vol}(M).$$

Here $\text{vol}(M(s_1, \dots, s_n), \sigma)$ denotes volume under the metric σ , and $\text{vol}(M)$ denotes the volume of M under its given hyperbolic metric.

Now, theorem 13.6 implies that the hyperbolic metric σ_{hyp} on the Dehn filled manifold $M(s_1, \dots, s_n)$ uniquely maximizes volume over the set S of all metrics whose sectional curvatures lie in the interval $[-a, 1]$. Thus:

$$\begin{aligned} \text{vol}(M(s_1, \dots, s_n), \sigma_{\text{hyp}}) &\geq \sup_{\sigma \in S} \text{vol}(M(s_1, \dots, s_n), \sigma) \\ &\geq \left(1 - \left(\frac{2\pi}{\ell_{\min}}\right)^2\right)^{3/2} \text{vol}(M). \quad \square \end{aligned}$$

13.2.2. Applications to knots. Recall the definitions of *twist-reduced*, definition 7.13 or definition 11.10, and *twist-number*, definition 11.13. We will denote the twist-number of a twist-reduced diagram K by $\text{tw}(K)$. An

application of theorem 13.14 is the following result, which first appeared in [FKP08].

THEOREM 13.15 (Volume bounds for highly twisted links). *Let $K \subset S^3$ be a link with a prime, twist-reduced diagram. Assume the diagram has $\text{tw}(K) \geq 2$ twist regions, and that each twist region contains at least seven crossings. Then K is a hyperbolic link satisfying*

$$0.70734(\text{tw}(K) - 1) \leq \text{vol}(S^3 - K) < 10v_{\text{tet}}(\text{tw}(k) - 1),$$

where $v_{\text{tet}} = 1.0149\dots$ is the volume of a regular ideal tetrahedron.

The proof of theorem 13.15 uses a theorem due to Miyamoto, which in full generality gives a lower bound on the volume of an n -dimensional hyperbolic manifold with geodesic boundary [Miy94]. Here, we state only the 3-dimensional case, which is the case we will use.

THEOREM 13.16 (Miyamoto). *If N is a hyperbolic 3-manifold with totally geodesic boundary, then $\text{vol}(N) \geq -v_{\text{oct}}\chi(N)$, where $v_{\text{oct}} = 3.66\dots$ is the volume of a regular ideal octahedron, with equality if and only if N decomposes into $-\chi(N)$ ideal octahedra.*

PROOF SKETCH. Suppose N has totally geodesic boundary. Then the lift of N to the universal cover \mathbb{H}^3 is a subspace \tilde{N} of \mathbb{H}^3 bounded by disjoint hyperplanes, where each hyperplane is a lift of the geodesic surface ∂N .

Pick one such hyperplane O , and consider the set D_O consisting of points in \tilde{N} closer to O than to any other hyperplane in the lift of ∂N . The set D_O is convex, with boundary consisting of faces F made up of points equidistant from the hyperplane O and some other hyperplane. Define the truncated cone C_F to be all points in D_O that lie on a line running from F to meet O orthogonally. We may decompose all of \tilde{N} into truncated cones.

Now project to N . Because $\partial\tilde{N}$ is invariant under the action of the covering transformations, and distances along geodesics are preserved, the decomposition projects to a decomposition of N . The volume of N is obtained by summing the volumes of all the truncated cones decomposing N .

The main step of the proof is to bound the ratio $\text{vol}(C_F)/\text{area}(O \cap C_F)$, with notation as above. To do so, *truncated tetrahedra* are introduced.

Consider a combinatorial polyhedron P obtained by removing from a tetrahedron a small open neighborhood of each vertex. The faces of the tetrahedra become hexagonal faces of P , and four new triangular faces are added. A truncated tetrahedron, also called a *hyperideal tetrahedron* in the literature, is a compact polyhedron in hyperbolic space that realizes P , such that the triangle faces and hexagonal faces are totally geodesic, and such that hexagons meet triangles at right angles. See figure 13.3, left.

It can be shown that a truncated tetrahedron is determined by the lengths of the six edges between its triangular faces. When each of these is the same length, we say the truncated tetrahedron is regular, and we denote the regular truncated tetrahedron of edge length r by T_r . Denote its four

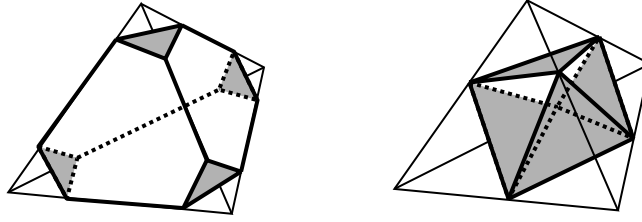


FIGURE 13.3. Left: a truncated tetrahedron, or hyperideal tetrahedron. Right: when lengths of edges between triangles go to zero, the truncated tetrahedron becomes a regular ideal octahedron.

triangular faces by τ_1, \dots, τ_4 . We will be considering the ratio

$$\rho(r) = \frac{\text{vol}(T_{2r})}{\text{area}(\tau_1 \cup \tau_2 \cup \tau_3 \cup \tau_4)}.$$

Observe that $r \geq 0$, and when r approaches 0, the triangles τ_j each become ideal triangles, and the truncated tetrahedron T_0 becomes a regular ideal octahedron. See figure 13.3, right. Miyamoto shows that $\rho(r)$ increases with r [Miy94, Lemma 2.1]. Thus $\rho(r) \geq \rho(0)$.

Now consider again the truncated cone C_F and its truncation face O . Consider geodesics in N with both endpoints on ∂N and orthogonal to ∂N . Such a geodesic is called a *return path*. Let ℓ be the length of the shortest return path in N ; note $\ell \geq 0$. The return path lifts to a collection of geodesics in \tilde{N} , each running between hyperplane lifts of ∂N , each perpendicular to the hyperplane, and each of length ℓ . If such a geodesic meets the cone C_F , its intersection with C_F has length $\ell/2$.

The main technical result in [Miy94] is a proof that

$$(13.2) \quad \frac{\text{vol}(C_F)}{\text{area}(O \cap C_F)} \geq \frac{\text{vol}(T_\ell)}{\text{area}(\tau_1 \cup \tau_2 \cup \tau_3 \cup \tau_4)} = \rho(\ell/2).$$

The proof is obtained by subdividing C_F into pieces, matching pieces making up T_ℓ , and observing relationships between volume and edge lengths for such pieces.

Assuming equation (13.2), we complete the proof. When N has shortest return path of length at least ℓ ,

$$\text{vol}(N) = \sum_C \text{vol}(C) \geq \rho\left(\frac{\ell}{2}\right) \sum_C \text{area}(C \cap O) = \rho\left(\frac{\ell}{2}\right) \text{area}(\partial N),$$

where the sum is over all truncated cones C in the decomposition, and $C \cap O \subset \partial N$ denotes the portion of C on ∂N .

Finally, note that the shortest return path always has length at least $\ell = 0$. Using the fact that ρ is increasing, the above equation becomes

$$\text{vol}(N) \geq \rho(0) \text{area}(\partial N) = \frac{v_{\text{oct}}}{4\pi} \cdot (-2\pi\chi(\partial N)) = -v_{\text{oct}}\chi(N).$$

Here we are using the fact that $\text{vol}(T_0) = v_{\text{oct}}$, that the area of an ideal triangle is π , the Gauss–Bonnet formula $\text{area}(\partial N) = -2\pi\chi(\partial N)$, and the fact that for a 3-manifold N with boundary, $\chi(\partial N) = 2\chi(N)$. \square

Given Miyamoto’s theorem, we prove theorem 13.15.

PROOF OF THEOREM 13.15. The fact that the link K is hyperbolic follows from theorem 8.47. The upper bound on volume comes from theorem 13.2.

To obtain the lower bound, we will consider fully augmented links. Let L be the fully augmented link obtained by adding a crossing circle encircling each twist region of K . By theorem 7.24, $S^3 - K$ is obtained from $S^3 - L$ by performing Dehn fillings on crossing circles, along a slopes of length at least $\sqrt{7^2 + 1} = \sqrt{50} > 2\pi$.

We will find a lower bound on the volume of $S^3 - L$. To do so, first remove all half-twists from the diagram of L . That is, recall L may have single crossings at twist regions. Replace L with a new fully augmented link L' that has no crossing at twist regions. Note the complement of L' is obtained from that of L by cutting along 2-punctured disks bounded by crossing circles and regluing, thus it follows from corollary 12.2 that the volume of $S^3 - L'$ is identical to the volume of $S^3 - L$.

Now cut $S^3 - L'$ along the plane of projection, separating it into two identical pieces, each with totally geodesic boundary coming from the white surface. Call one of these M . By Miyamoto’s theorem, $\text{vol}(M) \geq -v_{\text{oct}}\chi(M)$. Note that M is homeomorphic to a ball in S^3 with a tube drilled out for each crossing circle, and there are $\text{tw}(K)$ crossing circles. Thus the Euler characteristic of M is $\chi(M) = (1 - \text{tw}(K))$. Because we form $S^3 - L'$ by taking two copies of M , the volume satisfies

$$\text{vol}(S^3 - L) = \text{vol}(S^3 - L') \geq -2v_{\text{oct}}\chi(M) = 2v_{\text{oct}}(\text{tw}(K) - 1).$$

Now by theorem 13.14 (volume change under Dehn filling), the volume of $S^3 - K$ satisfies:

$$\begin{aligned} \text{vol}(S^3 - K) &\geq \left(1 - \left(\frac{2\pi}{\sqrt{50}}\right)^2\right)^{3/2} \text{vol}(S^3 - L) \\ &\geq \left(1 - \frac{2\pi^2}{25}\right)^{3/2} 2v_{\text{oct}}(\text{tw}(K) - 1) \\ &\geq 0.70735(\text{tw}(K) - 1). \end{aligned} \quad \square$$

13.3. Volume, guts, and essential surfaces

Theorem 13.15 gives volume bounds highly twisted knots and links, but only with at least seven crossings per twist region. A similar result holds for alternating knots and links, without a restriction on the number of crossings for twist regions, originally due to Lackenby [Lac04]. The method of proof is different, but illustrates another tool for bounding hyperbolic volume from

below, developed by Agol, Storm, and Thurston [AST07]. In this section, we explain the tool, and use it to bound volumes of alternating links.

The main theorem of the section is the following.

THEOREM 13.17 (Volume bounds for alternating links). *Let K be a hyperbolic knot or link with a twist-reduced alternating diagram with twist number $\text{tw}(K)$. Then*

$$\text{vol}(S^3 - K) \geq \frac{v_{\text{oct}}}{2}(\text{tw}(K) - 2).$$

We will prove theorem 13.17 by considering again the checkerboard surfaces of the alternating link, and the bounded polyhedral decomposition of the link complement cut along those surfaces, theorem 11.6 and lemma 11.25. To describe our main tool, we need additional terminology.

First, recall the JSJ-decomposition of a 3-manifold, theorem 8.23 and definition 8.24. We will apply a special form of this decomposition to a 3-manifold M cut along an essential surface S . Recall that $M \setminus\!\!\setminus S$ is the closure of the manifold obtained by removing a regular neighborhood of S (definition 11.23). Its boundary consists of components of the parabolic locus, which are remnants of the torus boundary components of M , and \tilde{S} .

DEFINITION 13.18. Let M be a compact 3-manifold with torus boundary components, and let S be an essential surface properly embedded in M . The *double of $M \setminus\!\!\setminus S$* , denoted $D(M \setminus\!\!\setminus S)$ is the manifold obtained by taking two copies of $M \setminus\!\!\setminus S$ and gluing them by the identity map on \tilde{S} .

Note the double of $M \setminus\!\!\setminus S$ will have torus boundary components coming from the parabolic locus of the boundary of $M \setminus\!\!\setminus S$. We will consider the JSJ-decomposition of the double, as in definition 8.24.

LEMMA 13.19. *Let M be a hyperbolic 3-manifold, homeomorphic to the interior of a compact manifold with torus boundary. Let S be a properly embedded essential surface in M . Consider the double $D(M \setminus\!\!\setminus S)$, and let \mathcal{T} denote the JSJ-decomposition of $D(M \setminus\!\!\setminus S)$. Finally, slice \mathcal{T} and $D(M \setminus\!\!\setminus S)$ along \tilde{S} , obtaining two copies of $M \setminus\!\!\setminus S$. The following hold.*

- (1) *The tori in the collection \mathcal{T} can be isotoped to be preserved by the reflection of $D(M \setminus\!\!\setminus S)$ in the surface \tilde{S} ; thus cutting $D(M \setminus\!\!\setminus S)$ along \tilde{S} cuts \mathcal{T} into two identical pieces.*
- (2) *Each essential torus $T \in \mathcal{T}$ is sliced into essential annuli in $M \setminus\!\!\setminus S$ with boundary on \tilde{S} .*
- (3) *The characteristic submanifold of $D(M \setminus\!\!\setminus S)$ intersects $M \setminus\!\!\setminus S$ in components that are either I -bundles over a subsurface of \tilde{S} , or Seifert fibered solid tori.*

PROOF. The first item follows from the equivariant torus theorem, due to Holzmann [Hol91]. It is an exercise to prove the remaining two items; exercise 13.5. \square

DEFINITION 13.20. Let M , S , \mathcal{T} be as in lemma 13.19. We say that the intersection of the characteristic submanifold of $D(M \setminus S)$ with $M \setminus S$ is the *characteristic submanifold of $M \setminus S$* . Its complement in $M \setminus S$ is the *guts* of S , denoted $\text{guts}(M \setminus S)$ or sometimes simply $\text{guts}(S)$.

EXAMPLE 13.21. Recall from example 12.26 that the figure-8 knot complement M contains a surface S that is a fiber, shown in figure 12.4. This surface S is essential and properly embedded. The manifold $M \setminus S$ is homeomorphic to $S \times I$. Thus in this case, all of $M \setminus S$ is an I -bundle. Thus $\text{guts}(M \setminus S)$ is empty.

By contrast, later in this section we will find examples of alternating knot complements M and surfaces S such that $\text{guts}(M \setminus S) = M \setminus S$, that is the characteristic submanifold is empty.

LEMMA 13.22. *Let M , S , and \mathcal{T} be as in lemma 13.19. Then the manifold $\text{guts}(M \setminus S)$ admits a hyperbolic metric with totally geodesic boundary.*

PROOF. If we double $\text{guts}(M \setminus S)$ along the portion of the boundary on \tilde{S} , i.e. take two copies of $\text{guts}(M \setminus S)$ and glue by the identity along their common boundary on \tilde{S} , we obtain the complement of the characteristic submanifold of the manifold $D(M \setminus S)$. This admits a finite volume hyperbolic metric. It also admits an involution fixing the surface $\text{guts}(M \setminus S) \cap \tilde{S}$ pointwise. It follows from the proof of the Mostow–Prasad rigidity theorem that an embedded surface fixed pointwise by an involution of a finite volume hyperbolic 3-manifold must be totally geodesic. Hence cutting along it yields a hyperbolic structure on $\text{guts}(M \setminus S)$ with totally geodesic boundary. \square

The following theorem, from [AST07], gives us a tool to bound volumes from below using the guts of surfaces.

THEOREM 13.23 (Agol, Storm, and Thurston). *Let S be a π_1 -essential surface properly embedded in an orientable hyperbolic 3-manifold M . Then*

$$\text{vol}(M) \geq -v_{\text{oct}} \chi(\text{guts}(M \setminus S)),$$

where $v_{\text{oct}} = 3.66\dots$ is the volume of a regular ideal octahedron.

PROOF SKETCH. The essential surface S can be isotoped to be minimal in M . Cut along the minimal surface isotopic to S , and denote $M \setminus S$ by N . Note that N inherits from M a Riemannian metric for which the mean curvature on its boundary \tilde{S} is 0. Denote this metric by g . Then $\text{vol}(M) = \text{vol}(N, g)$.

Let $D(N)$ denote the double of N , i.e. the manifold obtained by taking two copies of N and identifying them along their common boundary. By lemma 13.22, $D(\text{guts}(N)) \subset D(N)$ inherits a complete hyperbolic metric with $\tilde{S} \cap \text{guts}(N)$ a totally geodesic surface embedded in $D(\text{guts}(N))$; denote this metric by h . On the other hand, $D(N)$ inherits a singular Riemannian metric with singularities on S obtained from the metric g ; denote

this metric by g as well. Agol, Storm, and Thurston show that this singular metric g can be approximated by smooth Riemannian metrics $\{g_i\}$ with restricted curvature properties. The volumes $\text{vol}(D(N), g_i)$ under the smooth metrics g_i converge to the volume $\text{vol}(D(N), g)$ under its singular metric, with $\text{vol}(D(N), g) = 2 \text{vol}(N, g) = 2 \text{vol}(M)$.

First suppose M is closed. Use Ricci flow with surgery to evolve the metric, as in Perelman's proof of the geometrization theorem [Per02, Per03]. The evolution will give $D(\text{guts}(N))$ the hyperbolic metric h . Perelman's techniques imply a monotonicity result, in particular that

$$\text{vol}(D(N), g) \geq \text{vol}(D(\text{guts}(N)), h),$$

with equality if and only if S is totally geodesic in $(D(N), g)$. Then

$$\text{vol}(M) = \frac{1}{2} \text{vol}(D(N), g) \geq \text{vol}(\text{guts}(M \setminus S)),$$

with equality if and only if S is totally geodesic in M .

If M has torus boundary, then similar techniques can be used to approximate the metric on compact sets, giving the same result.

Finally, $(\text{guts}(M \setminus S), h)$ is a hyperbolic manifold with totally geodesic boundary. Thus by Miyamoto's theorem, theorem 13.16,

$$\text{vol}(\text{guts}(M \setminus S)) \geq -v_{\text{oct}} \chi(\text{guts}(M \setminus S)). \quad \square$$

We will be considering the guts of the checkerboard surfaces in an alternating link. By theorem 11.31, the checkerboard surfaces are essential, and thus satisfy the hypotheses of theorem 13.23.

LEMMA 13.24. *Let S be one of the checkerboard surfaces of a link with a twist-reduced alternating diagram K , whose hyperbolic complement we denote by $S^3 - K = M$. Without loss of generality say S is shaded, with W the other checkerboard surface, colored white. Suppose in the polyhedral decomposition of M that there are white bigon faces. Then a neighborhood of each white bigon face is part of an I -bundle in $M \setminus S$, and thus any bigon face of W does not belong to $\text{guts}(M \setminus S)$.*

PROOF. The I -bundle components of $M \setminus S$ have the form $Y \times I$, with $Y \times \{0\}$ and $Y \times \{1\}$ subsets of $\tilde{S} \subset \partial(M \setminus S)$. Recall that $Y \times \{0\}$ and $Y \times \{1\}$ form the *horizontal boundary* of the I -bundle. The subset $\partial Y \times I$ forms the *vertical boundary*.

A white bigon region of the polyhedral decomposition of M is bounded by two edges and two vertices; recall that edges are crossing arcs, and lie in the intersection $W \cap S$, and the vertices are ideal, forming portions of the parabolic locus. Thus a regular neighborhood of a white bigon face can be visualized as a thickened square, with two sides of its boundary on S and two sides of its boundary on the parabolic locus. Note such a thickened square is a portion of an I -bundle, with horizontal boundary a neighborhood in S of the two crossing arcs of $W \cap S$ that form the boundary of the bigon, and vertical boundary on the parabolic locus. We can complete this thickened

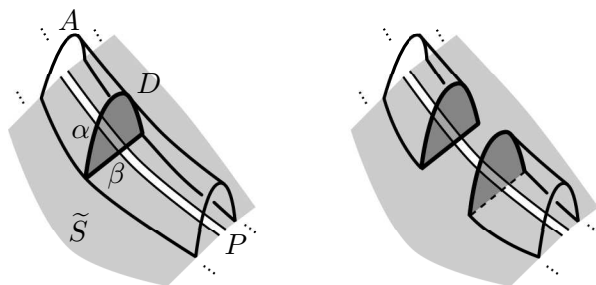


FIGURE 13.4. A portion of a parabolically compressible annulus on the left, and a parabolic compression on the right.

square to an I -bundle over a subsurface of S with boundary by attaching a neighborhood of the annulus that forms the parabolic locus. This annulus has boundary components on S , and is parallel to a link component. Its neighborhood can be given the structure of an I -bundle with fibers I parallel to those of the bigon. Thus the union of the neighborhood of the bigon and the neighborhood of this annulus (or possibly two annuli in the case of a link) forms an I -bundle in $M \setminus S$. \square

COROLLARY 13.25. *Let K be a twist-reduced diagram of a hyperbolic alternating link. Let K' be the diagram obtained from K by removing all crossings but one in each twist region of K . Let S denote a checkerboard surface of K , and let S' denote the corresponding checkerboard surface of K' . Then*

$$\text{guts}((S^3 - K) \setminus S) = \text{guts}((S^3 - K') \setminus S').$$

13.3.1. Essential annuli. Our method of proving the volume bound on alternating links, theorem 13.17, is to apply the volume bound via guts, theorem 13.23, to the modified diagram K' of K , as in corollary 13.25. We will determine the Euler characteristic of the guts of checkerboard surfaces of K' . Recall that to identify guts, we must first cut along essential annuli. Thus the next step in the proof is to find essential annuli in the cut manifold.

Suppose there is an essential annulus. Then the proof most easily breaks into two cases, depending on whether the annulus is *parabolically compressible* or not, in the sense of the following definition.

DEFINITION 13.26. Let M be a hyperbolic 3-manifold with a properly embedded essential surface S . Let P denote the parabolic locus of $M \setminus S$, as in definition 11.23. An annulus A , properly embedded in $M \setminus S$ with $\partial A \subset \tilde{S}$, is *parabolically compressible* if there exists a disk D with interior disjoint from A , with ∂D meeting A in an essential arc α on A , and with $\beta = \partial D - \alpha$ lying on $\tilde{S} \cup P$, with β meeting P transversely exactly once. We may surger along such a disk; this is called a *parabolic compression*, and it turns the annulus A into a disk meeting P transversely exactly twice, with boundary otherwise on \tilde{S} . See figure 13.4.

DEFINITION 13.27. Let D be a disk properly embedded in $M \setminus \setminus S$ with boundary consisting of two arcs on \tilde{S} and two arcs on the parabolic locus P . We say D is a *essential product disk (EPD)*.

A proof nearly identical to that of lemma 13.24 shows that EPDs belong to the I -bundle of $M \setminus \setminus S$ (exercise 13.6).

LEMMA 13.28. *Let S be the shaded checkerboard surface of a link with a twist-reduced alternating diagram K , whose hyperbolic complement we denote by $S^3 - K = M$. Suppose there are no white bigon regions, and suppose A is an essential annulus properly embedded in $M \setminus \setminus S$, disjoint from the parabolic locus and not parallel to the parabolic locus, with $\partial A \subset \tilde{S}$. Then A is not parabolically compressible.*

The proof of lemma 13.28 is completed by considering how a parabolically compressible annulus intersects the polyhedra in the decomposition of an alternating link, similar to several proofs in chapter 11. The following lemma will be useful.

LEMMA 13.29. *Let K be a link with a prime, twist-reduced alternating diagram, with corresponding ideal polyhedral decomposition. Let D_1 and D_2 be normal disks in the polyhedra such that ∂D_1 and ∂D_2 meet exactly four interior edges. Isotope ∂D_1 and ∂D_2 to minimize intersections $\partial D_1 \cap \partial D_2$ in faces. If ∂D_1 intersects ∂D_2 , then ∂D_1 intersects ∂D_2 exactly twice, in two faces of the same color.*

PROOF. The boundaries ∂D_1 and ∂D_2 are quadrilaterals, with sides of ∂D_i between intersections with interior edges. Note that ∂D_1 can intersect ∂D_2 at most once in any of its sides by the requirement that the number of intersections be minimal (else isotope through a face). Thus there are at most four intersections of ∂D_1 and ∂D_2 . If ∂D_1 meets ∂D_2 four times, then the two quads run through the same faces, both bounding disks, and can be isotoped off each other using the fact that the diagram is prime. Since the quads intersect an even number of times, there are either zero or two intersections. If zero intersections, we are done.

So suppose there are two intersections. Suppose ∂D_1 intersects ∂D_2 exactly twice in faces of the opposite color. Then an arc $\alpha_1 \subset \partial D_1$ has both endpoints on $\partial D_1 \cap \partial D_2$ and meets only one intersection of ∂D_1 with an interior edge of the polyhedron. Similarly, an arc $\alpha_2 \subset \partial D_2$ has both endpoints on $\partial D_1 \cap \partial D_2$ and meets only one intersection of ∂D_2 with an interior edge of the polyhedral decomposition. Then $\alpha_1 \cup \alpha_2$ is a closed curve on the boundary of the polyhedron meeting exactly two interior edges. This gives a curve in the diagram of K meeting K exactly twice. Because the diagram is prime, there must be no crossings on one side of the curve. In the polyhedron, this means the arcs α_1 and α_2 are parallel, and we can isotope them to remove the intersections of D_1 and D_2 . \square

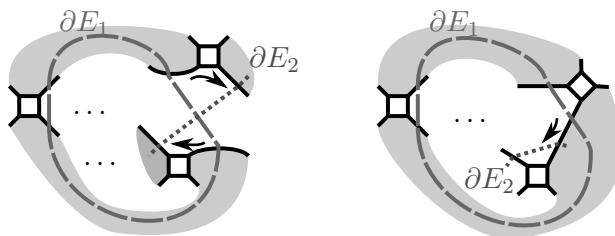


FIGURE 13.5. Left: ∂E_1 is not parallel to a boundary edge in U , hence ∂E_1 meets ∂E_2 in U . Right: ∂E_1 is parallel to a boundary edge.

PROOF OF LEMMA 13.28. Suppose by way of contradiction that A is an essential, parabolically compressible annulus properly embedded in $M \setminus S$ with $\partial A \subset \tilde{S}$. Perform a parabolic compression to obtain an EPD E . Put E into normal form with respect to the polyhedral decomposition of $M \setminus S$.

Suppose E intersects a white face V of W . Consider the arcs $E \cap V$; such an arc has both endpoints on \tilde{S} . If one cuts off a disk on E that does not meet the parabolic locus, then there will be an innermost such disk. Its boundary consists of an arc in W and an arc in S . We may sketch the boundary of the disk on the diagram of K , since the graph on the polyhedra is identical to the projection graph of the diagram (see theorem 11.6). Thus this innermost disk has boundary intersecting the link diagram exactly twice. Because the diagram of K is prime, this disk bounds a region containing no crossings. But then the original innermost disk in the polyhedron it is not normal: its boundary runs from a single edge back to that edge. This is a contradiction.

So $E \cap W$ consists of arcs running from \tilde{S} to \tilde{S} , cutting off disks on either side meeting the parabolic locus. Thus the white surface cuts E into normal quadrilaterals $\{E_1, \dots, E_n\}$, with $n \geq 2$ by assumption that E intersects a white face. On the end of E , the quadrilateral E_1 has one side on W , two sides on \tilde{S} and the final side on the parabolic locus (a boundary face). Isotope slightly off the boundary face into the adjacent white face so that E_1 remains normal. Do the same for E_n . Then all quadrilaterals E_1, \dots, E_n have two sides on S and two sides on W .

Superimpose E_1 and E_2 onto the boundary of one of the (identical) polyhedra. An edge of E_1 in a white face V is glued to an edge of E_2 in the same white face, but by a rotation in the face V . Thus when we superimpose, $\partial E_2 \cap V$ is obtained from $\partial E_1 \cap V$ by a rotation in V .

If $E_1 \cap V$ is not parallel to a single boundary edge, then $\partial E_1 \cap V$ must intersect $\partial E_2 \cap V$; see figure 13.5. Then lemma 13.29 implies that ∂E_1 and ∂E_2 also intersect in another white face. But ∂E_1 is parallel to a single boundary edge in its second white face, so ∂E_2 cannot intersect it. This is a contradiction.

So $E_1 \cap V$ is parallel to a single boundary edge (and hence so is $E_2 \cap V$). But then E_1 meets both white faces in arcs parallel to boundary edges. Isotoping ∂E_1 slightly into these boundary faces and transfer the curve to the diagram of the link. This gives a closed curve in the link diagram meeting the projection graph of K in exactly two crossings, running to opposite sides of the crossings. If the crossings are distinct, then because the diagram is twist-reduced, the two crossings must bound white bigons between them, contradicting the fact that there are no white bigon regions in the diagram. So the crossings are not distinct. Returning to the polyhedron, ∂E_1 encircles a single ideal vertex of the polyhedron. Repeating the argument with E_2 and E_3 , and so on, we find that each ∂E_i encircles a single ideal vertex. Gluing these together, the original annulus A is parallel to the parabolic locus. This contradicts our assumption on A .

So if there is an EPD E , it cannot meet W . Then it lies completely in a single polyhedron of the decomposition. Its boundary runs through two shaded faces and two boundary faces. Transfer to the link diagram; its boundary defines a curve meeting the link diagram in exactly two crossings, running to opposite sides of the crossings. Because the diagram is twist-reduced, the curve ∂E encloses a string of white bigons. But there are no white bigons, so ∂E must run in and out of the same boundary face. This contradicts the fact that it was normal. \square

LEMMA 13.30. *Let K be a hyperbolic alternating link with a prime, twist-reduced diagram and corresponding polyhedral decomposition. Let M denote $S^3 - K$ and let S denote the shaded checkerboard surface. Suppose that there are no white bigons in the polyhedra. Suppose A is an essential annulus embedded in $M \setminus S$, disjoint from the parabolic locus and not parallel to it, with $\partial A \subset \tilde{S}$. Then A bounds a Seifert fibered solid torus.*

PROOF. By lemma 13.28 we may assume that A is not parabolically compressible. Put it into normal form with respect to the polyhedral decomposition. Because the Euler characteristic of an annulus is 0, each normal disk making up A must have combinatorial area 0 by the Gauss–Bonnet lemma, lemma 8.35. Because A does not meet the parabolic locus, each such disk must meet exactly four interior edges; see definition 8.30. Thus the white surface W cuts A into squares E_1, \dots, E_n . Note that if a component of intersection of $E_i \cap W$ is parallel to a boundary edge, then the disk of W bounded by $E_i \cap W$, the boundary edge, and portions of edges of $\tilde{S} \cap W$ defines a parabolic compression disk for A , contradicting the fact that A cannot be parabolically compressible. So no component of $E_i \cap W$ is parallel to a boundary edge.

Again superimpose all squares E_1, \dots, E_n on one of the polyhedra. The squares are glued in white faces, and cut off more than a single boundary edge in each white face, so ∂E_i must intersect ∂E_{i+1} in a white face; see again figure 13.5. Then lemma 13.29 implies ∂E_i intersects ∂E_{i+1} in both of the white faces it meets. Similarly, ∂E_i intersects ∂E_{i-1} in both its white

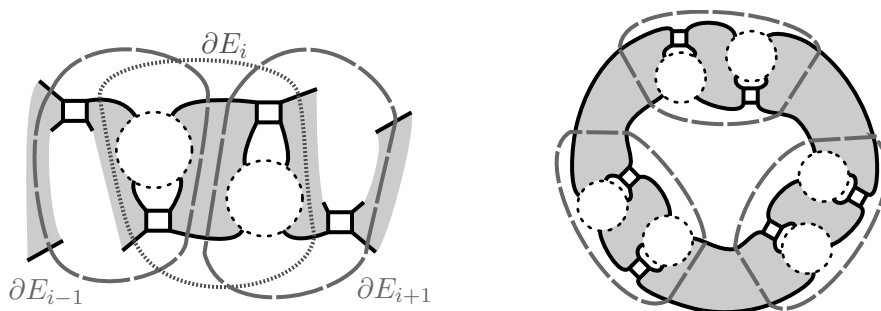


FIGURE 13.6. Left: E_{i-1} , E_i , and E_{i+1} must intersect as shown. Right: cycle of three such tangles.

faces. Because E_{i-1} and E_{i+1} lie in the same polyhedron, they are disjoint (or $E_{i-1} = E_{i+1}$, but this makes A a Möbius band rather than an annulus; see exercise 13.7). This is possible only if E_{i-1} , E_i , and E_{i+1} line up as in figure 13.6 left, bounding portions of the polyhedron as shown. These transfer to the link diagram to bound tangles; Lackenby calls such tangles *units* in [Lac04]. Then all E_j form a cycle of such tangles, as in figure 13.6 right.

Observe from figure 13.6 that each disk E_i encircles two units, with a band of shaded surface between E_i and E_{i+2} in the same polyhedron. Then in each polyhedron, these disks of A bound a solid cylinder (a ball) with top and bottom on white faces — one the central region of figure 13.6, right, and one the unbounded region — and sides along disks E_j and shaded faces. The two solid cylinders glue across white faces with a twist, to form a solid torus. As each cylinder can be written as $D^2 \times I$, with $D^2 \times \{0\}$ and $D^2 \times \{1\}$ on white faces, the gluing by a twist in the white face gives the solid torus a Seifert fibering. Thus A bounds a Seifert fibered solid torus. \square

THEOREM 13.31 (Lackenby, [Lac04]). *Let K be a link with a prime, twist-reduced alternating diagram, and corresponding polyhedral decomposition. Let M denote the complement of K , let S and W denote the checkerboard surfaces, and let r_S and r_W denote the number of non-bigon regions of S and W respectively. Then*

$$\chi(\text{guts}(M \setminus S)) = 2 - r_W, \quad \chi(\text{guts}(M \setminus W)) = 2 - r_S.$$

PROOF. Suppose first that the diagram has no white bigon regions. Then lemma 13.28 implies there is no embedded essential annulus that is parabolically compressible, and lemma 13.30 implies any parabolically incompressible annulus bounds a Seifert fibered solid torus. Thus

$$\chi(\text{guts}(M \setminus S)) = \chi(M \setminus S).$$

Since $M \setminus S$ is obtained by gluing two balls along white faces, $\chi(M \setminus S) = 2 - r_W$.

If the diagram contains white bigon regions, then replace each string of white bigons in the diagram by a single crossing, obtaining a new link K' . Let M' denote $S^3 - K'$ and let S' be the checkerboard surface coming from the same shaded regions as S in K . By corollary 13.25, $\text{guts}(M \setminus S) = \text{guts}(M' \setminus S')$. Hence $\chi(\text{guts}(M \setminus S)) = \chi(\text{guts}(M' \setminus S')) = 2 - r_W$.

An identical argument applies to $M \setminus W$, replacing S with W . \square

Theorem 13.17 is now almost an immediate consequence of theorem 13.31 and theorem 13.23.

PROOF OF THEOREM 13.17. Let Γ be the 4-regular diagram graph associated to K by replacing each twist-region with a vertex. Let $|v(\Gamma)|$ denote the number of vertices of Γ , and $|f(\Gamma)|$ the number of regions. Because Γ is 4-valent, the number of edges is $2|v(\Gamma)|$, so

$$\chi(S^2) = 2 = -|v(\Gamma)| + |f(\Gamma)| = -\text{tw}(K) + r_S + r_W.$$

Then applying Theorems 13.23 and 13.31 gives

$$\begin{aligned} \text{vol}(S^3 - K) &\geq -\frac{1}{2}v_{\text{oct}}\chi(\text{guts}(M \setminus S)) - \frac{1}{2}v_{\text{oct}}\chi(\text{guts}(M \setminus W)) \\ &= -\frac{1}{2}v_{\text{oct}}(2 - r_S - r_W) \\ &= \frac{1}{2}v_{\text{oct}}(\text{tw}(K) - 2). \end{aligned} \quad \square$$

13.4. Exercises

EXERCISE 13.1. Show the upper bound of theorem 13.2 is asymptotically sharp, in two steps. First, show there is a sequence of fully augmented links L_i with $t(L_i)$ crossing circles such that $\text{vol}(S^3 - L_i)/t(L_i)$ approaches $10v_{\text{tet}}$ as i goes to infinity. (Hint: take white faces to be regular hexagons.) Then show that there is a sequence of links K_i with twist number $t(K_i)$ such that $\text{vol}(S^3 - K_i)/t(K_i)$ approaches $10v_{\text{tet}}$ as i goes to infinity.

EXERCISE 13.2. Use theorem 9.10 to give an upper bound on the volume of a 2-bridge knot with continued fraction expansion $[0, a_{n-1}, \dots, a_1]$. Find an example of a 2-bridge knot such that your upper bound becomes $2v_{\text{tet}}(\text{tw}(K) - 1)$. Use this to show that the lower bound of theorem 13.4 is asymptotically sharp: The ratio of upper and lower bounds goes to 1 as $\text{tw}(K) \rightarrow \infty$.

EXERCISE 13.3. The volume of a regular ideal octahedron is denoted by v_{oct} . In exercise 7.10, it was shown that a fully augmented 2-bridge link decomposes into regular ideal octahedra. Use this to prove that the volume of a 2-bridge link with twist number $\text{tw}(K)$ is at most $2v_{\text{oct}}(\text{tw}(K) - 1)$.

EXERCISE 13.4. Suppose K is a link complement that admits a rotational symmetry about an axis, with order p . That is, suppose there is a

curve γ in S^3 such that a rotation of order p about γ preserves K . Show that if $p \geq 7$,

$$\text{vol}(S^3 - K) \geq \left(1 - \frac{4\pi^2}{49}\right)^{3/2} \text{vol}(S^3 - (K \cup \gamma)).$$

EXERCISE 13.5. Prove lemma 13.19.

EXERCISE 13.6. (EPDs lie in the characteristic submanifold) Prove that an essential product disk in $M \setminus S$ is a subset of the I -bundle of $M \setminus S$, thus cannot be part of the guts.

EXERCISE 13.7. Let K be a hyperbolic alternating knot with a prime twist-reduced diagram, and corresponding polyhedral decomposition. Let S denote the shaded checkerboard surface, and suppose that A is an essential surface with boundary on \tilde{S} such that A is the union of exactly two normal squares E_1 and E_2 , and such that the sides of ∂E_1 and ∂E_2 in white faces are not parallel to boundary edges of the polyhedra. Then prove that A is a Möbius band.

EXERCISE 13.8. We obtain lower bounds on volumes of highly twisted 2-bridge knots with at least seven crossings per twist region from three theorems in this chapter, namely theorem 13.4, theorem 13.15, and theorem 13.17. Compare the bounds coming from each theorem. Which gives the best volume estimate?

EXERCISE 13.9. How sharp are theorem 13.15 and theorem 13.17? By tracing through the proofs, find conditions that must be satisfied for the lower bound on volume to be sharp.

Ford Domains and Canonical Polyhedra

We have noted that there is (currently) no guarantee that every finite volume cusped hyperbolic 3-manifold admits a decomposition into positively oriented ideal tetrahedra. However, we can guarantee that every cusped hyperbolic 3-manifold admits a decomposition into convex ideal polyhedra. This is the canonical decomposition, first studied by [EP88], which we describe in this chapter. The canonical decomposition is dual to another decomposition, the Ford domain (sometimes called the Ford–Voronoi domain), which we will describe first. Our exposition is similar to that of [LP14], also [ASWY07], and [Bon09].

Before we begin, we give a few words motivating the canonical decomposition. In the case of a hyperbolic knot, if two knot complements have the same canonical decomposition, then they must necessarily be isometric, and hence equivalent by theorem 0.4, the Gordon–Luecke theorem. This result follows from theorem 14.33, below. Thus for hyperbolic knots, the canonical decomposition is a *complete* knot invariant. Unfortunately, it is not easy to compute in general. However, in this chapter we will explain how it is defined, and give a few examples.

Both Ford domains and canonical polyhedra arise from natural geometric ideas. However, they are somewhat difficult to describe in words because of various choices that must be made. If a hyperbolic 3-manifold has more than one cusp, they depend on a choice of horoball neighborhood of the cusp. For this reason, we begin this chapter by describing choices of horoball neighborhoods and the sets equidistant from horoballs, in section 14.1.

Moreover, the definition of a Ford domain differs in the literature, although all definitions are closely related. Perhaps the simplest definition is the one given by Guéritaud and Schleimer [GS10]: they define a Ford domain (or Ford–Voronoi domain) to be the set S of points in M that have a unique shortest path to the fixed horoball neighborhood. The drawback to this definition is that the resulting set S is not a fundamental domain for the manifold in the sense that not every point of M has a preimage in S . Additionally, the components of S are not simply connected, because each component admits a deformation retraction to a horoball neighborhood, which is homeomorphic to the thickened torus. We will give a closely related definition of the Ford domain in section 14.2 that overcomes these

difficulties, but at the cost of being slightly more complicated and dependent upon an additional choice (of fundamental domain for the horoball neighborhood). Still, throughout the discussion it is useful to keep Guéritaud and Schleimer's definition in mind.

However, all the different definitions of Ford domain in the literature still have the same geometric dual: the canonical polyhedral decomposition. This convex cell decomposition does depend on choice of horoball neighborhood, but it is independent of all other choices involved in defining the Ford domain. We describe the canonical polyhedral decomposition in section 14.3.

14.1. Horoballs and isometric spheres

Throughout, our setup is the following. We let M be an orientable 3-manifold admitting a complete hyperbolic structure with at least one cusp. The universal cover of M is then \mathbb{H}^3 . We may apply an isometry so that the point at infinity $\infty \in \partial_\infty \mathbb{H}^3$ maps to a cusp of M under the covering map. Then $M \cong \mathbb{H}^3/\Gamma$, where $\Gamma \leq \mathrm{PSL}(2, \mathbb{C})$ is a discrete group of isometries isomorphic to $\pi_1(M)$ via the holonomy representation $\rho: \pi_1(M) \rightarrow \mathrm{PSL}(2, \mathbb{C})$.

Because the point at infinity projects to a cusp of M , there will be a parabolic subgroup Γ_∞ of Γ fixing the point at infinity. If the cusp of M is a rank-1 cusp, then Γ_∞ will be isomorphic to \mathbb{Z} . If it is a rank-2 cusp, Γ_∞ will be isomorphic to $\mathbb{Z} \times \mathbb{Z}$; see definition 5.13. Only a rank-2 cusp can occur in a finite volume hyperbolic manifold such as a knot complement, and so this is the case we will consider in this chapter. However, much of the discussion here generalizes to the infinite volume case.

PROPOSITION 14.1. *A complete hyperbolic 3-manifold contains an embedded horoball neighborhood. That is, there is an embedded neighborhood N of the cusps of M such that N lifts to a disjoint collection of embedded horoballs in \mathbb{H}^3 .*

PROOF. This result follows immediately from the structure of the thin part, theorem 5.20. By that theorem, for any $0 < \epsilon \leq \epsilon_3$, where ϵ_3 is a universal constant, the ϵ -thin part of M consists of tubes around short geodesics and rank-1 and rank-2 cusps. Ignore the tubes; the cusps are embedded. Their lift to \mathbb{H}^3 consists of disjoint embedded horoballs as required. \square

LEMMA 14.2. *Suppose N is an embedded horoball neighborhood of a cusp of M that lifts to the horoball about $\infty \in \partial_\infty \mathbb{H}^3$. Then all the lifts of N to \mathbb{H}^3 give countably many horoballs in \mathbb{H}^3 , with centers at the points*

$$\{g(\infty) \mid g \in \Gamma\}.$$

PROOF. Let H_∞ denote the horoball about ∞ that projects to N . Note that for all $g \in \Gamma$, the horoball $g(H_\infty)$ must also project to N , and its center is $g(\infty)$. On the other hand, if H is a horoball in \mathbb{H}^3 that projects to N , then there must exist $h \in \Gamma$ such that $h(H) = H_\infty$, and so H has center $h^{-1}(\infty)$. Thus the set $\{g(H_\infty) \mid g \in \Gamma\}$ is exactly the set of horoballs projecting to N .

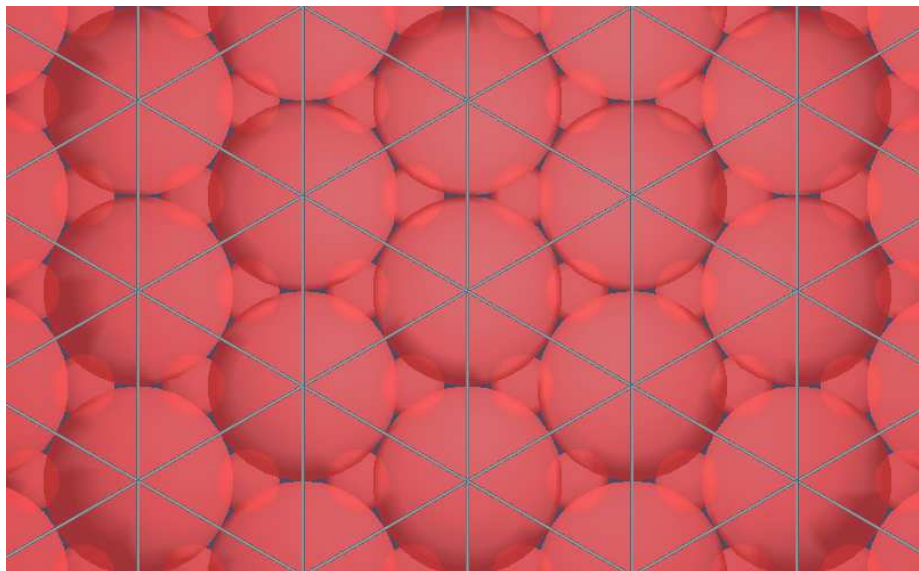


FIGURE 14.1. The horoballs in the lift of an embedded cusp of the figure-8 knot complement, from SnapPy [CDGW16].

Because Γ is a discrete group, it has countably many elements (exercise 14.1). Thus all lifts of N to \mathbb{H}^3 is a countable set of horoballs. \square

COROLLARY 14.3. *Let M be finite volume. Any embedded horoball neighborhood about all cusps of M lifts to countably many disjoint horoballs in \mathbb{H}^3 .*

PROOF. Lemma 14.2 shows that an embedded horoball neighborhood of one cusp of M lifts to countably many disjoint horoballs. Proposition 14.1 implies that all horoball lifts from all cusps are embedded. Since M has finite volume, it has only finitely many cusps. Hence the collection of all lifts of horoball neighborhoods is countable. \square

The software SnapPy [CDGW16] has a feature ‘Cusp Neighborhoods’ that shows the horoballs making up the lift of an embedded horoball neighborhood of M — or at least those that have Euclidean diameter larger than some specified lower bound. For example, the pattern arising from the figure-8 knot is shown in figure 14.1.

Now consider an embedded cusp neighborhood of a manifold with a single cusp, for example the figure-8 knot complement. Proposition 14.1 and 14.2 imply that the cusp lifts to a countable collection of embedded horoballs in \mathbb{H}^3 . If we adjust the size of the initial cusp neighborhood of M , the sizes of the horoball lifts will also be adjusted. For example, if we shrink the cusp of M , the horoball about infinity H_∞ will also shrink, which we see as an increase in Euclidean height of the horoball. All its translates $\gamma(H_\infty)$ will also shrink, which we see as a shrinking of the Euclidean diameters of the horoballs with centers away from ∞ .

On the other hand, if we increase the size of the cusp of M , the horoballs will grow. We can increase their sizes, keeping the cusp embedded, up until the point where the cusp neighborhood becomes tangent to itself. In the lift of the horoball neighborhood, at this point two horoballs are tangent.

If M has multiple cusps, then we can grow and shrink the sizes of cusps independently. However, we can still increase sizes of embedded cusps only until each is tangent either to itself or to another cusp.

DEFINITION 14.4. A *maximal cusp neighborhood* is an (open) embedded cusp neighborhood for M that is maximal in the sense that no cusp can be expanded while keeping the set of cusps embedded and disjoint.

DEFINITION 14.5. Consider the lift of an embedded maximal cusp neighborhood to \mathbb{H}^3 , with one cusp lifting to a horoball at infinity. A *full-sized horoball* is a horoball in this pattern that is tangent to the horoball at infinity. Viewed from infinity, it has maximal Euclidean diameter.

EXAMPLE 14.6. The complement of the figure-8 knot admits four full-sized horoballs, distinct up to translation by Γ_∞ ; see again figure 14.1. For this manifold, each full-sized horoball is tangent to the other three, in a pattern that is known to be the densest possible horoball packing. (This follows from a theorem of Böröczky [**Bör78**]: the 3-dimensional analogue of theorem 8.45.)

Recall that a *fundamental domain* for the action of a group on a space is a subset of the space that contains a point from each orbit, whose interior contains exactly one point from each orbit. In this chapter, we will restrict to complete (G, X) -structures on a manifold M , where X is the metric space \mathbb{E}^2 or \mathbb{H}^3 and G acts by isometries. In this case, we require a fundamental domain R to be cut out by geodesic planes. Distinct points in the interior of R project to distinct points in the manifold. The boundary of R is made up of faces intersecting in edges and vertices, and the interior of each face is paired by an isometry of G to exactly one other face; this is called a *face-pairing isometry*. Finally, the quotient of the fundamental domain under the action of face-pairing isometries, which agrees with the restriction of the covering map $X \rightarrow M$, is all of M .

For example, a Euclidean structure on a torus has fundamental domain a single (closed) parallelogram. It follows that the boundary of a cusp of a hyperbolic 3-manifold has a fundamental domain that is a parallelogram on a horosphere in \mathbb{H}^3 .

LEMMA 14.7. Let $M \cong \mathbb{H}^3/\Gamma$ be a hyperbolic 3-manifold with at least one cusp. In a horoball pattern in \mathbb{H}^3 given by lifting an embedded maximal cusp neighborhood for M , apply any isometry taking a desired horoball to the one at infinity. Then in the new pattern obtained by applying this isometry, there is at least one full-sized horoball meeting a fundamental domain for the boundary of the horoball about infinity.

Moreover, if M has only one cusp, then there are at least two full-sized horoballs in a fundamental domain. The second is often called the Adams horoball.

PROOF. By definition, an embedded maximal cusp neighborhood cannot be expanded or the cusp will no longer be embedded. Thus its lift to \mathbb{H}^3 will no longer consist of disjoint horoballs. That means that for each cusp, one horoball in its fundamental domain must be tangent to another. Hence when we apply an isometry taking a horoball projecting to that cusp to a horoball about infinity, another horoball becomes tangent to the one at infinity, hence full-sized.

In the case that M has exactly one cusp, let H_∞ denote the horoball at infinity and let H_f denote the full-sized horoball. Because there is only one cusp of M , the two horoballs must project to the same cusp of M . Thus there must be a covering transformation, i.e. an isometry $g \in \Gamma$, taking H_f to H_∞ . Consider the image $g(H_\infty)$. This is a horoball tangent to $g(H_f) = H_\infty$, hence it must be a full-sized horoball. Apply an isometry of $w \in \Gamma_\infty \leq \Gamma$ fixing ∞ , if necessary, so that $wg(H_\infty)$ lies in the same fundamental domain of the cusp as H_f , and replace g with wg . Now either H_f and $g(H_\infty)$ are disjoint full-sized horoballs, as desired, or possibly $H_f = g(H_\infty)$. We now rule out the latter case.

Suppose $g(H_\infty) = H_f$. Consider the effect of g on the geodesic from the center of H_f to ∞ . If g takes ∞ to the center of H_f , then this geodesic is mapped to itself, with the point of tangency between H_f and H_∞ mapped to the point of tangency between the two horoballs; hence g has a fixed point in the interior of \mathbb{H}^3 , so it is elliptic. But M is a manifold, hence proposition 5.10 implies the action of Γ is fixed point free, so g cannot have a fixed point. Thus H_f and $g(H_\infty)$ are disjoint full-sized horoballs. \square

The Adams horoball is so-called because it appears prominently in work of Adams, e.g. [Ada02].

COROLLARY 14.8. *The volume of any cusp component in a maximal cusp neighborhood of M is at least $\sqrt{3}/4$. If M has only one cusp, the volume of a maximal cusp neighborhood is at least $\sqrt{3}/2$.*

PROOF. Exercise 14.4. \square

We learn a great deal of information from a 3-manifold by considering its cusp neighborhoods, and lifts of maximal cusp neighborhoods to \mathbb{H}^3 . However, because there are countably infinitely many horoballs in such a pattern, it is difficult to compute this pattern and it can be difficult to work with. We can reduce the difficulty of the problem by considering points closer to one lift than another, and their boundaries in \mathbb{H}^3 .

LEMMA 14.9. *The set of points equidistant from two horoballs in \mathbb{H}^3 forms a geodesic plane in \mathbb{H}^3 .*

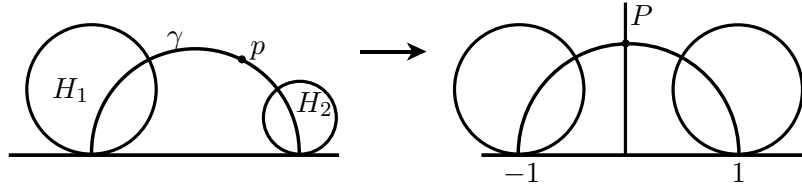


FIGURE 14.2. Map horoballs H_1 and H_2 to lie over -1 and 1 , respectively, with the point equidistant from them on the geodesic between their centers mapped to the point over 0 with height 1 .

PROOF. Let H_1 and H_2 be the two horoballs, and consider the geodesic γ between their centers. There exists a unique point p on γ equidistant from the boundaries of H_1 and H_2 ; see figure 14.2.

Apply the hyperbolic isometry ϕ taking the center of H_1 to $-1 \in \mathbb{C}$, taking the center of H_2 to $1 \in \mathbb{C}$, and taking p to the point lying over $0 \in \mathbb{C}$ of height 1 . Under this isometry, H_1 and H_2 are mapped to horoballs of the same Euclidean diameter, centered at -1 and 1 . We claim that the set of points equidistant from two horoballs of the same Euclidean diameter and centers -1 and 1 is the vertical plane P that meets \mathbb{C} in the imaginary axis. This can be seen as follows. There is a reflection isometry fixing P pointwise and exchanging the two horoballs. Thus the shortest path from a point $q \in P$ to one of the two horoballs will be mapped under the reflection to the shortest path from q to the other horoball. Thus the horoballs are equidistant from P .

Now apply ϕ^{-1} to this picture. The geodesic plane P is mapped to a geodesic plane in \mathbb{H}^3 that is equidistant to the original horoballs. \square

In the case that the two horoballs H_1 and H_2 project to the same cusp, the totally geodesic plane is known as an isometric sphere, as in the following definition.

DEFINITION 14.10. Let $g \in \text{PSL}(2, \mathbb{C})$ be an element that does not fix ∞ . Let H denote a horosphere about ∞ in \mathbb{H}^3 . Then $g^{-1}(H)$ is a horosphere centered at a point of $\mathbb{C} \subset (\mathbb{C} \cup \{\infty\}) = \partial\mathbb{H}^3$. Define the set $I(g)$ to be the set of points in \mathbb{H}^3 equidistant from H and $g^{-1}(H)$:

$$I(g) = \{x \in \mathbb{H}^3 \mid d(x, H) = d(x, g^{-1}(H))\}$$

The set $I(g)$ is the *isometric sphere* of g .

Note that $I(g)$ is well-defined, independent of H , even if H and $g^{-1}(H)$ overlap (exercise 14.3).

LEMMA 14.11. For $g \in \Gamma - \Gamma_\infty$, g maps $I(g)$ isometrically to $I(g^{-1})$, taking the half ball bounded by $I(g)$ to the exterior of the half ball bounded by $I(g^{-1})$.

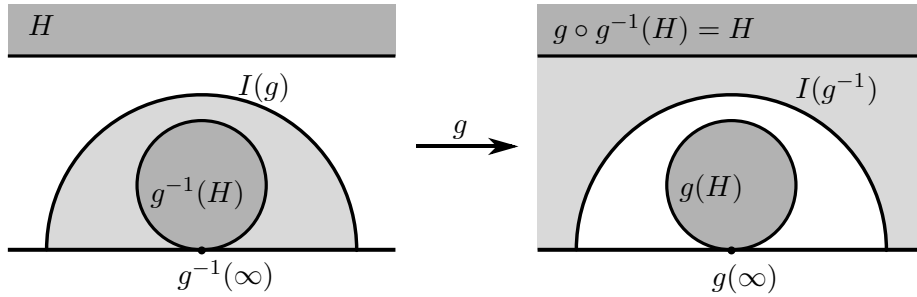


FIGURE 14.3. The horoballs H and $g^{-1}(H)$ are shown, along with the isometric sphere $I(g)$. The effect of applying g to this picture is shown on the right: $g \circ g^{-1}(H)$ maps to H , H to $g(H)$, and $I(g)$ maps to $I(g^{-1})$.

See figure 14.3.

PROOF OF LEMMA 14.11. Let H denote a horosphere about ∞ in \mathbb{H}^3 . Note that g takes the horoball $g^{-1}(H)$ to H , and takes H to $g(H)$. Thus g maps $I(g)$ isometrically to the set of points equidistant from H and $g(H)$. This is $I(g^{-1})$. The half-space bounded by $I(g)$, which contains $g^{-1}(H)$, is mapped to the exterior of the half-space bounded by $I(g^{-1})$, which contains H . \square

LEMMA 14.12. *As a set, $I(g^{-1})$ (and hence $I(g)$) is a Euclidean hemisphere orthogonal to \mathbb{C} . If $g = \begin{pmatrix} a & b \\ c & d \end{pmatrix} \in \text{PSL}(2, \mathbb{C})$, then the center of the Euclidean hemisphere $I(g^{-1})$ is $g(\infty) = a/c$. Its Euclidean radius is $1/|c|$.*

PROOF. The fact that $I(g^{-1})$ is a Euclidean hemisphere follows immediately from lemma 14.9: it must be a geodesic plane in \mathbb{H}^3 . Moreover, it cannot meet the point ∞ , since H is centered at that point. Thus it is a Euclidean hemisphere.

As for the center and radius of the hemisphere, note that $g(\infty) = a/c$, and this must be the center. Consider the geodesic running from ∞ to $g(\infty)$. It consists of points of the form $(a/c, t)$ in $\mathbb{C} \times \mathbb{R}^+ \cong \mathbb{H}^3$. It will meet the horosphere H about infinity at some height $t = h_1$, and the horosphere $g(H)$ at some height $t = h_0$. The radius of the isometric sphere $I(g^{-1})$ is the height of the point equidistant from points $(a/c, h_0)$ and $(a/c, h_1)$.

Note that $g^{-1}(g(H)) = H$, and hence h_1 is given by the height of $g^{-1}(a/c, h_0)$, which can be computed to be $(-d/c, 1/(|c|^2 h_0))$. Thus $h_1 = 1/(|c|^2 h_0)$. Then the point equidistant from $(a/c, h_0)$ and $(a/c, 1/(|c|^2 h_0))$ is the point of height $h = 1/|c|$. \square

LEMMA 14.13. *If $p = (x + iy, t) \in \mathbb{H}^3$ lies in $I(g)$, then $g(p)$ has third coordinate t . That is, g preserves the heights of points on $I(g)$.*

PROOF. Let $p \in I(g)$. If $p \in I(g)$ lies on the geodesic from ∞ to $g^{-1}(\infty)$, then the third coordinates of p and $g(p)$ can both be determined to be $1/|c|$

from lemma 14.12, and so they agree. If p is another point on $I(g)$, construct a 2/3-ideal triangle with vertices ∞ , $g^{-1}(\infty)$, and p . Then g maps this 2/3-ideal triangle to a triangle with the same area, hence the same angle at its finite vertex (see exercise 2.9). Since p and $g(p)$ also both lie on Euclidean hemispheres of the same radius (again by lemma 14.12), it follows that p and $g(p)$ have the same third coordinate. \square

LEMMA 14.14. *Let $\Gamma \leq \text{PSL}(2, \mathbb{C})$ be a nonelementary discrete group with a parabolic subgroup Γ_∞ fixing the point at infinity. Then the set of all isometric spheres $\{I(g) \mid g \in \Gamma - \Gamma_\infty\}$ is locally finite, meaning that for any $x \in \mathbb{H}^3$, there exists $\epsilon > 0$ such that the ball of radius ϵ centered at x meets only finitely many isometric spheres $I(g)$ for $g \in \Gamma - \Gamma_\infty$.*

In fact we show that for all $x \in \mathbb{H}^3$, and all $\epsilon > 0$, the ball $B_\epsilon(x)$ of radius ϵ centered at x meets only finitely many $I(g)$.

PROOF OF LEMMA 14.14. Suppose there exists $x \in \mathbb{H}^3$ and $\epsilon > 0$ so that $B_\epsilon(x)$ meets infinitely many distinct isometric spheres $I(g_n)$, for elements $g_n \in \Gamma - \Gamma_\infty$. Let $q_n \in B_\epsilon(x) \cap I(g_n)$, and let H be a horoball about infinity. By definition of $I(g_n)$, the point q_n is equidistant from H and $g_n^{-1}(H)$. Then $g_n(q_n)$ is equidistant from $g_n(H)$ and H , and by lemma 14.13 $g_n(q_n)$ has the same third coordinate as q_n , hence its third coordinate lies in an interval of length at most 2ϵ centered at the third coordinate of x .

Consider next the first and second coordinates of $g_n(q_n)$. The group Γ_∞ is isomorphic to $\mathbb{Z} \times \mathbb{Z}$, generated by two parabolics translating along the Euclidean plane ∂H . Choose a (closed) parallelogram on ∂H that forms a fundamental domain for the action of Γ_∞ . There exists some $w_n \in \Gamma_\infty$ taking $g_n(q_n)$ to lie in this parallelogram. Then the points $w_n g_n(q_n)$ have first and second coordinates lying within this parallelogram. Since w_n does not affect height, the height of $w_n g_n(q_n)$ agrees with that of q_n , and thus also lies in a bounded region. So all points $\{w_n g_n(q_n)\}$ lie within a bounded parallelepiped in \mathbb{H}^3 . Thus they all lie within some bounded distance of our original point x , say $d(x, w_n g_n(q_n)) \leq R$ for some $R > 0$.

Now consider the points $\{(w_n g_n)^{-1}(x)\}$. We have

$$\begin{aligned} d(x, (w_n g_n)^{-1}x) &\leq d(x, q_n) + d(q_n, (w_n g_n)^{-1}x) \\ &= d(x, q_n) + d(w_n g_n(q_n), x) \\ &\leq \epsilon + R. \end{aligned}$$

Let B denote the closed ball of radius $R + \epsilon$ centered at x . The above calculation shows that each point $(w_n g_n)^{-1}(x)$ lies within this ball.

Then for each n , $(w_n g_n)^{-1}(B) \cap B$ contains $(w_n g_n)^{-1}(x)$, so is nonempty. Because each of the g_n are distinct, each of the $(w_n g_n)^{-1}$ must be distinct, and therefore we have found an infinite set of elements of Γ which take B to a ball intersecting B . It follows that Γ is not properly discontinuous, as in definition 5.7. But Γ is a discrete group, contradicting lemma 5.9. \square

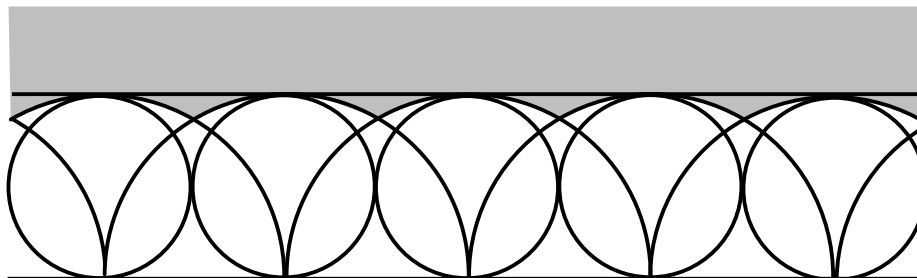


FIGURE 14.4. The shaded region is 2-dimensional cross section of the equivariant Ford domain corresponding to the maximal cusp neighborhood of the Figure-8 knot complement.

14.2. Ford domain

In this section, we define a special fundamental domain for a hyperbolic 3-manifold, called a Ford domain. We will build this fundamental domain for a hyperbolic 3-manifold with at least one cusp. It will not be unique or canonical, although in the case M has only one cusp, a cover will be unique and canonical. Because of the non-uniqueness of domains for multiple cusps, and the consequent additional difficulties to keep track of in that case, we will first treat the case that M has exactly one cusp.

14.2.1. The case of one cusp. When M has a unique cusp, we define a fundamental domain in terms of isometric spheres of M .

DEFINITION 14.15. Define $B(g)$ to be the open half ball bounded by $I(g)$ in \mathbb{H}^3 , and let $\mathcal{F}(\Gamma)$ be the set

$$\mathcal{F}(\Gamma) = \mathbb{H}^3 - \bigcup_{g \in \Gamma - \Gamma_\infty} B(g) = \bigcap_{g \in \Gamma - \Gamma_\infty} (\mathbb{H}^3 - B(g)).$$

We call $\mathcal{F}(\Gamma)$ the *equivariant Ford domain*. Notice that $\mathcal{F}(\Gamma)$ is invariant under the action of Γ_∞ .

An example is shown in figure 14.4.

LEMMA 14.16. *Fix a maximal cusp neighborhood of M , and let H be the horoball that is lift of the maximal cusp neighborhood to \mathbb{H}^3 with center at infinity. Then*

$$B(g) = \{x \in \mathbb{H}^3 \mid d(x, g^{-1}(H)) < d(x, H)\}, \quad \text{and}$$

$$\mathcal{F}(\Gamma) = \{x \in \mathbb{H}^3 \mid d(x, H) \leq d(x, g(H)) \text{ for all } g \in \Gamma - \Gamma_\infty\}.$$

PROOF. This follows from the definitions. By definition 14.10, $I(g)$ is the set of points equidistant from H and $g^{-1}(H)$. Thus $B(g)$ consists of points strictly closer to $g^{-1}(H)$ than to H . Then $\mathcal{F}(\Gamma)$ consists of points at least as close to H as to any of its translates under $\Gamma - \Gamma_\infty$. \square

LEMMA 14.17. *The equivariant Ford domain $\mathcal{F}(\Gamma)$ satisfies the following.*

- (1) $\mathcal{F}(\Gamma)$ is a convex subset of \mathbb{H}^3 .
- (2) $\partial\mathcal{F}(\Gamma)$ consists of points on $I(g)$ for at least one $g \in \Gamma - \Gamma_\infty$, and admits a decomposition into convex faces, edges, and vertices.
- (3) $\mathcal{F}(\Gamma)$ is invariant under the action of Γ_∞ . In particular, Γ_∞ takes faces, edges, and vertices of $\mathcal{F}(\Gamma)$ to faces, edges, and vertices, respectively.

PROOF. For convexity, $\mathcal{F}(\Gamma)$ is the intersection of half-spaces in \mathbb{H}^3 , which are convex, thus $\mathcal{F}(\Gamma)$ is convex.

Any point on the boundary of $\mathcal{F}(\Gamma)$ must lie on the boundary of $B(g)$ for some $g \in \Gamma - \Gamma_\infty$. But $\partial B(g) = I(g)$. Thus the decomposition into faces, edges, and vertices is via isometric spheres and their intersections: The faces of $\partial\mathcal{F}(\Gamma)$ are those points that lie on $I(g)$ for a fixed g . The interior of the face consists of points that do not lie on any other $I(h)$ for $h \in \Gamma - \Gamma_\infty$. Edges are points in the intersection of $I(g_1)$ and $I(g_2)$, for some $g_1, g_2 \in \Gamma - \Gamma_\infty$. Vertices lie in the intersection of three or more isometric spheres. Because faces are subsets of Euclidean hemispheres cut out by other Euclidean hemispheres, they are convex.

Finally, let $w \in \Gamma_\infty$. A point $x \in \mathbb{H}^3$ lies in $\mathcal{F}(\Gamma)$ if and only if x lies in the exterior of all open half balls $B(h)$ for $h \in \Gamma - \Gamma_\infty$. This holds if and only if $w(x)$ lies in the exterior of all open half balls $B(hw^{-1})$ for $hw^{-1} \in \Gamma - \Gamma_\infty$. This is the same set of open half balls. Thus $w(x)$ lies in $\mathcal{F}(\Gamma)$ if and only if x does, and so $\mathcal{F}(\Gamma)$ is invariant under Γ_∞ .

Suppose that x lies on a face of $\mathcal{F}(\Gamma)$, which is a subset of $I(g)$ for some $g \in \Gamma - \Gamma_\infty$. Then x is equidistant from a horoball H at infinity and its translate $g^{-1}(H)$. Thus $w(x)$ is equidistant from $w(H) = H$ and $w(g^{-1}(H)) = (gw^{-1})^{-1}(H)$. It follows that $w(x)$ lies on the isometric sphere $I(gw^{-1})$, and so w takes isometric spheres to isometric spheres. Because w preserves $\mathcal{F}(\Gamma)$, w takes the face to a subset of the isometric sphere $wI(g)$, which must be a face. Similarly, if x lies on an edge or vertex, then it lies on the intersection of isometric spheres, and so does $w(x)$. Since w preserves $\mathcal{F}(\Gamma)$, $w(x)$ lies on an edge or vertex. \square

The faces of $\mathcal{F}(\Gamma)$, which are contained in isometric spheres $I(g)$, can be glued in pairs using the group elements g , as in the following lemma.

LEMMA 14.18. *Suppose a subset f_g of $I(g)$ is a face of $\mathcal{F}(\Gamma)$. Then $g(f_g)$ is a face of $\mathcal{F}(\Gamma)$.*

PROOF. Any point x in the interior of f_g is equidistant from H and $g^{-1}(H)$, and because x is in the interior, x lies further away from $h(H)$ for any $h \neq g^{-1}$ in $\Gamma - \Gamma_\infty$. By lemma 14.11, g maps x to $g(x) \in I(g^{-1})$. Then $g(x)$ is equidistant from H and $g(H)$, but further away from $gh(H)$ for any $h \neq g^{-1}$ in $\Gamma - \Gamma_\infty$. Equivalently, $g(x)$ is equidistant from H and $g(H)$ but further from $k(H)$ for any $k \neq g$ in $\Gamma - \Gamma_\infty$. It follows that $g(x)$ lies in the interior of a face of $\mathcal{F}(\Gamma)$. \square

Lemma 14.18 implies that if $I(g) \cap \mathcal{F}(\Gamma)$ is a face for some g , then g is a face-pairing isometry of $\mathcal{F}(\Gamma)$ in the sense that it maps a face isometrically to a face. At this point, we could take the quotient of $\mathcal{F}(\Gamma)$ by its face pairing isometries and obtain a manifold that is a covering space of M . However, we really want a fundamental domain of M , so we restrict $\mathcal{F}(\Gamma)$ further.

DEFINITION 14.19. A *vertical fundamental domain* for Γ_∞ is a connected convex fundamental domain for the action of Γ_∞ on \mathbb{H}^3 that is cut out by finitely many vertical geodesic planes in \mathbb{H}^3 .

For example, a vertical fundamental domain for the figure-8 knot is cut out by four vertical planes whose boundary on \mathbb{C} at infinity is the parallelogram bounding the triangles shown in figure 4.12.

DEFINITION 14.20. A *Ford domain* for M is the intersection of $\mathcal{F}(\Gamma)$ and a vertical fundamental domain for Γ_∞ .

A Ford domain is not canonical; that is, it is not uniquely defined for the manifold, because the choice of vertical fundamental domain is not unique. However, the equivariant Ford domain is canonical. For this reason, sometimes in the literature the Ford domain is actually defined to be $\mathcal{F}(\Gamma)$; this is the definition in [Bon09], for example. However, $\mathcal{F}(\Gamma)$ is not a finite sided region, and its interior maps to M in an infinite-to-one manner rather than a one-to-one manner, meaning it is not a fundamental domain for M . Thus we have chosen to define the Ford domain as in definition 14.20.

PROPOSITION 14.21. *Let \overline{M} be a compact orientable 3-manifold with a single torus boundary component whose interior admits a complete finite-volume hyperbolic structure. Then any Ford domain F for M is a convex finite-sided polyhedron, cut out by finitely many geodesic planes in \mathbb{H}^3 . Moreover, it is a fundamental domain for M , in the sense that M is obtained as a quotient of the Ford domain by face-pairing isometries.*

PROOF. Both the equivariant Ford domain and a vertical fundamental domain are convex, and thus their intersection is convex.

To see that F is a fundamental domain for M , we must prove that when we restrict the covering map $\mathbb{H}^3 \rightarrow \mathbb{H}^3/\Gamma \cong M$ to $F \subset \mathbb{H}^3$, the projection surjects onto M , and that no two points in the interior of F project to the same point of M .

First, note that if x is in the interior of F , then $x \in \mathcal{F}(\Gamma)$, so $g(x) \notin \mathcal{F}(\Gamma)$ for all $g \in \Gamma - \Gamma_\infty$. Since x also lies in the interior of a vertical fundamental domain V for the action of Γ_∞ , all $g(x) \notin V$ for all nontrivial $g \in \Gamma_\infty$. Thus $g(x)$ lies in F only if g is the identity, therefore no two points in the interior of F project to the same point under the covering projection $\mathbb{H}^3 \rightarrow M$.

Now we show that the image of F under the covering map surjects onto M . Choose a maximal cusp neighborhood for M , and let H be a horoball about infinity that projects onto the cusp. Let $x \in M$. Let δ be the minimal distance from x to the maximal cusp neighborhood in M . Then there exists

a lift \tilde{x} of x in \mathbb{H}^3 that is distance δ from H . Since this distance is minimal, it follows that \tilde{x} lies in $\mathcal{F}(\Gamma)$. There exists $w \in \Gamma_\infty$ such that $w\tilde{x}$ lies in V . Thus $w\tilde{x}$ lies in $\mathcal{F}(\Gamma) \cap V = F$, and $w\tilde{x}$ projects to x . So F is a fundamental domain for M .

Next we show that the Ford domain is a finite-sided polyhedron. First, remove a small embedded horoball neighborhood from the cusp of M to obtain a compact 3-manifold \overline{M} . The lift of the horoball neighborhood lifts to \mathbb{H}^3 ; remove it from F , and call the result \overline{F} . By lemma 14.14, for any x in \mathbb{H}^3 , there is a ball B_x centered at x meeting only finitely many isometric spheres. The set of all such balls for $x \in \overline{F}$ cover \overline{F} . Since F is a fundamental domain for M , these balls map to a set of balls covering the compact manifold \overline{M} . Thus there is a finite subcollection of balls covering \overline{M} , which lift to give a finite cover of \overline{F} . Then the total collection of these balls meet only finitely many faces of F . Thus F is finite sided.

Finally consider face-pairings. By definition, a face of V is paired to another face of V by an isometry $w \in \Gamma_\infty$. Any x in the interior of the intersection of that face with $\mathcal{F}(\Gamma)$ is mapped by w to the point $w(x)$ in $V \cap \mathcal{F}(\Gamma)$. So w is a face-pairing isometry of F .

If $x \in F$ lies in the interior of a face $I(g) \cap F$, then x is glued to $g(x)$ in $I(g^{-1})$ in the interior of a face in $\mathcal{F}(\Gamma)$. The face may be disjoint from V , but because V is a fundamental domain for the action of Γ_∞ , there exists some $w \in \Gamma_\infty$ such that $wg(x) \in V$. Thus $wg(x) \in I(g^{-1}w^{-1}) \cap F$. By continuity, the same w maps $g(y)$ to F for any y in a small neighborhood of x . Thus wg is a face-pairing isometry. \square

EXAMPLE 14.22. We can compute explicitly a Ford domain for M the figure-8 knot complement. From example 5.4 of chapter 5, we have a description of three generators of the holonomy group Γ of the figure-8 knot complement, namely

$$T_B = \frac{i}{\sqrt{\omega}} \begin{pmatrix} 1 & 1 \\ 1 & -\omega^2 \end{pmatrix}, \quad T_C = \begin{pmatrix} 1 & \omega \\ 0 & 1 \end{pmatrix}, \quad T_D = \begin{pmatrix} 2 & -1 \\ 1 & 0 \end{pmatrix},$$

where recall $\omega = \frac{1}{2} + i\frac{\sqrt{3}}{2}$ is a cube root of unity. The transformation T_C fixes the point at infinity, so it plays a part in defining a vertical fundamental domain V , but it does not give isometric spheres. Note isometric spheres corresponding to $T_B^{\pm 1}$ and $T_D^{\pm 1}$ all have radius 1. The center of $I(T_B^{-1})$ is 1, that of $I(T_B)$ is ω^2 , that of $I(T_D)$ is 2, and that of $I(T_D^{-1})$ is 0. These are equidistant to the full-sized horoballs of example 14.6, up to translation in Γ_∞ . Take a vertical fundamental domain V for M cut out by planes meeting \mathbb{C} as shown in figure 4.12. Then V has face-pairing isometries T_C and $T = \begin{pmatrix} 1 & 4 \\ 0 & 1 \end{pmatrix}$. The ten isometric spheres $I(T_D^{-1})$, $I(T_B^{-1})$, $I(T_D)$, $I(T_C^{-1}TT_B)$, $I(T(T_D^{-1}))$, and their translates under T_C all intersect V . In fact, along with V they cut out a Ford domain. See figure 14.5.

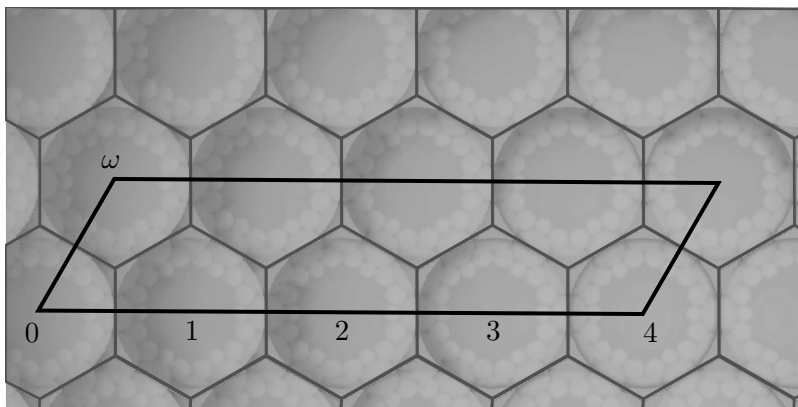


FIGURE 14.5. A Ford domain for the figure-8 knot complement. The vertical fundamental V domain meets \mathbb{C} in the parallelogram shown with vertices 0 , 4 , ω and $4 + \omega$. The isometric spheres intersect to form hexagon faces of the equivariant Ford domain $\mathcal{F}(\Gamma)$. The ford domain is the intersection $\mathcal{F}(\Gamma) \cap V$.

DEFINITION 14.23. Let $M \cong \mathbb{H}^3/\Gamma$ and $M' \cong \mathbb{H}^3/\Gamma'$ be one-cusped hyperbolic 3-manifolds, and let $\mathcal{F}(\Gamma)$ and $\mathcal{F}(\Gamma')$ be their respective equivariant Ford domains. Suppose there is a bijection between faces, edges, and vertices of $\mathcal{F}(\Gamma)$ and faces, edges, and vertices of $\mathcal{F}(\Gamma')$ such that:

- (1) An edge of $\mathcal{F}(\Gamma)$ is contained in a given face if and only if the corresponding edge of $\mathcal{F}(\Gamma')$ is contained in the corresponding face, and a vertex of $\mathcal{F}(\Gamma)$ is contained in a given edge if and only if the corresponding vertex of $\mathcal{F}(\Gamma')$ is contained in the corresponding edge.
- (2) A face f_1 of $\mathcal{F}(\Gamma)$ is mapped to a face f_2 by a parabolic translation in $\Gamma_\infty \leq \Gamma$ if and only if the face of $\mathcal{F}(\Gamma')$ corresponding to f_1 is mapped by a parabolic translation in $\Gamma'_\infty \leq \Gamma'$ to the face corresponding to f_2 .
- (3) A face pairing isometry of $\mathcal{F}(\Gamma)$ matches faces, edges, and vertices if and only if a face pairing isometry of $\mathcal{F}(\Gamma')$ matches corresponding faces, edges, and vertices.

Then the equivariant Ford domains $\mathcal{F}(\Gamma)$ and $\mathcal{F}(\Gamma')$ are said to be *combinatorially equivalent*.

THEOREM 14.24. *Suppose $M \cong \mathbb{H}^3/\Gamma$ and $M' \cong \mathbb{H}^3/\Gamma'$ are one-cusped hyperbolic 3-manifolds with combinatorially equivalent Ford domains $\mathcal{F}(\Gamma)$ and $\mathcal{F}(\Gamma')$. Then M and M' are isometric.*

In particular, if $M \cong S^3 - K$ and $M' \cong S^3 - K'$ are knot complements, then K and K' are isomorphic knots, up to reflection.

PROOF. Because $\mathcal{F}(\Gamma)$ and $\mathcal{F}(\Gamma')$ are combinatorially equivalent, the quotients $\mathcal{F}(\Gamma)/\Gamma$ and $\mathcal{F}(\Gamma')/\Gamma'$ are homeomorphic as 3-manifolds. Mostow–Prasad rigidity, theorem 6.1, then implies that the quotients are actually isometric.

If M and M' are knot complements, then the fact that they come from isomorphic knots follows from Gordon and Luecke’s knot complement theorem, theorem 0.4 [GL89]. \square

14.2.2. The case of multiple cusps. When there are multiple cusps, we still build a Ford domain by considering points closer to one cusp than another. However, there will be a choice involved. We will first give the definitions, then explain how the choices affect the domain.

Let $M \cong \mathbb{H}^3/\Gamma$ be a complete hyperbolic 3-manifold, and let C_0, \dots, C_k denote its cusps. Start by choosing a horoball neighborhood of all the cusps of M . The neighborhood does not necessarily need to be embedded for the definitions to work. In practice, however, we often consider a choice of maximal cusp neighborhood.

Lift the horoball neighborhood to the universal cover \mathbb{H}^3 . This gives a countable collection of horoballs in \mathbb{H}^3 , which will be disjoint if and only if the choice of horoball neighborhood is embedded in M . Apply an isometry of \mathbb{H}^3 so that the horoball H_0 about infinity projects to the cusp C_0 under the covering map.

Let $\Gamma_\infty \leq \Gamma$ denote the subgroup fixing the cusp at infinity. We may choose a vertical fundamental domain V_0 for the action of Γ_∞ , and we still have isometric spheres $I(g)$ for $g \in \Gamma - \Gamma_\infty$. These will form some of the faces of the Ford domain, but not all. In particular, isometric spheres only give points equidistant from lifts of the cusp C_0 . We also need to consider points equidistant from the horoball H_0 and lifts of cusps C_1, \dots, C_k . These are not isometric spheres, so must be defined separately.

For each C_j , $j = 1, \dots, k$, choose a horoball H_j such that the distance from H_0 to H_j is the distance from the cusp C_0 to C_j in M . For convenience, we may choose H_j such that its center lies inside the vertical fundamental domain V_0 . For a horoball H with center on \mathbb{C} , let $P(H)$ denote the set of points equidistant from H_0 and H . (Thus for $g \in \Gamma - \Gamma_\infty$, the isometric sphere $I(g)$ is the plane $P(g^{-1}(H_0))$.) Let $B(H)$ denote the open half ball bounded by $P(H)$, so $B(g^{-1}(H_0)) = B(g)$ in the notation of the previous subsection.

Define \mathcal{F}_0 to be the set

$$\mathcal{F}_0 = \mathbb{H}^3 - \left(\bigcup_{g \in \Gamma - \Gamma_\infty} B(g) \cup \bigcup_{j=1}^k \bigcup_{g \in \Gamma} B(g(H_j)) \right).$$

Define F_0 to be the set $\mathcal{F}_0 \cap V_0$.

Now repeat the entire construction above, only replacing C_0 with C_j . Thus we start by applying an isometry so that H_j is a horoball about infinity projecting to C_j . Define a vertical fundamental domain V_j , and obtain sets

\mathcal{F}_j and $F_j = \mathcal{F}_j \cap V_j$. Note that under the isometry taking C_j to the cusp at infinity, the sets \mathcal{F}_0 and F_0 created before are mapped to some other region of \mathbb{H}^3 whose interior will be disjoint from \mathcal{F}_j and F_j .

DEFINITION 14.25. Let M be a complete hyperbolic 3-manifold with cusps C_0, \dots, C_k . For each cusp, construct subsets \mathcal{F}_j and F_j of \mathbb{H}^3 as above. The (disjoint) union of the sets \mathcal{F}_j is the *equivariant Ford domain* \mathcal{F} . The (disjoint) union of the sets F_j is the *Ford domain* of M .

Observe that each F_j is a convex polyhedron. Faces of \mathcal{F} are paired by isometries of \mathbb{H}^3 that map the appropriate horoballs H_i, H_j to be equidistant from the given face.

Also note that the polyhedra F_j will depend on the choice of expansion of horoballs. An example is shown in figure 14.6 for the complement of the Borromean rings. The figures are adapted from SnapPy [CDGW16]. Three different choices of maximal cusp neighborhood are given, and their effect on the combinatorics of the corresponding subset \mathcal{F}_0 of the equivariant Ford domain is shown. At the top, the cusp C_0 has been chosen to be as large as possible. That is, first C_0 was expanded until it bumped itself, then C_1 and C_2 were expanded to meet C_0 . For this choice of maximal cusp neighborhood, the faces of \mathcal{F}_0 are squares oriented horizontally. In the middle, C_0 still has larger volume than that of C_1 and C_2 , but is not as large as possible. The faces of \mathcal{F}_0 are now octagons and squares. At the bottom, all three cusps have been chosen to have the same volume. The faces of \mathcal{F}_0 are squares again, but oriented on a diagonal. Akiyoshi has shown there are at most finitely many combinatorially inequivalent Ford domains for any given manifold [Aki01].

14.3. Canonical polyhedra

We now describe how to construct the canonical polyhedral decomposition of a finite volume 3-manifold.

Throughout this section, let $M \cong \mathbb{H}^3/\Gamma$ be a finite volume hyperbolic 3-manifold with a choice of maximal cusp neighborhood, and corresponding equivariant Ford domain \mathcal{F} .

We begin by describing the 1-cells, or edges of the polyhedral decomposition. Take a component \mathcal{F}_j of the equivariant Ford domain, embedded in \mathbb{H}^3 such that it contains a horoball H about infinity. Consider a face f of \mathcal{F}_j with nonempty interior. Points in the interior of f are exactly those points in \mathbb{H}^3 that are equidistant from H and from another horoball lift H' of a cusp of M . For each such face, take the geodesic from the center of H' on $\partial_\infty \mathbb{H}^3$ to ∞ . This geodesic is the *geometric dual* to the face f . For each face f of each \mathcal{F}_j , the geometric dual will be identified to a 1-cell of the canonical polyhedral decomposition. Two such geodesics are identified to the same 1-cell if they are identified by an element of Γ .

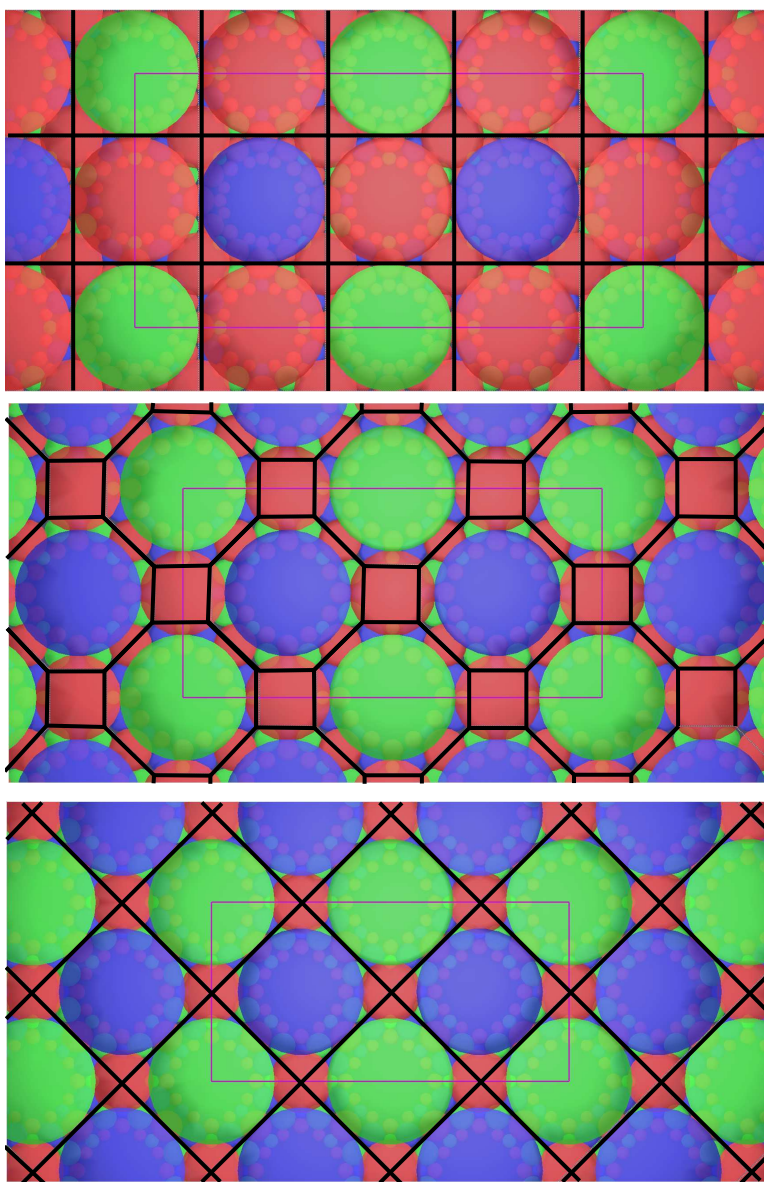


FIGURE 14.6. Three different Ford domains for the Borromean rings. The boundary of a vertical fundamental domain V_0 is in magenta. Faces of \mathcal{F}_0 have boundaries shown in black.

EXAMPLE 14.26. For the figure-8 knot complement, with equivariant Ford domain $\mathcal{F}(\Gamma)$ shown in figure 14.5, the geometric dual edges are those edges running from the points on \mathbb{C} at the centers of the hexagon faces to the point at infinity, intersecting the faces of the Ford domains in their centers.

REMARK 14.27. Note: A geometric dual edge does not necessarily intersect the face of \mathcal{F} that it is dual to, although the dual edges in the case of the figure-8 knot intersect their corresponding faces in example 14.26. For example, a geodesic may be the geometric dual to a face f_1 of the Ford domain, but the highest point of the Euclidean hemisphere containing f_1 might be covered by another face f_2 . Then the geometric dual to f_1 , which runs through this highest point, would not intersect f_1 . This phenomenon is not common, especially in the small examples that one sees using SnapPy, but it does occur in practice.

We now construct the 2-cells. Consider an edge e of \mathcal{F}_j with nonempty interior. The interior points on such an edge lie on faces f' and f'' of \mathcal{F}_j , where f' consists of points equidistant from H and a horoball H' , and where f'' consists of points equidistant from H and a horoball H'' . Denote the geometric dual of the face f' by γ' , and the geometric dual of the face f'' by γ'' . Thus γ' and γ'' are infinite geodesics running from H' to H and from H'' to H , respectively. Consider the vertical plane containing γ' and γ'' . Form a portion P of a 2-cell by taking the region of this plane lying between γ' and γ'' and its intersection with the exterior of the faces f' and f'' . For example, in figure 14.7, the lightly shaded region lying above two isometric spheres and running into infinity forms the portion P of the 2-cell. Two such portions of planes are identified if they are identified by a parabolic translation of Γ fixing the point at infinity.

The region P and its translates under Γ_∞ do not form the entire 2-cell; the 2-cell is formed by gluing portions of such regions P along their intersections with isometric spheres. Note that each P meets the faces f' and f'' at right angles. Form a 2-cell by gluing portions of planes via the face-pairing isometries of \mathcal{F}_j . That is, if f' is glued to \bar{f}' by a face-pairing isometry, then $P \cap f'$ is glued to \bar{f}' by the same isometry. Similarly for $P \cap f''$. In figure 14.7, the darker shaded regions form additional portions of the 2-cell; they are obtained by such gluings.

LEMMA 14.28. *The 2-cells constructed as above are totally geodesic ideal polygons with $n \geq 3$ sides, where n is the number of cusps equidistant from the image of the edge e in the component of the Ford domain \mathcal{F}_j of M .*

PROOF. Exercise 14.7. □

The totally geodesic ideal polygon thus constructed is the *geometric dual* of the edge e .

EXAMPLE 14.29. For the figure-8 knot complement, with equivariant Ford domain shown in figure 14.5, each portion P of a 2-cell lies over two faces of the Ford domain, running between their centers. A cross sectional view is shown on the left of figure 14.7. In this example, three distinct portions P glue to form an ideal triangle. Thus the 2-cells in this case are all ideal triangles.

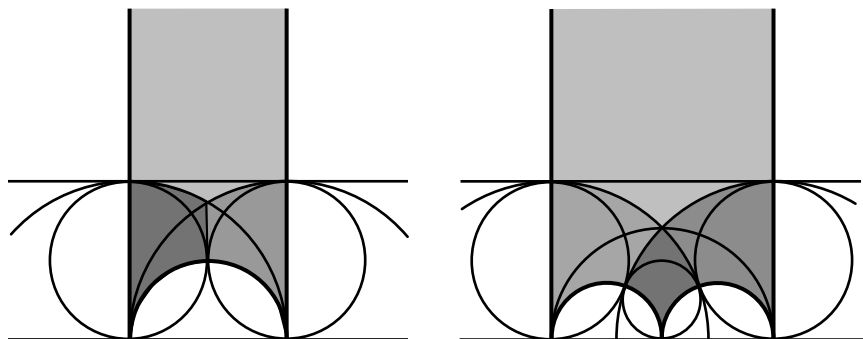


FIGURE 14.7. Left: Cross-sectional view of a 2-cell dual to an edge of the equivariant Ford domain for the figure-8 knot complement. Right: In different examples, the dual 2-cell may have more sides.

An example for an edge equidistant from more than three horoballs is shown on the right in figure 14.7.

As in the case of the 1-cells, two 2-cells are identified if they differ by an element of Γ .

Finally we construct the 3-cells. For each vertex of \mathcal{F}_j , there are finitely many adjacent edges of \mathcal{F}_j . The intersection of \mathcal{F}_j with the region bounded by the corresponding 2-cells forms a portion of a 3-cell C . The full 3-cell is formed by gluing $C \cap \partial\mathcal{F}_j$ by face-pairing isometries. The 3-cell is the *geometric dual* to the vertex. Again 3-cells are identified if they differ by an element of Γ . Note each 3-cell is bounded by a finite number of ideal polygons, thus it is an ideal polyhedron.

DEFINITION 14.30. The *canonical polyhedral decomposition* of M , or simply the *canonical decomposition* of M is the disjoint union of the 3-cells dual to the vertices of each \mathcal{F}_j , along with their ideal faces and ideal edges. The faces are paired by isometries of Γ .

THEOREM 14.31. *If M is a finite volume, orientable, cusped 3-manifold, with fixed embedded horoball neighborhood H of all cusps, then the canonical polyhedral decomposition associated with H decomposes M uniquely into a finite number of convex ideal polyhedra. That is, M is the quotient of the polyhedra with faces identified via face-pairing isometries, and the interiors of the polyhedra are mapped in a one-to-one manner to a subset of M .*

PROOF SKETCH. The fact that there are finitely many such polyhedra follows from the fact that Ford domains are finite sided. Convexity follows from the fact that the polyhedra are cut out by finitely many ideal polygons dual to the convex Ford domain. All translates of the polyhedra under Γ cover each \mathcal{F}_j , by their definition, thus the polyhedra project surjectively to M . If x lies in the interior of a polyhedron, projecting to some $y \in M$, then any other point \tilde{x} in a 3-cell projecting to y differs from x by an element of

Γ. By our definition of the 3-cells, it follows that the two 3-cells must agree. Thus x is the only point in the polyhedra that projects to y . \square

EXAMPLE 14.32. The 3-cells in the canonical polyhedral decomposition of the figure-8 knot are finite sided polyhedra whose faces are ideal triangles, by example 14.29. In fact, they are two regular ideal tetrahedra. The canonical polyhedral decomposition of the figure-8 knot is exactly the decomposition we obtained in chapter 1 and chapter 4.

THEOREM 14.33. *Suppose M and M' are hyperbolic 3-manifolds, each with a single cusp, and suppose M and M' have combinatorially equivalent canonical decompositions. Then M and M' are isometric.*

In particular, if M and M' are knot complements, then K and K' are equivalent knots, up to reflection.

PROOF. The canonical decomposition is geometrically dual to the Ford domain, and so this result follows from theorem 14.24. \square

In his thesis, Guéritaud showed that the canonical polyhedral decomposition of 2-bridge knots are the tetrahedra in the triangulation we described in chapter 10 [Gue06a]; see also [ASWY07]. There are a few other families of 3-manifolds whose canonical polyhedral decompositions are now known; for example Sakuma and Weeks find canonical polyhedra for some families of link complements using symmetry [SW95]. SnapPy computes canonical polyhedral decompositions of most reasonably sized 3-manifolds [CDGW16], but at the date of writing this book, such decompositions were not rigorously verified. In general it seems to be a difficult problem to determine canonical polyhedral decompositions of important families of link complements. For example, as of the writing of this book, the following is unknown, asked as a question in [SW95].

CONJECTURE 14.34. *For any hyperbolic alternating knot and any alternating diagram of the knot, each crossing arc is isotopic to an edge of the canonical polyhedral decomposition of the knot complement.*

In fact, to date it is not even known if crossing arcs of alternating knots are isotopic to geodesics in general.

14.4. Exercises

EXERCISE 14.1. Prove that a discrete subgroup of $\mathrm{PSL}(2, \mathbb{C})$ is countable.

EXERCISE 14.2. Prove that a complete hyperbolic surface contains an embedded neighborhood of its cusps that lifts to countably many horodisks in \mathbb{H}^2 .

EXERCISE 14.3. Prove that the definition of the set $I(g)$ is independent of choice of horosphere H .

EXERCISE 14.4. Prove corollary 14.8, that the volume of a cusp component in a maximal cusp neighborhood of M is at least $\sqrt{3}/4$, and that if M has only one cusp, then the volume of a maximal cusp neighborhood is at least $\sqrt{3}/2$.

Hints: If desired, you may use exercise 2.13. You may also apply the following theorem of Böröczky [Bör78], generalizing theorem 8.45.

THEOREM 14.35 (Böröczky density of disks in the torus). *Let D be a collection of disks of the same radius, embedded disjointly in the torus T . Then*

$$\frac{\text{area}(T \cap D)}{\text{area}(T)} \leq \frac{\pi}{2\sqrt{3}}.$$

EXERCISE 14.5. Extend the definition of a Ford domain to complete hyperbolic surfaces, first for those with one cusp, then generalize to finitely many cusps. Using the natural extension of the definition of a fundamental domain to hyperbolic surfaces, prove that the object you have defined is a convex fundamental domain for the surface.

EXERCISE 14.6. This exercise uses SnapPy [CDGW16] to investigate the combinatorics of Ford domains associated with different choices of maximal cusp neighborhoods. The manifold `m125` in the SnapPy census is a hyperbolic manifold with two cusps, isometric to the complement of the $(-2,3,8)$ -pretzel link.

- (1) Using SnapPy, find at least five different combinatorially inequivalent Ford domains for `m125`.
- (2) Find a Ford domain for `m125` where the dual canonical decomposition is a triangulation. Find a Ford domain where it is not a triangulation.

EXERCISE 14.7. Prove lemma 14.28: that the 2-cell dual to an edge of \mathcal{F} is a totally geodesic ideal polygon with $n \geq 3$ sides, where n is the number of cusps equidistant from the projection of the edge to M .

Algebraic Sets and the A -Polynomial

In this chapter, we introduce a polynomial invariant of a knot that is obtained from hyperbolic geometry. There are three closely related polynomials that appear in the literature and in calculations. We introduce all three in this chapter and discuss the relationships between them. We need to introduce a small amount of algebraic geometry, to consider how hyperbolic structures deform. M. Culler and P. Shalen were the first to investigate this material [CS83]. The A -polynomial was originally introduced in [CCG⁺94]. However, we start with a slightly different perspective.

15.1. The gluing variety

Suppose M is a 3-manifold with a topological ideal triangulation, as in definition 4.1. We have seen that associated with each ideal tetrahedron is an edge invariant, namely a complex number $z(e)$ corresponding to an edge of the tetrahedron, as in definition 4.4, with all edge invariants of a tetrahedron satisfying the relations of lemma 4.6. Finally, we have seen in theorem 4.7 that a choice of edge invariants gives a hyperbolic structure on M if and only if the $z(e)$ satisfy the edge gluing equations.

Suppose that n ideal tetrahedra form the topological ideal triangulation of M . Then we obtain $3n$ edge invariants: z_1, \dots, z_n , as well as $z'_i = 1/(1-z_i)$ and $z''_i = (z_i - 1)/z_i$ for $i = 1, \dots, n$. The edge gluing equations tell us that the product of those edge invariants that glue to the same edge of M must be 1. Clearing denominators, each edge gluing equation becomes a polynomial equation in z_1, \dots, z_n .

DEFINITION 15.1. An *affine algebraic set* is a subset of \mathbb{C}^N that is defined as the set of zeros of a system of polynomial equations with coefficients in \mathbb{C} and N variables.

The union of two affine algebraic sets is an affine algebraic set, and the intersection of arbitrarily many affine algebraic sets is an affine algebraic set (exercise 15.1). We define a topology on \mathbb{C}^N , called the *Zariski topology*, by taking affine algebraic sets to be closed sets. As a very simple preliminary example, the subset of \mathbb{C}^2 defined by $xy = 0$ is an affine algebraic set.

DEFINITION 15.2. An affine algebraic set is *reducible* if it can be expressed as the union of two proper affine algebraic sets. It is *irreducible* if not.

It is a corollary of the Hilbert basis theorem (says Shalen [Sha02]) that any affine algebraic set is a finite union of irreducible affine algebraic sets; we call these the *irreducible components*.

An irreducible affine algebraic set is called an *affine variety*.

The affine algebraic set defined by $xy = 0$ is not an affine variety; it is reducible, with irreducible affine algebraic sets defined by polynomials $x = 0$ and $y = 0$. These form irreducible components. Note they are not disjoint. In general, irreducible components of affine algebraic sets are not necessarily disjoint.

COROLLARY 15.3. Let \mathcal{T} be a topological ideal triangulation of a 3-manifold M , with n ideal tetrahedra. Then the set of points in \mathbb{C}^n satisfying the edge gluing equations associated with \mathcal{T} forms an affine algebraic set. \square

DEFINITION 15.4. Suppose M has ideal triangulation \mathcal{T} made up of n ideal tetrahedra (so n gluing equations by exercise 4.2). The *gluing variety* associated with \mathcal{T} , denoted $\mathcal{D}(\mathcal{T})$, is the affine algebraic subset of $\mathbb{C}^n \times \mathbb{C}$ consisting of points (z_1, \dots, z_n, t) satisfying the edge gluing equations as in corollary 15.3, as well as the equation

$$t \prod_{i=1}^n z_i(1 - z_i) = 1.$$

This last equation is called the *degeneracy equation*, and ensures that the parameters z_i do not degenerate to 0 or 1.

REMARK 15.5. Degeneracy is handled differently by different authors in the literature. For example, rather than including one degeneracy equation, some authors require that for each i , the equations

$$z_i(1 - z_i'') = 1, \quad z_i'(1 - z_i) = 1, \quad z_i''(1 - z_i') = 1$$

hold, in addition to gluing equations. This also rules out $z_i = 0, 1$.

Similarly, some authors require that for each i , the following equations hold in addition to the gluing equations:

$$z_i z_i' z_i'' = -1 \quad \text{and} \quad z_i + (z_i')^{-1} - 1 = 0.$$

Encoded in these equations are the relationships between z_i , z_i' , and z_i'' from lemma 4.6. Again a solution does not allow $z_i = 0, 1$.

Note that the gluing variety is an affine algebraic set, but it is not necessarily irreducible. In particular, the gluing variety may not satisfy the definition of an affine variety, so the terminology is somewhat misleading.

In the case that M has a complete hyperbolic structure, and \mathcal{T} can be given a collection of edge invariants to form a geometric ideal triangulation for this structure, as in definition 4.3, then the gluing variety is nonempty.

That is, there is an irreducible component of the gluing variety that contains this complete hyperbolic structure. The irreducible component containing the complete hyperbolic structure (when it exists) really is an affine variety.

DEFINITION 15.6. Suppose \mathcal{T} is an ideal triangulation of M that can be assigned edge invariants to form a geometric ideal triangulation, as in definition 4.3. Then the irreducible component of $\mathcal{D}(\mathcal{T})$ containing the geometric triangulation is called the *canonical component* of the gluing variety, and it is denoted $\mathcal{D}_0(\mathcal{T})$.

Some examples are in order.

EXAMPLE 15.7 (Figure-8 knot). Take the figure-8 knot complement with the ideal triangulation of chapter 1. This has two ideal tetrahedra, with edge invariants determined by z and w in \mathbb{C} . The two edge gluing equations of the figure-8 knot actually both give a single polynomial equation, which we calculated in equation (4.1):

$$(15.1) \quad z(z-1)w(w-1) = 1, \quad \text{or} \quad z^2w^2 - z^2w - zw^2 + zw - 1 = 0.$$

Note that in this case, the degeneracy equation $tz(1-z)w(1-w) = 1$ becomes simply $t = 1$, and so the gluing variety is therefore the set of points $(z, w, 1)$ in $\mathbb{C}^2 \times \mathbb{C}$ satisfying equation (15.1).

Note that the complete hyperbolic structure occurs when

$$z = w = (1 + i\sqrt{3})/2,$$

as shown in example 4.16. The triple

$$\left((1 + i\sqrt{3})/2, (1 + i\sqrt{3})/2, 1 \right) \in \mathbb{C}^2 \times \mathbb{C}$$

satisfies equation (15.1).

EXAMPLE 15.8 (6_1 knot). In chapter 4, we found a triangulation \mathcal{T}_1 of the 6_1 knot with five tetrahedra. There is also a triangulation \mathcal{T}_2 of the 6_1 knot with only four tetrahedra, for example this triangulation is stored in the SnapPy database of manifold [CDGW16]. Note that the gluing variety corresponding to \mathcal{T}_1 is a subset of \mathbb{C}^6 , while that corresponding to \mathcal{T}_2 is a subset of \mathbb{C}^5 . Thus even though the triangulations give the same manifold, the gluing varieties are different, living in different spaces.

EXAMPLE 15.9 (Triangulation with inessential edge). Dunfield notes that the figure-8 knot complement admits a topological ideal triangulation \mathcal{T} consisting of five tetrahedra where one of the edges E is 1-valent: it meets only one of the tetrahedra [Dun05]. Moreover, this edge E is *inessential*, meaning for any horoball neighborhood H of the knot, the arc $E \cap (S^3 - H)$ is homotopic rel endpoints $E \cap H$ into ∂H . For this triangulation \mathcal{T} , note that the edge gluing equation corresponding to the inessential edge is the equation $z_1 = 1$. Because it is impossible for this equation to hold simultaneously with the degeneracy equation, for this triangulation the gluing variety $\mathcal{D}(\mathcal{T})$ is empty.

REMARK 15.10. Suppose M is the interior of a compact manifold with torus boundary. Segerman and Tillmann showed that for any ideal triangulation \mathcal{T} of M , the gluing variety associated with \mathcal{T} is nonempty if and only if all edges in the triangulation are essential [ST11].

15.1.1. The A_{Hyp} -polynomial. We now describe a two-variable polynomial $A_{\text{Hyp}}(\ell, m)$ associated with any triangulated knot complement, or indeed any triangulated 3-manifold that is the interior of a compact manifold with a single torus boundary component. It was introduced by Champanerker in [Cha03], and there related to a more common polynomial, which we will describe later in this chapter. For now, we have the tools to understand the A_{Hyp} -polynomial and compute examples, so we do this first.

For a fixed triangulation \mathcal{T} , the gluing variety $\mathcal{D}(\mathcal{T})$ is defined using edge gluing equations only. Recall that we also have two completeness equations for each cusp, by proposition 4.15. That is, given a knot complement $S^3 - K$, with meridian $[\mu]$ and longitude $[\lambda]$, for $[\mu], [\lambda] \in \pi_1(\partial N(K))$, there are associated equations $H(\mu)$ and $H(\lambda)$, which are rational functions in the z_i . Define a map $\mathcal{H}: \mathcal{D} \rightarrow \mathbb{C} \times \mathbb{C}$ by

$$\mathcal{H}(z_1, \dots, z_n) = (H(\lambda)(z_1, \dots, z_n), H(\mu)(z_1, \dots, z_n)) = (\ell, m).$$

DEFINITION 15.11. Let Y_i be an irreducible component of $\mathcal{D}(\mathcal{T})$ for which the closure of $\mathcal{H}(Y_i)$ in $\mathbb{C} \times \mathbb{C}$ (in the Zariski topology) is an affine algebraic set, and let Z be the union of all such components. The image of Z under \mathcal{H} is called the *holonomy variety* with respect to the triangulation \mathcal{T} . The defining polynomial of the closure of the image is denoted by $A_{\text{Hyp}}^{\mathcal{T}}(\ell, m)$. We occasionally omit the notation \mathcal{T} when the triangulation is understood. The polynomial is called the *A_{Hyp} -polynomial* or *hyperbolic A -polynomial*.

EXAMPLE 15.12 (Figure-8 knot). For \mathcal{T} the usual two tetrahedra triangulation of the figure-8 knot K , the $A_{\text{Hyp}}^{\mathcal{T}}$ -polynomial satisfies equation (15.1) as well as two rational equations in m and ℓ that come from the completeness equations. We computed completeness equations in example 4.14, for curves α and β . The curve β is the meridian of the figure-8 knot. The curve α generates $\pi_1(\partial N(K))$ along with β , but it is not the standard longitude as defined in remark 6.9. Still, we may use it to compute a polynomial. That is, we require

$$m = z_2^{-1}w_1 = (1 - z)w, \quad \text{and}$$

$$\ell = \left(\frac{z_2 z_3}{w_2 w_3} \right)^2 = \frac{1}{(1 - z)^2} \frac{(z - 1)^2 (1 - w)^2}{z^2} \frac{w^2}{1} \frac{w^2}{(w - 1)^2} = \frac{w^2}{z^2}$$

Finding the polynomial A_{Hyp} , as an equation in m and ℓ only, is now a problem in elimination theory. One way to solve it is to form an ideal generated by the above equations in the ring $\mathbb{Z}[z, w, \ell, m]$ and compute a Groebner basis that eliminates z and w using tools from computational

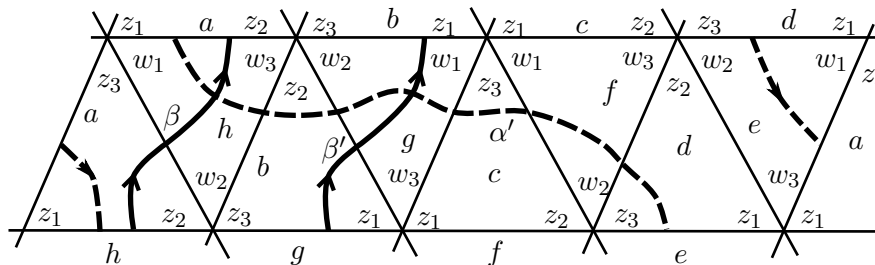


FIGURE 15.1. The cusp triangulation of the figure-8 knot complement, along with isotopic meridians β and β' , and a longitude α' .

algebraic geometry. For our examples, we did the latter, using Mathematica. The following command returns a polynomial in m and ℓ .

```
system := {z*(z-1)*w*(w-1)==1, M==w*(1-z), L*z^2==w^2};
elim := {z,w}; keep := {M,L};
GB := GroebnerBasis[system, keep, elim];
Print[GB];
```

This computation yields the following 2-variable polynomial:

$$A_{\text{Hyp}}(\ell, m) = \ell - 2\ell m - 3\ell m^2 - \ell^2 m^2 + 2\ell m^3 + 6\ell m^4 + 2\ell m^5 - m^6 - 3\ell m^6 - 2\ell m^7 + \ell m^8.$$

There were several choices made in the last example, particularly concerning representatives for the curves that give the completeness equations. We could change these in several different ways.

In the cusp triangulation of the figure-8 knot, reproduced in figure 15.1, a representative β for the meridian was chosen to run from the bottom of the triangle labeled a , across the triangle labeled h , back to the triangle labeled a , giving $H(\beta) = w_1/z_2$. We could have chosen a parallel curve, for example the curve β' running from the base of b , across g to the base of b , giving the curve $H(\beta') = w_2/z_1$.

Recall that in chapter 4, to define $H([\gamma])$ we require that a curve γ on a cusp triangulation cuts off a single corner of each triangle it enters. Such a curve is called a *normal curve*.

PROPOSITION 15.13. *Suppose $\alpha, \alpha' \in [\lambda]$ are distinct normal curves in the homotopy class of λ . Then the polynomial obtained by replacing $H(\alpha)$ by $H(\alpha')$ leaves A_{Hyp} unchanged. Similarly for $[\mu]$.*

PROOF. This follows from exercise 4.11: $H([\alpha])$ is independent of choice of α . The reason why is that if normal curves α and α' are ambient isotopic on a triangulated torus, then they differ by sliding past edges of the triangulation. Because the product of all tetrahedron edge parameters z_i meeting at an edge is 1, and the edge gluing equations are satisfied for the parameters

z_i , it follows that the two polynomials in the definition of A_{Hyp} will differ by a factor of 1. \square

We also could have chosen a different basis for $H_1(\partial N(K))$. For example, if α' denotes the standard longitude of the figure-8 knot, shown in figure 15.1, then it can be shown that

$$H(\alpha') = z_1^{-1} \cdot w_3 \cdot z_2 \cdot w_3^{-1} \cdot z_3 \cdot w_2^{-1} \cdot z_3^{-1} \cdot w_1.$$

Changing the basis for $H_1(\partial N(K))$ does affect A_{Hyp} , but in a well-understood way.

PROPOSITION 15.14. *Suppose p, q, r, s are integers satisfying $ps - rq = 1$, so that $\langle \ell^p m^q, \ell^r m^s \rangle$ is another basis for $H_1(\partial N(K))$. Then there exist integers a, b such that*

$$A_{\text{Hyp}}(\ell^p m^q, \ell^r m^s) = \pm \ell^a m^b A_{\text{Hyp}}(\ell, m).$$

EXAMPLE 15.15. The standard longitude of the figure-8 knot can be shown to be represented by the curve α' of figure 15.1, which is isotopic to $\alpha\beta^2$. Replacing α by α' yields the polynomial:

$$\begin{aligned} A_{\text{Hyp}}'(\ell, m) := & \ell - 2\ell m - 3\ell m^2 + 2\ell m^3 - m^4 + 6\ell m^4 \\ & - \ell^2 m^4 + 2\ell m^5 - 3\ell m^6 - 2\ell m^7 + \ell m^8. \end{aligned}$$

Note that this new polynomial satisfies $A_{\text{Hyp}}'(\ell, m) = m^{-2} A_{\text{Hyp}}(\ell m^2, m)$.

15.2. Representations of knots

The original A -polynomial was defined in [CCG⁺94] using representations of the fundamental group of a knot complement into the group $\text{SL}(2, \mathbb{C})$. In this section, we work our way up to the original definition of the A -polynomial. Our goals are first, to give a taste of the interesting mathematics along the way, but more importantly, to relate the polynomial A_{Hyp} to the original A -polynomial.

15.2.1. Wirtinger presentation. We take a bit of a detour in this subsection, to recall a few important results on presentations of knot groups. The tools we need follow almost immediately from the *Wirtinger presentation*, which we review now. See also [Rol90].

To obtain the presentation, start with a diagram of the knot, which we view as a collection of arcs, with each arc starting and ending at undercrossings and running along only overcrossings (if any) between them. To simplify the discussion, and to fix notation, choose an orientation of the knot (either orientation is fine). We say that a crossing is *positive* or *negative* based on the orientation of the arcs at the crossing, as in figure 15.2.

Now each arc a_i of the diagram is oriented. There will be one generator g_i of the fundamental group for each arc a_i ; the generator can be viewed as a loop beginning at a basepoint that lies high above the plane of projection, looping around a_i in a positive direction, then running back to the basepoint.

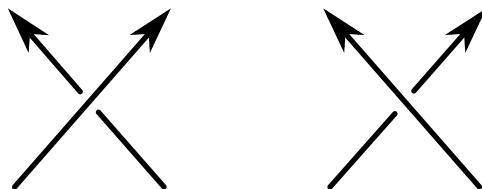


FIGURE 15.2. A positive crossing (left), and a negative crossing (right).

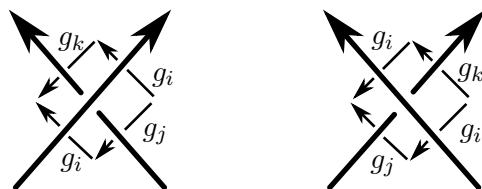


FIGURE 15.3. Relators for positive (left) and negative (right) crossings

Relators for the group presentation come from crossings, as follows. Suppose arc a_i runs along an overcrossing, meeting endpoints of arcs a_j and a_k at the crossing. If it is a positive crossing, then we have the relation $g_j g_i g_k^{-1} g_i^{-1} = 1$. If it is a negative crossing, we have instead $g_j g_i^{-1} g_k^{-1} g_i = 1$. See figure 15.3.

THEOREM 15.16 (Wirtinger presentation). *If K has a diagram with n crossings, then the group $\langle g_1, \dots, g_n \mid r_1, \dots, r_n \rangle$ obtained as above forms a presentation for the fundamental group of the knot complement. Moreover, one of the relators is redundant and can be removed from the presentation.*

PROOF. The proof is a standard exercise in algebraic topology, using the Seifert–Van Kampen theorem. We include it as exercise 15.3. \square

We give a few immediate corollaries.

COROLLARY 15.17. *The first homology group of a knot complement is always isomorphic to \mathbb{Z} , generated by (the class of) the meridian.*

PROOF. The first homology group $H_1(S^3 - K)$ is the abelianization of the fundamental group $\pi_1(S^3 - K) \cong \langle g_1, \dots, g_n \mid r_1, \dots, r_n \rangle$. Under the abelianization, each relator becomes $g_j = g_k$. Thus the presentation reduces to $\langle g_1, \dots, g_n \mid g_1 = \dots = g_n \rangle \cong \mathbb{Z}$, generated by the class of the meridian g_1 . \square

Note that each generator of the Wirtinger presentation is a curve that bounds a disk in S^3 , and can be isotoped to an embedded curve on the boundary of a neighborhood of the knot.

Generators of the Wirtinger presentation are meridians (definition 11.4). This leads to another corollary.

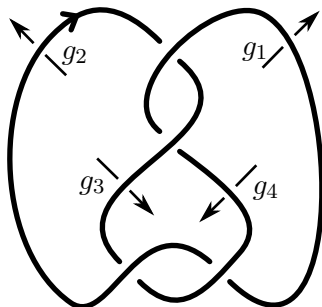


FIGURE 15.4. Generators of the fundamental group of the figure-8 knot complement

COROLLARY 15.18. *Let K be a knot whose complement admits a hyperbolic structure. Then the holonomy group of the complement of K has a presentation in which all generators are parabolic.*

Recall from definition 3.11 that the holonomy group is the image of the holonomy map $\rho: \pi_1(S^3 - K) \rightarrow \mathrm{PSL}(2, \mathbb{C})$, encoding the hyperbolic structure.

PROOF OF COROLLARY 15.18. Each generator of the Wirtinger presentation is a meridian. Each meridian is mapped by the holonomy map to an element of $\mathrm{PSL}(2, \mathbb{C})$ that commutes with a longitude. Then corollary 5.14 ($\mathbb{Z} \times \mathbb{Z}$ subgroups) implies that meridian and longitude are mapped to parabolic elements fixing the same point on $\partial\mathbb{H}^3$. \square

LEMMA 15.19. *Given a Wirtinger presentation of the fundamental group of a knot complement, we may compute the longitude as a product of generators as follows.*

- (1) *Beginning on an arc a_k of the knot, travel along it.*
- (2) *Write g_i when traversing an undercrossing under arc a_i in the positive direction, and write g_i^{-1} when traversing in the negative direction.*
- (3) *Finally, multiply by g_k^p where the power p is chosen such that the total exponent sum is zero.*

PROOF. The loop obtained as the product of generators corresponding to undercrossings as above will be homotopic to some longitude. We want to ensure it is homologically trivial. Consider its image in the abelianization of the fundamental group $H_1(S^3 - K) \cong \mathbb{Z}$. Each g_i maps to the generator g of \mathbb{Z} in homology. Therefore if the sum of the exponents in the product is zero, the image of the element in homology is trivial. \square

EXAMPLE 15.20. We use the Wirtinger presentation to compute the fundamental group of the figure-8 knot complement. See figure 15.4.

The generators are g_1, g_2, g_3, g_4 . The relators are

$$g_2 g_1^{-1} g_3^{-1} g_1 = 1 \quad g_4 g_3^{-1} g_1^{-1} g_3 = 1 \quad g_3 g_2 g_4^{-1} g_2^{-1} = 1 \quad g_1 g_4 g_2^{-1} g_4^{-1} = 1.$$

Use the first and third equations to eliminate g_3 and g_4 , respectively. Substitute into the fourth equation to obtain the single relation

$$g_1 g_2^{-1} g_1 g_2 g_1^{-1} g_2 = g_2^{-1} g_1 g_2 g_1^{-1} g_2 g_2.$$

Choose the meridian M to be g_1 .

Now starting on the arc of g_1 (right side of the diagram), traverse the knot by running up the arc, obtaining a longitude of the form

$$\begin{aligned} L &= g_3 g_2^{-1} g_1 g_4^{-1} \\ &= (g_1 g_2 g_1^{-1}) g_2^{-1} g_1 (g_2^{-1} g_1 g_2^{-1} g_1^{-1} g_2). \end{aligned}$$

Note that the sum of exponents in the example is zero, so this is the homologically trivial longitude.

15.2.2. Representation space and character varieties. In this subsection, we discuss representations of fundamental groups of 3-manifolds, particularly knot complements. We will only touch upon some of the details here; see [Sha02] for a more comprehensive survey.

Suppose M is a 3-manifold that is the interior of the compact manifold \overline{M} with a single torus boundary component, and suppose that M admits an ideal triangulation \mathcal{T} . Then associated to M is a gluing variety. Any point in the gluing variety gives a representation of $\pi_1(M)$ into $\mathrm{PSL}(2, \mathbb{C})$, as follows. A point in the gluing variety gives a collection of edge parameters for the tetrahedra in \mathcal{T} that satisfy the edge gluing equations. These lead to a (G, X) -structure on M , where $G = \mathrm{PSL}(2, \mathbb{C})$ and $X = \mathbb{H}^3$, by setting each tetrahedron in \mathcal{T} to be the ideal hyperbolic tetrahedron with given edge parameters. Then there is an associated developing map as in definition 3.9. A group element $\alpha \in \pi_1(M)$ determines a holonomy element $g_\alpha \in \mathrm{PSL}(2, \mathbb{C})$, as in definition 3.11. We have seen that the holonomy gives a homomorphism $\rho: \pi_1(M) \rightarrow \mathrm{PSL}(2, \mathbb{C})$. Thus holonomy is a representation

$$\rho: \pi_1(M) \rightarrow \mathrm{PSL}(2, \mathbb{C}) \cong \mathrm{SL}(2, \mathbb{C}) / \pm \mathrm{Id}.$$

In fact, the original study of A -polynomials in [CCG⁺94] considered representations to $\mathrm{SL}(2, \mathbb{C})$ rather than $\mathrm{PSL}(2, \mathbb{C})$, to avoid certain difficulties that arise. We begin with this perspective as well.

As usual, we focus on 3-manifolds that arise as knot complements. The following ensures that we have interesting representations to work with.

PROPOSITION 15.21. *Any representation $\rho: \pi_1(S^3 - K) \rightarrow \mathrm{PSL}(2, \mathbb{C})$ lifts to two representations $\tilde{\rho}, \tilde{\rho}': \pi_1(S^3 - K) \rightarrow \mathrm{SL}(2, \mathbb{C})$.*

PROOF. Let $\langle g_1, \dots, g_n \mid r_1, \dots, r_n \rangle$ be a Wirtinger presentation for $\pi_1(S^3 - K)$. Starting with g_1 , the representation ρ assigns $\rho(g_1)$ an element of $\mathrm{PSL}(2, \mathbb{C})$. This lifts to two matrices, say A_1 and $-A_1$ in $\mathrm{SL}(2, \mathbb{C})$. Choose $\tilde{\rho}(g_1) = A_1$, and $\tilde{\rho}'(g_1) = -A_1$. Now consider the arc a_1 of the knot diagram corresponding to the generator g_1 . Follow that arc to its endpoint. This will be an undercrossing, with an associated relator $g_1 = g_j^{\pm 1} g_k g_j^{\mp 1}$. Thus there is a unique choice for $\tilde{\rho}(g_k)$ and $\tilde{\rho}'(g_k)$. Continue along the arc

associated with g_k , obtaining a unique choice for the representations at its endpoint. Continuing in this manner, we traverse the entire knot, and obtain a unique choice for each generator, obtaining two well-defined lifts $\tilde{\rho}$ and $\tilde{\rho}'$. \square

In fact, it can be shown that for any complete hyperbolic manifold M the holonomy representation always lifts to a representation into $\mathrm{SL}(2, \mathbb{C})$ [CS83], but we only present the result above on knot complements.

We now consider representations of a group G into $\mathrm{SL}(2, \mathbb{C})$.

Suppose G has finite presentation $\langle g_1, \dots, g_n \mid r_1, \dots, r_m \rangle$. Then a representation $\rho: G \rightarrow \mathrm{SL}(2, \mathbb{C})$ is determined by $(\rho(g_1), \dots, \rho(g_n))$, each of which is a matrix in $\mathrm{SL}(2, \mathbb{C})$:

$$\rho(g_i) = \begin{pmatrix} a_i & b_i \\ c_i & d_i \end{pmatrix}.$$

We therefore may view the space of representations $R_{\mathrm{SL}}(G)$ as a subset of the complex space \mathbb{C}^{4n} .

Any representation of G must satisfy the relators. Each relator r_i is a word in the generators of G . Let $r_i(\rho(g_1), \dots, \rho(g_n))$ be the word with $\rho(g_j)^{\pm 1}$ substituted for each $g_j^{\pm 1}$ in r_i . Then

$$(a_1, b_1, c_1, d_1, \dots, a_n, b_n, c_n, d_n) \in \mathbb{C}^{4n}$$

lies in $R_{\mathrm{SL}}(G)$ if and only if the following hold:

$$(15.2) \quad a_i d_i - b_i c_i = 1 \quad \text{for } i = 1, \dots, n,$$

(15.3)

$$r_j \left(\begin{pmatrix} a_1 & b_1 \\ c_1 & d_1 \end{pmatrix}, \dots, \begin{pmatrix} a_n & b_n \\ c_n & d_n \end{pmatrix} \right) = \begin{pmatrix} 1 & 0 \\ 0 & 1 \end{pmatrix} \quad \text{for } j = 1, \dots, m.$$

The equations in (15.2) come from the determinant condition, to ensure each matrix $\begin{pmatrix} a_i & b_i \\ c_i & d_i \end{pmatrix}$ lies in $\mathrm{SL}(2, \mathbb{C})$.

The equations in (15.3) come from the relators; we claim that each such equation gives four polynomial equations in the variables $\{a_i, b_i, c_i, d_i\}_{i=1}^n$. To see this, in the word on the left of (15.3), replace each instance of $\begin{pmatrix} a_i & b_i \\ c_i & d_i \end{pmatrix}^{-1}$ with $\begin{pmatrix} d_i & -b_i \\ -c_i & a_i \end{pmatrix}$. Then matrix multiplication, followed by setting each position in the matrix on the left of (15.3) equal to the corresponding position in the identity matrix on the right of (15.3) gives four polynomial equations for each relator.

PROPOSITION 15.22. *The space $R_{\mathrm{SL}}(G)$ consisting of representations of G into $\mathrm{SL}(2, \mathbb{C})$ is an affine algebraic set.*

PROOF. By the above discussion, a point in \mathbb{C}^{4n} lies in $R_{\mathrm{SL}}(G)$ if and only if it satisfies the polynomial equations coming from (15.2), and the polynomial equations coming from each entry of each matrix equation (15.3). \square

DEFINITION 15.23. For G a finitely presented group, its *representation variety* is the affine algebraic set $R_{\text{SL}}(G)$.

Notice that a different presentation of G will have different relators, and hence different polynomial equations. However, we will see that the corresponding affine algebraic sets are not very different in this case, which we formalize with the following definition.

DEFINITION 15.24. A *polynomial map* is a map completely defined by polynomials. A *morphism* between affine algebraic sets is a polynomial map from one to the other. It is an isomorphism if it is bijective and its inverse function is also a morphism.

PROPOSITION 15.25. *Suppose G has presentations*

$$G = \langle g_1, \dots, g_n \mid r_1, \dots, r_m \rangle = \langle h_1, \dots, h_k \mid s_1, \dots, s_\ell \rangle.$$

Then the affine algebraic sets $R_{\text{SL}}^1(G)$ and $R_{\text{SL}}^2(G)$ corresponding to the two presentations are isomorphic.

PROOF. We may write each h_i as a word in the generating set g_1, \dots, g_n ; denote this by $h_i = w_i(g_1, \dots, g_n)$. Define a map $\phi: R_{\text{SL}}^1(G) \rightarrow R_{\text{SL}}^2(G)$ by setting $\phi(\rho)$ to be the representation defined on the generators h_1, \dots, h_k by $\phi(\rho)(h_i) = w_i(\rho(g_1), \dots, \rho(g_n))$. This map only involves multiplication and addition of matrix coordinates, hence it is completely defined by polynomials, and hence the map is a morphism of affine algebraic sets. By symmetry, we also have a polynomial map $\psi: R_{\text{SL}}^2(G) \rightarrow R_{\text{SL}}^1(G)$ defined similarly. Then ϕ and ψ are inverses; these are isomorphisms of affine algebraic sets. \square

EXAMPLE 15.26. The space $R_{\text{SL}}(\pi_1(S^3 - K))$ for any knot K will always contain a simple irreducible affine algebraic set, which we now describe.

Recall that the abelianization of the fundamental group of any knot complement is $\mathbb{Z} = H_1(S^3 - K)$, generated by the (homology class of the) meridian (corollary 15.17). Thus any representation of \mathbb{Z} into $\text{SL}(2, \mathbb{C})$ gives an induced representation of $\pi_1(S^3 - K)$ into $\text{SL}(2, \mathbb{C})$ via

$$\pi_1(S^3 - K) \rightarrow \mathbb{Z} \rightarrow \text{SL}(2, \mathbb{C}).$$

Any such representation is called an *abelian representation*.

Note that the standard longitude λ is trivial in $H_1(S^3 - K)$. Thus for any abelian representation ρ , we will have $\rho(\lambda) = \text{Id}$. On the other hand, the meridian μ can be mapped to any element of $\text{SL}(2, \mathbb{C})$.

We claim that abelian representations form an affine algebraic set as a subset of $R_{\text{SL}}(\pi_1(S^3 - K))$, and that this irreducible component is isomorphic to $\text{SL}(2, \mathbb{C})$. We leave this as an exercise (exercise 15.6).

We only wish to consider representations into $\text{SL}(2, \mathbb{C})$ up to conjugation. Changing the basepoint of G will change the fundamental group by conjugation, and hence will change any representation by conjugation. Thus we really want to consider two representations to be the same if they are conjugate.

A first idea would be to declare representations $\rho_1, \rho_2: G \rightarrow \mathrm{SL}(2, \mathbb{C})$ to be equivalent if they are conjugate. That is, $\mathrm{SL}(2, \mathbb{C})$ acts on $R_{\mathrm{SL}}(G)$ via conjugation as follows. If $\rho \in R_{\mathrm{SL}}(G)$ and $A \in \mathrm{SL}(2, \mathbb{C})$, then $A \cdot \rho = i_A \circ \rho$ where i_A is defined by $i_A(X) = AXA^{-1}$. We could consider the orbits of this action, which is a polynomial map from $\mathrm{SL}(2, \mathbb{C}) \times R_{\mathrm{SL}}(G)$ to $R_{\mathrm{SL}}(G)$, and take a quotient. However, a point may be in the closure of several orbits, so this can lead to a non-Hausdorff space. The way to fix this is to take what is sometimes called the algebro-geometric quotient, or the algebraic quotient of invariant theory. We will not go into the details of the construction here. Instead, we give a definition of the algebro-geometric quotient that is known to be equivalent.

DEFINITION 15.27. The *character* of a representation $\rho: G \rightarrow \mathrm{SL}(2, \mathbb{C})$ is the function $\chi_\rho: G \rightarrow \mathbb{C}$ given by $\chi_\rho(g) = \mathrm{tr}(\rho(g))$, where tr denotes the function that takes the trace of a matrix.

Note the character is the same for two conjugate representations. It is not quite true that representations with the same character are necessarily conjugate.

DEFINITION 15.28. The *character variety* $X_{\mathrm{SL}}(G)$ is the space of characters of all representations $R_{\mathrm{SL}}(G)$.

It is shown in [CS83] that the character variety is an affine algebraic set; a more elementary proof of this fact is also given in [GAMA93]. We refer you to those papers for the details. We note again that the standard terminology is a little misleading. In definition 15.2, we noted that an affine variety is an irreducible affine algebraic set. But the character variety is typically reducible, hence not an affine variety at all. One true variety that is frequently studied is the irreducible component of the character variety corresponding to a discrete faithful representation, i.e. the representation coming from a complete hyperbolic structure. This is called the *canonical component*.

The canonical component of a knot complement contains a great deal of information about the manifold, including information on Dehn filling and surfaces embedded in the 3-manifold. However, it can be very difficult to compute the character variety. At the time of writing this book, character varieties have been computed only for simple families of 3-manifolds and knot complements, including double twist knots and links, and some 2-bridge links [MPvL11], [PT15].

15.2.3. The case of PSL. We spent the last subsection considering representations to $\mathrm{SL}(2, \mathbb{C})$. Much of that work can be extended to $\mathrm{PSL}(2, \mathbb{C})$ with a little extra effort. The extension to $\mathrm{PSL}(2, \mathbb{C})$ has been done carefully by [BZ98]. See also [HP04] for a nice exposition.

Let G be a finitely presented group:

$$G = \langle g_1, \dots, g_n \mid r_1, \dots, r_m \rangle.$$

Let $R_{\text{PSL}}(G)$ denote the space of representations from G to $\text{PSL}(2, \mathbb{C})$.

The first thing to check is that R_{PSL} forms an algebraic set. As before, relators give polynomial equations, but now these are only defined up to multiplication by ± 1 . An easy way to avoid sign issues is to use the fact that the group $\text{PSL}(2, \mathbb{C})$ is isomorphic to $\text{SO}(3, \mathbb{C})$; this can be shown using standard tools from Lie groups, and we leave this to the reader (or see [HP04, Lemma 2.1]).

PROPOSITION 15.29. *The space R_{PSL} consisting of representations of G into $\text{PSL}(2, \mathbb{C})$ is an affine algebraic set.*

PROOF. Using the fact that $\text{PSL}(2, \mathbb{C}) \cong \text{SO}(3, \mathbb{C})$, this follows as in the proof of proposition 15.22. \square

DEFINITION 15.30. Let G be a finitely presented group. Define the *PSL-representation variety* of G to be the algebraic set $R_{\text{PSL}}(G)$.

Again we only wish to consider representations into $\text{PSL}(2, \mathbb{C})$ up to conjugation. In the PSL case, there is a natural geometric reason: conjugate holonomy representations give isometric hyperbolic structures on a 3-manifold. We want an algebraic theory that views these structures as the same. As in the SL case, we may take the algebro-geometric quotient, or alternatively, take the set of PSL -characters, defined below. [HP04] give a proof that this is equivalent.

DEFINITION 15.31. Let $\rho: G \rightarrow \text{PSL}(2\mathbb{C})$ be a representation. The *PSL-character* of ρ is the function $\xi_\rho: G \rightarrow \mathbb{C}$ given by $\xi_\rho(g) = \text{tr}(\rho(g))^2$, where tr denotes the trace of the matrix. Note that the trace of an element of $\text{PSL}(2, \mathbb{C})$ is only defined up to sign, but the square of the trace is well-defined.

DEFINITION 15.32. The *PSL-character variety* $X_{\text{PSL}}(G)$ is the space of PSL -characters of all representations $R_{\text{PSL}}(G)$.

15.3. The A -polynomial

The A -polynomial was first defined by Cooper, Culler, Gillet, Long, and Shalen in [CCG⁺94]. The authors noticed that for manifolds with a single torus boundary component, the difficult problem of computing the $\text{SL}(2, \mathbb{C})$ character variety could be replaced by a slightly simpler problem. Rather than considering the entire fundamental group of the knot complement, we focus on the subgroup corresponding to generators of the boundary of a regular neighborhood of the knot, $\partial N(K)$. This reduces a complicated algebraic set to a single polynomial, called the A -polynomial, which still encodes a great deal of geometric information. Our exposition in this section is based on that of Cooper and Long in [CL96], with thanks to Mathews [Mat03].

15.3.1. Classical definition. Denote the meridian and longitude of a knot by μ and λ , respectively. We will be considering representations of the fundamental group $\pi_1(\partial N(K))$ into $\mathrm{SL}(2, \mathbb{C})$ up to conjugation. Since μ and λ commute, for any representation $\rho: \pi_1(\partial N(K)) \rightarrow \mathrm{SL}(2, \mathbb{C})$, the matrices $\rho(\mu)$ and $\rho(\lambda)$ must have the same fixed points on $\partial\mathbb{H}^3$ (exercise 5.11). Hence they can be conjugated to fix either the point at infinity or the geodesic from 0 to ∞ in $\partial\mathbb{H}^3$. In the former case, the two matrices have the form $\begin{pmatrix} 1 & * \\ 0 & 1 \end{pmatrix}$, and in the latter, the matrices are diagonal. Thus there will be no loss of generality in restricting to representations for which $\rho(\mu)$ and $\rho(\lambda)$ are upper triangular.

Define $R_{\mathrm{SL}}^U(\pi_1(S^3 - K)) \subset R_{\mathrm{SL}}(\pi_1(S^3 - K))$ to be those representations ρ for which $\rho(\mu)$ and $\rho(\lambda)$ are both upper triangular. When the context is clear, we abbreviate to R^U .

LEMMA 15.33. *The set $R_{\mathrm{SL}}^U(\pi_1(S^3 - K))$ forms an affine algebraic set.*

PROOF. We need to show that R_{SL}^U , just like R_{SL} , is defined as the set of zeros of a system of polynomial equations.

Recall that $\rho \in R_{\mathrm{SL}}(\pi_1(S^3 - K))$ is determined by $\rho(g_1), \dots, \rho(g_n)$, where the g_i are generators, and we view each $\rho(g_i)$ as a matrix with coordinates $a_i, b_i, c_i, d_i \in \mathbb{C}$ satisfying equation (15.2) and equation (15.3). Then $\rho(\mu)$ and $\rho(\lambda)$ will be matrices whose coefficients are polynomials in the $\{a_i, b_i, c_i, d_i\}$. In particular, the lower left entries of $\rho(\mu)$ and $\rho(\lambda)$ are polynomials q_μ and q_λ , respectively. Thus $R_{\mathrm{SL}}^U(\pi_1(S^3 - K))$ is obtained by adjoining $q_\mu = 0$ and $q_\lambda = 0$ to the polynomials defining $R_{\mathrm{SL}}(\pi_1(S^3 - K))$. Hence R_{SL}^U is an algebraic set. \square

Next, because the determinants of $\rho(\mu)$ and $\rho(\lambda)$ are equal to 1, it must be the case that for some $m, \ell \in \mathbb{C}^2$, the matrices $\rho(\mu)$ and $\rho(\lambda)$ have the form

$$\rho(\mu) = \begin{pmatrix} m & * \\ 0 & m^{-1} \end{pmatrix}, \quad \rho(\lambda) = \begin{pmatrix} \ell & * \\ 0 & \ell^{-1} \end{pmatrix}.$$

Define functions $\xi_\mu, \xi_\lambda: R_{\mathrm{SL}}^U \rightarrow \mathbb{C}$ by letting $\xi_\mu(\rho)$ (respectively $\xi_\lambda(\rho)$) be the upper left entry of the matrix $\rho(\mu)$ (respectively $\rho(\lambda)$). That is, $\xi_\mu(\rho) = m$ and $\xi_\lambda(\rho) = \ell$. Each of these entries can be written as a polynomial in the a_i, b_i, c_i, d_i , so each map ξ_μ and ξ_λ is a polynomial map, and thus the map $\xi: R_{\mathrm{SL}}^U \rightarrow \mathbb{C}^2$ given by $\xi(\rho) = (\xi_\lambda(\rho), \xi_\mu(\rho)) = (\ell, m)$ is a morphism.

Consider the image $\xi(R_{\mathrm{SL}}^U) \subset \mathbb{C}^2$. This is the image of an algebraic set under a morphism, hence is an algebraic set. It may have several irreducible components. Let C be an irreducible component of R_{SL}^U and let $\overline{\xi(C)}$ be its closure (in the Zariski topology). The closure $\overline{\xi(C)}$ is the set of zeros of a family of polynomials. If there is a single such polynomial, then denote it by F_C .

EXAMPLE 15.34. Let $C \subset R_{\mathrm{SL}}^U$ be the component of abelian representations, as in example 15.26. Then $\rho(\mu)$ is an upper triangular matrix in

$\mathrm{SL}(2, \mathbb{C})$, but $\rho(\lambda) = \mathrm{Id}$ always. Thus $\xi_\mu(\rho)$ can be arbitrary, but $\xi_\lambda(\rho) = 1$. Thus the closure of $\xi(C)$ for C the component of abelian representations gives the polynomial $F_C = \ell - 1$.

Now consider all polynomials F_C arising from irreducible components of R_{SL}^U , aside from the abelian representation. Our preliminary definition of the A -polynomial is the polynomial obtained by multiplying all of these polynomials, or 1 if there are no such polynomials. Observe that since F_C is the set of zeros of a polynomial, it is only defined up to multiplication by a scalar and by powers of m and ℓ . It was shown in [CCG⁺94] that a scalar multiple can be chosen so that all coefficients are integers. We require integer coefficients with no common factors, and multiply by $\ell^a m^b$ for a, b integers such that the total degree is minimal. This defines the A -polynomial up to sign. We summarize:

DEFINITION 15.35. Let K be a knot. For every C an irreducible component of $R_{\mathrm{SL}}^U(\pi_1(S^3 - K))$ that is not abelian, and such that $\xi(C)$ is the set of zeros of a single polynomial, let F_C denote this polynomial. The *A-polynomial* (or $\mathrm{SL}(2, \mathbb{C})$ A -polynomial) of K is defined to be the product of 1 and any polynomials F_C as above, rescaled so that all coefficients are integers with no common factors. We normalize by multiplying by $\ell^a m^b$ so that the total degree is minimized, and denote the result by $A_{\mathrm{SL}}(\ell, m)$.

It is easiest to make sense of the definitions if we work with examples. The simplest example is given by the following.

PROPOSITION 15.36. *The A-polynomial of the unknot is 1.*

PROOF. The fundamental group G of the unknot is \mathbb{Z} , hence any representation of G into $\mathrm{SL}(2, \mathbb{C})$ is an abelian representation. Thus in definition 15.35, there are no polynomials F_C and the A -polynomial is 1. \square

EXAMPLE 15.37 (Figure-8 knot). We use the Wirtinger presentation of example 15.20 to compute the polynomial A_{SL} for the figure-8 knot.

There are two generators, g_1 and g_2 , satisfying

$$\rho(g_1) = \begin{pmatrix} a_1 & b_1 \\ c_1 & d_1 \end{pmatrix}, \quad \rho(g_2) = \begin{pmatrix} a_2 & b_2 \\ c_2 & d_2 \end{pmatrix}.$$

This initially gives the eight unknowns a_i, b_i, c_i, d_i for $i = 1, 2$. These must satisfy the following equations:

- (1) Two determinant equations $a_i d_i - b_i c_i = 1$.
- (2) Four equations coming from the four matrix entries of the relation

$$\rho(g_1 g_2^{-1} g_1 g_2 g_1^{-1} g_2) = \rho(g_2^{-1} g_1 g_2 g_1^{-1} g_2 g_2).$$

- (3) Equations coming from the matrix entries of $\rho(M)$ and $\rho(L)$:

$$\rho(L) = \rho(g_1^{-1} g_2 g_1 g_2^{-1} g_1^{-1} g_2^{-1} g_1 g_2 g_1^{-1} g_2) \quad \text{and} \quad \rho(M) = \rho(g_1).$$

There are two equations to ensure $\rho(M)$ and $\rho(L)$ are upper triangular, by setting their bottom left entry to be 0. In particular, this

requires the simple equation $c_1 = 0$, coming from $\rho(M)$. A more complicated equation will come from the bottom left entry of $\rho(L)$, since L is a more complicated product of $g_1^{\pm 1}, g_2^{\pm 1}$.

There is one equation ensuring the top left entry of $\rho(L) = \ell$, and one equation ensuring the top left entry of $\rho(M) = m$. In particular, again in the simpler $\rho(M)$ case this gives $a_1 = m$. Using one of the determinant equations, we also conclude $d_1 = m^{-1}$.

In all, this gives seven equations in the unknowns $\ell, m, b_1, a_2, b_2, c_2, d_2$.

Using computer software such as Mathematica, we find a polynomial describing the curve satisfying this system:

$$-\ell + \ell^2 + \ell m^2 - \ell^2 m^2 + m^4 + \ell m^4 - \ell^2 m^4 - \ell^3 m^4 + \ell m^6 - \ell^2 m^6 - \ell m^8 + \ell^2 m^8.$$

Note that $(\ell - 1)$ divides this polynomial, corresponding to the abelian representation. We divide out by $(\ell - 1)$, to obtain

$$A_{\text{PSL}}(\ell, m) = \ell - \ell m^2 - m^4 - 2\ell m^4 - \ell^2 m^4 - \ell m^6 + \ell m^8.$$

15.3.2. The A_{PSL} -polynomial. The work in the previous section can also be applied to representations of $\pi_1(S^3 - K)$ into $\text{PSL}(2, \mathbb{C})$ rather than $\text{SL}(2, \mathbb{C})$. That is, for fixed generators μ and λ of $\pi_1(\partial N(K))$ restrict to $R_{\text{PSL}}^U \subset R_{\text{PSL}}$, the subset of representations ρ for which $\rho(\mu)$ and $\rho(\lambda)$ are upper triangular in $\text{PSL}(2, \mathbb{C})$. Define $\xi_{\text{PSL}}: R_{\text{PSL}}^U(\pi_1(S^3 - K)) \rightarrow \mathbb{C}^2$ by

$$\xi_{\text{PSL}}(\rho) = (\xi_\lambda(\rho), \xi_\mu(\rho)) = (\ell^2, m^2),$$

where ξ_λ gives the square of the top left entry of $\rho(\lambda)$, and similarly for ξ_μ . Consider each irreducible component C of R_{PSL}^U such that the closure $\overline{\xi_{\text{PSL}}(C)}$ is defined by a single polynomial $F_{\text{PSL}}(C)$, and C is not abelian.

DEFINITION 15.38. The A_{PSL} -polynomial is defined to be the product of the polynomials $F_{\text{PSL}}(C)$ as above, or 1 if there are no such polynomials.

The A_{PSL} -polynomial and the A -polynomial are related, and we describe the relationship in the hyperbolic case. When K is hyperbolic, with $G = \pi_1(S^3 - K)$, let $X_{\text{PSL}}^0(G)$ be the irreducible component of $X_{\text{PSL}}(G)$ containing the complete hyperbolic structure. Similarly, let $X_{\text{SL}}^0(G)$ be the irreducible component of $X_{\text{SL}}(G)$ containing the lift of the complete hyperbolic structure. Then we may define polynomials A_{PSL}^0 and A_{SL}^0 by only considering C coming from these irreducible components. Note A_{PSL}^0 is a factor of the A_{PSL} -polynomial, and A_{SL}^0 is a factor of the A -polynomial.

PROPOSITION 15.39. *The polynomial $A_{\text{PSL}}^0(\ell^2, m^2)$ divides the polynomial*

$$A_{\text{SL}}^0(\ell, m)A_{\text{SL}}^0(\ell, -m)A_{\text{SL}}^0(-\ell, m)A_{\text{SL}}^0(-\ell, -m).$$

PROOF. The projection $\pi: \text{SL}(2, \mathbb{C}) \rightarrow \text{PSL}(2, \mathbb{C})$ induces a map on character varieties $\pi: X_{\text{SL}}^0(G) \rightarrow X_{\text{PSL}}^0(G)$, which is surjective by [Cul86].

Define $h: \mathbb{C}^2 \rightarrow \mathbb{C}^2$ by $h(x, y) = (x^2, y^2)$. Then the following diagram commutes.

$$\begin{array}{ccccc} X_{\text{SL}}^0(\pi_1(S^3 - N(K))) & \xrightarrow{r} & X_{\text{SL}}^0(\pi_1(\partial N(K))) & \xleftarrow{\xi^{-1} \circ \text{tr}} & (\mathbb{C}^*)^2 \\ \downarrow \pi & & \downarrow \pi & & \downarrow h \\ X_{\text{PSL}}^0(\pi_1(S^3 - N(K))) & \xrightarrow{r} & X_{\text{PSL}}^0(\pi_1(\partial N(K))) & \xleftarrow{\xi_{\text{PSL}}^{-1} \circ \text{tr}} & (\mathbb{C}^*)^2 \end{array}$$

Here r is a map induced by the inclusion of $\pi_1(\partial N(K))$ into $\pi_1(S^3 - N(K))$.

If D_{SL}^0 and D_{PSL}^0 are curves defined by $A_{\text{SL}}^0(\ell, m)$ and $A_{\text{PSL}}^0(\ell, m)$, respectively, then $h(D_{\text{SL}}^0) = D_{\text{PSL}}^0$. So $h^{-1}(D_{\text{PSL}}^0)$ is the union of the curves given by $A_{\text{SL}}^0(\pm\ell, \pm m)$. Thus $A_{\text{PSL}}^0(\ell^2, m^2)$ divides

$$A_{\text{SL}}^0(\ell, m)A_{\text{SL}}^0(\ell, -m)A_{\text{SL}}^0(-\ell, m)A_{\text{SL}}^0(-\ell, -m). \quad \square$$

15.3.3. Relation to A_{Hyp} -polynomial. Let $\{z_1, \dots, z_n\}$ be parameters for a triangulation coming from a point in the gluing variety. Then we obtain a well-defined developing map by attaching tetrahedra in \mathbb{H}^3 via a face-pairing isometry. This determines a holonomy representation, hence we obtain a map $D: \mathcal{DT} \rightarrow X_{\text{PSL}}(G)$. Champanerkar showed that this map is algebraic, i.e. a morphism, and thus $A_{\text{Hyp}}(\ell, m)$ divides $A_{\text{PSL}}(\ell, m)$ [Cha03].

It follows that $A_{\text{Hyp}}^0(\ell, m) = A_{\text{PSL}}^0(\ell, m)$.

EXAMPLE 15.40. We computed above in example 15.15 that for the figure-8 knot complement,

$$\begin{aligned} A_{\text{Hyp}}(\ell, m) = \ell - 2\ell m - 3\ell m^2 + 2\ell m^3 - m^4 + 6\ell m^4 \\ - \ell^2 m^4 + 2\ell m^5 - 3\ell m^6 - 2\ell m^7 + \ell m^8. \end{aligned}$$

And in example 15.37, its A -polynomial is

$$A_{\text{SL}}(\ell, m) = \ell - \ell m^2 - m^4 - 2\ell m^4 - \ell^2 m^4 - \ell m^6 + \ell m^8.$$

In this case, $A_{\text{Hyp}}(\ell^2, m^2) = -A_{\text{SL}}(\ell, m)A_{\text{SL}}(-\ell, m)$.

15.4. Exercises

EXERCISE 15.1. [Zariski topology]

- (1) Prove that the union of two affine algebraic sets and the intersection of arbitrarily many affine algebraic sets are both affine algebraic sets.
- (2) Describe the following sets as affine algebraic sets: \mathbb{C}^N , \emptyset , a single point (a_1, \dots, a_N) .
- (3) The *Zariski topology* is the topology on \mathbb{C}^N formed by taking affine algebraic sets to be closed sets. Prove that any Zariski-closed set is closed in the standard Euclidean topology. Find an example of a set that is Euclidean-closed but not Zariski-closed.

EXERCISE 15.2. SnapPy finds triangulations of knot complements and allows you to print out gluing and completeness equations.

- (1) Using SnapPy, find a set of polynomial equations that lead to the A_{Hyp} polynomials of the knots 5_2 , 6_1 , and 6_2 .
- (2) Using Mathematica (or other), compute the A_{Hyp} polynomials of these knots.
- (3) Use SnapPy to randomize the triangulations of the knots. What happens to the A_{Hyp} polynomial?
- (4) Use SnapPy to change the generators of $\pi_1(\partial N(K))$, i.e. the curves giving the completeness equations. What happens to the A_{Hyp} polynomial?

EXERCISE 15.3. Using the Siefert–Van Kampen theorem, or otherwise, prove that the group given by the Wirtinger presentation is isomorphic to the fundamental group of the knot complement.

EXERCISE 15.4. Find the Wirtinger presentation of the fundamental group of the 5_2 , 6_1 , and 6_2 knots. Also find a presentation for their longitudes.

EXERCISE 15.5. Let r_1, r_2, \dots, r_n denote the relators of the Wirtinger presentation coming from the n distinct crossings of a knot. Show that r_n is always redundant.

EXERCISE 15.6 (Abelian representations). Show that abelian representations form an affine algebraic set isomorphic to $\text{SL}(2, \mathbb{C})$. (Ensure your isomorphism is an isomorphism of affine algebraic sets, i.e. defined by polynomial maps.)

EXERCISE 15.7. Compute $A_{\text{SL}}(\ell, m)$ for the 5_2 , 6_1 , or 6_2 knot.

EXERCISE 15.8. The *support* of a polynomial $F(x, y)$ is the set $\{(a, b)\} \subset \mathbb{Z}^2$ such that the coefficient of the term $x^a y^b$ in $F(x, y)$ is nonzero. The convex hull of the support is the *Newton polygon* of F . The Newton polygon of the A -polynomial has a remarkable relationship with essential surfaces embedded in the knot:

THEOREM 15.41 ([CCG⁺94]). *Let K be a knot in S^3 with A -polynomial $A_{\text{SL}}(\ell, m)$. Suppose the Newton polygon of $A_{\text{SL}}(\ell, m)$ has a side of slope p/q . Then there is an essential surface S in $S^3 - N(K)$ with boundary that is a curve on the torus $\partial N(K)$ with slope $p/q \in H_1(\partial N(K))$.*

Champanerkar proved that the corresponding result holds for A_{Hyp} .

- (1) Compute the Newton polygon for $A_{\text{SL}}(\ell, m)$ for the figure-8 knot.
- (2) Compute the Newton polygon for $A_{\text{Hyp}}(\ell, m)$ for the figure-8 knot.

EXERCISE 15.9. Repeat the previous exercise for the 5_2 , 6_1 , or 6_2 knot.

Bibliography

- [AB27] J. W. Alexander and G. B. Briggs, *On types of knotted curves*, Ann. of Math. (2) **28** (1926/27), no. 1-4, 562–586. MR 1502807 [5]
- [Ada85] Colin C. Adams, *Thrice-punctured spheres in hyperbolic 3-manifolds*, Trans. Amer. Math. Soc. **287** (1985), no. 2, 645–656. [243]
- [Ada02] ———, *Waist size for cusps in hyperbolic 3-manifolds*, Topology **41** (2002), no. 2, 257–270. [295]
- [Ada05] Colin Adams, *Hyperbolic knots*, Handbook of knot theory, Elsevier B. V., Amsterdam, 2005, pp. 1–18. MR 2179259 [250]
- [Ago00] Ian Agol, *Bounds on exceptional Dehn filling*, Geom. Topol. **4** (2000), 431–449. [166, 167]
- [Ahl78] Lars V. Ahlfors, *Complex analysis*, third ed., McGraw-Hill Book Co., New York, 1978, An introduction to the theory of analytic functions of one complex variable, International Series in Pure and Applied Mathematics. MR 510197 [34]
- [AKC⁺17] Colin Adams, Alexander Kastner, Aaron Calderon, Xinyi Jiang, Gregory Kehne, Nathaniel Mayer, and Mia Smith, *Volume and determinant densities of hyperbolic rational links*, J. Knot Theory Ramifications **26** (2017), no. 1, 1750002, 13. MR 3597249 [243]
- [Aki01] Hirotaka Akiyoshi, *Finiteness of polyhedral decompositions of cusped hyperbolic manifolds obtained by the Epstein-Penner’s method*, Proc. Amer. Math. Soc. **129** (2001), no. 8, 2431–2439. MR 1823928 [305]
- [And05] James W. Anderson, *Hyperbolic geometry*, second ed., Springer Undergraduate Mathematics Series, Springer-Verlag London Ltd., London, 2005. MR MR2161463 (2006b:51001) [29]
- [AS05] Colin Adams and Eric Schoenfeld, *Totally geodesic Seifert surfaces in hyperbolic knot and link complements. I*, Geom. Dedicata **116** (2005), 237–247. MR 2195448 [250]
- [AST07] Ian Agol, Peter A. Storm, and William P. Thurston, *Lower bounds on volumes of hyperbolic Haken 3-manifolds*, J. Amer. Math. Soc. **20** (2007), no. 4, 1053–1077, with an appendix by Nathan Dunfield. [280, 281]
- [ASWY07] Hirotaka Akiyoshi, Makoto Sakuma, Masaaki Wada, and Yasushi Yamashita, *Punctured torus groups and 2-bridge knot groups. I*, Lecture Notes in Mathematics, vol. 1909, Springer, Berlin, 2007. MR 2330319 [291, 309]
- [BBP⁺19] Benjamin A. Burton, Ryan Budney, William Pettersson, et al., *Regina: Software for low-dimensional topology*, <http://regina-normal.github.io/>, 1999–2019. [6]
- [BCG95] G. Besson, G. Courtois, and S. Gallot, *Entropies et rigidités des espaces localement symétriques de courbure strictement négative*, Geom. Funct. Anal. **5** (1995), no. 5, 731–799. MR 1354289 [267]
- [BCS05] Jeffrey Boland, Chris Connell, and Juan Souto, *Volume rigidity for finite volume manifolds*, Amer. J. Math. **127** (2005), no. 3, 535–550. MR 2141643 [267]

- [BGS85] Werner Ballmann, Mikhael Gromov, and Viktor Schroeder, *Manifolds of non-positive curvature*, Progress in Mathematics, vol. 61, Birkhäuser Boston, Inc., Boston, MA, 1985. MR 823981 [100, 267]
- [BH96] Steven A. Bleiler and Craig D. Hodgson, *Spherical space forms and Dehn filling*, *Topology* **35** (1996), no. 3, 809–833. [268, 269]
- [Bon86] Francis Bonahon, *Bouts des variétés hyperboliques de dimension 3*, *Ann. of Math. (2)* **124** (1986), no. 1, 71–158. MR 847953 (88c:57013) [254]
- [Bon09] ———, *Low-dimensional geometry*, Student Mathematical Library, vol. 49, American Mathematical Society, Providence, RI; Institute for Advanced Study (IAS), Princeton, NJ, 2009, From Euclidean surfaces to hyperbolic knots, IAS/Park City Mathematical Subseries. MR 2522946 [291, 301]
- [Bör78] K. Böröczky, *Packing of spheres in spaces of constant curvature*, *Acta Math. Acad. Sci. Hungar.* **32** (1978), no. 3-4, 243–261. MR MR512399 (80h:52014) [168, 294, 310]
- [BP92] Riccardo Benedetti and Carlo Petronio, *Lectures on hyperbolic geometry*, Universitext, Springer-Verlag, Berlin, 1992. MR MR1219310 (94e:57015) [vii, 100, 105, 111, 118]
- [Bur16] Stephan D. Burton, *The spectra of volume and determinant densities of links*, *Topology Appl.* **211** (2016), 38–55. MR 3545288 [243]
- [Bur20] Benjamin A. Burton, *The next 350 million knots*, to appear in the proceedings of the 36th International Symposium on Computational Geometry (SoCG 2020), 2020. [vii, 6, 8]
- [BW83] Joan S. Birman and R. F. Williams, *Knotted periodic orbits in dynamical systems. I. Lorenz's equations*, *Topology* **22** (1983), no. 1, 47–82. MR 682059 [3]
- [BZ85] Gerhard Burde and Heiner Zieschang, *Knots*, de Gruyter Studies in Mathematics, vol. 5, Walter de Gruyter & Co., Berlin, 1985. MR 808776 (87b:57004) [vii, 195]
- [BZ98] S. Boyer and X. Zhang, *On Culler-Shalen seminorms and Dehn filling*, *Ann. of Math. (2)* **148** (1998), no. 3, 737–801. MR 1670053 [322]
- [CCG⁺94] D. Cooper, M. Culler, H. Gillet, D. D. Long, and P. B. Shalen, *Plane curves associated to character varieties of 3-manifolds*, *Invent. Math.* **118** (1994), no. 1, 47–84. MR 1288467 [311, 316, 319, 323, 325, 328]
- [CDGW16] Marc Culler, Nathan M. Dunfield, Matthias Goerner, and Jeffrey R. Weeks, *SnapPy, a computer program for studying the geometry and topology of 3-manifolds*, Available at <http://snappy.computop.org>, 2016. [8, 12, 14, 15, 78, 81, 115, 146, 207, 293, 305, 309, 310, 313]
- [CDW99] Patrick J. Callahan, John C. Dean, and Jeffrey R. Weeks, *The simplest hyperbolic knots*, *J. Knot Theory Ramifications* **8** (1999), no. 3, 279–297. MR 1691433 [3, 12]
- [CEG06] R. D. Canary, D. B. A. Epstein, and P. L. Green, *Notes on notes of Thurston*, Fundamentals of hyperbolic geometry: selected expositions, London Math. Soc. Lecture Note Ser., vol. 328, Cambridge Univ. Press, Cambridge, 2006, With a new foreword by Canary, pp. 1–115. MR 2235710 [118, 254]
- [CGHN00] David Coulson, Oliver A. Goodman, Craig D. Hodgson, and Walter D. Neumann, *Computing arithmetic invariants of 3-manifolds*, *Experiment. Math.* **9** (2000), no. 1, 127–152. MR 1758805 [79, 146]
- [Cha02] Ken Chan, *Constructing hyperbolic 3-manifolds from ideal triangulations*, 2002, Honours thesis, University of Melbourne. [183]
- [Cha03] Abhijit Ashok Champanerkar, *A-polynomial and Bloch invariants of hyperbolic 3-manifolds*, ProQuest LLC, Ann Arbor, MI, 2003, Thesis (Ph.D.)—Columbia University. MR 2704573 [314, 327]

- [CHK00] Daryl Cooper, Craig D. Hodgson, and Steven P. Kerckhoff, *Three-dimensional orbifolds and cone-manifolds*, MSJ Memoirs, vol. 5, Mathematical Society of Japan, Tokyo, 2000, With a postface by Sadayoshi Kojima. [113, 114, 118]
- [Cho04] Young-Eun Choi, *Positively oriented ideal triangulations on hyperbolic three-manifolds*, *Topology* **43** (2004), no. 6, 1345–1371. MR 2081429 [68]
- [CJ94] Andrew Casson and Douglas Jungreis, *Convergence groups and Seifert fibered 3-manifolds*, *Invent. Math.* **118** (1994), no. 3, 441–456. MR 1296353 [155, 156]
- [CKM14] Abhijit Champanerkar, Ilya Kofman, and Timothy Mullen, *The 500 simplest hyperbolic knots*, *J. Knot Theory Ramifications* **23** (2014), no. 12, 1450055, 34. MR 3298204 [3, 12]
- [CKP04] Abhijit Champanerkar, Ilya Kofman, and Eric Patterson, *The next simplest hyperbolic knots*, *J. Knot Theory Ramifications* **13** (2004), no. 7, 965–987. MR MR2101238 (2005k:57010) [3, 12]
- [CL96] D. Cooper and D. D. Long, *Remarks on the A-polynomial of a knot*, *J. Knot Theory Ramifications* **5** (1996), no. 5, 609–628. MR 1414090 [323]
- [Con70] J. H. Conway, *An enumeration of knots and links, and some of their algebraic properties*, *Computational Problems in Abstract Algebra* (Proc. Conf., Oxford, 1967), Pergamon, Oxford, 1970, pp. 329–358. MR 0258014 (41 #2661) [197]
- [Con78] John B. Conway, *Functions of one complex variable*, second ed., *Graduate Texts in Mathematics*, vol. 11, Springer-Verlag, New York-Berlin, 1978. MR 503901 [61]
- [CS83] Marc Culler and Peter B. Shalen, *Varieties of group representations and splittings of 3-manifolds*, *Ann. of Math. (2)* **117** (1983), no. 1, 109–146. MR 683804 [311, 320, 322]
- [Cul86] Marc Culler, *Lifting representations to covering groups*, *Adv. in Math.* **59** (1986), no. 1, 64–70. MR 825087 [326]
- [dC92] Manfredo Perdigão do Carmo, *Riemannian geometry*, *Mathematics: Theory & Applications*, Birkhäuser Boston Inc., Boston, MA, 1992, Translated from the second Portuguese edition by Francis Flaherty. [29]
- [DeB06] Jason DeBlois, *Totally geodesic surfaces and homology*, *Algebr. Geom. Topol.* **6** (2006), 1413–1428 (electronic). MR MR2253453 [250]
- [DP19] Vinh Dang and Jessica S. Purcell, *Cusp shape and tunnel number*, *Proc. Amer. Math. Soc.* **147** (2019), no. 3, 1351–1366. MR 3896079 [243]
- [Dun05] Nathan M. Dunfield, *Appendix to mahler’s measure and the dilogarithm ii*, *ArXiv:math/0308041*, 2005. [313]
- [EP88] D. B. A. Epstein and R. C. Penner, *Euclidean decompositions of noncompact hyperbolic manifolds*, *J. Differential Geom.* **27** (1988), no. 1, 67–80. MR 918457 [68, 291]
- [Epp98] Moritz Epple, *Topology, matter, and space. I. Topological notions in 19th-century natural philosophy*, *Arch. Hist. Exact Sci.* **52** (1998), no. 4, 297–392. MR 1611730 [vii, 4]
- [FG11] David Futer and François Guéritaud, *From angled triangulations to hyperbolic structures*, *Interactions between hyperbolic geometry, quantum topology and number theory*, *Contemp. Math.*, vol. 541, Amer. Math. Soc., Providence, RI, 2011, pp. 159–182. MR 2796632 [184]
- [FKP08] David Futer, Efstratia Kalfagianni, and Jessica S. Purcell, *Dehn filling, volume, and the Jones polynomial*, *J. Differential Geom.* **78** (2008), no. 3, 429–464. MR MR2396249 (2009c:57010) [122, 268, 275, 277]
- [FKP13] ———, *Guts of surfaces and the colored Jones polynomial*, *Lecture Notes in Mathematics*, vol. 2069, Springer, Heidelberg, 2013. [257]

- [FP07] David Futer and Jessica S. Purcell, *Links with no exceptional surgeries*, Comment. Math. Helv. **82** (2007), no. 3, 629–664. MR MR2314056 (2008k:57008) [135, 140, 170]
- [FS14] David Futer and Saul Schleimer, *Cusp geometry of fibered 3-manifolds*, Amer. J. Math. **136** (2014), no. 2, 309–356. MR 3188063 [167]
- [Gab92] David Gabai, *Convergence groups are Fuchsian groups*, Ann. of Math. (2) **136** (1992), no. 3, 447–510. MR 1189862 [155, 156]
- [GAMA93] F. González-Acuña and José María Montesinos-Amilibia, *On the character variety of group representations in $SL(2, \mathbf{C})$ and $PSL(2, \mathbf{C})$* , Math. Z. **214** (1993), no. 4, 627–652. MR 1248117 [322]
- [GHL04] Sylvestre Gallot, Dominique Hulin, and Jacques Lafontaine, *Riemannian geometry*, third ed., Universitext, Springer-Verlag, Berlin, 2004. MR 2088027 [267]
- [GL89] Cameron McA. Gordon and John Luecke, *Knots are determined by their complements*, J. Amer. Math. Soc. **2** (1989), no. 2, 371–415. [viii, 2, 304]
- [GMM01] David Gabai, G. Robert Meyerhoff, and Peter Milley, *Volumes of tubes in hyperbolic 3-manifolds*, J. Differential Geom. **57** (2001), no. 1, 23–46. MR 1871490 [103]
- [Goe34] Lebrecht Goeritz, *Bemerkungen zur knotentheorie*, Abh. Math. Sem. Univ. Hamburg **10** (1934), no. 1, 201–210. MR 3069625 [5]
- [Gor02] C. McA. Gordon, *Links and their complements*, Topology and geometry: commemorating SISTAG, Contemp. Math., vol. 314, Amer. Math. Soc., Providence, RI, 2002, pp. 71–82. MR 1941623 [3]
- [Gre17] Joshua E. Greene, *Alternating links and definite surfaces*, Duke Math. J. **166** (2017), no. 11, 2133–2151, with an appendix by András Juhás and Marc Lackenby. [241]
- [Gro99] Misha Gromov, *Metric structures for Riemannian and non-Riemannian spaces*, Progress in Mathematics, vol. 152, Birkhäuser Boston, Inc., Boston, MA, 1999, Based on the 1981 French original [MR0682063 (85e:53051)], With appendices by M. Katz, P. Pansu and S. Semmes, Translated from the French by Sean Michael Bates. MR 1699320 (2000d:53065) [118]
- [GS10] François Guéritaud and Saul Schleimer, *Canonical triangulations of Dehn fillings*, Geom. Topol. **14** (2010), no. 1, 193–242. MR 2578304 [291]
- [Gue06a] Francois Gueritaud, *Hyperbolic geometry and canonical triangulations in dimension three*, ProQuest LLC, Ann Arbor, MI, 2006, Thesis (Ph.D.)–University of Southern California. MR 2710030 [14, 309]
- [Gué06b] François Guéritaud, *On canonical triangulations of once-punctured torus bundles and two-bridge link complements*, Geom. Topol. **10** (2006), 1239–1284, With an appendix by David Futer. MR 2255497 [199, 205, 207, 220, 221, 265]
- [Hak61] Wolfgang Haken, *Theorie der Normalflächen*, Acta Math. **105** (1961), 245–375. MR 0141106 [157]
- [Hat02] Allen Hatcher, *Algebraic topology*, Cambridge University Press, Cambridge, 2002. MR 1867354 [51]
- [Hat07] ———, *Notes on basic 3-manifold topology*, available at <http://www.math.cornell.edu/~hatcher>, 2007. [149, 155]
- [Hem04] John Hempel, *3-manifolds*, AMS Chelsea Publishing, Providence, RI, 2004, Reprint of the 1976 original. MR 2098385 [149]
- [HIK⁺16] Neil Hoffman, Kazuhiro Ichihara, Masahide Kashiwagi, Hidetoshi Masai, Shin’ichi Oishi, and Akitoshi Takayasu, *Verified computations for hyperbolic 3-manifolds*, Exp. Math. **25** (2016), no. 1, 66–78. MR 3424833 [14, 79]

- [HK05] Craig D. Hodgson and Steven P. Kerckhoff, *Universal bounds for hyperbolic Dehn surgery*, Ann. of Math. (2) **162** (2005), no. 1, 367–421. MR MR2178964 [111, 122]
- [Hod86] Craig D. Hodgson, *Degeneration and regeneration of geometric structures on 3-manifolds*, Ph.D. thesis, Princeton Univ., 1986. [113]
- [Hol91] W. H. Holzmann, *An equivariant torus theorem for involutions*, Trans. Amer. Math. Soc. **326** (1991), no. 2, 887–906. MR MR1034664 (91k:57022) [280]
- [How17] Joshua A. Howie, *A characterisation of alternating knot exteriors*, Geom. Topol. **21** (2017), no. 4, 2353–2371. MR 3654110 [241]
- [HP04] Michael Heusener and Joan Porti, *The variety of characters in $\mathrm{PSL}_2(\mathbb{C})$* , Bol. Soc. Mat. Mexicana (3) **10** (2004), no. Special Issue, 221–237. MR 2199350 [322, 323]
- [HP17] Joshua A. Howie and Jessica S. Purcell, *Geometry of alternating links on surfaces*, ArXiv:1712.01373, 2017. [257]
- [HTW98] Jim Hoste, Morwen Thistlethwaite, and Jeff Weeks, *The first 1,701,936 knots*, Math. Intelligencer **20** (1998), no. 4, 33–48. MR MR1646740 (99i:57015) [vii, 6]
- [Jac80] William Jaco, *Lectures on three-manifold topology*, CBMS Regional Conference Series in Mathematics, vol. 43, American Mathematical Society, Providence, R.I., 1980. MR 565450 [251]
- [JK82] Troels Jørgensen and Peter Klein, *Algebraic convergence of finitely generated Kleinian groups*, Quart. J. Math. Oxford Ser. (2) **33** (1982), no. 131, 325–332. MR 668178 [97]
- [Joh79] Klaus Johannson, *Homotopy equivalences of 3-manifolds with boundaries*, Lecture Notes in Mathematics, vol. 761, Springer, Berlin, 1979. MR MR551744 (82c:57005) [155]
- [Jør76] Troels Jørgensen, *On discrete groups of Möbius transformations*, Amer. J. Math. **98** (1976), no. 3, 739–749. MR 0427627 [97]
- [JS79] William H. Jaco and Peter B. Shalen, *Seifert fibered spaces in 3-manifolds*, Mem. Amer. Math. Soc. **21** (1979), no. 220, viii+192. MR MR539411 (81c:57010) [155]
- [Kap01] Michael Kapovich, *Hyperbolic manifolds and discrete groups*, Progress in Mathematics, vol. 183, Birkhäuser Boston, Inc., Boston, MA, 2001. MR 1792613 [100, 118, 120, 154]
- [KM68] D. A. Kazdan and G. A. Margulis, *A proof of Selberg’s hypothesis*, Mat. Sb. (N.S.) **75** (117) (1968), 163–168. MR 0223487 [92, 99]
- [Kne29] Hellmuth Kneser, *Geschlossene Flächen in dreidimensionalen Mannigfaltigkeiten*, Jahresbericht der Dent. Math. Verein. **28** (1929), 248–260. [157]
- [Koe36] Paul Koebe, *Kontaktprobleme der konformen abbildung*, Ber. Sächs. Akad. Wiss. Leipzig, Math.-Phys. Kl. **88** (1936), 141–164. [138]
- [Lac00] Marc Lackenby, *Word hyperbolic Dehn surgery*, Invent. Math. **140** (2000), no. 2, 243–282. [166]
- [Lac04] ———, *The volume of hyperbolic alternating link complements*, Proc. London Math. Soc. (3) **88** (2004), no. 1, 204–224, With an appendix by Ian Agol and Dylan Thurston. [135, 263, 264, 279, 287]
- [Lei06] Christopher J. Leininger, *Small curvature surfaces in hyperbolic 3-manifolds*, J. Knot Theory Ramifications **15** (2006), no. 3, 379–411. MR MR2217503 (2007a:57025) [250]
- [Lic62] W. B. R. Lickorish, *A representation of orientable combinatorial 3-manifolds*, Ann. of Math. (2) **76** (1962), 531–540. [108]
- [Lic97] W. B. Raymond Lickorish, *An introduction to knot theory*, Graduate Texts in Mathematics, vol. 175, Springer-Verlag, New York, 1997. MR 1472978 [vii]

- [LP14] Marc Lackenby and Jessica S. Purcell, *Geodesics and compression bodies*, Exp. Math. **23** (2014), no. 2, 218–240. MR 3223775 [291]
- [LST08] Feng Luo, Saul Schleimer, and Stephan Tillmann, *Geodesic ideal triangulations exist virtually*, Proc. Amer. Math. Soc. **136** (2008), no. 7, 2625–2630. MR 2390535 [193]
- [Mar07] A. Marden, *Outer circles*, Cambridge University Press, Cambridge, 2007, An introduction to hyperbolic 3-manifolds. MR MR2355387 (2008i:57001) [29, 37, 83, 88, 92, 97, 120]
- [Mar16] Bruno Martelli, *An introduction to geometric topology*, 2016. [111]
- [Mas88] Bernard Maskit, *Kleinian groups*, Grundlehren der Mathematischen Wissenschaften [Fundamental Principles of Mathematical Sciences], vol. 287, Springer-Verlag, Berlin, 1988. MR 959135 [250]
- [Mat03] Daniel Mathews, *Mahler's unfinished symphony: etudes in knots, algebra and geometry*, 2003, Honours thesis, University of Melbourne. [323]
- [Men83] William W. Menasco, *Polyhedra representation of link complements*, Low-dimensional topology (San Francisco, Calif., 1981), Contemp. Math., vol. 20, Amer. Math. Soc., Providence, RI, 1983, pp. 305–325. MR MR718149 (85e:57006) [8, 19]
- [Men84] William Menasco, *Closed incompressible surfaces in alternating knot and link complements*, Topology **23** (1984), no. 1, 37–44. MR MR721450 (86b:57004) [213, 225, 230]
- [Mey87] Robert Meyerhoff, *A lower bound for the volume of hyperbolic 3-manifolds*, Canad. J. Math. **39** (1987), no. 5, 1038–1056. MR 918586 (88k:57049) [92]
- [Mil82] John Milnor, *Hyperbolic geometry: the first 150 years*, Bull. Amer. Math. Soc. (N.S.) **6** (1982), no. 1, 9–24. MR 634431 [174]
- [Mil94] ———, *Collected papers. Vol. 1*, Publish or Perish, Inc., Houston, TX, 1994, Geometry. MR 1277810 [190]
- [Mil17] Christian Millichap, *Mutations and short geodesics in hyperbolic 3-manifolds*, Comm. Anal. Geom. **25** (2017), no. 3, 625–683. MR 3702548 [243]
- [Miy94] Yosuke Miyamoto, *Volumes of hyperbolic manifolds with geodesic boundary*, Topology **33** (1994), no. 4, 613–629. MR 1293303 [277, 278]
- [Mos73] G. D. Mostow, *Strong rigidity of locally symmetric spaces*, Princeton University Press, Princeton, N.J., 1973, Annals of Mathematics Studies, No. 78. [vii, 105]
- [Mos09] Harriet Moser, *Proving a manifold to be hyperbolic once it has been approximated to be so*, Algebr. Geom. Topol. **9** (2009), no. 1, 103–133. MR 2471132 [79]
- [MPvL11] Melissa L. Macasieb, Kathleen L. Petersen, and Ronald M. van Luijk, *On character varieties of two-bridge knot groups*, Proc. Lond. Math. Soc. (3) **103** (2011), no. 3, 473–507. MR 2827003 [322]
- [MR92] William Menasco and Alan W. Reid, *Totally geodesic surfaces in hyperbolic link complements*, Topology '90 (Columbus, OH, 1990), Ohio State Univ. Math. Res. Inst. Publ., vol. 1, de Gruyter, Berlin, 1992, pp. 215–226. MR MR1184413 (94g:57016) [250]
- [MSW02] David Mumford, Caroline Series, and David Wright, *Indra's pearls*, Cambridge University Press, New York, 2002, The vision of Felix Klein. MR 1913879 [248]
- [Mun00] James R. Munkres, *Topology, second edition*, Prentice Hall, Upper Saddle River, NJ, 2000. [51]
- [Mur96] Kunio Murasugi, *Knot theory and its applications*, Birkhäuser Boston Inc., Boston, MA, 1996, Translated from the 1993 Japanese original by Bohdan Kurpita. [vii, 195]

- [Mye93] Robert Myers, *Excellent 1-manifolds in compact 3-manifolds*, *Topology Appl.* **49** (1993), no. 2, 115–127. MR 1206219 [113]
- [NZ85] Walter D. Neumann and Don Zagier, *Volumes of hyperbolic three-manifolds*, *Topology* **24** (1985), no. 3, 307–332. MR 815482 [111, 122, 183]
- [Pap57] C. D. Papakyriakopoulos, *On Dehn's lemma and the asphericity of knots*, *Ann. of Math. (2)* **66** (1957), 1–26. MR 0090053 [171]
- [Per02] Grisha Perelman, *The entropy formula for the Ricci flow and its geometric applications*, arXiv:math.DG/0211159, 2002. [156, 282]
- [Per03] ———, *Ricci flow with surgery on three-manifolds*, arXiv:math.DG/0303109, 2003. [156, 282]
- [PP00] Carlo Petronio and Joan Porti, *Negatively oriented ideal triangulations and a proof of Thurston's hyperbolic Dehn filling theorem*, *Expo. Math.* **18** (2000), no. 1, 1–35. MR 1751141 [111]
- [Pra73] Gopal Prasad, *Strong rigidity of \mathbf{Q} -rank 1 lattices*, *Invent. Math.* **21** (1973), 255–286. [vii, 105]
- [Pre43] Alexandre Preissmann, *Quelques propriétés globales des espaces de Riemann*, *Comment. Math. Helv.* **15** (1943), 175–216. MR 0010459 [267]
- [Prz98] Józef H. Przytycki, *Classical roots of knot theory*, *Chaos Solitons Fractals* **9** (1998), no. 4-5, 531–545, *Knot theory and its applications*. MR 1628740 [vii]
- [PT15] Kathleen L. Petersen and Anh T. Tran, *Character varieties of double twist links*, *Algebr. Geom. Topol.* **15** (2015), no. 6, 3569–3598. MR 3450771 [322]
- [Pur07] Jessica S. Purcell, *Volumes of highly twisted knots and links*, *Algebr. Geom. Topol.* **7** (2007), 93–108. MR MR2289805 (2007m:57011) [135]
- [Pur08] ———, *Cusp shapes under cone deformation*, *J. Differential Geom.* **80** (2008), no. 3, 453–500. MR MR2472480 [135]
- [Pur11] ———, *An introduction to fully augmented links*, *Interactions between hyperbolic geometry, quantum topology and number theory*, *Contemp. Math.*, vol. 541, Amer. Math. Soc., Providence, RI, 2011, pp. 205–220. MR 2796634 [135]
- [Rat06] John G. Ratcliffe, *Foundations of hyperbolic manifolds*, second ed., *Graduate Texts in Mathematics*, vol. 149, Springer, New York, 2006. MR MR2249478 (2007d:57029) [vii, 29, 105]
- [Rei27] Kurt Reidemeister, *Elementare Begründung der Knotentheorie*, *Abh. Math. Sem. Univ. Hamburg* **5** (1927), no. 1, 24–32. MR 3069462 [4]
- [Ril75] Robert Riley, *A quadratic parabolic group*, *Math. Proc. Cambridge Philos. Soc.* **77** (1975), 281–288. MR 0412416 [vii, 85, 101]
- [Riv94] Igor Rivin, *Euclidean structures on simplicial surfaces and hyperbolic volume*, *Ann. of Math. (2)* **139** (1994), no. 3, 553–580. MR 1283870 [183, 190]
- [Rol90] Dale Rolfsen, *Knots and links*, *Mathematics Lecture Series*, vol. 7, Publish or Perish, Inc., Houston, TX, 1990, Corrected reprint of the 1976 original. MR 1277811 [vii, 108, 316]
- [Rub87] Daniel Ruberman, *Mutation and volumes of knots in S^3* , *Invent. Math.* **90** (1987), no. 1, 189–215. MR 906585 [243, 246, 247]
- [Sch50] Ludwig Schläfli, *Gesammelte mathematische Abhandlungen. Band I*, Verlag Birkhäuser, Basel, 1950. MR 0034587 [178]
- [Sch53] ———, *Gesammelte mathematische Abhandlungen. Band II*, Verlag Birkhäuser, Basel, 1953. MR 0053873 [178]
- [Sch56] Horst Schubert, *Knoten mit zwei Brücken*, *Math. Z.* **65** (1956), 133–170. MR 0082104 (18,498e) [11, 195]
- [Sch61] ———, *Bestimmung der primfaktorzerlegung von verkettungen*, *Mathematische Zeitschrift* **76** (1961), no. 1, 116–148. [157]

- [Sch14] Jennifer Schultens, *Introduction to 3-manifolds*, Graduate Studies in Mathematics, vol. 151, American Mathematical Society, Providence, RI, 2014. MR 3203728 [149, 155]
- [Sco83] Peter Scott, *The geometries of 3-manifolds*, Bull. London Math. Soc. **15** (1983), no. 5, 401–487. MR MR705527 (84m:57009) [155]
- [Sha02] Peter B. Shalen, *Representations of 3-manifold groups*, Handbook of geometric topology, North-Holland, Amsterdam, 2002, pp. 955–1044. MR 1886685 [312, 319]
- [Sil06] Dan Silver, *Knot theory's odd origins*, American Scientist **94** (2006), no. 2, 158 – 165. [vii]
- [Sim73] Jonathan Simon, *An algebraic classification of knots in S^3* , Ann. of Math. (2) **97** (1973), 1–13. MR 0310861 [230]
- [SS09] Saul Schleimer and Henry Segerman, *Dehn surgery images*, Available at website https://math.okstate.edu/people/segerman/dehn_surgery_images.html, 2009. [115, 116]
- [ST98] Carl Sundberg and Morwen Thistlethwaite, *The rate of growth of the number of prime alternating links and tangles*, Pacific J. Math. **182** (1998), no. 2, 329–358. MR 1609591 [13, 225]
- [ST11] Henry Segerman and Stephan Tillmann, *Pseudo-developing maps for ideal triangulations I: essential edges and generalised hyperbolic gluing equations*, Topology and geometry in dimension three, Contemp. Math., vol. 560, Amer. Math. Soc., Providence, RI, 2011, pp. 85–102. MR 2866925 [314]
- [SW95] Makoto Sakuma and Jeffrey Weeks, *Examples of canonical decompositions of hyperbolic link complements*, Japan. J. Math. (N.S.) **21** (1995), no. 2, 393–439. MR 1364387 [199, 309]
- [Tai98] Peter Guthrie Tait, *Scientific papers*, vol. 1, Cambridge University Press, Cambridge, 1898. [1, 13]
- [Tai 4] Peter G. Tait, *On knots. part ii*, Trans. Roy. Soc. Edinburgh **32** (1883-4), 327–342. [4]
- [Tai 5] ———, *On knots. part iii*, Trans. Roy. Soc. Edinburgh **32** (1884-5), 493–506. [4]
- [Thi98] Morwen Thistlethwaite, *On the structure and scarcity of alternating links and tangles*, J. Knot Theory Ramifications **7** (1998), no. 7, 981–1004. MR 1654669 [13, 225]
- [Thu79] William P. Thurston, *The geometry and topology of three-manifolds*, Princeton Univ. Math. Dept. Notes, 1979, Available at <http://www.msri.org/communications/books/gt3m>. [vii, xii, 8, 19, 40, 72, 80, 90, 111, 113, 121, 122, 124, 174, 254]
- [Thu82] ———, *Three-dimensional manifolds, Kleinian groups and hyperbolic geometry*, Bull. Amer. Math. Soc. (N.S.) **6** (1982), no. 3, 357–381. [vii, 6, 8, 154, 248, 249]
- [Thu97] ———, *Three-dimensional geometry and topology. Vol. 1*, Princeton Mathematical Series, vol. 35, Princeton University Press, Princeton, NJ, 1997, Edited by Silvio Levy. [vii, 19, 29, 50, 60, 61]
- [Wad16] Masaaki Wada, *Opti, a computer program for studying punctured torus groups*, Available at <http://delta-mat.ist.osaka-u.ac.jp/OPTi/index.html>, 2016. [248]
- [Wal60] Andrew H. Wallace, *Modifications and cobounding manifolds*, Canad. J. Math. **12** (1960), 503–528. [108]
- [Wan69] Hsien-chung Wang, *Discrete nilpotent subgroups of Lie groups*, J. Differential Geometry **3** (1969), 481–492. MR 0260930 [92]
- [Wee85] Jeffrey R. Weeks, *Hyperbolic structures on three-manifolds*, Ph.D. thesis, Princeton University, 1985. [8, 65, 78]

- [Wee05] Jeff Weeks, *Computation of hyperbolic structures in knot theory*, Handbook of knot theory, Elsevier B. V., Amsterdam, 2005, pp. 461–480. MR 2179268 [78, 92]
- [Wie81] Norbert J. Wielenberg, *Hyperbolic 3-manifolds which share a fundamental polyhedron*, Riemann surfaces and related topics: Proceedings of the 1978 Stony Brook Conference (State Univ. New York, Stony Brook, N.Y., 1978), Ann. of Math. Stud., vol. 97, Princeton Univ. Press, Princeton, N.J., 1981, pp. 505–513. MR 624835 [243]
- [Yam12] Yasushi Yamashita, *Creating software for visualizing Kleinian groups*, Geometry, topology and dynamics of character varieties, Lect. Notes Ser. Inst. Math. Sci. Natl. Univ. Singap., vol. 23, World Sci. Publ., Hackensack, NJ, 2012, pp. 159–190. MR 2987618 [248, 260]
- [Zag07] Don Zagier, *The dilogarithm function*, Frontiers in number theory, physics, and geometry. II, Springer, Berlin, 2007, pp. 3–65. MR 2290758 [175]
- [Zas37] Hans Zassenhaus, *Beweis eines satzes über diskrete gruppen*, Abh. Math. Sem. Univ. Hamburg **12** (1937), no. 1, 289–312. MR 3069692 [99]

Index

- (G, X) -structure, 45, 47, 50, 60, 61, 294, 319
- 2/3-ideal triangle, 40, 297
- 2π -theorem, 271
- A -polynomial, 14, 325–327
 - A_{PSL} , 326
 - $\text{SL}(2, \mathbb{C})$, 325–327
 - hyperbolic, A_{HYP} , 314–316, 327
- I bundle
 - twisted, 258
- I -bundle, 253, 256–258, 280–283, 289
 - horizontal boundary, 253, 282
 - twisted, 253
 - vertical boundary, 253, 282
- $I(g)$, 296–300, 304, 309
- A_{PSL} -polynomial, 326
- A_{HYP} -polynomial, 314–316, 327
- PSL-character variety, 323
- PSL-representation variety, 323
- $\text{SL}(2, \mathbb{C})$ A -polynomial, 325–327
- π_1 -essential, 240, 241, 251, 281
- π_1 -injective, 152, 171, 240–242
- $d(v)$, 54, 55, 58, 59, 62, 106
- 2-bridge knot or link, 11–14, 147, 173, 189, 195, 197–199, 202, 206, 208, 213, 214, 222, 223, 265
 - angle structure, 208, 214
 - cusp triangulation, 206, 207, 223
 - definition, 197
 - hyperbolic, 213
 - triangulation, 202, 208
 - volume bound, 265
- 6-theorem, 166, 170
- 6-theorem, weaker, 165, 169, 170

- abelian representation, 321, 324–326, 328
- accidental parabolic, 248, 250, 251
- accidental surface, 248, 251–254, 259
- Adams horoball, 294, 295

- affine algebraic set, 311, 320, 321, 323, 324, 327, 328
 - morphism, 321, 324, 327, 328
 - reducible, irreducible, 311
- affine torus, 47, 53, 61, 62, 106
- affine transformation, 45, 47
- affine variety, 312, 322
- algebraically ∂ -incompressible, 164
- alternating diagram, 13, 26, 208, 225, 227–231, 235–237, 240–242, 250, 251, 257, 259, 265, 280, 282, 284, 287, 309
 - checkerboard surface, 284
 - definition, 13
 - example with no alternating diagram, 25, 26
 - tangle, 197
- alternating knot or link, 13–15, 25–27, 132, 208, 225, 228–231, 235–237, 240, 243, 250, 257, 259, 279, 289, 309
 - anannular, 235
- angled polyhedral structure, 229
- atoroidal, 237
- bounded polyhedral decomposition, 238
 - checkerboard surface, 238, 240, 241, 251, 259, 282, 283, 287
 - definition, 13
 - hyperbolic, 230, 237
 - polyhedral decomposition, 26, 228
 - twist-number, 231
 - volume bounds, 280
- ambient isotopic, 2, 22, 315
- ambient isotopy, 2, 147, 149
- analytic continuation, 52, 61, 175
- anannular, 153, 154, 163, 164, 166, 170, 230, 235, 237

- angle structure, 159–163, 182–184, 188, 189, 191–193, 208–210, 212–216, 222, 265, 266
 - angled polyhedral structure, 161–163, 229, 230
 - bounded, 239, 240
 - annulus theorem, 251, 252
 - approximate inverse, 118
 - arc length, 30, 31
 - arithmetic link, 146
 - asymptotically sharp volume bound, 264, 265, 288
 - atoroidal, 153, 154, 156, 163, 166, 170, 237, 267
 - augmented link, 134, 135
 - definition, 134
 - fully, 137
 - fully augmented, 134
 - augmenting link diagram, 134

 - belted sum, 245, 259
 - belted tangle, 245, 259
 - bigon, 9, 11, 27, 66, 67, 72, 79, 127, 130, 136, 137, 228, 230, 232–234, 242, 257, 258, 264, 282–284, 286, 287
 - Borromean family, 132, 134, 136
 - Borromean rings, 132, 136, 146, 147, 305, 306
 - Borromean twisted sisters, 132
 - boundary π_1 -injective, 240–242
 - boundary at infinity, 32, 37, 40, 90, 109, 139
 - boundary bigon, 161, 163, 234, 235
 - boundary compressible, 152, 166, 167
 - boundary compression disk, 152, 153, 159, 167, 227, 241, 253
 - boundary incompressible, 152–154, 164, 167, 239, 240, 242, 252, 253
 - boundary irreducible, 153–155, 157–159, 163, 166, 170, 172, 230, 237, 239, 251, 252
 - boundary parallel, 151, 153, 154, 163, 166, 167, 227, 237, 241
 - bounded angled polyhedral structure, 239, 240
 - Böröczky cusp density theorem
 - 2-dimensional, 168
 - 3-dimensional, 294, 310

 - Cabling conjecture, 114
 - canonical component, 313, 322
 - gluing variety, 313
 - canonical decomposition, 14, 168, 292, 308
 - canonical triangulation, 115
 - Casson’s conjecture, 191
 - Cauchy sequence, 44
 - center, 100
 - chain link, 259
 - character
 - PSL, 323
 - representation, 322
 - character variety, 322, 326
 - PSL, 323
 - canonical component, 322
 - characteristic submanifold, 156, 280, 281, 289
 - chart, 45–53, 61, 62
 - checkerboard coloring, 26, 237
 - checkerboard surface, 237, 238, 240, 250, 256, 257, 282–284, 286, 287
 - π_1 -essential, 240, 241
 - fiber, 256, 257
 - not accidental, 251
 - quasifuchsian, 259
 - circle at infinity, 32
 - circle packing, 137–139
 - intersection graph, 137–139
 - circle packing theorem, 137, 139
 - combinatorial area, 160, 161, 163, 229, 230, 232, 239–241, 252, 286
 - disk, 160
 - surface, 160
- combinatorially equivalent, 303
 - commutator, 99
 - companion knot, 152
 - complete metric space, 44, 50, 54–60, 62, 65, 68, 74, 76, 78, 79, 84, 105
 - completeness equations, 76, 78–80
 - complex length, 110, 123
 - complexity of essential surface, 158
 - compressible, 150, 151, 166, 167, 227
 - parabolically compressible, 283
 - compression disk, 150–152, 166, 167, 171, 240, 241
 - cone angle, 108–110, 113, 270
 - cone manifold, 108, 109, 113, 117
 - conjugate, 83
 - connected diagram, 225
 - connected sum, 6, 15, 226, 227
 - continued fraction, 195
 - convexity equation, 213
 - Conway sphere, 246, 247
 - coordinate change map, 46
 - cross ratio, 40, 41

- crossing
 - horizontal, 199
 - negative, 196, 316, 317
 - positive, 196, 316, 317
 - vertical, 199
- crossing arc, 21, 228, 233, 236, 237, 253, 282, 309
- crossing circle, 134
- crossing disk, 135
- crossing number, 5
- cuspidal neighborhood, 5
 - maximal cuspidal neighborhood, 294, 295, 299, 301, 304, 305, 309, 310
 - rank-1, 89
 - rank-2, 90
- cuspidal density theorem
 - 2-dimensional, 168, 310
 - 3-dimensional, 294
- cuspidal neighborhood, 74
- cuspidal torus, 74
- cuspidal triangulation, 74
- cut along surface Σ , 238
- cylindrical coordinates, 268

- degeneracy equation, 312, 313
- degenerate tetrahedron, 69, 115
- Dehn filling, 107, 108, 112, 114, 121, 122, 128, 129, 131, 132, 145, 147, 166, 170, 191–193, 264, 271, 276
 - exceptional, 113, 122
 - fundamental theorem of Wallace and Lickorish, 108
 - trivial, 112
- Dehn filling coefficient, 110
- Dehn filling equation, 115
- Dehn filling space, 110, 111, 113–118, 123
- denominator closure, 197
- developing map, 52, 319
- diffeomorphism
 - real analytic, 46
- dilogarithm function, 174
- discrete group, 84
- double of $M \setminus S$, 280

- edge gluing equations, 71, 311
- edge invariant, 69, 311
- elementary, 97
- elementary group, 88–93, 101, 102
- elliptic, 37, 38, 40, 70, 83, 84, 87, 88, 92, 101, 109, 295
- EPD, 284–286, 289
- equivariant Ford domain, 299
 - combinatorially equivalent, 303
 - multiple cusps, 305
- essential, 153, 156, 157, 163, 164, 166, 169, 171, 225, 227, 230, 232, 234–236, 239, 240, 242–244, 246, 248, 250, 254, 280–283, 286, 289, 328
 - essential meridional annulus, 227, 235, 236, 241
 - essential product disk (EPD), 284–286, 289
- Euclidean structure, 43, 46, 47, 53, 61, 74, 79, 106, 122, 131, 140, 165, 188, 189, 210, 294
- Euler characteristic, 162, 279, 283, 286
- exceptional Dehn filling, 113, 122
- exceptional fiber, 155

- face, 20
- face-pairing isometry, 48, 84, 102, 120, 139, 294, 300–302, 307, 308
- fiber, 155, 253
 - virtual, 254
- first fundamental form, 30
- flat tetrahedron, 69, 115
- flype, 10, 231
- Ford domain, 291, 301
 - equivariant
 - combinatorially equivalent, 303
 - equivariant Ford domain, 299
 - multiple cusps, 305
- Ford–Voronoi domain, 291
- framing of solid torus, 147
- free group action, 87, 88, 92, 102
- Fuchsian, 248, 249, 254
- full-sized horoball, 294
- fully augmented link, 134, 136, 137, 140, 143, 145, 147, 149, 164, 170, 243, 263, 265, 279, 288
 - cuspidal, 140, 143, 145
 - hyperbolic, 139
 - polyhedral decomposition, 135, 137
 - reduced, 136, 137, 139
 - volume bound, 263, 288
- fundamental domain, 291, 294

- gear rotation, 26
- geodesic, 32
 - infinite, 32
- geometric convergence, 119
- geometric convergence of groups, 120
- geometric dual, 305, 307, 308
- geometric ideal triangulation, 68

- geometric limit, 119
- geometric polygonal decomposition, 44
- geometric structure, 46
- geometric topology, 119
- geometric triangulation, 12, 13, 68, 69, 189, 195, 208, 213, 266
 - exist virtually, 193
- Geometrization theorem for closed
 - 3-manifolds, 156
- gluing, 44, 48
- gluing equations
 - edge equations, 71, 311
- gluing variety, 312, 313
- Gordon–Luecke knot complement
 - theorem, 2, 105, 304
- Gromov–Hausdorff topology, 119
- group action
 - free, 87, 88, 92, 102
 - properly discontinuous, 87, 88, 102
- guts, 281–283, 287, 289

- hairpin turn, 206
- half-twist, 135
- highly twisted, 10, 11, 170, 277, 279, 289
 - hyperbolicity, 170
 - volume bounds, 277
- hinge equation, 213
- hinge tetrahedron, 205
- holonomy, 53, 55–58, 62, 65, 74, 76, 77, 84, 106, 107, 109–111, 189, 253, 292, 317–320, 323, 327
- holonomy group, 53, 62, 78, 83–87, 102, 184, 302, 317
- holonomy variety, 314
- homogeneous space, 99
- homotopically ∂ -incompressible, 164
- homotopically boundary incompressible, 164
- horizontal boundary, 253, 282
- horizontal crossing, 199
- horoball, 36, 39
 - Adams, 294, 295
 - full-sized, 294
- horocycle, 36
- horosphere, 39
- hyperbolic A -polynomial, 314
- hyperbolic 3-manifold, 127
- hyperbolic cone, 108
- hyperbolic cone manifold, 108, 109, 113, 117
- hyperbolic Dehn filling space, 110, 111, 113–118, 123
- hyperbolic Dehn filling theorem, 111
 - geometric convergence, 120
- hyperbolic knot or link, 7, 127
- hyperbolic structure, definition, 47
- hyperideal tetrahedron, 277

- ideal octahedron, regular, 130, 131, 134, 193, 277, 278, 281, 288
- ideal polyhedron, definition, 20
- ideal tetrahedron, definition, 38
- ideal triangle, 35, 36, 40, 55, 57, 58, 65–67, 84, 142, 143, 164, 165, 168, 172, 201, 263, 278, 279, 307, 309
- ideal triangulation, definition, 12
- ideal vertex, 54
- incomplete 3-punctured sphere, 57
- incompressible, 150–154, 156, 164, 171, 226, 227, 239, 240, 242, 243, 245, 251, 259
- incompressible torus, 122, 151, 156, 226
- inessential edge, 313
- injectivity radius, 91–93
- interior edge, 238
- intersection graph, 137
- irreducible, 153–159, 163, 166, 170–172, 230, 237, 239, 251, 252, 267
- irreducible affine algebraic set, 311, 312, 321, 322
- irreducible component, 312–314, 321, 322, 324–326
- irreducible components, 312
- isometric sphere, 296–300, 302–304, 307
- isometry, definition, 33

- Jaco annulus theorem, 251, 252
- JSJ-decomposition, 156, 280

- Každan–Margulis Theorem, 100
- Kleinian group, 84
- knot complement theorem, 304
- knot complement, definition, 2
- knot diagram, definition, 3
- knot exterior, definition, 2
- knot invariant, definition, 6
- knot strand, 134
- knot sum, 5, 6, 226
- knot, definition, 1
- Koebe–Andreev–Thurston theorem, 137, 139
- Kubert identities, 176, 192

- leading–trailing deformation, 184
- lens space, 112, 123

- Lickorish, fundamental Dehn filling theorem, 108
- limit set, 90, 244, 248
- linear fractional transformation, 33
- link complement, definition, 2
- link diagram, definition, 3
- link exterior, definition, 2
- link invariant, 6
- link, definition, 1
- Lobachevsky function, 174
- locally finite, 298
- longitude, 147, 227
 - standard, 109, 227
- loop theorem, 171
- loxodromic, 37, 38, 40, 83, 84, 87, 89, 90, 93, 95, 96, 98, 100, 101, 103, 109, 111
- Möbius transformation, 37, 38, 41, 70, 137, 178
- Margulis constant, 91
- Margulis lemma, 92
- Margulis number for M , 91
- maximal cusp neighborhood, 294, 295, 299, 301, 304, 305, 309, 310
- Menasco–Reid conjecture, 250
- meridian, 109, 147, 227
- midpoint, 142–145
- Miyamoto’s theorem, 277
- morphism of affine algebraic sets, 321
- Mostow–Prasad rigidity, 105, 129, 192, 303
- mutation, 246, 247
- negative crossing, 196
- negatively oriented tetrahedron, 69, 113, 115
- Newton polygon, 328
- nilpotent group, 99
- nonelementary group, 88, 91, 95, 97
- normal, 157, 160–163, 229, 230, 232, 234–236, 239–242, 252, 253, 284–286, 289
 - disk, 156
- normal curve, 315
- normal fiber, 155
- normal form, 157, 163, 232, 234, 236, 240–242, 252, 285, 286
- nugatory crossing, 4, 27
- numerator closure, 197
- orthoscheme, 178
- parabolic, 37, 38, 40, 83, 84, 86–90, 93, 96, 98, 100–103, 109–111, 153, 154, 244, 248, 250, 251, 292, 298, 303, 307, 317, 318
 - parabolic compression, 283, 285, 286
 - parabolic locus, 238, 251, 252, 256, 257, 280, 282–286
 - parabolically compressible, 283, 284, 286, 287
 - plane of projection, definition, 3
 - pleated surface, 140, 165–167, 169, 210, 246, 247
 - pleating angle, 210
 - polyhedral convergence, 120
 - polyhedron, definition, 20
 - polynomial map, 321
 - positive crossing, 196
 - positively oriented tetrahedron, 68, 69, 113, 115, 173, 183, 189, 190, 193, 208, 222
 - prime, 6, 226
 - diagram, 6, 136, 226
 - knot or link, 226
 - projection plane, definition, 3
 - proper embedding, definition, 149
 - properly discontinuous, 87, 88, 102
 - quasi-isometric embedding, 118
 - quasi-isometric topology, 119
 - quasi-isometry, 118
 - quasifuchsian group, 248, 250
 - quasifuchsian surface, 248, 253, 254, 259
 - rank-1 cusp, 89
 - rank-2 cusp, 90
 - rational tangle, 195
 - real analytic diffeomorphism, 46
 - reduced diagram, 4
 - reduced fully augmented link, 136, 137
 - reducible 3-manifold, 114, 123, 166, 169, 239
 - reducible affine algebraic set, 311
 - reducible crossing, 4, 225
 - reducible Dehn filling, 114
 - reflection through a geodesic, 39
 - regular ideal octahedron, 130, 131, 134, 193, 277, 278, 281, 288
 - volume, 131
 - volume, 277, 281, 288
 - regular neighborhood, 149
 - regularly fibered solid torus, 155
 - Reidemeister move, 9
 - Reidemeister moves, 4

- representation variety, 320
 - PSL, 323
- Riemannian metric, 30
- satellite knot, 7, 15, 151, 153
- Schläfli's formula, 190
- Seifert fibered solid torus, 155
 - exceptional fiber, 155
 - normal fiber, 155
 - regularly fibered solid torus, 155
- Seifert fibered space, 155
- semifiber, 253, 257
- shearing, 160
- singular locus, 108
- slope, 107, 165
- slope length, 165, 166
- smooth category, 149
- SnapPea, 78
- SnapPy, 8, 78
- solid torus
 - Seifert fibered, 155
- standard longitude
 - Whitehead link, 147
- straightening edges and triangles, 164
- strict semifiber, 254
- surface
 - checkerboard, 237
 - fiber, 253
 - Fuchsian, 248
 - quasifuchsian, 248, 253, 254, 259
 - semifiber, 253
 - strict semifiber, 254
 - totally geodesic, 248
- surface edge, 238
- surface faces, 238
- surger, 150, 158
- swallow–follow torus, 226
- tangle, 195
 - rational tangle, 195
- tetrahedron
 - degenerate, 69, 115
 - flat, 69, 115
 - negatively oriented, 69, 113, 115
 - positively oriented, 68, 69, 113, 115, 173, 183, 189, 190, 193, 208, 222
- thick part, 91
- thin part, 91
 - structure of thin part, 91
- Thurston's hyperbolic Dehn filling
 - theorem, 111
 - geometric convergence, 120
- topological ideal triangulation, 65, 311
- topological polygonal decomposition, 44
- torus decomposition, 156
- torus knot, 7, 152, 154
 - $(2, q)$ -torus knot, 231
- totally geodesic surface, 248
- trace, 83
- transition map, 46
- transverse intersection, 149
- triangulation, definition, 12
- trivial Dehn filling, 112
- truncated tetrahedron, 12, 277
- tubular neighborhood, 2, 107, 149–151
- twist knot, 9, 127
- twist region, 9, 127
- twist-number, 11, 231, 276
- twist-reduced, 11, 136, 230, 276
- twisted I -bundle, 253
- twisted band, 237
- two-bridge links, 147
- unknot, 5
- valence, 26
- vertex triangle, 161, 163
- vertical boundary, 253, 282
- vertical crossing, 199
- vertical fundamental domain, 301
- virtual fiber, 254
- volume bound
 - lower bound from angle structures, 190
 - lower bound on Dehn filling, 122, 276
 - upper bound on Dehn filling, 121
- volume form, 31
- volume functional, 183, 184, 188–192, 208, 214, 215, 217, 218, 222, 265
- Wallace, fundamental Dehn filling
 - theorem, 108
- Weil rigidity theorem, 192
- Whitehead link, 10, 112, 123, 127–130, 146, 147
- wild knot, 2
- Wirtinger presentation, 316, 318, 319, 328
- Zariski topology, 311, 327
- Zassenhaus Theorem, 99
- zig-zag, 207